26 May 2006 | $10

Science

Cancer Treatment gets Personal

AAAS

LESS WASTE.

MORE BAND.

PCR so reliable, we guarantee your results. Get successful PCR the first time with AccuPrime™ enzymes and primers from Invitrogen. Put an end to waste: reduce rework, optimization, and repeat reactions. Start getting used to PCR you can count on. And if something goes wrong, we'll troubleshoot it and make it right—even redesign and synthesize primers at no charge. See how dependable PCR can be at **www.invitrogen.com/accuprime**.

illumina | invitrogen™

Don't let temperature hold you back.

Only StrataScript® 5.0 RT delivers reliable results at any temperature.

Our new StrataScript® 5.0 Multi-Temperature Reverse Transcriptase (RT) delivers high cDNA yield over a broader cDNA synthesis temperature range (37–60°C). This unique, multi-temperature capability allows you to use the optimal reaction temperature for your template and primers without having to change your reverse transcriptase. Achieve 10-fold greater yield of amplifiable cDNA from lower RNA input levels and up to four-fold better yields of full-length cDNA.

Choose the Temperature You Need

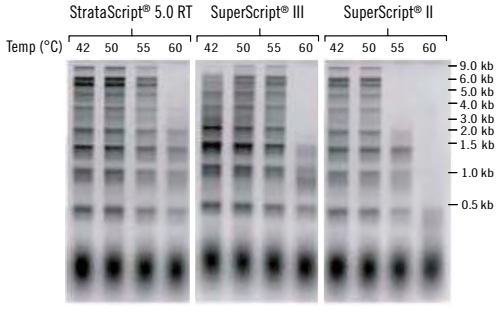

Need More Information? Give Us A Call:

Stratagene US and Canada
Order: 800-424-5444 x3
Technical Service: 800-894-1304 x2

Stratagene Europe
Order: 00800-7000-7000
Technical Service: 00800-7400-7400

Stratagene Japan K.K.
Order: 3-5821-8077
Technical Service: 3-5821-8076

www.stratagene.com

Ask Us About These Great Products:

StrataScript® 5.0 Multi-Temperature Reverse Transcriptase	**2,000U**	**600098**
	10,000U	**600100**

STRATAGENE®

GE Healthcare

Bringing science to life

When it comes to life sciences, GE Healthcare is setting the standard. Tens of thousands of scientists in over 100 countries around the world rely on our products every day. We have delivered more than 60 000 research protein purification systems, 1500 BioProcess™ systems and 12 000 BioProcess columns worldwide. Our Amersham family of consumables, with its 60-year heritage, is trusted to provide accurate results time and time again.

But we're never content to stand still. We constantly strive for new innovations for tomorrow's research and drug development. And the result is groundbreaking products like the ÄKTAdesign™ platform, IN Cell Analyzer, Ad-A-Gene Vectors, and MabSelect™ media. Thanks to our technological achievements and global presence, we're able to help you turn your scientific ideas into reality – bringing science to life and helping transform healthcare.

We call it Life Science Re-imagined.

Discover more at www.gehealthcare.com/life

imagination at work

Volume 312, Issue 5777

COVER

Advances in understanding the genetic basis of cancer have led to promising new therapies, which in turn have fueled discussions about a future model of cancer care in which treatment decisions are guided by the molecular attributes of the individual patient. A special section beginning on page 1157 examines this model and other emerging themes in cancer research.

Image: J. Moglia/Science; photos, (top) Getty Images, (bottom) Royalty-Free/Corbis

DEPARTMENTS

1099 *Science* Online
1101 This Week in *Science*
1107 Editors' Choice
1110 Contact *Science*
1113 NetWatch
1115 Random Samples
1135 Newsmakers
1154 AAAS News & Notes
1233 New Products
1234 *Science* Careers

EDITORIAL

1105 Health Roundup
by Donald Kennedy

SPECIAL SECTION

Frontiers in Cancer Research

INTRODUCTION

Celebrating a Glass Half-Full 1157

NEWS

Energy Deregulation: Licensing Tumors to Grow 1158
Autophagy: Is It Cancer's Friend or Foe? 1160

PERSPECTIVES

The New Era in Cancer Research 1162
H. Varmus

Poster: Cancer Treatment Gets Personal

Cancer Biomarkers—An Invitation to the Table 1165
W. S. Dalton and S. H. Friend

Molecular Imaging in Cancer 1168
R. Weissleder

Antiangiogenic Therapy: A Universal Chemosensitization Strategy for Cancer? 1171
R. S. Kerbel

Targeting Tyrosine Kinases in Cancer: The Second Wave 1175
J. Beselga

For related online content, see page 1099 or go to: www.sciencemag.org/sciext/cancer/

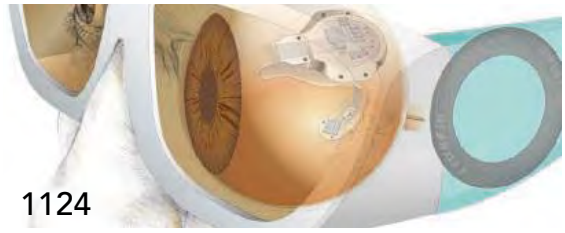

NEWS OF THE WEEK

Synthetic Biologists Debate Policing Themselves 1116
Pakistan Gives Geology Conference the Cold Shoulder 1117
Senate Panel Backs Social Sciences at NSF 1117
NIH Wants Its Minority Programs to Train More Academic Researchers 1119
SCIENCESCOPE 1119
High-Tech Materials Could Render Objects Invisible 1120
>>Science *Express reports by J. B. Pendry* et al. *and U. Leonhardt*
'Disappointed' Butler Exhausts Appeals 1120
RNAi Safety Comes Under Scrutiny 1121
Price Crash Rattles Europe's CO_2 Reduction Scheme 1123

NEWS FOCUS

A Vision for the Blind 1124
Universities Find Too Many Strings Attached to Foundation's Offer 1127
A Quiet Leader Unites Researchers in Drive for the Next Big Machine 1128
Why the International Linear Collider?
The HapMap Gold Rush: Researchers Mine A Rich Deposit 1131
Who Can Read the Martian Clock? 1132
Bombardment Looking "Possible"

CONTENTS continued >>

Systems Biology — Proteins and Proteomics

Standardized solutions for proteins

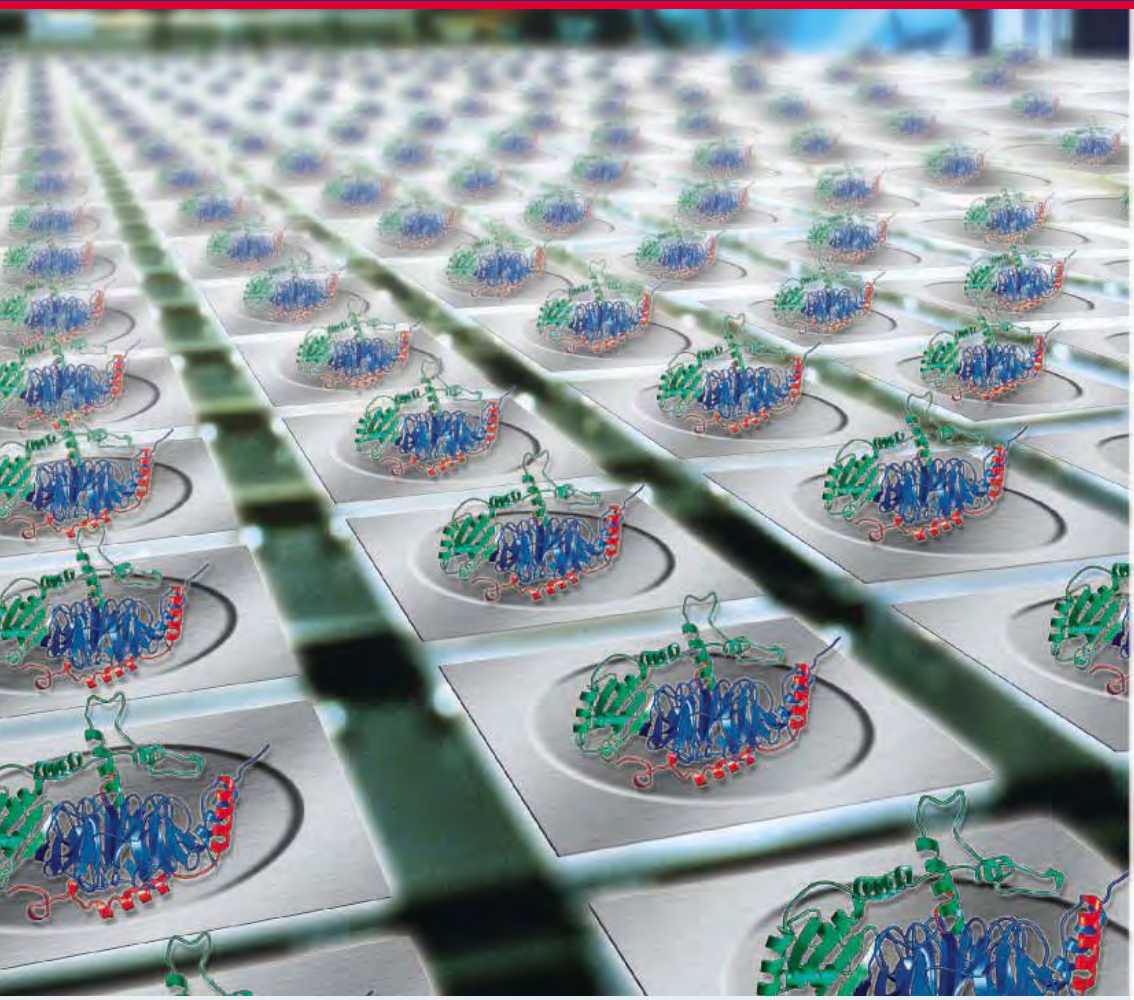

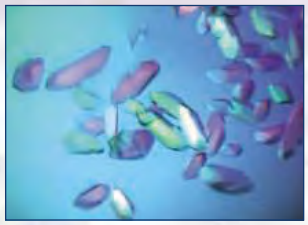

More reproducibility, streamlined crystallization*

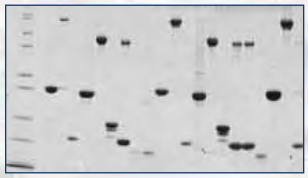

More proteins, purer, faster

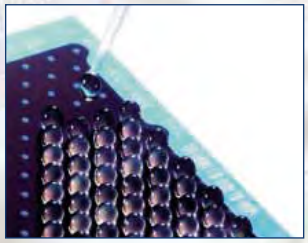

More peptide matches, more protein hits

Success with proteins — made possible by QIAGEN's expertise!

QIAGEN's comprehensive protein portfolio will help you rise to the challenge of working with proteins. QIAGEN provides easy-to-use, integrated solutions to help you succeed with:

- Expression
- Purification
- Detection
- Assay
- Crystallization
- MALDI sample prep
- Proteomics sample prep
- Automation
- Fractionation

Find a standardized solution for your protein challenge at www.qiagen.com/protein !

* Image shows *E. coli* gyrase A C-terminal domain crystals. Courtesy of Alex Ruthenburg from Prof. Verdine's laboratory, Harvard University, Boston, USA.

QIAGEN

Science

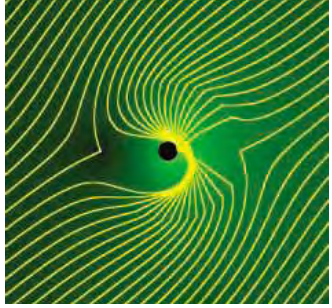

SCIENCE EXPRESS

www.sciencexpress.org

BIOCHEMISTRY

p53 Regulates Mitochondrial Respiration
S. Matoba et al.
Cancer cells can survive in low oxygen conditions because a defect in a common tumor suppressor inhibits mitochondrial respiration, allowing glycolysis to take place.
10.1126/science.1126863

MEDICINE

Chimpanzee Reservoirs of Pandemic and Nonpandemic HIV-1
B. F. Keele et al.
SIV, a close relative of the AIDS virus, infects up to 35 percent of the chimpanzees in a wild population in Cameroon, pointing to *Pan t. troglodytes* as the natural reservoir of HIV-1.
10.1126/science.1126531

PHYSICS

Controlling Electromagnetic Fields
J. B. Pendry, D. Schurig, D. R. Smith
The tunable dielectric and magnetic properties of metamaterials could be used in stealth technologies to cloak an object from view.
>> News story p. 1120; Science *Express article by U. Leonhardt*
10.1126/science.1125907

Optical Conformal Mapping
U. Leonhardt
In theory, the tunable dielectric and magnetic properties of metamaterials could be used in stealth technologies to pass light completely around an object and cloak it from view.
>> News story p. 1120; Science *Express article by J. B. Pendry* et al.
10.1126/science.1126493

LETTERS

Scientific Description Can Imperil Species 1137
B. L. Stewart, A. G. J. Rhodin, L. L. Grismer, T. Hansel
Tropical Deforestation and Global Warming *P. M. Fearnside*
Concern About Gag Rules *L. Pietrafesa*
Working Together for Communication *D. Acosta*
Response *D. Kennedy*
Revisiting the Age of the Sahara Desert *S. Kroepelin; C. S. Swezey* **Response** *M. Schuster* et al.

BOOKS *ET AL.*

Genesis The Scientific Quest for Life's Origin 1140
R. M. Hazen, reviewed by I. Fry

Browsings 1141

EDUCATION FORUM

Planning Early for Careers in Science 1143
R. H. Tai, C. Q. Liu, A. V. Maltese, X. Fan

PERSPECTIVES

How Many Ways to Make a Chordate? 1145
P. Lemaire >> Research Article p. 1183

Was the Younger Dryas Triggered by a Flood? 1146
W. S. Broecker

The Vacuum Energy Crisis 1148
A. Vilenkin >> Research Article p. 1180

High-Pressure Microscopy 1149
Z. Wang and Y. Zhao >> Report p. 1199

Bacteria Seize Control by Acetylating Host Problems 1150
C. A. Worby and J. E. Dixon >> Report p. 1211

Fluctuations in Plasticity at the Microscale 1151
M.-C. Miguel and S. Zapperi >> Report p. 1188

TECHNICAL COMMENT ABSTRACTS

GEOCHEMISTRY

Comment on "Heterogeneous Hadean Hafnium: Evidence of Continental Crust at 4.4 to 4.5 Ga" 1139
J. W. Valley, A. J. Cavosie, B. Fu, W. H. Peck, S. A. Wilde
full text at www.sciencemag.org/cgi/content/full/312/5777/1139a

Response to Comment on "Heterogeneous Hadean Hafnium: Evidence of Continental Crust at 4.4 to 4.5 Ga"
T. M. Harrison et al.
full text at www.sciencemag.org/cgi/content/full/312/5777/1139b

BREVIA

ATMOSPHERIC SCIENCE

Enhanced Mid-Latitude Tropospheric Warming in Satellite Measurements 1179
Q. Fu, C. M. Johanson, J. M. Wallace, T. Reichler
The pattern of tropospheric warming and stratospheric cooling visible in 26 years of satellite data indicates that the jet streams have been shifting poleward.

RESEARCH ARTICLES

ASTRONOMY

Why the Cosmological Constant Is Small and Positive 1180
P. J. Steinhardt and N. Turok
Models in which our universe repeatedly grows from a big bang and then collapse, produce a small cosmological constant consistently, not only as a special case. >> Perspective p. 1148

DEVELOPMENT

Regulatory Blueprint for a Chordate Embryo 1183
K. S. Imai, M. Levine, N. Satoh, Y. Satou
Sea squirts, among the simplest of extant chordates, now yield a glimpse at the network of regulatory gene interactions needed to generate a chordate animal.
>> Perspective p. 1145

CONTENTS continued >>

Hot Performance

Finnzymes' New Phusion™ Hot Start
The Number One DNA Polymerase

Accuracy	The highest fidelity of any available thermostable polymerase
Speed	Increased processivity allows reaction times to be reduced dramatically
Specificity	Reduces non-specific amplification and primer degradation
Robustness	Reduces reaction failures and minimizes optimization

Phusion - Extreme Performance

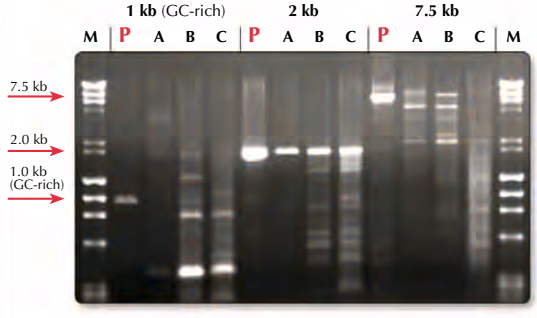

The following fragments were amplified from human genomic DNA: 1kb from CEBPB gene (GC-rich), 2 kb and 7.5 kb from human β-globin gene. Hot start high-fidelity DNA polymerases (P, A,B,C) were used according to suppliers' recommendations:

P) Phusion™ Hot Start High-Fidelity DNA Polymerase
A) novel *Pfu*-based fusion DNA polymerase
B) modified *Pfu* DNA polymerase
C) *T. kodakaraensis* DNA polymerase

Distributed in the US and Canada by New England Biolabs. For other countries visit www.finnzymes.com. PCR license notice: These products are sold under licensing arrangements of Finnzymes Oy with F. Hoffman-La Roche Ltd. The purchase of these products is accompanied by a limited license to use them in the Polymerase Chain Reaction (PCR) process in conjunction with a thermal cycler whose use in the automated performance of the PCR process is covered by the up-front fee, either by payment to Applied Biosystems or as purchased, i.e. an authorized thermal cycler.

FINNZYMES
TOOLS FOR MOLECULAR BIOLOGY

Finnzymes Oy • Keilaranta 16 A, 02150 Espoo, Finland • Tel. +358 9 584 121 • Fax +358 9 5841 2200 • fz@finnzymes.fi • www.finnzymes.com

REPORTS

MATERIALS SCIENCE

Scale-Free Intermittent Flow in Crystal Plasticity 1188
D. M. Dimiduk, C. Woodward, R. LeSar, M. D. Uchic
The relation between number and size of slip events in deforming nickel microcrystals follows a power law, like slip in ice and avalanches. *>> Perspective p. 1151*

APPLIED PHYSICS

Electronic Confinement and Coherence in Patterned Epitaxial Graphene 1191
C. Berger et al.
Thin graphene layers grown on silicon carbide can be patterned into ribbons that exhibit high electrical conductivity and quantum confinement effects at near zero kelvin.

CHEMISTRY

Imaging Bond Formation Between a Gold Atom and Pentacene on an Insulating Surface 1196
J. Repp, G. Meyer, S. Paavilainen, F. E. Olsson, M. Persson
A scanning tunneling microscope is used to form, break, control, and image a single bond between a gold atom and an organic molecule adsorbed on an insulating layer.

CHEMISTRY

Carbon Nanotubes as High-Pressure Cylinders and Nanoextruders 1199
L. Sun et al.
Induced defects on the walls of carbon nanotubes cause them to contract, producing a high-pressure chamber that can be probed with an electron microscope. *>> Perspective p. 1149*

GEOPHYSICS

Earthquake Rupture Stalled by a Subducting Fracture Zone 1203
D. P. Robinson, S. Das, A. B. Watts
In the great 2001 Peru earthquake, the rupture extended for 70 kilometers, skirted a barrier on the fault, then continued for another 200 kilometers, and 30 seconds later broke the barrier.

GEOPHYSICS

Reduced Radiative Conductivity of Low-Spin (Mg,Fe)O in the Lower Mantle 1205
A. F. Goncharov, V. V. Struzhkin, S. D. Jacobsen
Measurements show that a spin-pairing transition in iron causes iron oxide minerals in the Earth to become more opaque at high pressure, likely altering heat transfer in the deep mantle.

STRUCTURAL BIOLOGY

Structure of the Eukaryotic Thiamine Pyrophosphate Riboswitch with Its Regulatory Ligand 1208
S. Thore, M. Leibundgut, N. Ban
The structure of a common metabolite bound to a ubiquitous riboswitch shows how its ligand turns it off, suppressing translation of genes for the metabolite's synthesis.

MICROBIOLOGY

***Yersinia* YopJ Acetylates and Inhibits Kinase Activation by Blocking Phosphorylation** 1211
S. Mukherjee et al.
The plague-causing bacterium inhibits the innate immune responses of its infected host by blocking the phosphorylation and activation of key signaling enzymes. *>> Perspective p. 1150*

MEDICINE

A Regulatory SNP Causes a Human Genetic Disease by Creating a New Transcriptional Promoter 1215
M. De Gobbi et al.
A type of anemia is caused by a change in a single nucleotide, creating a new promoterlike sequence that disrupts transcription of downstream red blood cell genes.

PLANT SCIENCE

AXR4 Is Required for Localization of the Auxin Influx Facilitator AUX1 1218
S. Dharmasiri et al.
An intracellular protein directs a hormone transporter to a specific destination in the plant's root that allows it to grow selectively downward in response to gravity.

CELL BIOLOGY

CRACM1 Is a Plasma Membrane Protein Essential for Store-Operated Ca^{2+} Entry 1220
M. Vig et al.
Two membrane proteins that control calcium flow into cells upon depletion of intracellular calcium stores are either part of the elusive calcium release–activated calcium channel or act as its regulators.

DEVELOPMENTAL BIOLOGY

Regulation of Adult Bone Mass by the Zinc Finger Adapter Protein Schnurri-3 1223
D. C. Jones et al.
A newly identified regulatory protein maintains the proper proportion of growing bones by controlling the degradation of a bone cell growth factor.

MEDICINE

Pituitary Adenoma Predisposition Caused by Germline Mutations in the *AIP* Gene 1228
O. Vierimaa et al.
Molecular and genealogical data from a Finnish population show that benign but health-threatening tumors of the pituitary gland are caused by mutations in a regulatory gene.

ECOLOGY

Strong Top-Down Control in Southern California Kelp Forest Ecosystems 1230
B. S. Halpern, K. Cottenie, B. R. Broitman
The community structure and biomass of California kelp forests are largely controlled by top-down factors such as predatory fish, rather than by levels of dissolved nutrients.

1151 & 1188

ADVANCING SCIENCE, SERVING SOCIETY

SCIENCE (ISSN 0036-8075) is published weekly on Friday, except the last week in December, by the American Association for the Advancement of Science, 1200 New York Avenue, NW, Washington, DC 20005. Periodicals Mail postage (publication No. 484460) paid at Washington, DC, and additional mailing offices. Domestic individual membership and subscription (51 issues): $139 ($74 allocated to subscription). Domestic institutional subscription (51 issues): $650; Foreign postage extra: Mexico, Caribbean (surface mail) $55; other countries (air assist delivery) $85. First class, airmail, student, and emeritus rates on request. Canadian rates with GST available upon request, GST #1254 88122. Publications Mail Agreement Number 1069624. **Printed in the U.S.A.**

Change of address: Allow 4 weeks, giving old and new addresses and 8-digit account number. **Postmaster:** Send change of address to *AAAS*, P.O. Box 96178, Washington, DC 20090–6178. **Single-copy sales:** $10.00 current issue, $15.00 back issue prepaid includes surface postage; bulk rates on request. The identification code for *Science* is 0036-8075. *Science* is indexed in the *Reader's Guide to Periodical Literature* and in several specialized indexes.

CONTENTS continued **>>**

Break the midiprep and maxiprep speed limit.

New **PureYield**™ plasmid preps deliver transfection-quality DNA in record time. Recover up to 1mg of plasmid DNA in less than 60 minutes (maxiprep) or up to 200µg in only 30 minutes (midiprep). No post-elution alcohol precipitation required. Race through your next plasmid prep.

Request a FREE SAMPLE* at: www.promega.com/pureyield

*Samples to qualified customers where available, while supplies last.

PROMEGA CORPORATION • www.promega.com

Promega

SCIENCE**NOW**

www.sciencenow.org DAILY NEWS COVERAGE

Addicted by Sex?
Brain rewards men and women differently in response to illegal drug use.

Planning of the Apes
Bonobos and orangutans know the value of thinking ahead.

Emergence of the Galactic Heavyweights
How dwarf galaxies changed the face of the universe.

Marriage, science, or both?

SCIENCE **CAREERS**

www.sciencecareers.org CAREER RESOURCES FOR SCIENTISTS

GLOBAL: Are Science and Marriage Mutually Exclusive?
I. S. Levine
Our Mind Matters expert studies the personal and professional pros and cons of tying the knot.

US: The Food-Network Effect
S. Webb
Shows like the Food Network's Foods Unwrapped are drawing new blood into the food industry.

UK: Testing Hypotheses on the Stock Market
A. Forde
Ex-astronomer Keith Lipman uses his physics training as a hedge-fund manager.

MISCINET: Educated Woman, Chapter 51—Search. Scour. Capture. Job
M. P. DeWhyse
Micella has finally decided what she's going to do next.

SPECIAL CONTENT

Frontiers in Cancer Research

POSTER: Cancer Treatment Gets Personal
An interactive version of the pull-out poster in this issue.
www.sciencemag.org/sciext/cancerposter/

SCIENCE'S **STKE**

www.stke.org SIGNAL TRANSDUCTION KNOWLEDGE ENVIRONMENT

EDITORIAL GUIDE: Turning the Corner in Cancer Therapy?
E. M. Adler, N. R. Gough, L. B. Ray
New insights into the molecular bases of cancer and the behavior of cancer cells may lead to pivotal changes in diagnosis and treatment.

PERSPECTIVE: HIFing the Brakes—Therapeutic Opportunities for Treatment of Human Malignancies
J. A. Garcia
Epidermal growth factor receptor signaling acts through the hypoxia-inducible factors to contribute to cancer progression.

PERSPECTIVE: p19^{ras} Brings a New Twist to the Regulation of p73 by Mdm2
K. L. Harms and X. Chen
An alternatively spliced form of the oncogene c-H-ras promotes activity of the p73 tumor suppressor.

SCIENCE'S **SAGE KE**

www.sageke.org SCIENCE OF AGING KNOWLEDGE ENVIRONMENT

PERSPECTIVE: Stem Cell Aging and Cancer
J. Fuller
Do stem cells age? Cancer studies may bring us closer to an answer.

PERSPECTIVE: The Age of Skin Cancers
A. Desai, R. Krathen, I. Orengo, E. E. Medrano
Why are older men at greater risk for melanoma than older women?

NEWS FOCUS: Shortcut to Death
M. Leslie
Stubby protein spurs cancer cells to eat themselves.

SCIENCE**PODCAST**

Listen to a special all-cancer ***Science*** Podcast for 26 May, including stories about a new model of cancer treatment, cancer biomarkers, tumor bioenergetics, and the role of the "microenvironment."
www.sciencemag.org/about/podcast.dtl

Separate individual or institutional subscriptions to these products may be required for full-text access.

Taq DNA Polymerase from New England Biolabs

HIGH YIELD, ROBUST AND RELIABLE PCR REACTIONS IN CONVENIENT FORMATS

Looking for the right solution for your high yield PCR? Choose recombinant *Taq* DNA Polymerase from New England Biolabs. As the leader in enzyme technology, New England Biolabs provides the highest quality recombinant *Taq* at exceptional value. Our expanded selection of *Taq* based products includes kits, master mixes, and a choice of reaction buffers. Choose *Taq* DNA polymerase from NEB for guaranteed Performance, Convenience and Results.

- ***Taq* with Standard Buffer** RH **M0273S/L**
  Compatible with existing assay systems and high throughput applications, is always detergent free and available with or without $MgCl_2$
- ***Taq* with ThermoPol Buffer** RH **M0267S/L**
  Promotes high yields under demanding conditions, available with or without $MgSO_4$ and detergent

RH = Recombinant

- ***Taq* 2X Master Mix** RH **M0270S/L**
  Just add template and primers
- ***NEW* Quick-Load™ *Taq* 2X Master Mix** RH **M0271S/L**
  Load PCR products directly onto agarose gels
- ***Taq* PCR Kits** RH **E5000S/E5100S**
  Contains reagents for 200 PCR reactions, available with or without controls

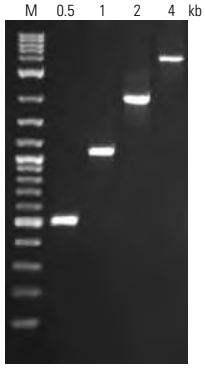

Selective and specific PCR amplification from Human Genomic DNA: Specific amplicons of 0.5, 1, 2, and 4 kb from human genomic DNA were amplified by *Taq* DNA Polymerase with Standard Buffer for 30 cycles. Marker (M) shown is 2-Log DNA Ladder (NEB #N3200).

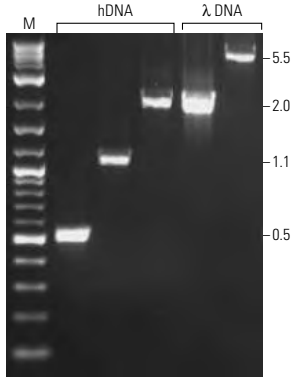

Versatility of the *Taq* 2X Master Mix: 30 ng human genomic DNA (hDNA) or 0.1 ng lambda DNA (λ DNA) was amplified in the presence of 200 nM primers in a 25 µl volume. Marker (M) shown is 2-Log DNA Ladder (NEB #N3200).

For more information and international distribution network, please visit www.neb.com

- **New England Biolabs Inc.** 240 County Road, Ipswich, MA 01938 USA 1-800-NEB-LABS Tel. (978) 927-5054 Fax (978) 921-1350 info@neb.com
- **Canada** Tel. (800) 387-1095 info@ca.neb.com
- **Germany** Tel. 0800/246 5227 info@de.neb.com
- **UK** Tel. (0800) 318486 info@uk.neb.com
- **China** Tel. 010-82378266 beijing@neb-china.com

NEW ENGLAND BioLabs® Inc.
the leader in enzyme technology

EDITED BY STELLA HURTLEY AND PHIL SZUROMI

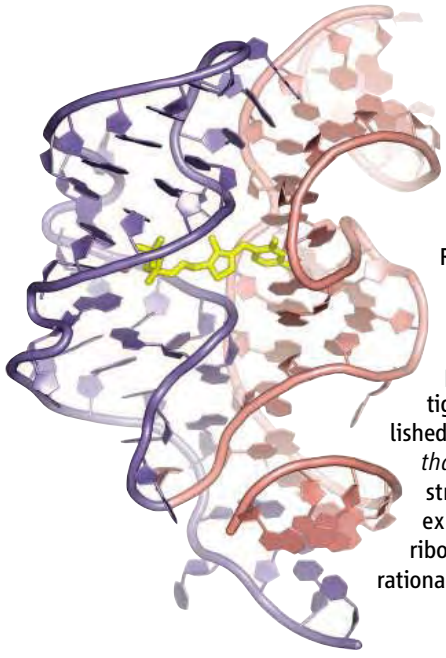

Making the Switch

Riboswitches are regions of untranslated messenger RNA that switch their conformations when they bind specific metabolites to regulate the expression of proteins involved in the biosynthesis of the bound metabolites. For example, in bacteria, archaea, and eukaryotes, the production of the essential cofactor thiamine pyrophosphate (TPP) is tightly regulated by TPP-binding riboswitches. **Thore *et al.*** (p. 1208, published online 4 May) determined the structure of the eukaryotic *Arabidopsis thaliana* TPP riboswitch bound to TPP at 2.9 angstrom resolution. The structure shows how the bound "off" conformation, which suppresses expression of a gene involved in TPP biosynthesis, is stabilized. TPP riboswitches are attractive targets for antimicrobial drugs, and the structure rationalizes the mechanism of resistance to the antibiotic pyrithiamine.

Jumping the Barrier

The rupture of faults causing earthquakes may be complicated by local tectonic conditions, but to date these subtleties have been difficult to disentangle. **Robinson *et al.*** (p. 1203) show that the rupture of the 23 June 2001 Peru earthquake (moment magnitude 8.4), the world's third largest since 1965, jumped a seismic barrier. After traveling for 70 kilometers, the rupture detoured around a hard block with an area 6000 square kilometers before continuing on for another 200 kilometers along the original fault. After a delay of half a minute, the block itself ruptured and released most of the earthquake's energy. The barrier is identified as a fracture zone on the subducting oceanic plate.

Deforming Slip by Slip

By recording nanoscale slip events in nickel microcrystals, **Dimiduk *et al.*** (p. 1188; see the Perspective by **Miguel and Zapperi**) quantitatively observe the critical dynamics in the plastic deformation of crystalline metals. Under a very slow loading rate, the sample deformed intermittently and the events followed a power-law distribution over more than two orders of magnitude in event size. This deviation from smooth laminar flow confirms the predictions of a number of models and acoustic measurements made on ice samples. The results may lead to an improved theoretical understanding of microscale deformation and may also relate to the behavior of magnetic noise and avalanches.

Why So Small?

In the standard Big Bang model, the amount of dark energy in the universe is roughly the same order of magnitude as energy in the form of matter, but this need not have been the case. Dark energy, parameterized as the cosmological constant, could have been trillions of times greater or smaller. This fine tuning has been explained by the anthropic principle—we would not be here if the cosmological parameters had been much different. **Steinhardt and Turok** (p. 1180, published online 4 May; see the Perspective by **Vilenkin**) propose an alternative way to tune the cosmological constant down to a small value. They model dark energy in a cyclic universe—a repeating succession of universes growing from big bangs and collapsing into big crunches—and find that most of the time the value of the cosmological constant is small and positive.

Making and Breaking a Metal Atom–Molecule Bond

Molecular electronics tries to exploit changes in conductivity of molecules held between metal electrodes, but the nature of the metal-molecule contact is not well understood. **Repp *et al.*** (p. 1196) followed the interaction of a gold atom with a pentacene molecule, both adsorbed on a thin NaCl film grown on a metal substrate. A scanning tunneling microscope (STM) tip was used to bring the Au atom into close contact with the molecule. Resonant inelastic electron tunneling (IET) through the lowest unoccupied orbital of pentacene led to bond formation, and the resulting changes in bond hybridization could be imaged. The bond could be broken by IET through the molecular complex. The resulting changes could be understood by comparison with density functional calculations.

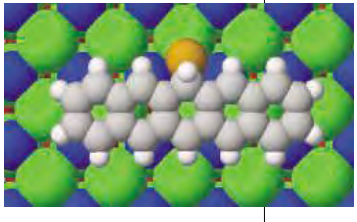

The In and Outs of Carbon Nanotubes

The inherent strength of carbon nanotubes has made them candidate materials for reinforcing composites. It is also possible to put a second material into the core of a nanotube for electronic applications or for use as contrast agents. **Sun *et al.*** (p. 1199; see the Perspective by **Wang and Zhao**) exploit both these properties and use carbon nanotubes as state-of-the-art high-pressure chambers that allow in situ observations of pressure-induced processes at atomic scale. Defects induced on the surface of the nanotubes moved and coalesced, which caused the tubes to contract and squeeze out metal particles that had been trapped inside.

Pathogen Puts a Spanner in the Works

So-called bacterial effector proteins usurp or mimic a eukaryotic activity and contribute to virulence. Many of the known virulence factors from the pathogenic bacterium *Yersinia pestis*, the causal agent of plague, have been assigned mechanisms, but YopJ has remained a mystery. **Mukherjee *et al.*** (p. 1211; see the Perspective by **Worby and Dixon**) now show that YopJ acts as an acetyltransferase that modifies serine or threonine residues in the activation loop of the MAPKK superfamily of signaling kinases. This modification prevents these residues from being

Continued on page 1103

CREDITS (TOP TO BOTTOM): THORE *ET AL.*; REPP *ET AL.*

FastStart Taq DNA Polymerase

Set Your Sights on The New Standard for Everyday PCR

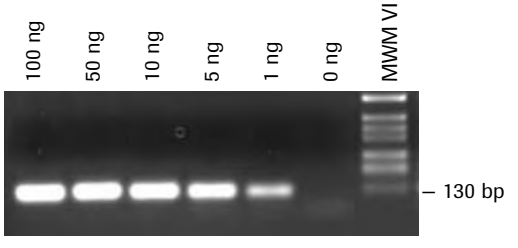

FastStart Taq DNA Polymerase†

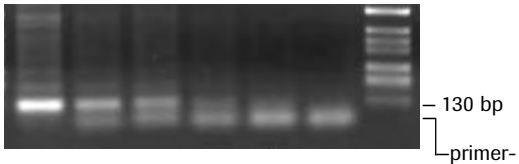

Taq DNA Polymerase†

Detect products from 100-fold less template DNA, without the primer-dimers that plague Taq DNA Polymerase.

Still using standard Taq DNA Polymerase for everyday PCR applications? It's time to upgrade to hot start PCR with FastStart Taq DNA Polymerase:

- **Achieve 100-fold higher sensitivity, and easily detect low-abundance genes.**
- **Obtain results that are easy to interpret** by minimizing nonspecific amplification products and primer-dimers.
- **Save time, effort, and money** by utilizing the same robust, economical enzyme in all your applications; use the supplied buffers and additives to optimize for virtually any template up to 3 kb.
- **Select the best product for your lab's needs:** Choose from the versatile polymerase, a convenient new master mix, or economical dNTPacks combining the enzyme, all buffers, and Roche's unmatched PCR-Grade Nucleotides.

Upgrade from basic Taq for a lot less than you would expect

Raise your standards for everyday PCR applictions. Start your upgrade today by **requesting a free sample* at *www.start-faststart-fast.com***

* Some conditions apply. Samples are limited. See website for details.

Roche Diagnostics

Roche Diagnostics GmbH
Roche Applied Science
68298 Mannheim
Germany

† Purchase of this product is accompanied by a limited license to use it in the Polymerase Chain Reaction (PCR) process for the purchaser's life science research in conjunction with a thermal cycler whose use in the automated performance of the PCR process is covered by the up-front license fee, either by payment to Applied Biosystems or as purchased, *i.e.,* an authorized thermal cycler.

FASTSTART is a trademark of Roche.

Continued from page 1101

phosphorylated by upstream signaling machinery and interferes with innate immune responses.

How a SNP Promotes Disease

Single-nucleotide polymorphisms (SNPs) are one-base variations in DNA sequence that can often be helpful when trying to find genes responsible for inherited diseases. **De Gobbi *et al.*** (p. 1215) have discovered a SNP in a gene regulatory region that causes a human genetic disease through an unusual mechanism. In a study of individuals with α thalassemia, a blood disease characterized by reduced production of hemoglobin, the authors identified a SNP between the upstream regulatory region and the promoter sequences of the α-globin gene cluster on human chromosome 16. The disease-associated allele creates a new promoter-like element whose activity appears to disrupt transcription of the downstream globin genes. Thus, SNPs that fall within intergenic regions, while seemingly innocuous, can occasionally have medically important functional consequences.

CRACing Calcium Channels

Calcium release–activated calcium (CRAC) channels mediate influx of calcium across the plasma membrane when intracellular stores of calcium are depleted, an important event in receptor-stimulated calcium signaling in many cells. **Vig *et al.*** (p. 1220, published online 27 April) moved the search for the molecular identity of the CRAC channel one step closer by completing a high-throughput RNA interference screen for gene products required for CRAC channel function in *Drosophila*. Two membrane proteins, CRAC modulators 1 and 2 (CRACM1 and CRACM2), could be part of the CRAC channel itself or part of the regulatory machinery that controls it.

The Dance of Development

The path from an egg into an adult requires a complex dance of thousands of genes. **Imai *et al.*** (p. 1183; see the Perspective by **Lemaire**) tracked the expression of regulatory genes on a cell-by-cell basis in the developing embryo of the sea squirt, *Ciona intestinalis*. The authors generated a map of the network of gene interactions from which they extract information about specific developmental pathways, such as the formation of notochord, or brain. The results give a snapshot of development in an organism that stands between invertebrates and vertebrates.

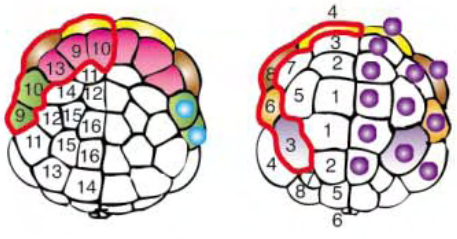

CREDIT: IMAI *ET AL.*

Bigger Bones

Adult bone mass is determined by the rates of bone formation by osteoblasts and bone resorption by osteoclasts. Genetic mutations that disrupt the function of these cells can lead to problems with skeletal development, including excessive postnatal bone formation. Pivotal in osteoblast differentiation is the transcriptional regulator Runx2. **Jones *et al.*** (p. 1223) reveal how this master control protein is itself regulated. Mice lacking the adapter protein Schnurri-3 accumulated bone mass because of increased osteoblast activity resulting from abnormal Runx2 turnover within the cell. Runx2 is normally regulated by ubiquitin-mediated degradation through the Schnurri-3–dependent association with the E3 ubiquitin ligase WWP1. The identification of this upstream pathway regulating postnatal bone formation might help reveal therapeutic avenues for treating bone abnormalities and deficiencies, such as osteoporosis.

Fisheries' Effects on Coastal Marine Ecosystems

Fishing removes top predators, and runoff from the land deposits large amounts of excess nutrients into coastal waters. The relative impact of these top-down and bottom-up factors on marine species and communities has been assessed by **Halpern *et al.*** (p. 1230), who used a database of species' abundances from southern California kelp forest communities spanning multiple years and a broad spatial scale. There is 7- to 10-fold greater influence of top-down control, despite wide-ranging levels of primary production, an effect that is strongest for the algae in the system. This result contradicts the idea that giant kelp are strongly regulated by nutrient levels. Instead, it seems top-down control is having a much greater impact on coastal ecosystems than bottom-up regulation, which argues that management strategies should focus on control of fisheries.

Unlimited!

INNOVATION @ WORK

With Sigma, the potential from a single cell is infinite

Unlock unlimited potential from a single cell with Sigma's GenomePlex® Single Cell Whole Genome Amplification Kit. This rapid and straightforward method provides million-fold amplification yielding microgram quantities of genomic DNA from a single cell.

- Robust and accurate amplification – abundant DNA yield within 4 hours with no detectable allele or locus bias
- Maximum flexibility – amplify DNA from any source including lymphocytes, cancer cells, epithelial cells, fibroblast amniotic cells, polycarbonate fixed cells, and plant cells
- Unlimited genetic analysis – GenomePlex Single Cell WGA DNA is suitable for use with downstream applications including gel electrophoresis, QPCR, CGH microarray, STR analysis, and SNP analysis

To discover the unlimited potential from a single cell visit:

sigma.com/wga4

Donald Kennedy is Editor-in-Chief of *Science*

Health Roundup

LOTS OF THINGS ARE HAPPENING ALL AT ONCE IN THE HEALTH SECTOR, SO IT'S A GOOD TIME FOR a roundup. Let's saddle up and start with intriguing news from the United Kingdom. As reported in the 3 May issue of the *Journal of the American Medical Association* by Banks *et al.*, Britons in the 55 to 64 age cohort are significantly healthier than their U.S. counterparts despite much lower per-capita health expenditures. The U.S.-UK difference for several diseases exists at all socioeconomic levels, and it's large: Diabetes prevalence is twice as high in the U.S. sample. The differences are not attributable to behavioral risk factors (drinking, smoking, and obesity), but they do depend on self-reporting, which may explain why they are minimally reflected in mortality differences.

This reminded me that in his splendid 1974 book *Who Shall Live?* the economist Victor Fuchs compared two neighboring U.S. states that had approximately equal health expenditures and physician coverage. Despite this similarity, he showed that one of them—Utah—had a much healthier population than its neighbor, Nevada. Although Fuchs believes that behavioral factors are important in this comparison but not in the British analysis, the similarity between the two is worth noticing. It made me want to entitle this editorial "Brits Are from Utah, Yanks From Nevada." But that would have left out other issues, which follow.

Last week saw the looming deadline for U.S. seniors to register for the Medicare prescription drug benefit, which might have made everyone more health policy–conscious. Maybe that's why a campaign is under way to give Americans with life-threatening diseases access to therapies that are untested for efficacy or safety. An organization called the Abigail Alliance, supported by the conservative Washington Legal Foundation, recently appealed an adverse district court decision to the U.S. Court of Appeals for the District of Columbia Circuit. A 2:1 majority there ruled that Food and Drug Administration (FDA) regulations that would withhold drugs from terminally ill patients violated the Due Process clause of the Constitution. The majority decision, as both the dissent and a scathing *Washington Post* editorial pointed out, invented a new patient right: one asserting that if you're terminally ill and have tried everything else, the government cannot interfere with your right to an unapproved therapy.

Well, this is not exactly a novel claim; it's a hardy perennial. Twenty-five years ago, the unapproved therapy in vogue was Laetrile, a purported cancer remedy made from apricot pits. Some doctors brought suit in district court on behalf of a plaintiff named Rutherford, who had wanted to try those apricot pits, and sued the FDA for getting in his way. The Tenth Circuit Court saw no right of access to Laetrile, whereupon plaintiffs appealed the case to the Supreme Court, which supported the FDA position in a unanimous 9-0 decision. Even if I hadn't been a defendant, I would have applauded it as a powerful statement on behalf of the public health.

The majority in the Abigail Alliance case made an attempt to dismiss the Rutherford precedent by pointing out that Phase I clinical trials had not been done on Laetrile. But Phase I testing simply seeks to determine appropriate dosage ranges; it does not establish safety. And safety is determined not just by toxicity but by a favorable relationship between risk and benefit. The dissent made the point that the majority had missed by quoting from Supreme Court Justice Thurgood Marshall's opinion for the majority in Rutherford: "For the terminally ill, as for anyone else, a drug is unsafe if its potential for inflicting death or physical injury is not offset by the possibility of therapeutic benefit."

Laetrile Redux is going legislative in a hurry. A pending Senate bill, cosponsored by Senators Brownback and Imhofe, would embed in statute the rights envisioned by the Abigail Alliance and (temporarily, at least) by the DC Circuit majority. Here is what it would mean. Drugs that have passed Phase I testing and some animal studies could be given to terminally ill patients whose doctors certify that they have sought other approved therapies to no avail. Despite some fig-leaf patient protections in this bill, it will do almost exactly what the Alliance would like. The interesting question now is whether this current Supreme Court would endorse Rutherford, support the DC Circuit majority's newly invented right, or take a pass. Place your bets.

Donald Kennedy

10.1126/science.1130059

ISI Web of Knowledge℠

Take the next step

When you use *ISI Web of Knowledge*, your path is clear. This powerful, renowned research platform offers an intuitive search environment that helps users focus on the destination instead of the journey … on the results instead of the process.

It's a fact …

- *ISI Web of Knowledge* provides a variety of search options from Quick Search to Cross Search — to suit users at every level.
- *ISI Web of Knowledge* adds six million keywords each year to help users get the right search results the first time.
- *ISI Web of Knowledge* offers a depth and breadth of cited reference searching capabilities unmatched elsewhere, with 25 million cited references added annually.

Still the best. ***ISI Web of Knowledge***.

http://www.scientific.thomson.com/webofknowledge/

THOMSON™

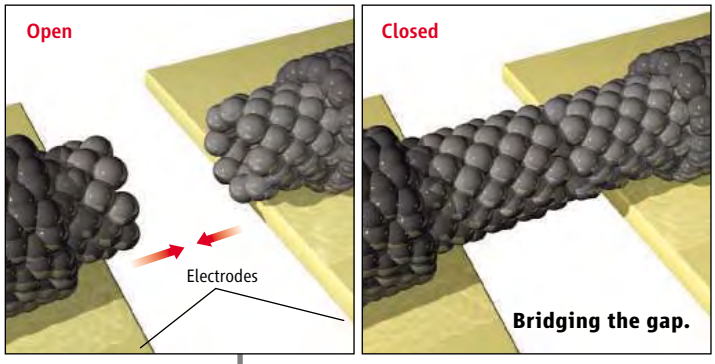

HIGHLIGHTS OF THE RECENT LITERATURE

MATERIALS SCIENCE

Tubular Switches

The mechanical strength and resilience of carbon nanotubes (CNTs) have prompted investigations of their use in applications ranging from fibers to molecular switches. A less commonly exploited property is the unusually low sliding friction characterizing the relative motion of the concentric hollow cylinders that make up double- or multiwalled CNTs—an action analogous to the extension or contraction of a collapsible spyglass.

Deshpande *et al*. have taken advantage of this property in fabricating nanotube-based voltage-gated switches. First, they mounted low-resistance (10 to 20 kilohms) CNTs on gold leads over a silicon gate region. Application of a 4.5-V bias across the leads cleaved the tubes in two, leaving an insulating gap of 5 to 20 nm in the middle and thereby creating an "off" state. Subsequent application of a higher bias (5 to 10 V) reestablished electrical contact, creating a conductive "on" state. The authors attributed this behavior to a charge-induced sliding of the inner tubes through the outer shells and across the gap, an explanation supported by the observation that the outer shells remained rigidly fixed to the leads. For double-walled CNTs, successive application of a 9-V bias across the leads and a 110-V gate potential cycled the device between on and off states. — PDS

Nano Lett. **6**, 10.1021/nl052513f (2006).

CELL BIOLOGY

Easing the Way Out

During animal development, proteins of the Wnt family act as morphogens, establishing gradients of molecules that control gene expression and cell fate. Many players in the Wnt signaling pathway have been identified in a variety of animal systems, including the morphogen itself and its cognate receptor, and also the many downstream components. Bänziger *et al.* and Bartscherer *et al*. have independently identified a new player in the pathway, respectively calling it *wntless* (*wls*) or *evenness interrupted* (*evi*). Wls/Evi is a conserved multipass transmembrane protein specifically found in Wnt-secreting cells, and it appears to promote the secretion of Wnt proteins in *Drosophila*, *C. elegans,* and humans. Wnt signaling relies on a functional interaction with Wls/Evi in the secretory pathway, which may involve the regulation of intracellular trafficking or covalent modification of Wnt. — SMH

Cell **125**, 509; 523 (2006).

APPLIED PHYSICS

A Liquid Mirror

Beyond the capacity to amuse carnival patrons, deformed mirrors can be highly useful in the field of adaptive optics. As light travels through the atmosphere, variations in temperature, density, and refractive index distort the optical wavefront. The cumulative effect of these distortions is a blurring of the image when, for example, the light is collected in the viewfinder of a telescope. If the extent of the wavefront distortion is measured, which can be done with the aid of an artificial guide star created using a laser beam, an adaptively deformable mirror can be tuned to iron out the distortions and restore the image clarity.

Vuelban *et al.* describe such a mirror, with a design based on electrocapillary actuation. A reflective membrane is placed atop a viscous dielectric liquid, which in turn floats above an aqueous electrolyte solution in a two-dimensional array of ~350-μm-diameter microchannels. The liquid levels in each microchannel can be independently adjusted by application of a voltage, thereby inducing precise local deformations in the mirror surface above. An advantage of the liquid system is the large dynamic range of inducible deformation. The authors demonstrate a prototype device with an ~2-ms response time. — ISO

Opt. Lett. **31**, 1717 (2006).

BIOTECHNOLOGY

It's Easy Being Green

Porous solids are widely used in chromatographic separations based on size and shape. Some pores are as large as proteins (for instance, in dextran- or agarose-based gel filtration), whereas others are as small as water molecules (as in molecular sieves used to keep organic solvents dry). Paukstelis has assessed the permeation properties of a self-assembled three-dimensional lattice constructed from four assembly strands [each 24 nucleotides (nt) long] and an 11-nt spacer strand. The estimated diameter of the largest internal solvent channel in crystals of this DNA array was 9 nm, which corresponds to a globular protein of 300 kD, but the measured size cutoff for negatively charged proteins appeared to be only one-10th this size (ovalbumin, no; carbonic anhydrase, yes), perhaps as a result of electrostatic interactions. Confocal microscopy revealed that the interior of a crystal soaked in a mixture of green fluorescent protein and a much bigger red maltose-binding protein was green and not red. — GJC

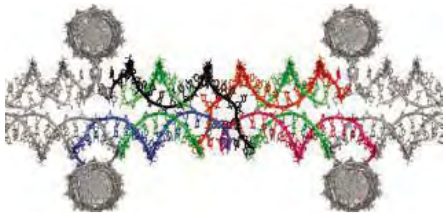

Model of DNA lattice showing spacer (green) and assembly (black, red, blue, and orange) strands.

J. Am. Chem. Soc. **128**, 10.1021/ja061322r (2006).

VIROLOGY

A Most Discerning Host

Viruses can inadvertently announce their presence by displaying tell-tale patterns—often in the form of their own double-stranded (ds) RNA—and hosts have evolved a panoply of

Continued on page 1109

CREDITS (TOP TO BOTTOM): C. BICKEL/*SCIENCE*; PAUKSTELIS *ET AL*., *J. AM. CHEM. SOC.* **128**, 10.1021/JA061322R (2006)

PathFinder

INNOVATION @ WORK

Discover Your Path to Innovation

On your path to innovation, Sigma is with you every step of the way. PathFinder is an online collection of interactive, interconnected maps showing biological signaling and metabolic pathways. For you to explore the relationships between different pathway elements, individual components are linked with related high-quality products.

You know your destination. PathFinder will get you there.

With Sigma's broad range of products, you will discover that we offer everything from small molecules to antibodies and enzymes. You will also be able to use PathFinder to locate qPCR components and siRNAs for gene knockdown. A valuable resource, PathFinder provides fast and accurate information on numerous levels, all in one place – and all linked to the important products that are key to the success of your research. In addition to products and services, you'll have immediate access to these helpful tools:

- Specific workflow analysis
- In-depth technical information
- Detailed product descriptions
- Relevant technical articles

Learn how PathFinder can help you discover your path to innovation by visiting us at:

sigma-aldrich.com/pathfinder

Accelerating Customers' success through Leadership in Life Science, High Technology and Service
SIGMA-ALDRICH CORPORATION • BOX 14508 • ST. LOUIS • MISSOURI 63178 • USA

SIGMA®

Continued from page 1107

intracellular factors to detect and decode these signals and to set in motion a cascade of antiviral responses. Recently two pattern recognition receptors, RIG-1 and MDA-5, were found to act as RNA helicases and signaling adaptor proteins.

Kato *et al.* and Gitlin *et al.* show that RIG-1 and MDA-5 are distinct in their tastes for viral dsRNAs. Thus, mice lacking the *MDA5* gene lost the ability to generate a type I interferon response to the dsRNA analog polyinosinic acid:polycytidylic acid [poly(I):poly(C)] and were more susceptible to infection with picornavirus. Kato *et al.* further compared this *MDA5*-dependent response with what happened in mice deficient in *RIG-1* and found a requirement for *RIG-1* in generating immunity to other dsRNA viruses, such as influenza and paramyxoviruses. With further antiviral dsRNA detectors likely to be discovered in mice and humans, elucidating the conformational or other features of dsRNA species important for selective pattern recognition would seem a useful avenue in the study of viral pathogenesis. — SJS

Nature **441**, 101 (2006); *Proc. Natl. Acad. Sci. U.S.A.* **103**, 10.1073/pnas.0603082103 (2006).

ARCHAEOLOGY

Did Climate Rock the Cradle?

The earliest cities and centralized state-level societies arose in Mesopotamia between 8000 and 5000 years ago. Anthropological archaeologists have long sought to uncover the factors underlying the Mesopotamian region's singular place in history as the cradle of civilization. In general, studies have focused on such contributing influences as technological and agricultural innovation, the rise of bureaucracy and political hierarchies, increased trade, and religious or military pressures. Fewer studies have examined the significance of environmental influences, such as climate patterns and shoreline movements due to shifting sea level.

Kennett and Kennett compare local climatic and geographical changes with concurrent societal developments in specific regions of the Persian Gulf between 15,000 and 6000 years ago. They suggest that early development was shaped by the formation of productive estuaries,

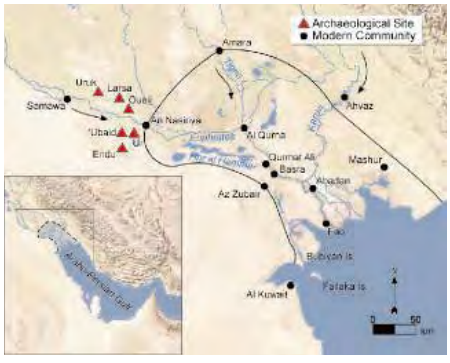

Mesopotamia, then and now (the coastline as it was 6000 years ago is outlined in black).

the availability of ample fresh water, and the ability to transport goods over water. They also discuss the potential role of climate—particularly the increase in aridity between 6000 and 5000 years ago—in fostering the consolidation of settlements. Thus, they argue that the emergence of highly organized urban society was at least in part a consequence of the glacial-interglacial cycle and related climate changes. — HJS

J. Island Coastal Archaeol. **1**, 67 (2006).

Science stke AAAS

www.stke.org

<< The GABA Defense

During infection of plants by *Agrobacterium tumefaciens*, plants are wounded and then a tumor is induced, which becomes a source of opines: chemicals that stimulate the production of the quorum-sensing (QS) signal *N*-(3-oxooctanoyl) homoserine lactone (OC8-HSL). γ-aminobutyric acid (GABA) is produced by plants as part of the response to wounding. Chevrot *et al*. show that GABA stimulates expression of the *attKLM* operon in *A. tumefaciens*, which produces a lactonase that opens the ring and inactivates OC8-HSL. Consequently, OC8-HSL was undetectable in cultures of *A. tumefaciens* exposed to GABA. Proteins encoded by the *attKLM* operon were identified in a screen for proteins synthesized in response to the addition of GABA to cultures of *A. tumefaciens*. The induction of the *attKLM* operon was also monitored using a reporter assay, and in *A. tumefaciens* deficient for the GABA transporter system, GABA did not induce the reporter. The importance of GABA for the plant response was verified using transgenic tobacco plants that expressed a glutamate decarboxylase (GAD, the enzyme that makes GABA from glutamate) that was not inhibited by Ca^{2+}/calmodulin (GADΔC). Compared with wild-type tobacco, the plants with the GADΔC mutant developed less severe disease symptoms in two different virulence assays. Thus, GABA appears to serve as a communication signal between the plant and the pathogen. — NRG

Proc. Natl. Acad. Sci. U.S.A. **103**, 7460 (2006).

CREDIT: JACOB BARTRUFF, UNIVERSITY OF OREGON

www.sciencemag.org

Science

1200 New York Avenue, NW
Washington, DC 20005
Editorial: 202-326-6550, FAX 202-289-7562
News: 202-326-6500, FAX 202-371-9227

Bateman House, 82-88 Hills Road
Cambridge, UK CB2 1LQ
+44 (0) 1223 326500, FAX +44 (0) 1223 326501

Subscription Services For change of address, missing issues, new orders and renewals, and payment questions: 866-294-0062 or 202-326-6417, FAX 202-842-1065. Mailing addresses: AAAS, P.O. Box 96178, Washington, DC 20090-6178 or AAAS Member Services, 1200 New York Avenue, NW, Washington, DC 20005

Institutional Site Licenses please call 202-326-6755 for any questions or information

Reprints: Author Inquiries 800-635-7181
Commercial Inquiries 803-359-4578
Corrections 202-326-6501

Permissions 202-326-7074, FAX 202-682-0816

Member Benefits Bookstore: AAAS/BarnesandNoble.com bookstore www.aaas.org/bn; Car purchase discount: Subaru VIP Program 202-326-6417; Credit Card: MBNA 800-847-7378; Car Rentals: Hertz 800-654-2200 CDP#343457, Dollar 800-800-4000 #AA1115; AAAS Travels: Betchart Expeditions 800-252-4910; Life Insurance: Seabury & Smith 800-424-9883; Other Benefits: AAAS Member Services 202-326-6417 or www.aaasmember.org.

science_editors@aaas.org	(for general editorial queries)
science_letters@aaas.org	(for queries about letters)
science_reviews@aaas.org	(for returning manuscript reviews)
science_bookrevs@aaas.org	(for book review queries)

Published by the American Association for the Advancement of Science (AAAS), *Science* serves its readers as a forum for the presentation and discussion of important issues related to the advancement of science, including the presentation of minority or conflicting points of view, rather than by publishing only material on which a consensus has been reached. Accordingly, all articles published in *Science*—including editorials, news and comment, and book reviews—are signed and reflect the individual views of the authors and not official points of view adopted by the AAAS or the institutions with which the authors are affiliated.

AAAS was founded in 1848 and incorporated in 1874. Its mission is to advance science and innovation throughout the world for the benefit of all people. The goals of the association are to: foster communication among scientists, engineers and the public; enhance international cooperation in science and its applications; promote the responsible conduct and use of science and technology; foster education in science and technology for everyone; enhance the science and technology workforce and infrastructure; increase public understanding and appreciation of science and technology; and strengthen support for the science and technology enterprise.

Information for Contributors

See pages 102 and 103 of the 6 January 2006 issue or access www.sciencemag.org/feature/contribinfo/home.shtml

EDITOR-IN-CHIEF **Donald Kennedy**
EXECUTIVE EDITOR **Monica M. Bradford**
DEPUTY EDITORS **R. Brooks Hanson, Katrina L. Kelner**
NEWS EDITOR **Colin Norman**

Editorial supervisory senior editors Barbara Jasny, Phillip D. Szuromi; **senior editor/perspectives** Lisa D. Chong; **senior editors** Gilbert J. Chin, Pamela J. Hines, Paula A. Kiberstis (Boston), Marc S. Lavine (Toronto), Beverly A. Purnell, L. Bryan Ray, Guy Riddihough (Manila), H. Jesse Smith, Valda Vinson, David Voss; **associate editors** Jake S. Yeston, Laura M. Zahn; **online editor** Stewart Wills; **associate online editor** Tara S. Marathe; **book review editor** Sherman J. Suter; **associate letters editor** Etta Kavanagh; **information specialist** Janet Kegg; **editorial manager** Cara Tate; **senior copy editors** Jeffrey E. Cook, Cynthia Howe, Harry Jach, Barbara P. Ordway, Jennifer Sills, Trista Wagoner; **copy editors** Alexis Wynne Mogul, Peter Mooreside; **editorial coordinators** Carolyn Kyle, Beverly Shields; **publication assistants** Ramatoulaye Diop, Chris Filiatreau, Joi S. Granger, Jeffrey Hearn, Lisa Johnson, Scott Miller, Jerry Richardson, Brian White, Anita Wynn; **editorial assistants** Lauren Kmec, Patricia M. Moore, Brendan Nardozzi, Michael Rodewald; **executive assistant** Sylvia S. Kihara

News senior correspondent Jean Marx; **deputy news editors** Robert Coontz, Jeffrey Mervis, Leslie Roberts, John Travis; **contributing editors** Elizabeth Culotta, Polly Shulman; **news writers** Yudhijit Bhattacharjee, Adrian Cho, Jennifer Couzin, David Grimm, Constance Holden, Jocelyn Kaiser, Richard A. Kerr, Eli Kintisch, Andrew Lawler (New England), Greg Miller, Elizabeth Pennisi, Robert F. Service (Pacific NW), Erik Stokstad; Katherine Unger (intern); **contributing correspondents** Barry A. Cipra, Jon Cohen (San Diego, CA), Daniel Ferber, Ann Gibbons, Robert Irion, Mitch Leslie (NetWatch), Charles C. Mann, Evelyn Strauss, Gary Taubes, Ingrid Wickelgren; **copy editors** Linda B. Felaco, Rachel Curran, Sean Richardson; **administrative support** Scherraine Mack, Fannie Groom **bureaus:** Berkeley, CA: 510-652-0302, FAX 510-652-1867, New England: 207-549-7755, San Diego, CA: 760-942-3252, FAX 760-942-4979, Pacific Northwest: 503-963-1940

Production director James Landry; **senior manager** Wendy K. Shank; **assistant manager** Rebecca Doshi; **senior specialists** Jay Covert, Chris Redwood; **specialist** Steve Forrester **Preflight director** David M. Tompkins; **manager** Marcus Spiegler; **specialist** Jessie Mudjitaba

Art director Joshua Moglia; **associate art director** Kelly Buckheit; **illustrators** Chris Bickel, Katharine Sutliff; **senior art associates** Holly Bishop, Laura Creveling, Preston Huey; **associate** Nayomi Kevitiyagala; **photo editor** Leslie Blizard

***Science* International**

Europe (science@science-int.co.uk) **editorial: international managing editor** Andrew M. Sugden; **senior editor/perspectives** Julia Fahrenkamp-Uppenbrink; **senior editors** Caroline Ash (Geneva: +41 (0) 222 346 3106), Stella M. Hurtley, Ian S. Osborne, Stephen J. Simpson, Peter Stern; **associate editor** Joanne Baker **editorial support** Alice Whaley; Deborah Dennison **administrative support** Janet Clements, Phil Marlow, Jill White; **news: international news editor** Eliot Marshall **deputy news editor** Daniel Clery; **correspondent** Gretchen Vogel (Berlin: +49 (0) 30 2809 3902, FAX +49 (0) 30 2809 8365); **contributing correspondents** Michael Balter (Paris), Martin Enserink (Amsterdam and Paris), John Bohannon (Berlin); **intern** Laura Blackburn

Asia Japan Office: Asca Corporation, Eiko Ishioka, Fusako Tamura, 1-8-13, Hirano-cho, Chuo-ku, Osaka-shi, Osaka, 541-0046 Japan; +81 (0) 6 6202 6272, FAX +81 (0) 6 6202 6271; asca@os.gulf.or.jp; **asia news editor** Richard Stone +66 2 662 5818 (rstone@aaas.org) **japan news bureau** Dennis Normile (contributing correspondent, +81 (0) 3 3391 0630, FAX 81 (0) 3 5936 3531; dnormile@gol.com); **china representative** Hao Xin, + 86 (0) 10 6307 4439 or 6307 3676, FAX +86 (0) 10 6307 4358; haoxin@earthlink.net; **south asia** Pallava Bagla (contributing correspondent +91 (0) 11 2271 2896; pbagla@vsnl.com) **Africa** Robert Koenig (contributing correspondent, rob.koenig@gmail.com)

EXECUTIVE PUBLISHER **Alan I. Leshner**
PUBLISHER **Beth Rosner**

Fulfillment & Membership Services (membership@aaas.org) **director** Marlene Zendell; **manager** Waylon Butler; **systems specialist** Andrew Vargo; **specialists** Pat Butler, Laurie Baker, Tamara Alfson, Karena Smith, Vicki Linton; **circulation associate** Christopher Refice; **data entry supervisor** Cynthia Johnson

Business Operations and Administration director Deborah Rivera-Wienhold; **business manager** Randy Yi; **senior business analyst** Lisa Donovan; **business analyst** Jessica Tierney; **financial analyst** Michael LoBue, Farida Yeasmin; **rights and permissions: administrator** Emilie David; **associate** Elizabeth Sandler; **marketing: director** John Meyers; **marketing managers** Darryl Walter, Allison Pritchard; **marketing associates** Julianne Wielga, Mary Ellen Crowley, Catherine Featherston, Alison Chandler, Lauren Lamoureux; **director of international marketing and recruitment advertising** Deborah Harris; **international marketing manager** Wendy Sturley; **marketing/member services executive:** Linda Rusk; **japan sales** Jason Hannaford; **site license sales: director** Tom Ryan; **sales and customer service** Mehan Dossani, Kiki Forsythe, Catherine Holland, Wendy Wise; **electronic media: manager** Lizabeth Harman; **production associates** Sheila Mackall, Amanda K. Skelton, Lisa Stanford, Nichele Johnston; **applications developer** Carl Saffell

Advertising director worldwide ad sales Bill Moran

Product (science_advertising@aaas.org)**; midwest** Rick Bongiovanni: 330-405-7080, FAX 330-405-7081 • **west coast/w. canada** Teola Young: **650-964-2266 east coast/e. canada** Christopher Breslin: 443-512-0330, FAX 443-512-0331 • **uk/europe/asia** Tracey Peers (Associate Director): +44 (0) 1782 752530, FAX +44 (0) 1782 752531 **japan** Mashy Yoshikawa: +81 (0) 33235 5961, FAX +81 (0) 33235 5852 **traffic manager** Carol Maddox; **sales coordinator** Deiandra Simms

Classified (advertise@sciencecareers.org); **u.s.: sales director** Gabrielle Boguslawski: 718-491-1607, FAX 202-289-6742; **inside sales manager** Daryl Anderson: 202-326-6543; **west coast/midwest** Kristine von Zedlitz: 415-956-2531; **east coast** Jill Downing: 631-580-2445; **canada, meetings and announcements** Kathleen Clark: 510-271-8349; **line ad sales** Emnet Tesfaye: 202-326-6740; **sales coordinators** Erika Bryant; Rohan Edmonson Christopher Normile, Joyce Scott, Shirley Young; **international: sales manager** Tracy Holmes: +44 (0) 1223 326525, FAX +44 (0) 1223 326532; **sales** Christina Harrison, Svitlana Barnes; **sales assistant** Helen Moroney; **japan:** Jason Hannaford: +81 (0) 52 789 1860, FAX +81 (0) 52 789 1861; **production: manager** Jennifer Rankin; **assistant manager** Deborah Tompkins; **associates** Christine Hall; Amy Hardcastle; **publications assistants** Robert Buck; Mary Lagnaoui

AAAS Board of Directors retiring president, chair Gilbert S. Omenn; **president** John P. Holdren; **president-elect** David Baltimore; **treasurer** David E. Shaw; **chief executive officer** Alan I. Leshner; **board** Rosina M. Bierbaum; John E. Dowling; Lynn W. Enquist; Susan M. Fitzpatrick; Alice Gast; Thomas Pollard; Peter J. Stang; Kathryn D. Sullivan

AAAS
ADVANCING SCIENCE, SERVING SOCIETY

Now Available!
SNPlex™ Genotyping System on the 3130*xl* Genetic Analyzer.

Accept No Limitations.

The improved SNPlex Genotyping System now performs cost effective and customizable genotyping projects on the 3130*xl* Genetic Analyzer.

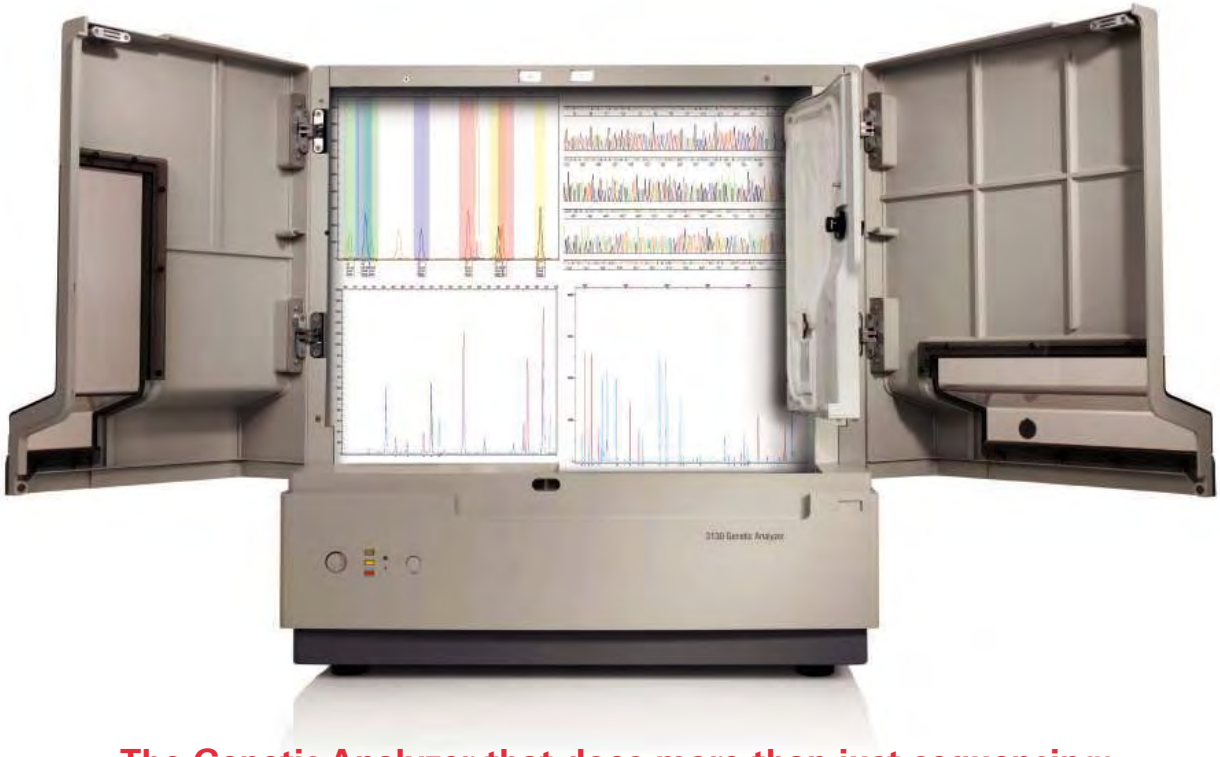

The Genetic Analyzer that does more than just sequencing:

SNPlex Genotyping System* • *De novo* sequencing • Resequencing • Comparative sequencing
Mutation/heterozygote detection • SAGE • SNP validation and screening • Genotyping • Microsatellite analysis
AFLP • Conformation analysis • T-RFLP • MLST • Relative fluorescent quantitation

Applied Biosystems 3130 and 3130*xl* Genetic Analyzers

The 4-capillary 3130 and 16-capillary 3130***xl*** Genetic Analyzers provide reference-standard data quality and sophisticated, hands-free automation capabilities across a wider range of sequencing, resequencing and fragment analysis applications. The 3130 Series systems leverage the same technology, reagents, and software interface that make our larger production-scale systems so successful, bringing superior performance within the reach of almost any lab. Learn more at: http://info.appliedbiosystems.com/3130series.

Applied Biosystems

25 YEARS ADVANCING SCIENCE

*Not supported on the 3130 Genetic Analyzer.

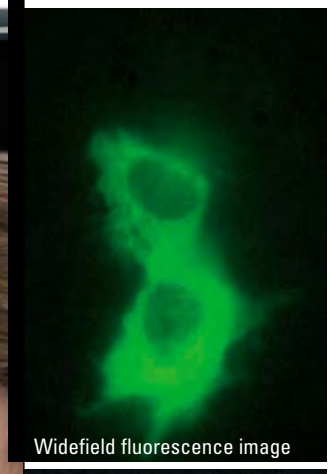

Widefield fluorescence image

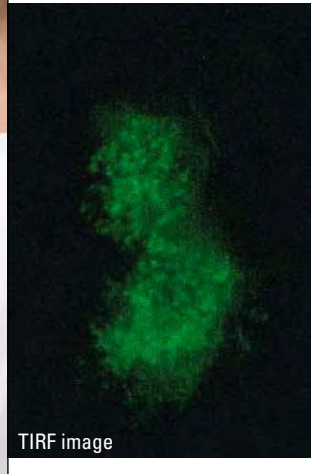

TIRF image

Visualize Life's Secrets with Complete, Automated TIRF

New! Complete, automated microscope system for precise TIRF. The Leica AM TIRF system gives accurate results for all research examinations of close-to-membrane specimen structures. Minimum light stress, high-sensitivity, and the most favorable signal-to-noise ratio combine to assure exact spatial resolution.

Leica's innovative auto-alignment functions automatically find the correlation between the penetration depths of the evanescent field and the TIRF angles. The system's dynamic scanner can be used to precisely position the laser beam and determine the exact penetration depth. Leica's TIRF objective offers maximum apochromatic correction for high-performance imaging.

www.leica-microsystems.com/AM_TIRF

Leica

MICROSYSTEMS

RESOURCES

Twisted Logic

German chemist Friedrich August Kekulé claimed that he discovered the ring structure of the molecule benzene during his sleep, when he dreamed of a snake eating its own tail. Do the odd origins of Kekulé's hypothesis make the structure any less plausible? If you answered yes, you need a remedial session with the Fallacy Files. Gary Curtis, a philosophy Ph.D. in Austin, Texas, compiled this encyclopedia that dissects more than 100 common logical blunders, using cases from the media, books, politics, and other sources. For instance, attacking Kekulé's notion—or any idea—based on its history is an example of the genetic fallacy. Another gaffe to avoid is the Texas sharpshooter fallacy, which involves mistaken conclusions about disease clusters. >> www.fallacyfiles.org

DATABASES

Fat Finders

They tantalize our palates, jam our arteries, and hold our cells together. They are the lipids, the chemical family that includes fats, oils, steroids, and related compounds. Biochemists and other scientists can dig up data on the heavyweight molecules at this pair of sites. Lipid Metabolites and Pathways Strategy* comes from a U.S. consortium that aims to identify all the lipids in one cell type and measure their quantities. Along with a catalog of more than 7600 lipids, the site features lab protocols, research results from consortium members, and a database of proteins that interact with lipids. Lipid Bank,† from the International Medical Center of Japan and the Japan Science and Technology Agency, houses data contributed by researchers on more than 6000 molecules. The pages offer a rich mix of information, from ultraviolet and infrared spectrometry results to synthesis recipes. >>

* www.lipidmaps.org
† lipidbank.jp

IMAGES

Redrawing the World

Russia is the largest country by land area. But on a map that scales nations according to total births (below), it practically disappears, dwarfed by India and China. The stark contrast in childbearing comes from Worldmapper, created by researchers at the University of Sheffield, U.K., and the University of Michigan, Ann Arbor. The site turns drab demographic and economic statistics into eye-catching maps. One hundred figures size each country according to variables such as past and predicted population, number of elderly people, and oil imports. >> www.sasi.group.shef.ac.uk/worldmapper/index.html

IMAGES

Bug-Eyed Beauties

Wander along a stream anywhere from Canada to Honduras, and you might see the glittering American rubyspot damselfly (*Hetaerina americana*; below) perched on vegetation. At OdonataCentral from entomologist John Abbott of the University of Texas, Austin, you can net data on the taxonomy and distribution of damselflies and their relatives the dragonflies. For North American states and provinces, the site offers checklists that feature interactive range maps. A field guide showcases species that buzz into Texas and neighboring states. >> **odonatacentral.bfl.utexas.edu**

EDUCATION

Touching the Void >>

It's like the ultimate adventure game: Board a spaceship, fly to a warped part of spacetime, and drop into a black hole. Welcome to the visually stunning Black Holes: Gravity's Relentless Pull. This month, astronomers Roeland van der Marel of the Space Telescope Science Institute in Baltimore, Maryland, and Gijs Verdoes Kleijn of the University of Groningen in the Netherlands received the €25,000 Pirelli INTERNETional Award for the educational Web site. Its encyclopedia offers background information on how black holes form, how long they last, and more. Chairborne astronauts can zip off to destinations such as Cygnus X-1, where a black hole is sucking matter from a nearby star (above). There, you can perform virtual experiments such as dropping a clock into the void: It ticks progressively slower and freezes on the edge of the black hole. >> hubblesite.org/go/blackholes

Send site suggestions to >> netwatch@aaas.org
Archive: www.sciencemag.org/netwatch

CREDITS (TOP TO BOTTOM): JOHN ABBOTT/UNIVERSITY OF TEXAS; SPACE TELESCOPE SCIENCE INSTITUTE; SASI GROUP/UNIV. OF SHEFFIELD AND MARK NEWMAN/UNIV. OF MICHIGAN

GRAPPLING WITH THE CHICKEN GENOME

Hoping to get their roosters in a row, chicken researchers gathered earlier this month at Cold Spring Harbor Laboratory in New York and hatched plans for analyzing the first bird genome. Eighteen months after an initial draft of the chicken sequence was released, bioinformaticists are still struggling to identify the fowl's 20,000 or so genes.

Chicken genome researchers face a host of obstacles including insufficient funding, confusing new gene names, conflicting computer predictions, and the need to nudge other chicken scientists into the genomics world. The ancestor of domesticated chickens, the red jungle fowl (*Gallus gallus*), is the lone avian among a dozen vertebrates already sequenced, and comparison with other genomes is difficult because the chicken evolved 300 million years ago—much, much earlier than humans or mice.

David Burt, a molecular biologist at the Roslin Institute in Edinburgh, U.K., has asked U.S. and British science agencies for money to set up a consortium to characterize the bird's genes. But getting organized is tough, says Wes Warren of Washington University in St. Louis, Missouri. "We have two different communities"—agricultural poultry scientists and biomedical researchers using chickens to study diseases—who have had little in common.

Exxon Valdez: Many-Leveled Disaster

Memories of the 1989 *Exxon Valdez* disaster in Alaska may have dimmed, but its menace endures. A new study suggests that ducks and otters are still being affected by a persistent oil presence.

The Knight Island region of Prince William Sound was hard hit when the supertanker *Exxon Valdez* leaked 40 million liters of oil, killing thousands of otters, seals, birds, and other marine species. Earlier studies confirmed that oil persisted in the area, but the surveys only looked for oil high on shore and not in the wetter low tidal zones where marine mammals dig for food.

Environmental chemist Jeffrey Short of the National Marine Fisheries Service in Alaska and colleagues recently surveyed 32 shorelines in the region, checking for oil both on the surface and in half-meter-deep pits. They found oil in 59 of 662 quadrants; subsurface oil appeared in 51 quadrants, distributed in lower and middle as well as higher tidal zones.

Oil in the lower tidal zone is bad news for animals such as ducks and otters, which forage in wet sand, says Short. The team, reporting online last week in *Environmental Science and Technology*, say run-ins with oil probably are why local otter and sea duck populations in the area haven't fully recovered since the spill. "This work is going to be useful for other oil spill sites," says marine chemist Christopher Reddy of the Woods Hole Oceanographic Institution in Massachusetts.

Oily hole in the sand.

Andean frowny face.

Early American Astronomy

Two recent finds suggest that early South Americans may have been more attuned to the cosmos than commonly believed.

In Peru, archaeologist Robert Benfer, retired from the University of Missouri, and colleagues have unearthed a 4200-year-old temple in the Andean foothills that may be the oldest astronomical observatory yet found in the Western Hemisphere, built about the same time as Stonehenge.

Benfer found that certain features, such as this frowning face (above), aligned with other geographic features at precise angles. Consulting with a physicist, he learned that the angles are related to where the sun would rise or set during seasonal solstices and equinoxes. Benfer, who reported the discovery at a meeting of the Society for American Archaeology in Puerto Rico last month, says these features suggest that the temple was used to help plan crops. "It's the most sophisticated early public art that has been encountered up to now anywhere in the Central Andes," says archaeologist Richard Burger of Yale University.

Another recently announced find, in the Brazilian Amazon, has also drawn comparisons to Stonehenge. It consists of 127 evenly placed stones, each weighing several tons, driven into the ground in a pattern that might help pinpoint the date of the winter solstice. Archaeologists with the Amapa Institute of Scientific and Technological Research in Brazil say ceramics in the area date back 2000 years.

The Amazon contains few clues to past civilizations because people rarely built in stone, says archaeologist John Walker of the University of Central Florida. But researchers are "coming around to the notion that there were some large-scale and pretty sophisticated societies throughout the Amazon."

CREDITS (TOP TO BOTTOM): NEIL A. DUNCAN; PHOTOS.COM; NOAA

Invisibility for real? 1120

The carbon market crash 1123

BIOSECURITY

Synthetic Biologists Debate Policing Themselves

BERKELEY, CALIFORNIA—Despite its reputation for free living, California seems to be the place biologists gather to debate whether—and how—to regulate themselves. Three decades after geneticists convening in Asilomar agreed to voluntary guidelines on recombinant DNA experiments, synthetic biologists meeting here this week* began hammering out a "community declaration" to promote security and safety in their nascent field.

Advances in synthetic biology are making it possible to easily mix and match parts from organisms and synthesize potentially dangerous microbes from scratch. This has raised a host of concerns including bioterrorism and ecological contamination. Against a backdrop of such worries, synthetic biologists have for the past 2 years consulted ethicists and legal experts and launched studies to explore ways to reduce the risks of their research—and to forestall possibly intrusive legislation by governments.

Yet the synthetic biologists in Berkeley only took baby steps toward self-regulation, suggesting but not voting on a pair of recommendations related to preventing DNA synthesis companies from supplying sequences that might be used for a bioweapon. "It's a good thing to start with," says Harvey Rubin, an infectious-disease specialist and biosecurity expert at the University of Pennsylvania. (As *Science* went to press, the complete list of declarations was still being worked out and was expected to be available for comment at pbd.lbl.gov/sbconf.)

Unlike conventional recombinant DNA technology, in which researchers tend to manipulate individual genes and proteins, synthetic biologists are increasingly able to alter large swaths of genomes at once and assemble new ones from scratch. Synthesizing complete organisms, even potentially dangerous ones, is already a reality. In 2002, a research team recreated the poliovirus by stitching together DNA ordered from companies (*Science*, 9 August 2002, p. 1016). And last year, another group recreated the pandemic flu strain that killed tens of millions of people worldwide in 1918 (*Science*, 7 October 2005, p. 77). "There are very real concerns that we must face," says Drew Endy, a synthetic biologist at the Massachusetts Institute of Technology (MIT) in Cambridge.

The Synthetic Biology 1.0 meeting held 2 years ago brought these issues to the forefront and helped prompt the Alfred P. Sloan Foundation to back a security study by researchers at MIT, the J. Craig Venter Institute, and elsewhere, the results of which are expected by the end of the summer. Last year, the U.S. National Institutes of Health also set up a National Science Advisory Board for Biosecurity to look at synthetic biology issues. And in April, Berkeley public policy expert Stephen Maurer and colleagues released a white paper outlining six possible early steps the field can take to boost security.

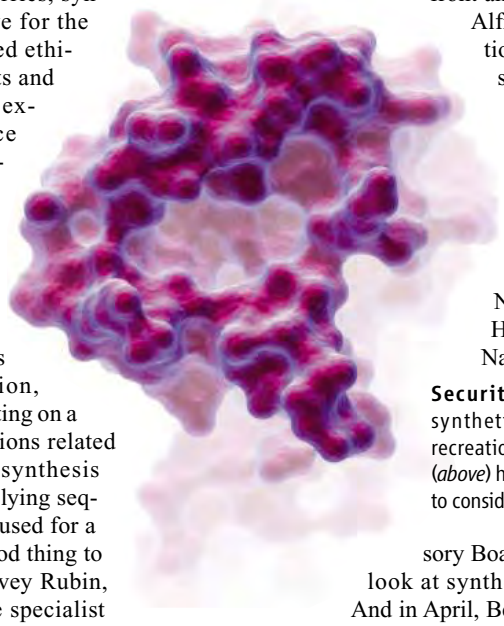

Security concerns. Feats of synthetic biology such as the recreation of the 1918 flu virus (*above*) have prompted researchers to consider self-regulation.

One issue highlighted in the white paper is the growing number of companies around the world that can synthesize stretches of DNA tens of thousands of bases long, within range of recreating viruses in one fell swoop, though still considerably below the 4-million-or-so-base length of a bacterial genome. Given such skills, DNA synthesis companies should monitor commercial orders and report suspicious sequences to government agencies, says George Church, a synthetic biologist at Harvard University. That's already required in Germany, says Hans Buegl, a sales manager with GeneArt, a DNA synthesis company based in Regensberg. But such rules have yet to be adopted in the United States and many other countries. The Berkeley meeting's attendees' proposed declaration would call for such monitoring efforts to be standard procedure. A second recommendation is expected to call for the development of software programs that spot efforts to evade the scans, such as modifying suspect strands with extra DNA that could later be clipped off.

Also suggested in the white paper were establishing a clearinghouse for community members to identify and track potential biosafety and biosecurity concerns and creating a confidential hotline from which researchers could seek advice from experts before proceeding with experiments about which they may be uneasy. But with it still unclear who should oversee such efforts, those proposals don't seem likely to be on any declaration for now.

Expecting Asilomar-like results was unrealistic, say some. "Our society is a different place, and it's unlikely you could go to the monastery without everyone following behind," says David Baltimore, who helped organize the 1975 conference and is president of the California Institute of Technology in Pasadena. Indeed, on 19 May, a group of 35 environmental organizations, trade unions, and ethicists wrote an open letter to the Berkeley meeting attendees imploring them to forgo self-governance in favor of an international discussion of more strict national and international controls. "Scientists creating new life forms cannot be allowed to act as judge and jury," says Sue Mayer, director of GeneWatch UK, one of the signatory groups. The letter also suggests that synthetic biologists have a conflict of interest because several have helped launch companies in the field.

Researchers counter that their intention was never to prevent a broader societal discussion or governmental oversight. "Look, we're trying to take a step forward here," says Church. "If you stop someone from doing something that is noble because you want something even more noble, what you wind up with is worse." By starting to propose a code of conduct for the field, he says, "we're beginning to develop some momentum."

–ROBERT F. SERVICE

CREDIT: KENNETH EWARD/PHOTO RESEARCHERS INC.

* Synthetic Biology 2.0, Berkeley, California, 20–22 May 2006.

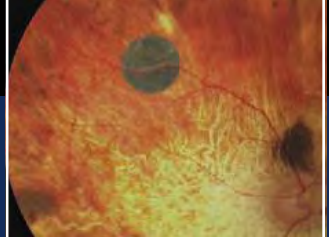

Restoring visual connections
1124

Midwife to the next big accelerator
1128

SCIENCE FOR PEACE

Pakistan Gives Geology Conference The Cold Shoulder

NEW DELHI—Pakistan has pulled the plug on a high-profile conference next week that would have brought together scientists from India and Pakistan in a session designed to set aside hostilities and forge a research plan for the high Himalayas. The blow has left organizers of the science-for-peace event reeling. The cancellation "is completely unexpected and unwarranted," says co-organizer Jack Shroder, a geologist at the University of Nebraska, Omaha.

The joint project was to focus on the Karakoram range of the Himalayan mountains of northern Kashmir, a high-altitude graveyard for soldiers from the Indian and Pakistani armies, who in reality are far more likely to die from exposure and accidents than enemy fire. Topping the agenda of the conference, funded in part by a $70,000 grant from the U.S. National Science Foundation and scheduled for 29 to 31 May, was a discussion of how to turn one iconic battleground, the 6100-meter-high Siachen Glacier, into a science peace park. The first step would require that the two countries strike an accord and withdraw their troops. More than 100 scientists from eight countries had registered for the conference, sponsored by Pakistan's Higher Education Commission (HEC).

Glacial progress? Pakistan has scuttled a meeting on turning Siachen Glacier into a research "peace park."

On 23 May, however, a geologist at the University of Peshawar e-mailed Shroder that the conference would be postponed "due to unavoidable circumstances." The decision, he stated, was taken "in consultation" with HEC. A driving force for the cross-border initiative, environmental planner Saleem H. Ali of the University of Vermont in Burlington, told *Science* that Pakistan's Interior Ministry had pressured HEC to bow out, citing "security reasons." Ali says HEC did not elaborate on the reasons, although he says HEC officials told him they were keen to go ahead with the event but were overruled. The abrupt postponement came, however, on the opening day of the 10th round of talks between senior officials from the defense ministries of India and Pakistan on how to demilitarize Siachen. As *Science* went to press, the talks were not expected to yield a breakthrough.

The 11th-hour cancellation has caused a major headache for Shroder, who broke the news to participants on 23 May. Some scientists, he noted, were already in transit to Islamabad, where the conference was to be held. "We can only hope that the recovery from this blow to good science will be ultimately redeemed in either Pakistan or India, whichever country steps firmly into the breach and decides to at last do things right," Shroder says. For now, however, the researchers, like the troops at Siachen, have been left out in the cold.

–PALLAVA BAGLA

U.S. SCIENCE POLICY

Senate Panel Backs Social Sciences at NSF

A U.S. senator has blunted her attack on the value of social science research, calming fears that the National Science Foundation (NSF) might be ordered to reduce its support for the discipline.

On 2 May, Senator Kay Bailey Hutchison (R–TX), chair of the research panel within the Senate committee that oversees NSF and several other science agencies, used a hearing on NSF's 2007 budget request to harshly criticize several grants funded by NSF's social, behavioral, and economic sciences directorate (*Science*, 12 May, p. 829). She said such research should be excluded from the president's proposed doubling of NSF's budget as part of an initiative to strengthen U.S. competitiveness.

Last week, the full committee approved a bill (S. 2802) that included NSF's role in the initiative. But after drafting language that would have restricted NSF's budget increase to the physical sciences, Hutchison instead introduced an amendment—passed unanimously—that preserves NSF's mission to fund the breadth of nonmedical scientific research across its $5.5 billion portfolio. The amendment highlights the importance of the "physical and natural sciences, technology, engineering, and mathematics" and explains that "nothing in this section shall be construed to restrict or bias the grant selection process against funding other areas of research deemed by the foundation to be consistent with its mandate, nor to change the core mission of the foundation."

NSF officials especially welcomed the last phrase, which allows them to stay the course. Senator Frank Lautenberg (D–NJ), who struck the compromise with Hutchison, says the words are intended to reflect "the importance of the social sciences to U.S. economic competitiveness" and their value in applying technology to societal needs.

Despite her softened stance, Hutchison made it clear that some grants still rankle. Speaking before the committee voted, Hutchison declared that "these projects should not be funded by NSF at a time when we are focusing on trying to increase the number of scientists and engineers," improve U.S. math and science education, and stay ahead of global competitors. The bill awaits action by the full Senate. The House of Representatives has not yet acted on a similar measure. **–JEFFREY MERVIS**

CREDIT: GALEN ROWELL/CORBIS

new!

The power of small²

NanoDrop introduces a Fluorospectrometer

1 µl samples ▪ No cuvettes ▪ 10-second measurements ▪ Broad spectral output

Small footprint. Revolutionary technology. The NanoDrop® ND-3300 Fluorospectrometer is a powerful new tool for fluorescence spectrometry. Choose from many pre-defined methods or configure your own.

- **Nucleic acids:** Determine concentration of dsDNA using PicoGreen® assay (2 pg), Quant-iT™ DNA assay or Hoechst 33258 dye; RNA using RiboGreen® dye.
- **Proteins:** Determine concentration using Quant-iT™ protein assay.
- **More:** FITC (fluorescein), Cy-Alexa Fluor dyes, B-Phycoerythrin, Quinine Sulfate, Sulforhodamine and 4-MU.

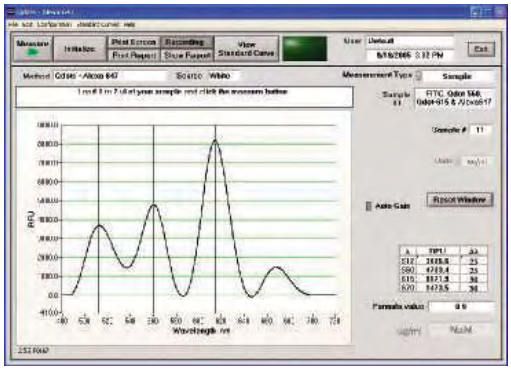

Measurement is as easy as pipette and read, requiring only 1-2 µl of sample. No cuvettes are necessary — simply wipe the optical surfaces and you're ready for your next sample. A broad excitation range is achieved using UV, blue and white LED sources. The uniquely clean optics of the patented retention system, combined with proprietary white LED signal processing, enables measurements across a wide range of wavelengths without the need for filter changes. The ND-3300 is small, simple and powerful enough for your most challenging and precious samples.

And for the power of small in absorbance measurement, the NanoDrop® ND-1000 UV/Vis Spectrophotometer can detect down to 2ng/µl and up to 3700 ng/µl of dsDNA without dilutions.

Ready to experience the power of small? Contact us today and try the ND-3300 or ND-1000 in your own lab.

FREE one week evaluation

Call for details **(302)479-7707** **www.nanodrop.com**

NanoDrop

BIOMEDICAL TRAINING

NIH Wants Its Minority Programs to Train More Academic Researchers

The U.S. National Institutes of Health (NIH) says it's time to get serious about producing more minority biomedical scientists. Admitting that they have been missing their target, NIH officials said at a public meeting last week that they will revise the rules of a flagship undergraduate program that serves mostly African Americans, Hispanics, and Native Americans. At the same meeting, a key advisory panel urged NIH and the academic community to go even further, proposing an 8-year doubling of minority candidates seeking doctoral degrees in the biomedical and behavioral sciences.

"We realize [the doubling] is a huge number," says Richard Morimoto of Northwestern University in Evanston, Illinois, co-chair of a working group that last week delivered a report on minority programs to the advisory council of the National Institute of General Medical Sciences (NIGMS), which oversees NIH's minority advancement programs. "But we felt that if we didn't raise the bar, a lot of programs would be content to keep serving the same number of students and achieving the same results."

At the core of the debate is how to get more mileage from several programs (see table) within the institute's $158-million-a-year division of Minority Opportunities in Research (MORE). (Given NIH's tight budget, nobody is talking about significant growth.) A staff white paper notes, for example, that fewer than 15% of the undergraduates in the Minority Access to Research Careers U*STAR program wind up with Ph.D.s in the biomedical or behavioral sciences, meaning that each doctorate-bound student costs NIH as much as $1 million. At the same time, the institute council's working group noted that nearly 40% of MORE's budget goes to a program helping faculty members at minority-serving institutions rather than directly to budding scientists.

Some argue that MORE's programs might be more successful if they moved beyond their traditional base—schools with largely minority student populations that focus on undergraduate education and do relatively little research—and embraced major research universities with fewer minorities but more resources. Minorities are increasingly being educated at the latter, the working group points out. But some training program directors believe that such a policy could shift money toward schools that don't really need the funding. "A $250,000 training grant may not be a big deal if you've got a multibillion-dollar budget, but it's vital to a school like ours," says Thomas Landefeld of California State University, Dominguez Hills. He and others believe that minority-serving institutions also plant the seeds for a scientific career among students who might not otherwise be aware of the opportunities.

How to measure success is another hot-button issue. Focusing on how many students become academic researchers, for example, could work against programs enrolling large numbers of students who pursue medical or pharmacy degrees, for example, or even those who go on to work for industry. "We are defining success more clearly," says NIGMS Director Jeremy Berg, "to mean greater diversity in the pool that trains the next generation of scientists and is eligible for NIH grants."

Morimoto admits there's no baseline for measuring progress toward the council's call for a 10% annual increase in filling the graduate school pipeline. The National Academies' National Research Council said in a report last year that NIH data fall woefully short of answering even basic questions about what its minority programs have accomplished (*Science*, 20 January, p. 328). But Morimoto says data alone aren't enough: "The training of more minority scientists needs to become the responsibility of the entire community."

–JEFFREY MERVIS

NIH's Major Efforts to Train Minority Scientists*

- **Minority Biomedical Research Support**
  - **SCORE:** Faculty research at minority-serving institutions ($60 million)
- **Minority Access To Research Careers**
  - **U*STAR:** Upper level undergraduates ($20 million)
  - **BRIDGES:** Transition from 2-year to 4-year schools, and for graduate training ($14 million)
- **RISE:** Institutional grants for student development ($20 million)
- **IMSD:** Programs to boost minority participation ($16 million)
- **Minority supplements** to R01 grants ($9.3 million)
- **Predoctoral fellowships** (N/A)

* 2005 funding levels.

SOURCE: NIGMS

Antiquities Bill Decried

German archaeologists say a law introduced to regulate sales of cultural artifacts won't reduce trade in looted objects.

The law would allow Germany to become one of the last countries to ratify a 1970 UNESCO convention designed to prevent illicit trade in stolen or looted artifacts. But critics claim that its loopholes—exempting illicit objects already in Germany and applying only to objects registered as stolen—would render it toothless. Freshly looted objects would not be covered, complains Michael Müller-Karpe of the Roman-Germanic Museum in Mainz. German archaeologist Susanne Osthoff, who was held captive earlier this year in Iraq, says the proposed law would abet terror groups that fence looted antiquities. The law could be adopted by fall. **–GRETCHEN VOGEL**

Alarm on Biohazard Lab

Construction work is already under way in Boston on an advanced biological research facility, but opponents of the $128 million project aren't giving up.

Last week, the Washington, D.C.–based Lawyers' Committee for Civil Rights Under Law sued the main funder, the National Institutes of Health (NIH), in federal court saying it had failed to look closely enough at the potential environmental risks of the biosafety level 4 lab, which is being built by Boston University (BU) in a densely populated neighborhood with a high percentage of minority residents and will handle highly infectious agents. "They said the *Titanic* was supposed to be safe, and an iceberg showed us that was not true," said Executive Director Charles Walker Jr. BU and NIH officials declined comment. **–ANDREW LAWLER**

Pachón Is Catchin' On

A proposed see-it-all telescope has found a home, but backers still need $300 million to build it.

The Large Synoptic Survey Telescope (LSST) would detect menacing asteroids and galaxies and probe space-stretching dark energy. Last week, a siting committee decided that LSST should perch atop Cerro Pachón, a Chilean peak that is already home to two other big telescopes. The site beat out one with poor infrastructure in Baja California, Mexico. Project leader J. Anthony Tyson of the University of California, Davis, hopes that the National Science Foundation will pony up enough to begin construction in 2009 on the telescope, whose novel design features a digital camera with 3 billion pixels. **–ADRIAN CHO**

PHYSICS

High-Tech Materials Could Render Objects Invisible

No, this isn't the 1 April issue of *Science*, and yes, you read the headline correctly. Materials already being developed could funnel light and electromagnetic radiation around any object and render it invisible, theoretical physicists predict online in *Science* this week (www.sciencemag.org/cgi/content/abstract/1125907 and … 1126493). In the near future, such cloaking devices might shield sensitive equipment from disruptive radio waves or electric and magnetic fields. Cloaks that hide objects from prying eyes might not be much further off, researchers say.

No see? Forget the Invisible Man's transparency potion; new materials might ferry light around an object, making it invisible.

The papers are "visionary," says George Eleftheriades, an electrical engineer at the University of Toronto in Canada. "It's pioneering work that sets the stage for future research." Greg Gbur, a theoretical physicist at the University of North Carolina, Charlotte, notes that others have studied invisibility but says the new papers describe more precisely how to achieve it. "Each gives specific examples of how you might design an invisibility device," he says.

From spaceships that vanish in *Star Trek* movies to Harry Potter hiding beneath his imperceptible cloak, invisibility has been a mainstay of science fiction and fantasy. But it might become a reality thanks to emerging "metamaterials," assemblages of tiny rods, c-shaped metallic rings, etc., that respond to electromagnetic fields in new and highly controllable ways. John Pendry of Imperial College London and colleagues, and Ulf Leonhardt of the University of St. Andrews, U.K., independently calculated how the properties of a shell metamaterial must be tailored to usher light around an object inside it. An observer would see whatever is behind the object as if the thing weren't there, Leonhardt says.

The theorists exploit the fact that light is always in a hurry, taking the quickest route between two points. That's not always a straight line, because light travels at different speeds in different materials, and it opts for the path that minimizes the total time of transit. So when light passes from, say, air into glass, its path may bend, which is why ordinary lenses focus light.

Pendry and colleagues and Leonhardt calculated how the speed of light would have to vary from point to point within a spherical or cylindrical shell to make the light flow around the hole in the middle. Light must travel faster toward the inner surface of the shell. In fact, along the inner surface, light must travel infinitely fast. That doesn't violate Einstein's theory of relativity because within a material, light has two speeds: the one at which the ripples in a wave of a given frequency zip along, and the one at which energy and information flow. Only the second must remain slower than light in a vacuum, as it does in a metamaterial.

The invisibility isn't perfect: It works only in a narrow range of wavelengths.

The authors map out the necessary speed variations and leave it to others to design the materials that will produce them. But researchers already know how to design metamaterials to achieve such bizarre properties, at least for radio waves, says Nader Engheta, an electrical engineer at the University of Pennsylvania. "It's not necessarily easy, but the recipes are there," says Engheta, who last year proposed using a metamaterial coating to counteract an object's ability to redirect light, making combination nearly transparent.

Cloaking devices for radio waves could appear within 5 years, Gbur says, and cloaks for visible light are conceivable. Pendry notes that even a cloak for static fields would, for example, let technicians insert sensitive electronic equipment into a magnetic resonance imaging machine without disturbing the machine's precisely tuned magnetic field.

Alas, even if invisibility proves possible, it may not work the way it does in the movies. For example, a cloaking device would be useless for spying, Pendry says. "Nobody can see you in there, but of course you can't see them, either." Keeping track of your always-invisible device might be a pain, too.

–ADRIAN CHO

U.S. COURTS

'Disappointed' Butler Exhausts Appeals

Thomas Butler's legal journey has come to an end. On 15 May, the U.S. Supreme Court declined to take up the case of the physician and microbiologist who received a 2-year prison sentence for shipping plague samples to Tanzania without the required permits and for defrauding his employer, Texas Tech University in Lubbock (*Science*, 19 December 2003, p. 2054).

Butler declined to be interviewed, but his wife Elizabeth says her husband is "very disappointed." Butler is working in Lubbock at a job unrelated to his professional training, she says, and weighing offers to rebuild his career. "This has been a tremendous blow," she adds, "but we are healing little by little."

In January 2003, Butler reported vials containing the plague bacterium *Yersinia pestis* missing from his lab; after questioning by the FBI, he signed a statement, which he later withdrew, saying he had accidentally destroyed the samples. In his trial, the jury dismissed all but one of the government's charges relating to illegal shipping and handling of plague samples but found Butler guilty of fraud involving fees for clinical trials he had conducted at Texas Tech. Last fall, a three-judge panel on the U.S. Court of Appeals for the Fifth Circuit upheld his conviction (*Science*, 4 November 2005, p. 758); the full appeals court declined to review the case.

"I have never in my career seen someone who was handed such a gross injustice," says his attorney, George Washington University law professor Jonathan Turley. Turley says that the fraud charges, which the government added after Butler refused to accept a plea bargain, concerned a dispute between the researcher and his employer that would not otherwise have been prosecuted criminally.

Butler, 64, was transferred to a halfway house in November after having served 19 months of his sentence and came home in late December. His supporters, including chemistry Nobelist Peter Agre of Duke University in Durham, North Carolina, are hoping against hope for a presidential pardon, if not from George W. Bush then possibly from his successor.

–MARTIN ENSERINK

MOLECULAR BIOLOGY

RNAi Safety Comes Under Scrutiny

What began as an effort to craft a better hepatitis therapy using a strategy called RNA interference has ended in the deaths of dozens upon dozens of mice—a harsh safety alarm for biomedical researchers looking to RNAi as a treatment for HIV, cancer, neurodegenerative diseases, and more.

The results, from gene therapist Mark Kay of Stanford University in California, come 3 years after he reported that a treatment based on the gene-silencing technique inhibited replication of the hepatitis B virus in mouse livers. This time around, Kay's team administered a refined version of the RNAi treatment to more than 50 infected mice.

"We saw for the first couple days exactly what we expected," says Kay's postdoctoral fellow Dirk Grimm, who helped lead the studies. But within a week or two, the mice began falling sick, their skin turning yellow from liver damage. More than 150 animals died, and many others suffered liver toxicity. Lowering the amount of virus given eliminated the harsh effects but also erased the treatment's success.

"There's something that we don't understand going on here," says Timothy Nilsen, who heads the Center for RNA Molecular Biology at Case Western Reserve University in Cleveland, Ohio. Although Kay and Grimm were taken aback by the devastating toxicity, they and others retain confidence in RNAi. "I really think it can still work," says Kay.

RNAi has become enormously popular in the last few years. It involves blocking the activity of genes, including those linked to disease, with short sequences of RNA complementary to a gene's sequence. Companies are already testing in people RNAi treatments for a respiratory virus and for macular degeneration.

Those trials, for which no significant safety problems have been disclosed so far, rely on simply introducing RNA molecules into the body. In contrast, Kay's team packages genes encoding small RNA molecules into viruses stripped of other genetic material, a strategy much like traditional gene therapy. Once injected, the viruses infect cells and keep producing the small RNAs, allowing a single dose to go a long way.

For its RNAi tests, Kay's team uses an adeno-associated virus (AAV), which homes to the liver. Indeed, 90% of the virally delivered RNA genes ended up there, says Grimm. Yet the virus is probably blameless; injections of an empty virus didn't cause problems in the mice. To explore whether specific RNA sequences might be the culprits, the Stanford team created dozens of viruses making other RNA sequences and injected them into mice without hepatitis B, some genetically altered and some normal. Out of all 49 sequences tested, 23 were lethal in every case, killing the animals within 2 months. Another 13 were "severely toxic" to the liver, they write in *Nature*. As with many treatments, dosing seems to correlate with risk: Kay's team safely thwarted hepatitis B in mice by injecting an AAV that makes fewer RNA sequences.

The results are "not surprising in retrospect," says John Rossi of City of Hope in Duarte, California, who's working on an RNAi therapy for HIV. Too many extra RNA molecules may disrupt a cell's own internal RNAi machinery, he explains. Kay's group suggests that the extra small RNAs compete for a protein that transports a cell's own RNAs.

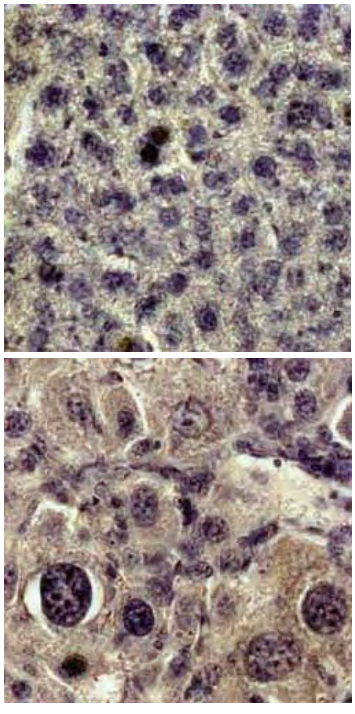

Interference problem. Compared to the liver of a healthy mouse (*above*), an RNAi treatment destroys the liver of a treated animal (*below*).

CREDIT: M. KAY/STANFORD UNIVERSITY

A company called Sirna Therapeutics in San Francisco, California, still plans to test a nonviral RNAi strategy on people with hepatitis C next year. The firm "has spent a hell of a lot of time and effort putting [small RNAs] into animals and nonhuman primates … looking for toxicity, and we haven't seen anything like this," says Barry Polisky, Sirna's chief scientific officer. Like Kay and others, Polisky worries that these new findings will be seen as an indictment of RNAi therapy, even though he is confident that injecting small RNAs alone is less hazardous than the viral approach. Not everyone's convinced. "I think it's premature to say anything is safer at this point," says Nilsen.

–JENNIFER COUZIN

Boycott Faces U.K. Vote

CAMBRIDGE, U.K.—For the fourth time in 5 years, a U.K. university union has proposed a boycott of Israeli academics. At a meeting beginning 27 May, the 67,000-member National Association of Teachers of Further and Higher Education (NATFHE) will vote on a motion to penalize Israel for "apartheid policies, including construction of the exclusion wall" that's meant to keep out terrorists. The motion calls on NATFHE members to "consider their own responsibility" for boycotting Israeli "institutions or individuals." The motion is likely to pass, says Ronnie Frazier, a U.K. representative of the Academic Friends of Israel, who calls the proposal discriminatory and the union generally biased. A union spokesperson declined comment, and the motion's sponsor remains unknown.

–ELIOT MARSHALL

WHO Suffers Loss

GENEVA—The unexpected death Monday of the head of the World Health Organization has brought forth tributes to the leadership of Lee Jong-Wook—and speculation that the next director could be someone Lee bested when he took the top job in 2003.

Lee, 61, collapsed 2 days before the start of the 59th World Health Assembly here. He died after undergoing emergency surgery to remove a blood clot in his brain. "Lee not only had long experience with global health but real energy and drive," says William Foege, a senior investigator at the Task Force for Child Survival and Development. "It's a great loss."

Among candidates rumored to succeed Lee are Belgian UNAIDS head Peter Piot, who was runner-up for the position in 2003, and Mexican Health Minister Julio Frenk Mora, who introduced universal health care coverage in his country. "[Mora] is very smart," says Boston University's Gerald Keusch, "and it would be good for someone from a developing country to take the leadership."

–MARTIN ENSERINK

House Preserves Toxics Rules

The Environmental Protection Agency won't be able to proceed with plans to relax rules for reporting information about hazardous chemicals (*Science*, 20 January, p. 319), under the terms of an amendment to an appropriations bill passed last week by the House of Representatives. The Senate has yet to act on its version of the bill.

–ERIK STOKSTAD

GREENHOUSE GASES

Price Crash Rattles Europe's CO_2 Reduction Scheme

LONDON—Dumping carbon into the atmosphere became very cheap last week. Or so it seemed, as the cost of licenses to emit carbon dioxide came tumbling down in Europe on 15 May. The price crash in the Emissions Trading Scheme fed doubts about the setup of this new market, launched in 2005 to help meet targets for CO_2 in the Kyoto Protocol on greenhouse gas emissions. Experts are now discussing what went wrong and what can be done to shore up the system.

The European Union (E.U.) invented the market to create incentives for cutting CO_2 emissions. Companies can meet specific targets by investing in green technology that lowers CO_2 emissions directly or by buying permits that allow them to emit CO_2. In theory, those with the best technology will have surplus credits, which they can sell to the laggards—making a profit while improving the environment. Under this scheme, the price of one allocation unit—equivalent to 1 metric ton of CO_2—soared to an all-time high of €31.5 in April. Then in a matter of days it dropped to €8. Prices were on the rise again as *Science* went to press but seem unlikely to climb back to where they were. The heaviest impact of the crash, ironically, may fall on developing countries, which had begun to benefit from investments in clean technology encouraged by the European CO_2 market.

CO_2 trading prices fell after the European Commission announced that European industries had emitted more than 60 million tons of greenhouse gases less than predicted. With more than enough emissions allowances to go around, demand vanished. The events confirmed what had been suspected for some time: European governments may have been too generous in granting credits.

"We know for sure that one of two things happened," says climate policy expert Michael Grubb of Imperial College London. "Either industrial emissions were never going to be as high as projections said they would be, or it turned out to be far easier for industries to cut back on emissions than they had been saying." The general consensus favors the first theory.

Before the E.U. launched its trading scheme last year, its governing body, the European Commission, agreed on a total number of emissions allowances. To come to this number, nations tallied up estimates of their own CO_2 emissions, subtracted a portion to create an incentive for industries to reduce their emissions, and handed over these targets in National Allocation Plans to the commission. Many governments, it appears, relied on company estimates of historical emissions.

In April, news started to trickle out that various countries had not only met their targets for 2005 but also had allowances to spare. Drawing up allocation plans based on industry projections "inflated the trading system and sent out the signal that industries just have to lobby to get what they need," says Grubb. But backers of the E.U. trading scheme point out that it is still in a teething period that runs from 2005 to 2007. The real deal begins in Phase II, from 2008 to 2012, corresponding to the time when the European Union must fulfil its Kyoto Protocol pledge to reduce greenhouse gas emissions to 8% below 1990 levels.

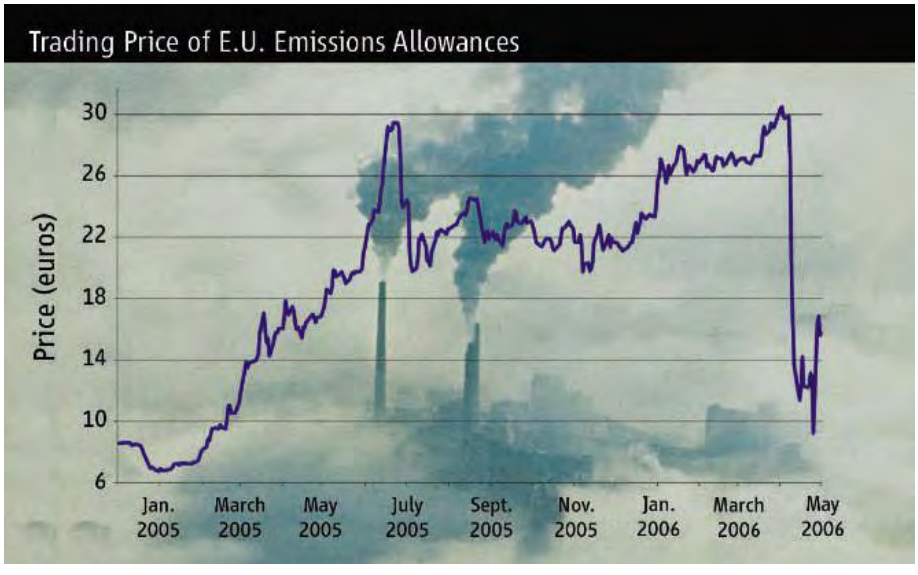

Member nations must give the European Commission their National Allocation Plans for the second phase on 30 June. This time, estimates will be based on real emissions data, installation by installation. According to Shell carbon trader Garth Edward, they are the one tool policymakers have to ensure that the movements of the market translate into reduced global emissions.

For Grubb, there's still a significant problem. The E.U. trading scheme covers slightly less than half of all E.U. emissions. Not included, for example, are the transport and domestic sectors. Countries need to justify how they will meet their Kyoto Protocol commitments both through their National Allocation Plans and by using technology and other measures such as taxes to reduce emissions in those nontrading sectors. "This is not a simple clear-cut matter," says a European Commission official. "It requires an in-depth review of emissions trends across all sectors and all measures being used to limit them." But Grubb believes it has been too easy for countries to claim they will achieve their Kyoto commitments by reducing emissions in sectors not covered by the trading scheme; he hopes the next allocations under the scheme will be more stringent.

Some policymakers see the drop in the price of allowances as potentially good news. Says Halldor Thorgeirsson, deputy executive secretary of the United Nations Framework Convention on Climate Change, many "will be looking to the market for indicators of the cost" when negotiating post-2012 climate change policy. "The price drop is a bonus as far as post-2012 goes," agrees Benito Müller, director of Oxford Climate Policy in the U.K. "The message is: 'See? It's not that expensive; we can tighten the limits.' "

Ultimately, developing countries may lose the most from the recent price crash. Investment surged in 2005 and 2006 in green projects in the south, partly stimulated by the high price of E.U. emissions allowances. Through a Kyoto Protocol instrument known as the Clean Development Mechanism (CDM), these projects offer companies in developed countries an opportunity to offset emissions at home by reducing emissions abroad. According to a World Bank report, CDM allowed approximately $2.5 billion in investments, or 350 million tons of reduced emissions, last year. More than half the volume was from European investment in developing countries.

When CO_2 emission prices were high in Europe, governments seemed ready to allow their industries to clean up southern skies as much as they wished. Now that prices have dropped to what most agree is a more realistic level, governments may decide to cap the external credits.

–CATHERINE BRAHIC

Catherine Brahic is a writer for SciDev.Net.

SOURCE: POINT CARBON; PHOTO: GETTY IMAGES

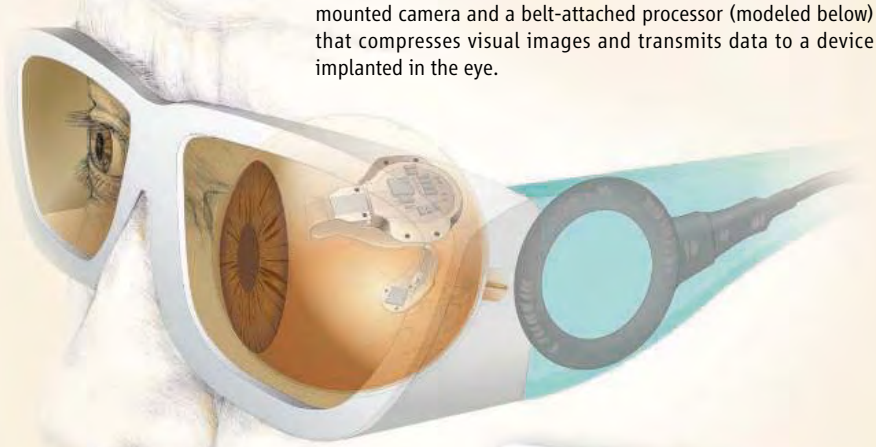

New views. A visual prosthesis (artist's illustration) developed by Intelligent Medical Implants in Germany employs a goggles-mounted camera and a belt-attached processor (modeled below) that compresses visual images and transmits data to a device implanted in the eye.

Early-stage artificial "eyes" are competing in the clinic, giving blind volunteers a glimpse of the future

A Vision for The Blind

WHEN STEFFAN SUCHERT, A LAWYER IN Nuremberg, Germany, learned that his two sons, who had been born deaf, were also going blind from a degenerative eye disorder, friends told him to pray and wait. Instead, he quit his law practice in 1998 and has spent nearly €3 million ($4.2 million) to found a company to develop a device that might return limited eyesight to his sons.

Researchers at that company, Intelligent Medical Implants (IMI) Group in Bonn, have since designed a gold implant containing a chip about the size of a small coin that sends signals to a pupil-sized patch of 49 electrodes, exciting cells in the retina at the back of the eye. Since November, ophthalmic surgeon Gisbert Richard of the University Clinic of Hamburg has implanted these chips on the eyeballs of four totally blind patients and tacked the electrodes onto their paper-thin retinas. The chips, which will ultimately be connected via an infrared receiver to a video camera, are now being tested with simulated visual input. When a computer sent each patient's chip infrared signals encoding simple patterns such as lines and spots, three of the patients saw the lines and identified the locations of the spots. In addition, one patient could see horizontal movement in either direction simulated by the computer, IMI's Chief Medical Officer Thomas Zehnder reported 2 May at the meeting of the Association for Research in Vision and Ophthalmology (ARVO) in Fort Lauderdale, Florida.

IMI is racing a growing cadre of companies and research groups to develop the first artificial "eye" that can supply useful vision to a subset of blind people. Just a few years ago, some artificial-vision investigators were lamenting that hype had outpaced clinical data in their field (*Science*, 8 February 2002, p. 1022). But now at least five teams have implanted experimental devices into people, and a sixth plans human tests within the next year or two. The pipeline of preclinical systems is also growing. At least 23 different devices are under development, a doubling in the past 4 years. "A critical mass" of research teams using innovative approaches has developed, says Joseph Rizzo, a Harvard Medical School neuroophthalmologist at the Massachusetts Eye and Ear Infirmary in Boston: "That kind of momentum makes it more likely that something will emerge that can really help blind people."

So far, even the most advanced of the experimental devices has provided blind people with only the crudest of black-and-white images, inadequate for navigating unfamiliar surroundings. Most of the artificial eyes currently under development would benefit just the minority of blind people who suffer from diseases such as retinitis pigmentosa (RP) and macular degeneration that degrade retinal cells but leave some of the retina intact. Much farther out are brain-implanted artificial-vision systems that can help people who have lost their eyes in accidents; none of today's devices will work for people who were born blind and whose visual system as a whole remains underdeveloped.

Chip in the eye. IMI's implant sends visual data via gold wires to a tiny electrode array tacked onto the human retina.

Lucian Del Priore, a retinal surgeon at Columbia Presbyterian Medical Center in New York City, warns that the field of visual prosthetics is still in its infancy. It is not realistic, he says, "to expect that a retina chip will restore vision to anything close to 20/20 in the near future."

Nevertheless, a combination of improved surgical techniques, miniaturization of electronics, advances in electrode design, and knowledge about how to safely encapsulate electronics in the body are inching the dream of artificial vision closer to reality. "It's very exciting for all of us to see the progress," says neuroophthalmologist Eberhart Zrenner of the University of Tübingen in Germany.

Entering the eye

Researchers have investigated the use of electricity to stimulate vision for nearly half a century. In the 1960s, physiologist Giles Brindley of the Medical Research Council in London and his colleagues implanted 80 electrodes on the surface of a blind person's visual cortex, a region at the back of the brain that is the first stop for

CREDITS: G. RICHARD/UNIVERSITY EYE CLINICAL CENTER, HAMBURG

visual signals coming from the eye. Wireless stimulation of the electrodes made the patient, an adult who had recently become blind from glaucoma and a retinal detachment in the right eye, see spots of light known as phosphenes. "That was the first bold demonstration of what one might be able to do," says Philip Troyk, a biomedical electrical engineer at the Illinois Institute of Technology (IIT) in Chicago.

By the 1980s, a crop of ophthalmologists began considering a narrower and seemingly easier-to-solve problem: making prostheses for the eye. Many of these physicians wanted a way to help patients with incurable degenerative retinal diseases such as RP and macular degeneration. Research suggested that such disorders, which degrade photoreceptor cells called rods and cones, still leave large portions of the retina intact even after a patient has become totally blind. On this assumption, researchers aimed to stimulate the remaining functional cells.

In the mid-1990s, ophthalmologist Mark Humayun, along with biomedical engineer James Weiland, then at Johns Hopkins Hospital in Baltimore, Maryland, and their colleagues, showed that this was feasible. When they stimulated the retinas of five blind people using handheld electrodes, the people saw spots of light in locations that matched the site of the stimulation.

Humayun, Weiland, and their colleagues then developed a more permanent prosthesis in conjunction with Second Sight Medical Products in Sylmar, California. The device consists of a small video camera perched on the bridge of a pair of glasses, a belt-worn video processing unit, and an electronic box implanted behind the patient's ear that has wires running to a grid of 16 electrodes affixed to the output layer of the retina. The video processor wirelessly transmits a simplified picture of what the camera images to the box, and then the retinal implant stimulates cells in a pattern roughly reflecting that information.

In normal vision, the rods and cones at the back of the retina detect light, and the retinal ganglion cells (RGCs), which actually sit closest to the vitreous—the eye's gelatinous interior—relay the visual signal to the brain. The electrodes of Second Sight's prosthesis directly excite RGCs—a so-called epiretinal approach—by sitting between them and vitreous. The stimulated RGCs then send signals along their axonal fibers, which make up the optic nerve.

Since 2002, Humayun's group, now at the University of Southern California in Los Angeles, has implanted its array into six people blinded by RP. After some training with the device, all of them could distinguish between the light patterns given off by a plate, cup, and spoon by moving their head-mounted cameras to scan the objects, the group reported at ARVO this month. Some of the people could also detect motion when a bar of light was moved in different directions in a darkened room. Their perceptions are crude, admits Weiland, "but for them, it's a pretty big deal."

Weiland, Humayun, and their colleagues are now working on epiretinal implants containing hundreds of electrodes, which they hope will provide enough points of light to enable patients to recognize faces and read large print. The group is also developing a tiny video camera that would be embedded in an artificial lens and implanted in the eye. That lens would replace the eye's natural lens and would enable scanning using natural eye movements instead of awkward head shifting. In the meantime, Second Sight plans to start testing a 60-electrode implant by the end of the year.

That technology will compete head-to-head with IMI's 49-electrode array, also implanted in the epiretinal space. Next to the IMI electrodes is a tiny infrared receiver, which enables the chip to receive video input from a glasses-mounted camera and "pocket processor," the size of a small paperback book. In August, the company will begin implanting this upgraded device into 10 people. The prosthesis should enable them to find large objects in a room such as a table, chair, door, and perhaps even a cup of coffee, according to Hans-Jürgen Tiedke, an electrical engineer who heads the IMI group.

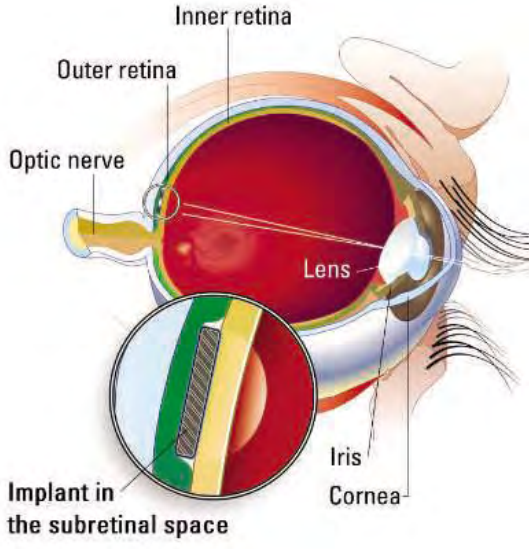

Silicon sandwich. A silicon-based subretinal implant is wedged (*inset*) into the photoreceptor layer of the retina at the back of the eye, near the eyeball's perimeter. An epiretinal implant would sit on the other side of the retina, facing the eye's gelatinous interior.

CREDIT: A. CHOW/OPTOBIONICS

Under the retina

Whereas epiretinal devices such as IMI's and Second Sight's require extraocular cameras and video processors to capture images, other teams elect to use light-sensitive chips designed to tap into more of the retina's image processing. In the retina, about 125 million rods and cones connect, through intermediate cell layers, to just 1.2 million optic nerve fibers, a 100-to-1 compression of information. Placing electrodes directly where photoreceptors are being lost, against the lining of the eyeball, enables the electrodes to excite the retina's intermediate cell layers and allows those layers to perform their normal processing of visual signals. These so-called subretinal implants also have the advantage of stimulating the retina in its natural topography, theoretically provoking more natural perceptions.

Ophthalmologist Alan Chow and his team at Optobionics in Naperville, Illinois, were the first to try this approach in people in 2000. In 30 people so far, they have implanted in one eye a silicon disk the size of a nail head that is studded with 5000 microscopic solar cells, or photodiodes. The solar cells capture ambient light and translate it into pulses of electricity intended to stimulate the retina's intermediate layer of cells.

Most of the implant recipients, including all 10 in the first clinical trial, have reported moderate to significant improvements in at least one aspect of visual function, such as light sensitivity, size of visual field, visual acuity, movement, or color perception. One of the first subjects, for example, had virtually no light perception before the surgery but could see human shadows after receiving the implant. A person in a more recent trial, who had very poor central vision and was legally blind, could thread a needle 6 months after the surgery, Chow says.

Such improvements pose a mystery to some. Many of them are unlikely to be a direct result of the chip's electricity on retinal cells, according to William Heetderks, who directs extramural sciences at the National Institute of Biomedical Imaging and Bioengineering in Bethesda, Maryland. "The amount of current you need to actively stimulate retinal ganglion cells is known," he notes, "and it is not in the same range as the amount you get off a photodiode."

Chow insists that some of his patients do see light at the implant site, but he agrees that the visual improvements are too widespread and complex to come solely from electrical stimulation of retinal cells by the tiny chip. He suggests that the implants somehow induce the release of growth factors that improve the function of remaining retinal cells. In rats with a genetic disorder that causes retinal degeneration, both active and inactive retinal implants delayed the degeneration of photoreceptor cells, Chow, Machelle Pardue of Emory University School

Solar-powered sight. Optobionics co-founders, and brothers, Alan and Vincent Chow work on their silicon eye implant (*above*), an array of 5000 microscopic solar cells (*below,* magnified). These are implanted in the human eye (*center*).

of Medicine in Atlanta, Georgia, and their colleagues reported at ARVO.

Retina Implant GmbH in Reutlingen, Germany, the company founded by Zrenner and his colleagues, has created its own subretinal implant, a 40 × 40 array of microscopic solar cells. Each photodiode links up with a small amplifier, to boost the power of incoming light. In October, ophthalmic surgeons spent 7 hours putting the Tübingen team's chip into a blind person and have since repeated the surgery on a second patient. So far, Zrenner's team has only revealed data from the use of the chip's 16 test electrodes, which can be controlled externally via a cable that leaves the body behind the ear. Activating those electrodes elicited predictable images in both patients. Stimulating single electrodes produced pea-sized spots of light an apparent arm's length away. Switching on all 16 electrodes created a square; flipping on four in a row lit up a line the size of a large match, Zrenner and his colleagues reported at ARVO. "In principle, if you have enough electrodes working, you can put together an object," he says.

Looking ahead

Although Zrenner's and Chow's prostheses are designed to work without cameras, subretinal devices don't have to operate solo. Physicist Daniel Palanker of Stanford University in California and his colleagues have developed an array of photodiodes that receive infrared input from goggles displaying a projection from a video camera. In this setup, the infrared "scene" changes as the eyes move inside the goggles' virtual reality display. This may provide more natural visual input than people can get from ordinary head-mounted displays, in which the view stays static unless a patient moves his or her head.

The Stanford team's chips, which are not yet in human trials, also have unique structures that enable electrodes to get closer to retinal cells. That enables each electrode to stimulate a narrow area of tissue distinct from that triggered by a neighboring electrode, an advance that could be critical for developing high-resolution artificial vision. In one of the chips, cells migrate toward electrodes through pores. In another, cells travel between pillars such that electrodes at the tips of the pillars penetrate into the retina without apparent harm. When implanted in the retinas of blind rats with an RP-like disorder, both chips put retinal cells within just a few micrometers from electrodes. That should be close enough for 20/80 vision, enabling a person to read large print, the group reported at ARVO. By comparison, other groups' chips are basically flat, and their electrodes are typically tens to hundreds of micrometers away from retinal cells, limiting resolution to about 20/400, the level of legal blindness, or worse.

Brindley's strategy of bypassing the eye completely also continues to be studied. IIT's Troyk and his colleagues are developing an array of 1000 microelectrodes that they hope eventually to implant in the visual cortex of a blind person. Such an implant could, in theory, help the many blind people who do not have intact optic nerves or retinas. One challenge is finding the best way to use an electronic link to put visual information into the brain, Troyk says.

There are still big hurdles to cross before any of the prosthetic eyes under development can be put to everyday use. For example, no one knows for sure how much of the retina remains intact in the late stages of RP and similar retinal disorders, or what happens to neural tissue after it's stimulated repeatedly over months or years. In addition, researchers still don't have devices that can illuminate any of the world's fine print—details of faces or the texture of a flower. Nor do they have eye chips that can adapt to variations in natural lighting as the eye does. Stimulating color perception remains an even more distant dream. "One of the realizations I've come to is that artificial vision is not a restoration of natural vision," Weiland says.

Still, Suchert remains optimistic that IMI's chip or a similar device will one day help his sons. Matthias, who is 30, sees the world through a narrow tunnel, as if he were looking through the bore of a paper-towel roll. Andreas, 32, has a wider field of view but has lost his peripheral and night vision. "I insist on being successful," says Suchert.

–INGRID WICKELGREN

CREDITS (TOP TO BOTTOM): EEMA FREDERIC/CORBIS SYGMA; A. CHOW/OPTOBIONICS

TECHNOLOGY TRANSFER

Universities Find Too Many Strings Attached to Foundation's Offer

The Alfred Mann foundation says professors need help to commercialize their inventions. But some experts say the charity is asking for too much in return

Billionaire entrepreneur and biochemist Alfred Mann, 81, thinks the commercialization of biomedical technologies is too important to be left to academics. He wants to set up multimillion-dollar campus-based R&D institutes to help turn inventions into marketable medical innovations—with the institutes calling the shots.

But Mann is having trouble selling the idea. This month, a proposed $100 million deal with the University of North Carolina (UNC), Chapel Hill, and North Carolina State University in Raleigh fell through, and discussions with several other universities have yet to result in agreements. Many technology transfer experts say they aren't surprised: What the Alfred E. Mann Foundation for Biomedical Research is proposing, they say, would force a university to surrender too much control over its intellectual property (IP).

Universities have been trying for the past 20 years to beef up their technology transfer operations, ever since Congress opened the door for them to make money off the fruits of federally funded research. Mann, who made a fortune starting and then selling off several high-tech companies, created his foundation in 1985 to speed the development of university-based biomedical inventions into treatments. In 1998, Mann gave $100 million to the University of Southern California (USC) in Los Angeles to create an Alfred Mann Institute.

A similar-sized gift to the two North Carolina universities was expected to be the first in a second generation of Mann institutes that would commercialize discoveries at a dozen or more campuses. The two universities were hoping the state would finance two $25 million buildings to house the institute; that request has been withdrawn after the talks collapsed and Mann withdrew his offer.

The arrangement Mann is promoting is a novel hybrid that would confer all power to a separate nonprofit institute. The university and the foundation would each appoint half the institute's board members, and the revenues and royalties would be divided among the original inventor, the university, the institute, and the Mann foundation. Although professors and graduate students will participate in the work, the institutes are to be staffed largely by experts in product development recruited from industry.

Tony Waldrop, vice chancellor for research at UNC, says the foundation "wanted much more far-reaching [IP rights] than what we were willing to give." The university "wanted to have some ability to pick and choose" which faculty research products would be licensed to the new institute, he adds, and more freedom for inventors to choose their commercial partners.

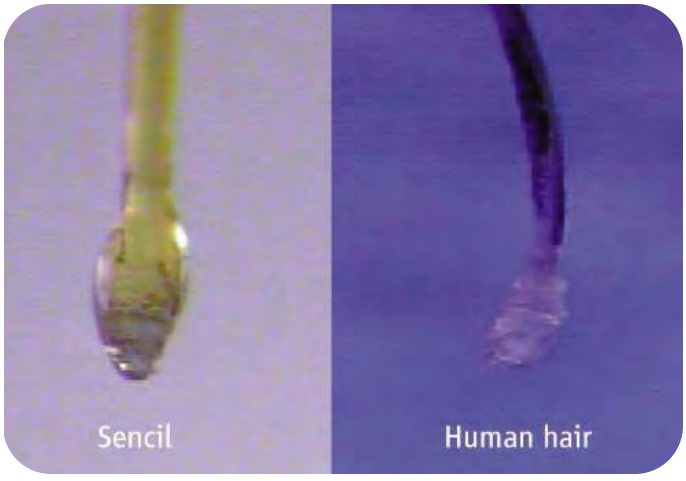

In by a hair. A subcutaneous miniprobe is one project at USC's Mann Institute.

Waldrop declined to be more specific, but a copy of the proposed agreement (obtained by *Science* under the state's open records law) explains that the university would have been required to give the Alfred Mann Institute the first crack at any biomedical technology or drug the institute wanted to develop that wasn't already bound by a prior agreement with the funder. The university would have been allowed two exemptions every 5 years.

IP experts who have seen the proposed agreement expressed surprise at its sweeping IP provisions. "I can't think of a major U.S. research university that would sign" such an agreement, says Karen Hersey of Franklin Pierce Law Center in Concord, New Hampshire, a former IP lawyer at the Massachusetts Institute of Technology. "The university is being asked to abandon its right to decide" what to do with its "uncommitted" IP. In fact, she says, the proposed scheme flies in the face of a host of accepted practices and constitutes a "massive reach" into federally funded research—possibly even violating a federal prohibition on discrimination by universities in making available the results of federally funded research. It's an "aggressive" proposal, agrees Robert Cook-Deegan of the Duke Institute for Genome Sciences & Policy in Durham, North Carolina. "It calls for the university to give the institute pretty much worldwide exclusive rights to anything that hasn't already been licensed to somebody else."

Mann foundation CEO Stephen Dahms, a former chemistry professor at San Diego State University, says that those who would reject the philanthropy's proposal don't know what's good for them. He says the institutes would cherry-pick only "a very limited subset of university IP"—perhaps two projects a year. The North Carolina institutions, he asserts, suffer from a "limited perspective on intellectual property access and other factors. … The lawyers warned us, but we thought we could overcome their traditional conservative ways of doing things."

"Universities are just not capable of making these business decisions," says Dahms. In a 21 April letter to the *Chronicle of Higher Education*, which reported in March that several universities had bristled at the IP provisions, Mann explained that universities are getting low rates of return on research investments because "professors have no concept of what it takes to bring a product to market" and technology transfer offices "often don't know how to find the right partner." A number of universities, including Johns Hopkins in Baltimore, Maryland, Emory in Atlanta, Georgia, and the University of Minnesota, have held preliminary discussions with the Mann foundation, but Dahms says no formal proposals have been made.

USC's institute, which has received $170 million from the foundation, has several projects nearing the marketing stage, including a noninvasive heart-output monitor and a hair follicle–sized chemical biosensor. But the IP arrangements are less rigorous than those in the proposed North Carolina agreement. "Under no conditions would I undertake something without cooperation of the inventor," says institute director Peter Staudhammer. Although proposed IP policies have become more rigorous since the USC agreement—"Mr. Mann wants to be certain these institutes are kept in an evergreen mode," says Dahms—he emphasizes that the foundation is further revising its policies.

–CONSTANCE HOLDEN

CREDIT: ALFRED MANN INSTITUTE FOR BIOMEDICAL ENGINEERING/UNIVERSITY OF SOUTHERN CALIFORNIA

Straight shooter. Barish (*second from left*) draws praise for his openness and integrity.

HIGH-ENERGY PHYSICS

A Quiet Leader Unites Researchers In Drive for the Next Big Machine

As head of the design team for the International Linear Collider, Barry Barish has physicists around the globe pulling together. But can the governments of the world afford their enormous particle smasher?

BATAVIA, ILLINOIS—Three years ago, particle physics was, like Julius Caesar's Gaul, divided into three parts. Physicists around the world agreed that they should build an International Linear Collider (ILC), a 30-kilometer-long particle smasher that would blast electrons into their antimatter partners, positrons, to produce new particles and probe a new high-energy frontier. But researchers in North America, Europe, and Asia had different conceptions of the multibillion-dollar machine, and accelerator physicists were developing two different technologies for its twin accelerators.

Now, researchers from the three regions are working together, thanks in good measure to the efforts of Barry Barish, a soft-spoken 70-year-old who wears his silver curls down to his collar and lives near the beach in Santa Monica, California. A particle physicist at the California Institute of Technology (Caltech) in Pasadena, Barish chaired the panel that settled the divisive technology issue and heads the ILC's Global Design Effort (GDE). But Barish is no Caesar. He leads not through force and intimidation but through a subtle combination of personal persuasion and masterful organization.

"You don't have to have a frown on your face and be a tough guy to get things done," Barish says. Nevertheless, Barish's leadership skills mystify others. "When Barry works with a group, people come away feeling that they've arrived at an answer that they discovered for themselves," says Michael Turner, a cosmologist at the University of Chicago in Illinois who has known Barish since Turner was a Caltech undergrad. "He has an ability to guide things with an invisible hand."

Barish will need a deft touch to manage the GDE, a largely virtual collaboration that stretches around the world and is itself a bold experiment in how science is done. By year's end, the GDE aims to produce a preliminary design. More important, the team intends to calculate a price—a figure that may determine whether the ILC ever gets out of the starting blocks politically.

That number has to be reliable. Physicists are haunted by the demise of the Superconducting Super Collider (SSC), an even bigger machine in Waxahachie, Texas, whose cost ballooned from $4 billion to $10 billion before the U.S. Department of Energy (DOE) axed it, unfinished, in 1993. Barish says the ILC cost estimate will be certain to within plus or minus 20%. That claim may make some of his colleagues' palms sweat.

Both outsider and insider

Barish received his doctorate from the University of California, Berkeley, in 1962 and has tackled ever-larger projects throughout his career. In the 1970s, he led one of the first experiments at the Fermi National Accelerator Laboratory (Fermilab) in Batavia, Illinois, a study of particles called neutrinos that cemented his reputation as a physicist. In the 1980s, he directed MACRO, an experiment in a cave in Gran Sasso, Italy, that searched for exotic particles called magnetic monopoles. In the early 1990s, he spearheaded GEM, an experiment that would have run at the SSC.

Barish may be known best for his work with the Laser Interferometer Gravitational-Wave Observatory (LIGO), a pair of exquisitely sensitive detectors in Hanford, Washington, and Livingston, Louisiana, designed to detect ripples in the fabric of spacetime. Run by Caltech and the Massachusetts Institute of Technology (MIT) in Cambridge, LIGO foundered in the early 1990s because of dissension within and friction between management and the National Science Foundation (NSF). The agency considered killing the $500 million project and pressured Caltech to find a new director. In early 1994, Caltech administrators asked Barish to take the job.

LIGO had been a "skunk works," in which a few leaders made decisions secretively, says MIT experimental physicist and LIGO member Rainer Weiss. Barish immediately implemented a more open management structure, he says. Barish brought in more people and had every collaboration member write a description of his or her part of the project, Weiss says. Those became the "LIGO baseline," a document that defined the experiment. Barish also made key decisions, such as changing the type of laser, that helped LIGO meet design specifications and start taking data, as it did last year.

Barish has followed a circuitous path to the GDE directorship. In 2001, he co-chaired a DOE-sponsored committee that concluded that the United States should push to host the ILC. At the time, the global community was split over the "radio frequency cavities" that would accelerate particles in such a machine. Researchers in Germany were developing a design, dubbed TESLA, that used cavities made of chilly superconducting niobium; their counterparts in the United States and Japan were developing more-conventional copper cavities (*Science*, 21 February 2003, p. 1168). Community leaders formed an International Technology Recommendation Panel to choose between the "cold" and "warm" technologies and ultimately asked Barish, who had no ties to either side, to chair it.

Many doubted that accelerator physicists would accept the panel's decision, as some had invested decades in one technology or the other. But when, in August 2004, the panel recommended the less powerful but also less demanding superconducting technology, the decision stuck—in large measure because Barish made the review exceptionally thorough and transparent, says NSF's Moishe Pripstein: "He focused on the process and was

CREDIT: FERMILAB

very open from the beginning so that people knew what the steps would be."

When it came time to pick a director for the design effort, Barish's name came up because he was familiar with the project but still had no ties to any particular camp, says Nobu Toge, an accelerator physicist at the Japanese particle physics laboratory KEK in Tsukuba. "Barry had the fewest enemies in this business," Toge quips. So in March 2005, the ILC Steering Committee tapped Barish to direct the GDE. He now spends between a third and a half of his days flitting all over Europe, Asia, and North America on ILC-related work. "I need to see everybody, so I travel a lot," he says. "Right now, I'm the face of this."

The process is personal

Ask Barish's colleagues why he's an effective leader, and they invariably point to his interpersonal skills. "When I interact with him, I can tell he's listening to me," Toge says. "He might answer yes, or he might answer no, but I can tell he's thought about what I said." Chris Walter of Duke University in Durham, North Carolina, did his graduate work under Barish and says he has a knack for persuasion. "You would go into a conversation with him thinking that you did or didn't want to do something," Walter says, "and you'd walk out agreeing with what Barry wanted and being somewhat baffled how that happened."

At the same time, Barish has a keen feel for process and organization, as his efforts with LIGO and the ILC technology panel demonstrate. Barish says he learned those skills through experience seasoned with a little purposeful study. "When we're talking about building a big project, we're talking about a bastardized version of how you build a bridge," he says. "The trick is to inject just enough process so the project works, but not so much that it becomes so disciplined that people feel their work isn't their own." Most important, Barish says, he strives to surround himself with talented people with whom he can work.

Those closest to Barish attribute his success to particular personality traits. "He's extremely, rigidly ethical, and I think that underlying ethics is part of what makes him effective," says Barish's daughter Stephanie, a multimedia producer in Venice, California. Samoan Barish, Barry's wife of 45 years and a social worker–psychoanalyst, says her husband possesses a self-confidence that lets him function under pressure. "Sometimes we're our own worst enemies; we put obstacles in front of ourselves," she says. "Barry doesn't do that. He's not afraid."

For his part, Barish says he's comfortable making decisions because a scientific collaboration is not a democracy and because it's almost always better to keep a project moving than to sweat every detail. Barish admits he makes mistakes. But most mistakes can be overcome, he says.

The ILC: How much?

That may be, but physicists say they must get the cost of the ILC right the first time. "We're being conservative, because we know it's better to have the cost come down than go up," says Peter Garbincius, a particle physicist at Fermilab and the GDE's lead cost engineer. "On the other hand, you can't start with too high a number and give [funding agencies] a chance to say no at the beginning." Some say they need more time, but Brian Foster, a particle physicist at Oxford University in the U.K., says, "The time is about right to start injecting a real element of price so people can begin the process of eliminating bells and whistles."

In December, the GDE adopted a baseline document for the collider, and researchers are fleshing it out in a more detailed reference design. A few key technical questions remain, but work now centers on production issues, such as how to manufacture the ILC's 16,000 cavities—and at what cost.

Above all, physicists vow not to repeat the mistakes made with the SSC. The cost of the SSC exploded in part because physicists did not design it for a specific site, and Waxahachie proved unexpectedly expensive, Barish says. Moreover, the original design pushed the technological limits, he says, and to ensure that the machine would work, researchers changed it in small but expensive ways. When estimating the cost of the ILC, physicists will consider specific "sample" sites, preferably close to existing labs, and will start with a conservative design, Barish says. "We're working much harder to capture all the costs in the beginning," he says. "The only design changes we can envision are likely to help, not hurt."

Ironically, if the GDE succeeds, the unity Barish has helped forge is likely to recede, as nations vie to host the machine and haggle over how much each will pay for it. That struggle would be fought at the highest levels of government, but it's at least a couple of years away. For the moment, particle physicists are working toward a common goal, guided by the sure hand of a quiet gent who can tell you a thing or two about building bridges.

–ADRIAN CHO

Tunnel visions. The ILC will lay bare the new physics on the horizon, researchers say.

CREDIT: SHIGEMI NUMAZAWA/ATLAS PHOTO BANK

Why the International Linear Collider?

Next year, physicists will start up the Large Hadron Collider (LHC) at the European particle physics laboratory CERN near Geneva, Switzerland. Most expect it to blast out the long-sought Higgs boson, the particle thought to give others their mass, and perhaps a slew of other finds. But only the International Linear Collider (ILC) could precisely measure the new particles' properties and chart the conceptual terrain, researchers say (*Science*, 21 February 2003, p. 1171). The LHC will collide protons, which consist of smaller particles called quarks and gluons, and produce immense sprays of particles. By smashing fundamental electrons and positrons, the ILC would produce much simpler collisions and give physicists far greater control over the energy and spin of the colliding bits of matter. **–A.C.**

Every
great idea
goes
through
an
evolution.

Introducing New Poly Bottles for Mallinckrodt® Solvents.

For over 130 years, Mallinckrodt Baker has delivered breakthrough solutions for chemists and researchers. Our latest is a high density polyethylene (HDPE) poly bottle for our Mallinckrodt brand ACS and histological grade solvents.

Our new poly bottles are designed to enhance laboratory safety while helping to reduce shipping and disposal costs compared to traditional glass containers. And with specifications that meet or exceed ACS and histology standards, our new reagent grade solvents in poly bottles are your best choice for quality and value.

So the next time your application calls for reagent grade solvents, remember Mallinckrodt Laboratory Chemicals.

For a copy of the latest Mallinckrodt Laboratory Chemicals catalog, visit www.mallbaker.com/sci

tyco / Specialty Products

Mallinckrodt® CHEMICALS

Mallinckrodt Baker

GENOMICS

The HapMap Gold Rush: Researchers Mine a Rich Deposit

Scientists are parsing a raft of new data on genetic variation for clues to disease and evolution

CAMBRIDGE, MASSACHUSETTS—For a conference on the next generation in genomics, the setting was just right: a pristine auditorium in a gleaming new building near the Massachusetts Institute of Technology (MIT). More than 200 people gathered here at the Broad Institute earlier this month to discuss the HapMap, a database cataloging human genetic variation. Begun in 2002, the map has been assembled primarily to boost the analysis of inheritance using pieces of DNA that are often transmitted as intact blocks.

Nearly complete, the HapMap is now being tested for a number of uses: to find genetic variants behind common diseases, to examine the genome's architecture, and to study natural selection. The human HapMap has even inspired the launch of a parallel effort for *Plasmodium falciparum*, the deadly malaria parasite.

Five countries kicked in about $138 million to fund the human project, properly known as the International HapMap Project. One early challenge was to allow for the fact that haplotypes differ somewhat across populations. To include a sweep of variants, the HapMap gathered DNA from 270 individuals of African, Japanese, Chinese, and European ancestry.

The final version, which will be completed this fall, is slated to include more than 4.5 million single-nucleotide polymorphisms (SNPs). Although the SNPs themselves aren't necessarily contributors to disease, they may travel alongside other SNPs that are. Most of the map is already freely available online (www.hapmap.org). And it is being used "a lot," says Francis Collins, director of the U.S. National Human Genome Research Institute (NHGRI) in Bethesda, Maryland, who is one of the map's biggest proponents. Collins says various National Institutes of Health institutes are being "flooded" with funding applications that involve using HapMap data.

Despite such enthusiasm, some researchers say they're not certain just how the HapMap will aid their own genetic studies. The map's central goal is to help identify genes behind common diseases such as cancer, but it's not always clear how to apply it. When it comes to evolution studies, for example, the map may be biased because it prefers common SNPs to rare ones. "The HapMap project was not about studying population history," says NHGRI's James Mullikin. But it's being used often by researchers in that area.

Deciphering disease. Aided by the HapMap, researchers are finding gene variants that may help explain diabetes and other conditions.

As for disease genes, "it's still a bit early" to expect new findings, says Aravinda Chakravarti of Johns Hopkins University in Baltimore, Maryland, one of the project's leaders. HapMap-related studies are just ramping up, however, and a few are hitting on new results. At the meeting, for example, a postdoc at the Broad Institute, Robert Graham, reported a gene variant linked to lupus that he's found while working in the Broad lab of David Altshuler, one of the HapMap's leaders.

John Todd of Cambridge University in the U.K. and postdoc Jason Cooper described a variant associated with type 1 diabetes, discovered by scanning more than 6500 SNPs in samples from thousands of type 1 diabetes patients and controls. With help from HapMap data, Todd's group homed in on a SNP on chromosome 2 that they believe may help drive diabetes, although they couldn't rule out effects from other SNPs nearby. The work appeared 14 May in the online edition of *Nature Genetics*.

Another test for the HapMap will come this fall when David Hafler, a multiple sclerosis (MS) researcher at Harvard Medical School in Boston and the Broad Institute, and colleagues worldwide plan to complete the initial phase of the first HapMap-guided whole genome scan for a human disease, MS. The outcome "will provide a map for what to study" in MS basic research, Hafler predicts.

The massive HapMap database is inspiring large collaborations as well as projects that take a big-picture look at the genome. Some search for changes in gene expression, inherited gaps in DNA, or patterns among so-called recombination hotspots, where matching chromosomes swap DNA more often than usual. Simon Myers, formerly a postdoc with statistician Peter Donnelly at Oxford University and now at the Broad Institute, examined more than 9000 hotspots found using the HapMap and a similar map by Perlegen Sciences Inc. in Mountain View, California.

Myers and his Oxford colleagues matched each of their hotspots to a nearby "coldspot" where DNA rarely recombines. They found two DNA motifs in particular that were common in hotspots. One seven-base sequence explained 10% of hotspots examined. The motif appeared to boost the chance of a hotspot in certain DNA stretches by up to five times.

Another group at the Broad Institute is examining data that were sequenced and publicly released by HapMappers but didn't make it into the final HapMap because they were deemed erroneous. "This project is kind of a dumpster dive," says the Broad Institute's Steven McCarroll. He and his colleagues found that thousands of the flaws are actually inherited DNA deletions. They've identified 10 commonly deleted genes, including two for sex steroid hormone metabolism and three for drug metabolism. They're now studying whether those deletions might contribute to disease.

Finally, in answer to the commonly asked question, "What now?" several groups are turning from humans to parasites. Dyann Wirth of Harvard School of Public Health in Boston is leading this latest haplotyping effort, which seeks to index genetic variation in *P. falciparum* by examining DNA samples collected from South and Central America, Asia, and Africa. So far, the group has identified 55,000 potential SNPs. Data like these, if they hold up, may help uncover new drug targets and explain drug resistance and the "functional effects of mutations," says Philip Awadalla of North Carolina State University in Raleigh, who's also studying *P. falciparum*'s gene variation.

–JENNIFER COUZIN

CREDIT: GETTY IMAGES

A local. Debris from a larger impact blasted open 210-meter Bonneville crater on Mars.

PLANETARY SCIENCE

Who Can Read the Martian Clock?

Researchers squabble over how to date martian geology by tallying impact craters. They're down for the count

HOUSTON, TEXAS—The concept sounds simple enough: To decipher the geologic history of other bodies in the solar system, count craters formed by the slow rain of bombarding rocks. The more craters on a lava flow, glacial debris, or a flood deposit, the farther back in time a volcano erupted, ice flowed, or water gushed. In practice, however, telling geologic time beyond Earth has proved tricky. For the earliest days of the solar system, researchers are even wrangling over the way the impacts took place (see sidebar, p. 1133).

At a "microsymposium"* here in March, about 125 planetary scientists deadlocked over how to apply crater-dating techniques to recent Mars history. There was "no real progress in terms of mutual understanding," laments Gerhard Neukum of the Free University Berlin in Germany.

For more than 30 years, Neukum has been building the case that the overwhelming majority of craters planetary scientists can see resulted from a steady, uniform rain of impactors from the asteroid belt. If you count craters carefully on the moon, where rocks brought back to Earth have been used to date impacts, then crater counts on Mars—or Mercury, or the asteroids—will produce good ages, he has argued. Lately, however, other scientists, both relative newcomers and old hands in the cratering business, have challenged that view. "Gerhard has a very fixed way of looking at things," says asteroid specialist Clark Chapman of the Southwest Research Institute (SwRI) in Boulder, Colorado. "I don't believe it."

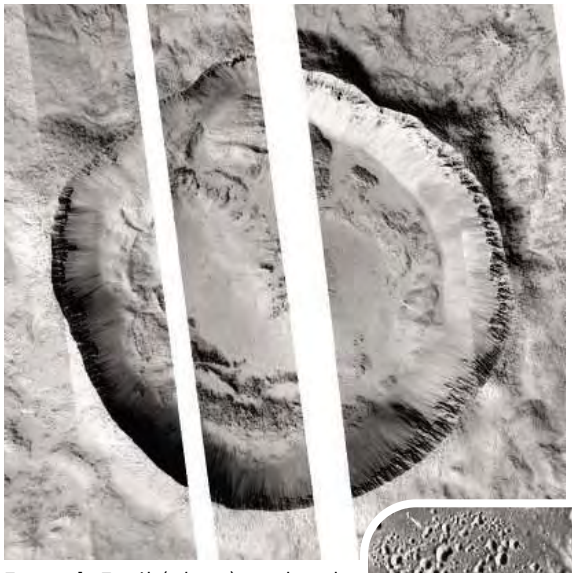

Fecund. Zunil (*above*) produced millions of secondary craters, like the moon's (*right*).

Chapman and some other American researchers argue that most of the smaller craters in Neukum's counts were created not by rocks from the asteroid belt but by impact debris falling back to Mars, and therefore have little to do with telling time. In that case, Neukum could be off by orders of magnitude in his ages of younger features such as icy flows and gullies, which speak of an active Mars in the geologic here and now.

"I really don't understand what is going on over there," responds Neukum, referring to his American critics. "It's absolutely stupid nonsense. Somewhere, they are making a terrible mistake."

Mother of millions

When meteoriticists noticed in the 1980s that a handful of meteorites in their collections had been blasted off Mars by impacts, researchers wondered how many more chunks of impact debris fall back on Mars and create craters. The more of these smaller, secondary craters scientists counted as asteroidal, the less accurate the crater-counting clock would be.

Planetary scientist Alfred McEwen of the University of Arizona in Tucson and eight colleagues reported last year in *Icarus* that at least one impact on Mars created a huge number of secondaries. They counted secondary craters created by the debris from the formation of a 10-kilometer-wide crater named Zunil. Secondary craters can be hard to distinguish from so-called primary craters made by rocks coming out of the asteroid belt. But Zunil's secondary craters are so young that erosion has yet to obliterate their distinctive blankets of debris thrown out when they formed. At the workshop, McEwen and his colleagues upped their earlier estimate of the number of Zunil's 10-meter-and-larger debris chunks from 10 million to 100 million.

Zunil "is just one little 10-kilometer crater," says McEwen. If other primary craters produce as many secondary craters, he says, then most craters 10 meters to a few hundred meters in diameter on Mars are secondaries. That is just the size range that crater counters must use to date small geologic features such as glacial deposits and very young features such as water-cut gullies. Neukum and his colleagues have dated glacial flows at 4 million years ago, a geologic yesterday, and lava flows at 5 million years.

"I give [Neukum] credit for doing the best job that can be done," McEwen says, but adds,

* Microsymposium 43, The Martian Time Scale: Craters, Meteorites, Processes, and Stratigraphy, 11–12 March, sponsored by Brown University and the Vernadsky Institute, Moscow.

CREDITS (TOP TO BOTTOM): NASA/JPL; A. MCEWEN, UNIVERSITY OF ARIZONA/NASA

"I'm really concerned. It's very hard to distinguish primaries and secondaries. Given a few million years, you'd never know which is which." Neukum is inevitably mistaking secondary craters for primaries both on the moon and on Mars, McEwen says. As a result, when Neukum sees a sparsely cratered feature, he thinks it's very young. In fact, it could be much older—as old as 100 million years, said McEwen. It may just not yet have been splattered by a large, infrequent primary crater.

Returning fire

Neukum disagrees. At the meeting, he and Stephanie Werner, a student of his who just received her Ph.D., argued that only a few percent of small craters result from secondary impacts. "So we don't care," said Neukum. "They are not important." Their evidence comes from the source of primary impactors, the asteroid belt. Neukum has counted craters on the 18-kilometer-long asteroid Gaspra, imaged by the Galileo spacecraft. "There are no secondaries on this body," he says. That's because Gaspra's feeble gravity can't pull impact ejecta back onto itself to form secondaries, Neukum notes. The craters pockmarking it must reflect the sizes of the rocks produced by eons of colliding asteroids. By Neukum's count, the number of Gaspra craters goes up sharply with decreasing crater size. For example, for every 1-kilometer crater on the asteroid, there are about 1000 100-meter craters.

Neukum and Werner see the same preponderance of small primary craters on the moon and on Mars. They've counted secondary craters from Zunil and those from "many Zunils" on the moon. Despite the differences in gravity, the results are the same as in the asteroid belt. "We had one kind of impactor cratering the inner solar system in the same way," says Neukum, down to 10-meter craters. Because the proportions of small and large craters stay the same as on Gaspra, he says, "the admixture of secondaries cannot be true." In addition, Neukum's cratering rates produce good matches between small-crater dating and sample-dating of young impacts on the moon. "It fits extremely well," he says. "It all fits."

Crater counter William Hartmann of the Planetary Science Institute in Tucson agrees that it fits—at least well enough. Hartmann, who co-authored the now-standard 2001 cratering chronology with Neukum, throws out the obvious secondaries—the ones clustered together—and counts the rest as a rough guide to the age of the youngest features. "I think things look reasonably good," he says.

Where other crater counters err, says Neukum, is in the geology. "Many people have not been very careful," he says. "Mars is [geologically] complicated. You find very few areas you can use in crater counting." Erosion may have erased some craters, or crater counters may have unwittingly included surfaces of two different ages. "You can get any kind of [crater size] distribution," he says.

Signs of secondaries?

At the symposium, some researchers begged to differ over the fine points of crater counting. Chapman and his SwRI colleague planetary dynamicist William Bottke reported on their new perspective on Gaspra. "One of Gerhard's biases is being conservative about recognizing something as a crater," says Chapman. "Gerhard doesn't see [craters] if they aren't sharp and fresh. We now believe the fresh craters have got to be an anomaly due to very recent cratering." Perhaps ejecta from an impact on a nearby asteroid hit Gaspra, Bottke suggests. In any case, the fresh craters are in fact secondaries of a sort, Chapman and Bottke say, contrary to Neukum's contention. The remaining craters represent the asteroidal source of Mars impactors, they say, and show no sign of Neukum's preponderance of small impactors.

Close-up images from the Mars rover Spirit also suggest that secondaries dominate small craters on Mars, too. Geologist Matthew Golombek of the Jet Propulsion Laboratory in Pasadena, California, a Spirit team member, reported on a survey of impact craters measuring from 10 centimeters to a couple of hundred meters across. Spirit found that they are all far shallower and less bowllike than primary craters tend to be. The high speed of impactors falling in from the asteroid belt makes for relatively deeper craters than those made by slower ejecta blocks of the same size. "Almost every crater you see looks like a secondary," said Golombek.

So who's right? McEwen, who is a co-investigator on the Lunar Reconnaissance Orbiter (LRO) camera team, proposed a test to find out. LRO could image the same areas of the moon as Apollo orbiters did at the same resolution and under the same lighting. If Neukum is right about small bits of asteroids being so abundant, LRO should find about 50 new craters formed during the 39 years since Apollo. If impact ejecta from rare large impacts form most small craters, as McEwen believes, LRO will find no new craters. LRO launches in October 2008.

–RICHARD A. KERR

Bombardment Looking "Possible"

Although researchers at the symposium deadlocked over Mars's recent cratering history (see main text), they may have made progress with a related question: how cratering took place during the planet's first billion years.

Since Apollo astronauts brought rocks back from the moon, planetary scientists have debated two diametrically opposite views of early cratering. One interpretation of lunar sample ages describes a "late heavy bombardment" 3900 million years ago, in which a swarm of debris with chunks ranging in size up to 100 kilometers across pummeled the moon and the rest of the inner solar system for a brief 80 million years. The other camp holds that cratering slowly declined after the formation of the solar system 800 million years earlier and that the battering recorded on the moon just marks the tail end of a drawn-out process.

At the symposium, cataclysm versus decline came in for considerable discussion. The cataclysm hypothesis "cannot be true. There is a flaw in the interpretation," declared cratering specialist Gerhard Neukum of the Free University Berlin. Geochronologist Donald Bogard of NASA's Johnson Space Center in Houston, Texas, then offered a compromise scenario: a much broader spike in cratering about 3900 million years ago, lasting a few hundred million years. "I admit it's a possibility," Neukum conceded, eliciting a ripple of applause.

A few days later, at March's Lunar and Planetary Conference in Houston, geochemist Dustin Trail of the University of Colorado, Boulder, and colleagues offered new support for a cataclysm in their analyses of six zircon grains over 4 billion years old from western Australia. Zircon is a highly durable mineral, but when severely heated, as by a large impact, it can form an enveloping overgrowth. Four of the six Australian grains had such rims, all dating to 3900 million years ago. None had rims older than that—evidence for a concentrated bombardment rather than a leisurely tapering off.

At the Planetary Chronology Workshop in Houston this week, planetary dynamicists William Bottke of Southwest Research Institute in Boulder and Alessandro Morbidelli of the Observatory of the Côte d'Azur in Nice, France, described their computer simulation in which the new planets sweep up or fling away the leftovers from planetary formation. In the model, the pool of available impactors shrinks too fast to produce all the craters recorded on the moon 3900 million years ago. If that was the case, the decline scenario "cannot work," Bottke says.

"I feel that I'm getting pushed toward a cataclysm by data," says geochronologist Timothy Swindle of the University of Arizona, Tucson. "The pause [in cratering] is there and then a spike that hangs around longer. I think we're getting there." **–R.A.K.**

No one understands your laboratory and research needs more than Sigma-Aldrich, because no one listens harder.

By appreciating your individual requirements, our customized approach delivers highly innovative solutions in order to ensure your expectations are always met.

Renowned for providing the highest levels of service and science, we also understand the need to control costs and maintain quality.

With a product line extending from the most frequently used solvents and reagents to the rarest chemical and biological specialties – you can count on us.

By listening to you, Sigma-Aldrich has changed. Why not hear how we can better meet your needs?

SIGMA-ALDRICH

www.sigma-aldrich.com/listening3

Unusual Paths

INVALUABLE ASSISTANT. Vincent Santana was a 19-year-old security guard in a New York City hospital when he saw an ad seeking an escort for Alzheimer's disease researchers doing interviews in dangerous neighborhoods. He got the job, and 15 years later he's still working with the same Columbia University–based team. But now he conducts the interviews himself.

He spent years gathering family histories and testing individuals in northern Manhattan whose relatives suffer from Alzheimer's disease. Now Santana (above, right) oversees an Alzheimer's epidemiology project of Dominican families, following roughly 600 of them in search of the genes behind the disease.

Santana praises his boss, Columbia's Richard Mayeux, for giving him "on-the-job training" in lab research and fieldwork. Since joining the Columbia team, Santana has picked up a bachelor's degree in finance and economics, and this month he will receive an MBA. "He's one of these kids who never stops learning," says Mayeux, who half-jokingly predicts that Santana will one day run a hospital.

That's not too far off from where Santana envisions himself. Among other things, he'd welcome becoming the administrator of "a major genetics department," melding his dual interests in business and science.

CREDITS (TOP TO BOTTOM): VINCENT SANTANA; M. ENSERINK/*SCIENCE*; FEATURE PHOTO SERVICE

POLITICAL SCIENCE

HERE TODAY ... The French scientific establishment raised a toast to the country's young talent last week with an event aimed at showcasing the promise of the next generation of scientists. But it also ended up raising a thorny question: Can France retain its most talented researchers?

The 339-year-old Academy of Sciences heard from six young biomedical scientists at the 16 May event, which was designed to show that, despite its current budget woes, French research can still excel. "It was an opportunity you couldn't pass up," says Jérôme Gros (below, left) of the Developmental Biology Institute of Marseille, who presented his work on muscular stem cells. But Gros may not be around long: He's off to apply for jobs at five U.S. universities. A second speaker, cellular microbiologist Emmanuel Boucrot (right), is already an expatriate: He left Marseille's Center for Immunology for a postdoc at Harvard Medical School in Boston last year.

But the event's organizer, Pasteur Institute microbiologist Pascale Cossart, is confident a number of recent initiatives—including France's National Research Agency (*Science*, 26 August 2005, p. 1316)—will help lure them back. "They are fantastic scientists, and there's a future for them in France," she says.

MONEY MATTERS

MUSIC FOR UCSF. When Ray Dolby says something sounds good, people listen. This month, the physicist who pioneered noise-reduction techniques and whose name is synonymous with stereo sound, gave the University of California, San Francisco (UCSF), $16 million to support the construction of a new stem cell research facility. Dolby's prodding also helped persuade UCSF officials to change the name of their center from the Institute for Stem Cell and Tissue Biology to the Institute for Regeneration Medicine, in order to make its mission clear. Officials briefly considered "regenerative" instead of "regeneration" in the institute's name. But, says Dolby, "to my ear, the word regenerative sounded too much like heavy machinery." The design for the institute's new building, which will bring under one roof 15 UCSF labs involved in stem cell research, is expected to be completed this summer.

This isn't Dolby's first gift to stem cell science: Last year, he gave $5 million to help create the administrative infrastructure for the California Institute for Regenerative Medicine, the state's $3 billion stem cell initiative.

Got a tip for this page? E-mail people@aaas.org

Rising Stars >>

TOP OF THE HEAP. Hannah Wolf (left) of Allentown, Pennsylvania, Madhavi Gavini (center) of Stakville, Mississippi, and Meredith MacGregor (right) of Boulder, Colorado, rose to the top in the 2006 Intel International Science and Engineering Fair, which drew 1500 high school contestants from 47 countries. Wolf won for her study of formations caused by ancient earthquakes in the Grand Staircase-Escalante National Monument; Gavini discovered a novel method to destroy a bacterium that causes secondary infections in patients with cancer, AIDS, and other conditions involving weakened immunity; and MacGregor earned the prize for her investigation of the Brazil nut effect: the phenomenon that makes the largest-sized particles in a container rise to the top when the container is shaken. Each of the three women will receive a $50,000 scholarship.

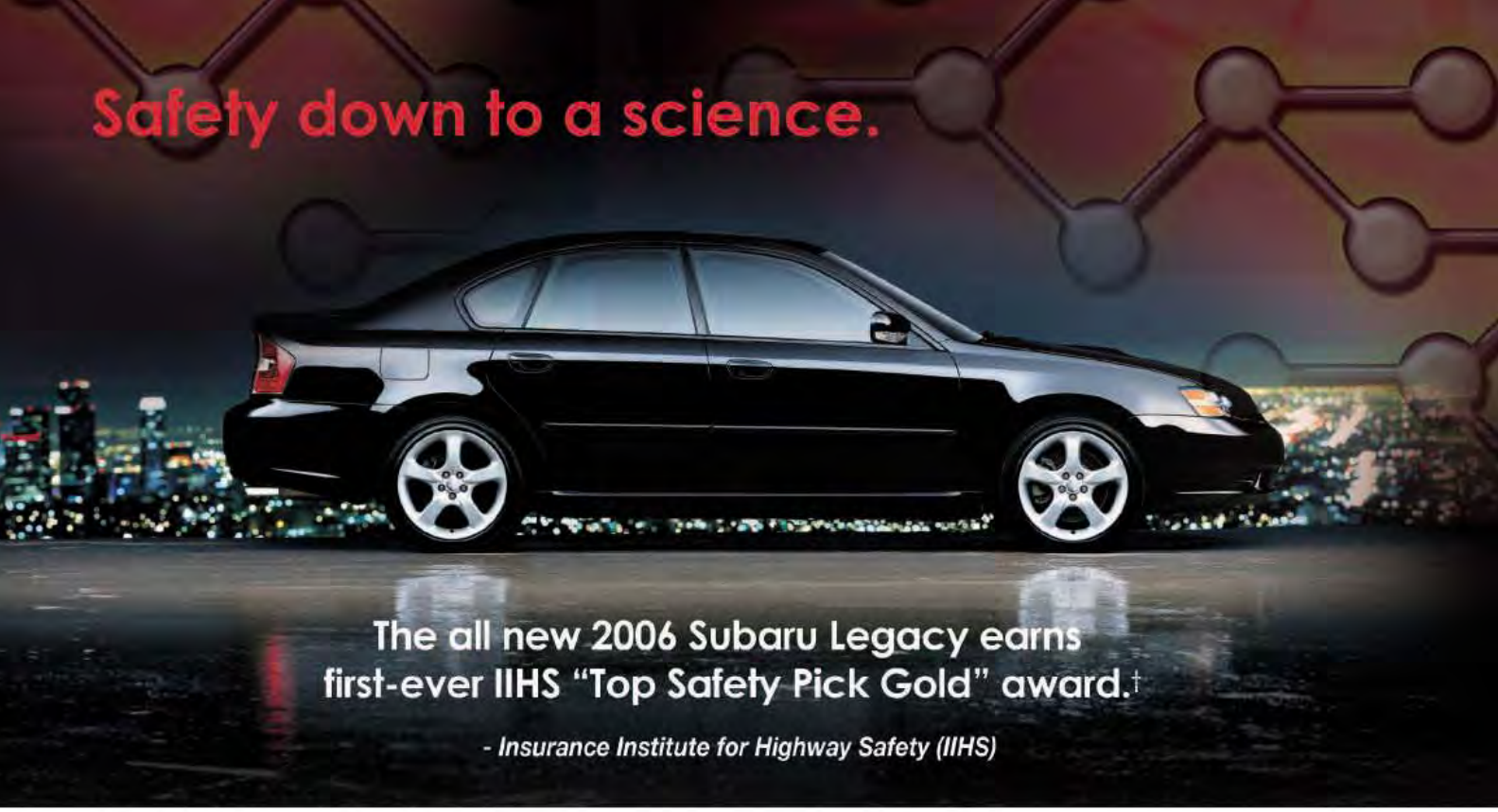

Subaru's sponsorship of the American Association for the Advancement of Science (AAAS) highlights our advanced design of symmetrical all-wheel drive technology to our target markets and underscores Subaru's commitment to further science, engineering and technology education both at the annual meeting and programs throughout the year. Subaru is proud to be the Premier Automotive Sponsor of the AAAS.

In a continuing effort to offer our partners unique and valuable benefits, we provide special offers for AAAS Members, the Subaru VIP Partners Program. AAAS Members can **save up to $3,000*** off the manufacturer's suggested retail price (depending on model and accessories) on the purchase or lease of a new Subaru from participating dealers. To qualify, you must be a AAAS member in good standing for at least six consecutive months prior to participation in this program. Please contact AAAS Member Services at 202.326.6417 or e-mail membership@aaas.org **BEFORE** visiting your local Subaru dealer. Access subaru.com to find a nearby dealer or learn more about Subaru vehicles.

Science
AAAS

Think. Feel. Drive.™

SUBARU

*From MSRP to dealer invoice. MSRP does not include tax, title, and registration fees. Limited time offer subject to change without notice. Terms and conditions apply. This offer replaces all other existing offers, cannot be redeemed for cash and is not applicable in Canada and Hawaii. † Based on Insurance Institute for Highway Safety 40 mph offset frontal crash test, 31 mph side impact test, and 20 mph rear impact test.

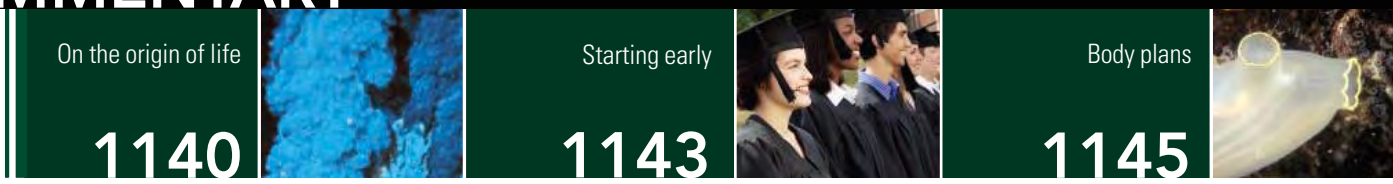

LETTERS

edited by Etta Kavanagh

Scientific Description Can Imperil Species

SCIENTISTS ARE RACING TO DISCOVER AND describe new species in the face of a global biodiversity crisis. Ironically, in cases of commercially valuable taxa, publishing new species descriptions may inadvertently facilitate their extinctions. These descriptions advertise "novelties" for hobbyists and drive new markets. Most modern descriptions provide detailed information on the locality and habitat where the new species occurs, turning a scientific article into a treasure map for commercial collectors. Researchers in fields with application to bioterrorism are debating codes of conduct to ensure that their findings do not fall into the wrong hands, the so-called "dual-use dilemma" (*1*). Taxonomists describing new species that have the potential to become commercially valuable are also faced with a dual-use dilemma.


A *Goniurosaurus luii* gecko

Three of us have published descriptions of new species of restricted-range reptiles and amphibians that tragically aided their commercial exploitation. Immediately after being described, the turtle *Chelodina mccordi* from the small Indonesian island of Roti (*2*) and the gecko *Goniurosaurus luii* from southeastern China (*3*) became recognized as rarities in the international pet trade, and prices in importing countries soared to highs of $1500 to $2000 each. They became so heavily hunted that today *C. mccordi* is nearly extinct in the wild (*4*) and *G. luii* is extirpated from its type locality (*3*). The salamander *Paramesotriton laoensis* from northern Laos was not known in the international pet trade prior to its recent description as a new species (*5*). Over the past year, Japanese (*6*, *7*) and German collectors used the published description to find these salamanders, and they are now being sold to hobbyists in those countries for $170 to $250 each. Similar cases are known from elsewhere in the world and from other taxa.

Withholding locality information from new species descriptions (*8*) might hamper profiteers, but it also hampers science and conservation. However, with the aid of the Internet, scientists can now monitor commercial demand for species just as commercial collectors can monitor scientific journals. This means prior information exists on which taxa will likely become commercial commodities (we should become concerned for any newly described species of *Chelodina* and *Goniurosaurus*). In such cases, taxonomists should work closely with relevant governmental agencies to coordinate publication of the description with legislation or management plans that thwart overexploitation of the new species. Of course, this will not always be easy or successful, and may lengthen publication time, but alternative solutions that allow taxonomists to continue their work without contributing to species decline are wanting.

BRYAN L. STUART,[1,2] ANDERS G. J. RHODIN,[3] L. LEE GRISMER,[4] TROY HANSEL[5]

[1]Department of Zoology, The Field Museum, 1400 South Lake Shore Drive, Chicago, IL 60605–2496, USA. [2]Department of Biological Sciences, University of Illinois at Chicago, 845 West Taylor Street, Chicago, IL 60607–7060, USA. [3]Chelonian Research Foundation, 168 Goodrich Street, Lunenburg, MA 01462, USA. [4]Department of Biology, La Sierra University, 4500 Riverwalk Parkway, Riverside, CA 92515, USA. [5]Wildlife Conservation Society, Post Office Box 6712, Vientiane, Lao People's Democratic Republic.

References

1. M. A. Somerville, R. M. Atlas, *Science* **307**, 1881 (2005).
2. A. G. J. Rhodin, *Breviora* **498**, 1 (1994).
3. L. L. Grismer, B. E. Viets, L. J. Boyle, *J. Herpetol*. **33**, 382 (1999).
4. C. R. Shepherd, B. Ibarrondo, "The trade of the Roti Island snake-necked turtle *Chelodina mccordi*" (TRAFFIC Southeast Asia, Selangor, Malaysia, 2005).
5. B. L. Stuart, T. J. Papenfuss, *J. Herpetol*. **36**, 145 (2002).
6. H. Masumitsu, *Daily Yomiuri*, 24 Apr. 2006, p. 3.
7. K. Chang, *N.Y. Times*, 25 Apr. 2006, p. D1.
8. For an example, see G. Nilson, C. Andrén, B. Flärdh, *Amphibia-Reptilia* **11**, 285 (1990).

Tropical Deforestation and Global Warming

THE NEWS FOCUS ITEM "ALONG THE ROAD FROM Kyoto" (E. Kintisch, 24 Mar., p. 1702) dramatically reveals the contrasts among countries in their impact on global warming and correctly identifies countries such as the United States as the greatest emitters of carbon. However, the news report fails to mention that the numbers used in its graphs of "total emissions" and "global emissions" refer only to fossil-fuel combustion and cement manufacture (*1*)—they do not include deforestation. The bar representing 2002 emissions from Brazil would be about five times longer if Amazonian deforestation at the 2002 annual rate of 23.3×10^3 km^2 were included (*2*, *3*). Recognizing the substantial contribution of tropical deforestation is important if action is to be taken to reduce the rate of forest loss through measures that could be financed on the basis of the climatic benefits of keeping forests standing (*4*).

PHILIP M. FEARNSIDE

Department of Ecology, INPA, C.P. 478, Manaus, Amazonas 69011-970, Brazil. E-mail: pmfearn@inpa.gov.br

References

1. World Resources Institute (WRI), CAIT, the Climate Analysis Indicators Tool, http://cait.wri.org/ (2006).
2. P. M. Fearnside, *Clim. Change* **46**, 115 (2000).
3. P. M. Fearnside, W. F. Laurance, *Ecol. Applic.* **14**, 982 (2004).
4. P. M. Fearnside, in *Emerging Threats to Tropical Forests*, W. F. Laurance, C. A. Peres, Eds. (Univ. of Chicago Press, Chicago, Il, in press).

Concern About Gag Rules

WITH REGARD TO DONALD KENNEDY'S EDITORial "The new gag rules" (17 Feb., p. 917), the National Oceanic and Atmospheric Administration's (NOAA) Science Advisory Board

(SAB) is deeply concerned about reports of attempts to suppress and/or distort the reporting or representation of scientific findings by federal agency scientists. However, the SAB is also concerned about misrepresentations of NOAA actions, particularly when the agency has been scientifically proactive.

At a public meeting of the SAB in March 2005, NOAA Administrator C. C. Lautenbacher Jr. requested that the SAB create an external Hurricane Intensity Research Working Group (HIRWG). He requested that the group be charged with assessing the status of NOAA's hurricane intensity forecasting and making recommendations on ways to improve operational forecasting. Through a public, open nomination process, the SAB created the HIRWG, consisting of 12 U.S. hurricane experts. The HIRWG presented its preliminary findings and recommendations to the SAB on 7 March 2006.

Thus, NOAA requested this external study of the agency's hurricane intensity modeling and forecasting, including the relationships of intensity and intensity change to sea surface temperatures and ocean-atmospheric exchange, several months before hurricanes Katrina and Rita appeared in September 2005. The timing of the request also was well in advance of the publication of the manuscripts to which your Editorial alludes. NOAA and its SAB await the rollout of the final report. Thank you for your continued vigilance.

LEN PIETRAFESA

Department of Marine, Earth, and Atmospheric Sciences, College of Physical and Mathematical Sciences, North Carolina State University, Raleigh, NC 27695, USA, and Chair, NOAA Science Advisory Board.

Working Together for Communication

DONALD KENNEDY'S EDITORIAL "THE NEW GAG rules" (17 Feb., p. 917) was quite disturbing. I was offended, not by the unfounded allegations of conspiracy at the National Aeronautics and Space Administration (NASA), but by the Editorial's reckless disregard for the truth.

The *New York Times* article (*1*) upon which the Editorial is based contains no references whatsoever to any personal involvement by me in any sort of conspiracy or political influence. Is Kennedy's citing of these nonexistent allegations a deliberate fabrication of "facts" to fit his editorial position—or is it just shoddy journalism?

I know scientists often feel they are eloquent writers and expert communicators, but often they are not. Nor are public affairs officers always experts in science. This is why public affairs officers and scientists must work together in explaining their work in a way that laymen can understand. That is the best way to communicate their incredible science discoveries to the public.

DEAN ACOSTA

National Aeronautics and Space Administration, Office of Public Affairs, Washington, DC 20546, USA.

Reference

1. A. C. Revkin, "Climate expert says NASA tried to silence him," *N.Y. Times*, 29 Jan. 2006, p. 1.

Response

ACOSTA OFFERS NOT A SINGLE INSTANCE OF misrepresentation, fabrication, inaccuracy, or shoddy journalism in my Editorial. Readers can check the *New York Times* article we both cited to see whether I misrepresented it. His letter is short on facts but rich in rhetoric, presumably to support his central point: that public affairs types need to collaborate with scientists because the latter can't write well.

DONALD KENNEDY

Revisiting the Age of the Sahara Desert

IN THEIR BREVIA "THE AGE OF THE SAHARA Desert" (10 Feb., p. 821), M. Schuster *et al.* state that the oldest terrestrial records for desert conditions in the Sahara are only 86 thousand years old (ka). This is not correct. For example, U/Th dating from the Eastern Sahara gives dates of >300 ka (*1*). The lack of older geochronological data can be explained by the extreme eolian and fluvial erosion during the many arid-humid cycles, which lasted about 100,000 years each and which have deleted most of the sediments deposited during the preceding cycle. A wealth of paleoclimatic, geomorphological, archaeological, astronomical, and other evidence and reasoning suggests that the origin of the Sahara desert is closely linked to the Quaternary Ice Age, which began about 2.5 million years ago (Ma).

Dunes have existed in subtropical Africa since plate tectonics drifted it to its present latitudinal position. A 7-Ma dune complex (according to biostratigraphic correlation) at 16°N (which is not even in the Sahara but in the sahelian transition zone at its southern fringe) is therefore not a serious base for postulating such an early age, which contradicts decades of field research in the Sahara. At best, it shows an arid or semi-arid period, which may not at all have persisted over 7 Ma.

STEFAN KROEPELIN

University of Cologne, Collaborative Research Centre 389 (ACACIA), Forschungsstelle Afrika, Jennerstrasse 8, 50823 Cologne, Germany. E-mail: s.kroe@uni-koeln.de

Reference

1. B. J. Szabo *et al.*, *Science* **243**, 1053 (1989).

IN THEIR BREVIA "THE AGE OF THE SAHARA Desert" (10 Feb., p. 821), M. Schuster *et al.* interpret Upper Miocene sandstones in Chad as eolian dune deposits, they claim that these sandstones provide the earliest in situ record for arid climates and eolian sand accumulation in the Sahara, and they claim that this interpretation indicates that desert conditions started in the Sahara at least 7 million years ago. There are several concerns about these claims:

1) The photographs and descriptions provided by Schuster *et al.* are not sufficient for a reader to evaluate the interpretation of an eolian origin for the sandstones. Detailed photographs of grainfall deposits and ripple strata would provide more convincing evidence for the interpretation (*1*, *2*).

2) The Upper Eocene Hadida Formation in southern Morocco is the oldest Cenozoic stratigraphic interval in the Sahara that has been given an eolian interpretation (*3*).

3) Most Miocene strata in the Sahara consist of sandstones with cross-bedding that have been interpreted as fluvial deposits that accumulated under humid climate conditions. Specifically in Chad, previous studies suggest that the climate during most of the Miocene was relatively humid and that the first appearance of persistent and widespread arid conditions occurred during the Pliocene (*4*–*6*).

4) Data from marine cores off the west coast of Africa suggest that persistent and widespread desert conditions first appeared in the Sahara during the Early Pliocene (*7*, *8*).

In addition, there are errors in the Brevia. The oldest thermoluminescence date reported from an eolian sandstone in Tunisia of >86 thousand years ago (ka) (*9*, *10*) may not be "the oldest terrestrial record for desert conditions in the Sahara." Several claims of pre-Quaternary eolian strata need to be examined more closely, including the Upper Eocene Hadida Formation of southern Morocco (*3*) and the Pliocene-Pleistocene Garet Uedda Formation of northern Libya (*11*, *12*).

Contrary to the claim that Callot provided "firm evidence … for a pre-Quaternary Great Western Sand Sea in Algeria," a closer reading

CREDIT: CORBIS

shows that Callot postulated that the age of the Great Western Sand Sea is pre-Holocene and that the Sand Sea was probably initiated during the late Neogene and (or) early Quaternary (*13*). The age that Callot postulated is based on observations of sand grain sizes, eolian dune geomorphology, and stratigraphic relations with a "hamada" surface.

CHRISTOPHER S. SWEZEY

U.S. Geological Survey, 12201 Sunrise Valley Drive, MS 956, Reston, VA 20192, USA. E-mail: cswezey@usgs.gov

References

1. R. E. Hunter, *Sedimentology* **24**, 361 (1977).
2. C. Swezey, *C.R. Acad. Sci. (Sér. IIa)* **327**, 513 (1998).
3. A. El Harfi *et al.*, *Int. J. Earth Sci.* **90**, 393 (2001).
4. Y. Coppens, J.-C. Koeniguer, *Bull. Soc. Géol. Fr. (Sér. 7)* **18**, 1009 (1976).
5. S. Servant-Vildary, *Trav. Doc. ORSTOM (Off. Rech. Sci. Tech. Outre-Mer)* **84** (Tome I), 346 (1978).
6. M. Servant, *Trav. Doc. ORSTOM (Off. Rech. Sci. Tech. Outre-Mer)* **159**, 573 (1983).
7. W. F. Ruddiman *et al.*, *Proc. Ocean Drilling Program Sci. Results* **108**, 463 (1989).
8. P. B. deMenocal, *Science* **270**, 53 (1995).
9. C. Swezey, *Science* **286**, 243 (1999).
10. C. Swezey *et al.*, *Holocene* **9**, 141 (1999).
11. F. Di Cesare *et al.*, *Rev. Inst. Fr. Pétrole* **18**, 1344 (1963).
12. E. Tawadros, *Geology of Egypt and Libya* (A. A. Balkema, Rotterdam, Netherlands, 2001).
13. Y. Callot, *Bull. Soc. Géol. Fr. (Sér. 8)* **4**, 1073 (1988).

Response

THE BOUNDARIES OF THE SAHARA, BASED ON an isohyet distribution and not on latitude, have changed with time (*1*). Our study area (Toros-Menalla) is located in the "Erg du Djourab" (i.e., Djurab sand-sea), which is clearly part of the Sahara.

It is easy to postulate, as Kroepelin does, that ancient sediments were deposited and then eroded, but that is not a satisfying answer. The "paleoclimatic, geomorphological, archaeological, astronomical, and other evidence" he mentions has systematically failed to precisely date processes older than a few 100,000 years. The U/Th dating mentioned in the comment has been performed on carbonates, deposited during "humid climates." However, paleontological discoveries over the past 10 years in the Chad Basin [e.g., (*2*–*5*)] show that a pre-Quaternary succession (upper Miocene and Pliocene deposits) can be well preserved in the Sahara. Some of these deposits are eolian in origin, with a minimum preserved area of 1000 km^2. Our data clearly show that a sand sea existed at 16°N as long ago as 7 million years ago (Ma). It was made clear in our Brevia that arid desert conditions have not persisted since 7 Ma but existed repetitively.

It was beyond the scope of our Brevia to discuss sedimentary interpretations based on photographs. We are preparing a paper that will properly illustrate depositional facies and successions, including "ripple strata and grain fall deposits." However, the interpretation of an old eolian deposit is much more than the occurrence of such primary sedimentary structures. For example, in the Chadian eolian deposit, the similarity of Miocene and modern wind orientations, perpendicular to regional paleoslope, is also convincing evidence.

The Upper Eocene Hadida Formation in Southern Morocco (*6*) comprises deposits interpreted as eolian in origin (there were no photographs in this paper). However, these deposits are of very limited spatial and temporal extent. In addition, they are intercalated between coastal sebkha deposits and alluvial-fan sediments and therefore represent coastal eolian sand dunes. Such coastal eolian sedimentation cannot be used to ascertain the start of desert conditions in the Sahara (many examples are developed along the Atlantic French coast to the Dutch and German North Sea area).

Dating of the sedimentary succession based on the discovery of abundant Pliocene and Miocene vertebrate faunas is now available (*3*–*5*) and replaces less reliable age attributions. Dealing with facies interpretations, cross-bedding is not sufficient to identify fluvial deposition, and we consider that some of the cross-bedded units can be re-interpreted in eolian sediments (see our Brevia). Recent research (1995–2006) in the Chad Basin has greatly challenged the pioneering works used by Swezey, which were done in the 1970s. Marine cores off the west coast of Africa can produce proxies for the onset of arid conditions in the Western Sahara but cannot be used if dealing with the Central Sahara. As the latter area is known to be more arid than the former, the onset of desert conditions may have been earlier in the Chad Basin, and Miocene sand seas would thus be not surprising.

About Callot's work (*7*), whatever the late Neogene or early Quaternary age of the former Western Great Sand sea, it clearly reported the oldest eolian deposits known in the Sahara, until the discovery of the Miocene Chadian eolian sediments. We simply wrote pre-Quaternary as Hamada deposits are generally regarded as Neogene, even if later pedogenetic processes are probably post-Quaternary [(e.g., (*8*)].

MATHIEU SCHUSTER,[1,2]* PHILIPPE DURINGER,[2] JEAN-FRANÇOIS GHIENNE,[2] PATRICK VIGNAUD,[3] HASSAN TAISSO MACKAYE,[4] ANDOSSA LIKIUS,[4] MICHEL BRUNET[3]

[1]Université Bretagne Occidentale, Institut Universitaire Européen de la Mer, Domaines Océaniques CNRS Unité Mixte de Recherche (UMR) 6538, 1 place Nicolas Copernic, 29870 Plouzané, France. [2]Université Louis Pasteur, Ecole et Observatoire de Sciences de la Terre, Centre de Géochimie de la Surface CNRS UMR 7517, 67084 Strasbourg, France. [3]Université de Poitiers, Laboratoire de Géobiologie, Biochronologie et Paléontologie Humaine CNRS UMR 6046, 86022 Poitiers, France. [4]Département de Paléontologie, Université de N'Djaména, BP 1117, N'Djaména, Chad.

*To whom correspondence should be addressed. E-mail: mathieumailbox@gmail.com

References

1. P. Rognon, *C. R. Acad. Sci.* **323**, 549 (1996).
2. M. Brunet *et al.*, *Nature* **378**, 273 (1995).
3. M. Brunet *et al.*, *J. Vertebr. Paleontol.* **20**, 199 (2000).
4. M. Brunet *et al.*, *Nature* **418**, 145 (2002).
5. P. Vignaud *et al.*, *Nature* **418**, 152 (2002).
6. A. El Harfi *et al.*, *Int. J. Earth Sci.* **90**, 393 (2001).
7. Y. Callot, *Bull. Soc. Géol. Fr.* **8**, 1073 (1988).
8. M. Thiry, M. Ben Brahim, *Geodin. Acta* **10**, 12 (1997).

TECHNICAL COMMENT ABSTRACTS

Comment on "Heterogeneous Hadean Hafnium: Evidence of Continental Crust at 4.4 to 4.5 Ga"

John W. Valley, Aaron J. Cavosie, Bin Fu, William H. Peck, Simon A. Wilde

Harrison *et al*. (Reports, 23 December 2005, p. 1947) proposed that plate tectonics and granites existed 4.5 billion years ago (Ga), within 70 million years of Earth's formation, based on geochemistry of >4.0 Ga detrital zircons from Australia. We highlight the large uncertainties of this claim and make the more moderate proposal that some crust formed by 4.4 Ga and oceans formed by 4.2 Ga.

Full text at www.sciencemag.org/cgi/content/full/312/5777/1139a

Response to Comment on "Heterogeneous Hadean Hafnium: Evidence of Continental Crust at 4.4 to 4.5 Ga"

T. M. Harrison, J. Blichert-Toft, W. Müller, F. Albarede, P. Holden, S. J. Mojzsis

Valley *et al*. review the lines of evidence on which we drew to conclude that continental crust formed much earlier than previously thought. Their comment contains some misrepresentations that we correct, but new information they provide appears to bolster our hypothesis. Nothing in their comment refutes the presence of continental crust or plate boundary processes prior to 4 billion years ago.

Full text at www.sciencemag.org/cgi/content/full/312/5777/1139b

Letters to the Editor

Letters (~300 words) discuss material published in *Science* in the previous 6 months or issues of general interest. They can be submitted through the Web (www.submit2science.org) or by regular mail (1200 New York Ave., NW, Washington, DC 20005, USA). Letters are not acknowledged upon receipt, nor are authors generally consulted before publication. Whether published in full or in part, letters are subject to editing for clarity and space.

ORIGIN OF LIFE

Search for Life's Beginnings

Iris Fry

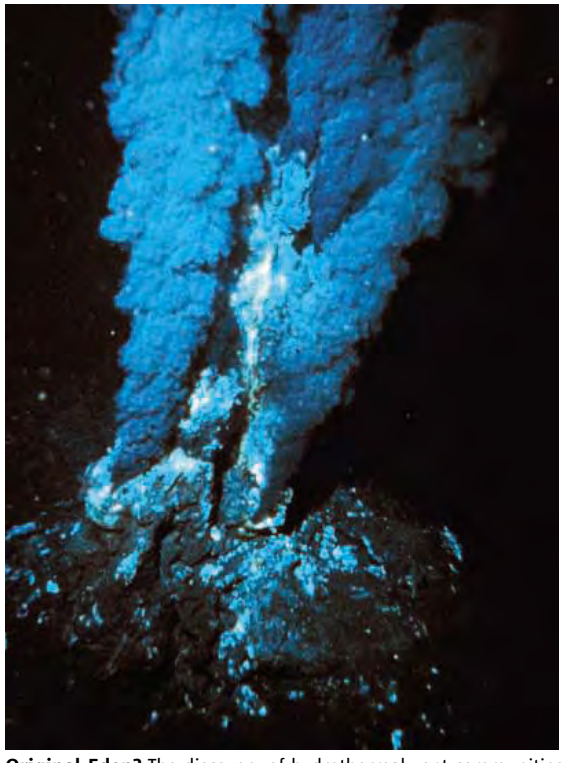

Original Eden? The discovery of hydrothermal vent communities led to the proposal that hydrothermal systems provided a site for the rapid emergence of life through a sequence of abiotic syntheses.

The scientific field devoted to the origin of life on Earth is very young, having taken its first experimental steps in the 1950s. Though the question has captivated human imagination since the dawn of history, its scientific pursuit has depended on several crucial conceptual developments during the 20th century. First, the emergence of life had to be conceived of as an integral part of the general process of evolution, leading from the geochemistry of the barren Earth to the universal common ancestor, which later diversified into the Darwinian tree of life. Following the rise of molecular biology in the 1950s and 1960s, the origin-of-life question could be formulated in biochemical and genetic terms, making it a subject of experimental investigation.

Early on, most scientists engaged in this research were chemists who attempted to formulate plausible scenarios for the prebiotic synthesis of organic building blocks, biologically relevant polymers, and the first metabolically or genetically functional chemical structures. In the late 1970s, however, geologists also became increasingly involved in the field. Their participation was associated with the rise of a new paradigm positing that the synthesis of organic building blocks and the emergence of life itself took place not in the "primordial soup" of the traditional hypotheses but in the vicinity of undersea hydrothermal vents, at high temperature and under extreme pressure. Supporters of this new conception claim that origin-of-life theories can now be subjected to more rigorous constraints posed by specific primordial physical settings (*1*). On the other hand, the "soup people"—in particular, Stanley Miller, renowned pioneer of the 1953 prebiotic simulation experiments, and his colleagues—reject the alternative paradigm as empirically untenable (*2*).

Genesis
The Scientific Quest for Life's Origin
by Robert M. Hazen
Joseph Henry Press, Washington, DC, 2005. 359 pp. $27.95, C$37.95. ISBN 0-309-09432-1.

In *Genesis*, Robert Hazen tells the story of these debates over the origin of life. There is no one better suited to examine recent developments in the experimental study of the topic. Trained in mineralogy and crystallography, he has been personally involved in the major lines of research through which Earth scientists have come to shape the field. Describing these contributions, he vividly portrays numerous experiments and observations. Hazen's academic home, the Geophysical Laboratory at the Carnegie Institution of Washington, which specializes in investigations of chemical reactions under extreme conditions, serves as an ideal setting for his experiments on the effects of high pressure and temperature on organic synthesis and particularly on the possible role of minerals abundant in hydrothermal vents in such synthesis. Describing the scientific status of this lab, its remarkable members, and their close professional and personal relationships, Hazen weaves the scientific and the personal into an engaging, sometimes dramatic tale. He highlights the excitement involved in research, the many setbacks and disappointments, and the inevitable internal politics within the origin-of-life community. In addition, his research team's membership in the NASA Astrobiology Institute allows him to comment on the role of geologists in the study of possible conditions for life on Mars and other extraterrestrial sites within the context of the new "deep-origin" paradigm.

An underlying theme of the book is Hazen's conception of the origin of life as part of a wider "theory of emergence" (*3*), a perspective based mainly on the ideas of theoretical biologist Harold Morowitz, a colleague of Hazen's at George Mason University. According to this ambitious theory, the growth of organization and complexity in physical, chemical, biological, and social systems follows a general, though as-yet-unknown, principle on a par with the universal laws of nature. Considering the origin of life as a quintessential process of emergence, Hazen suggests that uncovering "the missing law" should advance origin-of-life research. However, although various complex systems do share common features, the "new science of emergence" is in danger of downplaying the unique features of living systems as well as the distinction between physical and chemical selection on the one hand and natural selection on the other. Moreover, as Hazen acknowledges, the basic concepts underlying this grand scheme (e.g., complexity) are far from clear. Since the origin-of-life field itself lacks firm, unequivocal conclusions, it is doubtful whether such additional conceptual baggage offers much scientific value.

Among the many issues dividing the origin-of-life community, none is more crucial than the controversy between "RNA-first" and "metabolism-first" scenarios. This division stems from the difficulty of deciding which emerged earlier, genetic polymers or metabolic cycles. Because nucleic acids and protein enzymes are tightly interdependent in extant living cells, an adequate theory must establish how either could have originally functioned on its own. After describing the rival positions even-handedly, noting the pros and cons of both, Hazen commendably feels that he has to place his bets on the table. He comes down on the side of metabolism-first, probably in the form of a molecular layer on a surface of a rock. Interestingly, he bases his choice on the "theory of emergence" and the hypothesis that life emerged through stages of increasing complexity. But wouldn't a primitive genetic system, made of RNA or a simpler genetic polymer, also have to emerge through such stages?

The chemical requirements for the establishment of a self-replicating genetic system under prebiotic conditions are clearly extremely complex. Nonetheless, the support for the RNA-first notion, despite its difficulties, reflects the double realization that the emergence of life's com-

The reviewer is at the Cohn Institute for the History and Philosophy of Science and Ideas, Tel Aviv University, and the Department of Humanities and Arts, Technion–Israel Institute of Technology, Haifa 32000, Israel. E-mail: iris.fry@gmail.com

CREDIT: P. RONA/OAR/NATIONAL UNDERSEA RESEARCH PROGRAM (NURP); NOAA

plex organization depended on the formation of a reproducing, mutating, and evolving system and that a population of RNA molecules (perhaps enclosed within a membrane) could fulfill these conditions.

Compared to the requirements of a self-replicating genetic system, the prebiotic synthesis of organic molecules (such as amino acids, other carboxylic acids, and their polymers) that could have participated in primitive metabolism seems much simpler. Furthermore, empirical evidence lends support to several reactions involved in one of the field's most elaborate metabolic scenarios, that suggested by Günter Wächtershäuser (*4*). However, it is still not clear whether a metabolic cycle could spontaneously self-organize so as to reproduce itself, mutate, and evolve (*5*). Perhaps throughout the book Hazen should have more vigorously stressed that the origin of life had to involve the emergence of an infrastructure for the further evolution of a living system. No doubt, though, the author's empirical work—which he describes clearly and in detail—is aimed in this direction. With his Carnegie Institution colleagues, he has performed a series of experiments to explore whether the reverse citric acid cycle (proposed to have been the original metabolic system) could have self-replicated under specified geophysical conditions. As in so many other cases in the origin-of-life field, a final answer still awaits decisive experimental demonstration.

This informative and captivating book unfortunately includes some inaccuracies related to the history of ideas in the field. Most notably, vitalism and the belief in spontaneous generation did not, as Hazen suggests, necessarily overlap. Both the Greek atomists and the French materialists supported spontaneous generation as part of their anti-vitalistic systems; Pasteur saw in his refutation of spontaneous generation evidence that matter could not organize itself to form life.

The scientific study of the emergence of life is now under heavy attack by proponents of intelligent design, the latest representatives of the creationist movement. *Genesis*, written from the careful yet self-confident perspective of an experimentalist, serves as a solid rebuttal to such assaults. Candidly acknowledging that we have not yet reached a solution, Hazen convincingly demonstrates how he and his many colleagues are focused on obtaining a deeper understanding of a most fundamental problem.

References

1. N. R. Pace, *Cell* **65**, 531 (1991).
2. J. L. Bada, S. L. Miller, M. Zhao, *Origins Life Evol. Biosph.* **24**, 364 (1994).
3. H. J. Morowitz, *The Emergence of Everything: How the World Became Complex* (Oxford Univ. Press, Oxford, 2002).
4. C. W. Huber, S. Eisenreich, S. Hecht, G. Wächtershäuser, *Science* **301**, 938 (2003).
5. L. E. Orgel, *Proc. Natl. Acad. Sci. U.S.A.* **97**, 12503 (2000).

10.1126/science.1127301

BROWSINGS

The Box. How the Shipping Container Made the World Smaller and the World Economy Bigger. Marc Levinson. Princeton University Press, Princeton, NJ, 2006. 390 pp. $24.95. ISBN 0-691-12324-1.

Box Boats. How Container Ships Changed the World. Brian J. Cudahy. Fordham University Press, New York, 2006. 370 pp. $29.95. ISBN 0-8232-2568-2.

In late April 1956, a modified World War II tanker left the port of Newark, New Jersey, for Houston with 58 truck trailer bodies lashed above its deck. Fifty years on, the world's largest container ship—*MSC Pamela* (photographed during its inaugural call at Felixstowe, Britain)—can carry more than 4000 40-foot boxes, and Malcom McLean's innovation plays a crucial role in world trade. Business practices, government intervention, and opposition from longshoremen's unions impeded the adoption of containers, and Levinson describes the changes that led to the eclipse of traditional ports such as New York and the transformation of shipping. An economist, he argues that by slashing transport costs containerization helped manufacturers shift production around the world and increased the integration of the global economy. Cudahy, a maritime historian, charts the growth of McLean's line into Sea-Land Service and its successors while also sketching the evolution of other major container lines. His book is filled with details about these shipping firms and their vessels.

CREDIT: COURTESY PORT OF FELIXSTOWE

The Commercial and Political Atlas and Statistical Breviary. William Playfair. Edited and introduced by Howard Wainer and Ian Spence. Cambridge University Press, Cambridge, 2005. 162 pp. $39.99, £25. ISBN 0-521-85554-3.

Computer software has helped make the visual display of quantitative data a nearly universal feature of science, business, government, and the media. A surprising number of graphical constructions commonly used today—including time series line charts, bar graphs, and pie diagrams—were introduced in the late 18th century by William Playfair, who used annotated graphs of England's trade and national debt to present his economic and political arguments. This volume offers facsimiles of two of Playfair's most important books: the third (1801) edition of *The Commercial and Political Atlas* and the *Statistical Breviary* (also 1801). The editors provide a short account of Playfair's life and times. They also summarize his conceptual breakthroughs and discuss "some of the difficulties, idiosyncrasies, and infelicities" of his work. Playfair's approach was not accepted by his contemporaries, whose skepticism about the accuracy of graphical representation was reinforced by errors in his work, his outspoken opinions, and his disreputable reputation. But as the editors note, Playfair (again ahead of his times) seems to have recognized perceptual and cognitive aspects of his charts. He claimed two advantages for such graphical representation: "to facilitate the attainment of information, and aid the memory in retaining it."

CAREER CHOICE

Planning Early for Careers in Science

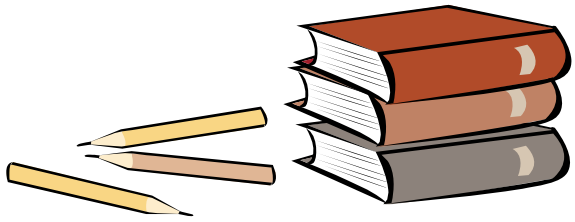

Robert H. Tai,* Christine Qi Liu, Adam V. Maltese, Xitao Fan

Young adolescents who expected to have a career in science were more likely to graduate from college with a science degree, emphasizing the importance of early encouragement.

Concern about U.S. leadership in science has captured the national spotlight once again (*1*). The physical sciences and engineering are at particular risk, with declines in the number of earned doctorates in these fields among U.S. citizens and permanent residents in the past decade (*2*) (figs. S1 to S3). Recommendations for improvement focus on education, particularly in improving the number of teachers and the quality of teacher training for primary and secondary schools (*1*). This is an attractive but expensive approach.

Enhanced online at www.sciencemag.org/cgi/content/full/312/5777/1143

How important is it to encourage interest in science early in children's lives? How early in their lives do students decide to pursue a science-related career? We used nationally representative longitudinal data to investigate whether science-related career expectations of early adolescent students predicted the concentrations of their baccalaureate degrees earned years later. Specifically, we asked whether eighth-grade students (approximately age 13) who reported that they expected to enter a science-related career by age 30 obtained baccalaureate degrees in science-related fields at higher rates than students who did not have this expectation. We analyzed students in the United States for years 1988 through 2000 and controlled for differences in academic achievement, academic characteristics, and students' and parents' demographics.

Survey and Analysis

We used the *National Education Longitudinal Study of 1988* (*NELS:88*) for this study. Designed and conducted by the National Center for Educational Statistics (NCES), *NELS:88* began in 1988 with a survey of 24,599 eighth graders. Researchers conducted additional surveys in 1990, 1992, 1994, and 2000. The overall sample size after five surveys was 12,144 participants. Our analysis focused on those students who responded to the question about their age 30 career expectation as eighth graders in 1988 and who also obtained baccalaureate degrees from 4-year colleges or universities by 2000. This reduced the sample to 3,743 participants. The sample was further reduced to a final size of 3,359 participants, because 384 participants were missing data in one or more of the variables used in the analysis.

MULTINOMIAL LOGISTIC REGRESSION ANALYSIS

Independent variable		Coefficients of nested models				
		Baseline	2	3	4	Final
Career expectation	Life sci.	0.6 (0.2)	0.7 (0.2)	0.7 (0.2)	0.6 (0.2)	0.7 (0.2)
	Phy. sci. /engr.	1.7 (0.2)	1.4 (0.2)	1.2 (0.2)	1.2 (0.2)	1.2 (0.2)
Covariate groups						
Student demographics			+	+	+	+
Achievement scores				+	+	+
Academic characteristics					+	+
Parent background						+

Regression analysis results. $P < 0.001$ for all data shown; + indicates inclusion of covariates in the model; standard errors are shown in parentheses; $n = 3359$. Dependent variables: nonscience = 0, life science = 1, and physical science/engineering = 2. See supporting online material for more details.

These variables included scores from mathematics and science achievement tests (designed by the Educational Testing Service) that were administered in the first three surveys of data collection, when students were mostly enrolled in the 8th, 10th, and 12th grades (*3*, *4*).

The baccalaureate degree concentrations—which were coded into three broad categories of physical science/engineering, life science, and nonscience—resulted in a categorical dependent variable (tables S1 and S2 and supporting online material text) (*5*). The independent variables used in this analysis came from data collected when participants were enrolled in the eighth grade.

In our analysis, we took into account students' backgrounds and natural propensities. For example, students with stronger performance in science and mathematics may be more likely to major in the sciences. We therefore included four covariate groups to account for (i) academic backgrounds (science and mathematics achievement scores); (ii) students' demographics (gender and ethnicity); (iii) students' academic characteristics (enrollment in advanced versus regular mathematics and science classes, attendance in these classes, and student-reported attitudes toward mathematics and science); and (iv) parents' background (highest educational level and professional versus nonprofessional employment) (*6*).

Our analysis focuses on the independent variable derived from the *NELS:88* survey question: "What kind of work do you expect to be doing when you are 30 years old?" Students were then given a list of employment options and required to select only one. We categorized the responses into two groups: science-related and nonscience career expectations, creating the Career Expectation independent variable (*4*).

We applied multinomial logistic regression, which handles categorical dependent variables with more than two outcomes. Our analysis included two outcome comparisons in earned baccalaureate degrees: (i) earning degrees in life sciences versus nonscience areas and (ii) earning degrees in physical sciences/engineering versus nonscience areas. We assessed the degree to which the independent variables could predict these two comparisons. In the *NELS:88* sampling design, two analytical issues require special attention: (i) the effect of purposeful

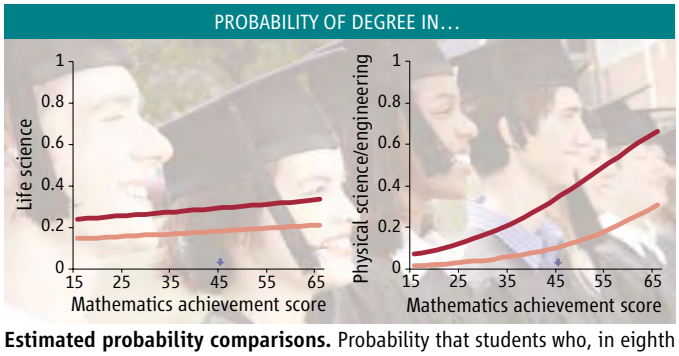

Estimated probability comparisons. Probability that students who, in eighth grade, expected (dark line) or did not expect (light line) a science career would achieve a life science degree (left) or a physical science/engineering degree (right). Blue arrow designates the average mathematics achievement score.

The authors are at the Curry School of Education, University of Virginia, 405 Emmet Street South, Charlottesville, VA 22904–4273, USA.

*To whom correspondence should be addressed. E-mail: rht6h@virginia.edu

oversampling of some ethnic and minority groups and (ii) the effect of multistage cluster sampling on standard error estimation. We followed the NCES guidelines by using sampling weights for statistical analyses (*3*). We accounted for the complex sampling design by using the STATA 9.0 statistical software package (*3*, *7*).

Results and Discussion

Our analysis began with a baseline model that included only the Career Expectation independent variable and continued with successively more complex models systematically accounting for each of the four covariate groups (see table on page 1143 and table S7).

As more independent variables were included in the nested models, the coefficient remained unchanged for the life science outcome. For the physical science outcome, the coefficient at first attenuated from its initial value and then settled into a robust value after model 3. This behavior is common in such analyses because variance accounted for by initially entered variables is subsumed by successive variables. We also checked for interactions between Career Expectations and the other independent variables and did not find them to be significant at the $P = 0.05$ level.

The odds ratios, calculated from the final model, were 1.9 for life sciences versus nonscience and 3.4 for physical sciences/engineering versus nonscience (table S7). This result suggests that, among the students who graduated with baccalaureate degrees from 4-year colleges, those who expected as eighth graders to have science-related careers at age 30 were 1.9 times more likely to earn a life science baccalaureate degree than those who did not expect a science-related career. Students with expectations for a science-related career were 3.4 times more likely to earn physical science and engineering degrees than students without similar expectations.

Next, we considered the estimated probabilities of earning science baccalaureate degrees produced by the final model comparison (see figure on page 1143). For life sciences, estimated probabilities nearly doubled for students who reported science-related career expectations compared with those who did not. For example, a prototypical student expecting a science-related career has an estimated probability of obtaining a life science degree of 29% compared with 18% for a prototypical student expecting a nonscience career, with all other predictors set to the means. Eighth-grade mathematics achievement was not a significant predictor for life science degrees.

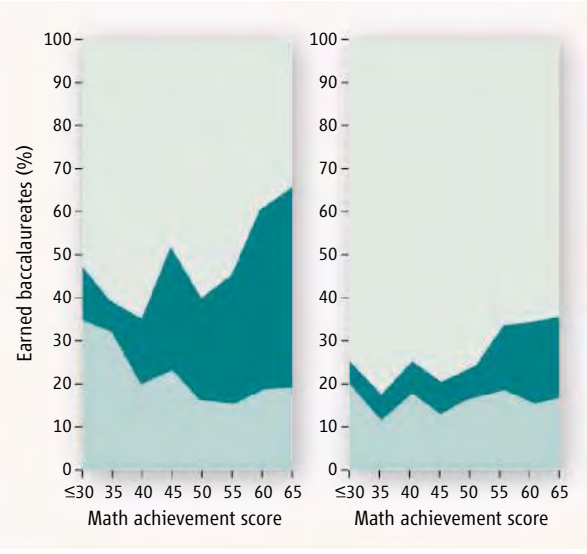

Proportion of earned baccalaureates. Degrees in life science (light green), physical science/engineering (dark green), and nonscience fields (gray). Students who in eighth grade expected a science degree are shown on the left ($n = 337$); those who did not expect a science degree are shown on the right ($n = 3022$).

However, for physical science/engineering degrees, the result was quite different (see figure on page 1143, right panel). High mathematics achievers were much more likely than low achievers to earn these degrees. For example, let us compare the estimated probabilities for two pairs of prototypical students with all other variables set to means. Suppose the first pair has average mathematics achievement scores (average math achievement score at eighth grade = 45, SD = 11). Here, the estimated probability of earning a physical science or engineering baccalaureate degree for the student who expected a science-related future career was 34%. In contrast, for the student who expected a nonscience career, the estimated probability was 10%. Suppose that for the second pair, we have high mathematics achievers whose test scores were one standard deviation above average. Here, the estimated probability of the student who expected a science-related future career was 51%, whereas the estimated probability of the student who expected a nonscience career was 19%. To the extent that taking courses encourages expectations, this result supports the National Science Board's contention (*8*) that mathematics courses taken in grades 7 and 8 have an impact on the physical sciences and engineering workforce.

There is an additional comparison across these pairs that should not go unnoted. An average mathematics achiever with a science-related career expectation has a higher probability of earning a baccalaureate degree in the physical sciences or engineering than a high mathematics achiever with a nonscience career expectation, 34% versus 19%. We make this comparison not to minimize the importance of academic achievement, but rather to highlight the importance of career expectations for young adolescents.

We analyzed (see figure at left) the proportion of students who earned the three types of baccalaureates degrees, according to eighth-grade expectations and math achievement scores. Most notable is the proportion of students who, in a sense, followed through on their eighth-grade science career choices—roughly half. In contrast, proportionally fewer students who reported nonscience career expectations switched into science—roughly a third.

Much effort has been focused on raising test scores and promoting advanced courses at later ages; however, we should not overlook the likelihood that life experiences before eighth grade and in elementary school may have an important impact on future career plans. Although our current analysis does not provide proof of an uninterrupted causal chain of influence, our study does suggest that to attract students into the sciences and engineering, we should pay close attention to children's early exposure to science at the middle and even younger grades. Encouragement of interest and exposure to the sciences should not be ignored in favor of an emphasis on standardized test preparation (*9*).

References and Notes

1. National Research Council, *Rising Above the Gathering Storm: Energizing and Employing America for a Brighter Future* (National Research Council, Washington, DC, 2005).
2. Data obtained through WebCASPAR (http://caspar.nsf.gov/).
3. National Center for Educational Statistics, *User's Manual: National Education Longitudinal Study of 1988* (NCES, Washington, DC, 2004).
4. D. A. Rock, J. M. Pollack, "Psychometric report for the *NELS:88* base test battery" (Tech. Rep. NCES 91-468, National Center for Educational Statistics, Washington, DC, 1991).
5. N. Hativa, M. Marincovich, *Disciplinary Differences in Teaching and Learning: Implications for Practice* (Jossey-Bass, San Francisco, CA, 1995).
6. Occupational classifications are highly complex and, in this analysis, only limited data were available on parents' specific occupations. We paid special attention to parental occupation in this analysis, because conventional wisdom suggests that children whose parents have careers in science may be more likely to choose similar careers. However, the existing data related to parents' occupations were reported in categories that did not specify whether jobs were science related. As a result, we chose to use the broad categories of professional versus nonprofessional.
7. For a more detailed discussion of this technique, please see J. S. Long, J. Freese, *Regression Models for Categorical Dependent Variables Using STATA®* (STATA, College Station, TX, 2001).
8. National Science Board, *An Emerging and Critical Problem of the Science and Engineering Labor Force: A Companion to the Science and Engineering Indicators 2004* (National Science Board, Washington, DC, 2004); available online (www.nsf.gov/statistics/nsb0407/ nsb0407.pdf).
9. S. Dillon, "Schools cuts back subjects to push reading and math," *The New York Times*, 26 March 2006 (www.nytimes.com/2006/03/26/education/26child.html).
10. This study was funded in part through a grant from NSF, Directorate of Education and Human Resources, Division of Research, Evaluation, and Communication, Research on Learning and Education Program (REC 0440002, Project Crossover). We thank L. E. Suter (NSF), D. Herschbach (Harvard University), and D. R. Webb (Proctor and Gamble) for their comments.

Supporting Online Material

www.sciencemag.org/cgi/content/full/312/5777/1143/DC1

10.1126/science.1128690

DEVELOPMENTAL BIOLOGY

How Many Ways to Make a Chordate?

The regulatory gene circuits that control the development of a protochordate are simpler than those of sea urchins or vertebrates, indicating that their similar tadpole-like body plan can be constructed in several ways.

Patrick Lemaire

Ascidians are invertebrate chordates that belong to the tunicates, the closest living sister group of vertebrates (*1*), from which they diverged more than 500 million years ago. On page 1183 of this issue, Imai and co-workers (*2*) report how they analyzed the ascidian *Ciona intestinalis* (sea squirt) to generate the first metazoan whole-embryo gene regulatory network. Surprisingly, it appears quite different from vertebrate networks despite the conservation of a common, tadpole-like larval body plan (see the figure).

Gene regulatory networks consist of functional linkages between transcription factors, cell signaling components, and the cis-regulatory modules that control their expression at the transcriptional level (*3*). The action of such networks is a major force driving animal development, from a simple egg to a complex larva. These networks are proposed to be free standing—that is, the regulation of each network component can be accounted for by the presence of other components. Ultimately, the networks control the precise expression of differentiation genes that confer specific attributes to each embryonic cell. The identification of networks in echinoderms (sea urchins) (*4*) and vertebrates (*5*, *6*) has illuminated the developmental logic underlying animal embryogenesis. In addition, comparing gene-regulatory networks that give rise to homologous anatomical structures across taxa or phyla have helped to elucidate the evolutionary origin of these structures (*3*).

Like lower vertebrates, developing *Ciona* make tadpole larvae. But these tadpoles have only 2600 cells, and the size of the *Ciona* genome is only 1/20 that of the mouse. In addition, ascidian genomes have not undergone the vertebrate-specific duplication events (*7*). The extreme genetic and cellular simplicity of *Ciona* is a boon to biologists attempting to reconstruct gene regulatory networks. It is, however, unlikely to reflect the condition of the ancestral chordate. Rather, most of it probably results from secondary simplification that has occurred since the tunicate and vertebrate lineages separated.

Thus, despite a shared larval body plan, the extent of conservation between ascidian and vertebrate gene regulatory networks has been uncertain. For instance, unlike in vertebrates, most ascidian tail muscle cells form cell autonomously, following the inheritance of the localized maternal Zic-family transcription factor Macho-1 (*8*). Notochord formation in ascidians and vertebrates involves the induced expression of the T-box transcription factor Brachyury by signals elicited by fibroblast growth factor (*9*). On the other hand, signals from bone morphogenetic protein play opposite roles in the formation of this tissue in ascidians and vertebrates (*10*). Neural tissue development is induced by fibroblast growth factor signals in ascidians and vertebrates, but it is unclear whether the transcription factors that act in the fibroblast growth factor signaling cascade are shared between ascidians and vertebrates (*11*). Finally, involvement of the transcription factors Mesp, Nkx, and HAND in heart formation appears to be conserved (*12*). These examples suggest a mixture of conservation and divergence between ascidian and vertebrate developmental strategies.

Look-alikes, early on. Although ascidians such as *Ciona intestinalis* have a very peculiar adult body plan that is adapted to their marine filter-feeding life-styles, their larvae are very similar to frog tadpoles (such as *Rana sylvatica*), demonstrating a close common evolutionary history. Nevertheless, their genetic circuits are different.

The extent to which different components of a large gene regulatory network are evolutionarily conserved may, however, differ. It was proposed that the only parts of the network that are well conserved, the "kernels," are highly connective subnetworks that specify the organization in space of different tissues (the body plan) rather than specifying precise cell types (*3*). The major function of kernels, and the reason for their high level of evolutionary conservation, would be to "lock" a given body plan in place (*3*). If this is true, chordate-specific kernels should be detected in ascidian gene regulatory networks despite the simplification of ascidian development.

Imai *et al*. provide the first whole-embryo gene regulatory network for a chordate, covering development from the 16-cell stage to the gastrula stage in *Ciona*. Previously, Imai and colleagues (*13*) generated a spatiotemporal atlas of gene expression of nearly 500 genes coding for transcription factors, signaling ligands, and receptors. They identified 65 genes encoding transcription factors and 26 genes encoding signaling molecules that are zygotically expressed up to the onset of gastrulation. In the present work, Imai *et al*. focus on those of these genes with no maternal expression and show that their expression patterns define an unambiguous transcriptional code for each blastomere up to the gastrula stage. This suggests that the combination of these genes is sufficient to give rise to the cellular diversity in the early embryo, and that they should therefore form a reasonably complete network. Imai *et al*. microinjected morpholino antisense oligonucleotides into *Ciona* eggs to inhibit the expression of most of these genes individually. Using quantitative polymerase chain reaction and in situ hybridization, they assessed the expression of all candidate genes (nodes of the network) in response to each perturbation. Only 27 out of 70 (39%) morpholinos tested produced a specific phenotype. This relatively low percentage reflects either imperfect morpholino design or the existence of genetic redundancy. The network constructed from these data is far from complete because the regulation of many genes cannot be accounted for by the presence of other genes from the collection. In particular, the network does not address how the expression of early zygotic genes is turned on by maternal factors. Finally, it does not include cis-regulatory analysis, so that the links established may be direct or indirect. Yet, it provides the first bird's-eye view of the regulatory circuitry that creates an early metazoan gastrula, at which stage most cell fates are restricted.

A first surprise is the low level of connectivity of the network in each embryonic territory. In contrast to the situation for the echinoderms and

The author is at the Institut de Biologie du Développement de Marseille Luminy, UMR6216 CNRS-Université de la Méditerranée, Campus de Luminy, F-13288 Marseille cedex 9, France. E-mail: lemaire@ibdm.univ-mrs.fr

vertebrate networks, only a small minority of signaling molecules (fibroblast growth factor, Nodal) and transcription factors (ZicL, FoxD, FoxA-a, Otx) affect the expression of a large fraction of the regulatory genes assayed. It will be interesting to test whether the majority of genes studied, which have few or no targets in the network, directly control differentiation genes. This would suggest that the simple and rapidly developing *Ciona* embryo may not need the cross-regulatory interactions used to stabilize gene expression patterns found in more slowly developing and also more complex embryos. Because extensive cross-regulatory interactions are a feature of kernels, the low level of connectivity of the *Ciona* network suggests their absence at the stages analyzed. Another surprise is the prevalent—though probably indirect—use of negative autoregulatory loops in the network. In contrast, very few positive autoregulatory loops were identified. This conflicts with the proposal that cell fate determination, which occurs very early in *Ciona*, is associated with the establishment of positive regulatory loops that lock in a given fate (*4*).

The structure of the current early *Ciona* network differs substantially from those of other deuterostomes. The maintenance of a chordate body plan in ascidians, in the absence of detectable kernels, may cast doubt upon the proposal that this type of subnetwork is important to stabilize a body plan across large evolutionary distances. It should, however, be considered that within a phylum, developmental strategies can be diverse in early embryos, converge at the phylotypic stage, and diverge again when terminally differentiated structures form. The network analyzed in the present work mainly covers pregastrula stages, and forms a necessary first step toward reconstructing networks for later stages in which chordate-specific kernels may be present. As it stands, the *Ciona* network has already allowed researchers to identify novel key regulators of specific fates and illustrates that whole-embryo reconstruction of gene regulatory networks is feasible provided that a suitable model organism is chosen. As was noted a few years ago, "Ascidians are back in the limelight, with a good chance of staying there" (*14*).

References

1. F. Delsuc, H. Brinkmann, D. Chourrout, H. Philippe, *Nature* **439**, 965 (2006).
2. K. S. Imai, M. Levine, N. Satoh, Y. Satou, *Science* **312**, 1183 (2006).
3. E. H. Davidson, D. H. Erwin, *Science* **311**, 796 (2006).
4. E. H. Davidson *et al.*, *Science* **295**, 1669 (2002).
5. M. Loose, R. Patient, *Dev Biol.* **271**, 467 (2004).
6. T. Koide, T. Hayata, K. W. Cho, *Proc. Natl. Acad. Sci. U.S.A.* **102**, 4943 (2005).
7. N. Satoh, Y. Satou, B. Davidson, M. Levine, *Trends Genet.* **19**, 376 (2003).
8. H. Nishida, K. Sawada, *Nature* **409**, 724 (2001).
9. K. S. Imai, N. Satoh, Y. Satou, *Development* **129**, 1729 (2002).
10. S. Darras, H. Nishida, *Development* **128**, 2629 (2001).
11. V. Bertrand, C. Hudson, D. Caillol, C. Popovici, P. Lemaire, *Cell* **115**, 615 (2003).
12. Y. Satou, K. S. Imai, N. Satoh, *Development* **131**, 2533 (2004).
13. K. S. Imai, K. Hino, K. Yagi, N. Satoh, Y. Satou, *Development* **131**, 4047 (2004).
14. O. Pourquie, *Nature* **409**, 679 (2001).

10.1126/science.1128784

GEOLOGY

Was the Younger Dryas Triggered by a Flood?

Draining of a huge lake into the Northern Atlantic may have triggered a cold period ~12,900 years ago. The route taken by the flood waters remains unknown.

Wallace S. Broecker

As Earth's surface warmed at the end of the last glacial period, the Laurentide ice sheet that covered much of North America retreated and a vast melt water lake—Lake Agassiz—formed in the area of today's Great Lakes. But the transition from glacial to interglacial conditions was not smooth: Between ~12,900 and ~11,500 years ago, cold conditions returned during the Younger Dryas.

It is widely believed that this cold event was triggered by a flood of fresh water that poured into the northern Atlantic (*1*) and disrupted the thermohaline ocean circulation (*2*). The accepted scenario (*3*) is that at some point during the retreat of the Laurentide ice sheet, the northern and eastern shorelines of Lake Agassiz were breached, diverting the outflow from the lake eastward through Lake Superior and into the northern Atlantic via the St. Lawrence lowlands (see the first figure). Teller *et al.* have argued that the initial flood caused by the sudden drop in outlet elevation, rather than the subsequent steady-state discharge from the lake, was instrumental in causing the Younger Dryas (*4*).

The author is at the Lamont-Doherty Earth Observatory, Columbia University, Palisades, NY 10964, USA. E-mail: broecker@ldeo.columbia.edu

However, an aerial search to the west of Lake Superior (*5*, *6*) yielded no visual evidence for flood channels or boulder fields that might support the flood scenario. This absence is particularly disconcerting, because lesser floods thought to have occurred after the Younger Dryas created spectacular canyons (see the second figure) and boulder fields. If not a flood, then what else might have triggered the Younger Dryas?

Before considering alternate scenarios, a brief summary of the evidence in support of an Agassiz flood is in order. I will use radiocarbon rather than calendar years, because the exact conversion factor to calendar years remains uncertain. The Younger Dryas occurred 11,100 to 10,000 radiocarbon years ago.

During the Bölling-Allerod warm interval that preceded the Younger Dryas, Lake Agassiz overflowed to the south over the Big Stone Moraine (see the first figure). Around 10,800 ± 200 radiocarbon years ago, this overflow ceased (*7*). At this time, the level of the lake must have dropped to that of a newly created alternate outlet. The new level may have been that of the "Moorhead lowstand," when Lake Agassiz stood more than 40 m below the level of the southern outlet; radiocarbon ages for wood from the Moorhead lowstand fall within the span of the Younger Dryas (*5*).

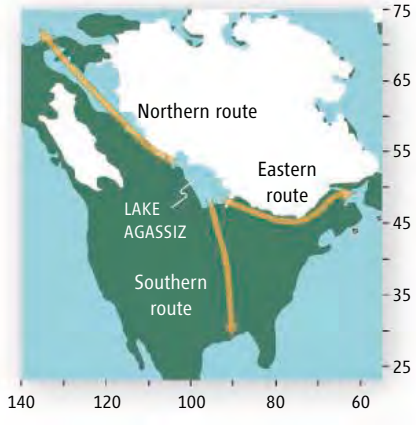

Drainage pathways from Lake Agassiz

Oxygen isotope records from sediment cores from the Gulf of Mexico support the contention that the new outlet did not empty into the Mississippi River drainage. Planktonic shells have yielded a radiocarbon age of 11,100 years, marking the onset of a time of decreased inflow of ^{18}O-depleted glacial melt water into the Gulf of Mexico (*8*). This interval lasted until about 10,000 radiocarbon years before the present and hence corresponds to the Younger Dryas time interval. But although the observed rise in ^{18}O is

consistent with a diversion of Agassiz outflow to an alternate pathway to the sea, it can also be explained by a decrease in the rate of ice-sheet melting during the cold Younger Dryas.

A complementary drop in the ^{18}O in shells from the St. Lawrence Valley at the onset of the Younger Dryas would provide support for the Lake Agassiz flood scenario. In a recent paper (*9*), Brand and McCarthy present evidence for such a drop in mollusks from two sites south of Ottawa, Canada. However, the time of this drop is poorly constrained, and the event may postdate the onset of the Younger Dryas. Furthermore, de Vernal *et al*. (*10*) find no evidence in sediments from the St. Lawrence Estuary for an eastward flow of melt water during the Younger Dryas.

New radiocarbon ages for organic material from the bottom of borings in small lakes in the area west of Thunder Bay (*5*) suggest that the area through which the proposed pre–Younger Dryas flood had to pass was not deglaciated until 10,200 radiocarbon years ago, late in the Younger Dryas. These new radiocarbon ages are younger than those for wood from the Moorhead lowstand of Lake Agassiz (up to 10,900 radiocarbon years before the present). The wood cannot be older than the time of diversion of melt water to the presumed eastern outlet. Thus, it has been suggested that the oldest Moorhead wood is reworked (that is, it was transported after growth) (*5*). But there is another explanation: The area may have been deglaciated during the Bölling-Allerod warm period and reglaciated during the Younger Dryas. If so, then the sediment cores likely terminated in impenetrable silt deposited during the ice retreat subsequent to the Younger Dryas.

In the absence of geomorphic evidence for an eastern outlet, an alternate trigger for the Younger Dryas cold episode must be found. There are several possibilities.

First, flood waters from Lake Agassiz may have escaped to the north rather than to the east. Indeed, there is clear evidence that a catastrophic flood passed through the Fort McMurray area (*11*). A 1-km-wide, 30-km-long channel marks the path taken by these waters. At the channel's mouth, there is a large gravel field and beyond that, a huge apron of sand. However, these deposits are around 9800 radiocarbon years old and thus postdate the Younger Dryas. Of course, an earlier flood predating the Younger Dryas may have passed through the same area, but, to date, no convincing physical evidence for such an event has been found.

Second, the water from Lake Agassiz may have escaped beneath the ice. Were this the case, then no radiocarbon-datable material recording the event would exist, because nothing could grow under the ice roof. Further, boulders put in place by the subice flood would have ^{10}Be ages reflecting the time of deglaciation rather than the time of the flood (radioactive ^{10}Be atoms are produced within exposed boulders by cosmic ray neutrons that shatter the nuclei of oxygen atoms; no such cosmic rays could penetrate the ice roof). Indeed, there are spectacular canyons (see the first figure) and boulder fields to the north of Thunder Bay (*3*). The 2-km-long, 100-m-deep Ouimet Canyon is situated just north of Lake Superior. But no quartz-bearing rock suitable for dating has yet been found (quartz crystals can be acid-leached to remove contaminating ^{10}Be atoms produced in the atmosphere and carried to the surface by rain. Hence quartz is the mineral of preference for ^{10}Be studies). ^{10}Be measurements on meter-size granitic boulders from west of Lake Nipigon yield an age of about 8400 years (*12*). This result provides a minimum age for the deglaciation of this area. Although a subice escape of water stored in Lake Agassiz may seem unlikely, it must be kept in mind that such an escape has been called on to explain the triggering of the 50-year cold snap that occurred 8200 years ago (*13*).

Evidence for lesser floods thought to have occurred after the Younger Dryas. (Bottom left) Ouimet Canyon appears to have been cut by flood waters escaping from Lake Agassiz. No material suitable for dating has been found. (**Bottom right**) Rabbit Canyon is one of the numerous channels to the west of present day Lake Nipigon. A granitic boulder from the mouth of a nearby channel has a ^{10}Be age of 8400 years, fixing the time of deglaciation of this site.

Third, the fresh water that triggered the Younger Dryas may have originated from the melting of an armada of icebergs rather than from the escape of stored melt water. In three marine sediment cores from southeast of Hudson Straits, a detrital $CaCO_3$-bearing horizon has been found (*14*–*16*). Such horizons are believed to be caused by armadas of icebergs shedding their debris upon melting. Although not precisely dated, this horizon appears to correlate with the Younger Dryas. However, no evidence for this iceberg armada is found in other sediment cores from the northern Atlantic, and the impact was therefore probably too small to have produced a shutdown of the ocean's circulation. In a variant on this scenario, the subice escape of Agassiz water may have passed through the Hudson Bay carrying debris-laden basal ice. In this case, the flood water rather than the melting of the entrained ice would have diluted the salt content of northern Atlantic waters.

Of course, the Younger Dryas may not have been triggered by a catastrophic freshening of northern Atlantic surface waters at all. Seager and Battisti have argued that a temperature anomaly in the tropics may have triggered a shift in the wind pattern over the northern Atlantic, in turn allowing sea ice to form (*17*). As a consequence, the thermohaline conveyor was shut down. Although these detractors disagree regarding the nature of the trigger, they agree that a reorganization of ocean circulation was necessary to stabilize climate during the 1400-year-long Younger Dryas.

The Younger Dryas is unique to the termination of the last glacial cycle. Ice cores from Greenland and Antarctica show that during the Younger Dryas, the atmosphere's methane content dropped from 680 to 460 parts per billion (*18*). The core from Greenland does not extend to previous terminations, but that from Antarctica records three earlier ones. None of these shows a Younger Dryas–like methane drop (*19*). Hence, the Younger Dryas was likely triggered by a freak event rather than by something common to each glacial termination. The sudden release of a large amount of stored fresh water qualifies as a freak event, because its occurrence depends on the detailed geometry of the retreating ice front.

Despite the flies in the flood ointment described above, my money remains on a flood of water stored in Lake Aggasiz. Otherwise, the confluence of dates for the cessation of the Big Stone Moraine overflow, the Moorhead lowstand, and the rise in $\delta^{18}O$ in the Gulf of Mexico would have to be attributed to coincidence. But our inability to identify the path taken by the flood is disconcerting. Given that the Younger Dryas holds the key to understanding abrupt climate change, further detailed studies of key areas must be conducted. Of critical importance is precise radiocarbon dating.

References and Notes

1. R. G. Johnson, B. T. McClure, *Quat. Res.* **6**, 325 (1976).
2. C. Rooth, *Prog. Oceanog.* **11**, 131 (1982).
3. J. T. Teller, L. H. Thorleifson, in *Glacial Lake Agassiz*, J. T. Teller, L. Clayton, Eds. (Geological Association of Canada, St. John's, Newfoundland, 1983), pp. 261–290.
4. J. T. Teller, D. W. Leverington, J. D. Mann, *Quat. Sci. Rev.* **21**, 879 (2002).
5. T. V. Lowell *et al*., *Eos* **86**, 365 (2005).

6. J. T. Teller, M. Boyd, Z. Yang, P. S. G. Kor, A. M. Fard, *Quat. Sci. Rev.* **24**, 1890 (2005).
7. T. G. Fisher, *Quat. Res.* **59**, 271 (2003).
8. W. S. Broecker *et al.*, *Nature* **341**, 250 (1989).
9. U. Brand, F. M. G. McCarthy, *Quat. Sci. Rev.* **24**, 1463 (2005).
10. A. de Vernal, C. Hillaire-Marcel, G. Bilodeau, *Nature* **381**, 774 (1996).
11. T. G. Fisher, D. G. Smith, *Quat. Sci. Res.* **13**, 845 (1994).
12. V. Rinterknecht *et al.*, *Eos* **85**, 47 (2004).
13. D. C. Barber *et al.*, *Nature* **400**, 344 (1999).
14. J. T. Andrews, H. Erlenkeuser, K. Tedesco, A. E. Aksu, A. J. T. Jull, *Quat. Res.* **41**, 26 (1994).
15. J. T. Andrews, K. Tedesco, W. M. Briggs, L. W. Evans, *Can. J. Earth Sci.* **31**, 90 (1994).
16. J. T. Andrews *et al.*, *Paleoceanography* **10**, 943 (1995).
17. R. Seager, D. S. Battisti, in *The General Circulation of the Atmosphere*, T. Schneider, A. S. Sobel, Eds. (Princeton Univ. Press, 2005).
18. J. Chappellaz *et al.*, *Nature* **366**, 443 (1993).
19. J. R. Petit *et al.*, *Nature* **399**, 429 (1999).
20. I am indebted to G. Comer for financial backing and for initiating and participating in field expeditions to the Agassiz outlets and the glaciated mountain ranges of eastern and southern Greenland. These field trips have substantially advanced my thinking with regard to the Younger Dryas. Discussions with T. Lowell, T. Fisher, G. Denton, J. Teller, S. Hemming, and J. Schaefer have also been extremely helpful.

10.1126/science.1123253

ASTRONOMY

The Vacuum Energy Crisis

Alexander Vilenkin

Even empty space has energy, but understanding its magnitude is a major puzzle. A cyclic series of big bangs has been proposed as a solution; anthropic selection offers another explanation

One of the stranger consequences of quantum mechanics is that even empty space has energy. The problem of how to calculate this vacuum energy is arguably the most intriguing mystery in theoretical physics. For decades, physicists have tried to understand why this energy is so small, but no definitive solution has yet been found. On page 1180 of this issue, Steinhardt and Turok propose a new approach (*1*).

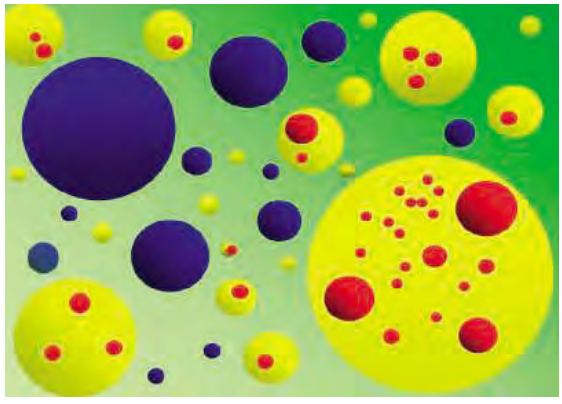

The inflationary multiverse. Bubbles with different properties nucleate and expand in the inflating high-energy background. We live in one of the bubbles and can observe only a tiny part of it.

Vacuum is empty space, but it is far from being "nothing." It is a complicated physical object in which particles such as electrons, positrons, and photons are being incessantly produced and destroyed by quantum fluctuations. Such virtual particles exist only for a fleeting moment, but their energies combine to endow each cubic centimeter of space with a nonzero energy. This vacuum energy density does not change in time; it is called the cosmological constant and is usually denoted by Λ. The trouble is that theoretical calculations of Λ give ridiculously large numbers, 120 orders of magnitude greater than what is observed. According to Einstein's theory of general relativity, vacuum energy produces a repulsive gravitational force, and if the energy were so large, its gravity would have instantly blown the universe apart.

It is conceivable that positive vacuum energy contributions from some particle species are compensated by negative contributions from other species, so that the net result is close to zero. But then the compensation must be amazingly precise, up to 120 decimal places. There seems to be no good reason for such a miraculous cancellation. Until recently, the majority of physicists believed that something so small could only be zero: some hidden symmetry should force the exact cancellation of all contributions to the cosmological constant. However, observations in the late 1990s of distant supernova explosions yielded the surprising discovery that the expansion of the universe accelerates with time (*2*, *3*)—a telltale sign of cosmic repulsion caused by a nonzero (positive) cosmological constant.

The observed magnitude of Λ has brought about another mystery: its value is roughly twice the average energy density (or, equivalently, the mass density) of matter in the universe. This is surprising because the matter and vacuum densities behave very differently with cosmic expansion. The vacuum density remains constant, whereas the matter density decreases; it was much greater in the past and will be much smaller in the future. Why, then, do we happen to live during the very special epoch when the two densities are so close to one another? This has become known as the cosmic coincidence problem.

Both puzzles can be resolved if one is prepared to assume that the cosmological constant is not a fixed number, but takes a wide variety of values in remote parts of the universe. In regions where it is much larger than the observed value, its repulsive gravity will be stronger and will prevent matter from clumping into galaxies and stars (*4*, *5*). Life is not likely to evolve in such regions.

The idea of "anthropic selection"—that certain features of the universe are selected by the requirement that observers should be there to detect them (*6*)—runs contrary to the physicist's aspiration to derive all constants of nature from first principles. It has been passionately resisted by the physics community, but has recently gained support from both string theory and cosmology. String theory, the most promising candidate for the fundamental theory of nature, predicts a multitude of vacuum states characterized by different values of Λ and other "constants." Inflationary cosmology, which now has substantial observational support, suggests that the universe on the largest scales is in a state of high-energy exponential expansion and is constantly spawning low-energy "bubbles" like the one we live in, with all possible values of the "constants" (see the figure). Galaxies and observers exist only in rare bubbles where Λ is small and other constants are also appropriately selected. Analysis shows that most of the galaxies are formed in regions where vacuum and matter densities are about the same at the epoch of galaxy formation (*7*–*9*). Our present time is close to that epoch, and this explains the coincidence (*10*, *11*).

Steinhardt and Turok propose an alternate explanation for the smallness of Λ. Building on an idea of Abbott (*12*), they postulate the existence of a long sequence of vacuum states, with Λ changing in small increments from one state to the next. If the universe starts with a large cosmological constant, its value will be gradually reduced through a sequence of quantum transitions to lower and lower values. Abbott showed that as Λ approaches zero, the transitions become increasingly slow, so the universe spends most of the time in the state with the smallest positive Λ. He found, however, that the descent to small values of Λ takes so long that

The author is in the Department of Physics and Astronomy, Tufts University, Medford, MA, 02155, USA. E-mail: vilenkin@cosmos.phy.tufts.edu

CREDIT: D. SCHWARTZ-PERLOV/TUFTS UNIVERSITY

all matter gets completely diluted by the cosmic expansion, and an empty universe results. To fix this flaw, Steinhardt and Turok combined Abbott's model with the cyclic cosmological scenario (*13*), in which the universe goes through multiple cycles of expansion and contraction. The high density of matter is regenerated at the start of each cycle, so the empty universe problem is solved. Most of the cycles will occur while the universe is in the lowest Λ state, and Steinhardt and Turok argue that this state is most likely to be observed.

The cyclic model is still being developed and is not widely accepted. More importantly, although Steinhardt and Turok's proposal may explain the smallness of Λ, it does not address the cosmic coincidence problem: Why should the smallest possible value of Λ be comparable to the present density of the universe? The anthropic explanation appears, therefore, to be more compelling.

References and Notes

1. P. J. Steinhardt, N. Turok, *Science* **312**, 1180 (2006); published online 4 May 2006 (10.1126/scence. 1126231).
2. A. G. Riess *et al*., *Astron. J.* **116**, 1009 (1998).
3. S. Perlmutter *et al*., *Astrophys. J.* **517**, 565 (1999).
4. S. Weinberg, *Phys. Rev. Lett.* **59**, 2607 (1987).
5. A. D. Linde, in *300 Years of Gravitation*, S. W. Hawking, W. Israel, Eds. (Cambridge Univ. Press, Cambridge, 1987).
6. M. Livio, M. J. Rees, *Science* **309**, 1022 (2005).
7. A. Vilenkin, *Phys. Rev. Lett.* **74**, 864 (1995).
8. G. Efstathiou, *Mon. Not. R. Astron. Soc.* **274**, L73 (1995).
9. H. Martel, P. R. Shapiro, S. Weinberg, *Astrophys. J.* **492**, 29 (1998).
10. J. Garriga, M. Livio, A. Vilenkin, *Phys. Rev.* **D61**, 023503 (2000).
11. S. Bludman, *Nucl. Phys.* **A663-664**, 865 (2000).
12. L. Abbott, *Phys. Lett.* **B150**, 427 (1985).
13. P. J. Steinhardt, N. G. Turok, *Science* **296**, 1436 (2002).

14. The author acknowledges the support of the NSF.

Published online 4 May 2006;
10.1126/science.1128570
Include this information when citing this paper.

10.1126/science.1128570

MATERIALS SCIENCE

High-Pressure Microscopy

When bombarded with electrons, carbon nanotubes shrink, creating high internal pressures. The effect on molecules within the tubes can be studied at atomic resolution.

Zhongwu Wang and Yusheng Zhao

When materials are put under pressure, their structures can change dramatically. Such pressure-induced structural changes occur in many contexts, from materials synthesis to geophysics. Studies of these structural changes have mainly relied on diffraction and spectroscopic techniques. Electron microscopy—the only means to view atomic structure directly—must be conducted in a vacuum. It would therefore seem impossible to directly observe pressure-induced atomic motion. But on page 1199 of this issue, Sun *et al*. (*1*) show that transmission electron microscopy (TEM) can be used to induce self-compression of carbon nanotubes and hence to study the effect of pressure on materials trapped within the nanotubes.

The diamond anvil cell is currently the most widely used device for applying extreme pressures on a material (see the figure, left panel). In this method, two perfectly aligned gem diamond anvils squeeze a sample loaded within the gasket hole to achieve megabar pressure under a moderate loading force. Diamond anvil techniques have been used, for example, to produce metallic hydrogen and to study the melting of iron under pressure/temperature conditions resembling those in Earth's core (*2*–*4*).

X-ray diffraction and Raman spectroscopic measurements can be performed within the diamond anvil cell, allowing crystal structures and transition pressures between different structures to be determined. For example, it has been shown that iron, which crystallizes in a cubic structure at ambient conditions, transforms to hexagonal phase at ~10 GPa (*3*, *4*). Upon release of pressure, the hexagonal iron transforms back to the starting cubic structure. However, the transformation mechanisms can only be conjectured. Recent syntheses of defect-free, nanometer-scale crystals have helped to elucidate the transformation mechanisms, but in situ spectroscopic measurements still cannot provide a definite answer (*5*, *6*). Molecular dynamics simulations can also be used to study the transition mechanism and the resulting kinetics. However, it has been difficult to replicate complicated dynamic processes, such as the pressure-induced transformations in iron and graphite, in simulations (*4*, *7*, *8*).

High-resolution TEM is the only analytical technique that provides a visual image of the atomic structure. Ten years ago, Banhart and Ajayan found that electron irradiation from a high-resolution TEM could induce self-compression of carbon onions (*9*). More recent high-resolution TEM studies have observed atomic deformations of Mo and W nanocrystals encapsulated in carbon onions, as a result of self-compression (*10*). These results provide important clues to

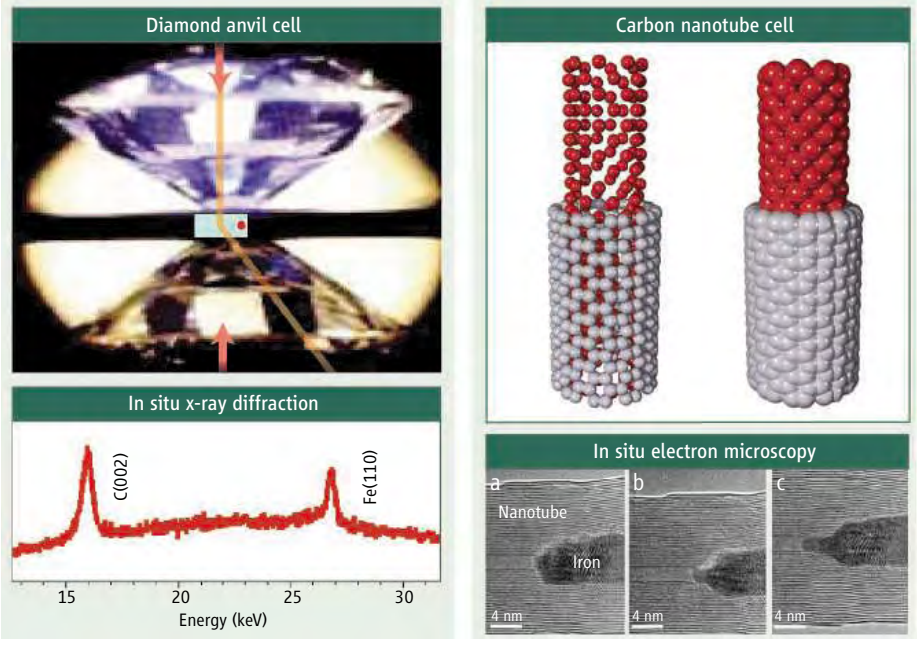

A matter of scale. (**Left**) A transparent diamond anvil cell allows in situ spectroscopic measurements of bulk samples. The red arrow represents an x-ray beam that is diffracted by the sample. (**Right**) A carbon nanotube self-compression cell enables in situ atomic-resolution snapshots at zero (**a**), intermediate (**b**), and high (~40 GPa) (**c**) pressure.

CREDIT: (TOP RIGHT PANEL) C. BICKEL/*SCIENCE*

The authors are at the Los Alamos Neutron Science Center, Los Alamos National Laboratory, Los Alamos, NM 87545, USA. E-mail: z_wang@lanl.gov

how a carbon nanotube pressure cell for in situ high-resolution TEM observation can be built.

Such a pressure cell must meet four requirements: a strong elastic modulus to achieve maximum pressure; a hollow core to encapsulate materials; the ability to compress the sample through electron radiation; and a sufficiently small sample size for high-resolution TEM characterization. Sun *et al*. confirm that multiwalled carbon nanotubes are suitable for this task and document the atomic deformation of materials within the nanotubes (see the figure, right panel).

The authors created multiwalled carbon nanotubes filled with iron carbide, iron, and/or cobalt and placed them in a heating stage within their TEM. At a temperature of ~600ºC, electron irradiation knocks carbon atoms off the nanotube lattices. Atomic-scale reconstruction results in the shrinkage of the nanotubes and consequently squeezes the encapsulated materials. Upon continuous electronic irradiation, the damage to and restructuring of the carbon lattice increases the pressure within the tubes; high-resolution TEM images recorded throughout this process provide a detailed record of the pressure buildup and resulting deformation of the encapsulated materials. The results show that even hard materials such as iron carbide can be deformed, extruded, and broken by this method. The detailed deformation mechanisms appear to differ from that of macroscopic crystals, where defects—not observed in the current study—are known to play an important role.

How high is the pressure within the tubes? One way to reach an estimate is to measure the lattice spacings between the nanotube sheets and within the encapsulated materials; another is to perform computer simulations. Sun *et al.* show that both methods yield similar estimates of up to ~40 GPa. Although this is an order of magnitude below the highest pressure achieved in a diamond anvil cell, the phase-transformation pressures of many materials fall within this range (*2*–*4*), providing a route to explore the atomic-scale dynamics of these materials under pressure.

Carbon nanotubes have been filled with a wide range of materials, including gases, liquids, and solids (*11*, *12*). The nanotube pressure cell opens up a window to directly watch atomic-scale development of pressure-induced phenomena in these samples, with applications in materials science, chemistry, condensed-matter physics, geophysics, planetary science, and nanotechnology. Understanding the driving mechanism of phase transformation at the atomic scale is important not only for optimizing the synthesis of novel functional materials, but also for developing robust theoretical models. Such insights will advance fundamental condensed-matter physics and will help to tune the properties of nanometer-scale crystals and composites and to explore the formation dynamics of Earth and other planets.

References

1. L. Sun *et al*., *Science* **312**, 1199 (2006).
2. G. L. Chiaroti R. J. Hemley, M. Bernasconi, L. Ulivi, Eds., *High Pressure Phenomena* (IOS Press/Soc. Ital. di Fis., Amsterdam, 2002).
3. C. S. Yoo *et al*., *Science* **270**, 1473 (1995).
4. R. J. Hemley, H.-K. Mao, V. V. Struzhkin, *J. Synchrotron Radiat*. **12,** 135 (2005).
5. L. Brus, *Science* **276**, 373 (1997).
6. Z. W. Wang *et al*., *Proc. Natl. Acad. Sci. U.S.A.* **101**, 13699 (2004).
7. J. C. Angus, C. C. Hayman, *Science* **241**, 913 (1988).
8. A. DeVita *et al*., *Nature* **379**, 523 (1996).
9. F. Banhart, P. M. Ajayan, *Nature* **382**, 433 (1996).
10. J. X. Li, F. Banhart, *Adv. Mater*. **17**, 1539 (2005).
11. P. M. Ajayan, S. Iijima, *Nature* **361**, 333 (1993).
12. S. C. Tsang *et al.*, *Nature* **372**, 159 (1994).

10.1126/science.1127181

MICROBIOLOGY

Bacteria Seize Control by Acetylating Host Proteins

The plague-causing bacterium *Yersinia pestis* injects toxic proteins into its hosts' cells. One of these interferes with the host's secretion of a protective factor by adding acetyl groups to a signaling kinase, blocking its activation.

Carolyn A. Worby and Jack E. Dixon

The devastation wreaked by the infamous bacterium *Yersinia pestis* in the Middle Ages altered the course of human history, as the plague or "black death" accounted for millions of deaths in what has been called one of the worst epidemics in history (*1*). Our molecular understanding of this bacterium and its pathogenic effects is helping us understand how it accomplished such a feat. *Y. pestis*, along with two related pathogens, *Y. pseudotuberculosis* and *Y. enterocolytica*, harbors a plasmid that encodes a secretion system that effectively delivers virulence factors into eukaryotic cells, where they can subvert key cellular systems for their own purposes. On page 1211 of this issue, Mukherjee *et al.* (*2*) report how one such virulence factor, YopJ, blocks the host's immune response, allowing infection to prevail.

Yersinia's type III secretion system is commonly described as a molecular pore or syringe-like structure that the bacterium uses to penetrate a host cell and inject virulence factors (referred to as *Yersinia* outer proteins or Yops). There are six well-defined Yops in *Yersinia*: YopO/YpkA, YopE, YopH, YopM, YopT, and YopJ. Early studies on YopJ showed that it prevents release of the cytokine tumor necrosis factor–α from host cells, thereby circumventing the body's ability to mount an effective immune response (*3*).

Previous work demonstrated that YopJ blocks several cellular signaling pathways, including the extracellular signal-regulated kinase, c-Jun NH_2-terminal kinase, p38 mitogen-activated protein kinase (MAPK), and nuclear factor κB (NFκB) pathways (*4*, *5*). Each of these pathways signals through a series of kinases, enzymes that catalyze protein phosphorylation. In the case of the MAPK signaling cascade (see the figure), an extracellular stimulus normally activates the pathway by inducing the phosphorylation of specific MAPK kinase kinases (MAPKKK or MKKK). These activated enzymes then phosphorylate their respective substrates, MAPK kinases (MAPKK or MKK) or IκB kinase β (IKKβ) in the case of the NFκB pathway. The MKKs and IKKβ are activated by phosphorylation on two serine residues or a serine and threonine residue found in their activation loops. These activated kinases in turn phosphorylate and activate MAPK and NFκB, resulting in the production of cytokines and antiapoptotic signals. Orth and colleagues (*6*) previously determined that YopJ can block these phosphorylation cascades. Using yeast two-hybrid analysis, they demonstrated that YopJ binds directly to MKK1. It turns out that YopJ also binds to several members of the MAPK kinase superfamily, but how this interaction blocks kinase activation has remained unresolved until now.

A search for proteins with amino acid sequence identity to YopJ identified several proteins from plant and animal pathogens, including adenovirus protease-2 (AVP), fowl *monas campestris* pv. *vesicatoria*, adenovirus 8-like-protease, AvrBst from *Xantho*AvrA from *Salmonella typhimurium*, and a potential protease from hemorrhagic enteritis virus (*7*). All of these proteins contain a conserved catalytic triad of amino acids (His, Asp/Glu, Cys) that is simi-

The authors are in the Departments of Pharmacology, Cellular and Molecular Medicine, and Chemistry and Biochemistry, University of California at San Diego, 9500 Gilman Drive, La Jolla, CA 92093, USA. E-mail: jedixon@ucsd.edu

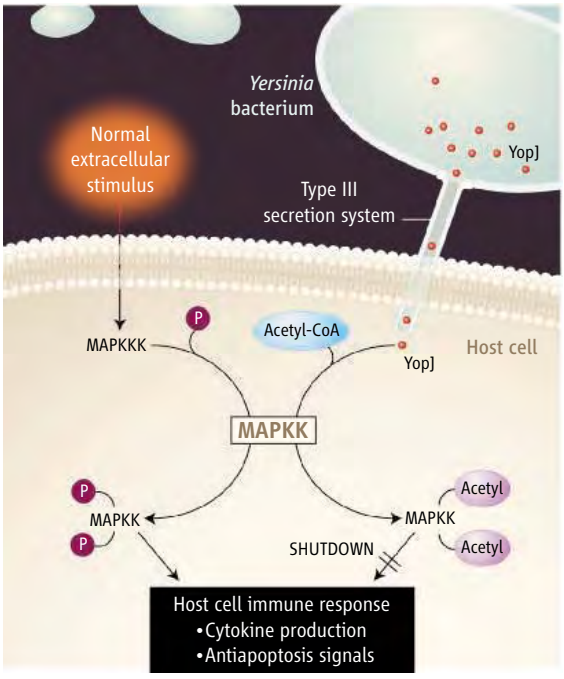

Virulence factor interference. YopJ that is deployed into a host cell blocks a signaling pathway by modifying the enzyme MAPK kinase (MAPKK) with acetyl moieties. This prevents activation of MAPKK by phosphorylation (P) via MAPKKK, and shuts down the immune response.

lar to a triad found in ClanCE cysteine proteases, which include AVP and the ubiquitin-like protease (Ulp-1) (*8*). Orth *et al*. (*7*) showed that YopJ can hydrolyze SUMO-1, a ubiquitin-like protein, from SUMO-1–conjugated proteins. Using a similar rationale, Zhou *et al*. (*9*) demonstrated that YopJ can function as a deubiquitinase. Neither of these observations, however, explains the ability of YopJ to specifically inhibit the MAPK pathways at the level of the MKKs. In light of the new data, it seems likely that the above observations may represent global cellular effects that can be obtained when a protein, usually expressed at low levels, is overexpressed in cells.

Mukherjee *et al.* show that YopJ is an acetyltransferase that blocks activation of the MAPK and NFκB pathways by acetylating serine and threonine residues on MKK6 and IKKβ. The authors used an in vitro system to recapitulate the ability of YopJ to inhibit the phosphorylation of MKK6. Subsequent analysis of MKK6 demonstrated that YopJ acetylates MKK6 on the serine or threonine residues critical for kinase activation, thus directly blocking its activation by phosphorylation. In addition, IKKβ is also acetylated on the two residues that are normally phosphorylated in its signaling cascade. Therefore, in each case, acetylation effectively blocks the ability of upstream kinases to phosphorylate and activate these proteins, thereby preventing the activation of downstream effectors. Although the details of the enzymatic posttranslational modification are yet to be worked out, most likely the cysteine residue of YopJ catalyzes the transfer of the acetyl group from acetyl-CoA to YopJ, forming an acyl enzyme intermediate. The acetylated form of YopJ then transfers the acetyl group to the reactive serine or threonine residues of MKK6 and IKKβ.

This activity for YopJ elegantly explains its ability to block phosphorylation of MKK6 and IKKβ and raises the interesting question of whether other MKKs present in parallel MAPK pathways also undergo similar modifications. This in turn raises other questions: Do other members of the YopJ family function as acetyltransferases? Do eukaryotic cells have acetyltransferases whose normal function is to regulate fluxes through the MAPK pathways, and do novel acetyltransferases exist to block sites of phosphorylation in other pathways? Hart and colleagues have suggested that glycosylation plays a similar role in blocking phosphorylation (*10*). Taken together, the direct competition of one posttranslational modification for another may be a more common cellular strategy for regulation of flux through signal transduction pathways than previously recognized.

Knowing that YopJ functions as an acetyltransferase is not the end of the story. It is really the beginning of what is likely to be the exciting search for other acetyltransferases in bacterial pathogens and viruses as well as in eukaryotic cells.

References

1. R. R. Brubaker, *Curr. Top. Microbiol. Immunol.* **57**, 111 (1972).
2. S. Mukherjee *et al.*, *Science* **312**, 1211 (2006).
3. L. E. Palmer, S. Hobbie, J. E. Galan, J. B. Bliska, *Mol. Microbiol.* **27**, 953 (1998).
4. L. E. Palmer, A. R. Pancetti, S. Greenberg, J. B. Bliska, *Infect. Immun.* **67**, 708 (1999).
5. K. Ruckdeschel *et al.*, *J. Exp. Med.* **187**, 1069 (1998).
6. K. Orth *et al.*, *Science* **285**, 1920 (1999).
7. K. Orth *et al.*, *Science* **290**, 1594 (2000).
8. A. J. Barrett, N. D. Rawlings, *J. Biol. Chem.* **382**, 727 (2001).
9. H. Zhou *et al.*, *J. Exp. Med.* **202**, 1327 (2005).
10. K. Kamemura, G. W. Hart, *Prog. Nucleic Acid. Res. Mol. Biol.* **73**, 107 (2003).

10.1126/science.1128785

MATERIALS SCIENCE

Fluctuations in Plasticity at the Microscale

M.-Carmen Miguel and Stefano Zapperi

During deformation, microscale materials may flow or change shape abruptly as atomic-scale defects migrate and assemble. The abrupt episodes of deformation appear to have a power-law distribution, a finding that may help in the design of miniature devices.

A fundamental challenge in materials science today is the investigation of size effects that influence the mechanical properties of micrometer- to nanometer-scale devices. These small scales are ubiquitous in modern technological applications and pose new theoretical questions as a result of the crucial role played by fluctuations. These fluctuations are observed as step changes or discontinuities in the mechanical response caused by the inhomogeneous dynamics of defects at the microscale. Fluctuations of this kind become more important as the size of any physical system decreases, hence they can lead to substantial deviations from the system's average behavior. On page 1188 of this issue, Dimiduk and co-workers (*1*) report experimental results on metal microcrystals that provide direct evidence of scale-invariant intermittent plastic flow—that is, permanent deformation with strain bursts that have a power-law distribution. These high-resolution experiments call for a novel theoretical framework that could help unravel microscopic deformation behavior in crystalline materials.

Plastic deformation is often described as a smooth process occurring in an elastic continuum. Yet microscopically it is due to the nucleation and motion of discrete crystal defects, known as dislocations. Dislocations self-assemble into intricate structures that determine the mechanical properties of a crystalline material. When external forces are applied, these dislocation structures dis-

M.-C. Miguel is in the Departament de Física Fonamental, Universitat de Barcelona, 08028 Barcelona, Spain. S. Zapperi is with the Consiglio Nazionale delle Ricerche–Istituto Nazionale per la Fisica della Materia, Dipartimento di Fisica, Università "La Sapienza," 00185 Roma, Italy. E-mail: stefano.zapperi@roma1.infn.it

CREDIT: P. HUEY/*SCIENCE*

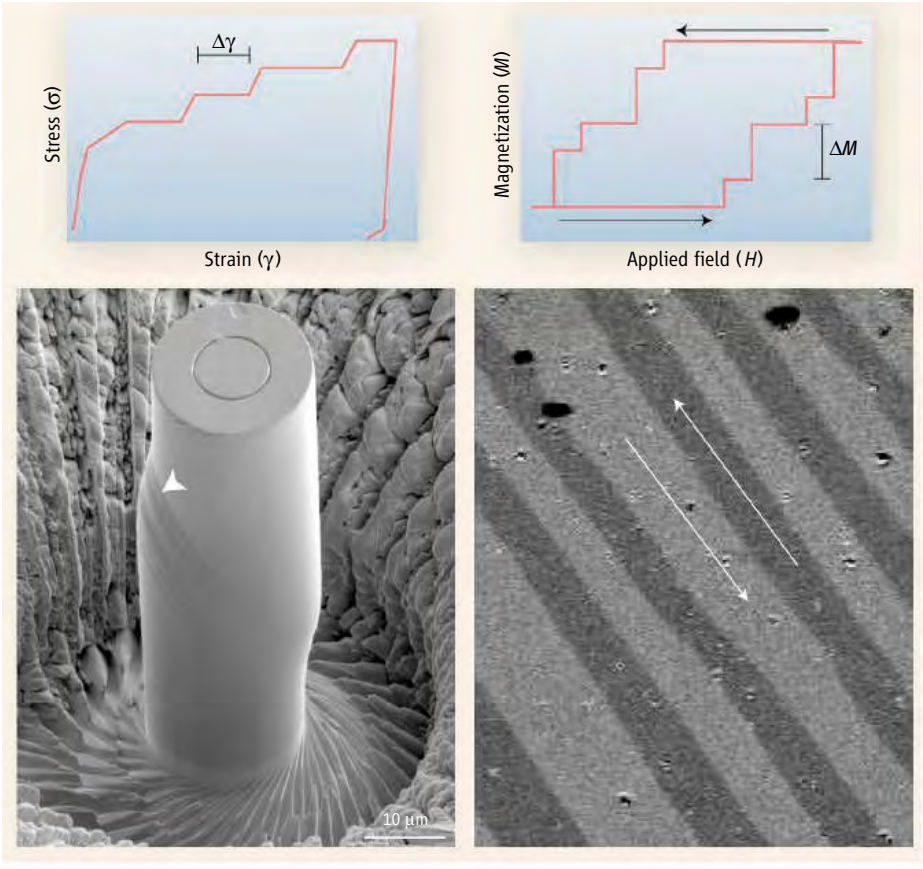

Plastic deformation of crystalline materials resembles ferromagnetic hysteresis. (**Top**) The bursts in a typical stress-strain curve from a micrometer-size sample (**left**) are analogous to the magnetization jumps in a hysteresis cycle of a ferromagnetic thin film (**right**). (**Bottom left**) A cylindrical nickel sample after compression shows sloping slip planes (arrowhead) formed by motion of dislocations. (**Bottom right**) A magneto-optical image of a ferromagnetic alloy, where magnetization is due to the motion of domain walls (arrows).

entangle and become mobile, giving rise to plastic strain. Conventional analysis based on continuum models presumes that the microscopic details of this flow average out above a given size scale, so that fluctuations can safely be ignored.

The powerful experimental methodology developed by Dimiduk *et al*. and Uchic *et al*. (*2*) to manipulate small crystals challenges this viewpoint. Uniaxial compression testing of nickel crystals gives rise to staircase-like stress-strain curves (see the figure, top left) and, at the same time, leads to the formation of slip bands on the sample's surface (figure, bottom left), indicating dislocation-mediated deformation. Moreover, the yield stress, which separates elastic and plastic behavior, increases, as does its fluctuation, as the sample size is decreased (*2*). These experimental results exhibit some common features characteristic of other systems driven out of equilibrium. Bursts of activity (avalanches) and power law–distributed crackling noise are observed in a wide variety of physical systems, but, in particular, they are expected in the close vicinity of a critical point (*3*). Are all these mechanical observations thus interpretable within the realm of statistical mechanics, or more precisely, within the scenario of nonequilibrium phase transitions?

Dislocation dynamics models suggest that the onset of plasticity corresponds to a nonequilibrium phase transition, controlled by the external stress, that separates a jammed phase, in which dislocations are immobile, from a flowing phase (*4*). When the external stress σ is raised toward the yield stress σ_Y, the material responds by larger and larger dislocation avalanches, whose characteristic size diverges at σ_Y. Right at this point, the plastic strain γ would grow indefinitely. We may wonder why macroscopic deformation looks smooth if the internal strain avalanches are scale-free. An important fact is that when most materials deform, the dislocation density increases, leading to strain hardening: The stress required to sustain plastic flow increases with deformation, as if an additional back-stress $\sigma_b = -\Theta\gamma$ were building up inside the crystal (where Θ is a phenomenological coefficient). The back-stress opposes the propagation of large plastic avalanches, inducing a finite characteristic size. For this reason, we do not normally see steps in the stress-strain curves, although dislocation avalanches can still be revealed when probing small scales in acoustic emission experiments (*5*).

The scale-invariant strain bursts observed in crystal plasticity have a counterpart in ferromagnetic materials. In thin films, for instance, irregular steps in the magnetization curve can be seen by magneto-optical methods (*6*) (see the figure, top right). These steps reflect the erratic dynamics of domain walls, separating regions of opposite magnetization M (figure, bottom right). Domain walls are pinned by the impurities present in the material and start to move, magnetizing the sample, when the applied magnetic field H overcomes the coercive field H_c, in a way analogous to dislocations at the yield stress. In addition, large domain wall avalanches are hindered by dipolar interactions that induce a demagnetizing field opposed to the magnetization: $H_d = -\kappa M$ (where κ is the demagnetization factor) (*7*). Thus, hysteresis loops appear smooth in thick samples but look more irregular in thin films where κ vanishes. The close analogy between plasticity and magnetism, which are two apparently very different problems, provides a vivid illustration of the principles of complexity: Collective phenomena often obey simple rules, regardless of the distinctive details.

The experimental results presented by Dimiduk *et al*. open the way to understanding and possibly controlling fluctuations in plastic deformation. This is a topic of great technological importance in view of the current trend toward device miniaturization. Furthermore, this understanding could pave the way for a microscopic theory of the yielding transition of interacting dislocation assemblies. Although this represents a formidable task, important steps in this direction have been taken recently by Zaiser and Moretti (*8*). The theoretical conditions they study are not far from those in the experiments by Dimiduk and co-workers, and indeed the value of the experimentally measured power-law exponent (*1*) is explained by the theory (*8*). These results confirm that plasticity is an excellent playground for statistical mechanics methods and ideas.

References

1. D. M. Dimiduk *et al*., *Science* **312**, 1188 (2006).
2. M. D. Uchic *et al*., *Science* **305**, 986 (2004).
3. J. P. Sethna *et al*., *Nature* **410**, 242 (2001).
4. M.-C. Miguel *et al*., *Phys. Rev. Lett*. **89**, 165501 (2002).
5. M.-C. Miguel *et al*., *Nature* **410**, 667 (2001).
6. E. Puppin, *Phys. Rev. Lett*. **84**, 5415 (2000).
7. S. Zapperi *et al*., *Phys. Rev. B* **58**, 6563 (1998).
8. M. Zaiser, P. Moretti, *J. Stat. Mech.* 10.1088/1742-5468/2005/08/P08004 (2005).
9. M.-C.M. acknowledges financial support from Ministerio de Educación y Ciencia (Spain) and DURSI (Generalitat de Catalunya).

10.1126/science.1127729

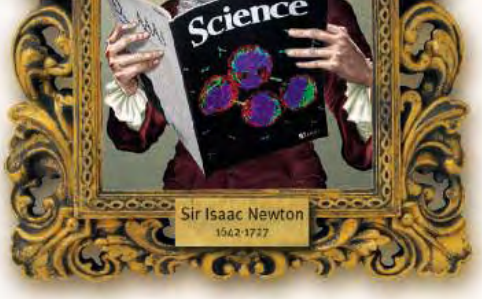

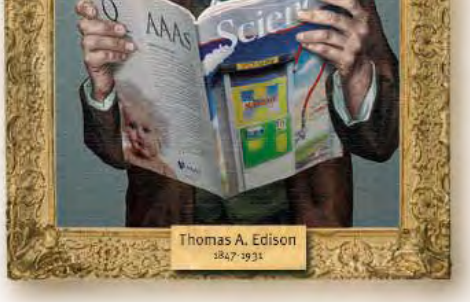

ScienceCareers.org now with Next Wave

IS BIGGER, BETTER AND FREE

ScienceCareers.org is the leading careers resource for scientists. And now it offers even more. In addition to a brand new website with easier navigation, ScienceCareers.org now includes Next Wave, the essential online careers magazine. Next Wave is packed with features and articles to help advance your science career – all for free.

- Hundreds of job postings
- Career tools from Next Wave
- Grant information
- Resume/CV Database
- Career Forum

ScienceCareers.org
We know science AAAS

SCIENCE DIPLOMACY

Iraqi Virtual Science Library Brings Data—and Hope—to the War Zone

The e-mail arrived this spring from a Ph.D. candidate in molecular spectroscopy. His note was brief, but there was no hiding his tension: Living in the Kurdish area of Northern Iraq, he finds it nearly impossible to meet with his adviser at the University of Baghdad—travel is too dangerous. The lack of a full library only compounds his isolation.

But for that scholar and for thousands of other scientists, engineers, and students in the embattled country, a new resource has emerged: The Iraqi Virtual Science Library (IVSL). Conceived by a small group of 2004–2005 AAAS Science & Technology Policy Fellows, the library has grown from a bright idea to a powerful new research tool backed by a spectrum of science and diplomatic interests in the United States and Iraq.

Samir Shakir Mahmud Al-Sumaydi, the Iraqi ambassador to the United States.

The library "provides us an important step toward rebuilding our scientific community," Samir Shakir Mahmud Al-Sumaydi, the Iraqi ambassador to the United States, said at a 3 May news briefing in Washington, D.C. "It … can serve as a vital tool for Iraq's economic growth and the betterment of Iraqi society for many generations to come."

Organizers say the IVSL will deliver scientific articles from over 17,000 journals, plus online educational material and access to funding opportunities. In the months ahead, organizers expect it to offer access to up to 80% of Iraqi S&T professionals and students. Over the next 2 years, control of the library will be transferred to the Iraqis.

Paula Dobriansky, undersecretary of state for Democracy and Global Affairs, used the news briefing to credit the AAAS S&T Policy Fellows for bringing "an extraordinary project" to fruition. The Fellowships were founded in 1973 as a way to make sound science more available to policy-makers. Nearly 2000 scientists and engineers have served as Fellows in a variety of federal departments and agencies.

Over the same three decades, Iraq's once-sophisticated science, engineering, and research sectors have been militarized by Saddam Hussein and further weakened by wars, sanctions, and looting. Since Saddam's fall in 2003, scientists and engineers have been prominent in recovery and rebuilding efforts—and frequently have been targeted by anti-democratic assassins.

Alex Dehgan, a field biologist, has seen the conditions firsthand. As a AAAS Diplomacy Fellow, he was assigned to the U.S. State Department and deployed in 2004 to Iraq to implement and oversee a program that sought to redirect weapons scientists into civil society. On his return, AAAS S&T Policy Fellow Susan Cumberledge, a molecular biologist assigned to the Defense Threat Reduction Agency (DTRA), suggested to Dehgan a digital effort to aid colleagues in Iraq.

A group coalesced to develop the idea. Despite the threatening conditions in Iraq, they saw opportunity: Electricity was scarce, but still, Internet access was growing. So was the culture of Internet cafés.

In addition to Cumberledge and Dehgan, organizers included Fellows D. J. Patil and Ben Perman at DTRA; Ranjiv Khush in the Office of the Science and Technology Adviser to the Secretary of State (STAS); Kwabena Boakye-Yiadon at the Office of the Secretary of Defense; 2001–2002 AAAS Diplomacy Fellow Barrett H. Ripin, the senior science diplomacy officer at State; and Bill McCluskey, director of the International Technology Policy Office at the Department of Defense.

In time, nearly 30 agencies, associations, and publishers joined to support the project, including the National Academies, the United Nations, and Sun Microsystems. The Academies parlayed a modest federal outlay into articles and journals valued at $11 million. Twenty nonprofit and commercial scientific publishers, including federal and academic organizations, are offering deeply discounted access. (*Science* is available to Iraqis through HINARI—the Health InterNetwork Access to Research Initiative.) Sun is donating eight servers to Iraqi research centers.

In beta testing before the rollout this month, about 700 Iraqis used the library. The Institute of Electrical and Electronic Engineers recorded 250 downloads at its electronic library from IVSL users in January; in March, there were more than 10,000.

Ripin said the early usage rates "have exceeded my wildest dreams and expectations and demonstrate how thirsty Iraqis are for information and inclusion in the world scientific community."

Organizers acknowledge the challenges ahead. But Patil noted the Kurdish doctoral student has signed up to use the IVSL, and in that he sees a sign of hope. "This project is all about scientists reaching out to help other scientists," Patil said. "Things will stabilize at some point—we hope they will—and at that point you need to have people ready to step forward."

SCIENCE AND SOCIETY

Science Policy Experts Stress Innovation to Address Challenges

Some of the nation's most influential science policy experts focused on U.S. innovation strategy at the annual AAAS Forum on Science and Technology Policy, urging a deeper commitment to research and development.

In 2 days of discussions and lectures, the experts identified a range of challenges facing the United States and the world in the years and decades ahead—energy, security, climate change, economic growth, education, and public health, among others. The issues are interrelated, they said, and innovation will be crucial to resolving all of them.

"We are at a moment of historic challenge and historic opportunity," said U.S. Energy Secretary Samuel Bodman. "A consensus is building … that this nation must act, and act decisively, to improve mathematics and science education at all levels and expand its support for basic research and development work in the physical sciences."

Other speakers worried that elected officials and the public lack the political will to make an investment that could someday pay

CREDIT: LONNIE SHEKHTMAN

historic dividends. Like Bodman, former AAAS President and Chair Shirley Ann Jackson compared the current era to the time of urgent soul-searching that followed the Soviet Union's launch of Sputnik in 1957.

The Administration and Congress must ensure "real investment in the components of an innovation agenda that are so critical to our nation's economic and national security," said Jackson, president of Rensselaer Polytechnic Institute in Troy, New York.

The 31st annual Forum on S&T Policy was held 20–21 April in Washington, D.C. More than 500 scientists, policy-makers, educators, students, journalists, and others came to hear science policy experts and government officials explore critical issues facing scientists and society.

AAAS President John P. Holdren.

Bodman and John H. Marburger III, director of the White House Office of Science and Technology Policy, emphasized the American Competitiveness Initiative offered by President George W. Bush. The plan would allocate $5.9 billion in the coming budget year, and $136 billion over the next decade, to basic research in the physical sciences, improved mathematics and science education, and tax incentives for private research.

In the Forum's opening address, Marburger predicted the initiative would "assure the future economic competitiveness of our nation."

A bipartisan panel of budget experts offered a more gloomy forecast. Unless escalating long-term costs for Social Security, Medicaid, and Medicare; interest on debt; and other mandatory expenses are offset by increased revenues, the nation faces a devastating debt build-up or crippling budget cuts. A huge tax increase might not be the answer—that could undermine economic growth. All such scenarios would put future R&D commitments at risk, the experts warned.

AAAS President John P. Holdren, the Teresa and John Heinz Professor of Environmental Policy and director of the Science, Technology, and Public Policy Program at Harvard University, moderated a panel on energy policy. To counter global climate change, he said, the world will need to continuously improve energy efficiency over the whole 21st century.

"Everybody who looks at this picture says our investments are inadequate in energy technology innovation in relation to the scale of the challenges and the opportunities," said Holdren, who also serves as director of the Woods Hole Research Center. "Everybody who looks at it says that's particularly true in terms of the climate challenge and also the demands of achieving sustainable prosperity for all the world's population."

In the annual William D. Carey Lecture, Princeton President-Emeritus Harold T. Shapiro struck a cautionary note. To build support for innovation, he suggested, science must call on its often overlooked humanistic dimension to more fully engage with a broad, diverse—and sometimes skeptical—society.

"Friends of science need to understand that ultimately scientists and nonscientists alike are part of a common moral community," Shapiro said. "As a result, the scientific community has an enormous stake not simply in the amount of resources made available to them, but in the nature and health of the society we are trying to build."

–Earl Lane contributed to this report.

CREDIT: (TOP) MARTHA STEWART

INTERNATIONAL

Japanese S&T Minister Details Bold Innovation Plan

Confronted by rising Asian competition and its dependence on foreign oil, Japan is embarking on a visionary plan to become a world innovation leader, Iwao Matsuda, Japan's minister of state for science and technology policy, said during a visit to AAAS.

In an animated and engaging lecture, Matsuda described initiatives that, if successful, would have global impact: gas-free automobiles, technology for monitoring Earth's environment, and medical technology for the detection of microscopic cancers.

The approach is detailed in the third 5-year phase of Japan's basic S&T plan, which began in April. It calls for government research and development investment of 25 trillion yen, or about $221 billion. The plan's guiding assumption: Economic productivity through the development of new technologies is essential to Japan's future competitiveness in the world market.

"This is the first time that such a clearly defined investment strategy has been introduced in the history of Japanese S&T policy," Matsuda said. "I hope very much that setting priorities in this way should lead to more effective R&D investment."

Matsuda, a veteran elected official in Japan, was appointed minister of state for S&T policy in 2005 and is also minister of state for information technology. The 3 May talk in Washington, D.C., was sponsored by the Japanese embassy, the Washington Science Policy Alliance, and AAAS.

"Minister Matsuda's speech provided us with an excellent overview of Japan's S&T plans," said Albert Teich, director of Science & Policy at AAAS. "Watching his energy and enthusiasm should serve as inspiration for our own efforts in the United States."

–Lonnie Shekhtman

SCIENCE POLICY

AAAS Staff Discuss NSF, Education on Capitol Hill

Senior AAAS staff members visited Capitol Hill in May to discuss two topics directly related to long-term U.S. innovation strategy: the National Science Foundation (NSF) budget and plans to improve Advanced Placement science curriculum in American high schools.

Alan I. Leshner, chief executive officer of AAAS and executive publisher of *Science,* told the Senate Commerce Subcommittee on Science and Space that despite an 8% budget increase proposed for NSF in 2007, the agency will be able to fund fewer than 25% of the research proposals it recieves.

"This matters because it means a great amount of very important work will still go unfunded," Leshner testified on 2 May.

He said he was further concerned that the NSF budget for education and human resources would increase just 2.5% in the proposed spending plan—leaving it 20% below 2004 funding in real terms.

Shirley Malcom, head of Education and Human Resources at AAAS, appeared later that day on an NSF/College Board panel convened to discuss new ways to teach Advanced Placement science courses in U.S. high schools. NSF is underwriting a redesign of the courses with a $1.8 million grant; the curriculum is slated for an autumn 2009 launch.

Malcom compared current instruction to teaching isolated scenes of a play without ever telling students the play's full story. "Let's go for things that are important, for the knowledge that is significant," Malcom said. "Can we set them up for a lifetime of learning?"

Improvement in AP curriculum would ripple through all high school science instruction, she said.

–Paul Recer

Isn't it time science discovered you?

GE & Science Prize for Young Life Scientists was established in 1995, and is presented by *Science*/AAAS and GE Healthcare. The prize was established to help bring science to life by recognizing outstanding PhDs from around the world and reward their research in the field of molecular biology.

GE & Science Prize for Young Life Scientists

This is your chance to gain international acclaim and recognition for yourself and your faculty, as well as to turn your scientific ideas into reality. If you were awarded your PhD in molecular biology* during 2005, describe your work in a 1,000-word essay. Then submit it for the 2006 GE & Science Prize for Young Life Scientists. Your essay will be reviewed by a panel of distinguished scientists who will select one grand prizewinner and four regional winners.

The grand prizewinner will get his or her essay published in *Science*, receive US$25,000, and be flown to the awards ceremony in Stockholm, Sweden. Entries should be received by **July 15, 2006**.

GE & Science Prize for Young Life Scientists: Life Science Re-imagined.

For more information on how to enter, go to www.gehealthcare.com/science

Dr. Ahmet Yildiz
Grand prizewinner 2005 for his essay, "Elucidating the Mechanism of Molecular Motor Movement."

Established and presented by:

Science AAAS

* For the purpose of this prize, molecular biology is defined as "that part of biology which attempts to interpret biological events in terms of the physico-chemical properties of molecules in a cell" (McGraw-Hill Dictionary of Scientific and Technical Terms, 4th Edition).

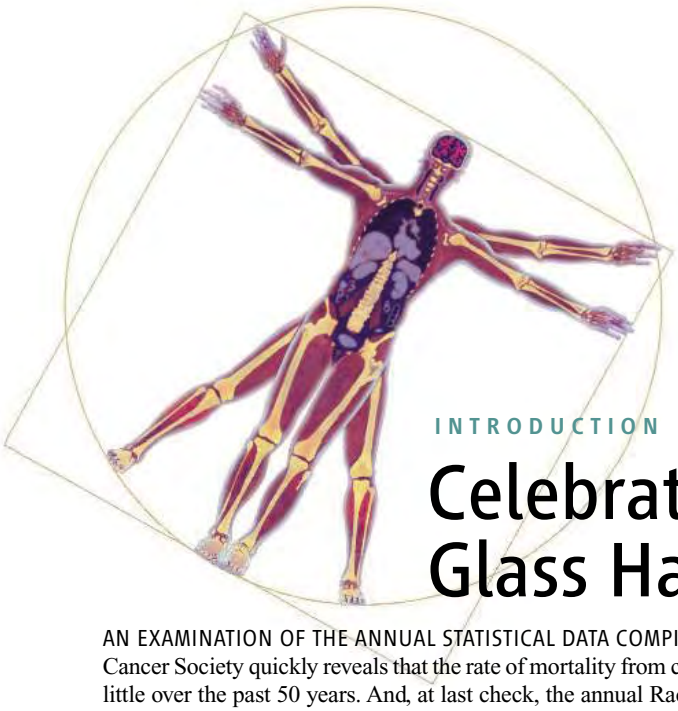

INTRODUCTION

Celebrating a Glass Half-Full

AN EXAMINATION OF THE ANNUAL STATISTICAL DATA COMPILED BY THE AMERICAN Cancer Society quickly reveals that the rate of mortality from cancer has changed very little over the past 50 years. And, at last check, the annual Race for the Cure is being scheduled well into the future. So why has *Science* chosen this particular moment to celebrate the cancer research field?

In part, it's because targeted cancer therapies, cancer biomarkers, and genomic medicine are in the midst of a transition from hype to clinical reality. As articulated by Varmus in the opening Perspective of our special section (p. 1162), ". . . a description of cancer in molecular terms seems increasingly likely to improve the ways in which human cancers are detected, classified, monitored, and (especially) treated." To help nonspecialist readers understand how the molecular description of cancer might one day form the basis of a new patient-centered model of cancer care, *Science* has prepared a foldout poster illustrating the concept and how it might be implemented. Several Perspectives expand on topics covered in the poster but also point out important obstacles to that vision. Varmus, for example, emphasizes the need for changes in the "culture" of oncology, including the formation of stronger collaborations among researchers, clinical oncologists, industry, and regulatory agencies. The pressing need for new working partnerships is a theme echoed by Dalton and Friend (p. 1165), who discuss the limitations of current efforts to identify and validate molecularly based biomarkers for cancer diagnosis and treatment, and by Weissleder (p. 1168), who outlines how new molecular imaging technologies might contribute to future models of cancer care.

Two additional Perspectives focus on new molecularly targeted drugs that have shown promise in the clinic. Kerbel (p. 1171) discusses several mechanistic models that might explain why antiangiogenesis drugs are most effective in cancer patients when delivered in combination with conventional chemotherapy, and Baselga (p. 1175) reviews the history and clinical activity of small-molecule and antibody-based drugs that inhibit protein tyrosine kinases.

Two News stories discuss emerging research areas that may one day occupy a prominent position on a revised version of our poster. Garber (p. 1158) describes how an old discredited idea—that tumor cells rely on glycolysis for energy—has been resurrected and is driving the development of new anticancer drugs. Exploring another contentious topic, Marx (p. 1160) details the debate over whether the cellular recycling process called autophagy is a tumor suppressor or promoter.

In related online resources, *Science*'s Signal Transduction Knowledge Environment (STKE) (stke.sciencemag.org) features a Perspective by Garcia that explores the role of hypoxia-inducible factor signaling in cancer progression and another by Harms and Chen that discusses a splice variant of the c-H-*ras* oncogene with potential tumor-suppressor activity. In Perspectives in *Science*'s Science of Aging Knowledge Environment (SAGE) (sageke.sciencemag.org), Fuller discusses the relationship between stem cell aging and cancer, and Medrano *et al*. examine why older men are at a greater risk for melanoma than are older women.

We hope that after perusing these articles, readers will come away feeling that in cancer research, the glass is indeed (at least) half-full.

–PAULA A. KIBERSTIS AND JOHN TRAVIS

CREDIT: K. SUTLIFF/*SCIENCE*

Frontiers in Cancer Research

CONTENTS

News

1158 Energy Deregulation: Licensing Tumors to Grow

1160 Autophagy: Is It Cancer's Friend or Foe?

Perspectives

1162 The New Era in Cancer Research
H. Varmus

Poster: Cancer Treatment Gets Personal

1165 Cancer Biomarkers—An Invitation to the Table
W. S. Dalton and S. H. Friend

1168 Molecular Imaging in Cancer
R. Weissleder

1171 Antiangiogenic Therapy: A Universal Chemosensitization Strategy for Cancer?
R. S. Kerbel

1175 Targeting Tyrosine Kinases in Cancer: The Second Wave
J. Baselga

See also related Report page p. 1228; Science *Express Report by S. Matoba* et al.; *STKE and SAGE KE material on p. 1099 or at www.sciencemag.org/sciext/cancer/ Poster at www.sciencemag.org/sciext/cancerposter/ Podcast at www.sciencemag.org/about/podcast.dtl*

Science

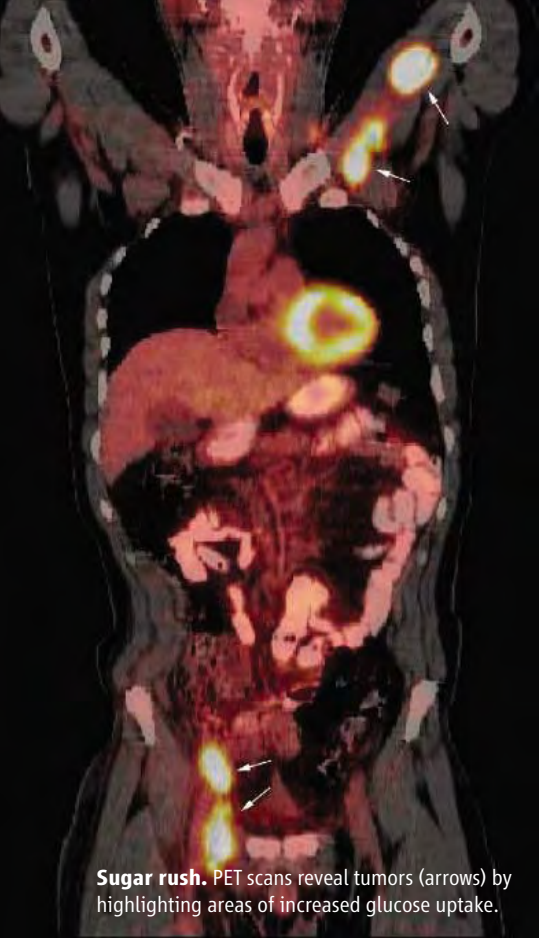

Sugar rush. PET scans reveal tumors (arrows) by highlighting areas of increased glucose uptake.

NEWS

Energy Deregulation: Licensing Tumors to Grow

Taking their cue from a controversial, 80-year-old theory of cancer, scientists are reexamining how tumors fuel their own growth and finding new ways to cut off their energy supply

In a widely cited paper published 6 years ago, cancer biologists Robert Weinberg of the Massachusetts Institute of Technology and Douglas Hanahan of the University of California, San Francisco, described six hallmarks of cancer cells, including their ability to invade other tissues and their limitless potential to replicate. Last month, at the annual meeting of the American Association of Cancer Research, Eyal Gottlieb launched a lecture with this provocative claim: "I believe I'm working on the seventh element, which is bioenergetics."

Gottlieb, a biologist at the Beatson Institute for Cancer Research in Glasgow, U.K., notes that tumor cells need an unusual amount of energy to survive and grow. "The overall metabolic demand on these cells is significantly higher than [on] most other tissues," he says.

Tumors often cope by ramping up an alternative energy production strategy. For most of their energy needs, normal cells rely on a process called respiration, which consumes oxygen and glucose to make energy-storing molecules of adenosine triphosphate (ATP). But cancer cells typically depend more on glycolysis, the anaerobic breakdown of glucose into ATP. This increased glycolysis, even in the presence of available oxygen, is known as the Warburg effect, after German biochemist Otto Warburg, who first described the phenomenon 80 years ago. Warburg thought this "aerobic glycolysis" was a universal property of cancer, and even its main cause.

Warburg won a Nobel Prize in 1931 for his earlier work on respiration, but his cancer theory was gradually discredited, beginning with the discovery of tumors that didn't display any shift to glycolysis. Ultimately, the ascendancy of molecular biology over the last quarter-century completely eclipsed the study of tumor bioenergetics, including Warburg's ideas. The modern view of cancer is that it's a disease of genes, not one of deranged energy processing.

Now, a revival in research on tumor bioenergetics suggests it could be both. A growing stream of papers is making the link between cancer genes and the Warburg effect, indicating that bioenergetics may lie at the heart of malignant transformation. For example, in a paper published online by *Science* this week (www.sciencemag.org/cgi/content/abstract/1126863), Paul Hwang's group at the National Heart, Lung, and Blood Institute in Bethesda, Maryland, reveals that *p53*, one of the mostly commonly mutated genes in cancer, can trigger the Warburg effect. And last year, Arvind Ramanathan and Stuart Schreiber of the Broad Institute in Cambridge, Massachusetts, reported that in cells genetically engineered to become cancerous, glycolytic conversion started early and expanded as the cells became more malignant. They concluded that the cancer-gene model and the Warburg hypothesis "are intimately linked and fully consonant."

This idea remains controversial. Weinberg, for example, is a prominent skeptic. In his view, the Warburg effect and related metabolic changes are consequences of cancer, not major contributors to it: "It is a stretch to say that all this lies at the heart of cancer pathogenesis." Nevertheless, several companies and labs are now testing anticancer drugs designed to exploit the bioenergetics of tumors.

A new model of cancer

The revival in cancer bioenergetics began in the mid-1990s when radiologists showed that positron emission tomography (PET) imaging could detect and map many tumors. In PET, an injected glucose analog highlights tumors, which are hungrier for glucose than normal cells are. "PET imaging," says Schreiber, "suggests that the glycolytic switch even precedes the angiogenic switch": the point at which tumors begin making their own blood vessels.

Other evidence for metabolic differences in cancer accumulated at about the same time. Gregg Semenza of Johns Hopkins School of Medicine in Baltimore, Maryland, showed that a protein, hypoxia-inducible factor-1 (HIF-1), raised levels of glycolytic enzymes in cells lacking oxygen, and many hypoxic tumors contain elevated levels of HIF-1 (*Science*, 5 March 2004, p. 1454). In 1997, Chi Dang, also at Johns Hopkins, reported that the *myc* oncogene could turn on glycolysis. Furthermore, genes involved in energy production are mutated in several rare familial cancer syndromes.

One way that cancer cells might increase glycolysis is through Akt, an important pro-survival signaling protein. In 2004, Craig Thompson, a cancer biologist at the University of Pennsylvania, reported that activated Akt, independent of HIF-1, could convert cancer cells to start using glycolysis. Akt had earlier been shown to induce glucose transporters to take glucose into the cell, and Nissim Hay of the University of Illinois, Chicago, showed that Akt signals a glycolytic enzyme, hexokinase, to bind tightly to mitochondria, the organelles in which most of the cell's ATP is normally made during respiration. This allows hexokinase to use ATP from mitochondria to jump-start glycolysis. Thompson has since linked Akt to other glycolytic functions.

Thompson's model of how tumors make energy starts with upstream gene mutations that activate Akt and ends with cancer cells continuously consuming glucose, both aerobically and anaerobically. Others propose that cancer cells rely almost completely on glycolysis and largely shut down respiration, as Warburg originally reported. Because glycolysis is far less efficient than respiration, producing two ATPs per glucose molecule versus roughly 36 for respiration, that raises the question of how cancer cells benefit from the Warburg effect. "Is there a selective advantage?" asks Ajay Verma, a biologist at the Uniformed Services University of the Health Sciences in Bethesda, Maryland. "That hasn't been answered very well."

Cancer cells could benefit from glycolysis in many ways. Gottlieb and Thompson contend that

CREDIT: RICHARD K. J. BROWN/UNIVERSITY OF MICHIGAN HEALTH SYSTEM

a boost in glycolysis, added to respiration—which continues unabated—generates more energy more quickly than in normal cells that overwhelmingly rely on respiration. And because a glycolytic cancer cell is constantly slurping up nutrients, whereas a normal cell typically needs outside signals for permission to do this, such energy independence "empowers the [cancer] cell to grow," says Thompson. It doesn't need to break down amino acids and fatty acids to generate energy as most normal human cells commonly do and can turn them instead into the proteins and lipids necessary for growth.

Other potential benefits: Verma's work suggests that glycolysis leads directly to HIF-1 activation, which further boosts metabolism, and also stimulates angiogenesis and invasiveness. And in cases in which respiration is impaired, Dang suggests that shutting it down protects cancer cells from mitochondria damage that occurs when cellular respiration functions abnormally under hypoxic conditions.

But does the Warburg effect cause cancer, as Warburg claimed? Probably not. "The glycolytic shift is not absolutely required for transformation," says Thompson. But, he adds, it gives cancer cells "a higher metastatic potential and a higher invasive potential … because they're now cell-autonomous for their own metabolism." Gottlieb agrees: "I believe [increased glycolysis] is important for sustaining tumors rather than inducing them."

Causality may not matter much when it comes to therapies. After all, angiogenesis doesn't cause cancer, but blocking it can stop cancer growth. Many early events in cancer "may not be relevant at the stages where we start treating those tumors," notes Gottlieb. "Well, the bioenergetic demand will always be there and will always be required."

Energy crisis

Drugs targeting tumor bioenergetics are on the way. Most exploit a tumor's increased reliance on glycolysis. Threshold Pharmaceuticals Inc., a biotech company in South San Francisco, California, is already testing two such drugs in cancer patients: a chemotherapy compound conjugated to glucose, and a glucose analog that cannot be metabolized, thus shutting down glycolysis.

Hexokinase, because it catalyzes the first step in glycolysis and can block cell death, is another key target. Hay, for example, proposes that drugs causing hexokinase to separate from mitochondria could treat cancer, by both damping down glycolysis, indirectly blocking a signaling molecule called mTOR and causing apoptosis by another mechanism. Directly inhibiting the enzyme is another strategy. In 2004, Johns Hopkins researchers reported that a hexokinase inhibitor, 3-bromopyruvate, completely eradicated advanced glycolytic tumors in all mice treated. Chemists at the M. D. Anderson Cancer Center in Houston, Texas, are now developing 3-bromopyruvate analogs for eventual clinical trials.

Other potential drug targets exist. Last year, Thompson identified an enzyme, ATP citrate lyase, that allows cancer cells to overcome a natural check on glycolysis. Inhibiting it blocks growth of tumors in mice. And this March, Dang and Nicholas Denko of Stanford University in California separately reported that another enzyme, pyruvate dehydrogenase kinase (PDK), acts to shut down mitochondrial respiration and protect cells in low-oxygen conditions. "One can imagine that by blocking PDK activity we can actually trigger cells to commit suicide," Dang says.

Compounds that limit glycolysis would, in theory, kill cancer cells while sparing normal cells, which can burn amino acids and fatty acids for energy. "When [cancer] cells are engaged in high-throughput aerobic glycolysis, they become addicted to glucose," says Thompson. "So if you suddenly take away their ability to do high-throughput glucose capture and metabolism, the cell has no choice but to die."

How prevalent are glycolytic tumors? Using PET imagery, which maps glucose uptake, as a surrogate for the Warburg effect, Thompson estimates that between 60% and 90% of tumors make the shift to glycolysis. Gottlieb contends that most tumors turn to glycolysis only after oxygen disappears. But their special bioenergetics, he agrees, make them targetable by drugs.

Some remain dubious. Michael Guppy, a biochemist recently retired from the University of Western Australia in Perth, even contends that the Warburg effect is a myth. Many researchers reporting the Warburg effect, Guppy says, do not accurately measure oxygen consumption in their cancer cells, sometimes ignoring the fact that cells can break down other molecules besides glucose to generate ATP. As a result, he contends, they overestimate the role of glycolysis. In a 2004 paper analyzing studies he found meeting his criteria for accuracy, Guppy reported that cancer cells, on average, were no more glycolytic than normal cells. So "a strategy for controlling cancer that relies on cancer cells being the sort of cell that cannot use oxygen when it's available … is wrong," he says. Dang agrees that oxygen consumption could be measured more carefully but says Guppy "has ignored some key work in high-impact journals that negate his contention." He adds that the fact that PET detects tumors is more evidence for a high level of glucose uptake.

Even those at the vanguard of tumor bioenergetics acknowledge, however, that they must fully demonstrate how tumors inherently switch to glycolysis to meet energy needs. "We're still in the middle of absolutely proving that [system]," says Thompson. "It's a much more complex and dynamically regulated thing than anything else that we study in biology today." Until the results are in, the seventh hallmark of cancer may have to wait.

–KEN GARBER

Ken Garber is a science writer in Ann Arbor, Michigan.

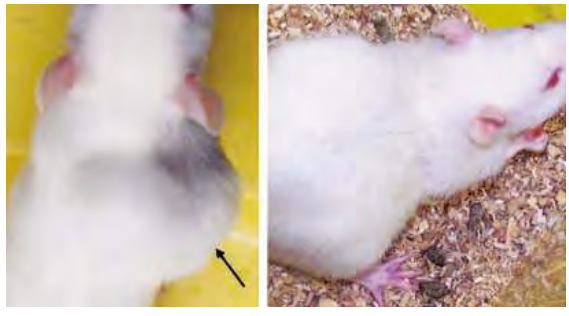

Energy blocker. The large tumor on a rat's back (*left*, arrow) disappeared (*right*) after treatment with an experimental drug that interferes with cellular energy production.

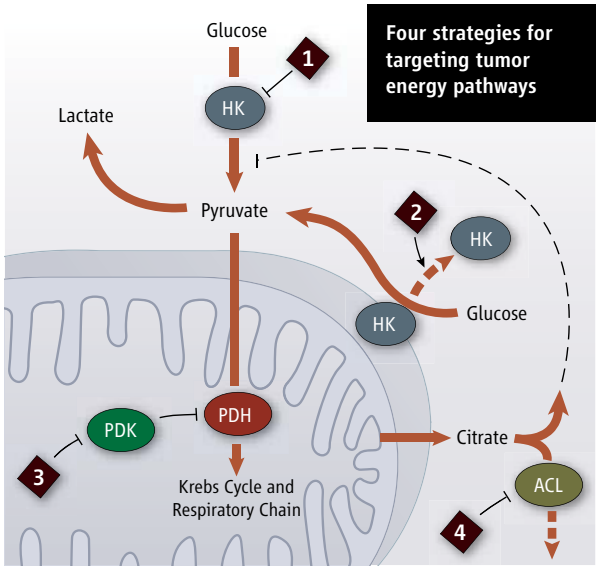

Powering down. (1) Hexokinase (HK) inhibitors interfere with the first step in glycolysis; (2) Drugs dissociating hexokinase from the mitochondrial membrane cause apoptosis and interfere with growth pathways; (3) Inhibitors of pyruvate dehydrogenase kinase (PDK) funnel pyruvate into defective respiratory machinery and cause apoptosis; (4) Inhibitors of ATP citrate lyase (ACL) cause citrate to build up, inhibiting glycolysis. (PDH = pyruvate dehydrogenase).

CREDIT (TOP): JOHNS HOPKINS MEDICINE/YOUNG KO

NEWS

Autophagy: Is It Cancer's Friend or Foe?

Cells rely on autophagy to recycle their components, and much evidence favors the idea that this "self-eating" suppresses tumor development. But other data suggest that autophagy fosters tumor development and actually protects cancer cells from treatments

Environmentalists have long proclaimed the importance of recycling. Now cell biologists are delivering a similar message. Within the past few years, they have been working out the genetic and biochemical underpinnings of a cellular recycling system known as autophagy, and what they are learning could shed light on a variety of diseases—cancer among them.

Autophagy has long been known for its roles in protecting cells against stresses such as starvation and in eliminating defective cellular constituents, including subcellular structures such as the energy-generating mitochondria. It is essentially a form of self-cannibalism—hence the name, which means "eating oneself"—in which the cell breaks down its own components. Cells can then recycle the resulting degradation products, using them to provide the energy and cellular building blocks necessary for their survival (*Science*, 5 November 2004, p. 990).

The cancer connection, which has cropped up more recently, comes from several research teams that have found that autophagy appears to suppress tumor development in animals. This includes demonstrations that some tumor-suppressor genes stimulate autophagy and that certain cancer-causing oncogenes inhibit it. But although such work suggests that boosting autophagy will prevent or treat cancers, "the situation is not so clear," cautions Patrice Codogno of the University of Paris-Sud in France.

Indeed, researchers continue to wrestle with the crucial question of whether some tumors exploit autophagy in order to survive. The process is known to kick in when cells encounter nutrient shortages. And because cancer cells in a growing tumor can find themselves short of needed nutrients, inducing autophagy could give them a hand. There's also evidence that in some cases autophagy helps cancer cells fight off chemotherapeutic drugs, although in others it may be part of the drugs' killing mechanisms. "There's controversy about whether one should be turning autophagy on or off to treat cancer," says Beth Levine of the University of Texas Southwestern Medical Center in Dallas.

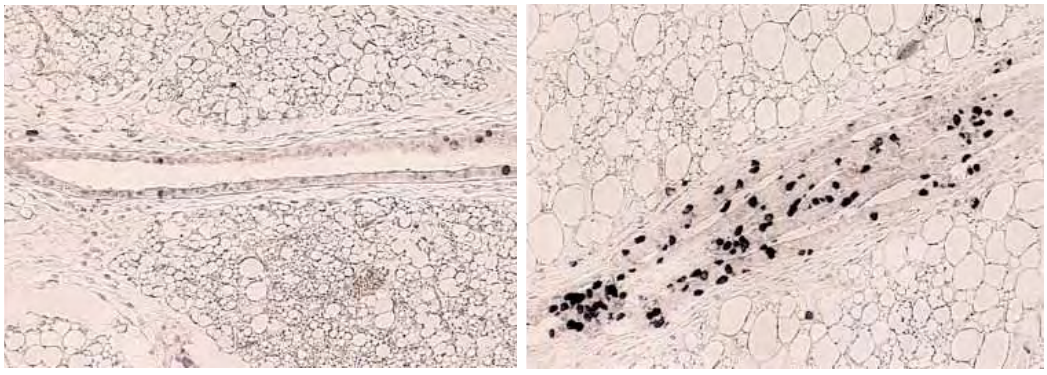

Boost for growth. As indicated by the black dots, which mark the nuclei of dividing cells, mammary duct cells from mice with one *beclin-1* gene inactivated (*right*) show increased growth compared to duct cells from normal mice (*left*).

Early neglect

Suspicions that autophagy plays a role in cancer first arose about 3 decades ago when researchers noted that cancer cells seemed deficient in the process compared to normal cells. They made this determination either by measuring the rates of degradation of long-lived proteins or by looking for the characteristic double-membraned vacuoles that form in cells undergoing autophagy. These vacuoles encircle the cellular cargo destined for degradation and then fuse with lysosomes, which carry a host of enzymes for digesting proteins and other materials.

At the time, however, researchers couldn't do much with the cancer connection, mainly because the genes involved in autophagy hadn't been identified. The early work implicating autophagy defects was "largely ignored by the cancer community because the evidence was mainly correlative," recalls Levine.

That didn't change until the early 1990s when yeast researchers, particularly Yoshinori Ohsumi of the National Institute for Basic Biology in Okazaki, Japan, Daniel Klionsky of the University of Michigan, Ann Arbor, and Michael Thumm of Georg-August University in Göttingen, Germany, began teasing out the genes needed for autophagy in that simple eukaryote. So far, more than 20 yeast autophagy genes have been unearthed, several of which have counterparts in mammals.

Levine, who didn't set out to study autophagy, identified one such counterpart in 1998, helping to spark the current wave of interest in autophagy's role in cancer. Her team found the gene, now called *beclin-1*, while screening for binding partners for the protein encoded by the mouse *bcl-2* oncogene. The sequence of the new gene, which also occurs in humans, resembled that of the yeast autophagy gene 6 (*ATG6*), and the Dallas group showed that *beclin-1* could repair the autophagy defect in yeast with no *ATG6* activity.

Even more interestingly, Levine and her colleagues noted that the human gene maps to a chromosomal location that's frequently deleted in ovarian, breast, and prostate cancers—an indication that the site harbors a tumor-suppressor gene. The Levine team also found that *beclin-1* expression is much reduced in invasive breast cancer cells compared to normal cells.

Unlike most tumor suppressors, only one copy of the cell's two *beclin-1* genes is usually lost in breast cancer. So Levine and her colleagues recreated this situation by knocking out a single copy of the gene in mice. The resulting animals showed both a decrease in autophagy and an increased frequency of cancers of the lungs and liver as well as lymphomas, the team reported in the December 2003 *Journal of Clinical Investigation*. The mice also developed benign breast tumors.

A team led by Arnold Levine (not related to Beth Levine) of the University of Medicine and Dentistry of New Jersey–Robert Wood Johnson Medical School in News Brunswick and Nathaniel Heintz of Rockefeller University in New York City reported similar results the same month in the *Proceedings of the National Academy of Sciences*. That "pinpoints that *beclin-1* is a tumor suppressor," says team member Shengkan Jin of the Robert Wood Johnson Piscataway campus.

Other researchers have connected previously identified tumor-suppressor genes to

CREDITS: BETH LEVINE/UT SOUTHWESTERN

autophagy regulation. Codogno's team showed that one of these is *PTEN*, which inhibits a major cell growth stimulatory pathway and, as a result of that, a protein called TOR. Because TOR normally curbs autophagy, the process gets ramped up. Jin, Arnold Levine, and their colleagues have shown that the well-known tumor-suppressor gene *p53* also increases autophagy by inhibiting TOR. And Adi Kimchi and her colleagues at the Weizmann Institute of Science in Rehovot, Israel, have found that the tumor suppressor known as DAPK (for death-associated protein kinase) is yet another autophagy stimulator.

Conversely, many oncogenes appear to inhibit autophagy. Codogno and his colleagues have found that overactivity of the oncogene *AKT* curbs autophagy—the expected result because it promotes TOR activity. And last month in Washington, D.C., at the annual meeting of the American Association for Cancer Research (AACR), John Cleveland of St. Jude Children's Research Hospital in Memphis, Tennessee, presented as-yet-unpublished data from his lab indicating that the carcinogenic effects of the well-known *myc* oncogene are at least partly due to its ability to decrease autophagy. The evidence, obtained in collaboration with Michael Kastan, also at St. Jude, includes the finding that *myc* activity suppresses the expression of *ATG* genes 8 and 9. "Oncogenes suppress autophagy during tumor development," Cleveland concludes.

Then there's *bcl-2*, the gene that helped Beth Levine and her colleagues identify *beclin-1*. This oncogene promotes the survival of cancer cells by inhibiting apoptosis, a process by which dysfunctional cells kill themselves. Evidence published by Levine and her colleagues last September in *Cell* raises the possibility that *bcl-2* prevents autophagic cell death as well. Although autophagy is often protective, it can kill cells in some circumstances; they essentially digest themselves to death.

The researchers showed that binding of the Bcl-2 protein to the protein product of *beclin-1* inhibits autophagy. Levine suggests that this suppression by Bcl-2 helps keep autophagy in check under normal conditions. But if *bcl-2* activity is excessive, as it is in some cancers, the consequent suppression of autophagy could allow damaged cells to complete a cancerous transformation.

Killing abnormal cells is not the only way that autophagy could protect against tumor development, however. Autophagy's recycling ability can eliminate damaged cell components, especially organelles such as the mitochondria. Indeed, Klionsky says, it "is virtually the only way to get rid of whole organelles." Getting rid of defective mitochondria, which release abnormally large amounts of DNA-damaging reactive oxygen species, could help protect cells against cancer-causing mutations, Jin and others suggest.

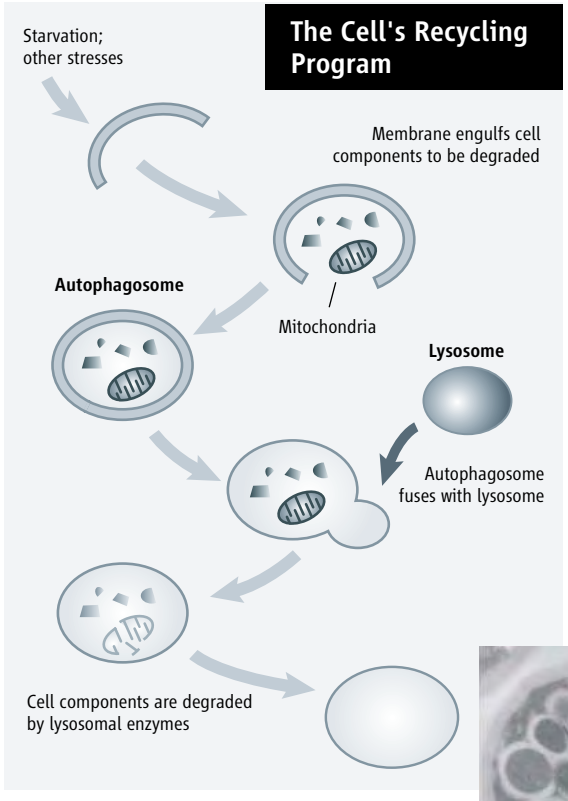

Autophagy in action. Stresses such as starvation lead to formation of double-membrane-bound autophagosomes that engulf cellular components destined for degradation by lysosome enzymes. The micrograph (*inset*) shows autophagosomes in yeast.

Heart of the controversy

Although many cancer therapies are thought to kill tumor cells by inducing apoptosis, researchers have begun to find signs of autophagy in tumor cells exposed to chemotherapy or radiation. The chemotherapeutic drugs that appear to trigger autophagy include tamoxifen, rapamycin, and arsenic compounds. "Many treatments induce autophagy rather than apoptosis," says Seiji Kondo of M. D. Anderson Cancer Center in Houston, Texas.

The crucial question, however, is whether autophagy helps kill tumor cells or instead protects them from the therapies' cell-damaging effects. There's evidence on both sides.

One example favoring a cancer-killing role for autophagy involves the chemotherapeutic drug rapamycin, which is a known TOR inhibitor. Kondo and his colleagues have found that the rapamycin sensitivity of cells derived from highly malignant brain tumors called gliomas correlates with the drug's ability to induce autophagy. The researchers also found that drugs that increase autophagy boost rapamycin's ability to kill glioma cells.

In contrast, at the AACR meeting, Ravi Amaravadi, who works in Craig Thompson's lab at the University of Pennsylvania, presented results supporting the idea that autophagy can protect against a chemotherapeutic drug. This work involved genetically engineered mice that overexpress the *myc* oncogene and develop lymphomas as a result. The animals also carried an altered *p53* gene that can be activated by treatment with tamoxifen. The resulting *p53* activity induces apoptosis, leading to a temporary regression of the animals' lymphomas.

The Pennsylvania team showed that chloroquine, a drug that previous studies had suggested was an autophagy inhibitor, enhanced the animals' responses to tamoxifen treatment. "Cancer cells, when faced with cytotoxic damage [from chemotherapy], turn to autophagy. It's a mechanism that cancer cells adopt to survive," Thompson maintains.

This situation is complicated by results Cleveland described in his AACR talk. His team found that chloroquine can suppress *myc*-induced lymphoma development in mice. But Cleveland and his colleagues also concluded that chloroquine is an autophagy inducer, not an inhibitor. So although their mouse results were similar, the two groups came to diametrically opposite interpretations about whether autophagy enables chemotherapies to kill cancer cells or instead protects them from the drugs.

The answer to the question of whether inducers of autophagy will be good or bad for cancer therapies may vary depending on the nature of the cancer, the drug, or both. The drug temozolomide (TMZ), which is currently in clinical trials for treating gliomas, provides an illustration of this kind of complexity. Kondo's team found that a drug that inhibits the late stages of autophagy enhanced TMZ's antitumor effects, whereas a different drug that blocks an early stage of autophagy suppressed them. "We have to understand all the players to predict whether a therapy [promoting autophagy] will protect the cells or kill them," Kimchi says. Obviously, autophagy researchers still have their work cut out for them.

–JEAN MARX

CREDITS (TOP TO BOTTOM): J. MOGLIA/*SCIENCE*; D. KLIONSKY/UNIVERSITY OF MICHIGAN

PERSPECTIVE

The New Era in Cancer Research

Harold Varmus

For many years, discoveries about the genetic determinants of cancer appeared to be having only minor effects on efforts to control the disease in the clinic. Following advances made over the past decade, however, a description of cancer in molecular terms seems increasingly likely to improve the ways in which human cancers are detected, classified, monitored, and (especially) treated. Achieving the medical promise of this new era in cancer research will require a deeper understanding of the biology of cancer and imaginative application of new knowledge in the clinic, as well as political, social, and cultural changes.

The conquest of cancer continues to pose great challenges to medical science. The disease is notably complex, affecting nearly every tissue lineage in our bodies and arising from normal cells as a consequence of diverse mutations affecting many genes. It is also widespread and lethal; currently the second most common cause of death in the United States, it is likely to become the most common in the near future. Despite large federal and industrial investments in cancer research and a wealth of discoveries about the genetic, biochemical, and functional changes in cancer cells, cancer is commonly viewed as, at best, minimally controlled by modern medicine, especially when compared with other major diseases. Indeed, the age-adjusted mortality rate for cancer is about the same in the 21st century as it was 50 years ago, whereas the death rates for cardiac, cerebrovascular, and infectious diseases have declined by about two-thirds (*1*).

A Perspective on the History of Cancer Research

The recent death of Joseph Burchenal (*2*), one of the pioneers in the use of chemotherapy, provides a vantage point for thinking about the history and the future of cancer research and its implications for control of the disease. Just over 50 years ago, Burchenal (Fig. 1) and his colleagues used analogs of folic acid, methotrexate, and of a nucleoside, 6-mercaptopurine, to induce profound and sustained remissions in children with aggressive leukemias (*3*). This event—viewed in combination with related, contemporaneous work by Sidney Farber and by Emil Frei and Emil Freireich—was revolutionary: For the first time, drugs of known chemical composition that interfered with enzymes engaged in a specific biological process, DNA replication, were used to treat cancers successfully in a rational manner. The several successful cases inspired the design of clinical trials, permitting the measurement of gradual improvements in treatment protocols. The resulting progress against childhood leukemias, despite the toxicity of the drugs and the lethality of the diseases, built confidence in the notion that biology and chemistry could be harnessed to benefit patients with cancer (*4*).

At the time that Burchenal began treating leukemias, little was known about the causes of cancers or about the genetic and molecular mechanisms by which they arise from normal cells. His therapeutic strategy was based largely on the premise that cancer cells replicate their DNA and divide more frequently than most normal cells and hence would be more sensitive to DNA damage. Although this concept has proven to be an overly simplistic explanation, an emphasis on damage to DNA and the mitotic apparatus has guided the development of the many chemotherapeutic regimens and radiotherapies that have been used for nearly all types of cancers over the past 50 years. The results have ranged from modest at best (in the advanced stages of some of the most common carcinomas of adults), to partially protective against subsequent metastasis (when used as an adjuvant to surgery in the early stages of such diseases), to highly effective (in the treatment of even advanced stages of testicular cancers, some lymphomas, and a few other tumor types).

During most of those 50 years, pharmaceutical chemistry continued to serve cancer patients much more effectively than did cancer biology. Laboratory-based investigations into the nature of cancer cells and clinical efforts to control cancer often seemed to inhabit separate worlds. In the world of laboratory research, the characterization of cancer viruses of animals in the 1960s and 70s, the discovery of the first proto-oncogenes and tumor suppressor genes in the 1970s and 80s, the integration of the products of those genes into cell signaling pathways in the 1990s, and even the repeated unveilings of mutant genes implicated in human cancers beginning in the early 1980s—all seemed to have little or no impact on the methods used by clinicians to diagnose and treat cancers.

The Rise of Molecular Oncology

During the past decade, perceptions about this situation have been changing rapidly. Understanding the genetic and biochemical mechanisms by which cancers arise and behave is now widely believed to portend improvements in the way we detect, classify, monitor, and treat these diseases. This message has been driven home, gradually but effectively, by a variety of new and less toxic agents for treating cancers—hormones, antibodies, and enzyme-inhibitory drugs—and, especially, by the dramatic arrival of a near-miraculous drug, imatinib (Gleevec), a "molecule-specific" agent that induces nearly complete and sustained remissions in nearly all patients in the early stages of chronic myeloid leukemia (CML), by blocking a protein-tyrosine kinase activated by a well-studied chromosomal translocation (*5*).

These new therapies are often called "targeted." But in a sense they are not any more targeted than the conventional chemotherapies that interfere with components of the DNA replication, DNA repair, or mitotic machineries or than radiotherapies that damage DNA in a focused field. The new breeds of treatments usually have specificity for individual cancers, reflecting the particular mutations responsible for that tumor or variations in gene expression—distinctive molecular attributes that are increasingly used to subdivide cancers assigned to the same standard histopathological subtype (*6*, *7*). These attributes include the presence or absence of receptors that bind to hormones or to derivative antagonists; the amplification or efficient expression of genes encoding cell surface proteins that are recognized by antibodies that may inhibit cancer cells (directly or through damaging toxins or isotopes); or the activation of intracellular signaling pathways by mutant proteins that are sensitive to molecule-specific drugs.

Therapeutic successes, however limited in some situations, have prompted optimism about other uses of genetic and biochemical information—to classify tumors, to detect them early and

Fig. 1. Joseph H. Burchenal. [Photo: courtesy of Memorial Sloan-Kettering Cancer Center]

Memorial Sloan-Kettering Cancer Center, New York, NY 10021, USA. E-mail: varmus@mskcc.org

Science

Cancer Treatment gets Personal

HISTORIANS OF CANCER RESEARCH HAVE OFTEN NOTED A DISCONNECT BETWEEN THE ACTIVITIES OF THE RESEARCH SCIENTISTS who study the biology of the disease in the laboratory and the work of the clinical oncologists who care for cancer patients. With the recent clinical success of new therapies that target the genetic causes of cancer, and with the advent of new technologies that permit comprehensive molecular evaluation of human tumors, the lines between these two disparate worlds have at long last begun to blur—and to do so in ways that benefit cancer patients. These developments have energized both cancer researchers and clinical oncologists alike and have fueled discussions about a new, patient-centered model of cancer care.

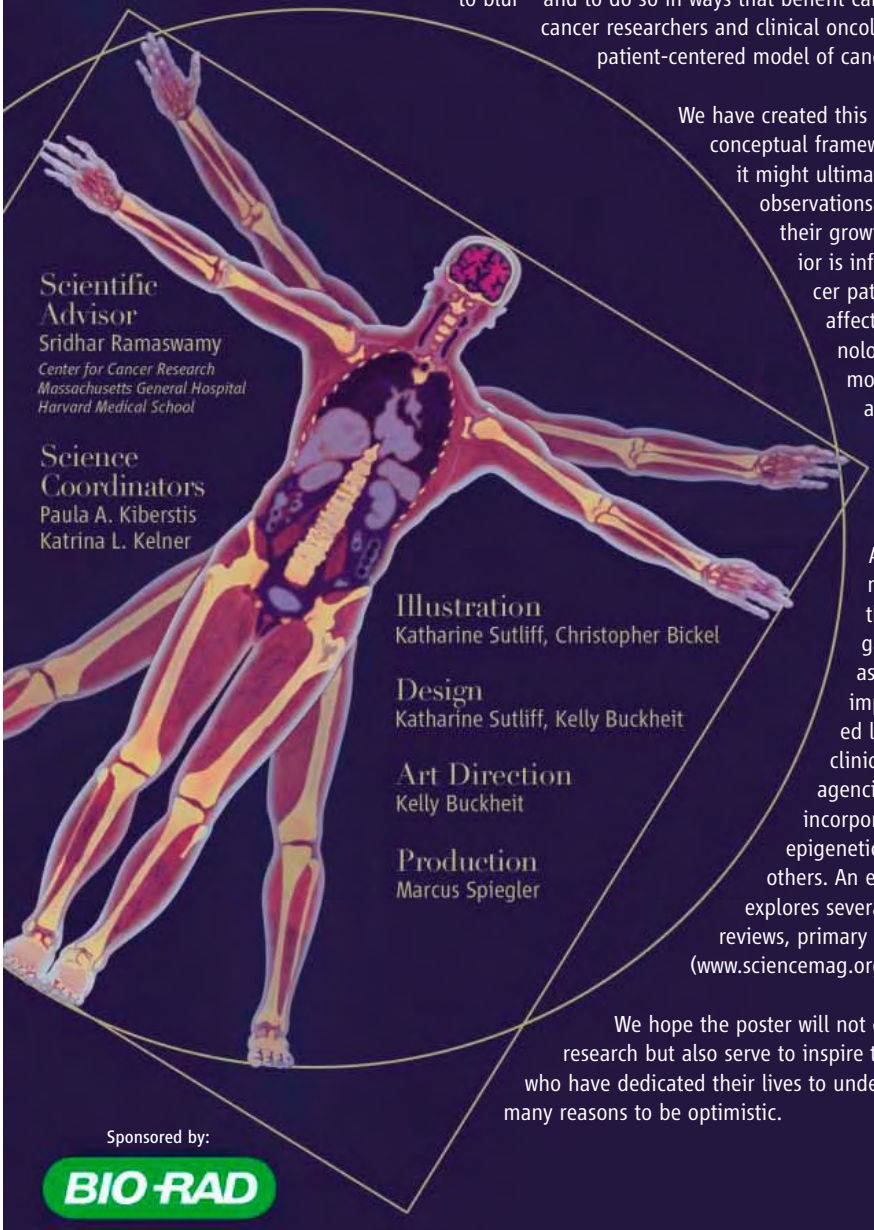

We have created this poster to help readers of *Science* understand the conceptual framework of this envisioned model of cancer care, and how it might ultimately be implemented. The model is based on three key observations: (i) that tumors harbor genetic alterations which drive their growth and/or mark their progression; (ii) that tumor behavior is influenced by surrounding host tissue; and (iii) that cancer patients show interindividual differences in (i) and (ii) that affect the clinical course of the disease. Because new technologies allow these differences to be identified at the molecular level, clinical oncologists will be able to evaluate the molecular attributes of the individual patient and his/her tumor, and use that information as a tool for more accurate diagnosis and for matching each patient with the best treatment.

Although progress is being made on many fronts, this model of cancer care remains a grand vision rather than a reality. There are still scientific and technological gaps that need to be addressed. More importantly—and as noted by authors of accompanying Perspectives—implementation of the model will require an unprecedented level of cooperation between laboratory researchers, clinicians, pharmaceutical companies, and regulatory agencies. In addition, the model will inevitably evolve to incorporate emerging research areas such as cancer stem cells, epigenetics, nanotechnology, and gene-based therapies, among others. An enhanced version of the poster on *Science* Online explores several of these areas and provides links to News stories, reviews, primary research reports, and other resources (www.sciencemag.org/sciext/cancerposter).

We hope the poster will not only educate readers outside the sphere of cancer research but also serve to inspire the legions of researchers and clinical oncologists who have dedicated their lives to understanding and treating this disease. There are many reasons to be optimistic.

–SRIDHAR RAMASWAMY AND PAULA KIBERSTIS

Cancer Treatment gets Person

Clinical oncology is poised to enter a new era in which cancer detection, diagnosis, and treatment will be guided increasingly by the molecular attributes of the individual patient.

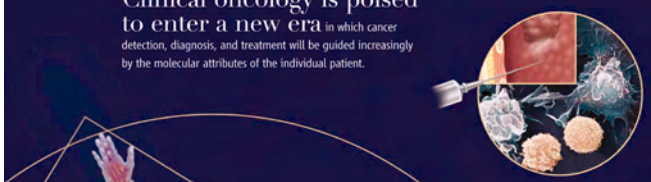

Host tissue

Body fluids

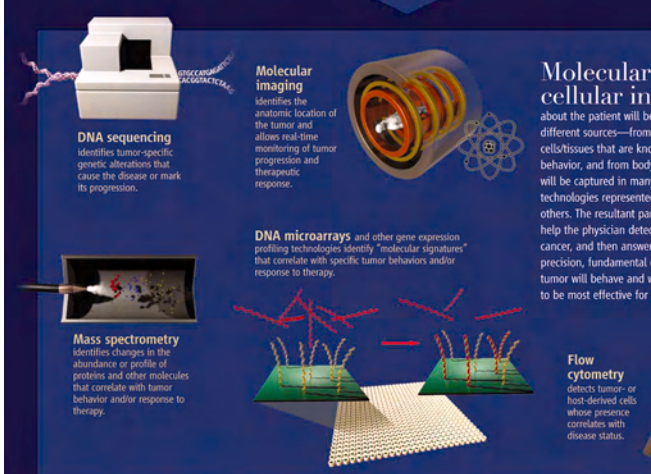

DNA sequencing
identifies tumor-specific genetic alterations that cause the disease or mark its progression.

Molecular imaging
identifies the anatomic location of the tumor and allows real-time monitoring of tumor progression and therapeutic response.

Molecular a
cellular info
about the patient will be ac
different sources—from tur
cells/tissues that are known
behavior, and from body flu
will be captured in many fo
technologies represented h
others. The resultant panel
help the physician detect a
cancer, and then answer, wi
precision, fundamental que
tumor will behave and whic
to be most effective for tha

DNA microarrays and other gene expression profiling technologies identify "molecular signatures" that correlate with specific tumor behaviors and/or response to therapy.

Mass spectrometry
identifies changes in the abundance or profile of proteins and other molecules that correlate with tumor behavior and/or response to therapy.

Flow cytometry
detects tumor- or host-derived cells whose presence correlates with disease status.

Who is at risk of developing cancer?

How aggressive is the tumor? Will it metastasize? To which organ?

How should the patient be treated?

How is the patient responding to the treatment?

Why has the tumor become resistant to treatment?

Science

Genes. . .

ONE OF THE MAJOR CONCEPTUAL advances driving the transformation of clinical oncology is the recognition that cancer is largely a genetic disease. Cancer cells display a diverse array of genetic alterations including (as depicted here) gene rearrangements, point mutations, and gene amplifications. Those alterations observed in a substantial fraction of patients with a given tumor type are causally involved in the disease and provide an entry point into specific molecular pathways that regulate tumor cell growth, survival, and metastatic capacity. When tumor cell growth and/or survival is dependent on these pathways, a phenomenon sometimes called "oncogene addiction," **targeted therapies** can be developed to exploit this vulnerability. In addition, genetic alterations can be used as **biomarkers** for early detection of cancer and for predicting the course of the disease and how it will respond to specific treatments.

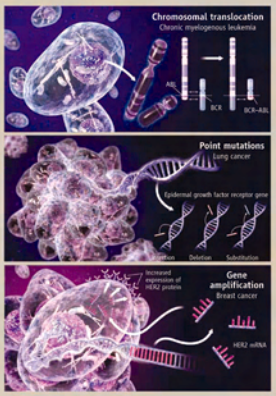

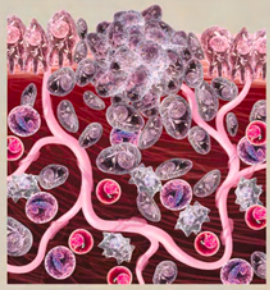

TUMOR CELLS ARE CONTINUALLY ENGAGED in a molecular conversation with surrounding host tissue, or "microenvironment." It has become increasingly clear that the details of this conversation can have profound effects on tumor behavior. Among the most influential cells in the microenvironment are those involved in the formation of blood vessels that supply oxygen and essential nutrients to the tumor; a variety of immune cells, some of which promote tumor growth and others that suppress it; and activated stromal cells such as fibroblasts. **Targeted therapies** directed against molecules expressed by these host cells are expected to augment the activity of therapies directed against tumor cell functions. Drugs targeting the tumor vasculature ("anti-angiogenic" agents) have already provided a proof-of-concept for this approach. Molecules that modulate the activity of inflammatory cells and stroma are likely to attract increasing attention as potential drug targets. As with tumor cells, the molecular characteristics of these influential host cells will vary from patient to patient. Thus, they too can serve as potential **biomarkers** for predicting the course of the disease and how the patient will respond to specific treatments.

. . . and Environment

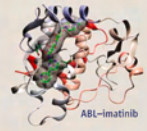

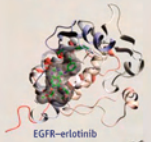

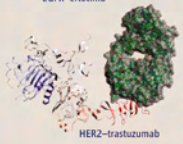

Targeted Therapies

CYTOTOXIC CHEMOTHERAPY AND RADIOTHERAPY REMAIN THE most effective treatments for cancer, but because they do not discriminate adequately between tumor and normal cells, they can cause serious side effects. Advances in understanding the molecular basis of cancer—made possible by the identification and functional analysis of tumor-specific genetic alterations—have opened up exciting new opportunities for the design of therapies that specifically target the molecular pathways that drive tumor cell growth. In principle, "targeted therapies" should display greater selectivity for tumor cells, and indeed several such therapies have already shown promise in the clinic. These include small-molecule drugs that inhibit the activity of protein-tyrosine kinases [e.g., imatinib and erlotinib, targeting ABL and the epidermal growth factor receptor (EGFR), respectively] and neutralizing antibodies that inhibit transmembrane signaling receptors (e.g., trastuzumab, targeting HER2). Other targeted therapies block the activity of molecules in the host microenvironment that support tumor growth (e.g., the antibody bevacizumab, which targets a growth factor that stimulates tumor blood vessel growth). To date many of these therapies have conferred only modest benefits on patient survival, but continuing refinements in how these drugs are used (e.g., as combination therapies and with biomarker-guided patient selection) are expected to improve their efficacy.

IMAGES: M. NOBLE/OXFORD UNIVERSITY

Biomarkers

CANCER BIOMARKERS ARE QUANTIFIABLE TRAITS THAT help physicians (i) identify who is at risk for the disease, (ii) diagnose the disease at an early stage, (iii) select the best treatment, and (iv) monitor response to treatment. These biomarkers exist in many different forms; traditional biomarkers include mammograms and circulating levels of PSA (prostate-specific antigen). With the completion of the human genome sequence, and with advances in key technologies such as high-throughput DNA sequencing, microarrays, and mass spectrometry, the universe of potentially informative cancer biomarkers has expanded dramatically to include the sequence and expression levels of DNA, RNA, and protein. The power of these newer molecular-based approaches lies in their direct applicability to human tissues and, in some cases, in their unbiased, multiplexed nature, which allows the identification of "patterns" of molecules that are potentially more accurate markers of disease status than measurements of single variables. Parallel advances in imaging technologies open up the possibility that pertinent molecular biomarkers (e.g., those marking response to therapy) can be monitored in cancer patients in real time. Together, these new biomarkers will play an increasingly important role in classifying cancers and guiding treatment decisions.

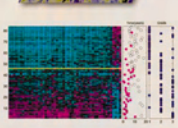

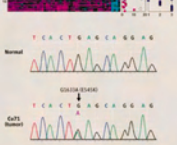

IMAGES (TOP TO BOTTOM): NEIL BOUDEN/PHOTO RESEARCHERS, INC.; H. DAI ET AL. CANCER RES. 63, 4859 (2003); SABOURIN ET AL., SCIENCE 304, 554 (2004)

One just right for you.

Find the cycler that best reflects your needs among the full line of Bio-Rad amplification products.

Bio-Rad is committed to providing you with the best tools for your PCR needs. This dedication is proven by our history of innovation, quality, and regard for researchers' needs.

- Flexible, space-saving dual blocks and multi-bay instruments
- The only modular real-time cycler upgrade with a thermal gradient; choose from 1 to 5 colors
- Innovative enzymes that work where others fail
- PCR tubes, plates, and sealers for any application
- Dedicated technical support by experienced scientists

Bio-Rad offers the most complete line of thermal cyclers anywhere.

For more information, visit us on the Web at **www.bio-rad.com/amplification/**

Visit us on the Web at **discover.bio-rad.com**
Call toll free at 1-800-4BIORAD (1-800-424-6723);
outside the US, contact your local sales office.

BIO-RAD

Make It Personal

Introducing the BioOdyssey™ Calligrapher™ miniarrayer from Bio-Rad. Now you can print the sample of your choice — DNA, proteins, or cell lysates — onto or into the substrate of your choice — slides, membranes, or 96-well plates — all from your laboratory benchtop.

Your Arrayer, Your Discovery

- Easy-to-use computer software to automatically create grids
- Flow-through wash station and vacuum
- Small footprint to fit easily on your benchtop
- Flexible options to empower your specific research needs — Humidity control module (HCM) to add or reduce humidity, a chilling unit for cooling the work surface, and a software upgrade to give total control of the robot

For more information on microarray systems from Bio-Rad, visit us on the Web at **www.bio-rad.com/ad/calligrapher/**

Visit us on the Web at **discover.bio-rad.com**
Call toll free at 1-800-4BIORAD (1-800-424-6723);
outside the US, contact your local sales office.

BIO-RAD

Bio-Rad and RNAi. Come have a look.

From delivery to detection, Bio-Rad supports your RNAi research.

With a broad range of proven delivery technologies, award-winning detection systems, and a suite of high-quality support products, it's clear that Bio-Rad has a vision for RNAi.

- Greatest choice of delivery technologies
- RNA and protein purification products
- Automated microfluidic RNA analysis
- Sensitive, optimized cDNA synthesis kits
- Systems for protein and mRNA detection

For a close look at Bio-Rad's tools for RNAi, visit us on the Web at **www.bio-rad.com/rnai/**

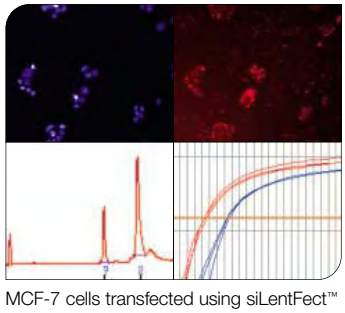

MCF-7 cells transfected using siLentFect™ reagent. RNA purified and analyzed using the Aurum™ total RNA kit and Experion™ system. Detection performed using iScript™ cDNA synthesis kit and the MyiQ™ system.

Visit us on the Web at **discover.bio-rad.com**
Call toll free at 1-800-4BIORAD (1-800-424-6723);
outside the US, contact your local sales office.

BIO-RAD

monitor their growth, and to devise more ingenious ways to inhibit or reverse their growth. Two broad areas of knowledge about cancer in general—and about individual cancers arising in different cell lineages—have been especially significant in this transformation of thinking about cancer:

1) The genetic basis of cancer. Mutations are now recognized to be the fundamental lesions driving neoplasia (*8*). The mutations are largely somatic, but sometimes hereditary; they affect proto-oncogenes, producing a dominant gain-of-function, and tumor suppressor genes, resulting in a loss of function. The Cancer Gene Census maintained by the Sanger Center of the Wellcome Trust (*9*) now lists over 350 genes, situated on every chromosome (except Y), that have been causally implicated in human cancer because they have been repeatedly encountered in mutant form—amplified, deleted, translocated, or damaged by missense, nonsense, or frameshift mutations—in one or more cancer types. The mutations are supplemented by epigenetic variations (methylation of DNA or modifications of histones or transcription factors) that affect gene expression (*10*). The mutations and the secondary changes in gene expression provide new tools for classifying tumors, for predicting their behavior, for anticipating means to detect them early, for designing new tools for imaging, and for developing therapeutic strategies. In addition, germ line mutations associated with cancers have been observed in 66 genes (*9*), making them candidates for assessment of genetic risks of certain cancers (*11*).

2) The physiology of cancer. The biological behavior of cancer cells has increasingly been linked to underlying mutations through an understanding of the signaling pathways that govern the cell cycle and cell growth, programmed cell death (apoptosis), longevity, motility, metabolism, and genome integrity. Furthermore, in addition to the physiological characteristics of cancer cells themselves, components of a cancer cell's environment are now recognized to be important for understanding cancer and considering new means to attack it. The so-called hallmarks of cancer (*12*) include the acquisition of self-sufficient signals for growth, the capacity for extended proliferation, resistance to growth-inhibiting signals, the ability to evade cell death signals, the potential for tissue invasion and metastasis, and the power to induce blood-vessel formation (angiogenesis). Some of these traits are the properties of the cancer cells themselves, but others depend on communication between the cancer cells and their cellular and macromolecular environments. Each property constitutes a vulnerability in a tumor, to be exploited by new therapies, especially when the underlying mutations and signaling aberrations are known.

Still, despite all this new knowledge and despite the startling success of imatinib in the treatment of CML, most of the effects of the new era in cancer research are promised, not achieved. Classification of tumors based on analysis of DNA and RNA is still an uncertain art and practiced only in a few academic centers, largely on an experimental basis. Development of reliable new biomarkers for detection of tumors and of novel, high-affinity ligands for imaging, based on evidence of changes in the structure or production of certain proteins in specific cancers, has yet to occur. The impact of the new generation of molecularly targeted therapies on overall cancer mortality rates remains negligible, because imatinib is effective only in CML and a few other relatively uncommon cancers; because other tyrosine kinase inhibitors dramatically shrink only those lung cancers with mutations in the epidermal growth factor receptor (*13*), and the impact on survival in this group of patients has yet to be established in prospective studies; and because antibodies against cell surface proteins that are effective as adjuvant therapies, such as anti-HER2 in early breast cancer (*14*, *15*), have not yet been used long and widely enough to affect public health data.

Oncogene Dependence

So why is there so much excitement about new cancer therapies? One reason is based on an unexpected consequence of interfering with activated oncogenes. The remarkable reduction in the number of cancer cells observed after treatment with imatinib and some other tyrosine kinase inhibitors implies that such drugs do not simply arrest tumor cell proliferation when they block oncogene activity; they eliminate tumor cells, most likely by programmed cell death. The idea that cancer cells are dependent on mutant oncogenes for viability, not just growth—often called "oncogene dependence" (*16*) or "oncogene addiction" (*17*)—is also supported by studies of cancer cell lines and animals. In mice carrying oncogenes as transgenes that can be regulated by transcriptional control, a wide variety of tumor types swiftly regress, mainly by apoptosis, when the oncogenic proteins are de-induced (*16*, *18*).

The concept of oncogene dependence encourages efforts to destroy cancer cells with new therapeutics directed specifically against the products of mutant oncogenes, but it is still a poorly understood phenomenon. At its heart is a vexing question: How did a cell that was originally content without an oncogene become ready to die if deprived of it? Answers to this question could guide strategies for exploiting a cancer cell's dependence on some of the most frequently encountered oncogenes, such as members of the *RAS* and *MYC* gene families, for which therapeutic agents are currently lacking. This will entail learning more about the vulnerabilities of cells dependent on oncogenic proteins that do not function as enzymes (e.g., Myc and other oncogenic transcription factors) or those that have lost a catalytic activity (e.g., mutant Ras proteins lacking guanosine triphosphatase activity).

Several other issues require attention before oncogene dependence can be adequately exploited for diagnostic and therapeutic purposes:

1) The mutational repertoire. Most obviously, the catalog of oncogenic mutations associated with the many forms of human cancer is far from complete. The Cancer Genome Atlas (TCGA) initiative, recently announced by the National Institutes of Health (NIH) (*19*), should substantially improve this situation over the next decade. The high-throughput technologies that make this initiative possible can, in principle, be used to survey sets of hundreds of tumors, each set representing one of the common malignancies, for determination of gene copy number, gene expression pattern, and sequences of the exons of 1000 to 2000 genes (*20*). Development of new methods for DNA sequencing (*21*) could appreciably drive down costs of TCGA, and faster methods for karyotyping could extend the project to detect chromosomal rearrangements, which are proving to be very common mechanisms of oncogenic mutation (*9*). TCGA is intended to assist the development of therapeutic strategies, but the portraits of molecular changes in many cancer types should also offer new ideas about diagnosing and classifying cancers, detecting them earlier with biomarkers, and monitoring them during therapy with novel imaging methods.

2) Mutational hierarchies. Most if not all tumors have multiple mutations affecting known cancer genes, but the relative importance of such mutant genes in maintaining the oncogenicity and viability of a cancer cell is not known. The loss of responsiveness to anti-HER2 antibody after a tumor suppressor gene (*PTEN*) is mutated in human breast cancers (*22*), and loss of dependence on the c-*Myc* oncogene in mouse breast tumors when a mutation occurs in another oncogene (*Ras*) (*23*), imply that therapies addressing multiple genetic changes will be required. On the other hand, in some genetically engineered mice, oncogene dependence is not affected by the coexistence of an oncogenic mutation in another gene (*24*). Experiments that explore the hierarchy of mutations in different types of tumors could guide the selection of the most appropriate molecular targets and the design of multi-agent therapies.

3) Secondary resistance. All targeted therapies are limited by the appearance of resistance to drugs or antibodies. In some highly instructive cases, resistance can be attributed to a limited repertoire of secondary mutations in targets such as oncogenic tyrosine kinases (*25*, *26*), providing a basis for screening for drug resistance and for seeking new agents that can prevent or overcome it. Deciphering mechanisms of resistance and developing multi-agent treatment protocols, resembling the anti-HIV combination therapies that reduce the likelihood that drug resistance will emerge, will be essential to achieve long-term control of cancers.

4) Heterogeneity and stem cells. The use of differentiation markers reveals heterogeneity among neoplastic cells in a single tumor (*27*, *28*). Some if not all tumors are thought to contain a minor population of cells (so-called cancer stem cells) that are responsible for the tumor's continued expansion and for its regeneration when once-effective therapies fail (*29*, *30*). Better characterization of cancer stem cells and the means to isolate them may help to monitor this subset of cells during treatment and to design treatments that selectively kill them, thereby eliminating a tumor's potential for regrowth.

This list is, of course, incomplete. It remains to be established, for example, whether all cancers show oncogene dependence; whether there is a relationship between oncogene dependence and metastatic potential; and whether components of signaling mechanisms "downstream" of mutant oncogenic proteins (*31*) can commonly serve as targets for therapeutic intervention.

Attacking Cancer Cells Indirectly

An enlarged understanding of the tissue environment in which cancers grow is providing new opportunities to develop therapies that are not targeted at the tumor cells themselves. Best known among these novel approaches is the anti-angiogenic strategy, for which drugs and antibodies have already been approved by the Food and Drug Administration (FDA) (*32*).

There are grounds for optimism about other approaches that address the tumor's milieu: (i) by interfering with growth-promoting signals supplied by non-neoplastic "stromal cells" that surround a tumor (*33*); (ii) by inhibiting specific proteases that mold a tumor's environs to promote the dangerous escape of tumor cells into the circulation (*34*, *35*) or by using those proteases to activate molecules useful for imaging tumors (*36*); and (iii) by promoting an immune response against tumor cells—for example, by inactivating factors, such as the T cell surface protein CTLA-4 (*37*), that restrict the immune response to cancer cells.

Placing Selective Therapies in Perspective

Despite these encouraging ideas, enthusiasm for harnessing new knowledge to combat cancer clinically can seem naïvely overpromising; simplistic about the medical and social attributes of cancer; unperceptive about the history of incorporating complex technical changes into the general practice of medicine; and neglectful of the many other ways cancer can be controlled. Surgery, chemotherapy, radiation, histopathology, and conventional imaging are likely to remain the staples of cancer care for many years. And they too are becoming more effective, even without any molecular advances, through image-guided and minimally invasive surgery, positron emission tomography–computed tomography scanning, dose-modulated radiotherapy, and other technologies.

Other means to control cancer have also been developed, improved, or more widely used in recent years. These include strategies for prevention [such as smoking cessation programs, vaccines against cancer-promoting viruses (hepatitis B and papilloma viruses), and methods for detection of premalignant lesions and early cancers (e.g., colonoscopies, mammography, and PAP smears)]; neurotropic medications to control the ancillary symptoms of cancer, most obviously pain and nausea; hematopoietic growth factors to blunt the side-effects of cytotoxic treatments, such as anemia and leukopenia; and psychosocial methods for managing the response of patients and families to the diagnosis and treatment of cancers.

Furthermore, as a recent inventory of U.S. cancer rates and trends makes evident (*38*), successful control of cancer will require more than just new technologies, whether molecularly based or not. It also calls for elimination of disparities in care—and in access to care—that are based on racial and economic factors.

Gauging the Future

It is difficult to appraise the progress that has been made against cancer over the past half-century, but even more so to predict the progress that should be anticipated over the next 10 or 50 years, because cancer is such a complex problem, with hundreds of forms, diverse means of controlling it, and daunting social barriers to reducing its burdens. To argue that the fight against cancer has been disappointing, one can simply recall that age-adjusted mortality rates now are about the same as they were 50 years ago. But it is also legitimate to support a more optimistic view by noting the recent annual 1% declines in mortality rates after several decades of steady increases (*38*); the enormous improvements in treatments of a few adult and several pediatric cancers; the large increases in 5-year patient survival rates for many cancers (*39*); the recent development and FDA approval of several narrowly targeted therapies with mild side-effects; and the several ways in which living with advanced cancer has been made better by controlling the symptoms of even resilient underlying disease.

Regardless of how the current situation is viewed, the United States and many other countries are faced with a daunting demographic reality: With the continued aging of the population, the absolute number of cancer diagnoses will very likely rise substantially in the coming decades. So, for the foreseeable future, we will need better ways to detect and treat cancers, especially the solid tumors of the lung, breast, prostate, colon, pancreas, ovary, and other organs that are common in older age groups. Articles in this issue provide grounds for optimism about the prospects for better means to control such cancers if new research opportunities are fully exploited. But science operates in a cultural context that affects the deployment of the limited financial resources and human talent devoted to cancer. From that perspective, there is a great deal to worry about.

The major public support for cancer research in the United States comes from the National Cancer Institute (NCI) and, to lesser degrees, from several other components of the NIH. Despite a much welcomed doubling of the NIH budget from 1998 to 2003, appropriations to the NCI specifically, and to the NIH generally, have not kept pace with inflation since then (*40*). As a result, the buying power of the NIH has been substantially eroded, and the success rates for grant applications have fallen to discouraging levels. In this atmosphere, it is difficult to take on new and expensive projects and to attract the best young talent even to this exciting and important area of research. Furthermore, the leadership of the nation's cancer efforts has been poorly defined in recent months and will remain so until a new NCI director is appointed (*41*, *42*).

Traditionally, the public has looked to the pharmaceutical and biotechnology industries for new tools to detect and treat a wide spectrum of diseases, based largely on the results of publicly funded basic science. But a number of factors raise questions about how, in oncology, this tradition may be challenged by a future increasingly influenced by a molecular view of cancer. Will industry lose incentives to develop targeted therapies that address small, precisely defined classes of tumors? Or will commonalities among tumors, such as the high frequency of mutations in *RAS* genes (*43*), sustain market sizes? Will the high prices of some recently approved cancer therapies (*44*) be sustainable, given increasing pressures on health care financing? Will government agencies and private insurers continue to provide adequate reimbursement for molecular methods for detecting, diagnosing, and monitoring tumors as the use of these currently expensive technologies expands? Will regulatory agencies and industry find common ground to allow affordable and interpretable clinical trials for drugs for uncommon cancers, perhaps by using early indicators of therapeutic success, such as biomarkers in serum? And will companies collaborate to test multi-agent therapies directed at multiple targets?

Finally, the new era in cancer research calls for changes in the culture of oncology. These include stronger working relationships between bench scientists and their clinical colleagues, between oncologists in academia and those in community hospitals, and between oncologists and other physicians; new training programs that provide graduate students in the basic sciences with an opportunity to understand the dilemmas posed by cancer as a human disease; grant mechanisms and criteria for advancement in academia that support the kind of teamwork traditionally associated with industry; and guarantees of access to the molecular data sets generated with public funding, to enhance their usefulness for investigators, practitioners, and patients and their advocates.

In sum, concerted national efforts to ensure the vitality of all of the components of modern oncology—academic research, industrial development, and the delivery of new methods throughout the health care arena—are essential to an optimistic view of the prospects for transforming an understanding of oncogenic mechanisms into therapeutic benefits for our entire society.

References

1. www.cancer.org/docroot/PRO/content/PRO_1_1_Cancer_Statistics_2006_ Presentation.asp.
2. J. Pearce, *New York Times*, 16 March 2006, p. A25.
3. J. H. Burchenal, M. L. Murphy, C. T. Tan, *Pediatrics* **18**, 643 (1956).
4. www.beyonddiscovery.org/content/view.article.asp?a=285.
5. B. J. Druker *et al.*, *N. Engl. J. Med.* **344**, 1031 (2001).
6. L. M. Staudt, S. Dave, *Adv. Immunol.* **87**, 163 (2005).
7. A. H. Bild *et al.*, *Nature* **439**, 353 (2006).
8. J. M. Bishop, *Cell* **64**, 235 (1991).
9. www.sanger.ac.uk/genetics/CGP/Census/.
10. C. B. Yoo, P. A. Jones, *Nat. Rev. Drug Discov.* **5**, 37 (2006).
11. J. E. Garber, K. Offit, *J. Clin. Oncol.* **23**, 276 (2005).
12. D. Hanahan, R. A. Weinberg, *Cell* **100**, 57 (2000).
13. W. Pao, V. A. Miller, *J. Clin. Oncol.* **10**, 2556 (2005).
14. E. H. Romond *et al.*, *N. Engl. J. Med.* **353**, 1673 (2005).
15. M. J. Piccart-Gebhart *et al.*, *N. Engl. J. Med.* **353**, 1659 (2005).
16. H. Varmus *et al.*, *Cold Spring Harbor Symp. Quant. Biol.* **70**, 1 (2006).
17. I. B. Weinstein, *Science* **297**, 63 (2002).
18. D. W. Felsher, *Curr. Opin. Genet. Dev.* **14**, 37 (2004).
19. http://cancergenome.nih.gov/index.asp.
20. www.genome.gov/Pages/About/NACHGR/May2005NACHGRAgenda/ReportoftheWorkingGrouponBiomedicalTechnology.pdf.
21. R. F. Service, *Science* **311**, 1544 (2006).
22. Y. Nagata *et al.*, *Cancer Cell* **6**, 117 (2004).
23. C. M. D'Cruz *et al.*, *Nat. Med.* **7**, 235 (2001).
24. G. H. Fisher *et al.*, *Genes Dev.* **15**, 3249 (2001).
25. M. E. Gorre *et al.*, *Science* **293**, 876 (2001).
26. W. Pao *et al.*, *PLoS Med.* **2**, e17 (2005).
27. M. Al-Hajj *et al.*, *Proc. Natl. Acad. Sci. U.S.A.* **100**, 3983 (2003).
28. Y. Li *et al.*, *Proc. Natl. Acad. Sci. U.S.A.* **100**, 15853 (2003).
29. M. Al-Hajj *et al.*, *Curr. Opin. Genet. Dev.* **14**, 43 (2004).
30. T. Reya, S. J. Morrison, M. F. Clarke, I. L. Weissman, *Nature* **414**, 105 (2001).
31. D. B. Solit *et al.*, *Nature* **439**, 358 (2006).
32. N. Ferrara, R. S. Kerbel, *Nature* **438**, 967 (2005).
33. N. A. Bhowmick, H. L. Moses, *Curr. Opin. Genet. Dev.* **15**, 97 (2005).
34. C. M. Overall, O. Kleifeld, *Nat. Rev. Cancer* **6**, 227 (2006).
35. C. Jedeszko, B. F. Sloane, *Biol. Chem.* **385**, 1017 (2004).
36. J. Grimm *et al.*, *Proc. Natl. Acad. Sci. U.S.A.* **102**, 14404 (2005).
37. J. G. Egen, M. S. Kuhns, J. P. Allison, *Nat. Immunol.* **3**, 611 (2002).
38. B. K. Edwards *et al.*, *J. Natl. Cancer Inst.* **97**, 1407 (2005).
39. A. Jemal *et al.*, *CA Cancer J. Clin.* **55**, 10 (2005).
40. www.aaas.org/spp/rd/nih07p.htm.
41. J. Couzin, *Science*NOW Daily News, 15 March 2006; http://sciencenow.sciencemag.org/cgi/content/full/2006/315/1.
42. R. Weiss, *The Washington Post*, 1 October 2005, p. A03.
43. J. L. Bos, *Cancer Res.* **49**, 4682 (1989).
44. A. Berenson, *The New York Times*, 15 February 2006, p. A1.

10.1126/science.1126758

PERSPECTIVE

Cancer Biomarkers—An Invitation to the Table

William S. Dalton[1]* and Stephen H. Friend[2]*

The allure of the emerging genomic technologies in cancer is their ability to generate new biomarkers that predict how individual cancer patients will respond to various treatments. However, productive implementation of cancer biomarkers into patient care will require fundamental changes in how we consider approvals for cancer indications and how we track patient responses. Here we briefly describe ongoing efforts to identify and to validate cancer biomarkers, discuss the technological hurdles that lie ahead, and then focus on the more pressing political and cultural issues that, if left unheeded, could derail many of the anticipated benefits of biomarker research.

In 2005, cancer became the leading cause of death in the United States for people under the age of 85 (*1*). Survival rates for patients with the most common cancers, especially those detected at an advanced stage, remain discouragingly low. For example, fewer than 10% of patients with metastatic colon cancer and about 5% of patients with pancreatic cancer survive 5 years or more (*1*). Cancer therapies are still essentially "one size fits all," with all patients within a given diagnostic category—typically based on tumor type and stage of disease—receiving the same treatment despite the biological heterogeneity known to exist from patient to patient. It is in the search for better ways to match the right treatment with the right patient that many investigators have turned to the promise of cancer biomarkers.

Biomarkers are quantifiable measurements of biologic homeostasis that define what is "normal," thereby providing a frame of reference for predicting or detecting what is "abnormal." Cancer biomarkers exist in many different forms, including physiologic (patient performance status), images (mammograms), specific molecules (prostate-specific antigen, PSA), genetic alterations (*BRCA* mutations), gene or protein expression profiles (serum protein electrophoresis for detection of monoclonal gammopathies), and cell-based markers (circulating tumor cells), among others. With recent technological advances in molecular biology, the range of cancer biomarkers has expanded dramatically to encompass identification of single-nucleotide polymorphisms (SNPs), genomic profiling, transcriptome analysis, and proteomic analysis (*2*). The new molecular technologies have allowed us to move from a linear, single event–based concept of cancer pathogenesis to a greater understanding of how alterations in entire biosystems may contribute to disease.

At least three major benefits can be anticipated from the implementation of molecularly based cancer biomarkers into patient care. First is their enormous potential to predict who will develop cancer and/or to detect the disease at an early stage (*3*). Their anticipated benefit in this setting is based on the assumption that interventions exist that either prevent cancer in high-risk individuals or more effectively eradicate cancer when individuals are diagnosed at a time of low tumor burden. The use of biomarkers to detect early cancers or to identify individuals at high risk has been discussed extensively elsewhere (*4*) and will not be covered here. Second, biomarkers can guide treatment decisions. For example, cancer patients with biomarkers that predict a poor outcome could be selected for aggressive treatments to increase their chance of survival, whereas patients with biomarkers predicting a good outcome could be spared unnecessary, potentially debilitating treatments. Biomarkers also provide an opportunity to identify subpopulations of patients who are most likely to respond to a given therapy and thus should allow more informed decisions about patient enrollment into clinical trials. Finally, biomarkers can help to identify new targets for drug development.

The emerging use of cancer biomarkers may herald an era in which physicians no longer make treatment choices that are based on population-based statistics but rather on the specific characteristics of individual patients and their tumor. Careful tracking of how individual patients with specific molecular alterations in their tumor respond to specific treatments could facilitate a continuous cycle of cancer care (Fig. 1), in which physicians are informed by the responses of all previously treated patients. At the same time, this information could drive the discovery and development of new drugs, as deficiencies are recognized in existing therapies.

The allure of these opportunities has driven a scientific race that spans academic laboratories, industry, and the government to design and to

[1]H. Lee Moffitt Cancer Center, University of South Florida, Tampa, FL 33613, USA. [2]Merck Research Laboratories, West Point, PA 19846, USA.

*To whom correspondence should be addressed. E-mail: dalton@moffitt.usf.edu (W.S.D.); stephen_friend@merck.com (S.H.F.)

implement the use of cancer biomarkers. Here we will briefly review some basic definitions, discuss metrics that suggest progress is being made, but most importantly, highlight some of the numerous misconceptions regarding the scientific, clinical, and political issues that, if left unheeded, will likely derail many of the anticipated benefits of the biomarker enterprise.

The Future of Biomarkers Based in Genomic and Proteomic Technologies

Although the various "omic" technologies are promising, the fact is that they have not yet produced widely applicable new approaches to patient therapy. The Food and Drug Administration (FDA) has recently approved several new drugs that would fall under the category of "target-based therapy." These agents include imatinib mesylate (Gleevec), gefitinib (Iressa), and trastuzumab (Herceptin). Imatinib is a tyrosine kinase inhibitor that blocks the activity of the kinase encoded by the *BCR/ABL* fusion gene that causes chronic myelogenous leukemia (CML). Mutations in and/or increased copy number of *BCR/ABL* predict response to the drug and the emergence of drug resistance (*5*). Gefitinib, another tyrosine kinase inhibitor, blocks the activity of the epidermal growth factor receptor (EGFR), and it has been approved for the treatment of non–small cell lung cancer. Clinical trials revealed that Japanese patients had a higher response rate to the drug than did patients of European descent, and this differential response was traced to a higher incidence of heterozygous missense mutations in the *EGFR* gene among the Japanese patients (*6*). Trastuzumab, a monoclonal antibody directed against the extracellular domain of the HER-2 cell surface receptor, is uniquely active in breast cancer patients with overexpression and/or amplification of the *HER-2* gene (*7*).

In all three cases, these agents were designed to target a specific molecule, and expression of these molecules is required for tumor response. However, with the exception of CML, targeting a single molecule is unlikely to result in a profound response or durable remission in cancer patients. More and more, we are recognizing that cancer pathogenesis is the result of multiple molecules or systems gone awry. Targeting systems, rather than single molecules, will likely result in more durable responses in cancers considered nonresponsive to treatment. Thus, the "omic" technology—because of its ability to identify abnormal patterns of expression associated with biosystems—is promising as an approach both to evaluate the heterogeneity of cancer patients and as a means of identifying biosystems as targets for new drug development.

So, what are we waiting for? Why hasn't the promise been fulfilled? We suggest that before these new technologies can be used productively to analyze the complexity of clinical cancer, the inherent complexities in the technologies themselves must first be addressed. A "future-user" case may be illustrative here. Imagine, for example, that a patient is diagnosed with stage II breast cancer anywhere in the USA. Hoping for guidance in the selection of the most appropriate adjuvant therapy for this particular patient, the treating physician sends a portion of the tumor specimen to a diagnostic laboratory for "molecular profiling." What must be in place for this molecular information to be of value in the decision-making process?

Intrinsic to the success of "omic" technology is an accurate clinical annotation of the tumor specimens being analyzed. Better understanding of cancer heterogeneity, including the variability in response to therapy, will require careful collection and analysis of clinical and pathologic data, as well as collection of outcome annotation for every patient whose tumor is profiled by genomic analysis. Comprehensive databases must be developed to relate individual genomic profiling analyses to individual clinical characteristics of the patient (e.g., survival time) and of the tumor (e.g., stromal infiltration). In the specific clinical scenario here, a large comprehensive database (requiring up to tens of thousands of patients and tumors to be highly informative) would have to be constructed to discover, to validate, and ultimately to apply molecular biomarkers to individual breast cancer cases. Construction of such a database will require standardization of methods and data analysis that is probably best conducted by combining retrospective data mining with prospective clinical trial designs and by following patients longitudinally throughout their lifetime. This relational database could then potentially be used to predict whether the newly diagnosed breast cancer patient would or would not respond to a given therapy on the basis of prior cases in the database that are characterized by the same set of biomarkers. Ideally, this approach will enable the treating physician to choose the optimal therapy for an individual patient on the basis of the evidence generated to date. Undoubtedly, this approach will also identify patients who are unlikely to respond to any known therapies. Such patients could be spared treatment with debilitating, but ultimately ineffective, therapies, and novel treatment options would have to be considered. Implicit in the functioning of this treatment scheme would be a health-care information system that allows community-based oncologists access to the comprehensive databases. At present, unresolved issues pertaining to patient privacy rights and public fears about genetic testing impede the ability to build these databases. To this end, solutions need to be suggested.

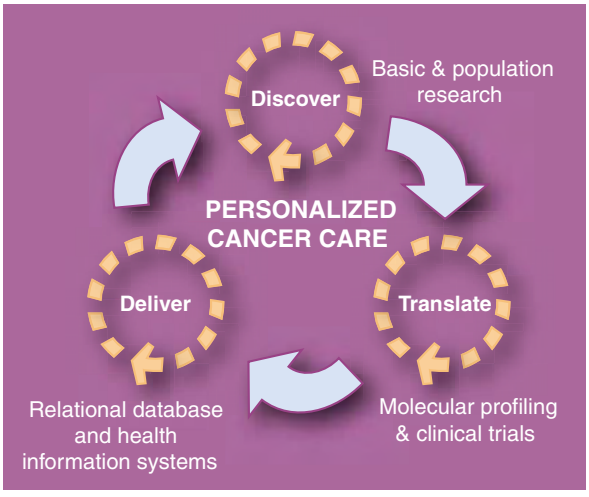

Fig. 1. Personalized cancer care as a continuous cycle. The cycle starts with the discovery of specific molecular alterations in tumors that are then linked to specific patient outcomes in clinical trials. The ability to capture molecular profiles and clinical information at the level of individual patients allows translation of the information into more personalized cancer care. The underlying relational databases and health information systems in turn ensure more informed delivery of cancer therapies to future patients and can also guide the discovery of new therapies.

Are Genomic Biomarkers Robust Enough?

Initial efforts to identify cancer biomarkers through genomic tools were focused on mining the variations in gene expression in tumors from patients whose disease later exhibited different degrees of aggressive behavior (*8*–*10*). These markers of disease progression in breast cancer, lymphoma, and other tumors were defined not in terms of classical single markers, but by sets of genes whose changes in expression, both up-regulation and down-regulation, correlated with the course of the disease. Earlier work with model organisms such as yeast (*11*) had documented how the use of multigene expression profiles, or "signatures," and pattern-matching technologies could be harnessed to learn new biology. Over the past 5 years, many groups have generated expression profiling signatures to predict aggressive disease. Unexpectedly, many of these new gene signatures have had only a marginal overlap with those identified in the original studies (*8*, *12*), even though subsequent work had validated pathway mechanisms identified in the original studies (*13*). Because these gene signatures are at the heart of the opportunities and risks that lie ahead for cancer biomarkers, it is worth exploring possible reasons for the variable results.

One possible source of variation in published signatures is poor study design. Studies with inadequate sample numbers can potentially lead to false-positive and false-negative conclusions. This is especially a risk when working with samples

numbering less than 100 and searching for changes in genes numbering more than 10,000. This problem is often adequately addressed through inclusion of independent validation sets. The importance of designing biomarker experiments to minimize problems of validity and bias has been highlighted by Ransohoff (*14*, *15*). A second possible reason for the variable results is the lack of a standard technology platform. Here, reference is made to all the methodologies required—from extraction of tumor RNA, to methods for amplifying mRNA, to the microarrays and techniques for hybridization—and to the diversity of existing products and protocols for each. Ongoing efforts to create standards for microarray experiments (*16*, *17*) are a step in the right direction. A third potential source of variation is the different ways that tumors are collected. Here there is both the natural variation in the mix between tumor and normal cells, and the variation in how surgeons and cancer research and treatment centers process their tumor samples. A fourth source is the different statistical methods used to analyze separate groups of patients. Imagine two common cases of selecting predictive biomarkers: The first laboratory uses correlation to an end point (or *t* test if it is a binary end point) and presents a group of biomarker genes highly associated with the end point. Most of the genes in the selected panel are similar to each other. The second laboratory uses a multivariate model to select and present the biomarkers. The multivariate model will start from the most predictive gene (likely to be the top gene from the first method) and then add on genes complementary (dissimilar) to the genes already in the model. In the extreme case, these two methods will have only one overlapping gene from the same data set and will create an impression in the clinical world of an inconsistent result. Finally, although the clinical questions are often framed in the same general way, such as which markers predict aggressive disease, the input cohorts used to generate these markers have significant effects on the outcome of the study. A good example of this can be found in the paired studies done at the same hospital to look at markers of disease progression in breast cancer where one study done at the same hospital enrolled only women under the age of 55 and the other study enrolled all available patients. The two studies yielded different results that most likely were linked to the age difference at enrollment (*8*, *18*).

When laboratories have made efforts to share samples, work on common platforms, ask similar questions, and use similar criteria for patient enrollment, the data are more robust. Under such conditions, there are variations, but they are more understandable in terms of real biology. The important point is that in these early days of biomarker discovery, the sources of variation noted above will impede the establishment of standards of care needed to maximize patient benefits. This issue will become even more urgent when we expand the discussion to the search for predictors of therapeutic response. There is real progress being made in the search for biomarkers to identify subpopulations of patients most likely to respond to therapy. Some of these early studies on predictors of response are linked to mutational analysis of the *EGFR* gene to parse responders and nonresponders to the EGFR inhibitors (*5*). Other studies have used expression profiles to identify response to paclitaxel, fluorouracil, and other cytotoxic drugs (*19*, *20*). The same issues regarding variation in the signatures of disease progression will likely accompany these new genomic signatures of response to therapy.

There are two critical lessons to remember. The first, noted above, is that as long as there is such diversity in the methods and technology platforms and the questions are loosely defined, it will be difficult to move toward standard markers, whether they are for disease progression or for predicting response. The second relates to improper simplification, that is, many investigators expect to use these markers to distill hard answers from the very complex biology of cancer, or they expect biomarker sets to emerge that will be broadly applicable to all patients regardless of the stage of their disease or their treatment history. Such expectations defy what we have painfully learned about the complexity of cancer over the past 30 years. It is time we embrace the complexity. When biomarkers give answers that vary depending on certain biological contexts, we should listen. If we are going to improve the prediction of response and better match the right drug with the right patient, we will need to live in a world in which predictive biomarkers are built from larger and more coherent data sets that include patient information collected over many years. This will apply equally to all the DNA-, RNA-, and protein-based tools we are currently designing.

For all these tools, we must acknowledge three different dimensions of complexity. First is the need to develop markers that track the molecular diversity of disease. These may be largely but not completely determined by the tissue of origin. There is also a need to develop molecular markers to monitor the progression of disease. Only when these first two are taken into account will it be possible to interface with the third group of markers that predict the response to therapies. Simply stated—to hope that a single marker for response to a drug will be independent of the context of that tumor as defined by its starting state and stage—may be naïve.

This leads to a fundamental question about the variety of the disease states we will need to monitor. If there exist hundreds to thousands of basic functional contexts for tumors, very large data sets will be required. Even if this is true, the problem is not insurmountable. A stepwise approach could be taken: A finite number of grids could be formed in the multidimensional biomarker space, and patients in the vicinity of the grid could be bucketed toward each grid so as to have a sufficient number of training and validation samples. As the database increases, finer resolution grids or more dimensions could be introduced. If on the other hand, as Hartwell and others have suggested, the basic contexts or functional modules within cancer cells are more thematic ones numbering in the dozens (*21*), the time we must wait to have a multitude of functional predictive markers is on a much shorter time scale—possibly within a decade.

Are We Ready to Build the Partnerships Required to Implement Biomarkers into Patient Care?

This takes us to the pressing and more political issues. We have laid out the multitude of realities surrounding the need to closely collaborate, share common platforms, and frame questions in similar formats. Current structures within academia, the pharmaceutical industry, and the government are not ones poised to enable the alliances needed to engage the type of model proposed in Fig. 1. Academic groups vie for original content to fortify rather elusive intellectual property positions, and primary investigators often compete against each other for the visibility needed for their promotion and funding. Pharmaceutical and biotechnology companies are required to identify and to protect advantages that allow them to take the serious risks required to develop their products and to generate adequate financial returns. Government agencies in the recent past have too often exhibited a somewhat overconfident attitude regarding their ability to coordinate all aspects of biomarker research. So where do we turn?

We would suggest it is worth taking lessons from the Internet industry, which needed to navigate massive problems of integration between academic groups, industry, and the government. Their success came from teamwork-based solutions developed at a project level, glued together by a standards-based common architecture not dictated by either government or industry (*22*). An example of how important such partnerships were to the Internet industry can be seen in the methods used to define the standards for their operating systems (*23*). In the world of cancer biomarkers, the constituent groups still too much at the periphery are the payers, the regulators, and the patients. As we bring them to the table, we should not promise simple, immediate solutions but instead build the long-term partnerships needed to implement new models of cancer care.

What if, instead of just focusing on clinical trials designed to prove that there is a survival benefit to a pool of patients, we also identified ways to run trials with the statistical power to examine the benefit to subpopulations of patients defined by response signatures? One possible scenario might be that in addition to conducting trials to examine the safety and benefit of new drugs for specific diseases, physicians and/or

investigators in cancer research and treatment centers, in partnerships with oncology drug companies, worked together on interactive trials that stored data prospectively from all patients being treated with a new drug, even after gaining FDA approval. Doing so would essentially create an evidence-based system where the next patient to be treated would have a better chance of receiving the optimal treatment because of information in the database about all previously treated patients.

Developing such a model of comprehensive oncology health care could potentially blur some of the current distinctions between academic groups, hospital care, government approvals, and the pharmaceutical industry. It will be enabled by reexamining the privacy issues around current HIPPA (Health Insurance Portability and Accountability Act) regulations and the manner in which academic centers sometimes structure their rights to intellectual property. It will require companies to search for ways to identify precompetitive projects and to collaborate. Focused projects run by coordinated partnerships between comprehensive cancer centers, industry, and the government might be very effective. There are many issues to tackle, but there are also real signs that all who might need to be at this table are eager to begin working together. Recent efforts by the FDA suggest the time is ripe for sending out these invitations (*24*).

References

1. American Cancer Society, Cancer statistics 2005 at (www.cancer.org).
2. R. Simon, S.-J. Wang, *Pharmacogenomics J.*, published online 17 January 2006 (10.1038/sj.tpj.6500349).
3. L. M. Hernandez, *Implications of Genomics for Public Health: Workshop Summary* (Committee on Genomics and the Public's Health in the 21st Century, Institute of Medicine, National Academies Press, Washington, DC, 2005); (www.nap.edu/catalog/11260.html).
4. S. G. Baker *et al.*, *Clin. Trials* **3**, 43 (2006).
5. M. E. Gorre *et al.*, *Science* **293**, 876 (2001).
6. J. G. Paez *et al.*, *Science* **304**, 1497 (2004).
7. M. A. Cobleigh *et al.*, *J. Clin. Oncol.* **17**, 2639 (1999).
8. L. J. van't Veer *et al.*, *Nature* **415**, 530 (2002).
9. T. R. Golub *et al.*, *Science* **286**, 531 (1999).
10. C. M. Perou *et al.*, *Nature* **406**, 747 (2000).
11. T. R. Hughes *et al.*, *Cell* **102**, 109 (2000).
12. S. Ramaswamy, K. N. Ross, E. S. Lander, T. R. Golub, *Nat. Genet.* **33**, 49 (2003).
13. J. A. Foekens *et al.*, *J. Clin. Oncol.* **24**, 1665 (2006).
14. D. F. Ransohoff, *Nat. Rev. Cancer* **5**, 142 (2005).
15. D. F. Ransohoff, *Nat. Rev. Cancer* **4**, 309 (2004).
16. P. L. Whetzel *et al.*, *Bioinformatics* **22**, 866 (2006).
17. S. C. Baker *et al.*, *Nat. Methods* **2**, 731 (2005).
18. M. J. van de Vijver *et al.*, *N. Engl. J. Med.* **347**, 1999 (2002).
19. M. Ayers *et al.*, *J. Clin. Oncol.* **22**, 2284 (2004).
20. P. Wagner *et al.*, *Cell Cycle* **4**, 1149 (2005).
21. L. Hartwell, J. J. Hopfield, S. Leibler, A. W. Murray, *Nature* **402**, C47 (1999).
22. J. J. Naughton, *A Brief History of the Future: From Radio Days to Internet Years in a Lifetime* (Overlook Press, Peter Mayer Publishers, Woodstock, NY, 2001).
23. Computers and Communications Standards (www.cmpcmm.com/cc/standards.html).
24. E. Russo, "FDA, NCI, and CMS announce agreement to build better cancer biomarkers" (Research Policy Alert, FDC Reports, Reed Elsevier Science, Chevy Chase, MD, 2006).

24 March 2006; accepted 20 April 2006
10.1126/science.1125948

PERSPECTIVE

Molecular Imaging in Cancer

Ralph Weissleder

Medical imaging technologies have undergone explosive growth over the past few decades and now play a central role in clinical oncology. But the truly transformative power of imaging in the clinical management of cancer patients lies ahead. Today, imaging is at a crossroads, with molecularly targeted imaging agents expected to broadly expand the capabilities of conventional anatomical imaging methods. Molecular imaging will allow clinicians to not only see where a tumor is located in the body, but also to visualize the expression and activity of specific molecules (e.g., proteases and protein kinases) and biological processes (e.g., apoptosis, angiogenesis, and metastasis) that influence tumor behavior and/or response to therapy. This information is expected to have a major impact on cancer detection, individualized treatment, and drug development, as well as our understanding of how cancer arises.

Modern clinical cancer treatments require precise positional information. Where is the tumor located? How large is it? Is it confined, or has it spread to lymph nodes? Does it involve any critical anatomical structures that would alter the treatment strategy? These questions are being answered, at ever-increasing spatial resolution, through the application of traditional anatomical imaging methods such as computed x-ray tomography (CT), magnetic resonance imaging (MRI), and ultrasound (US). Although these methods still represent the mainstay of clinical imaging, it has become clear that the acquisition of molecular and physiological information by nuclear magnetic resonance and optical imaging technologies could vastly enhance our ability to fight cancer (*1*–*3*).

Center for Molecular Imaging Research, Massachusetts General Hospital, Harvard Medical School, Charlestown, MA 02129, USA. E-mail: weissleder@helix.mgh.harvard.edu

Emerging genomic and proteomic technologies have the potential to transform the way in which cancer is clinically managed. Molecular imaging is poised to play a central role in this transformation, because it will allow the integration of molecular and physiological information specific to each patient with anatomical information obtained by conventional imaging methods. The hope is that clinical molecular imaging will one day be used to achieve the following: (i) the detection of molecular or physiological alterations that signal the presence of cancer when it is still at a curable stage, (ii) the ability to evaluate and adjust treatment protocols in real time, and (iii) the ability to streamline the cancer drug development process.

Molecular Imaging and Cancer Detection

There is tremendous incentive for developing technologies that detect cancer at its earliest stages. In most cases, detection of stage 1 cancers is associated with a >90% 5-year survival rate (*4*). When lesions are detected even earlier (at the premalignant stage), treatment is often curative. Conventional anatomic imaging techniques typically detect cancers when they are a centimeter or greater in diameter, at which point they already consist of $>10^9$ cells (including circulating and microscopic metastatic deposits). Molecular imaging is expected to play an important role in this setting, because it will allow sensitive and specific monitoring of key molecular targets and host responses associated with early events in carcinogenesis. In lung cancer, for example, potential molecular targets include activated oncogenes such as *KRAS* (*5*), as well as proteins whose expression or activity is consistently altered in tumor cells versus normal cells. An optical probe activated by cathepsins, a family of cysteine proteases that are overexpressed in lung tumors, has been used in mouse models to detect tumors as small as 1 mm in diameter (*6*). Similar fluorescent-based imaging agents can be used in conjunction with endoscopic confocal microscopy for the detection of microscopic epithelial precancerous lesions that elude conventional imaging methods (*7*–*9*). Endoscopic confocal microscopy produces high-magnification cross-sectional images of the gastrointestinal epithelium and could one day permit in vivo characterization of tumors without the need for multiple excisional biopsies. Figure 1, A to F, shows an application of this imaging technology in mice.

Other imaging technologies can provide information important for the staging and restaging of cancers. For example, magnetic nanoparticles targeted to macrophages in lymph nodes have been used to detect nodal metastases in patients with clinically occult cancers. Because of the exquisite spatial resolution of MRI, millimeter-sized metastases are detectable in nonenlarged

lymph nodes (*10*), a size which is beyond the detection threshold of many other imaging techniques (Fig. 1, G to I). This approach has already been validated for a number of genitourinary malignancies, as well as head and neck cancer and breast cancer.

Positron emission tomography (PET) imaging has emerged as a clinical cornerstone in cancer staging and restaging for a number of malignancies and is one of the few molecular imaging technologies approved by the Food and Drug Administration (FDA) (*1*). The most frequently used PET agent (>90% of all cancer-related scans) is [^{18}F]fluorodeoxyglucose (FDG), a glucose analog that is selectively taken up by cells with a high rate of glucose metabolism, which is a distinguishing feature of malignant cells (*11*). FDG-PET imaging has been approved for staging of breast cancer, colorectal cancer, esophageal cancer, head and neck cancer, non–small cell lung cancers, melanoma, and lymphoma (*1*, *11*, *12*).

Molecular Imaging and Cancer Treatment

FDG-PET imaging is also a valuable clinical tool for predicting tumor response to therapy and patient survival (*13*). The technique (Fig. 2 shows examples of specific applications) is particularly well established for lymphoma, gastrointestinal stromal tumors (GISTs), esophageal carcinomas, head and neck cancer, and ovarian cancer. In one recent prospective study of patients with advanced ovarian cancer, sequential FDG-PET imaging was reported to be a more accurate predictor of response to neoadjuvant chemotherapy than other clinical or histopathologic criteria, including changes in serum levels of the tumor marker CA-125 (*14*).

Whereas FDG-PET imaging has been successful for tumor staging and therapy assessment, there has been a continued search for imaging agents that more specifically monitor tumor cell growth and cell death as a means to follow treatment response. This search has driven the development of radiolabeled nucleoside analogs such as thymidine compounds, which, because they are incorporated into DNA, may serve as useful markers of cell proliferation. Such agents are now being tested in clinical trials. Radiolabeled monoclonal antibodies against tumor-specific antigens such as Her2 and carcinoembryonic antigen are also being explored, but these tracers can produce high background signals because of their slow clearance from the blood (*11*). Smaller engineered antibody fragments (minibodies and diabodies) may improve the signal-to-noise ratio because they are cleared more rapidly, but they may also have a reduced affinity for the target antigen. Other targeted radiolabeled imaging agents include proteins such as annexin-V (to measure cell death), nanoparticles targeted to avß3 or VCAM-1 (to measure angiogenesis), and peptides or small molecules including dihydrotestosterone, estrogen, and protein kinase inhibitors.

Molecular Imaging and Cancer Drug Development

The development of new cancer therapeutics is expensive, time-consuming, and often requires vast numbers of patients. These factors all contribute to the final cost of the therapies once they are approved for clinical use (*15*). On average, it takes 10 to 12 years to take a new drug from discovery to regulatory approval at costs that can exceed $880 million (*16*). In addition, many newer drugs (cytotoxic, cytostatic, and molecularly targeted) are often efficacious only in subgroups of patients (*17*), whereas others—despite robust scientific rationale and promising preclinical results—have failed to show efficacy in clinical trials (*18*). Reducing the number and cost of failed projects would benefit the pharmaceutical industry, the health care system, and, most importantly, the patient.

Molecular imaging has the potential to improve the efficiency and cost-effectiveness of drug development programs. Imaging-based biomarkers (specific molecular targets or biological cancer processes) can be used in all phases of the cancer drug development process, from target discovery and validation to the pivotal clinical trials that precede drug approval (*19*). Genetic reporter strategies involving bioluminescence and fluorescent-tagged proteins have been especially valuable for the study of cancer biology and preclinical drug evaluation in mouse models (*20*–*24*). For example, these types of imaging approaches have recently been used to test the antitumor efficacy of epothilones, drugs that disrupt mitosis (*25*), as well as novel constructs of tumor necrosis factor–related apoptosis-inducing ligand (TRAIL), a protein that induces tumor cell apoptosis (*26*). Although the reporter gene strategy cannot be directly translated into the clinic, high-resolution mouse imaging with injectable imaging agents can provide an important window into the effect of drugs on specific targets (*2*, *19*, *23*).

Molecular imaging can help identify new efficacy endpoints that are more easily monitored than currently used endpoints, such as histological analyses of tumor biopsies. For example, steady-state imaging of tumor blood flow can be obtained within minutes in living mice, whereas CD31

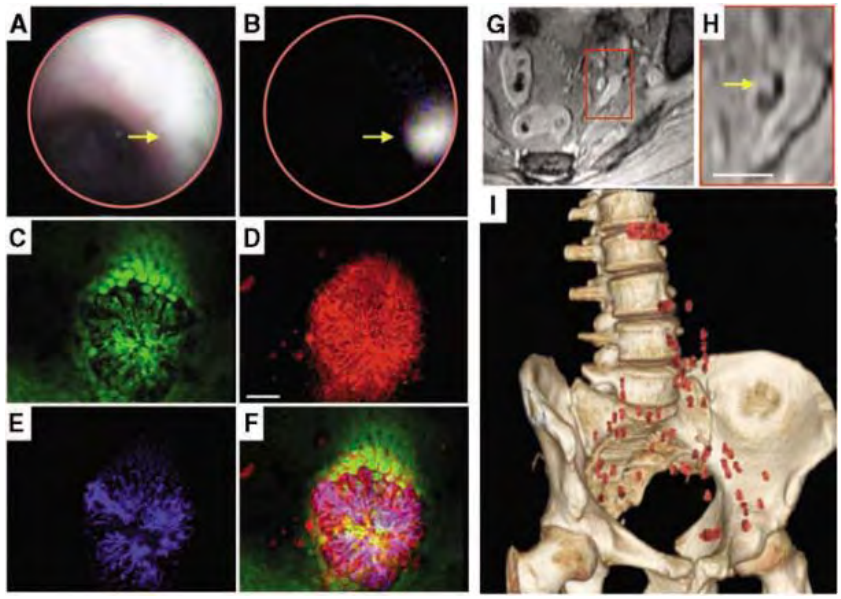

Fig. 1. Molecular imaging used for early detection of cancer in mice and humans. Dysplastic colonic adenoma in *Apc*$^{Min/-}$ mice imaged by fiberoptic endoscopy (**A** and **B**) and endomicroscopy (**C** to **F**). The 2-mm lesion is not detectable by regular colonoscopy (A) but becomes readily apparent by imaging cathepsin protease activity in the near infrared channel (B). Arrows indicate location of adenoma. [(C) to (F)] show that endomicroscopy of an adenomatous lesion in a living mouse provides cellular resolution of this early lesion (C), cathepsin expression (D) (scale bar, 1 mm), and microvascularity (E). (F) is a merged image. (**G** and **H**) MRI of a human male pelvis showing prostate cancer metastasis. (G) shows an axial MRI of the pelvis. The square highlights a region of nonenlarged lymph nodes and vessels. Magnetic nanoparticles with affinity for lymph node macrophages were administered systemically to detect intranodal metastases. (H) is a magnified region after nanoparticle administration, which shows 1.3-mm micrometastases in a 4 × 7 mm lymph node. Scale bar, 10 mm. Arrow points to micrometastases within dark lymph node. (**I**) Reconstruction of lymph node metastases detected in 34 patients by the above technique. The extensive, unpredictable spread of prostate cancer to these nodes (red) is one of the reasons that imaging in individual patients is so important.

microvascular density measurements are slower and more labor intensive. Furthermore, because molecular imaging is noninvasive, in the preclinical setting it allows for longitudinal studies in a single animal, which can reduce the number of animals required for an experiment without compromising statistical significance. In the clinical setting, molecular imaging endpoints could be used to identify the most appropriate patient populations in which to test new drugs.

Imaging of cancer drugs that have been labeled with ^{11}C or ^{18}F can facilitate clinical pharmacokinetic and pharmacodynamic assessments, as well as dosing and comparative efficacy studies of different lead compounds. In particular, microdosing studies (defined as 1% of the therapeutic dose, which typically has negligible toxicities in patients) have been advocated as a way to quickly obtain data on drug absorption, distribution, metabolism, excretion, and toxicity (*27*–*29*).

Impediments to Progress

Despite many recent advances in the field, there are still relatively few molecular imaging agents in the clinic. This can be attributed to several factors. First, as is the case with new cancer therapeutics, the attrition rate for new imaging agents is high. Fewer than 25% of new imaging agents survive rigorous preclinical testing in animal models. Suboptimal pharmacokinetics is one of the major reasons for failure. To be successful, imaging agents must display exquisite affinity for their molecular/biological targets, efficiently gain access to these targets, show minimal nonspecific uptake or retention (a major factor contributing to low target-to-background ratios), and have sufficiently long half-lives to be detectable/functional at trace concentrations (*20*). Designing a single imaging agent with all of these features is challenging. Recent efforts to boost target-to-background ratios have used sophisticated chemical signal amplification strategies with some success.

A second factor impeding progress is the regulatory hurdles that preclude rapid translation of molecular imaging technologies from the laboratory to the clinic. This problem has been recognized by the FDA, which has recently released newer, less-stringent criteria for exploratory investigational new drug (IND) studies (*30*). Such studies involve very limited human exposure and have no therapeutic or diagnostic intent. Nevertheless, the revised facilitating guidelines largely apply to isotope-based PET imaging agents and microdosing studies and do not address the use of diagnostic doses to test efficacy for particularly promising fluorescent or MRI agents. Basic fluorochrome structures such as indocyanine green have already been used safely for human breast imaging and other clinical applications (*31*), and, as mentioned above, nanoparticles detectable by MRI have been used to locate submillimeter lymph node metastases in patients with prostate cancer (*10*). Newer, molecularly targeted imaging agents based on the above will be particularly useful in settings where repeated or higher resolution imaging is necessary—for example, in efforts aimed at early detection of cancer.

A third factor impeding the clinical development of molecular imaging agents is economics. The development of an imaging agent currently costs 50 to 100 million dollars, and reimbursement levels from the Centers for Medicare and Medicaid Services for imaging studies are often lower than those for therapeutic drugs. Consequently, the pharmaceutical industry and venture capitalists have been reluctant to invest unless widespread clinical applications are immediately evident. The fact that there are so many competing imaging modalities and that these modalities are all evolving at such a rapid pace (which limits the window of marketability) has also served to diminish investor interest. Another economic consideration relates to the general problem of rising health care costs, which some feel would be exacerbated by the implementation of molecular imaging technologies into patient care. In fact, molecular imaging—if used appropriately—can potentially reduce health care costs. The average cost of new molecularly targeted cancer treatments has increased from about $20,000 per patient per year to ~$100,000 per patient per year (*32*). When such drugs are given as combination therapies (e.g., Avastin, Erbitux, and Eloxatin), the yearly cost can reach multiple hundreds of thousands of dollars per patient. Because molecular imaging techniques can help clinicians match specific therapies to the patient populations which are most likely to respond, they may lower costs by reducing the number of patients eligible for a given treatment combination. In addition, in some settings, molecular imaging techniques may eliminate costly surgical procedures altogether (*10*). In preliminary studies, FDG-PET imaging has been shown to have a high benefit/cost ratio for cancer staging (*1*, *33*).

A final impediment to progress, but one that is likely the easiest to overcome, is that the discovery of imaging agents is a complex multidisciplinary effort. It requires an infrastructure of experts from research fields as diverse as genomics, proteomics, chemical biology, engineering, image computation, and clinical trial design. Although such infrastructures are commonplace in large pharmaceutical companies, there are only a handful of academic centers in the world that have such a collection of experts or have access to appropriate resources.

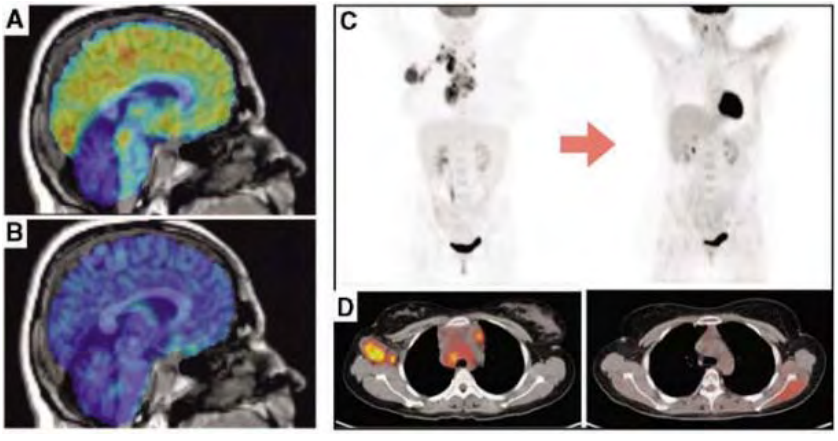

Fig. 2. Molecular imaging used for monitoring of patient response to therapy. (**A**) PET scan of brain substance P (neurokinin-1 receptor) using ^{18}F–substance-P antagonist–receptor quantifier (SPA-RQ) superimposed onto an MRI scan. (**B**) PET scan after receptor blockade with Aprepitant, a neurokinin-1 receptor antagonist. Blue indicates low levels of tracer binding; yellow and orange indicate high levels of tracer binding. The study shown here assessed the efficacy of Aprepitant as a treatment for depression; however, the drug is also used to treat cancer patients for chemotherapy-induced nausea. Panels (A) and (B) are reprinted with permission from (*42*) with permission from the Society of Biological Psychiatry. (**C**) FDG-PET scan of a patient with lymphoma before (left) and after (right) treatment. (**D**) Corresponding axial PET-CT axial sections show a decrease in FDG activity (yellow red) in axilla and mediastinum.

Near-Term Needs and Opportunities

What's needed to catalyze the field of molecular imaging in cancer and drive imaging agents into the clinic at a faster pace? Of utmost importance is the need to discover and validate new biomarkers optimally suited for cancer imaging, particularly those with amplification potential such as internalizing cell-surface receptors, enzymes, and abundant nonprotein targets (e.g., growth factor receptors). Recent technological developments that may hasten the biomarker discovery process are: "imaging filters" to screen existing databases for targets ideally suited for imaging, newer conjugation chemistries such as "click chemistry" (*34*), and the use of yeast/phage surface display to identify recombinant antibodies/peptides (*35*). There is also a pressing need for the synthesis of new imaging agents. There is an opportunity to

apply combinatorial methods, chemical biology, synthetic small molecule compounds, and newer nanomaterials as scaffolds to improve pharmacological behavior (*36*, *37*). The continued development of "smart" imaging reagents, whose signal depends on specific biochemical activities, also remains a top priority. For example, small-molecule prodrugs that change their imaging signal upon target interaction have been shown to dramatically boost target-to-background ratios in vivo (*38*, *39*). Additional opportunities exist for the development of fluorescence-based imaging agents, one of the most important growth areas in molecular imaging. Fluorochromes such as indocyanines are inexpensive, stable, involve no radiation, and have been used safely for the past 20 years. Just as in the in vitro setting where they have been key tools in both genomics and proteomics, fluorochromes can be uniquely converted into sensing agents in vivo (*40*). Continuing improvements in instrumentation including high–spatial resolution endomicroscopy, near-infrared intraoperative reflectance imaging, and fluorescence tomography will also be important. The latter technology is of particular interest because it allows accurate in vivo quantitation of near-infrared fluorochrome, which is important to differentiate target binding from pharmacokinetics (*41*).

Given the remarkable parallel progress in other research areas—including our deepening understanding of the molecular basis of human cancer, continued refinements of mouse tumor models, and advances in imaging instrumentation—we can be optimistic that molecular imaging will contribute in many important ways to the improved care of cancer patients.

References and Notes

1. M. E. Juweid, B. D. Cheson, *N. Engl. J. Med.* **354**, 496 (2006).
2. R. Weissleder, *Nat. Rev. Cancer* **2**, 11 (2002).
3. F. A. Jaffer, R. Weissleder, *JAMA* **293**, 855 (2005).
4. R. Etzioni *et al.*, *Nat. Rev. Cancer* **3**, 243 (2003).
5. A. Sweet-Cordero *et al.*, *Nat. Genet.* **37**, 48 (2005).
6. J. Grimm *et al.*, *Proc. Natl. Acad. Sci. U.S.A.* **102**, 14404 (2005).
7. K. Marten *et al.*, *Gastroenterology* **122**, 406 (2002).
8. H. Alencar, U. Mahmood, Y. Kawano, T. Hirata, R. Weissleder, *Neoplasia* **7**, 977 (2005).
9. J. A. Evans, N. S. Nishioka, *Curr. Opin. Gastroenterol.* **21**, 578 (2005).
10. M. G. Harisinghani *et al.*, *N. Engl. J. Med.* **348**, 2491 (2003).
11. A. Quon, S. S. Gambhir, *J. Clin. Oncol.* **23**, 1664 (2005).
12. U. Guller *et al.*, *Breast Cancer Res. Treat.* **71**, 171 (2002).
13. H. A. Wieder *et al.*, *J. Clin. Oncol.* **22**, 900 (2004).
14. N. Avril *et al.*, *J. Clin. Oncol.* **23**, 7445 (2005).
15. G. J. Kelloff, C. C. Sigman, *Eur. J. Cancer* **41**, 491 (2005).
16. The Biomedical Research and Development Guide is available at (www.biag.org/BIAG/rd.htm).
17. T. J. Lynch *et al.*, *J. Med.* **350**, 2129 (2004).
18. J. W. Park *et al.*, *Clin. Cancer Res.* **10**, 3885 (2004).
19. M. Rudin, R. Weissleder, *Nat. Rev. Drug Discov.* **2**, 123 (2003).
20. T. F. Massoud, S. S. Gambhir, *Genes Dev.* **17**, 545 (2003).
21. R. Weissleder, V. Ntziachristos, *Nat. Med.* **9**, 123 (2003).
22. S. Gross, D. Piwnica-Worms, *Cancer Cell* **7**, 5 (2005).
23. H. R. Herschman, *Science* **302**, 605 (2003).
24. P. R. Contag, *Drug Discov. Today* **7**, 555 (2002).
25. K. D. Wu *et al.*, *Proc. Natl. Acad. Sci. U.S.A.* **102**, 10640 (2005).
26. K. Shah, C. H. Tung, X. O. Breakefield, R. Weissleder, *Mol. Ther.* **11**, 926 (2005).
27. G. Lappin, R. C. Garner, *Nat. Rev. Drug Discov.* **2**, 233 (2003).
28. A. Saleem *et al.*, *J. Clin. Oncol.* **19**, 1421 (2001).
29. D. J. Propper *et al.*, *J. Clin. Oncol.* **21**, 203 (2003).
30. Information on IND studies is available at (www.fda.gov/cder/guidance/7086fnl.htm).
31. V. Ntziachristos, A. G. Yodh, M. Schnall, B. Chance, *Proc. Natl. Acad. Sci. U.S.A.* **97**, 2767 (2000).
32. E. Nadler, B. Eckert, P. J. Neumann, *Oncologist* **11**, 90 (2006).
33. S. Heinrich *et al.*, *Ann. Surg.* **242**, 235 (2005).
34. H. C. Kolb, K. B. Sharpless, *Drug Discov. Today* **8**, 1128 (2003).
35. J. A. Joyce *et al.*, *Cancer Cell* **4**, 393 (2003).
36. D. G. Anderson, S. Levenberg, R. Langer, *Nat. Biotechnol.* **22**, 863 (2004).
37. R. Weissleder, K. Kelly, E. Y. Sun, T. Shtatland, L. Josephson, *Nat. Biotechnol.* **23**, 1418 (2005).
38. T. J. Meade, A. K. Taylor, S. R. Bull, *Curr. Opin. Neurobiol.* **13**, 597 (2003).
39. M. Querol, J. W. Chen, R. Weissleder, A. J. Bogdanov, *Org. Lett.* **7**, 1719 (2005).
40. R. Weissleder, C. H. Tung, U. Mahmood, A. Bogdanov Jr., *Nat. Biotechnol.* **17**, 375 (1999).
41. V. Ntziachristos, J. Ripoll, L. V. Wang, R. Weissleder, *Nat. Biotechnol.* **23**, 313 (2005).
42. M. Keller *et al.*, *Biol. Psychiatry* **59**, 216 (2006).

43. The author is a founder of and holds shares of stock in VisEn Medical, a company that is developing experimental imaging technologies. The author thanks U. Mahmood, M. Harisinghani, and R. Hargreaves for figures and all members of the Center for Molecular Imaging Research for many helpful discussions.

10.1126/science.1125949

PERSPECTIVE

Antiangiogenic Therapy: A Universal Chemosensitization Strategy for Cancer?

Robert S. Kerbel

For more than 50 years, a major goal of research in cancer therapeutics has been to develop universally effective agents that render cancer cells more sensitive to cytotoxic chemotherapy without substantially increasing toxicity to normal cells. The results of recent clinical trials indicate that certain antiangiogenic drugs may produce this long-sought effect. Here, I describe three distinct mechanisms that may help to explain the chemosensitizing activity of these drugs: normalizing tumor vasculature, preventing rapid tumor cell repopulation, and augmenting the antivascular effects of chemotherapy. I then discuss how these potential mechanisms might be exploited to maximize therapeutic efficacy.

In 1971, Judah Folkman first articulated the concept behind what he called "antiangiogenic" drugs: Because progressive tumor growth is dependent on a blood supply, he proposed that treatment with drugs that prevent the formation of tumor blood vessels might be able to constrain cancer for prolonged periods (*1*). Over the next three decades, roughly 10,000 research papers on angiogenesis were published, culminating in a recent report of the first large-scale clinical success of an antiangiogenic drug for cancer treatment (*2*). In this phase III trial, patients with metastatic colorectal cancer who had been treated with a combination of conventional cytotoxic chemotherapy plus bevacizumab, a humanized monoclonal antibody directed against vascular endothelial growth factor (VEGF), showed prolonged survival compared with patients treated with chemotherapy alone (*2*). The combination of bevacizumab (Avastin) and chemotherapy is now approved in the United States and many other countries as a first-line treatment for colorectal cancer. Subsequent phase III trials with bevacizumab and chemotherapy in breast and non–small cell lung cancer have produced similarly promising results (Table 1). In addition, two small-molecule antiangiogenic drugs, SU11248/sunitinib (Sutent) and BAY-43-9006/sorafenib (Nexavar), have been approved as monotherapies for kidney cancer (*3*). Bevacizumab has also shown activity as a monotherapy in kidney cancer (*4*).

These clinical trial results and some others—e.g., in ovarian and pancreatic cancer (*5*, *6*)—underscore the expanding range of tumor types that respond to this class of drugs (Table 1). Although the survival benefits conferred are modest [generally between 2 and 5 months in the completed phase III bevacizumab trials (Table 1)], the results nonetheless represent one

Sunnybrook Health Sciences Centre, Departments of Medical Biophysics and Laboratory Medicine and Pathobiology, University of Toronto, Toronto, Ontario M4N 3M5, Canada. E-mail: robert.kerbel@sri.utoronto.ca

of the most notable advances in cancer research and treatment over the past 3 years (*7*). They raise the possibility that the addition of antiangiogenic drugs to chemotherapy agents might become standard practice in clinical oncology, thus making such drugs "universal" chemosensitizing agents.

This scenario raises a number of interesting questions. For example, although we know bevacizumab's precise molecular target (VEGF), do we really understand how this drug works as an antitumor agent? Why does it prolong survival of patients with advanced cancers primarily when it is combined with cytotoxic chemotherapy? This is especially puzzling because intuitively one would expect antiangiogenic agents to suppress the intratumoral delivery of coadministered drugs by reducing the number of tumor-associated blood vessels and/or by compromising their ability to perfuse blood. Moreover, these two effects would increase the degree and duration of tumor hypoxia, leading to suppression of tumor cell proliferation—yet, it is proliferating tumor cells that are most sensitive to chemotherapy.

This leads to more questions. Is combination with conventional, maximum tolerated dose (MTD) chemotherapy the optimal (or only) way to use chemotherapy with an antiangiogenic drug? Furthermore, why is it that small-molecule receptor tyrosine kinase inhibitors (RTKIs) with antiangiogenic activity have thus far not shown the same chemosensitizing prowess as antibody-based drugs in randomized clinical trials? For example, based on interim or final phase III clinical trial results, neither SU-5416 nor PTK787 (valatinib), which target the VEGF and/or platelet-derived growth factor (PDGF) receptors, enhanced the efficacy of chemotherapy regimens in metastatic colorectal cancer [cited in (*7*, *8*)]. Perhaps, in some cases, the answer lies in the ability of certain antibody-based drugs directed to cell surface antigens to induce antibody-dependent cell-mediated cytotoxicity, a mechanism that makes target cells more vulnerable to attack by the immune system (*9*). Alternatively, the activity differences might be related to differences in suboptimal potency, dosing, and/or pharmacokinetics. The results of ongoing trials with drugs such as sunitinib or sorafenib with chemotherapy should answer this question.

Chemotherapy will remain a mainstay of cancer treatment for many years to come, and it will be increasingly used with antiangiogenic agents, as well as other targeted therapies. Thus, research will focus on the mechanisms by which these drugs assist one another. Understanding these mechanisms will almost certainly lead to improvements in the efficacy of the combination therapies and may increase their cost effectiveness, an issue of growing concern. Indeed, the costs of many targeted cancer drugs can be so high as to threaten their widespread usage, thus potentially negating the decades of inspiring research and discovery that contributed to their development (*10*).

There are other important reasons for focusing on the mechanisms by which these different classes of drugs interact. Conventional chemotherapy can be very toxic, and many antiangiogenic drugs have their own set of toxicities, such as hypertension, blood clotting, and proteinurea, and more rarely, gastrointestinal perforations of the bowel (*4*). Although most of these complications are not severe (bowel perforations and arterial clots being exceptions), there is limited evidence that some (e.g., blood clot formation) may be exacerbated by combining antiangiogenic drugs with certain regimens of chemotherapy (*11*). Acquired resistance to antiangiogenic drugs is also emerging as an issue (*12*, *13*), and combinatorial drug strategies, some involving chemotherapy, are one potential approach for prolonging tumor responses to antiangiogenic drugs, just as antiangiogenic drugs may delay the onset of resistance to chemotherapy drugs. Finally, information about the mechanism of action of antiangiogenic drugs will be important for determining each one's optimal biologic dose, when used in combination treatment regimens.

Table 1. Results of recent clinical trials of antiangiogenic drugs in cancer. The table presents representative examples; it is not intended to be comprehensive. Bevacizumab is a humanized monoclonal antibody directed against VEGF. SU11248/sunitinib is an orally available small-molecule inhibitor of VEGF receptors 1, 2, and 3 and PDGF receptors alpha and beta c-kit and flt-3. BAY-43-9006/sorafenib is an orally available small-molecule inhibitor of VEGF receptors 2 and 3, PDGF receptor beta, and Raf kinase. The results of the following clinical trials were published (*2*, *4*, *18*) or presented at the American Society for Clinical Oncology (*50*–*53*) and are cited in several reviews and commentaries (*3*, *7*, *8*, *15*).

Drug	Trial type	Cancer type	Treatment regimen	Outcome
Bevacizumab	Phase II	Metastatic renal cell cancer	Monotherapy	Benefit in progression-free survival but not overall survival with higher dose (10 mg/kg) (*4*)
Bevacizumab	Phase III	Colorectal cancer	First-line treatment in combination with chemotherapy (5-FU/leucovorin plus irinotecan)	Benefit in both progression-free survival and overall survival (4.7 months) with addition of bevacizumab to chemotherapy (*2*)
Bevacizumab	Phase III	Colorectal cancer	Second-line treatment in combination with "FOLFOX4" chemotherapy (oxaliplatin, 5-FU/leucovorin)	Benefit in progression-free survival and overall survival (2.5 months), compared with chemotherapy (*50*) [cited in (*7*, *15*)]
Bevacizumab	Phase III	Non–small cell lung cancer	First-line treatment in combination with paclitaxel plus carboplatin chemotherapy	Benefit in progression-free survival and in overall survival (2.3 months) with addition of bevacizumab (*51*) [cited in (*7*, *8*, *15*)]
Bevacizumab	Phase III	Metastatic breast cancer	First-line treatment in combination with paclitaxel chemotherapy	Benefit in progression-free survival (about 5 months) based on interim analysis with addition of bevacizumab; overall survival results not yet known (*52*) [cited in (*7*, *8*, *15*)]
SU11248/ sunitinib	Phase II	Cytokine-refractory metastatic renal cell cancer	Monotherapy	Unusually high rate of objective tumor responses detected (40%); stable disease (27%) also seen; overall survival benefit not yet known (*18*) [cited in (*3*)]
BAY-43-9006/ sorafenib	Phase III	Metastatic renal cell cancer	Second-line monotherapy	Significant improvement in progression-free survival despite very low (2%) rate of partial tumor responses (*53*) [cited in (*3*, *8*)]

Here, I describe three distinct mechanistic models that may help to explain the chemosensitizing activity of antiangiogenic drugs, and I discuss some possible clinical implications of each.

Model 1: Antiangiogenic Drugs "Normalize" the Tumor Vasculature, Enhancing the Efficacy of Chemotherapeutic Drugs

Much of the vasculature in tumors is disorganized, leaky, and structurally abnormal (*14*, *15*). The structural eccentricities include absent, reduced, or altered basement membranes and periendothelial support cells such as pericytes; excessively dilated or constricted vessels; and corkscrew-like tortuosities. Tumor vessel leakiness can lead to extravasation of plasma proteins and fluid, producing high interstitial fluid pressures (IFPs) within tumors, which in turn may impede the delivery and diffusion of certain cancer drugs, especially large molecules or immune killer cells (*14*). In addition, the flow and perfusion of blood in many of the tumor vessels may be impaired, which, as noted above, can produce localized and transient areas of hypoxia. As a result, nearby tumor cells may enter a quiescent state that would reduce their inherent sensitivity to chemotherapy and radiation.

It has been postulated that treatment with antiangiogenic agents can transiently reverse some of these abnormalities, a phenomenon called "vessel normalization." For example, it has been proposed that because VEGF is a potent inducer of vascular permeability (*16*), agents that block VEGF activity, such as bevacizumab, would suppress vessel leakiness. Such drugs would also prune immature growing blood vessels—generally considered to be the vessels most sensitive to antiangiogenic drugs—leaving behind an increased proportion of mature, functional vessels. Remaining immature vessels might mature rapidly as a result of an influx of pericytes, driven by the action of PDGF acting on PDGF beta receptors expressed by these cells (*17*). Angiopoietin and the Tie-2 endothelial cell receptor tyrosine kinase may also be involved in this vessel normalization effect (*14*).

Jain and colleagues have hypothesized that these changes generate transient drops in intratumoral IFPs and decrease the level of tumor hypoxia, after the initial expected increase in hypoxia (*14*). Improved delivery of cytotoxic drugs to the tumor during this "normalization window" would coincide with a transient burst in tumor cell proliferation, conceivably leading to increased tumor cell killing (*15*). This hypothesis may explain the failure of certain multitargeted RTKIs to enhance the efficacy of chemotherapy when combined with conventional cytotoxic chemotherapy (*8*). It has been speculated that because pericyte-associated PDGF receptors contribute to vessel normalization, blocking them with PDGF receptor targeting drugs might suppress vessel normalization and thus reduce the efficacy of cytotoxic chemotherapy, or at least have no effect. Thus, counterintuitively, stimulating PDGF (or Tie-2) receptor activity may be an effective strategy in combination therapy situations involving chemotherapy or radiation, whereas inhibiting PDGF receptors would be beneficial when such drugs are used as monotherapies (*14*, *18*), as in the case of SU11248 or BAY-43-9006 for kidney cancer (Table 1).

The results of limited preclinical studies on the kinetics of vessel normalization suggest that the administration of an antiangiogenic agent should precede rather than coincide with chemotherapy; otherwise the normalization window could be missed (*17*). However, many of the successful randomized phase II and III trials of bevacizumab have used concurrent drug administration protocols where one might expect to observe, at least in some cases, a reduction in the efficacy of chemotherapy. In addition, the effects of chemotherapy can be enhanced by an antiangiogenic drug even during sustained increases in hypoxia, with little evidence of vessel normalization (*19*). Indeed, another class of vascular targeting drugs called vascular disrupting agents, which cause rapid occlusion of existing blood vessels in tumors and subsequent massive hypoxia and tumor necrosis, can nevertheless augment the efficacy of chemotherapy or radiation, even though these treatments are less effective against hypoxic tumor cells (*20*). Thus, additional or alternative mechanisms of chemosensitization are presumably involved in such cases. Moreover, almost all the randomized trials of bevacizumab have involved patients with advanced metastatic disease, so many of them would have had multiple metastases of varying size in different organs. Vessel normalization induced by an antiangiogenic drug would have to be precisely synchronized in virtually every such lesion in order to be successfully exploited to bring about an overall chemosensitization benefit and prolong patient survival. If so, exploiting vessel normalization to improve chemotherapy may be most practical in situations involving single localized tumors such as glioblastomas, or when using localized radiation therapy.

Model 2: Antiangiogenic Drugs Prevent Rapid Tumor Cell Repopulation After Cytotoxic Chemotherapy

Treatment of most types of cancer with conventional cytotoxic drugs initially induces tumor shrinkage (the so-called "objective tumor response"), but this is almost always followed by tumor cell repopulation. Moreover, the rate of tumor cell growth tends to be faster the smaller the tumor (as a result of "Gompertzian" growth kinetics), so major shrinkage of tumor mass does not necessarily lead to commensurate prolongation of patient survival times (*21*, *22*). In addition, the rate of tumor cell repopulation does not necessarily decline in proportion to the number of successive courses of cytotoxic chemotherapy or radiation; in fact, the observed trend suggests the opposite effect (*23*). Consequently, it has been argued that implementing therapeutic strategies that dampen the rate of tumor cell repopulation during the break periods between successive courses of MTD chemotherapy may prolong survival times (*22*, *23*). (Such breaks—usually about 3 weeks—permit patient recovery from myelosuppression and other side effects of the chemotherapy.) One way to achieve this goal is to administer the chemotherapy more frequently (e.g., every 2 weeks), a strategy referred to as "dose-dense" chemotherapy (*21*), along with agents that accelerate recovery from myelosuppression (*21*, *23*). Such dose-dense chemotherapy regimens have shown success in early-stage breast cancer as adjuvant therapy (*24*).

A second possible approach is to expose the tumor to an antiangiogenic drug during the break periods between courses of chemotherapy, as discussed by Hudis (*22*). In other words, one should "apply a brake during the break" (*22*, *23*). In a sense, this is the way that bevacizumab is currently used. Unlike most chemotherapy drugs, antibody-based drugs such as bevacizumab can persist in the circulation for 2 to 3 weeks and thus would continue to circulate at relatively high levels during the 3-week break periods. The rationale is that many of the repopulating tumor cells will require oxygen and nutrients delivered by the adjacent tumor vasculature. In this scenario, just when the antibody's inhibitory effects on tumor cell repopulation might begin to wane, the next dose of chemotherapy is administered. As with vessel normalization, this mechanistic model underscores the importance of timing and sequence in achieving the maximal therapeutic benefit from these combination therapies.

Model 3: Antiangiogenic Drugs Augment the Antivascular Effects of Chemotherapy

Many anticancer drugs, including cytotoxic chemotherapy, have been hypothesized to have antiangiogenic activities that contribute to their antitumor efficacy (*25*, *26*). There are at least two plausible explanations for the effect of cytotoxic drugs on the tumor vasculature. First, these drugs could damage or destroy the subset of endothelial cells that proliferate during the formation of new blood vessels (*27*). Research with preclinical models supports this hypothesis (*25*, *26*). Because VEGF is a potent survival factor for activated endothelial cells (*28*) neutralization of VEGF function

should amplify the ability of chemotherapy to damage such cells (*29*–*31*) in the local tumor microenvironment.

A second, more systemic way that chemotherapy might exert effects on the vasculature is by impairing the mobilization, function, or viability of circulating bone marrow–derived cell populations that contribute to angiogenesis. These cells include circulating endothelial progenitor cells (EPCs) that can incorporate into the lumens of nascent vessels and differentiate into mature endothelial cells (*32*, *33*), $CD45^+$ Tie-2–expressing monocytes (*34*), as well as other $CD45^+$ monocyte- and myeloid-like populations (*35*, *36*) that are home to sites of ongoing angiogenesis, adhere to blood vessels and further stimulate angiogenesis (e.g., by secretion of VEGF). Given the well-established myelosuppressive effects of cytotoxic chemotherapy, one might predict that at least some of these proangiogenic bone marrow cell types would be sensitive to chemotherapy. This hypothesis is supported by preclinical evidence showing that chemotherapy can substantially reduce the level of circulating EPCs (*37*, *38*). Moreover, because many of these cell populations can be mobilized into the peripheral blood by growth factors such as VEGF, the combination of a VEGF-targeting agent with chemotherapy would be expected to have an additive, if not synergistic, suppressive effect on these cells. In mice, MTD chemotherapy causes an acute drop in the level of circulating EPCs, but this is followed by a rapid rebound to normal or above normal levels during the subsequent drug-free rest period (*37*). This rebound has also been observed clinically (*39*) and is similar to the effects of chemotherapy on hematopoiesis, namely, a decline in hematopoietic ($CD34^+$) progenitor cells, and hence, neutrophils, followed by mobilization and recovery of such cells during the break period. Thus, the presence or administration of certain antiangiogenic drugs during the break period could, in principle, suppress the EPC rebound and thus increase the efficacy of the chemotherapy by maximizing its antivascular properties, without compromising recovery from myelosuppression. The impact of antiangiogenic drugs has not yet been tested in the context of dose-dense chemotherapy regimens that are supported by hematopoietic growth factors such as granulocyte colony-stimulating factor (G-CSF). There is a reason that this should be given consideration, however. Preclinical studies have shown that G-CSF can mobilize EPCs (*40*, *41*), which theoretically could stimulate tumor angiogenesis and tumor growth (*40*).

In the context of this third mechanistic model, it is interesting to consider a form of dose-dense chemotherapy called ''metronomic'' or ''antiangiogenic'' chemotherapy (*25*, *27*, *29*, *42*). Metronomic chemotherapy refers to the close, regular administration of low, nontoxic doses of chemotherapeutic drugs with no extended drug-free breaks, over prolonged periods (*25*). The antiangiogenic activity of metronomic chemotherapy appears to involve direct killing of endothelial cells in the tumor neovasculature (*27*, *29*) and suppression of circulating EPCs (*37*, *38*, *43*). At least in vitro, dividing endothelial cells are sensitive to very low doses of chemotherapy (*25*, *44*) that do not cause substantial myelosuppression in vivo (*45*, *46*). Because of its low toxicity, metronomic chemotherapy may be well suited for long-term combination with antiangiogenic drugs; such combinations have marked antitumor effects in preclinical models (*25*, *27*, *29*, *42*). Both antibody-based and small-molecule antiangiogenic drugs enhance the effects of metronomic chemotherapy in preclinical models (*29*, *42*). Phase II trials of metronomic chemotherapy (*46*, *47*), sometimes used in combination with antiangiogenic drugs, have yielded encouraging results in patients with advanced cancer (*48*), but larger randomized trials are needed to validate the concept. There is also a need for surrogate markers to help determine the optimal biologic dose of this therapy. Circulating EPCs have been used successfully as a marker in preclinical studies (*38*), but are not yet validated clinically.

Conclusions

Antiangiogenic drugs are on the cusp of fundamentally changing the practice of clinical oncology. While some have shown activity as monotherapies, most clinical trials to date indicate that they are most effective when piggybacked onto traditional therapies, especially chemotherapy. It may be possible to enhance their chemosensitizing activity by using chemotherapy protocols involving close regular dosing with shortened break periods. I have outlined several distinct mechanisms that might underlie their chemosensitizing activity, but these proposed mechanisms are not mutually exclusive; they may operate concurrently or sequentially. In addition, there may be other mechanisms at work that do not depend on the antiangiogenic or vasculature-modifying properties of these drugs. For example, drugs that target VEGF could act directly on tumor cells that aberrantly express VEGF receptors and depend in part on VEGF for their survival (*49*).

Considering the enormous, decades-long, but still mostly clinically unsuccessful efforts aimed at the development of effective chemosensitizers and radiation sensitizers, such as hypoxia-activated bioreductive prodrugs or agents that reverse drug efflux pumps, the chemosensitization prowess of antiangiogenic drugs stands out as a truly unexpected irony. The more we learn about the vascular-modifying properties of antiangiogenic drugs, the more effective they should become, not only as chemosensitizers but possibly as sensitizing agents for other types of cancer drugs, both old and new.

References and Notes

1. J. Folkman, *N. Engl. J. Med.* **285**, 1182 (1971).
2. H. Hurwitz *et al.*, *N. Engl. J. Med.* **350**, 2335 (2004).
3. N. J. Vogelzang, *J. Clin. Oncol.* **24**, 1 (2006).
4. J. C. Yang *et al.*, *N. Engl. J. Med.* **349**, 427 (2003).
5. H. L. Kindler *et al.*, *J. Clin. Oncol.* **23**, 8033 (2005).
6. D. E. Cohn *et al.*, *Gynecol. Oncol.* 10.1016/j.ygyno.2006.01.030 (2006).
7. N. Ferrara, R. S. Kerbel, *Nature* **438**, 967 (2005).
8. J. Marx, *Science* **308**, 1248 (2005).
9. R. A. Clynes *et al.*, *Nat. Med.* **6**, 443 (2000).
10. D. Schrag, *N. Engl. J. Med.* **351**, 317 (2004).
11. L. Ma *et al.*, *Cancer Res.* **65**, 5365 (2005).
12. J. L. Yu, J. W. Rak, B. L. Coomber, D. J. Hicklin, R. S. Kerbel, *Science* **295**, 1526 (2002).
13. O. Casanovas *et al.*, *Cancer Cell* **8**, 299 (2005).
14. R. K. Jain, *Science* **307**, 58 (2005).
15. R. K. Jain, D. G. Duda, J. W. Clark, J. S. Loeffler, *Nat. Clin. Pract. Oncol.* **3**, 24 (2006).
16. D. R. Senger *et al.*, *Science* **219**, 983 (1983).
17. F. Winkler *et al.*, *Cancer Cell* **6**, 553 (2004).
18. R. J. Motzer *et al.*, *J. Clin. Oncol.* **24**, 16 (2006).
19. M. Franco *et al.*, *Cancer Res.* **66**, 3639 (2006).
20. G. M. Tozer, C. Kanthou, B. C. Baguley, *Nat. Rev. Cancer* **5**, 423 (2005).
21. M. L. Citron, *Cancer Invest.* **22**, 555 (2004).
22. C. A. Hudis, *Oncology* **19**, 26 (2005).
23. J. J. Kim, I. F. Tannock, *Nat. Rev. Cancer* **5**, 516 (2005).
24. M. L. Citron *et al.*, *J. Clin. Oncol.* **21**, 1431 (2003).
25. R. S. Kerbel, B. A. Kamen, *Nat. Rev. Cancer* **4**, 423 (2004).
26. K. D. Miller, C. J. Sweeney, G. W. Sledge Jr., *J. Clin. Oncol.* **19**, 1195 (2001).
27. T. Browder *et al.*, *Cancer Res.* **60**, 1878 (2000).
28. T. Alon *et al.*, *Nat. Med.* **1**, 1024 (1995).
29. G. Klement *et al.*, *J. Clin. Invest.* **105**, R15 (2000).
30. J. Tran *et al.*, *Proc. Natl. Acad. Sci. U.S.A.* **99**, 4349 (2002).
31. C. J. Sweeney *et al.*, *Cancer Res.* **61**, 3369 (2001).
32. T. Asahara *et al.*, *Science* **275**, 964 (1997).
33. Y. Shaked *et al.*, *Cancer Cell* **7**, 101 (2005).
34. M. De Palma *et al.*, *Cancer Cell* **8**, 211 (2005).
35. M. Grunewald *et al.*, *Cell* **124**, 175 (2006).
36. T. Udagawa *et al.*, *FASEB J.* **20**, 95 (2006).
37. F. Bertolini *et al.*, *Cancer Res.* **63**, 4342 (2003).
38. Y. Shaked *et al.*, *Blood* **106**, 3058 (2005).
39. G. Furstenberger *et al.*, *Br. J. Cancer* **94**, 524 (2006).
40. T. Natori *et al.*, *Biochem. Biophys. Res. Commun.* **297**, 1058 (2002).
41. T. Okazaki *et al.*, *Int. Immunol.* **18**, 1 (2006).
42. K. Pietras, D. Hanahan, *J. Clin. Oncol.* **23**, 939 (2005).
43. R. Munoz *et al.*, *Cancer Res.* **66**, 3386 (2006).
44. J. Wang *et al.*, *Anticancer Drugs* **14**, 13 (2003).
45. U. Emmenegger *et al.*, *Cancer Res.* **64**, 3994 (2004).
46. M. Colleoni *et al.*, *Ann. Oncol.* **13**, 73 (2002).
47. M. W. Kieran *et al.*, *J. Pediatr. Hematol. Oncol.* **27**, 573 (2005).
48. C. Canady, *Oncol. News Int.* **14**, 8 (2005).
49. J. S. Wey *et al.*, *Br. J. Cancer* **93**, 233 (2005).
50. D. J. Giantonio *et al.*, *2005 ASCO Annu. Meet. Proc.* **23**, 1S (abstr. 2) (2005).
51. A. B. Sandler *et al.*, *2005 ASCO Annu. Meet. Proc.* **23**, 2S (abstr. 4) (2005).
52. K. Miller *et al.*, abstract presented at the 41st Annual Meeting of the American Society for Clinical Oncology, Orlando, FL, 13–17 May 2005.
53. B. Escudier *et al.*, *2005 ASCO Annu. Meet. Proc.* **23**, 380S (abstr. 4510) (2005).

54. I thank C. Cheng for assistance with manuscript preparation and G. Sledge for critical review of the manuscript. I apologize to the numerous investigators whose papers could not be cited because of space limitations. I am a recipient of sponsored research agreements from Taiho Pharmaceuticals, which is developing a drug for use in metronomic chemotherapy, and from ImClone Systems, Inc., which is developing antibody-based antiangiogenic drugs. I am also a paid consultant for both companies. I have received consulting fees and honoraria from Genentech, which markets the antiangiogenic drug bevacizumab, and honoraria from Roche, which markets bevacizumab outside the United States. I am on the Scientific Advisory Boards of and have stock options with Oxigene, Inc., which is developing vascular disrupting agents, and Compound Therapeutics and Attenuon LLC, which are developing antiangiogenic drugs. I have also received honoraria from the following companies developing antiangiogenic drugs: Pfizer, Amgen, Novartis, and Centocor. I do not have planned, pending, or awarded patents related to the work discussed here. I receive research support from the Canadian Institutes of Health, the National Cancer Institute of Canada, and the NIH.

10.1126/science.1125950

PERSPECTIVE

Targeting Tyrosine Kinases in Cancer: The Second Wave

Jose Baselga

One of the most exciting developments in cancer research in recent years has been the clinical validation of molecularly targeted drugs that inhibit the action of pathogenic tyrosine kinases. Treatment of appropriately selected patients with these drugs can alter the natural history of their disease and improve survival. The clinical validation of these "first-generation" tyrosine kinase inhibitors has been the prelude to a second wave of advances in molecular targeting that is expected to further change the way we classify and treat cancer. Efforts are now being directed at identifying the tumor subtypes and patients who will benefit the most from these drugs. In addition, new compounds that circumvent acquired resistance to the first-generation tyrosine kinase inhibitors are being tested in patients with refractory disease. Agents directed against new molecular targets are also being explored.

The rationale for targeting protein tyrosine kinases in human cancer is compelling. These enzymes regulate multiple cellular processes that contribute to tumor development and progression, including cell growth, differentiation, migration, and apoptosis. In model systems, perturbation of tyrosine kinase signaling can result in malignant transformation (*1*). The human genome encodes 90 proteins with tyrosine kinase domains (*2*), and many human tumors display aberrant activation of tyrosine kinases caused by genetic alterations. For tumors whose growth is driven by these activated kinases, targeted drugs can potentially inhibit or reverse malignant progression.

Clinical studies conducted over the past decade have established that tyrosine kinase inhibitors are safe and therapeutically active in selected populations of cancer patients, and several of these drugs are now part of the standard treatment regimen for specific tumor types. These include imatinib (directed against BCR-ABL and other kinases), trastuzumab (directed against the HER2/ErbB2 receptor), and cetuximab, erlotinib, and gefitinib [directed against the epidermal growth factor receptor (EGFR)]. Here, I provide a brief history of the first generation of tyrosine kinase inhibitors and discuss how the lessons learned from initial clinical experience is paving the way for the development of new and more effective drugs.

Oncology Program, Vall d'Hebron University Hospital and Vall d'Hebron Research Institute, Universidad Autónoma de Barcelona, Barcelona 08035, Spain. E-mail: jbaselga@vhebron.net

Imatinib (STI-571, Gleevec)

The discovery of imatinib is rooted in cytogenetic research performed more than 30 years ago on leukemic cells from patients with chronic myelogenous leukemia (CML). These cells display a characteristic reciprocal translocation between chromosomes 9 and 22 that generates the so-called "Philadelphia (Ph) chromosome." At the molecular level, this translocation juxtaposes the coding sequences of the *bcr* gene and *c-abl* genes. The *c-abl* gene encodes a nonreceptor tyrosine kinase, and the genetic fusion creates an oncoprotein, BCR-ABL, with constitutively active tyrosine kinase activity. BCR-ABL powers the rapid clonal expansion of pluripotent hematopoietic stem cells that underlies CML. The uncontrolled kinase activity of BCR-ABL is sufficient to cause leukemia, making it an ideal therapeutic target.

Identification of the causative genetic lesion in CML stimulated a search for inhibitors of the ABL kinase. Screening of compound libraries for molecules that had tyrosine kinase inhibitory activity resulted in the identification of 2-phenylamino pyrimidines as promising agents. From this initial lead, imatinib (STI-571) was synthesized and was found to potently inhibit the proliferation of BCR-ABL–expressing cells and their ability to form tumors in mice (*3*). In the initial trial in patients with CML, imatinib had minimal side effects, and almost all treated patients showed complete hematologic responses, defined as normalization of hematological parameters in the peripheral blood (*4*). Cytogenetic responses, defined as a major reduction in Ph-chromosome–positive cells in the bone marrow, occurred in half of the patients, and several had complete cytogenetic remissions. Responses were also seen in patients with Ph-chromosome–positive acute lymphoblastic leukemia (ALL) and patients with CML in blast crisis. Several later studies confirmed the results of these trials, culminating in the demonstration that imatinib is superior to interferon-α–based treatments in terms of cytogenetic response and likelihood of progression to accelerated-phase or blast crisis CML (*5*).

Imatinib is a "promiscuous" tyrosine kinase inhibitor in that it blocks the activity of additional tyrosine kinases, including the c-Kit receptor and the platelet-derived growth factor receptor (PDGFR). A subset of gastrointestinal stromal tumors (GISTs) display mutations in the *c-KIT* gene and express permanently activated forms of the c-Kit receptor. Patients with such tumors, who are largely unresponsive to conventional chemotherapy, show an excellent response to imatinib (*6*). Interestingly, almost one-third of GISTs lacking mutations in *c-Kit* have intragenic mutations in the *PDGFRA* gene, resulting in constitutively active PDGFRα, a finding that potentially explains the clinical responses to imatinib in GISTs with wild-type *c-Kit*. Imatinib also exhibits robust clinical activity in several other cancers associated with PDGFR alterations (*7*). These include chronic myelomonocytic leukemia (CMML), which is characterized by the constitutively active TEL-PDGFRβ fusion tyrosine kinase; hypereosinophilic syndrome, which is characterized by the FIP1L1-PDGFRα fusion protein; and dermatofibrosarcoma protuberans, which is characterized by a t(17,22) chromosomal translocation leading to constitutive production of PDGF ligand and subsequent PDGFR activation. Together, these results suggest that activating mutations in genes encoding the molecular targets of imatinib are reliable biomarkers of "kinase dependence" and thus may predict which patients are most likely to benefit from the drug.

Trastuzumab (Herceptin)

HER2 is a member of the HER (erbB) family of transmembrane receptor tyrosine kinases, which

also includes EGFR (HER1, erbB1), HER3 (erbB3), and HER4 (erbB4). Receptor-specific ligands bind to the ectodomains of EGFR, HER3, and HER4, resulting in the formation of homodimeric and heterodimeric kinase-active complexes to which HER2 is recruited as a preferred partner (*8*). Interestingly, HER2 does not directly interact with receptor ligands but can potently enhance signaling by HER2-containing heterodimers and/or increase the binding affinity of receptor ligands to EGFR and HER3/4. Overexpression of HER2 causes malignant transformation of mammary epithelial cells. Approximately 25% of invasive primary breast cancers exhibit *HER2* gene amplification, and this molecular feature correlates with reduced patient survival.

Trastuzumab is a humanized monoclonal antibody that binds to the extracellular region of HER2 and inhibits the growth of HER2-overexpressing cells (*9*). Its antitumor activity has been ascribed to several distinct mechanisms, including down-regulation of HER2 from the cell surface membrane, blockade of metalloprotease-induced proteolytic cleavage of HER2, antibody-dependent cell-mediated cytotoxicity (ADCC), and down-regulation of angiogenic factors. In initial clinical studies in the 1990s, trastuzumab was shown to induce tumor regressions in patients with advanced metastatic breast cancer for whom all available lines of therapy had failed. In subsequent studies, trastuzumab was found to offer significant clinical benefit for patients with HER2-positive metastatic breast cancer (*10*) and to improve survival when combined with chemotherapy (*11*). The survival benefits seen with combination therapy were particularly impressive and suggested that the impact of trastuzumab on the course of the disease might be even stronger with earlier treatment. This has now been confirmed in five large studies that together have included more than 14,000 women. The results show that the postoperative administration of trastuzumab to women with HER2-overexpressing breast cancer, given either in combination with chemotherapy or sequentially after chemotherapy has been completed, reduces local and distant (metastasic) recurrences by about one-half (*12*, *13*) and, as expected, improves patient survival by over one-third in those trials with sufficient follow-up (*13*).

It is worth emphasizing that if these pivotal tratuzumab trials had been conducted with breast cancer patients who had not been preselected according to their HER2 status, the therapeutic activity of the drug would likely have been missed, thus threatening its clinical development and approval. This is a recurring scenario in the clinical development of tyrosine kinase inhibitors.

Anti-EGFR Therapies

As noted above, the EGFR has a high degree of homology with HER2, and there are strong similarities in the development of drugs targeting the two receptors. Human tumors of epithelial origin express high levels of EGFR. For this and other reasons, this receptor tyrosine kinase was first proposed as a target for cancer therapy more than 20 years ago [summarized in (*14*)]. Intensive research performed over the ensuing years has resulted in the successful development of two distinct classes of anti-EGFR drugs that have recently received regulatory approval for the treatment of cancer. These are monoclonal antibodies directed against the extracellular domain of the receptor (anti-EGFR MAbs) and small-molecule inhibitors of the receptor's tyrosine kinase activity (TKIs).

The antibody-based drugs compete with ligand for binding to the extracellular domain of EGFR and, as with many other antireceptor antibodies, they induce receptor internalization. The small-molecule inhibitors, on the other hand, act intracellularly by competing with ATP for binding to the tyrosine kinase domain of EGFR, thereby abrogating the receptor's enzymatic activity. The small molecules also block the catalytic activity of EGFR mutants lacking the extracellular domain, and thus may prevent ligand-independent activation of EGF receptor kinase activity as well.

At the level of downstream receptor-dependent signaling pathways, anti-EGFR MAbs and small-molecule TKIs have many similar effects. Both strategies result in an efficient blockade of the major EGFR signal transduction pathways, including the mitogen-activated protein kinase (MAPK) and PI3K/Akt pathways and the Jak/Stat pathway. The mechanisms of action and the antitumor effects of the two drug classes do not completely overlap, however. For example, in addition to promoting receptor internalization, the anti-EGFR MAbs elicit ADCC, which renders tumor cells more vulnerable to attack by the immune system. Conversely, the small-molecule TKIs, but not the antibody-based drugs, are active against more than one ErbB receptor type. The two classes of drugs have additive growth inhibitory effects on cancer cells in vitro (*15*), a finding that has set the stage for ongoing clinical studies combining the two therapies.

Anti-EGFR MAbs have shown clinical activity in a variety of epithelial tumors and one of them, cetuximab, has been approved for the treatment of advanced colorectal cancer and, more recently, head-and-neck tumors. In the setting of colorectal cancer, cetuximab is active in patients whose illness has become refractory to chemotherapy (*16*). However, as with trastuzumab, cetuximab may be most valuable when used earlier in combination with chemotherapy, either as first-line therapy for metastatic disease or in the adjuvant setting. For example, up to 80% of patients respond to the combination of cetuximab and chemotherapy when given as the initial treatment in patients with metastatic colorectal carcinoma. In the setting of advanced head-and-neck tumors, a disease with high morbidity and for which there is a desperate need for new drugs, anti-EGFR MAbs are active in refractory patients previously treated with several lines of chemotherapy and radiation therapy (*17*). In a recent study, treatment of locoregionally advanced head-and-neck cancer with concomitant radiotherapy plus cetuximab was shown to improve locoregional control and reduce mortality without increasing the common toxic effects associated with radiotherapy of this cancer type (*18*). Head-and-neck cancer has been particularly resistant to systemic therapies, and it is noteworthy that cetuximab is the first new treatment approved for this cancer in 30 years.

EGFR TKIs are largely inactive in colorectal cancer; however, two of these drugs, gefitinib and erlotinib, have been approved for the treatment of non–small cell lung cancer (NSCLC). EGFR TKIs also improve survival in patients with advanced pancreatic cancer (*19*), and responses have been observed in head-and-neck cancer (*20*) and in glioblastoma (*21*).

I will discuss in some detail the development of the small-molecule TKIs in NSCLC, as this example best illustrates the progress being made in the field of molecularly targeted therapies. Initial studies of these drugs in patients with refractory disease revealed moderate but real response rates. As was the case with trastuzumab and cetuximab (see above), these agents were then combined with conventional chemotherapy in a series of large (phase III) studies [for review, see (*20*)]. Disappointingly, no additional survival benefit was evident when erlotinib or gefitinib was added to conventional chemotherapy regimens. The anti-EGFR TKIs do show varying degrees of antitumor activity when administered as single agents, however. In a phase III study comparing erlotinib with the best supportive care in NSCLC patients for whom first- or second-line chemotherapy had failed (*22*), those who received TKI showed a statistically significant improvement in response rate and overall survival (6.7 months versus 4.7 months). A similar response rate was observed in a phase III study of gefitinib in NSCLC, although in this case the results did not reach statistical significance (*23*). Although both studies demonstrated that TKIs have a modest level of activity in unselected patient populations, a small subset of patients in the studies appeared to benefit more substantially from the therapy. Patients with adenocarcinoma (particularly bronchioalveolar carcinoma), those who had never smoked, women, and Japanese patients had a higher response rate, which suggests that their particular tumors might be EGFR-dependent. These clinical findings were followed by the discovery that a subset of NSCLCs harbor somatic mutations in the EGFR gene, and the presence of these mutations correlates with a positive clinical response to

gefitinib and erlotinib (*24*, *25*). *EGFR* mutations affecting four exons of the gene have been described: substitutions for G719 in the nucleotide binding loop encoded by exon 18, in-frame deletions within exon 19, in-frame insertions within exon 20, and substitution for L858 or L861 in the activation loop encoded by exon 21.

The clinical benefit observed with anti-EGFR TKIs is not restricted to patients with tumors harboring *EGFR* gene mutations. Other potential markers of sensitivity/resistance to EGFR TKIs include the presence of *EGFR* gene amplification, expression levels of ErbB3, and possibly mutations in the *RAS* and *HER2* genes. Increased *EGFR* copy number and *EGFR* mutations are not mutually exclusive events: About 65% of patients with *EGFR* amplification also have *EGFR* mutations (*26*). On the other hand, the presence of *K-RAS* mutations, which are frequent in smokers, correlates with resistance to EGFR inhibitors (*27*). Mutations in the *HER2* gene have been observed in lung adenocarcinomas (*28*), although their ability to serve as markers of TKI response remains to be explored. Intriguingly, these mutations are small in-frame insertions located in exon 20 in a position analogous to the insertion mutations found in EGFR (codons 774-781). Another potential molecular predictor of response to EGFR TK inhibitors is ErbB-3 protein, which is expressed at high levels in gefitinib-sensitive NSCLC cell lines and in patients responsive to gefitinib therapy (*29*).

Acquired Resistance and Second-Generation Tyrosine Kinase Inhibitors

Despite the early successes with the tyrosine kinase inhibitors discussed above, the majority of responding patients will eventually develop resistance to the drugs. Resistance can be caused by amplification of the oncogenic protein kinase gene or other mechanisms, but in a high fraction of cases, resistance can be traced to the selection of cancer cells with secondary mutations in the gene encoding the targeted kinase. The resistance mutations often affect amino acids within the kinase catalytic domain, and they prevent or weaken interaction of this domain with the drug. Resistance mutations have been observed in the kinase domains of BCR-ABL, Kit, and the PDGFR in the tumor cells of patients treated with imatinib (*30*). Likewise, the tumors of patients who initially responded to gefitinib or erlotinib have been found to acquire secondary *EGFR* mutations that render them resistant to these agents (*31*).

In light of this new challenge, agents active against new mutations that arise during therapy with first-generation tyrosine kinase inhibitors are being rapidly developed (Fig. 1). Dasatinib (BMS-354825), for example, is a dual SRC-ABL inhibitor that binds ABL with less stringent conformational requirements than imatinib (*32*), and it has been shown to be active in patients with imatinib-resistant CML (*33*). In GISTs that have acquired mutations conferring resistance to imatinib, SU11248 (Sutent), a multitargeted tyrosine kinase inhibitor that blocks vascular endothelial growth factor receptor (VEGFR), PDGFR, and KIT activation, has shown substantial activity (*34*). In the case of acquired resistance to drugs targeting EGFR, there seems to be an added complexity because some of the resistance mutations are primary. Patients who initially respond to gefitinib or erlotinib may acquire secondary *EGFR* mutations, specifically the T790M mutation, which resides within the protein's catalytic ATP-binding site (*31*, *35*). However, T790M mutations can also arise in tumors of previously untreated patients; the same is true of an exon 20 insertion mutation that confers resistance (*36*). It is encouraging that tumor cells with acquired or primary mutations conferring resistance to gefinitib and erlotinib appear to be sensitive to a series of irreversible EGFR inhibitors, a group of small-molecule TKI that covalently cross-link the receptor (*37*). Clinical studies of these agents are ongoing in patients with NSCLC.

The molecular mechanisms underlying acquired resistance to trastuzumab are less well defined, although loss of PTEN function and absence or loss of the extracellular, antibody-binding domain of the receptor have been implicated. Lapatinib (GW572016) is a small-molecule dual inhibitor of EGFR and HER2 (*38*) that has shown activity in patients with HER2-overexpressing advanced breast cancer whose disease has progressed after treatment with trastuzumab (*39*). It has also shown activity when administered as a first-line therapy and seems to be synergistic when combined with trastuzumab (*40*, *41*). Large phase III studies are underway both in patients with advanced breast cancer and in the early postoperative setting.

Kinase Dependence in Other Tumor Types: Therapeutic Opportunities

Genome sequence analyses across different tumor types have identified additional tumor-specific activating mutations in tyrosine kinase genes that may drive tumor growth. These include *BRAF* mutations in melanoma (*42*) and mutations in the Flt3 receptor tyrosine kinase in one-third of acute myeloid leukemia (AML) and a smaller group of ALL (*43*). Somatic mutations in the *PI3KCA* gene, which encodes the p110α catalytic subunit of phosphoinositol-3-kinase (PI3K), have also been identified in a wide range of cancers (*44*). *BRAF* mutant tumors are exquisitely sensitive to small-molecule inhibitors of MAPK kinase (MEK) (*45*) and offer a rational therapeutic

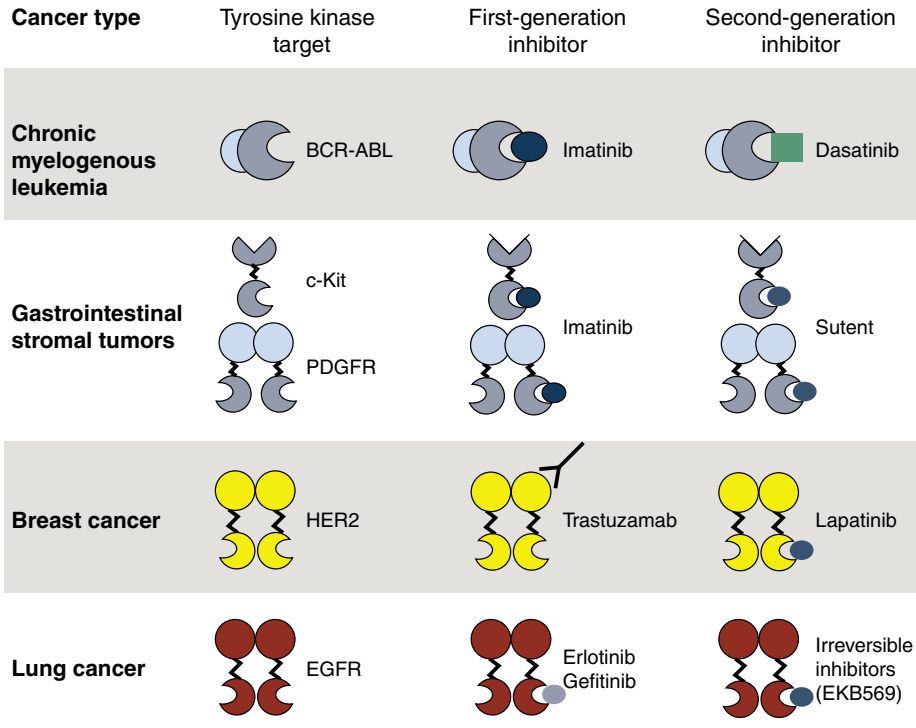

Fig. 1. First- and second-generation tyrosine kinase inhibitors for cancer treatment. Over time, tumors that respond to the first-generation inhibitors often develop resistance to the drugs, in some cases because of the appearance of secondary mutations in the gene encoding the targeted tyrosine kinase. Second-generation inhibitors have been developed to address this problem. The first-and second-generation drugs can be administered sequentially or as a combination therapy.

strategy for this genetically defined tumor subtype. The finding of clinical responses to MEK inhibitors in patients with advanced melanoma is highly encouraging (*46*). Activation of the insulin-like growth factor receptor 1 (IGF-1R) may be involved in abrogating the antitumor effect of EGFR TKIs and trastuzumab (*47*). Targeting of the IGF-1R is being explored in the clinic with small-molecule inhibitors as well as monoclonal antibodies.

Finally, mutations in the *PTEN* (phosphatase and tensin homolog deleted in chromosome 10) tumor suppressor gene are also of interest in the context of kinase dependence. PTEN is a phosphatase that selectively dephosphorylates the lipid phosphatidylinositol (3,4,5) trisphosphate. Loss of PTEN function occurs in a wide range of human cancers (*48*) and is associated with increased PI3K activity. Such tumors are likely dependent on this pathway, as PTEN-null cells are highly sensitive to mTOR and PI3K inhibitors in model systems (*49*). On the basis of these preclinical studies, PTEN mutational status is being used to select patients for enrollment into trials testing the clinical activity of mTOR inhibitors and, in the near future, PI3K inhibitors.

Riding the Second Wave of Tyrosine Inhibitors: Lessons from the Past

How the clinical development of tyrosine kinase inhibition in cancer will ultimately progress is not easy to predict, as the field will at times be driven by unanticipated findings along the way. This unpredictability is exemplified by the discovery of secondary mutations in tyrosine kinase genes in the tumors of patients who developed resistance to imatinib and erlotinib. Although acquired resistance to anticancer agents is an expected consequence of prolonged treatment, it was somewhat surprising that tumor cells with a large repertoire of growth-promoting mechanisms resort instead to reactivation of the same kinase that caused their malignant transformation.

That said, some of the lessons learned from initial clinical experience will surely influence how these drugs will be developed. The activity of imatinib in CML and GIST, trastuzumab in breast cancer, and anti-EGFR agents in NSCLC has validated the concept that certain tumors are "oncogene dependent" (*50*). This underscores the need to direct anticancer drugs to the subset of tumors whose growth depends on the oncogenic signals targeted by the molecular therapies. In other words, random testing of imatinib across tumor types without focusing on Bcr-Abl– and c-Kit–dependent cancers, or of trastuzumab in non-HER2 amplified tumors, would have been a clinical development strategy destined to fail. The second-generation inhibitors that are effective against tumors with acquired drug resistance illustrate the potential of mutation-specific therapies, but they also raise the question of whether secondary resistance might be avoided or delayed by the combined administration of tyrosine kinase inhibitors up front instead of a sequential approach. An answer to this question may come from ongoing clinical trials that are testing combinations of agents directed at a single tyrosine kinase.

The majority of advanced solid tumors are genetically complex and, with rare exceptions, it is unlikely that a given tumor will be entirely dependent on one abnormally activated kinase or signaling pathway for its malignant behavior. There is also a considerable level of compensatory "cross talk" between receptors within one signaling pathway, as well as cross talk between distinct signaling pathways regulating cell proliferation, trafficking, and survival. As with conventional chemotherapeutic agents, which are often most effective when administered as combination therapies, rationally developed combinations of molecularly targeted agents are likely to be more potent than single-agent therapies. In terms of combining molecularly targeted agents with conventional chemotherapy, the negative results of the anti-EGFR TKI studies in NSCLC have greatly limited the enthusiasm to embark on large studies in unselected patient populations.

From a practical standpoint, it will be mandatory to have tumor tissue available from patients participating in clinical trials in order to study the molecular features that correlate with sensitivity or resistance to these molecularly targeted agents. The availability of tissue and serum from all patients may allow retrospective identification of a molecular profile or surrogate marker characteristic of responding tumors, even when the demonstration of activity is limited to a small group of patients. In turn, this profile or marker could be used prospectively for patient enrollment into subsequent studies with selected patients. Ideally, such predictive biomarkers would encompass not only specific gene mutations but also gene expression signatures, which provide information about the activation status of several oncogenic pathways (*51*). At the time of tumor progression, one could also consider assessment of newly acquired mutations to select the next line of therapy. In early studies, incorporation of biomarkers of drug effects and drug sensitivity in tumors will also be coupled with noninvasive molecular imaging, which could provide early indications of clinical benefit (*52*).

Future research on molecularly targeted therapies will focus on the identification of new drugs and drug targets, improved selection of tumors sensitive to these drugs, and the rational design and optimization of combination therapies. The new wave of discoveries will help transform oncology from its current state of empirically based patient management to one in which treatment decisions are based on mechanistic approaches that successfully integrate molecular biology, pathology, imaging, and clinical medicine.

References and Notes

1. P. Blume-Jensen, T. Hunter, *Nature* **411**, 355 (2001).
2. G. Manning, D. B. Whyte, R. Martinez, T. Hunter, S. Sudarsanam, *Science* **298**, 1912 (2002).
3. B. J. Druker *et al.*, *Nat. Med.* **2**, 561 (1996).
4. B. J. Druker *et al.*, *N. Engl. J. Med.* **344**, 1031 (2001).
5. S. G. O'Brien *et al.*, *N. Engl. J. Med.* **348**, 994 (2003).
6. M. C. Heinrich *et al.*, *J. Clin. Oncol.* **21**, 4342 (2003).
7. J. Baselga, J. Arribas, *Nat. Med.* **10**, 786 (2004).
8. Y. Yarden, M. Sliwkowski, *Nat. Rev. Mol. Cell Biol.* **2**, 127 (2001).
9. P. Carter *et al.*, *Proc. Natl. Acad. Sci. U.S.A.* **89**, 4285 (1992).
10. C. L. Vogel *et al.*, *J. Clin. Oncol.* **20**, 719 (2002).
11. D. J. Slamon *et al.*, *J. Med.* **344**, 783 (2001).
12. M. J. Piccart-Gebhart *et al.*, *N. Engl. J. Med.* **353**, 1659 (2005).
13. E. H. Romond *et al.*, *N. Engl. J. Med.* **353**, 1673 (2005).
14. J. Mendelsohn, J. Baselga, *J. Clin. Oncol.* **21**, 2787 (2003).
15. P. Matar *et al.*, *Clin. Cancer Res.* **10**, 6487 (2004).
16. D. Cunningham *et al.*, *N. Engl. J. Med.* **351**, 337 (2004).
17. J. Baselga *et al.*, *J. Clin. Oncol.* **23**, 5568 (2005).
18. J. A. Bonner *et al.*, *N. Engl. J. Med.* **354**, 567 (2006).
19. M. J. Moore *et al.*, *ASCO Meeting Abstracts* **23**, 1 (2005).
20. J. Baselga, C. L. Arteaga, *J. Clin. Oncol.* **23**, 2445 (2005).
21. I. K. Mellinghoff *et al.*, *N. Engl. J. Med.* **353**, 2012 (2005).
22. F. A. Shepherd *et al.*, *N. Engl. J. Med.* **353**, 123 (2005).
23. N. Thatcher *et al.*, *Lancet* **366**, 1527 (2005).
24. T. J. Lynch *et al.*, *N. Engl. J. Med.* **350**, 2129 (2004).
25. J. G. Paez *et al.*, *Science* **304**, 1497 (2004).
26. F. Cappuzzo *et al.*, *J. Natl. Cancer Inst.* **97**, 643 (2005).
27. W. Pao *et al.*, *PLoS Med.* **2**, e17 (2005).
28. P. Stephens *et al.*, *Nature* **431**, 525 (2004).
29. N. Fujimoto *et al.*, *Cancer Res.* **65**, 11478 (2005).
30. H. Daub, K. Specht, A. Ullrich, *Nat. Rev. Drug Discov.* **3**, 1001 (2004).
31. W. Pao *et al.*, *PLoS Med.* **2**, e73 (2005).
32. N. P. Shah *et al.*, *Science* **305**, 399 (2004).
33. M. Talpaz *et al.*, *Blood* (American Society of Hematology annual meeting abstract, 10–13 December 2005, Atlanta, GA) **106**, 40 (2005).
34. G. D. Demetri *et al.*, *ASCO Meeting Abstracts* **22**, 3001 (2004).
35. S. Kobayashi *et al.*, *Cancer Res.* **65**, 7096 (2005).
36. H. Greulich *et al.*, *PLoS Medicine* **2** (2005).
37. T. A. Carter *et al.*, *Proc. Natl. Acad. Sci. U.S.A.* **102**, 11011 (2005).
38. W. Xia *et al.*, *Oncogene* **21**, 6255 (2002).
39. H. A. Burris III *et al.*, *J. Clin. Oncol.* **23**, 5305 (2005).
40. H. L. Gomez *et al.*, American Society of Clinical Oncology (ASCO) annual meeting abstract, 13–17 May 2005, Orlando, FL **23**, 203s, Abs. 3046 (2005).
41. A. M. Storniolo *et al.*, ASCO meeting abstract **23**, Abs. 559 (2005).
42. H. Davies *et al.*, *Nature* **417**, 949 (2002).
43. M. Nakao *et al.*, *Leukemia* **10**, 1911 (1996).
44. Y. Samuels *et al.*, *Science* **304**, 554 (2004).
45. D. B. Solit *et al.*, *Nature* **439**, 358 (2006).
46. P. Lorusso *et al.*, *ASCO Meeting Abstracts* **23**, 3011 (2005).
47. L. J. Chakravarti, *Cancer Res.* **62**, 200 (2002).
48. I. Vivanco, C. L. Sawyers, *Nat. Rev. Cancer* **2**, 489 (2002).
49. M. I. Neshat, *Proc. Natl. Acad. Sci. U.S.A.* **98**, 10314 (2001).
50. I. B. Weinstein, *Science* **297**, 63 (2002).
51. A. H. Bild *et al.*, *Nature* **439**, 353 (2006).
52. R. Weissleder, *Science* **312**, 1168 (2006).

53. The author apologizes to the many authors whose work could not be cited here because of space limitations.
Supported by a Spanish Science and Technology Ministry grant SAF2003-03818 and a Breast Cancer Research Foundation grant.

10.1126/science.1125951

Enhanced Mid-Latitude Tropospheric Warming in Satellite Measurements

Qiang Fu,[1,2]* Celeste M. Johanson,[1] John M. Wallace,[1] Thomas Reichler[3]

Boreal summers that follow strong El Niño events, like the one that occurred in 1997, are often characterized by anomalous tropospheric warmth in mid-latitudes of both the Northern and Southern Hemisphere. This warmth occurs in response to El Niño/Southern Oscillation (ENSO)–induced, positive–sea-surface temperature (SST) anomalies in the Indian and western Pacific Ocean "warm pool" regions (*1*). The anomalous mid-latitude tropospheric warmth is accompanied by an elevation of the pressure surfaces in the upper troposphere and an increased frequency of droughts, including in parts of the United States (*1*, *2*).

From 1979 onward, the most pronounced SST warming has occurred within this same "warm pool" region (*3*). If the planetary-scale atmospheric circulation responds to the multidecadal SST trends in the same way as it responds to ENSO-induced SST variability, one might expect to observe a multidecadal trend toward a warmer mid-latitude troposphere.

We examined atmospheric temperature trends for 1979 to 2005 based on satellite-borne microwave sounding unit (MSU) data (*4*–*6*). Figure 1 shows the global spatial patterns of stratospheric and tropospheric temperature trends for 1979 to 2005 and the corresponding zonal mean latitudinal profiles. To emphasize the spatial gradients in the trends, the reference (white) values in the color bars in (Fig. 1, A and B) are set equal to the respective global mean trends. The most pronounced feature is the enhanced stratospheric cooling and tropospheric warming in the 15 to 45° latitude belts in both hemispheres, relative to other latitudes. The atmospheric trends for 1979 to 1997 (fig. S1) exhibit features similar to those in Fig. 1, which indicates that existence of the trend is not contingent on the episode of record-high mid-latitude temperatures that occurred in summer 1998 in response to the 1997 El Niño (*1*) but is a robust feature of the period of record from 1979 onward (fig. S2). The same pattern is evident in the trend in radiances from MSU channel 2 (fig. S3), which is a further proof of the enhanced mid-latitude tropospheric warming corresponding to the enhanced stratospheric cooling.

Unless it is compensated by a drop in sea-level pressure in the same latitude belt, the observed pattern of temperature changes in Fig. 1 is indicative of a tendency toward an upward bulging of the upper tropospheric pressure surfaces centered around 30° latitude in both hemispheres. Because 30° latitude corresponds to the latitude of the tropospheric jet streams, it can be inferred that the downward slope of the pressure surfaces toward the poles has been increasing on the poleward flanks of the jet streams and decreasing on the equatorward flanks. Such a reshaping of the pressure surfaces would have the effect of shifting the jet streams poleward. Based on the observed temperature changes alone, we estimate that the jet streams in both hemispheres have shifted poleward by ~1° latitude in both summer and winter seasons (*6*). Because the jet streams mark the poleward limit of the tropical Hadley circulation, a systematic poleward shift of the jet streams implies that the tropical circulation has widened by ~2° latitude during this 27-year period (*7*). (Our analysis of the National Centers for Environmental Prediction/National Center for Atmospheric Research reanalyses suggests that sea-level pressures near 30°N and 30°S have risen relative to surrounding latitudes. Such pressure rises, if real, would cause an additional poleward shift in the jet streams.)

In contrast to the seasonally dependent circulation changes reported in association with the Northern and Southern Hemisphere annular modes, the changes reported here are occurring at somewhat lower latitudes, and the Northern Hemisphere trends are no less pronounced during the warm season (fig. S4) than during the cold season.

Whether the observed trends in Fig. 1 are an integral part of the response to greenhouse warming remains to be seen (*8*–*10*). Regardless of the cause, the poleward shift of the jet streams and the associated subtropical dry zone (*11*), if it continues, could have important societal implications.

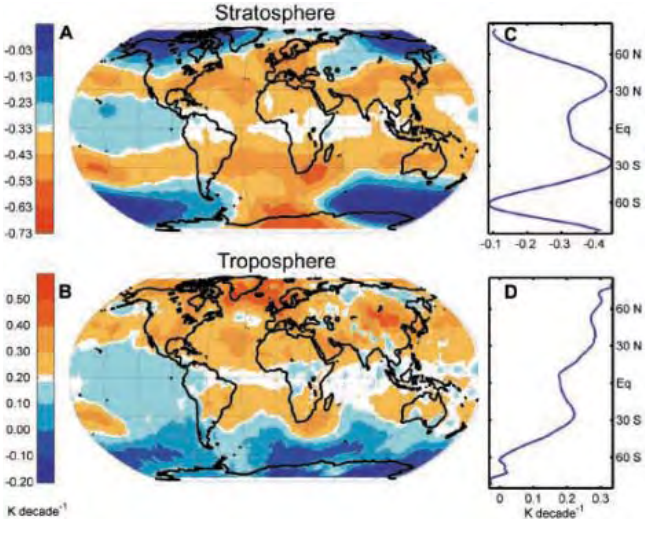

Fig. 1. Global and latitudinal distributions of atmospheric temperature trends for 1979 to 2005 based on satellite-borne MSU observations. (**A** and **C**) Stratospheric trends with a global mean of –0.33 K per decade. (**B** and **D**) Tropospheric trends with a global mean of +0.20 K per decade. Orange shading represents enhanced rates of stratospheric cooling and tropospheric warming relative to their respective global means, and blue shading represents suppressed rates. The polarity is reversed to facilitate comparison between (A) and (B).

References and Notes

1. N. C. Lau, A. Leetmaa, M. J. Nath, H. L. Wang, *J. Clim.* **18**, 2922 (2005).
2. M. P. Hoerling, A. Kumar, *Science* **299**, 691 (2003).
3. T. M. Smith, R. W. Reynolds, *J. Clim.* **18**, 2021 (2005).
4. C. A. Mears, M. C. Schabel, F. J. Wentz, *J. Clim.* **16**, 3650 (2003).
5. Q. Fu, C. M. Johanson, S. G. Warren, D. J. Seidel, *Nature* **429**, 55 (2004).
6. Materials and methods are available as supporting material on *Science* Online.
7. T. Reichler, I. Held, paper presented at the 17th Conference on Climate Variability and Change, Cambridge, MA, 13 to 17 June 2005.
8. State-of-the-art coupled ocean-atmospheric models predict stronger warming in the tropical troposphere than in mid-latitudes (*9*) and a poleward shift of the eddy-driven jets centered ~45° latitude (*10*). A pattern like the recent trends, with strongest tropospheric warming centered ~30° latitude, is not recovered in the simulations.
9. J. T. Houghton, *Climate Change 2001: The Scientific Basis* (Cambridge Univ. Press, Cambridge, 2001).
10. S. S. Leroy, J. G. Anderson, J. A. Dykema, paper presented at the 18th Conference on Climate Variability and Change, Atlanta, GA, 28 January to 3 February 2006.
11. S. D. Schubert *et al.*, *J. Clim.* **17**, 485 (2004).

12. This study is supported by the National Oceanic and Atmospheric Administration grant NA17RJ1232 and NASA grant NNG04GM23G. We thank D. L. Hartmann and J. Paegle for useful discussions.

Supporting Online Material

www.sciencemag.org/cgi/content/full/312/5777/1179/DC1
Materials and Methods
Figs. S1 to S4
References

30 January 2006; accepted 30 March 2006
10.1126/science.1125566

[1]Department of Atmospheric Sciences, University of Washington, Seattle, WA 98195, USA. [2]College of Atmospheric Sciences, Lanzhou University, Lanzhou, Gansu, 730000, China. [3]Department of Meteorology, University of Utah, 135 S 1460 E, Room 819 (WBB), Salt Lake City, UT 84112-0110, USA.

*To whom correspondence should be addressed. E-mail: qfu@atmos.washington.edu

Why the Cosmological Constant Is Small and Positive

Paul J. Steinhardt[1]* and Neil Turok[2]

Within conventional big bang cosmology, it has proven to be very difficult to understand why today's cosmological constant is so small. In this paper, we show that a cyclic model of the universe can naturally incorporate a dynamical mechanism that automatically relaxes the value of the cosmological constant, including contributions to the vacuum density at all energy scales. Because the relaxation time grows exponentially as the vacuum density decreases, nearly every volume of space spends an overwhelming majority of the time at the stage when the cosmological constant is small and positive, as observed today.

One of the greatest challenges in physics today is to explain the small positive value of the cosmological constant or, equivalently, the energy density of the vacuum. The observed value, 7×10^{-30} g/cm^3, is over 120 orders of magnitude smaller than the Planck density, 10^{93} g/cm^3, as the universe emerges from the big bang, yet its value is thought to be set at that time. Even more puzzling, the vacuum density receives a series of contributions from lower energy physical effects, including the electroweak and quantum chromodynamics (QCD) transitions, that only become important at a later stage. Explaining today's tiny value requires a mechanism capable of canceling many very different contributions with near-perfect precision.

One long-standing hope had been to find a symmetry (*1*) or quantum gravity effect (*2*, *3*) that forces the vacuum density to be zero. Another hope had been to find a relaxation mechanism driving it to zero in the hot early universe as the universe expands. These hopes have been hard to reconcile with cosmic inflation and, in any case, have been dashed by recent observations indicating that the vacuum density is small, positive, and very nearly constant (*4*, *5*). Now it is apparent that one does not want a complete cancellation of the cosmological constant. And, in order for a relaxation mechanism to operate within the standard inflationary picture, the relaxation time must at first be much longer than the Hubble time, so inflation can take place; then much shorter than the Hubble time so that nucleosynthesis and structure formation can occur; and then, after that, much longer than the Hubble time again so that the vacuum density is nearly constant today, as observed. Despite many attempts, no simple and compelling mechanism has been found. The frustration has been enough to drive many physicists to consider anthropic explanations (*6*, *7*), in which one assumes that the vacuum density takes on all possible values in different regions of space, but that life is only possible in one of the rare regions where the vacuum density is exponentially small.

In this paper, we point out that a cyclic model of the type described in (*8*, *9*) reopens the possibility of solving the cosmological constant problem with a natural, monotonic relaxation mechanism. In these models, each cycle consists of a hot big bang followed by a nearly vacuous period of dark energy domination, ending with a crunch that initiates the next bang. The duration of a cycle is typically on the order of a trillion years. There is no known limit to the number of cycles that have occurred in the past, so the universe today can plausibly be exponentially older than today's Hubble time and still form galaxies and stars as observed today. Within this cyclic framework, it is reasonable to consider mechanisms for relaxing the cosmological constant whose time scale is always far greater than today's Hubble time. The cosmological constant is exponentially smaller than one might have guessed on the basis of the big bang picture precisely because the universe is exponentially older than the big bang estimate, so the cosmological constant has had a very long time to reduce in value from the Planck scale to the miniscule value observed today. Furthermore, we will show that it is natural to have mechanisms in which the relaxation time increases exponentially as the vacuum density approaches zero from above, resulting in a universe in which nearly every volume of space spends an exponentially longer time in a state with small, positive cosmological constant than in any other state. This is in stark contrast to anthropic explanations, according to which the only regions of space ever capable of producing galaxies, stars, planets, and life are exponentially rare.

Dynamical relaxation: a worked example. As a specific example of a dynamical relaxation mechanism, we adapt an idea first discussed by Abbott (*10*) in the context of standard big bang cosmology [see also (*11*)]. In Abbott's model, the vacuum energy density of a scalar field gradually decays through a sequence of exponentially slow quantum tunneling events, relaxing an initially large positive cosmological constant to a small value. In spite of some appealing features, Abbott found that the mechanism failed, as we will explain, within the context of a big bang universe, essentially because the relaxation occurs far too slowly compared to a Hubble time. In this paper, however, we show that the mechanism becomes viable within the cyclic universe picture.

Abbott's proposal introduces an axion-like scalar field, ϕ, coupled to the hidden nonabelian gauge fields through a pseudoscalar coupling $(\phi/f)F^*F$, with f representing some high energy mass scale and where F is the field gauge strength and F^* is its dual. The theory is assumed to have a classical symmetry

$$\phi \rightarrow \phi + \text{constant} \qquad (1)$$

which is softly broken at low energies by various effects. Integrating out the gauge fields induces a potential of $-M^4 \cos(\phi/f)$, where M is the scale at which the gauge coupling becomes strong. [Fields of this type are commonly invoked to suppress charge-parity (CP) violation in the strong interactions (*12*–*14*) and are also ubiquitous in string theory.]

It is natural for M to be very small as a consequence of the slow (logarithmic) running of the coupling in a nonabelian gauge theory. For example, in QCD with six flavors, $\Lambda_{QCD} = M_{Pl}\exp[-2\pi/(7\alpha_{QCD}M_{Pl})]$ is about 100 MeV if the coupling strength at the Planck scale $\alpha_{QCD}(M_{Pl})$ is about 1/50. [Here and below, M_{Pl} is equal to $(8\pi G)^{-1/2}$.] In Abbott's model for the hidden axion field, M replaces Λ_{QCD} and is similarly expressed in terms of the relevant coupling to hidden gauge fields. For example, if the hidden sector were exactly like QCD, taking $\alpha(M_{Pl}) \sim 1/75$ would give $M \sim 10^{-3}$ eV, a viable value for our model. (Our choices are less extreme than those in Abbott's paper; in the 1980s, his goal was to obtain a very small vacuum density, whereas ours is to explain the observed value.)

The cosine potential breaks the continuous symmetry in Eq. 1 down to a discrete subgroup, $\phi \rightarrow \phi + 2\pi N$, where N is an integer. The discrete symmetry is also assumed to be softly broken by a term proportional to ε, resulting in a "washboard" effective potential:

$$V(\phi) = -M^4 \cos\left(\frac{\phi}{f}\right) + \varepsilon\frac{\phi}{2\pi f} + V_{\text{other}} \qquad (2)$$

where V_{other} includes all other contributions to the vacuum density. (The linearity of the second, soft breaking term is inessential: Any potential will do as long as it is very gently sloping in the region of interest, around $V = 0$.) Provided that $\varepsilon < M^4$, Eq. 2 has a set of equally spaced minima V_N, with effective cosmological constant Λ_{total} spaced by $V_N - V_{N-1} = \varepsilon$ (Fig. 1). No matter what V_{other} is, there is a minimum with $\Lambda_{\text{total}} = V_0$ in the range $0 \leq V_0 < \varepsilon$. Although ε must be chosen to be very small in order to account for today's tiny vacuum density, this choice is technically natural

[1]Joseph Henry Laboratories, Princeton University, Princeton, NJ 08544, USA. [2]Department of Applied Mathematics and Theoretical Physics (DAMTP), Center for Mathematical Sciences (CMS), Cambridge University, Wilberforce Road, Cambridge, CB3 0WA, UK.

*To whom correspondence should be addressed. E-mail: steinh@princeton.edu

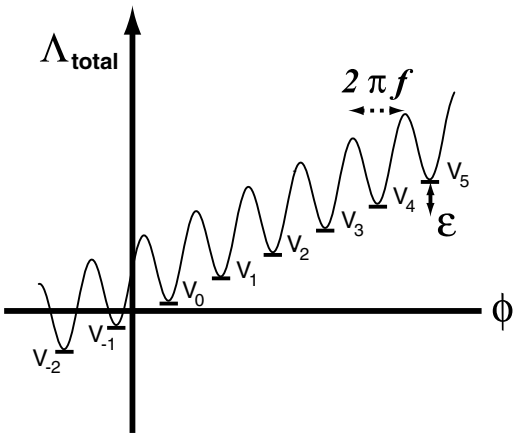

Fig. 1. The effective cosmological constant, Λ_{total}, for the washboard potential defined in Eq. 2 can take discrete values depending on which minimum ϕ occupies. In the scenario presented here, the time spent in the lowest positive minimum is exponentially greater than the entire time spent in all other minima.

within the model because all quantum corrections to ε are proportional to ε. Hence, Abbott's model is a self-consistent low-energy effective theory capable of cancelling contributions to the vacuum density coming from any other source.

In Abbott's scheme, the smallness of the cosmological constant today is related through the relaxation mechanism to the smallness of the parameters M and ε in the potential $V(\phi)$. Effectively, the intractable problem of naturally obtaining an exponentially small cosmological constant is transmuted into a tractable problem of naturally obtaining small axion interaction parameters.

Abbott assumed that the universe emerges from the big bang with some large positive value of ϕ and quickly settles into a minimum with large positive V_N, driving a period of de Sitter expansion that dilutes away any matter and radiation. Over time the field ϕ then works its way slowly but inexorably downhill. In flat spacetime, the tunneling events would occur at a constant rate independent of N. However, once the effects of gravity are included, the tunneling rate becomes slower and slower as V_N decreases. As we shall see, the universe remains in the last positive minimum for a relative eternity compared with the time spent in reaching it. This is the basis for our claim that the most probable value for the vacuum density in the model is that of the last positive minimum.

Assuming the field starts high up the potential, $V_N \gg M^2 M_{\rm Pl}^2$, de Sitter fluctuations overwhelm the energy barriers and the field makes its way quickly downhill. But as V_N falls below $M^2 M_{\rm Pl}^2$, the barriers become increasingly important and the field progresses downward by quantum tunneling via bubble nucleation (*15*). Upward tunneling is also allowed but hugely suppressed in the parameter range of interest (*16*).

For simplicity, we shall focus on the parameter range $f^2/M_{\rm Pl}^2 \ll \beta < 1$, where $\beta \equiv \varepsilon/M^4$ is the ratio of the difference between energy minima to the height of the energy barrier. In the semiclassical approximation, the rate for nucleating bubbles of vacuum energy density V_{N-1} beginning from the V_N phase is $\Gamma(N) \propto \exp[-B(N)]$, where $B(N)$ is the Euclidean action for the tunneling solution. In order to describe the scaling of $B(N)$ with N, we shall neglect unimportant numerical coefficients and approximate $V_N \approx \beta N M^4$.

As ϕ tunnels toward minima with decreasing N, the nucleation rate decreases monotonically through three scaling regimes that match smoothly onto one another:

1) For $N > M_{Pl}^2/(f^2\beta) \equiv N_{\rm HM}$, the de Sitter radius is smaller than the bubble wall thickness, $\sim fM^{-2}$, and the relevant instanton is the Hawking-Moss solution (*17*). In this regime, $B(N)$ is proportional to N^{-2}.

2) For $N_{\rm CD} < N < N_{\rm HM}$, where $N_{\rm CD} \equiv M_{\rm Pl}^2\beta/f^2$, the relevant instantons are of the Coleman-De Luccia type (*15*) and the thin wall approximation becomes increasingly accurate. The bubbles are in the scaling regime described by Parke (*18*), where the bubble radius is controlled by gravitational effects. In this regime, $B(N)$ is proportional to $N^{-3/2}$.

3) As N falls below $N_{\rm CD}$, the bubble radius becomes much smaller than the de Sitter radius, and the instantons are well approximated by the flat spacetime bubble solution. Although gravitational effects increase the action by only a small factor in this regime, the correction is very important because B_0 is so large. The leading gravitational correction is given by

$$B(N) = B_0\left(1 - \frac{3}{2}\frac{(V_N + V_{N-1})T^2}{M_{\rm Pl}^2\varepsilon^2}\right) \quad (3)$$

where the flat spacetime bubble action, B_0, equals $(27/8)\pi^2T^4/\varepsilon^3$, with T as the wall tension. In a cosine potential this is $8M^2f$. B_0 is an enormous number, $\sim 10^{110}$, for plausible parameters $f \sim 10^{14}$ GeV, $\beta \sim 0.1$, and $M \sim 10^{-3}$ eV. The gravitational correction causes the bubble action to decrease linearly with N in this final regime. Thus, as N approaches zero from above, the time spent at vacuum density V_N scales parametrically as $\exp[-B_0(N/N_{\rm CD})]$, where $N_{\rm CD}$ is given above. For example, with our chosen parameters the time spent at the last positive value of the vacuum energy density is more than $10^{10^{110}}$ times longer than the entire time spent before it.

The whole process ends when ϕ tunnels through to negative potential energy. Then, the negative potential causes the space within the bubble to collapse in a time of order one Hubble time. (For this reason, it makes no difference whether the field could have tunneled further downhill or not because the region will collapse before it tunnels further downhill.) Space outside the bubble continues to expand from cycle to cycle, so there always remain regions with positive cosmological constant. Hence, the relaxation process we have described naturally leads to a universe that is overwhelmingly likely to possess a small positive cosmological constant, in agreement with observation.

Despite its attractive features, the proposal proves to be fatally flawed in a standard big bang cosmology setting, as Abbott himself pointed out, because of the "empty universe problem." Each time the universe is caught in a minimum, it undergoes a period of inflation that empties out all matter and radiation. When a bubble is nucleated, its interior is nearly empty, too. At most, it contains an energy density, ε, and even if this is turned entirely into matter and radiation it is far too low to make planets, stars, or galaxies. In fact, whatever density does lie within the bubble is rapidly diluted away by the next bout of de Sitter expansion. The process continues; new bubbles are formed within the old, but at each stage the energy density is far too small to explain the observed universe. In effect, the problem is that the relaxation process is too slow for standard big bang cosmology, so that the universe is empty by the time the cosmological constant reaches the requisite value.

Cyclic model with dynamical relaxation. With this thought in mind, we now turn to the cyclic model of the universe (*8*, *9*). According to the cyclic picture, each big bang is a collision between orbifold planes (branes) along an extra dimension of space, as might occur in heterotic M-theory (*19*). A weak, springlike force draws the branes together at regular intervals, resulting in periodic collisions that fill the universe with new matter and radiation. After each collision, the branes separate and start to re-expand, causing matter and radiation to cool and spread out. Eventually, the matter and the radiation become so dilute that the potential energy associated with the interbrane force takes over.

In the low energy four-dimensional (4D) effective theory, the interbrane distance can be described by a modulus field, ψ, that moves back and forth along its effective potential. When the branes are far apart, the potential energy density is positive and acts as dark energy, causing the branes to expand at an accelerating rate and diluting away the matter and the radiation created at the bang. At the same time, the force draws the branes together, causing the potential energy density to decrease from positive to negative. As the branes accelerate toward one another, their expansion slows.

Ripples in the branes caused by quantum fluctuations are amplified by the interbrane force as the branes approach one another into a scale-invariant spectrum of growing energy density perturbations. The branes remain stretched out, though, and any matter and radiation within them remains dilute. So, after a period of a trillion years or so, the nearly

empty branes collide, creating new matter and radiation and initiating a new cycle of cosmic evolution. In dealing directly with the big bang singularity, the cyclic scenario poses new challenges to fundamental theory, and some aspects are still being actively debated (*20*–*24*). Here, we shall assume the cyclic picture is valid.

Now, let us suppose we add to this story the axion-like field ϕ and the associated hidden gauge sector as entities on one of the two branes. Surprisingly, although it was not invented for this purpose, the cyclic model has just the right properties to make Abbott's mechanism viable, leading to the prediction we have emphasized: a small, positive cosmological constant. Four features inherent to the cyclic model play a key role in rendering the combined model viable.

First and foremost, the cyclic model regularly replenishes the supply of matter and radiation, instantly solving the empty universe problem. Brane collisions occur every trillion years or so, an infinitesimal time compared with the eons it takes the universe to tunnel from one minimum to the next. So, between each step down the washboard potential, the universe undergoes exponentially many cycles. Each bubble that is nucleated fills with matter and radiation at the cyclic reheat temperature, $T_{\mathrm{reheat}} \sim 10^8$ GeV or so (*21*), at each new brane collision. The value of ε is far smaller than the energy scale associated with the collision, so the washboard potential has little effect on reheating. Instead, it controls the low energy density, de Sitter–like phase of each cycle, ensuring the cycling solution is a stable attractor (*9*). For $f \gg T_{\mathrm{reheat}}$, ϕ is only weakly coupled to the matter and radiation, and the reheating process does not significantly affect the evolution of ϕ.

A second essential element of the cyclic model is the orbifold (brane) structure. If ϕ were coupled to the usual 4D Einstein metric, its kinetic energy would be strongly blueshifted during the periods of Einstein-frame contraction. Instead of proceeding in an orderly manner down the washboard potential, it would be excited by the contraction and jump out of the minimum, accelerating off to infinity as the crunch approached. In the cyclic model, the behavior is quite different because ϕ couples to the induced metric on the brane, not the 4D effective Einstein-frame metric. The brane expands exponentially from cycle to cycle and never contracts to zero; only the extra dimension that separates the branes does that. Consequently, the kinetic energy of ϕ is red-shifted and diluted during every cycle, even during the phases when the extra dimension (and the Einstein-frame 4D effective scale factor) contracts to zero. Thus, ϕ remains trapped in its potential minimum for exponentially long periods until the next bubble nucleation occurs.

The reheating of the universe at the beginning of each cycle also does not excite ϕ because it is so weakly coupled. In fact, by causing the expansion to decelerate and hence suppressing the de Sitter fluctuations in ϕ, the matter and the radiation actually decrease the nucleation rate. The majority of tunneling events occur during vacuum energy domination, which is the longest phase of each cycle.

A third advantageous feature of the cyclic model is that, because the homogeneity and isotropy of the universe and the generation of density perturbations are produced by very low-energy physics, there is no inflation and, hence, no need to tune the relaxation to be slow and then fast.

A fourth critical aspect of the cyclic model is that dark energy acts as a stabilizer. By diluting the density of matter and radiation and any random excess kinetic energy of the branes produced at the previous bounce, the dark energy ensures that the cycling solution is a stable attractor (*9*). When we add the washboard potential, the dark energy density depends on $V(\phi)$. The value decreases by ε each time a bubble is nucleated. As long as the dark energy density is positive, the cyclic solution remains a stable attractor. Once the sum becomes negative, the periodic cycling comes to an end. Most likely, the interior of the negative potential energy bubble collapses into a black hole, detaching itself from the universe outside it and ending cycling in that small patch of space, but the rest of the universe continues to cycle stably.

Putting these ideas together, the cyclic model and Abbott's mechanism are merged into a new scenario that greatly modifies both. In the combined picture, there are two fundamental time scales that govern the long-term evolution of any patch of universe: the cycling time, τ_{cycle}, and the time it takes to nucleate bubbles, τ_N. The latter increases exponentially as the universe tunnels from large N toward $N = 0$, and, during each of the stages we have described, τ_N is exponentially greater than τ_{cycle}. So, for each jump in ϕ the universe undergoes many cycles and many big bangs. When V_N is large, the vacuum energy density dominates the universe at an earlier point in the cycle compared with when V_N is small, before matter has a chance to cool and form stars, planets, or life. But, nothing happens to disrupt the evolution. The universe simply continues cycling as ϕ continues to hop down the potential, each step taking exponentially longer than the one before. Finally, V_N becomes small enough that structure begins to form. How big N is before this occurs depends on ε; for our example above, galaxy formation occurs during the last few hundred steps or so. However, exponentially more time and more cycles are spent at $V = V_0$ than at any other value.

Discussion. We have focused on Abbott's particular mechanism, but we can extract from this case the conditions that are generally required: (i) a relaxation time much greater than today's Hubble time and (ii) a dynamics that collapses or recycles any regions with negative cosmological constant on a much shorter time scale. In our example, the relaxation time increases as the cosmological constant approaches zero, so that the system spends most of the time at the lowest positive value. However, it is also interesting to consider other parameter ranges or other forms for $V(\phi)$, including the pure linear potential invoked in the anthropic model of (*6*), which has no local minimum to be fixed. In this model, the relaxation time decreases as the cosmological constant approaches zero from above. By introducing cycling and restricting attention to the past light cone of any observer, we find that most galaxies are produced when the vacuum density is smaller, but not much smaller, than the matter density.

In either example, our result is a universe in which the cosmological constant $\Lambda(t)$ is an ultra-slowly varying function of time t and in which virtually every patch of space proceeds through stages of evolution that include ones in which $\Lambda(t)$ is small enough to be habitable for life. It is interesting to contrast this situation with the anthropic picture, especially versions based on inflationary cosmology, for which the fraction of habitable space is infinitesimally small. All other things being equal, a theory that predicts that life can exist almost everywhere is overwhelmingly preferred by Bayesian analysis (or common sense) over a theory that predicts it can exist almost nowhere.

Although the relaxation time scale is far too slow to be detectable, the general picture we have suggested here can be falsified. First, because it relies on the cyclic model, it inherits the cyclic prediction for primordial gravitational waves (*25*). Second, one might look for other implications of having an exponentially long time for fields or couplings to evolve. For example, axions in QCD and string theory with $f \gg 10^{12}$ GeV are well motivated theoretically but ruled out in conventional inflationary theory because de Sitter fluctuations typically excite the field to a value where its energy density overdominates the universe today (*26*). Some propose resolving this dilemma, also, using the anthropic principle (*27*, *28*), but then the same reasoning suggests that axions should contribute all or most of the dark matter density today (*29*). In the alternative picture we have presented, though, there is no inflation and axions are never excited. So, finding axions with large f and negligible density would be an embarrassment for the inflationary picture but would fit naturally in the picture outlined here. Similar considerations apply to other solutions to the strong CP problem (*30*) where a very long relaxation time may be useful.

References and Notes

1. A. D. Linde, *Phys. Lett. B* **200**, 272 (1988).
2. S. W. Hawking, *Phys. Lett. B* **134**, 403 (1984).
3. S. Coleman, *Nucl. Phys. B* **310**, 643 (1988).
4. S. Perlmutter *et al.*, *Ap. J.* **517**, 565 (1999).
5. A. G. Riess *et al.*, *Ap. J.* **116**, 1009 (1998).
6. A. D. Linde, in *300 Years of Gravitation*, S. W. Hawking, W. Israel, Eds. (Cambridge Univ. Press, Cambridge, 1987), pp. 604–630.
7. S. Weinberg, *Phys. Rev. Lett.* **59**, 2607 (1987).
8. P. J. Steinhardt, N. Turok, *Science* **296**, 1436 (2002); published online 25 April 2002 (10.1126/science.1070462).
9. P. J. Steinhardt, N. Turok, *Phys. Rev. D* **65**, 126003 (2002).
10. L. Abbott, *Phys. Lett. B* **150**, 427 (1985).
11. J. D. Brown, C. Teitelboim, *Phys. Lett. B* **195**, 177 (1987).
12. R. D. Peccei, H. R. Quinn, *Phys. Rev. Lett.* **38**, 1440 (1977).
13. S. Weinberg, *Phys. Rev. Lett.* **40**, 223 (1978).
14. F. Wilczek, *Phys. Rev. Lett.* **40**, 279 (1978).
15. S. R. Coleman, F. De Luccia, *Phys. Rev. D* **21**, 3305 (1980).

16. K. Lee, E. J. Weinberg, *Phys. Rev. D* **36**, 1088 (1987).
17. S. W. Hawking, I. G. Moss, *Phys. Lett. B* **110**, 35 (1983).
18. S. J. Parke, *Phys. Lett. B* **21**, 313 (1983).
19. J. Khoury, B. A. Ovrut, P. J. Steinhardt, N. Turok, *Phys. Rev. D* **64**, 123522 (2001).
20. G. Felder, A. Frolov, L. Kofman, A. Linde, *Phys. Rev. D* **66**, 023507 (2002).
21. J. Khoury, P. J. Steinhardt, N. Turok, *Phys. Rev. Lett.* **92**, 031302 (2004).
22. P. Creminelli, A. Nicolis, M. Zaldarriaga, *Phys. Rev. D* **71**, 063505 (2005).
23. T. J. Battefeld, S. P. Patil, R. Brandenberger, *Phys. Rev. D* **70**, 066006 (2004).
24. P. McFadden, N. Turok, P. J. Steinhardt, published online 12 December 2005 (http://arxiv.org/pdf/hep-th/0512123).
25. L. A. Boyle, P. J. Steinhardt, N. Turok, *Phys. Rev. D* **69**, 127302 (2004).
26. For a recent discussion, see P. Fox, A. Pierce, S. Thomas, published online 3 September 2004 (http://arxiv.org/pdf/hep-th/0409059).
27. M. S. Turner, F. Wilczek, *Phys. Rev. Lett.* **40**, 279 (1978).
28. A. D. Linde, *Phys. Lett. B* **259**, 38 (1991).
29. M. Tegmark, A. Aguirre, M. J. Rees, F. Wilczek, *Phys. Rev. D* **73**, 023505 (2006).
30. T. Banks, M. Dine, N. Seiberg, *Phys. Lett. B* **273**, 105 (1991).

31. We thank A. Upadhye, E. J. Weinberg, and the participants of the workshop Expectations of an Ultimate Theory held in Trinity College, Cambridge, in September 2005, for useful discussions. This work is supported in part by the Particle Physics and Astronomy Research Council (N.T.) and by U.S. Department of Energy grant DE-FG02-91ER40671 (P.J.S.).

14 February 2006; accepted 28 March 2006
Published online 4 May 2006;
10.1126/science.1126231
Include this information when citing this paper.

Regulatory Blueprint for a Chordate Embryo

Kaoru S. Imai,[1] Michael Levine,[2] Nori Satoh,[1] Yutaka Satou[1]*

Ciona is an emerging model system for elucidating gene networks in development. Comprehensive in situ hybridization assays have identified 76 regulatory genes with localized expression patterns in the early embryo, at the time when naïve blastomeres are determined to follow specific cell fates. Systematic gene disruption assays provided more than 3000 combinations of gene expression profiles in mutant backgrounds. Deduced gene circuit diagrams describing the formation of larval tissues were computationally visualized. These diagrams constitute a blueprint for the *Ciona* embryo and provide a foundation for understanding the evolutionary origins of the chordate body plan.

During the past three decades, there has been remarkable progress in identifying the regulatory genes and signaling pathways responsible for the development of a variety of tissues and organs in worms, fruit flies, sea urchins, zebrafish, frogs, chicks, and mice. However, there are just a few cases where this information has been integrated to produce gene regulation networks embodying the functional interconnections among the genes responsible for a given developmental process. The best success has been obtained for the specification of endomesoderm in the pregastrular sea urchin embryo (*1*) and the dorsal-ventral patterning of the early *Drosophila* embryo (*2*). Significant progress has also been made on the specification of the "Spemann organizer" in the *Xenopus* embryo (*3*).

The ascidian *Ciona intestinalis* provides an ideal experimental system to elucidate gene regulatory networks. The ascidian tadpole shares a common body plan with vertebrates (*4*), including a notochord centered in the tail that is flanked dorsally by the nerve cord, laterally by muscle, and ventrally by endoderm. The mature ascidian larva is composed of ~2600 cells, and the genome contains only 16,000 genes (*5*). This genetic and cellular simplicity offers the promise of superimposing gene networks onto the behavior of individual cells during specification and differentiation in early embryos. Such networks would provide a detailed understanding of complex morphogenetic processes and would establish a foundation for determining the evolutionary origins of chordate features in lower Deuterostomes (e.g., starfish and acorn worms) and their subsequent elaboration in vertebrates.

Here we present the systematic analysis of the 76 zygotic regulatory genes controlling *Ciona* embryogenesis during the time when the basic chordate tissues are specified and begin to differentiate. Particular efforts focus on the transcription factors and signaling components dedicated to the major tissues of the early tadpole. *Macho-1*, *Tbx6b*, and *ZicL* are expressed in the tail muscles (*6*–*9*); *β-catenin* and *Lhx3* in the endoderm (*10*, *11*); *Fgf9/16/20*, *FoxA-a*, *FoxD*, *ZicL*, and *Brachyury* in the notochord (*7*, *12*–*14*); and *Fgf9/16/20*, *Nodal*, *Otx*, and *GATA-a* in the CNS (*15*, *16*). Gene disruption and in situ hybridization assays were used to create circuit diagrams showing the functional interconnections among the signaling pathways and regulatory factors governing the dynamic cellular interactions underlying the formation of the nerve cord, notochord, heart, and other key chordate tissues. These circuit diagrams constitute a blueprint for *Ciona* embryogenesis.

Regulatory codes for defined lineages. Previous comprehensive in situ hybridization assays showed that the *Ciona* genome contains 65 genes encoding sequence-specific transcription factors (TFs) and 26 genes encoding components of cell signal transduction molecules (STs) that are zygotically expressed between the 16-cell and early gastrula stages of embryogenesis (*17*, *18*). Because of difficulties measuring zygotic transcription of genes expressed both maternally and zygotically, we excluded those genes exhibiting abundant maternal transcripts, thereby restricting the total to 53 TF genes and 23 ST genes (table S1). We do not regard the exclusion of maternal genes as a major limitation, because they are used to establish a regulatory prepattern in 16-cell embryos. The link between this prepattern and the establishment of definitive larval tissues is the major focus of the present study.

From the 16-cell to early gastrula (around 110-cell) stage, most of the blastomeres can be assigned a unique identity on the basis of the expression of specific combinations of TF genes (regulatory code; summarized in fig. S1). There is a close correspondence between establishing different regulatory codes and forming diverse cell lineages (Fig. 1). For example, the blastomeres that form the primitive gut (endoderm; A6.1, B6.1, and A6.3 at the 32-cell stage; and A7.1, A7.2, A7.5, B7.1, and B7.2 in 64-cell embryos) have slightly different regulatory codes during early cleaving embryos (fig. S2, A and B) but acquire identical codes at the early gastrula stage. The b5.3 and b5.4 blastomeres contain similar regulatory codes at the 16-cell stage. At the gastrula stage, descendants that give rise to nerve cord cells (b8.17 and b8.19) acquire a regulatory code that is distinct from their sister cells that give rise to epidermal cells (b8.18 and b8.20). The latter cells have a code that is similar to those of other epidermal cells, which indicates an inductive event at or before this stage. All lineages except the B7.5 blastomeres, which form the heart (trunk ventral cells) and anterior tail muscles, achieve clonal restriction before gastrulation. Thus, the hierarchical clustering of cell identities with similar regulatory codes accurately reflects cell lineages and the clonal restriction of cell fate and illuminates at what point key molecular interactions occur to establish a unique identity for each cell.

In order to define distinct neuronal cell identities, it was necessary to extend the analysis of regulatory codes beyond the early gastrula stage because of the complexity of neural cell types. Systematic in situ hybridization assays suggested that there are at least 13 distinct neuronal cell types composing the future central and peripheral nervous system at the late gastrula stage (Fig. 2, A and B;

[1]Department of Zoology, Graduate School of Science, Kyoto University, Sakyo-ku, Kyoto, 606-8502, Japan. [2]Department of Molecular and Cellular Biology, Division of Genetics and Development, University of California, Berkeley, CA 94720, USA.

*To whom correspondence should be addressed. E-mail: yutaka@ascidian.zool.kyoto-u.ac.jp

fig. S3A). There are also at least six different TF-ST combinations in the epidermis of tailbud stage embryos (Fig. 2C; fig. S3B). The TF-ST codes identified for the neuronal and epidermal cell types in the *Ciona* tadpole could be useful for determining whether comparable cells exist in the diffuse nervous systems of lower Deuterstomes, such as starfish (echinoderms) and acorn worms (hemichordates).

Elucidation of provisional gene networks. There are five distinct regulatory codes seen for the eight different blastomeres (paired blastomeres are identical across the left-right axis) in 16-cell embryos (Fig. 1, A and B): anterior animal blastomeres (a-line blastomeres), posterior animal blastomeres (b-line blastomeres), anterior vegetal blastomeres (A-line blastomeres; not identical to each other, but very similar), the posterior vegetal blastomere (B5.1 blastomeres), and the posteriormost blastomere (B5.2). *FoxA-a*, *FoxD*, *Tbx6a*, *Tbx6b/c/d* (fig. S1), and *Fgf9/16/20* (*13*) display restricted patterns of zygotic expression in 16-cell embryos. These restricted patterns constitute a prepattern that is used to produce the major larval tissues. For example, *FoxD* makes presumptive notochord cells competent for response to Fgf/9/16/20 by activating *ZicL* expression (see also supporting online text). The link between the 16-cell prepattern and the specification of basic chordate tissues is described below.

Perturbation of TF and ST gene function was achieved by microinjection of morpholino oligonucleotides (MOs; supporting online text) (*19*). MOs were designed for 70 of the 76 genes (table S2), but 30 of them failed to produce clear mutant phenotypes when microinjected into fertilized eggs (Table 1). Four of the MOs severely slowed cleavage; another nine produced additional nonspecific defects. The remaining 27 MOs produced unambiguous and specific mutant phenotypes (Table 1). The identification of specific mutant phenotypes for 27 of 70 MOs (~40%) is consistent with previously reported "hit-rates" using single MOs for a given gene (*20*).

Quantitative reverse transcription–polymerase chain reaction (qRT-PCR) assays were used to examine the expression profiles of 73 of the 76 TF and ST genes in 25 of the 27 mutants at the early gastrula stage (*21*) (table S3; fig. S4). In situ hybridization assays were used to determine the detailed expression profiles of subsets of the TF and ST genes in select mutant backgrounds (table S4; figs. S5 and S6). In addition, 39 TF and 12 ST genes were similarly examined in the 27 mutants at the late gastrula stage (tables S4 and S5; figs. S5, S6, and S7). Finally, 16 mutants were examined at tailbud stages using 17 different TF and ST in situ hybridization probes (table S4; figs. S5 and S6). Overall, the resulting analysis provided more than 3000 combinations of gene expression profiles and mutant backgrounds. This information, along with earlier results, was used to create a provisional circuit diagram showing the interconnections among 79 TF and 25 ST genes controlling cell-fate specification and the initial phases of tissue differentiation (Fig. 3A).

The entire analysis of TF and ST expression profiles in MO mutant embryos is available on a World Wide Web interface [(*22*) or Database S1]. The circuit diagrams are illustrated for individual blastomeres in successively older embryos extending to the early gastrula stage. At later stages, the diagrams encompass groups of cells forming discrete tissues.

Circuit diagram for the notochord. The prepattern seen in 16-cell embryos establishes the presumptive notochord through the activation of *Brachyury* expression. *Brachyury* encodes a T-box transcription factor that regulates a variety of target genes controlling the cell shape changes and intercalary movements accompanying notochord differentiation (*23*).

The anterior 32 notochord cells arise from the A7.3 and A7.7 blastomeres at the 64-cell stage. A-line activation depends on *ZicL* and *Fgf9/16/20* (*7*, *13*) (Fig. 3B). *Fgf9/16/20* signaling may be mediated by phosphorylation of the ETS-containing transcription factor, ets/pointed2. *ZicL* is

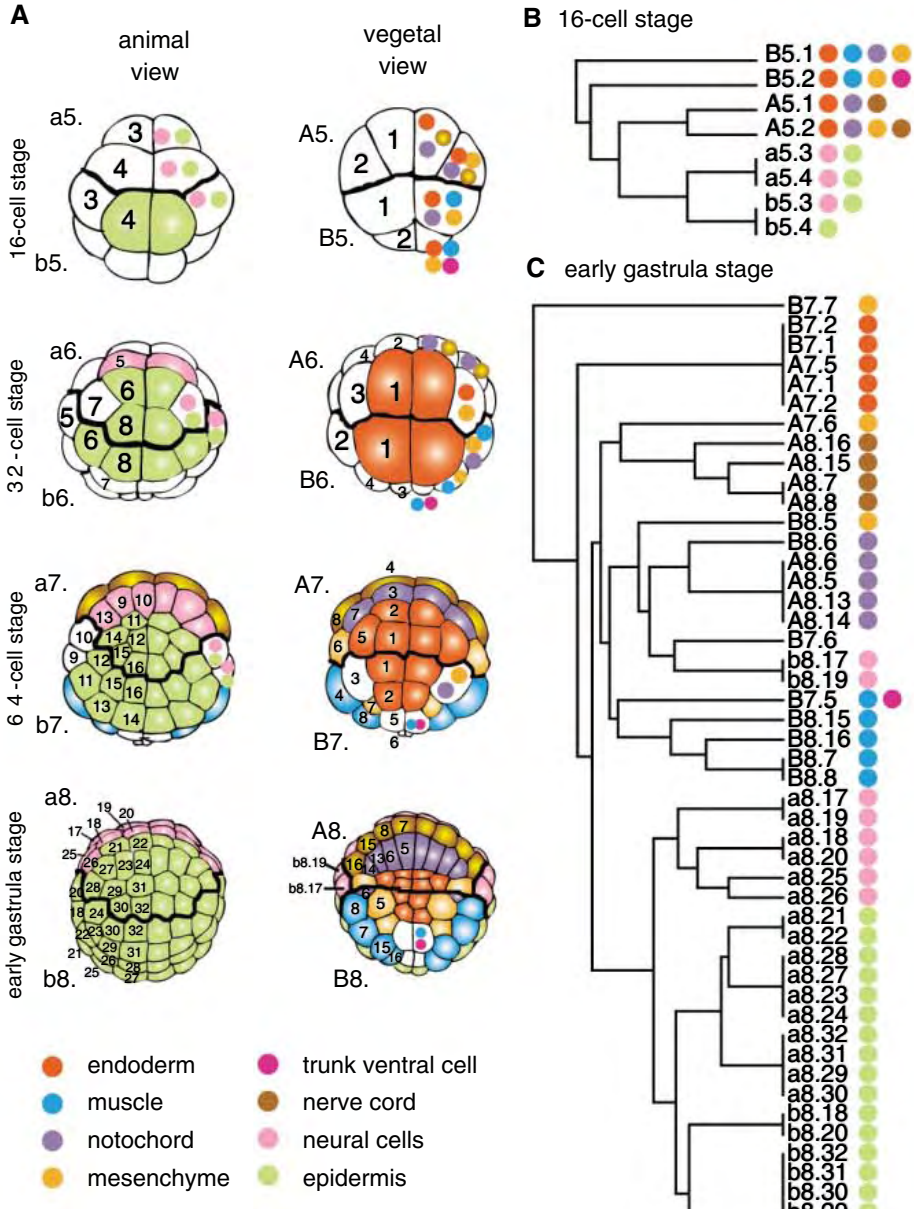

Fig. 1. Blastomere identities in terms of regulatory codes. (**A**) Schematic representations of early ascidian embryos. Blastomeres whose developmental fate is restricted to one specific tissue are colored; the pluripotent blastomeres are depicted as colored circles. Each color represents the tissue indicated at the bottom. The names of individual cells indicated in each illustration should be prefixed with IDs shown at the left. The anterior and posterior boundaries are shown as thick lines. (**B** and **C**) Hierarchical clusterings of blastomeres based on regulatory codes at the 16-cell (B) and early gastrula (C) stages. The developmental potentials of each cell are shown with the same color codes as in (A).

activated in the A-line progenitors by *FoxA-a* and *FoxD* (fig. S5, A and B), two of the early determinants of the 16-cell prepattern. It is conceivable that *FoxA-a* and *ZicL* function through a feed-forward loop, which is a common feature of previously characterized gene regulatory networks, including those controlling endomesoderm formation in sea urchin embryos and dorsal-ventral patterning of the *Drosophila* embryo (*1*, *2*). *FoxA-a* is expressed in the A-line progenitors at the 32-cell stage, A6.2 and A6.4. Expression persists in A7.3 and A7.7, but not in A7.4 and A7.8, which form A-line nerve cord derivatives (fig. S1). This asymmetric activity of *FoxA-a* might exclude *Brachyury* expression in nerve cord cells. The posterior eight notochord cells arise from the B8.6 blastomeres, where *Brachyury* is also activated by a distinct mechanism (see below; supporting online text).

The nodal network. Nodal is a member of the transforming growth factor β (TGFβ) superfamily of signaling molecules. It is conserved in Deuterostomes, including sea urchins, ascidians, and vertebrates, but not found in protostomes. In *Xenopus*, *Nodal* and *Nodal-related* genes (*XNRs*) are expressed predominantly in the dorsal endomesoderm (*24*). A different function is seen in sea urchins. *Nodal* is expressed in the oral ectoderm, but not endomesoderm, and it patterns the oral-aboral axis (*25*). The detailed analysis of *Nodal* function in *Ciona* raises the possibility that ascidians have hybrid properties of lower Deuterostomes and vertebrates (Fig. 4).

Nodal is first expressed in the b6.5 blastomere, which gives rise to the b7.9 and b7.10 daughters in 64-cell embryos (Fig. 4A). These cells form dorsal epidermal tissues and the dorsal-most ependymal cells of the nerve cord—the roof cells. The localized expression of *Nodal* depends on at least three regulatory influences. First, *Fgf9/16/20* signals, emanating from a wide range of the A-line and B-line vegetal cells, induce *Nodal* expression in the b6.5 lineage. Second, restricted expression depends on direct or indirect repression by SoxC and FoxA-a (Fig. 4B). Finally, *Nodal* is negatively autoregulated; there is more than a 10-fold elevation in the levels of expression in mutant embryos injected with the *Nodal* MO. It is highly likely that this auto-regulation is required for supplying the proper amount of Nodal ligand to the surrounding cells. Negative feedback loops are a common feature of other gene networks that have been examined (*25*, *26*).

Recent studies suggest that Nodal functions as an organizing signal, which patterns the developing nerve cord (*16*). Considered in cross section, the larval nerve cord contains four ependymal cells surrounding a hollow cord. The ventral-most ependymal cell has the properties of a simple floor plate. It expresses floor plate markers such as *hedgehog-2* (*hh-2*) and *FoxA-a* (*HNF3β*) (*27*, *28*). MO-mediated knockdown of *SoxC* activity results in ectopic expression of *Nodal* in the a-line neuronal cells and concomitant misexpression of *snail*, *Delta-like*, *Pax6*, *Cdx*, and *Neurogenin* in the floor plate (fig. S5E).

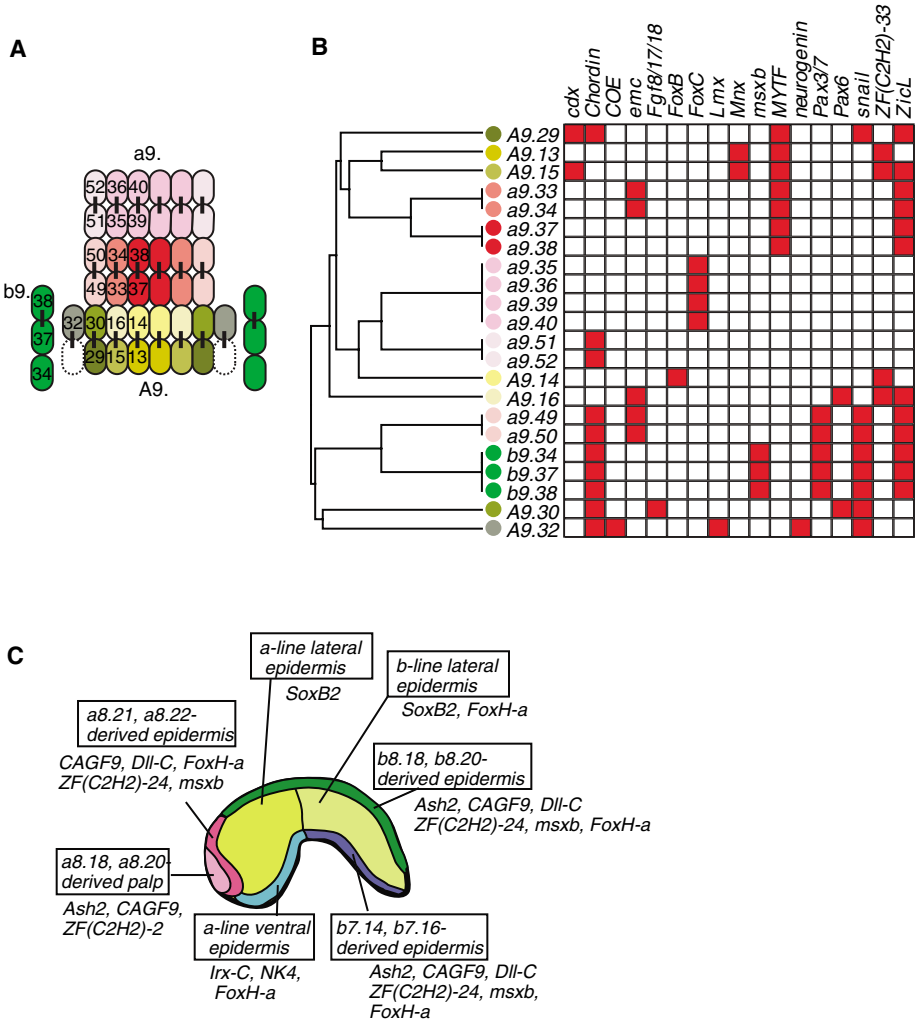

Fig. 2. (**A** and **B**) Cell identities in the neural plate at the late gastrula stage, characterized on the basis of the expression profiles of selected TF and ST genes. (**A**) Cells in the neural plates are shown in colors, with cell identities represented by a color code. The names of individual cells, indicated at the left half of each illustration, should be prefixed with the IDs shown at the outside of the illustration. Vertical bars indicate sister relations between blastomeres. (**B**) Hierarchical clustering of blastomeres in the neural plate (left) and gene expression profiles (right). The color code of the circles is the same as that used in (**A**). (**C**) A schematic representation of the epidermal territories of the tailbud embryo, defined by the expression profiles of 10 TF genes.

Table 1. Summary of knockdown experiments with morpholino oligonucleotides.

Gene	No. of genes
Genes analyzed in detail	
ADMP, AP-2-like2, Brachyury, dickkopf, Dll-B, DMRT1, ets/pointed2, FGF9/16/20, FoxA-a, FoxB, FoxC, FoxD-a/b, lefty/antivin, Mesp, msxb, MyoD, Neurogenin, nodal, NoTrlc, Otx, Snail, SoxC, Tbx2/3, Tbx6b/c/d, Twist-like1a/b, Wnt5, ZicL	27
Genes for which a morpholino oligonucleotide did not give any effects	
BMP2/4, BMP3, E(spl)/hairy-a, ELK, Emc, Eph1, FGF8/17/18, Fli/ERG1, Fli/ERG3, Fos, Fz4, Hedgehog1, HNF4, Irx-B, Lhx3, noggin, Orphan Fox-2, Orphan Wnt-e, RAR, sFRP1/5, SOCS1/2/3/CIS, SoxB1, SoxB2, SoxF, SMYD1, Tbx6a, TGFβ not assigned 1, TTF1, ZF (C2H2)-2, ZF (C2H2)-25	30
Genes for which a morpholino oligonucleotide evoked a nonspecific effect or a phenotype that was not expected from the zygotic gene expression pattern	
DUSP1.2.4.5, E(spl)/hairy-b, E12/E47, EphrinA-c, EphrinA-d, FoxH-b, FoxP, Jun, Mnx, PPAR, ROR, ZF (C2H2)-34, ZF (C3H)	13
Genes for which no cDNA clone could be obtained and that were not examined in this study	
Chordin, Delta-like, GATA-b, MyTF, Otp, Tolloid	6

Nodal activates *Msxb*, *Pax3/7*, *snail*, *Delta-like*, and *Chordin* within the b6.5 lineage that forms the roof nerve cord cells and dorsal epidermis (Fig. 4B). It also induces *Snail*, *Delta-like*, *Neurogenin*, and *E(spl)/Hairy-b* expression in the A7.8 lineage, which forms the lateral ependymal cells of the nerve cord (Fig. 4B). Localized repressors in the lateral cells help restrict gene expression within the floor plate. For example, *Snail* restricts *Mnx* expression to the floor plate and keeps it off in lateral ependymal cells.

The cellular simplicity of the *Ciona* embryo and tadpole permits the elucidation of "four-dimensional" gene networks, whereby cell-autonomous gene cascades can be linked to dynamic signaling interactions between neighboring cells. For example, Nodal emanating from the b6.5 lineage induces *NoTrlc* and *Delta-like* expression in the neighboring trunk lateral cell, A7.6, which gives rise to adult blood cells and muscles (*29*). It is possible that Delta-like relays Notch signaling in the B7.3 blastomere, which forms the secondary notochord and mesenchyme. Delta is a well-known ligand for the Notch receptor [e.g., (*30*)], and the primary transcriptional effector of Notch-signaling—Su(H)—replaces the ZicL activator to induce *Brachyury* expression in the B8.6 (secondary) notochord lineage (supporting online text). Thus, the b6.5 lineage has the properties of an organizer. It is essential for the patterning of the nerve cord and the induction of internal mesoderm derivatives, such as the secondary notochord (Fig. 4B).

Transcriptional repression. As in the case of Nodal negative feedback, repression is an important feature of gene networks. For example, the Snail repressor is expressed in the notochord. Earlier, when *Brachyury* is first activated in the A-line and B-line progenitors at the 64-cell stage, the Snail repressor is restricted to the trunk mesenchyme and developing tail muscles (*31*). *Snail* is activated in the tail muscles and helps exclude *Brachyury* expression in neighboring muscle cells when Delta-like and *Fgf 9/16/20* induce notochord formation. However, by the onset of gastrulation, *Snail* is expressed in notochord cells, where it might attenuate *Brachyury* expression. Peak *Brachyury* expression is seen at neurulation, but only low levels persist during elongation of the tail. It is conceivable that this down-regulation is important for normal notochord differentiation, because sustained expression of high levels of *Brachyury* causes defects in notochord intercalation and tail elongation.

Repression is also a prominent feature of other gene regulation networks. For example, the pMar repressor in the sea urchin micromere lineage permits localized expression of a Delta ligand, which induces Notch signaling in neighboring endomesoderm cells (*1*). Similarly, the Snail repressor in the presumptive mesoderm of early *Drosophila* embryos results in the activation of Notch signaling in neighboring mesectoderm cells in the ventral-most regions of the neurogenic ectoderm (*2*).

As shown in table S7, 22 of the 27 genes examined in this study negatively regulate themselves, directly or indirectly. Thus, it would appear that negative autoregulation loops are an essential property of ascidian gene regulatory networks.

Conclusions. The preceding analysis provides provisional circuit diagrams for the specification and initial differentiation of several tissues of the *Ciona* tadpole, including the gut, tail muscles, notochord, heart, nerve cord, and brain [supporting online text (fig. S8)]. Definitive gene networks will require integrating this information with lineage-specific enhancers from key patterning genes. For example, the characterization of a

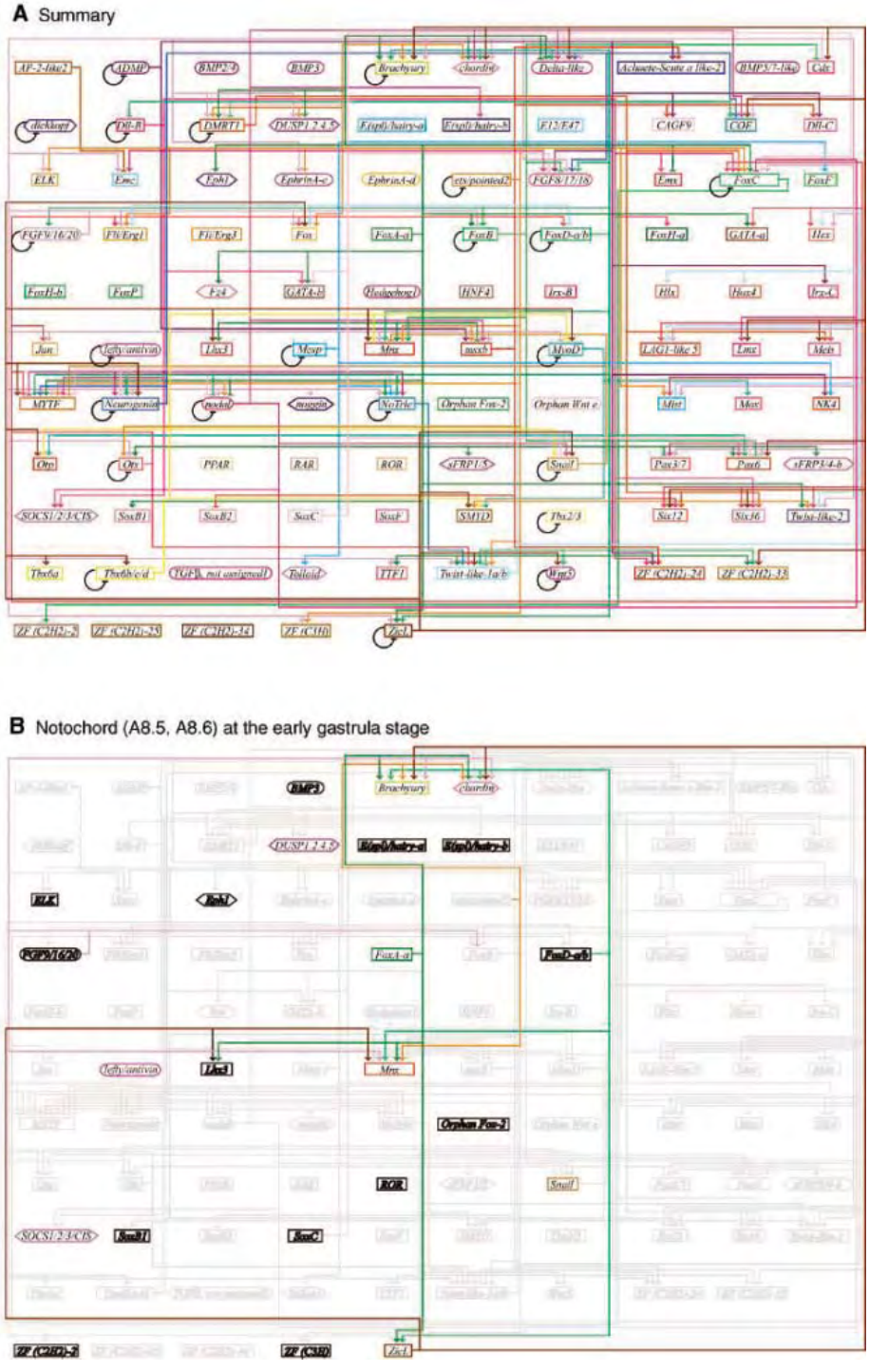

Fig. 3. Gene regulatory networks in the ascidian embryo. (**A**) Summary of all relations. (**B**) Relations in A-line notochord cells at the early gastrula stage. TF genes are indicated by rectangles. Signaling ligand genes and other ST genes are shown by ovals and hexagons. Arrows indicate transcriptionally regulatory interactions. The flat-head arrows indicate repression. Genes expressed in the ancestors of the cell, but not expressed at this stage, are enclosed by a black rectangle. Genes that are not expressed in either the specified cell or its ancestors are shown in light gray.

minimal notochord-specific enhancer from the *Brachyury* gene provides evidence that *ZicL*, *Fgf9/16/20*, and Notch jointly establish the prospective notochord, rather than functioning in a sequential pathway (see Fig. 4B).

The current study provides a foundation for determining the evolutionary origins of chordate structures, and their elaboration in vertebrate systems. It also provides insights for evolutionary plasticity and conservation, as ascidians are simple chordates that might retain some of the ancestral properties of the first chordates, as well as emergent properties of vertebrates. The circuit diagrams provide a glimpse of the genetic and cellular interactions that might have operated in the earliest ancestors of the vertebrates. For example, we have argued that Nodal signal emanating from the b6.5 lineage might represent a "transitional organizer," with hybrid properties seen in sea urchins and vertebrates.

One of the great mysteries in evolutionary biology is the origin of the chordate body plan. The closest nonchordate relatives of ascidians, the hemichordates (e.g., acorn worms) and echinoderms (e.g., starfish), do not display a tadpole-like organization at any point in their life cycles. It should be possible to use the genetic circuits governing the formation of the *Ciona* tadpole to identify homologous structures in hemichordates and echinoderms. For example, *FGF9/16/20*, *Mesp*, *FoxF*, and *Tolloid* constitute specialized components of the early chordate heart network (supporting online text), and it will be interesting to see if this pathway is used in echinoderms or hemichordates. Similarly, it should be possible to determine whether any of the circuits governing the compartmentalization of the *Ciona* nerve cord or cerebral vesicle are used within the apparently more diffuse nervous systems of lower Deuterostomes.

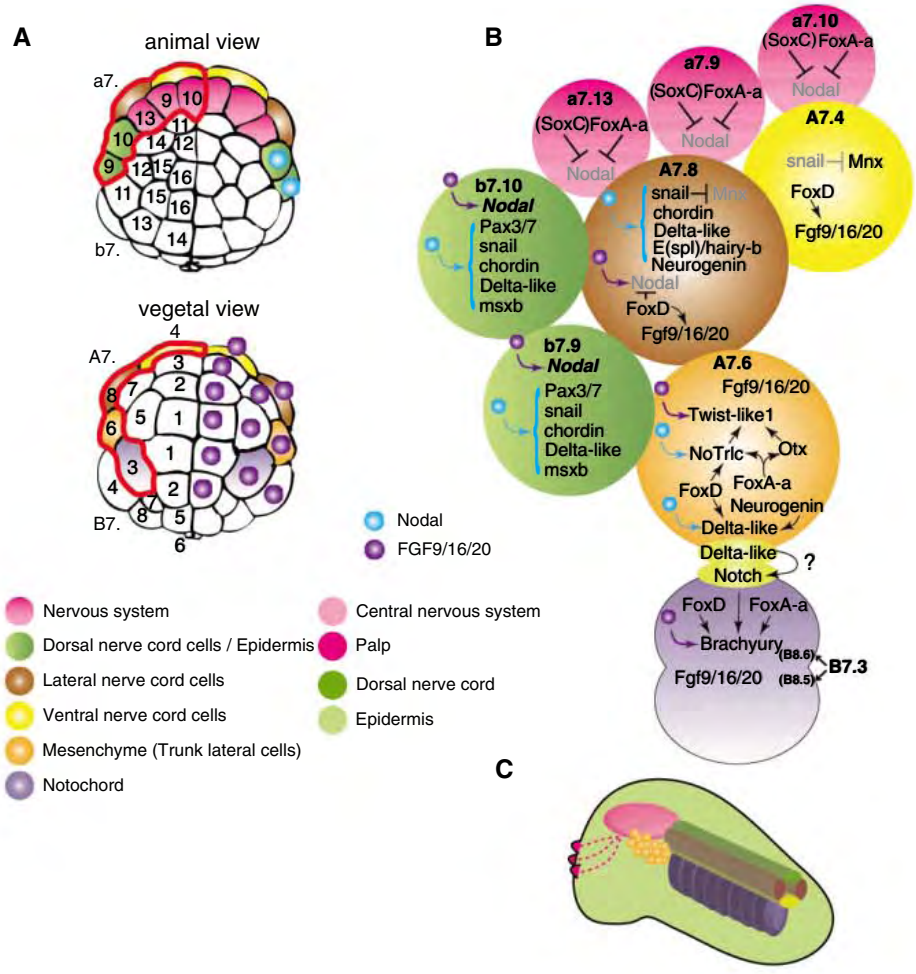

Fig. 4. The Nodal network. (**A**) The 64-cell embryos depicting cells secreting Nodal and FGF9/16/20 and developmental fates of selected blastomeres shown in (**B**). Note that cells whose ancestors express the FGF are also depicted. (B) Nodal-centered gene networks. Arrows and flattend arrows show activation and repression of downstream genes. Genes shown in gray or in parentheses are not expressed there. (**C**) A schematic representation of tissues of the tailbud embryo differentiated from the blastomeres shown in (B). The color codes in (A) are applied in the same way to (B) and (C). Note that only the networks related to Nodal are depicted, and some regulatory interactions seen in their ancestral cells and descendants are also included for better understanding. See the text for the details.

References and Notes

1. E. H. Davidson *et al.*, *Science* **295**, 1669 (2002).
2. A. Stathopoulos, M. Levine, *Dev. Cell* **9**, 449 (2005).
3. M. Loose, R. T. Patient, *Dev. Biol.* **271**, 467 (2004).
4. N. Satoh, *Nat. Rev. Genet.* **4**, 285 (2003).
5. P. Dehal *et al.*, *Science* **298**, 2157 (2002).
6. H. Nishida, K. Sawada, *Nature* **409**, 724 (2001).
7. K. S. Imai, Y. Satou, N. Satoh, *Development* **129**, 2723 (2002).
8. K. Yagi, N. Takatori, Y. Satou, N. Satoh, *Dev. Biol.* **282**, 535 (2005).
9. Y. Satou *et al.*, *Dev. Genes Evol.* **212**, 87 (2002).
10. K. Imai, N. Takada, N. Satoh, Y. Satou, *Development* **127**, 3009 (2000).
11. Y. Satou, K. S. Imai, N. Satoh, *Development* **128**, 3559 (2001).
12. J. C. Corbo, M. Levine, R. W. Zeller, *Development* **124**, 589 (1997).
13. K. S. Imai, N. Satoh, Y. Satou, *Development* **129**, 1729 (2002).
14. K. S. Imai, N. Satoh, Y. Satou, *Development* **129**, 3441 (2002).
15. V. Bertrand, C. Hudson, D. Caillol, C. Popovici, P. Lemaire, *Cell* **115**, 615 (2003).
16. C. Hudson, H. Yasuo, *Development* **132**, 1199 (2005).
17. K. S. Imai, K. Hino, K. Yagi, N. Satoh, Y. Satou, *Development* **131**, 4047 (2004).
18. Because *Ci-Delta-like* (*Ci-Delta2*) (*16*) was missed in our previous screen and a new cDNA was obtained for *Pax3/7*, detailed expression profiles are now available for both genes (fig. S9), which revealed that *Ci-Delta-like* is expressed at and before the early gastrula stage.
19. Materials and methods are available as supporting material on *Science* Online.
20. L. Yamada *et al.*, *Development* **130**, 6485 (2003).
21. We examined effects of the MO-mediated knockdown of 25 genes, with the exception of *FoxC* and *Mesp*, on the expression of 73 genes at the various cleavage stages. *FoxC*, *Mesp*, and *Jun* were not included in the expression analysis, because *FoxC*, *Mesp*, and *Jun* begin to be expressed late in the early gastrula stage; thus, their functions and expression patterns are better evaluated at later stages.
22. The *Ciona* Integrated Database, GHOST (http://ghost.zool.kyoto-u.ac.jp/network/TFSTgenes.html).
23. H. Takahashi *et al.*, *Genes Dev.* **13**, 1519 (1999).
24. E. Agius, M. Oelgeschlager, O. Wessely, C. Kemp, E. M. De Robertis, *Development* **127**, 1173 (2000).
25. V. Duboc, E. Rottinger, L. Besnardeau, T. Lepage, *Dev. Cell* **6**, 397 (2004).
26. M. Whitman, *Dev. Cell* **1**, 605 (2001).
27. J. C. Corbo, A. Erives, A. Di Gregorio, A. Chang, M. Levine, *Development* **124**, 2335 (1997).
28. N. Takatori, Y. Satou, N. Satoh, *Mech. Dev.* **116**, 235 (2002).
29. M. Tokuoka, N. Satoh, Y. Satou, *Dev. Biol.* **288**, 387 (2005).
30. K. Katsube, K. Sakamoto, *Int. J. Dev. Biol.* **49**, 369 (2005).
31. S. Fujiwara, J. C. Corbo, M. Levine, *Development* **125**, 2511 (1998).

32. This research was mainly supported by Grants-in-Aid from MEXT, Japan, and from Japan Society for the Promotion of Science (JSPS) to Y.S. (17687022 and 13044001). K.S.I. was supported by a postdoctoral fellowship from the JSPS for Japanese junior scientists with a research grant (15004751). M.L. is supported by a grant from the NIH. This research was also supported in part as a Core Research for Evolutional Science and Technology (CREST) project by the Japan Science and Technology Agency to N.S.

Supporting Online Material

www.sciencemag.org/cgi/content/full/312/5777/1183/DC1
Materials and Methods
SOM Text
Figs. S1 to S9
Tables S1 to S7
References and Notes
Database S1

5 December 2005; accepted 27 March 2006
10.1126/science.1123404

Scale-Free Intermittent Flow in Crystal Plasticity

Dennis M. Dimiduk,[1]* Chris Woodward,[2] Richard LeSar,[3] Michael D. Uchic[1]

Under stress, crystals irreversibly deform through complex dislocation processes that intermittently change the microscopic material shape through isolated slip events. These underlying processes can be revealed in the statistics of the discrete changes. Through ultraprecise nanoscale measurements on nickel microcrystals, we directly determined the size of discrete slip events. The sizes ranged over nearly three orders of magnitude and exhibited a shock-and-aftershock, earthquake-like behavior over time. Analysis of the events reveals power-law scaling between the number of events and their magnitude, or scale-free flow. We show that dislocated crystals are a model system for studying scale-free behavior as observed in many macroscopic systems. In analogy to plate tectonics, smooth macroscopic-scale crystalline glide arises from the spatial and time averages of disruptive earthquake-like events at the nanometer scale.

The vivid images of radiant-hot metal being forged on a blacksmith's anvil, or being formed between rolls and dies, support a view of crystal deformation as analogous to viscous fluid flow. Such deformation is often described via a set of continuum-level parameters, which, in contrast to those describing fluids, evolve with deformation to reflect the increasing resistance to flow that occurs with increasing distortion (work hardening). Although continuum approaches are selectively useful for describing deformation, especially at high temperatures, they completely fail to account for well-known intermittent deformation phenomena such as the spatial localization of dislocation flow into "slip bands" [described in 1900 (*1*)] and the temporal fluctuations in load-versus-time curves (the Portevin–Le Chatelier effect first reported in the 1920s) (*2*, *3*).

From the late 1950s to the 1970s, numerous investigators sought to account for the heterogeneous nature of crystal deformation. Studies ranged from examining the motion of individual dislocations to describing the development and propagation of dislocation aggregates to form deformation bands (*4*). Those studies demonstrated the importance of both topological (crystallographic) constraints and the complex, long-range interactions between dislocations that determine collective dislocation motion, thus distinguishing crystal plasticity from continuum flow. For example, Pond convincingly showed that crystal slip in metals can be intermittent and heterogeneous at multiple length and time scales through cinematographic studies of deformation band formation and growth (*5*). Studies of dislocation motion, slip-line formation, and the collective intermittent nature of slip continued, providing a detailed view of dislocation motion and crystal glide (*6*–*8*). Despite much effort, a quantitative understanding of intermittency and collective dislocation flow has remained elusive. As a consequence, our ability to predict critical deformation behavior is often limited, impeding our understanding of such phenomena as work hardening (*9*–*11*).

Recent studies of intermittency in crystal plasticity were based on measurements of acoustic emissions that arise from the motion of dislocations through large (tens to hundreds of mm) ice crystals (*12*–*16*). The essence of the technique is the detection of the acoustic waves that are generated by dislocation glide and their subsequent analysis based on models of dislocation motion. Under some conditions, it has been argued that the amplitudes of the acoustic signals are related to the area swept by the fast-moving dislocations and hence to the energy dissipated during deformation events. These results were used to suggest intermittency of flow (*12*), scale-free dissipation processes (*13*), spatial clustering of flow avalanches (*14*), and, most recently, conditions for "supercritical" flow in polycrystalline ice (*15*, *16*). However, the results from these measurements can only be interpreted via models and under certain key assumptions about the deformation processes. Other reports also show the characteristics of scale-free flow for crystals through simulation (*17*–*19*) and models of dislocation glide at low temperature (*20*, *21*). These studies conclude that deformation of crystals having highly mobile dislocations exhibits the attributes of a self-organized critical (SOC) process.

We report the direct measurement of scale-free intermittent flow within micrometer-scale pure metal crystals loaded above the elastic-plastic transition. Using the ultrahigh displacement resolution offered by modern nanoindentation systems (effectively a nanoscale seismometer), we examined the frequency of displacement events as a function of their magnitude for several sample sizes and applied loads. The results were analyzed following the suggestion that dislocations form a SOC system, as briefly reviewed in (*22*, *23*). Bak *et al*. (*24*) introduced this concept to describe dynamical systems that arrange themselves such that they are always at a critical point irrespective of their initial state, that is, they self-organize to the critical point of the system (*25*). An important aspect of SOC behavior is that it is self-similar or scale-free. That is, structures at one scale appear the same (at least in a statistical sense) as structures at other scales. If dislocations are indeed self-organized critical systems, then the statistics that describe these ensembles can be used to develop homogenization schemes for mapping between groups of dislocations and macroscopic deformation.

The experimental techniques used for this study were reported in (*26*–*28*) [see also (*29*)]. Microcrystals of pure Ni were prepared by isolating cylindrical columns via focused ion-beam machining, with one end of each column attached to the bulk material, within the surface of an electropolished macroscopic crystal. The microcrystals were transferred to a nanoindenter and aligned for axial compression testing. Samples ranging in diameter from 18 to 30.7 μm, with length-to-diameter ratios ranging from ~1.9:1 to 2.8:1, were loaded via a flattened diamond tip platen at a nominal axial strain rate of 10^{-4}/s at room temperature. For each sample a variety of parameters were measured, including load (±50 nN) and displacement (±0.02 nm), and digitally stored at a frequency of 5 Hz. The displacement-versus-time data were differentiated by a simple two-point forward-derivative method. The resultant loading platen velocity profiles were correlated with the displacement-versus-time data to identify displacement events larger than a chosen "noise threshold." The shear-stress versus shear-strain curves measured for the present experiments and a typical plot of detected displacements versus time are shown in Fig. 1, A and B. Note that the displacements reflect dissipated energy and are intermittent in both space and time, despite the programmed continuous loading rate.

For the scaling analysis, a noise threshold for detecting displacements was established for each test by monitoring the standard deviation from ideal of the detected displacements during the unloading portion of the test. For these tests, the noise values ranged from 0.13 to 0.68 nm. Thus, for Ni crystals with ⟨–2, 6, 9⟩ orientation, a typical minimum detected event corresponds to ~0.3 nm or ~4 dislocations leaving the crys-

[1]Air Force Research Laboratory, Materials and Manufacturing Directorate, AFRL/MLLM, Wright-Patterson AFB, OH 45433, USA. [2]Department of Materials Science and Engineering, Northwestern University, Evanston, IL 60208, USA. [3]Theoretical Division, Los Alamos National Laboratory, Los Alamos, NM 87545, USA.

*To whom correspondence should be addressed. E-mail: dennis.dimiduk@wpafb.af.mil

tal. For events exceeding the noise threshold, the displacement magnitude was recorded and sorted into bins for each sample as well as for the collective set of samples. A plot of the number of events at a given displacement magnitude, $n(x)$, versus magnitude x (in nm) for events isolated from a single sample (Fig. 2) reveals that a linear regime exists in which the probability of observing a displacement event of a given magnitude decreases as the event size increases. Also shown in Fig. 2 are the displacements for all of the samples analyzed collectively. Both data sets demonstrate power-law scaling. The data were fit to a power-law expression $n(x) = Cx^{-\alpha}$, producing a measured value of $\alpha = \sim 1.5$ where C is a constant. This scale-free flow was observed over a range of displacements from ~0.5 nm to more than ~150 nm per event—more than two orders of magnitude. Values for α derived from log-log plots are known to underestimate this parameter. Using alternative approaches as suggested by Newman (*25*), we estimated a power-law slope of 1.60 ± 0.02 by a bootstrap method (*29*). Note that the value of 1.6 is identical to that found through acoustic emission experiments (*13*) and from theory (*19*). Further, the scaling relationship is independent of sample size over the range examined as well as the gradually increasing stress over the range of the test (i.e., there is no work-hardening effect for single slip-plane flow).

Closer inspection of a typical sequence of events (Fig. 3) shows several important features of the data. First, the individual events take place at a rate that is much faster than the programmed displacement rate of the test. This demonstrates that dissipation is much faster than the rate of change of the driving force. Second, the largest displacement events typically occur after an increment of the remote stress. Note that the magnitude of a stress increment is a vanishingly small percentage of the total applied stress. This observation of "large" events (displacement shocks) after a small change of driving force indicates that the system is near critical. Third, these large events are frequently followed by a succession of additional displacement events of much smaller magnitude (aftershocks) that occur in the absence of further detectable remote stress rise; this suggests self-organization back to a critical state. Fourth, a post mortem examination of the deformed samples by transmission electron microscopy (TEM) (Fig. 4) shows a substructure containing many dislocations that is characteristic of those seen after similar deformation of large Ni crystals (*28*, *30*, *31*). Finally, the displacement-versus-time plots show intervals having a small positive slope that indicates additional displacements not accounted for within the detected bursts. These extra displacements occur even under conditions of no increase in the applied load, consistent with these samples exhibiting creep at or near criticality.

Our data and analysis explicitly show that crystalline glide in metals exhibits the characteristic attributes of self-organized criticality under the appropriate control of the driving force (in this case an applied displacement rate or load). These results support an emerging view that a statistical framework that creates a coarse-grained description of dislocation response is needed to bridge the

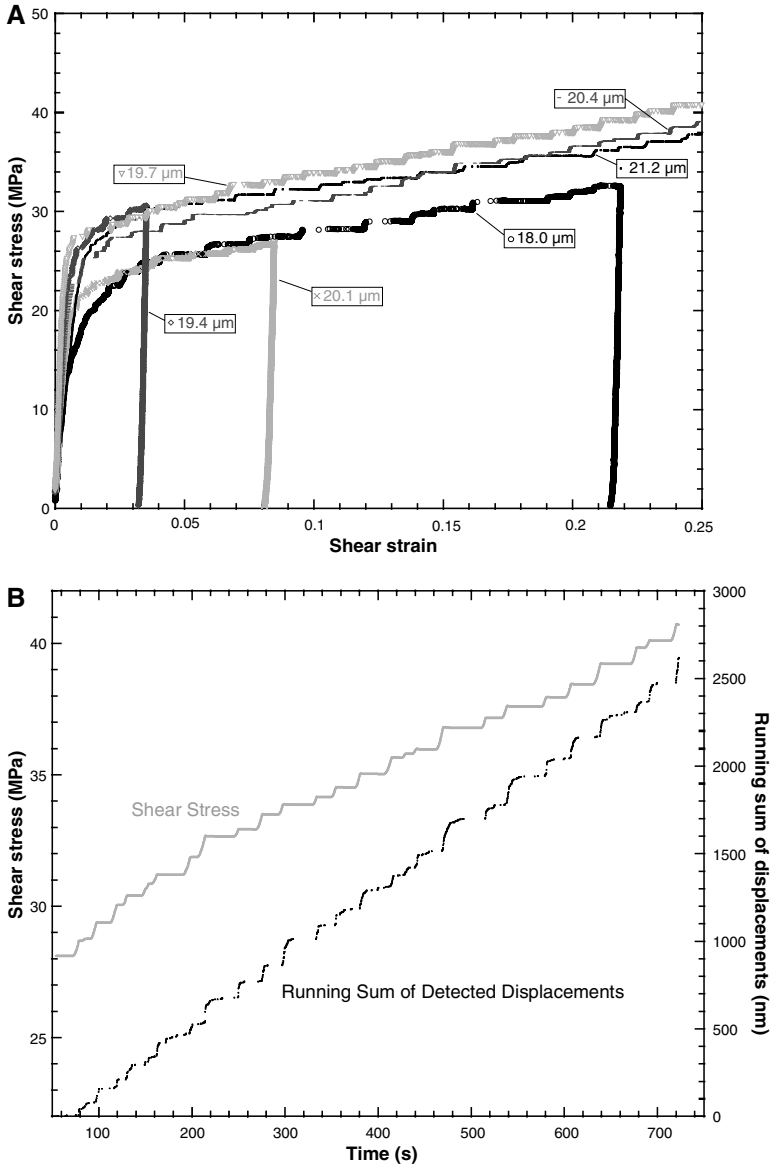

Fig. 1. (**A**) Selected shear-stress versus shear-strain curves for Ni samples with ⟨−2, 6, 9⟩ orientation, ~20 μm in diameter, showing intermittency of strain and stress. (**B**) Plot of shear stress and the cumulative sum of detected displacements as functions of time for a single sample 19.7 μm in diameter. See (*29*) for additional sample data from these and from samples ~30 μm in diameter.

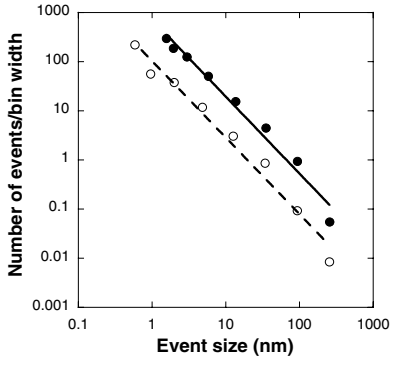

Fig. 2. Event frequency distribution showing the number of slip events of a certain size, $n(x)$, versus event size, x, plotted on logarithmic scales. Power-law scaling over more than two orders of magnitude is exhibited for both a single sample ~20 μm in diameter (open circles and dashed line fit) and the aggregate data from several samples (solid circles and solid line fit).

gap between the behavior of individual dislocations and the ensemble of dislocations that govern macroscopic metal plasticity. Further, the existence of a scale-free set of variables that describe deformation suggests that such a coarse-graining variable set exists (*23*). This assessment puts dislocation motion in the same class as earthquakes, sand pile avalanches, magnetic domain dynamics, and a wide variety of other dynamical systems. The picture that emerges is that crystal deformation has more in common with plate tectonics than with viscous fluid flow, at least in selected commonly experienced regimes.

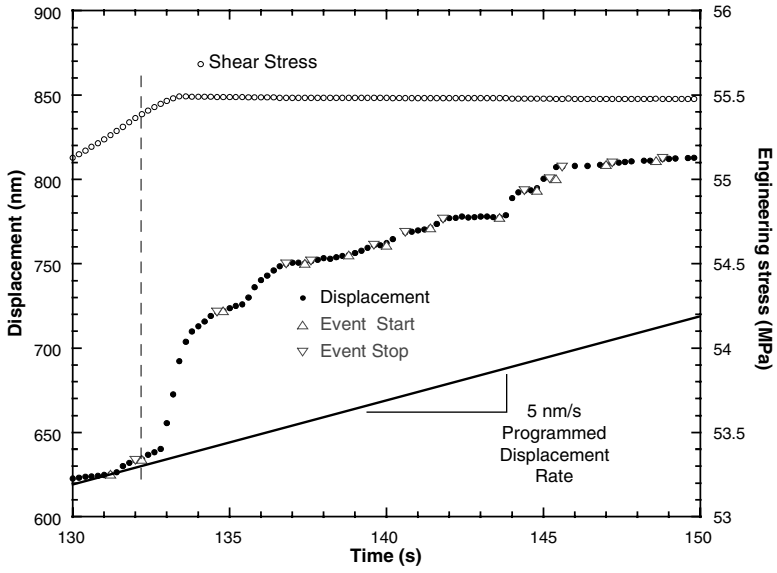

Fig. 3. A detailed example of the stress-versus-time and displacement-versus-time curves taken from the data for the sample 30.7 μm in diameter. The displacement curve shows superimposed markers for detected event start and stop times. Note that the large event beginning at the vertical dashed line occurs as a shock under a rising stress but continues under constant stress, as do the vast number of aftershocks at smaller magnitudes.

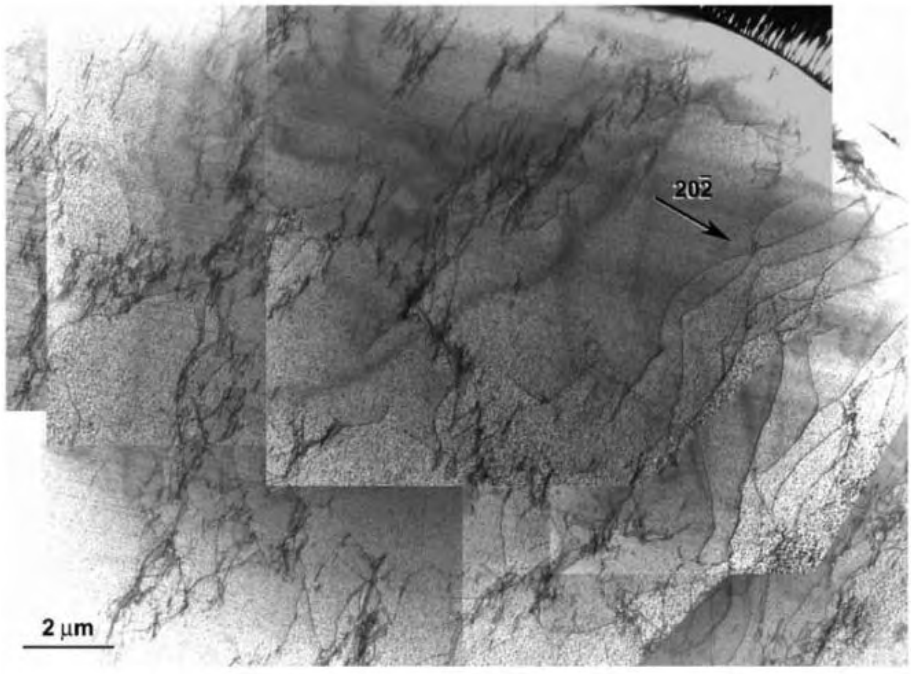

Fig. 4. Bright-field TEM image showing the dislocation structure for the sample 20.1 μm in diameter after 8.1% plastic shear strain. The plane of view is parallel to the {111} slip planes, and the field of view includes most of the sample cross section. The crystallographic direction marker indicates both the imaging vector and the direction of the dislocation Burgers vector. The montage image was digitally assembled from seven individually leveled micrographs, the edges of which can be seen.

References and Notes

1. J. A. Ewing, W. Rosenhain, *Philos. Trans. R. Soc. London Ser. A* **193**, 353 (1900).
2. A. Portevin, F. Le Chatelier, *C. R. Acad. Sci.* **176**, 507 (1923).
3. M. A. Lebyodkin, Y. Estrin, *Acta Mater.* **53**, 3403 (2005).
4. J. J. Gilman, in *Micromechanics of Flow in Solids* (McGraw-Hill, New York, 1969), pp. 185–199.
5. R. B. Pond, in *The Inhomogeneity of Plastic Deformation* (American Society for Metals, Metals Park, OH, 1973), pp. 1–18.
6. H. Neuhauser, in *Dislocations in Solids* (North-Holland, Amsterdam, 1983), vol. 6, pp 319–440.
7. E. M. Nadgorny, *Prog. Mater. Sci.* **31**, 434 (1988).
8. M. Zaiser, F. Madani, V. Koutos, E. C. Aifantis, *Phys. Rev. Lett.* **93**, 195507 (2004).
9. R. Madec, B. Devincre, L. Kubin, T. Hoc, D. Rodney, *Science* **301**, 1879 (2003).
10. P. Gumbsch, *Science* **301**, 1857 (2003).
11. A. H. Cottrell, in *Dislocations in Solids* (North-Holland, Amsterdam, 2002), vol. 11, pp. vii–xvii.
12. J. Weiss, J.-R. Grasso, *J. Phys. Chem. B* **101**, 6113 (1997).
13. M.-C. Miguel, A. Vespignani, S. Zapperi, J. Weiss, J.-R. Grasso, *Nature* **410**, 667 (2001).
14. J. Weiss, D. Marsan, *Science* **299**, 89 (2003).
15. T. Richeton, J. Weiss, F. Louchet, *Nat. Mater.* **4**, 465 (2005).
16. T. Richeton, J. Weiss, F. Louchet, *Acta Mater.* **53**, 4463 (2005).
17. M. Koslowski, R. LeSar, R. Thomson, *Phys. Rev. Lett.* **93**, 125502 (2004).
18. M. Koslowski, R. LeSar, R. Thomson, *Phys. Rev. Lett.* **93**, 265503 (2004).
19. M. Zaiser, P. Moretti, *J. Stat. Mech.*, 10.1088/1742-5468/2005/08/P08004 (2005).
20. I. Groma, F. F. Csikor, M. Zaiser, *Acta Mater.* **51**, 1271 (2003).
21. M.-C. Miguel, P. Moretti, M. Zaiser, S. Zapperi, *Mater. Sci. Eng. A* **400–401**, 191 (2005).
22. P. Sammonds, *Nat. Mater.* **4**, 425 (2005).
23. J. P. Sethna, K. A. Dahmen, C. R. Myers, *Nature* **410**, 242 (2001).
24. P. Bak, C. Tang, K. Wiesenfeld, *Phys. Rev. Lett.* **59**, 381 (1987).
25. M. E. J. Newman, *Contemp. Phys.* **46**, 323 (2005).
26. M. D. Uchic, D. M. Dimiduk, J. N. Florando, W. D. Nix, *Science* **305**, 986 (2004).
27. M. D. Uchic, D. M. Dimiduk, *Mater. Sci. Eng. A* **400–401**, 268 (2005).
28. D. M. Dimiduk, M. D. Uchic, T. A. Parthasarathy, *Acta Mater.* **53**, 4065 (2005).
29. See supporting material on *Science* Online.
30. S. Mader, in *Electron Microscopy and Strength of Crystals* (Interscience, New York, 1963), pp. 183–229.
31. J. Gil-Sevillano, in *Materials Science and Technology, Vol. 6, Plastic Deformation and Fracture of Materials* (Weinheim, New York, 1993), pp. 19–88.

32. We thank T. A. Parthasarathy and D. Trinkle for many useful discussions and for bringing reference (*25*) to our attention, and S. Polasik for the image of the dislocation structure in Fig. 4. Supported by the Defense Advanced Research Projects Agency and the Air Force Office of Scientific Research. The work of R.L. was performed under the auspices of the U.S. Department of Energy under contract W-7405-ENG-36.

Supporting Online Material

www.sciencemag.org/cgi/content/full/312/5777/1188/DC1
Materials and Methods
Figs. S1 to S4
Tables S1 and S2
References

15 December 2005; accepted 20 March 2006
10.1126/science.1123889

Electronic Confinement and Coherence in Patterned Epitaxial Graphene

Claire Berger,[1,2] Zhimin Song,[1] Xuebin Li,[1] Xiaosong Wu,[1] Nate Brown,[1] Cécile Naud,[2] Didier Mayou,[2] Tianbo Li,[1] Joanna Hass,[1] Alexei N. Marchenkov,[1] Edward H. Conrad,[1] Phillip N. First,[1] Walt A. de Heer*

Ultrathin epitaxial graphite was grown on single-crystal silicon carbide by vacuum graphitization. The material can be patterned using standard nanolithography methods. The transport properties, which are closely related to those of carbon nanotubes, are dominated by the single epitaxial graphene layer at the silicon carbide interface and reveal the Dirac nature of the charge carriers. Patterned structures show quantum confinement of electrons and phase coherence lengths beyond 1 micrometer at 4 kelvin, with mobilities exceeding 2.5 square meters per volt-second. All-graphene electronically coherent devices and device architectures are envisaged.

The fundamental limitations of silicon-based microelectronics have inspired searches for new processes, methods, and materials. We show here that the properties of epitaxial graphene are suitable for coherent nanoscale electronics applications (*1*). In particular, an ultrathin graphite layer grown on a commercial single-crystal silicon carbide by thermal decomposition has high structural integrity. The single graphene layer at the graphite-SiC interface has impressive two-dimensional (2D) electron gas properties, including long phase coherence lengths (even at relatively high temperatures) and elastic scattering lengths that are determined primarily by the micrometer-scale sample geometry. Magnetotransport measurements of patterned structures reveal signatures of quantum confinement, thus demonstrating that graphene ribbons act as electron waveguides. The material can be patterned, and intricate submicrometer structures can be constructed using standard microelectronics lithography methods, in contrast to the closely related carbon nanotube electronics. The transport properties show that electrons in the interfacial graphene layer dominate the transport and that they are Dirac fermions, as recently observed in mechanically exfoliated graphene layers (*2*, *3*). The properties of Dirac fermions, which are also responsible for transport in carbon nanotubes (*4*), can be conveniently explored in epitaxial graphene.

The electronic properties of sp^2-bonded carbon structures (which include bulk graphite, graphene ribbons, carbon nanotubes, and aromatic molecules) result from the overlap of p_z atomic orbitals on neighboring carbon atoms. Simple tight-binding calculations show that in graphene, π-bands are formed, with electronic energy dispersion $E(p) = \pm v_0|p|$, where the carrier momentum $p = \hbar\sqrt{(k_x^2 + k_y^2)}$ (*5*–*7*), v_0 is the velocity, and $\hbar$ is Planck's constant divided by 2π. Consequently, like photons, the velocity of electrons is independent of energy. The predicted velocity $v_0 = 3a_0\gamma_0/2\hbar \approx 10^6$ m/s, where $\gamma_0 \sim 3$ eV is the interatomic overlap energy and $a_0 = 1.42$ Å is the interatomic spacing. The Fermi surface of neutral graphene (Fermi energy $E_F = 0$) shrinks to a point, so that it is a zero-band-gap semiconductor (*6*). When carriers in graphene are confined, their properties depend on the confinement geometry, as is true for other 2D electron gases (*8*). However, in contrast to conventional 2D electron systems, which are electrostatically confined at a buried interface, epitaxial graphene (*1*, *9*, *10*) is a well-defined material that is robust, so that in principle it can be sculpted down to the molecular level.

We present production methods for epitaxial graphene (EG) and show that the transport properties of a representative patterned EG structure are due to carrier confinement and coherence. From magnetoresistance (MR) and Hall-effect measurements, we find that the material that dominates the transport is in fact graphene. This conclusion follows from the following measured properties: Berry's phase $\Phi_B = \pi$, Fermi temperature $T_F = 2490$ K, Fermi velocity $v_0 = 1.0 \times 10^6$ m/s, mobility

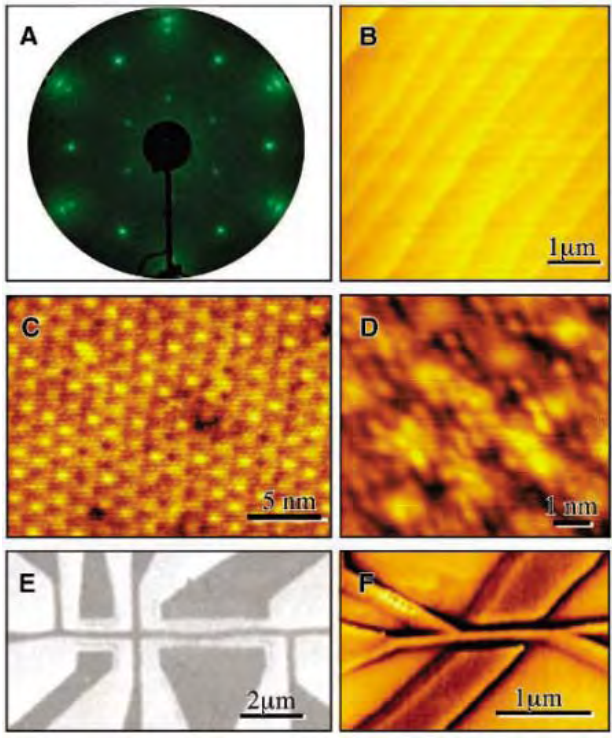

Fig. 1. Production and characterization of EG. (**A**) LEED pattern (71 eV) of three monolayers of EG on 4H-SiC(000$\bar{1}$) (C-terminated face). The outermost hexagon (spots aligned on the vertical) is graphene 1×1 diffraction. Bright sixfold spots aligned on the horizontal are SiC 1×1. The smallest hexagon is the result of a $\sqrt{3} \times \sqrt{3}$ reconstruction of the interfacial layer, as are the spots lying just inside the graphene pattern. Graphene thickness is determined via Auger spectroscopy (attenuation of Si peaks). (**B**) AFM image of graphitized 4H-SiC, showing extended terraces. STM studies indicate that the graphite is continuous over the steps (*1*). (**C**) STM image of one monolayer of EG on SiC(0001). Tunneling conditions (tip bias –0.8 V, current 100 pA) preferentially image structure beneath the graphene layer. Two interface corrugations are apparent, with periods 6×6 (1.8-nm triangular superlattice) and $\sqrt{3} \times \sqrt{3}$ (smaller spots with 0.54-nm spacing) relative to the SiC surface unit cell. (**D**) STM image of interface reconstruction beneath one monolayer of graphene on SiC(0001) obtained after lithography. General features are as seen in (C). (**E**) SEM of patterned EG. Dark regions are the EG (still coated with electron-beam resist). (**F**) EFM of another patterned EG sample, showing a horizontal ribbon (bright contrast) with tapered voltage contacts left and right, which is flanked by diagonally oriented side gates above and below the ribbon. Contrast is obtained through electrostatic forces between the probe and the graphene structure to which potentials are applied, thus allowing functioning devices to be measured.

[1]School of Physics, Georgia Institute of Technology, Atlanta, GA 30332, USA. [2]Laboratoire d'Études des Propriétés Électroniques des Solides, CNRS, BP166, 38042 Grenoble Cedex 9, France.

*To whom correspondence should be addressed. E-mail: walt.deheer@physics.gatech.edu

$\mu = 2.7\ m^2/V{\cdot}s$, carrier diffusion constant $D = 0.3\ m^2/s$, elastic mean free path $l_s = 600$ nm, and phase coherence lengths of $l_\phi = 1.1$ μm at 4 K and 500 nm at 58 K. Furthermore, quantum-confined states are observed.

The production of EG on diced (3 mm by 4 mm) commercial SiC wafers (*11*) is illustrated in Fig. 1. In summary, the steps are (i) hydrogen etching to produce atomically flat surfaces (*12*), (ii) vacuum graphitization to produce an ultrathin epitaxial graphite layer (*9*, *10*), (iii) application of metal contacts (Pd, Au), (iv) electron-beam patterning and development, (v) oxygen plasma etch to define graphite structures, and (vi) wire bonding. To date, more than 200 SiC sample blanks have been processed, of which 22 have been patterned and measured in detail [see also (*1*)]. The structural order has been characterized by low-energy electron diffraction (LEED), Auger electron spectroscopy, x-ray diffraction (*13*), and scanning tunneling microscopy (STM) (*1*). The electronic structure has been characterized by angle-resolved photoelectron spectroscopy [ARPES (*14*)], scanning tunneling spectroscopy (STS) (*1*), and electronic transport [see below and (*1*)]. Patterned surfaces are routinely measured by atomic force microscopy (AFM) and electrostatic force microscopy (EFM) under ambient conditions. The results are summarized in Fig. 1. As evident from LEED, an ultrathin graphite layer grows epitaxially on the SiC(000$\bar{1}$) surface. X-ray diffraction shows that graphene grown on the 000$\bar{1}$ face has a structural coherence of at least 90 nm (*13*). On the Si-terminated SiC(0001) surface, LEED and STM measurements reveal a $(6\sqrt{3} \times 6\sqrt{3})$R30° interface reconstruction. STS measurements reveal the graphitic band structure, and STM and STS together suggest that graphene layers can remain continuous over steps on the SiC surface (*1*). The ARPES data (for two EG layers on 0001 SiC) suggest a Dirac electronic dispersion and a Fermi temperature of 2700 K (*14*). This relatively large energy indicates that the interface layer is charged, with a charge density $\sigma \sim 1 \times 10^{12}$ electrons/cm^2 (see below). As usual for such interfaces, the electric field caused by the surface charge compensates the work function difference between the materials. Only the interface layer is expected to be highly charged (*15*, *16*); the (few) other layers are essentially neutral. Thus, the interface layer should dominate the transport properties, which are essentially identical to those of isolated graphene (see below). The interface layer is further distinguished from any others by a weak superlattice structure imposed by the epitaxial match to SiC (*1*).

We briefly summarize some relevant properties of confined Dirac electrons in graphene. For a graphene ribbon of width W, the boundaries impose a constraint on the transverse motion so that (for not too small n) k_y is quantized: $k_y = n\pi/W$, where n is an integer (*17*). Hence, the energy of the nth electronic subband is $E_n(p_x) = v_0|p| = \hbar v_0\sqrt{(k_x^2 + k_y^2)} = \sqrt{(E_x^2 + n^2\Delta E^2)}$, where $\Delta E = \Delta E(W) = \pi\hbar v_0/W \sim (2\ \text{eV}{\cdot}\text{nm})/W$, and $E_x = \hbar v_0 k_x$. Hence, these electrons propagate like electromagnetic waves in waveguides. A more detailed analysis shows that undoped graphene (i.e., $E_F = 0$) can be tuned to be either a metal or a semiconductor with a band gap on the order of $\Delta E(W)$ (*18*, *19*). This is an important property that undoped graphene ribbons share with undoped carbon nanotubes.

For any 2D electron system (*20*–*22*), a perpendicular magnetic field B creates a discrete energy spectrum (Landau levels) due to quantization of the cyclotron orbits (radius $R_c = p/eB$). The energy states for Dirac electrons are given by $E_n(B) = \sqrt{(2neBv_0^2\hbar)}$ (*2*, *3*, *23*) where n is the integer Landau level index [by contrast, $E_n^*(B) = (n + \frac{1}{2})\hbar eB/m^*$ for "normal" electrons, where m^* is the effective mass (*20*)]. Shubnikov–de Haas (SdH) MR maxima were observed at magnetic fields B_n such that $E_n(B_n) = E_F$. Hence, $B_n = B_0/n$, where $B_0 = E_F^2/(2ev_0^2\hbar) = \hbar k_F^2/2e$ (*24*–*26*).

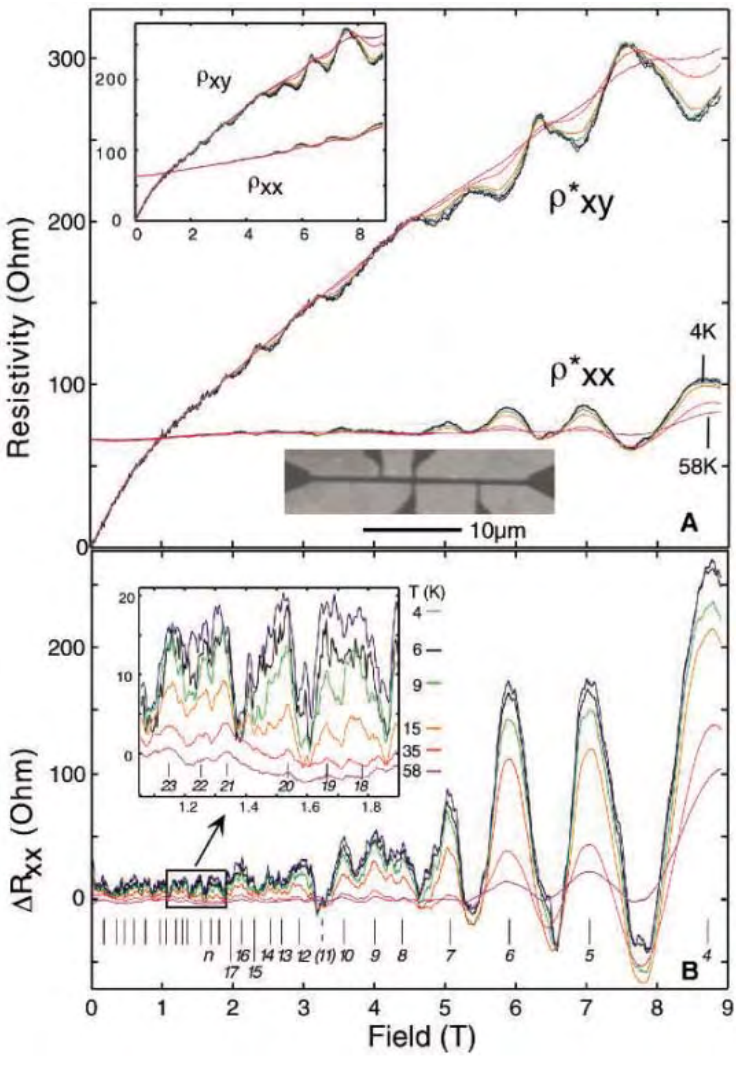

Fig. 2. Magnetotransport of a lithographically patterned graphene Hall bar (SEM micrograph, lower inset) measured at temperatures $T = 4$, 6, 9, 15, 35, and 58 K, and magnetic fields $-9\ \text{T} \le B \le 9\ \text{T}$. (**A**) Components of the resistivity tensor ρ are shown (inset; $\rho_{xx} = R_{xx}W^*/L$, $\rho_{xy} = R_{xy}$). ρ* is derived from ρ: $(\rho^*)^{-1} = \rho^{-1} - (\rho^0)^{-1}$, where $\rho^0_{xx} = 1125$ ohms and $\rho^0_{xy} = 0$. Hence, the slight slope in ρ_{xx} appears to be caused by a conducting layer ρ^0 on top of the graphene layer. The graphene mobility is $\mu^* = 2.7\ m^2/V{\cdot}s$. (**B**) ΔR_{xx} obtained from the measured R_{xx} by subtracting a smooth background. Peak positions are indicated (peak 11 is missing). The peak character changes near $B = 4.5$ T. The peak amplitudes are essentially constant below 2 T and increase above 2 T. Inset: Detail of the oscillations near $B = 1$ T. The amplitude of the universal conductance fluctuations (noise-like structures) increases with decreasing temperature.

Next, consider a graphene ribbon of width W in a magnetic field. It is intuitively clear that for low magnetic fields, when $W < 2R_c$ the ribbon cannot support a cyclotron orbit, so the above picture needs to be modified (*20*, *22*). For graphene, $2R_c = 4n/k_F$, which is 260 nm for $n = 20$. Quantitatively, Berggren *et al*. (*27*) found that for a normal 2D electron system confined to a strip of width W, $E_n(B,W) \approx \sqrt{[E_n(W)^2 + E_n(B)^2]}$, where $E_n(W) = (n\pi\hbar/W)^2/2m^*$ (*20*). Analogously, for graphene ribbons, $E_n(W) = n\pi\hbar v_0/W$, and an approximate expression for the energy levels can be obtained (*28*):

$$E_n(B,W) \approx [E_n(W)^4 + E_n(B)^4]^{1/4} = \{[n\pi\hbar v_0/W]^4 + [2neBv_0^2\hbar]^2\}^{1/4} \quad (1)$$

Recent numerical results agree very well with this analytical form (*29*). As for normal electrons, SdH peaks are expected when $E_n(B_n,W) = E_F$. Consequently $B_n = B_0/n$ for small n, whereas for large $n \sim n_{max}$ the peak spacing becomes more regular: $B_n - B_{n+1} \sim B_0/n_{max}$, where $n_{max} = E_F/\Delta E(W)$ is the number of populated transverse modes.

To illustrate the properties of carrier confinement and coherence, we next present magnetotransport data from a representative patterned EG structure. The sample is a Hall bar (ribbon) of width W = 500 nm created on the graphitized $000\bar{1}$ face of a high-quality semi-insulating 4H-SiC substrate (Fig. 2A, lower inset). Contacts are bonded on Pd/Au deposited pads. Four-point measurements were made using standard lock-in methods, with excitation currents through the ribbon limited to 100 nA. Voltages were measured over a 6-μm length L of the ribbon. MR and Hall-effect data were acquired at six temperatures from 4 to 58 K and in magnetic fields from –9 to +9 T. Field sweeps were repeated to verify reproducibility.

Figure 2A shows that $\rho_{xx} = R_{xx}\, W^*/L$ (where ρ_{xx} is the resistivity and W^* the effective ribbon width), and the Hall resistance $R_{xy} = \rho_{xy}$ of the sample. ρ_{xx} increases approximately linearly with increasing field. At high fields, SdH oscillations are clearly seen in the ρ_{xx} curves and step-like features are observed in ρ_{xy}. Subtracting a common smooth curve from the MR data reveals a rich, reproducible, and temperature-dependent structure (Fig. 2B). Pronounced, regularly spaced SdH maxima are distinguished clearly at high fields, whereas at low fields MR peaks are visible but are less well defined. Increasing the temperature decreases the amplitude of the peaks, with the high-field peaks decreasing more slowly than the low-field peaks. At a given temperature the amplitudes are relatively constant for $B < 2$ T and increase uniformly for $B > 2$ T. Positions of 29 distinct SdH peaks B_n have been identified and are indicated in Fig. 2B. Features are identified as SdH peaks when they present a clear maximum, and they are present at all of the measured temperatures. A complication is the reproducible fine structure observed throughout the MR spectra, which can obscure the SdH peaks for small fields. These are (universal) conductance fluctuations. As discussed below, the temperature dependences of universal conductance fluctuations (UCFs) and SdH oscillations are well understood and quite distinct. Incorporating this information results in an ambiguity of less than 10% in the number of peaks assigned according to the above criteria.

A Landau plot of the peaks [i.e., B_n^{-1} versus n (*20*, *24*, *30*)] is shown in the inset of Fig. 3B. The low index peaks (n = 4 to 12) define a straight line: $B_n^{-1} = (n + \gamma)B_0^{-1}$ with $B_0 = 35.1 \pm 0.8$ T and $\gamma = -0.05 \pm 0.14$. This value of γ is consistent with a Berry phase $\Phi_B = \pi$, as expected for Dirac fermions and previously observed in graphene (*2*, *3*, *23*, *26*). It is specifically not consistent with $\gamma = \pm 0.5$, as would

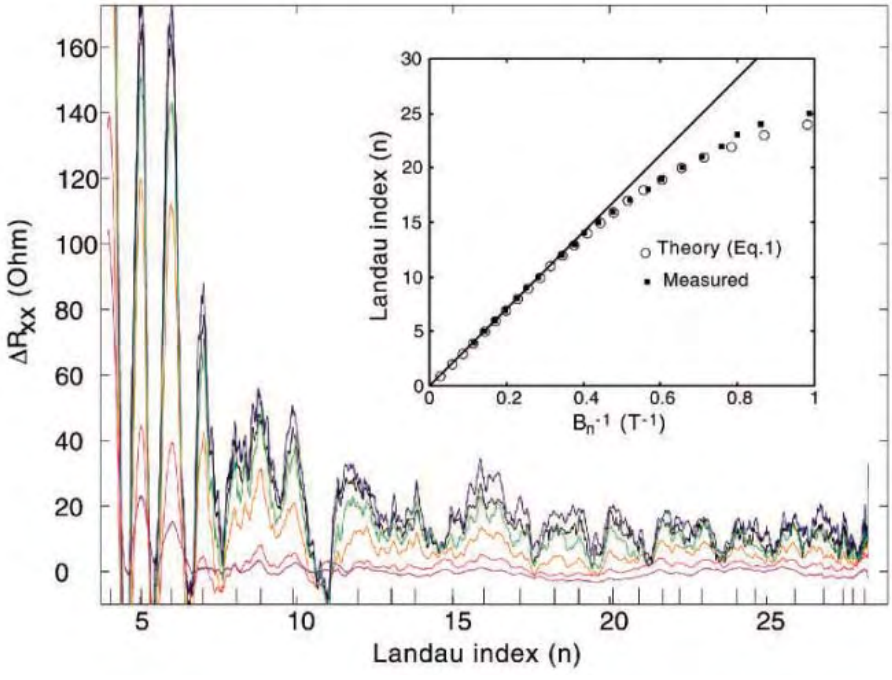

Fig. 3. Demonstration of confinement. Inset: Landau plot demonstrating the linear dependence of the measured inverse MR peak positions $1/B_n$ on the peak index n when the cyclotron diameter is smaller than the ribbon width. The linear fit for small n (bold line) intercepts the ordinate at n = 0.05, consistent with the graphene value $\gamma = 0$ and Berry's phase $\Phi_B = \pi$ (the slope of the fit corresponds to B_0, which determines k_F). The observed deviations from linearity occur for larger n when confinement becomes important; these correspond well with Eq. 1 predictions. The confinement is further illustrated by plotting ΔR_{xx} in terms of the variable $n(B)$ from Eq. 1, which shows that the peak positions approximately coincide with integers. For color code, see Fig. 2.

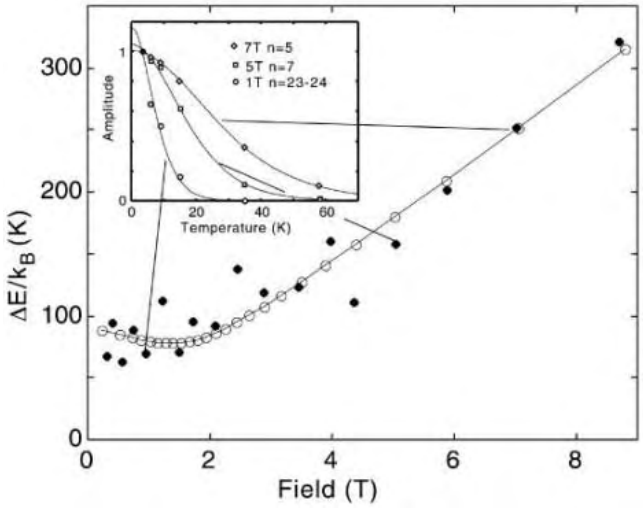

Fig. 4. Landau level excitation energies $\Delta E(B)$. Inset: Normalized MR amplitudes $\Delta R_{xx}(B,T)/\Delta R_{xx}(B,T = 4\ K)$ are fitted to Eq. 2; fit examples are shown for B = 7 T (n = 5), 5 T (n = 7), and 1 T (n = 23–24). Note that $\Delta E(B)$ increases approximately linearly for $B > 2$ as predicted theoretically (open circles from Eq. 1). In this region $\Delta E(B_n) \sim E_F/2n$. For smaller fields $\Delta E(B_n) \rightarrow E_F/n_{max}$, where n_{max} is the number of subbands in zero field. Good correspondence with theory is found for W^* = 270 nm.

be the case for normal electrons (*23*). Note that the same result was found for various subsets of peaks in the interval $n = 4$ to 12. For a 2D electron gas in general, we have $k_F = \sqrt{(2eB_0/\hbar)}$. From B_0 we find $k_F = 3.3 \times 10^8$/m, and the carrier density $n_s = g_s g_v k_F^2/4\pi = 3.4 \times 10^{16}$ electrons/m^2 (where $g_s = 2$ and $g_v = 2$ are the spin and valley degeneracies) (*20*, *21*). The deviation from linearity for the larger index peaks ($n > 14$; $B < 2.5$ T; $2R_c > 170$ nm) indicates confinement (*20*, *27*), as explained below.

We next analyze the individual SdH peaks. The amplitudes of SdH peaks decrease with increasing temperature because higher Landau levels are thermally populated. The temperature dependence of the peak amplitudes is given by the Lifshitz-Kosevich (LK) equation (*23*, *31*):

$$A_n(T)/A_n(0) = u/\sinh(u) \qquad (2)$$

where $A_n(T)$ is the peak amplitude (or peak area) of the nth SdH peak at temperature T, and $u = 2\pi^2 k_B T/\Delta E(B)$, where $\Delta E(B) = E_{n+1}(B) - E_n(B)$. Experimental values for $\Delta E(B)$ were determined by fitting SdH peaks to the LK equation for six different temperatures. In Fig. 4 the results are plotted as solid circles; values of $\Delta E(B)$ calculated from Eq. 1 are shown as open circles. A nearly linear increase for $B > 4$ T and saturation at low fields is observed in both theory and experiment. For large B, $\Delta E(B) \sim E_F B/2B_0 = E_F/2n$; for small B, $\Delta E(B) = \hbar\pi v_0/W$. Consequently, the data in Fig. 4 can be used to find $E_F/k_B = 2490 \pm 80$ K and $v_0 = E_F/\hbar k_F = E_F/\hbar\sqrt{(2eB_0/\hbar)} = (1.00 \pm 0.03) \times 10^6$ m/s. Our experimental v_0 agrees remarkably well with the accepted value for graphene (*6*). Furthermore, E_F is also consistent with recent ARPES measurements (*14*) on two-layer EG grown on SiC(0001), which found $E_F/k_B = 2700$ K. Hence, experimental evidence (measured Φ_B, v_0, E_F) strongly supports the conclusion that the material is indeed graphene.

For small B, the saturation of $\Delta E_n(B)/k_B$ at 80 ± 10 K indicates quantum confinement. The number of confined subbands should be $n_{max} \sim E_F/\Delta E(B \rightarrow 0) = 31 \pm 3$, consistent with the observed $n_{max} = 29 \pm 3$. However the hard wall boundary condition would predict that $n_{max} = Wk_F/\pi = 52$. This discrepancy suggests that the carrier confinement width of the ribbon is less than the lithographic width $W = 500$ nm (subsequent AFM and EFM studies confirmed that the physical width of the ribbon is compatible with the lithographic width; this does not preclude edge roughness effects). In fact, the best fit to the data using Eq. 1 is for $W^* = 270$ nm, as shown in Fig. 4 (see below for further evidence of reduced width). Similar discrepancies have been observed in several ribbons. The smaller effective width may be related to carrier scattering from steps on the substrate (Fig. 1; steps tend to run parallel to the ribbon) or to a stronger confinement potential caused by charge transfer to states at the ribbon edges (edge roughness, chemisorbed molecules, and intrinsic edge states could contribute), or it may have a more fundamental origin. In Fig. 3 the MR data are presented with the Landau index $n(B)$ as the abscissa, obtained by inversion of Eq. 1 (for $E_n = E_F$), where the experimental values $v_0 = 1.0 \times 10^6$ m/s, $E_F = 2490$ k_B, and $W^* = 270$ nm were used. If Eq. 1 is correct, the measured SdH peaks should coincide with integers. The correspondences up to $n = 22$ are remarkable (note that the $n = 11$ peak is missing at low T), providing additional support for our conclusion that the SdH peaks are determined by both Landau orbital quantization and transverse quantum confinement.

The overall linear increase in the MR (Fig. 1A, inset) may result from a conducting layer on top of the graphene [i.e., a thin graphite layer, consistent with independent x-ray measurements on similar samples (*13*)]. The slope is removed completely by subtracting from the measurement the conductivity of a layer with resistivity $\rho^0_{xx} = 1125$ ohms/square, and with negligible Hall coefficient. This procedure results in ρ^*_{xx} and ρ^*_{xy} values that are similar to those reported for isolated graphene. Hence, the resistivity of the graphene layer is $\rho^*_{xx} = 68$ ohms/square, versus 63 ohms/square for the sample before correction. The integrated carrier density derived from the Hall resistance is $n_{Hall} = 6.5 \times 10^{16}$/m^2, compared with $n_s = 3.4 \times 10^{16}$/m^2 found for the graphene layer (see above). The difference can be attributed to the integrated carrier density of the conducting (presumably neutral graphite) layer. Hence, we find the graphene mobility $\mu^* = (n_s e\rho^*)^{-1} = 2.7$ m^2/V·s, and carrier diffusion constant $D = E_F/2n_s e^2\rho^* = 0.30$ m^2/s. From $D = l^* v_0/2$, we obtain $l^* = 600$ nm, where l^* is the carrier mean free path in the graphene. This value is in excellent agreement with the limiting value $l^* \sim 3\pi W^*/4 = 635$ nm for a ribbon 270 nm wide with only diffuse elastic boundary scattering (*20*), which implies that the resistance is determined primarily by the confining geometry and not by defect scattering in the material.

Alternatively, the conductance of a graphene ribbon can be estimated from the Landauer equation (*21*): $G = (e^2/h) g_s g_v \Sigma T_n$, where ΣT_n is the sum over transmission coefficients of the nth modes ($0 \le T \le 1$). The T_n values are obtained approximately as $T_n = l_n/L$, where l_n is the mean free path of the nth mode (*21*). If we assume elastic scattering at the boundaries without mode mixing, then l_n is the distance along the wire between scattering events for the nth mode—that is, $l_n = k_x/k_n W = W[(k_F W/n\pi)^2 - 1]^{1/2}$. Hence, $G = (e^2/h)(g_s g_v W^*/L) \Sigma[(n_{max}/n)^2 - 1]^{1/2}$.

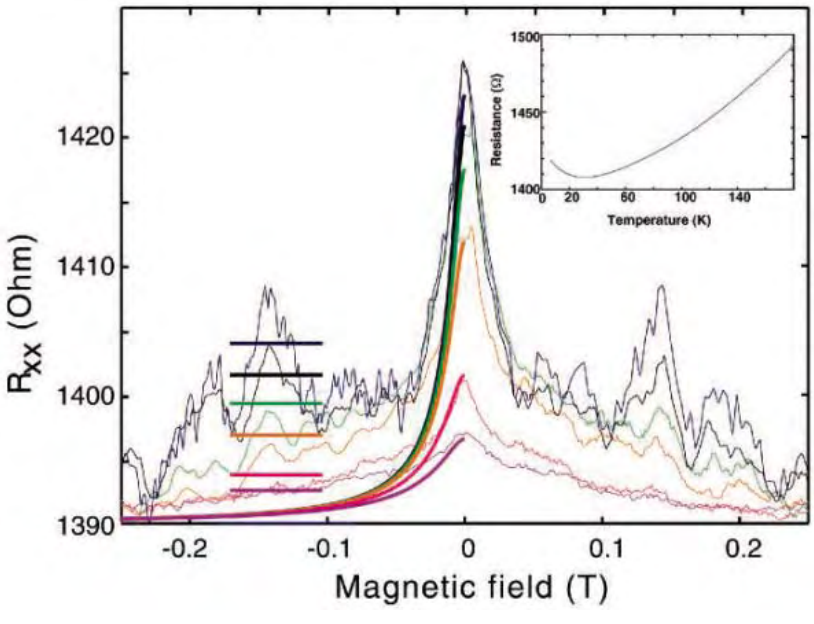

Fig. 5. Electronic coherence determined from weak localization and conductance fluctuations. The weak localization peak observed in the MR near $B = 0$ results from electronic coherent backscattering effects. The temperature dependence of the absolute amplitudes and the widths depend on the phase coherence length $l_\phi(T)$ and the geometry [note the low-temperature saturation of $l_\phi(T) \sim 1.1$ μm]. The UCF structures have widths that are similar to the WL peak (~0.03 T, considerably narrower than the SdH peaks). The theoretical fits (bold lines, plotted only for $B < 0$), using only $l_\phi(T)$ as a parameter, describe reasonably well both the WL peaks and the UCF amplitudes (bold horizontal lines). Inset: Sample resistance as a function of temperature for $B = 0$.

With $W^* = 270$ nm, $L = 6$ μm, and $n_{max} = 29$, we find $R = 1/G = 1430$ ohms, or $\rho_g = RW^*/L = 64$ ohms/square, in remarkable agreement with experiment.

The sample resistance decreased uniformly from 1490 ohms at $T = 180$ K to a minimum of 1410 ohms at $T = 30$ K, below which it increased (Fig. 5, inset). From 300 to 30 K, the resistance decreased only 13%, which indicates [from Matthiessen's rule (*20*, *21*)] that the electron phonon-scattering time is $\sim 4 \times 10^{-12}$ s at 300 K. The increase of resistance below 30 K is caused by the increasing phase coherence length l_ϕ (*20*, *22*, *32*). The resistance increase is a manifestation of constructive quantum interference between time-reversed trajectories, which enhances the probability for an electron to be localized at a scattering site (*20*, *22*, *32*). This well-understood weak localization (WL) effect is undone in a magnetic field because time reversal symmetry is lifted (*20*, *22*). The pronounced peak in the low-field MR at $B = 0$ shows this WL effect (Fig. 5). Clear universal conductance fluctuations flank the peak. The reproducible UCFs are caused by quantum interference from elastic scatterers (e.g., at the ribbon edges). For all fields, the widths of UCF features are similar to the WL peak width, in contrast to the SdH peaks, which are much wider. The WL peak saturates at low temperatures (peaks for 4, 6, and 9 K are similar), whereas the amplitude of the UCFs increases very rapidly with decreasing temperature (which also distinguishes UCFs from SdH peaks).

Weak localization and UCFs have been exhaustively investigated in 2D electron systems. Before saturation below 9 K, the observed decrease of the WL peak with increasing T fits a $T^{-2/3}$ dependence, which indicates that electron-electron scattering is the primary dephasing mechanism (*22*). The decrease in amplitude of the UCFs with increasing T is caused by a reduction of l_ϕ combined with "thermal smearing," which is characterized by the thermal length $l_T = \sqrt{(\hbar D/k_B T)}$.

On the other hand, the WL is not sensitive to l_T. Its width ΔB is essentially determined by the field for which an electron trajectory of length l_ϕ encloses one flux quantum (for this sample $l_\phi \gg W$, so that flux cancellation effects also need to be taken into account). Following the thorough development reviewed by Beenakker and van Houten (*20*), the field is parameterized in terms of $l_B = \sqrt{D\tau_B}$, where $\tau_B = 3l_m^2 l^*/(W^2 v_0)(4\pi l_m^2/3Wl^* + 1)$, and $l_m = (\hbar/eB)^{1/2}$ is the magnetic length. The WL contribution to the conductance (for $l_\phi \gg l^* \gg W$) is

$$\Delta G_{WL} = -4(G_0/L)[(l_\phi^{-2} + l_B^{-2})^{-1/2} - (l_\phi^{-2} + l_B^{-2} + l^{*-2})^{-1/2}] \quad (3)$$

and the root mean square amplitude of the UCFs is given by

$$\Delta G_{UCF} = \sqrt{24} G_0 (l_\phi/L)^{3/2}[1 + (9/2\pi)(l_\phi/l_T)^2]^{-1/2} \quad (4)$$

The only free parameter in these expressions is $l_\phi(T)$. The origin of the commonly observed low-temperature saturation of the WL is still debated intensely (*22*). Here we assume that it is caused by a physical limitation to l_ϕ, which appears to be the finite sample length. The effective phase coherence length $l_\phi^* = [l_\phi(T)^{-2} + (L_{sat}/2\pi)^{-2}]^{-1/2}$ saturates at $L_{sat}/2\pi$ (*22*). The fits shown in Fig. 5 correspond to $L_{sat} = 7$ μm and $l_\phi(T) = (7\ \mu m)T^{-2/3}$ [at 4 K, $l_\phi^* = 1.1$ μm, and $\tau_\phi = (l_\phi^*)^2/D = 4 \times 10^{-12}$ s; at 58 K, $l_\phi^* = 430$ nm, and $\tau_\phi = 6 \times 10^{-13}$ s].

This analysis clearly shows that the resistance of the graphene ribbon is determined primarily by boundary scattering, with a coherence length far larger than the effective ribbon width, even at 58 K. Therefore, as also shown in our analysis of SdH oscillations, the low-field resistance depends directly on the eigenmodes of laterally confined carriers in the graphene ribbon. Other samples indicate that the width dependence of resistance can persist up to room temperature. Because electron-phonon scattering is weak even at room temperature (see above), electron-electron scattering should continue to be the dominant dephasing mechanism under ambient conditions (such scattering affects the resistance only through phase-breaking, i.e., by limiting l_ϕ). Accordingly, on the basis of the measurements presented here, we expect to see quantum interference effects over distances exceeding 100 nm at room temperature (and beyond 400 nm at liquid nitrogen temperature). Moreover, quantum confinement should be observable at room temperature in ribbons as wide as 50 nm. In this context, we also note that a ribbon 100 nm wide has been observed to sustain a current of >100 μA at room temperature, and that, like nanotubes (*33*), the conductance of graphene ribbons increases approximately linearly with bias voltage at high bias.

These results raise new possibilities for coherent EG electronics on an attractive size scale and at relatively high temperatures. The demonstrated material and transport properties of EG could allow electronic devices and interconnects to be designed that rely on the wave properties of electrons and holes, so that interference-based electronic switches can be envisioned. Nanotubes, on the other hand, require metallic interconnects that destroy phase coherence. Furthermore, graphene is an extremely robust material that has the potential to be patterned with atomic precision down to the molecular level. Such precision might be achieved through a combination of standard lithographic and chemical methods, enabling a wide variety of coherently connected molecular structures. Finally, we note that it has been previously determined that the carrier density can be controlled electrostatically (*1*, *16*, *34*) and that chemical doping of the edges also is feasible (*1*, *35*). Consequently, epitaxial graphene provides a platform for the science and technology of coherent graphene molecular electronics.

References and Notes

1. C. Berger *et al.*, *J. Phys. Chem. B* **108**, 19912 (2004).
2. K. S. Novoselov *et al.*, *Nature* **438**, 197 (2005).
3. Y. B. Zhang, Y. W. Tan, H. L. Stormer, P. Kim, *Nature* **438**, 201 (2005).
4. T. Ando, T. Nakanishi, R. Saito, *J. Phys. Soc. Jpn.* **67**, 2857 (1998).
5. P. R. Wallace, *Phys. Rev.* **71**, 622 (1947).
6. B. T. Kelly, *Physics of Graphite* (Applied Science, London, 1981).
7. The momentum is with reference to the K point in graphene, i.e., $E = v_0\hbar|k - k(K)|$, where k is the wave vector.
8. Carbon nanotubes are a specific example of confined graphene, where the momentum perpendicular to the axis is quantized according to $k_{perp} = n/D$, where D is the diameter.
9. I. Forbeaux, J. M. Themlin, J. M. Debever, *Phys. Rev. B* **58**, 16396 (1998).
10. A. Charrier *et al.*, *J. Appl. Phys.* **92**, 2479 (2002).
11. Cree Inc., High Purity, R Grade 4H SiC.
12. V. Ramachandran, M. F. Brady, A. R. Smith, R. M. Feenstra, D. W. Greve, *J. Electron. Mater.* **27**, 308 (1998).
13. J. Hass *et al.*, arxiv.org/abs/cond-mat/0604206 (2006).
14. E. Rollings *et al.*, arxiv.org/abs/cond-mat/0512226 (2005).
15. P. B. Visscher, L. M. Falicov, *Phys. Rev. B* **3**, 2541 (1971).
16. Y. B. Zhang, J. P. Small, M. E. S. Amori, P. Kim, *Phys. Rev. Lett.* **94**, 176803 (2005).
17. M. Fujita, K. Wakabayashi, K. Nakada, K. Kusakabe, *J. Phys. Soc. Jpn.* **65**, 1920 (1996).
18. K. Nakada, M. Fujita, G. Dresselhaus, M. S. Dresselhaus, *Phys. Rev. B* **54**, 17954 (1996).
19. K. Wakabayashi, *Phys. Rev. B* **64**, 12 (2001).
20. C. W. J. Beenakker, H. van Houten, *Quantum Transport in Semiconductor Nanostructures*, vol. 44 (Academic Press, New York, 1991), and reference therein (also available at arxiv.org/abs/cond-mat/0412664).
21. S. Datta, *Electronic Transport in Mesoscopic Systems* (Cambridge Univ. Press, Cambridge, 1995).
22. J. J. Lin, J. P. Bird, *J. Phys. Condens. Matter* **14**, R501 (2002).
23. S. G. Sharapov, V. P. Gusynin, H. Beck, *Phys. Rev. B* **69**, 075104 (2004).
24. D. E. Soule, J. W. McClure, L. B. Smith, *Phys. Rev. A.* **134**, A453 (1964).
25. D. E. Soule, *Phys. Rev.* **1**, 708 (1958).
26. I. A. Luk'yanchuk, Y. Kopelevich, *Phys. Rev. Lett.* **93**, 166402 (2004).
27. K. F. Berggren, G. Roos, H. van Houten, *Phys. Rev. B* **37**, 10118 (1988).
28. Equation 1 is obtained by applying the interpolation scheme of (*27*) to Dirac electrons. Applying the Schrödinger equation $H|\Psi\rangle = E|\Psi\rangle$ twice gives $H_{eff}|\Psi\rangle = E_{eff}|\Psi\rangle$ with $H_{eff} = H^2$ and $E_{eff} = E^2$. It can be shown that $H_{eff} = H^2$ describes free-like electrons close to the band edges (either from the Dirac equation or the tight-binding model; the origin of energies is taken at the band edges). Using the square root interpolation formula of (*27*) applied to $H_{eff} = H^2$ gives $E_n = \sqrt{E_{eff_n}}$ for the energies at the bottom of band n.
29. N. M. R. Peres, A. H. Castro Neto, F. Guinea, arxiv.org/abs/cond-mat/0603771 (2006).
30. We follow the convention of indexing the MR peaks (*24*, *25*) rather than the valleys.
31. I. M. Lifshitz, A. M. Kosevich, *Sov. Phys. JETP* **2**, 636 (1956).

32. B. L. Altshuler, A. G. Aronov, Eds., *Electron-Electron Interactions in Disordered Systems* (Elsevier, Amsterdam, 1985).
33. P. Poncharal, C. Berger, Y. Yi, Z. L. Wang, W. A. de Heer, *J. Phys. Chem. B* **106**, 12104 (2002).
34. K. S. Novoselov *et al.*, *Science* **306**, 666 (2004).
35. N. M. R. Peres, F. Guinea, A. H. Castro Neto, arxiv.org/abs/cond-mat/0512091 (2005).

36. Supported by NSF grant 0404084, U.S. Department of Energy grant DE-FG02-02ER45956, a grant from Intel Research Corporation, and a USA-France travel grant from CNRS. We acknowledge discussions with J. D. Meindl and help from the staff of the Georgia Tech MIRC clean room. Any opinions, findings, and conclusions or recommendations expressed in this material are those of the authors and do not necessarily reflect the views of the research sponsors.

7 February 2006; accepted 5 April 2006
Published online 13 April 2006;
10.1126/science.1125925
Include this information when citing this paper.

Imaging Bond Formation Between a Gold Atom and Pentacene on an Insulating Surface

Jascha Repp,[1]* Gerhard Meyer,[1] Sami Paavilainen,[2] Fredrik E. Olsson,[3] Mats Persson[4]

A covalent bond between an individual pentacene molecule and a gold atom was formed by means of single-molecule chemistry inside a scanning tunneling microscope junction. The bond formation is reversible, and different structural isomers can be produced. The single-molecule synthesis was done on ultrathin insulating films that electronically isolated the reactants and products from their environment. Direct imaging of the orbital hybridization upon bond formation provides insight into the energetic shifts and occupation of the molecular resonances.

Electron transport through single molecules in contact with metal electrodes has turned out to depend crucially on the details of the contact geometry (*1*), resulting in poor reproducibility of experiments in different setups. Control on the contact formation will not only have to include the atomic-scale geometry itself, but also coherent (strong coupling) versus incoherent (weak coupling) electron transport, coupling with respect to the molecular orbitals, and possibly also the phase of the orbital wave function at the contact point.

We show here that such control can be achieved for connecting metal atoms to π-conjugated molecules on insulating NaCl films by means of single-molecule chemistry (*2*–*5*) in a scanning tunneling microscope (STM) junction. The atomic precision in STM manipulation and single-molecule chemistry can be exploited to create different kinds of contacts between a gold atom and a pentacene molecule. The gold atom can be brought into various positions a few angstroms away from the molecule, which facilitates an electron tunneling current between the atom and the molecule (weak coupling). Alternatively, the gold atom can be covalently bound to the pentacene molecule to form a metal-organic complex, which is accompanied by a strong and coherent electronic coupling between the two constituents, as can be deduced from STM images. Moreover, the possibility of creating different structural isomers by bringing together the reactants in different orientations enables control of the phase of the molecular orbital at the contact point. The influence of the contact formation on the electronic structure of the complex is evident from the different frontier orbitals of the different isomers, which can be directly seen in the corresponding STM images (*6*). Frontier orbitals have previously been imaged for the case of pentacene alone. We complement our results by using density functional theory (DFT) calculations.

The experiments were carried out with a home-built low-temperature STM operated at 5 K. NaCl was evaporated thermally onto clean Cu(111) and Cu(100) single-crystal samples at room temperature so that defect-free, (100)-terminated NaCl islands of two atomic layers in thickness were formed (*7*). Individual pentacene molecules and gold atoms were adsorbed at a sample temperature of $T \sim 5$ K, with the sample located in the STM. Bias voltages refer to the sample voltage with respect to the tip. All experimental data refer to the NaCl/Cu(100) system, except where stated otherwise.

Single-molecule chemistry by means of STM on an insulating surface follows a different route compared with the well-established manipulations on metal substrates, on which a single-

[1]IBM Zurich Research Laboratory, 8803 Rüschlikon, Switzerland. [2]Institute of Physics, Tampere University of Technology, 33720 Tampere, Finland. [3]Department of Applied Physics, Chalmers, 41296 Göteborg, Sweden. [4]Surface Science Research Centre and Department of Chemistry, The University of Liverpool, Liverpool L69 3BX, UK.

*To whom correspondence should be addressed. E-mail: jre@zurich.ibm.com

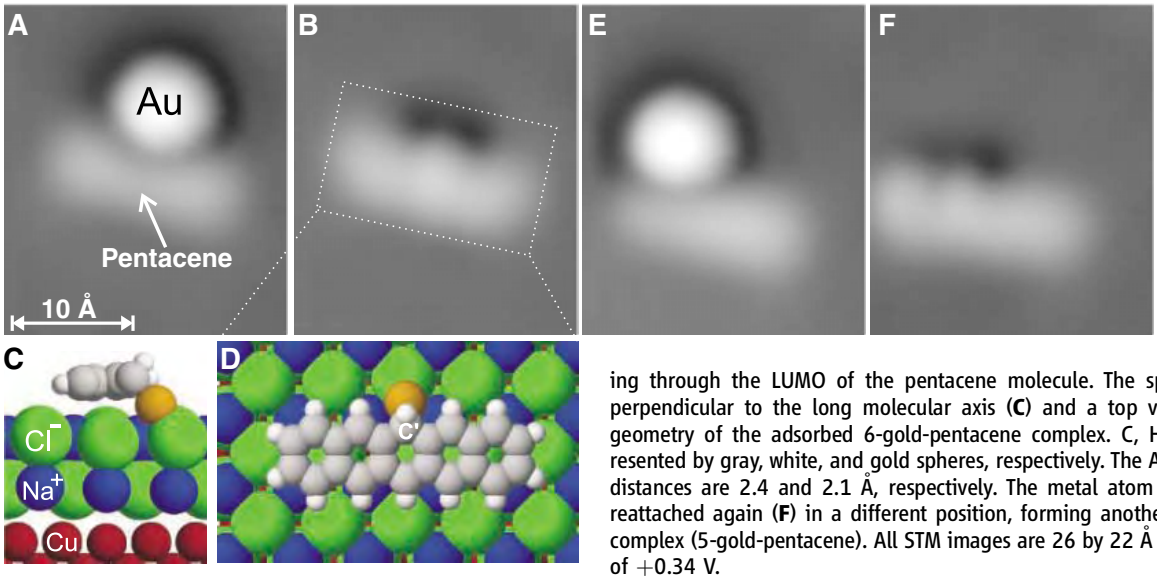

Fig. 1. Making and breaking a chemical bond between a single pentacene molecule and gold atom on an NaCl bilayer supported by a Cu(100) substrate. (**A**) STM image showing the molecule and the gold atom before bond formation. (**B**) Image showing a molecule-metal complex (6-gold-pentacene) after resonant tunneling through the LUMO of the pentacene molecule. The sphere models show a cut perpendicular to the long molecular axis (**C**) and a top view (**D**) of the calculated geometry of the adsorbed 6-gold-pentacene complex. C, H, and Au atoms are represented by gray, white, and gold spheres, respectively. The Au-Cl and Au-C interatomic distances are 2.4 and 2.1 Å, respectively. The metal atom can be detached (**E**) and reattached again (**F**) in a different position, forming another structural isomer of the complex (5-gold-pentacene). All STM images are 26 by 22 Å in size and taken at a bias of +0.34 V.

molecule synthesis can be separated into two distinct steps (*3*–*5*). On a flat metal surface, the first step, in which the reactants are brought close to each other by lateral manipulation (*8*), is relatively easily achieved because of the small diffusion barrier–to–binding energy ratio. In the second, more-complex bond-formation step, much higher energy barriers must be overcome. Thus, this step is initiated by means of nonthermal excitation of the reactants with inelastic electron tunneling (IET). In the case of an insulating substrate, as discussed here, the diffusion barrier–to–binding energy ratio is much larger, thus requiring an excitation by IET to induce the lateral movement. Such IET excitation is most efficient on insulating films, because of the longer electronic lifetimes (*7*, *9*, *10*). The actual bond formation between the metal atom and the molecule, however, requires a smaller activation energy, such that the IET excitation process applied to achieve lateral movement is already sufficient to also initiate the synthesis.

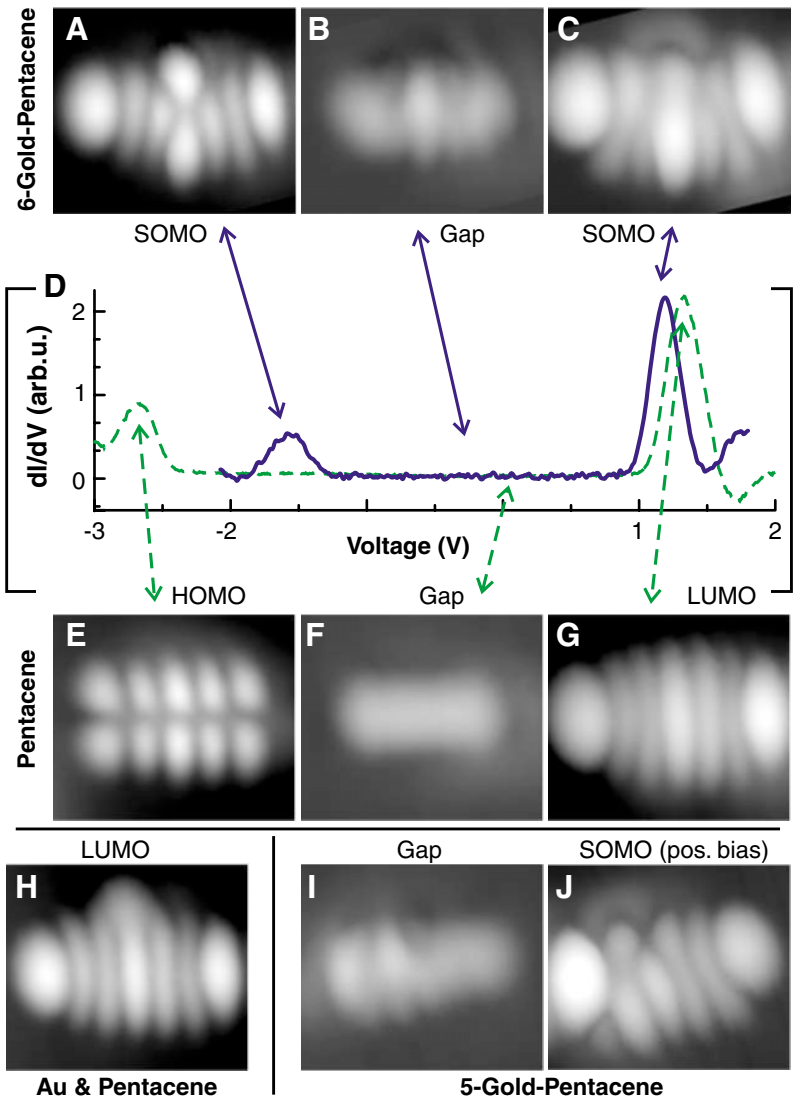

Fig. 2. Bias-dependent STM images and differential conductance (*dI*/*dV*) spectra of various structures of a gold atom and a pentacene molecule on the NaCl film. The d*I*/d*V* spectrum of the 6-gold-pentacene complex (**D**) exhibits two distinct peaks at -1.5 and +1.2 V (solid line). For easy reference, the plot also shows the *dI*/*dV* signal of an isolated pentacene molecule (dashed line). At biases corresponding to the two peaks and the broad gap region of the *dI*/*dV* spectrum, the 6-gold-pentacene complex and the isolated pentacene molecule yield three different STM images: (**A** to **C**) and (**E** to **G**), respectively. The 5-gold-pentacene isomer shows an almost identical *dI*/*dV* spectrum, but the corresponding in-gap (**I**) and resonance (**J**) images are different from those of the other complex. For comparison, in an arrangement of the Au atom and molecule corresponding to Fig. 1A, the image of the molecular resonance (**H**) shows just the unperturbed LUMO of the pentacene molecule and the protrusion of the Au atom, indicating a nonbonded arrangement. All images are 22-by-19 Å in size and acquired with a pentacene molecule attached to the tip (*6*) to enhance the intramolecular resolution. pos., positive; arb. u., arbitrary units.

Figure 1 shows the bond formation between a pentacene molecule and a gold atom on a bilayer of NaCl. In Fig. 1A, the reactants are already located close to each other. The bond was formed by IET (*11*), and the resulting complex (Fig. 1B) has a mirror plane that is perpendicular to the long axis of the molecule, indicating that the gold atom is attached to the central ring of pentacene (6-gold-pentacene) (Fig. 1, C and D). The bond was broken again by IET-induced excitation of the entire complex. The next image (Fig. 1E) shows the two constituents separated again; namely, the gold atom and the pentacene molecule. In a subsequent step, they were bonded to each other again, but this time the gold atom was attached to the pentacene molecule in a different position. Judging from the dark feature in the STM image of the complex (Fig. 1F), the gold atom is slightly off-center (5-gold-pentacene).

The reversibility of the complex formation suggests that it is an addition reaction of the gold atom to one of the pentacene's aromatic rings and involves neither the substitution of a hydrogen atom nor a defect creation in the substrate. The complete reversibility was substantiated in an experiment in which, after forming and breaking the bond again (as seen in the STM image of Fig. 1E), the molecular orbitals of the pentacene (*6*) and the charge bistability of the gold atom (*7*) on the NaCl/Cu(111) surface could be observed at unchanged experimental parameters. This finding indicates that the gold atom, the pentacene molecule, and the underlying substrate were not permanently modified.

The differential conductance signal (*dI*/*dV*, where *I* is current and *V* is voltage) acquired with the STM tip above the 6-gold-pentacene complex in Fig. 2D exhibits two pronounced peaks at –1.5 and +1.2 V and a broad gap in between. As in the case of isolated pentacene (*6*), images taken at different bias voltages corresponding to the gap region (in-gap conditions) and to the peaks in *dI*/*dV* spectra (resonance conditions) differ greatly. The images in Fig. 2, A and C, show pronounced intramolecular resolution and a large apparent height of 2.0 and 2.6 Å, respectively. In contrast, for in-gap conditions, the apparent height measures only 1.0 Å (Fig. 2B). The orbital structure of the complex is delocalized over the entire complex including the gold atom, indicating a covalent bond between the pentacene molecule and the gold atom. For comparison, Fig. 2, E to G, show the STM images of an isolated pentacene molecule for bias voltages corresponding to the highest occupied molecular orbital (HOMO), in-gap conditions, and the lowest unoccupied molecular orbital (LUMO), respectively. When the gold atom is very close to a pentacene molecule but not bound to it, the corresponding STM image (Fig. 2H) exhibits no sign of bonding or common orbital structure but is just a super-

position of the unperturbed LUMO of the pentacene molecule and the protrusion of the gold atom. In this configuration, the Au atom is adsorbed at a distance of 6 Å from the long molecular axis.

The 5-gold-pentacene complex (Fig. 2I) exhibits two peaks in its *dI*/*dV* spectrum, almost identical to those of the 6-gold-pentacene isomer (the peak at positive bias is slightly lower in energy by ~0.05 V). The corresponding image in Fig. 2J also shows a covalent bond formation, with distinct differences to the pentacene's LUMO, which are predominant near the gold atom. In addition, there is a very strong enhancement of the orbital structure at the end of the complex that is closer to the gold atom. This enhancement in the STM image is expressed in a height difference of about 1 Å of the two outmost protrusions.

Because electrons can still tunnel through the ultrathin NaCl film, the charge state of the complex after its formation is not clear a priori (*7*, *12*). Therefore, the charge state of the 6-gold-pentacene complex was experimentally investigated and found to be neutral because of the absence of scattering of the NaCl/Cu(111) interface-state electrons at the complex (*9*). Thus, the complex accommodates an odd number of electrons and has a singly-occupied molecular orbital (SOMO) near the Fermi level (E_F). This result explains why the orbital structure looks almost the same for both polarities of the bias voltage in Fig. 2, A and C. In both cases, the electrons tunnel through the same orbital, either temporarily emptying it ($V < 0$) or temporarily filling it with a second electron ($V > 0$) (*13*, *14*).

Thus, the broad gap in the *dI*/*dV* spectra of the complexes is not a HOMO-LUMO gap, but is solely attributed to the Coulomb energy associated with adding or removing an electron to or from the same orbital of the complex. Thus, the separation of the two peaks labeled SOMO gives a simple and direct measure of this important parameter. In the case of isolated pentacene, the HOMO-LUMO peak separation is much larger [4.1 eV (*6*)]. This value can be regarded as the sum of the energy needed to excite an electron from the HOMO to the LUMO, plus a similar Coulomb energy associated with adding or removing an electron to or from the very same orbital.

To gain deeper insight into the nature of the 6-gold-pentacene complex on the NaCl film, we have carried out spin-polarized DFT calculations (*15*) of the complex adsorbed on an NaCl bilayer supported by a Cu(100) surface (*7*, *16*). We used the projector augmented wave method (*17*) as implemented in the Vienna Ab initio Simulation Package (VASP) code (*18*). STM images were simulated in the Tersoff-Hamann approximation (*19*) as topographies of constant, local density of (Kohn-Sham) states (LDOS) integrated over the range of energies allowed by the applied bias.

With the DFT calculations, we have identified a geometrically stable configuration of the 6-gold-pentacene complex (Fig. 1, C and D) with an interesting metal-ligand interaction. The pentacene molecule in the complex has the same adsorption site on the NaCl film as does the single molecule in previous studies (*6*). The molecule is aligned parallel to one of the polar <011> directions of the NaCl(100) films with its center located on top of a Cl^- ion. The Au atom is bonded to both a Cl^- and a C atom in the central ring of the molecule (Fig. 1, C and D). This C atom is henceforth referred to as the C′ atom. The H atom is tilted upward so that the C′ atom is in a nearly tetrahedral bond configuration with respect to its four neighbors—the Au atom, the H atom, and the two adjacent C atoms—indicating a sp^2-to-sp^3 rehybridization of the C′ atom. The bonding of the Au atom to the pentacene molecule results in sizeable relaxations in the NaCl film only for the Cl^- bonded to the Au atom and the Na^+ below.

A comparison between simulated and observed STM images of the complex provides strong support that the calculated geometry corresponds to the one imaged in experiments. The simulated image (Fig. 3A) reproduces all of the details of the experimental image (Fig. 2C). An analysis of the LDOS reveals that the "half-moon" around the Au atom in the STM image originates from the Au 6s state and the protrusion above the Au atom from one of the C′ sp^3-hybridized states. To understand the detailed molecular orbital character of the STM image and the formation of the complex and its bonding to the surface, we need to scrutinize the electronic structure of the complex and its fragments.

First we need to understand the bonding of the fragments to the NaCl film. The closed-shell structure of the pentacene molecule results in a weakly adsorbed state for the molecule on the NaCl bilayer. The HOMO and the LUMO experience small energy shifts and have a negligible overlap with the metal substrate states. The characteristic nodal structures of these π-orbitals are shown in the left column of Fig. 3C. The bonding of the Au atom to the NaCl film can result in two different charge states (*7*). In the (nearly) neutral state, the Au atom is weakly adsorbed on the film and the Au(6s) state of the adsorbed gold atom [henceforth referred to as Au(6ŝ)] is partially occupied and pinned to E_F of the substrate.

The addition of an Au atom in its neutral state to the pentacene molecule results in a radical complex with an odd number of electrons, with predominant orbital interactions being among their frontier orbitals. The HOMO and LUMO of the molecule and the Au(6ŝ) state (Fig. 3C) interact and form three new orbitals whose characters can be rationalized in a

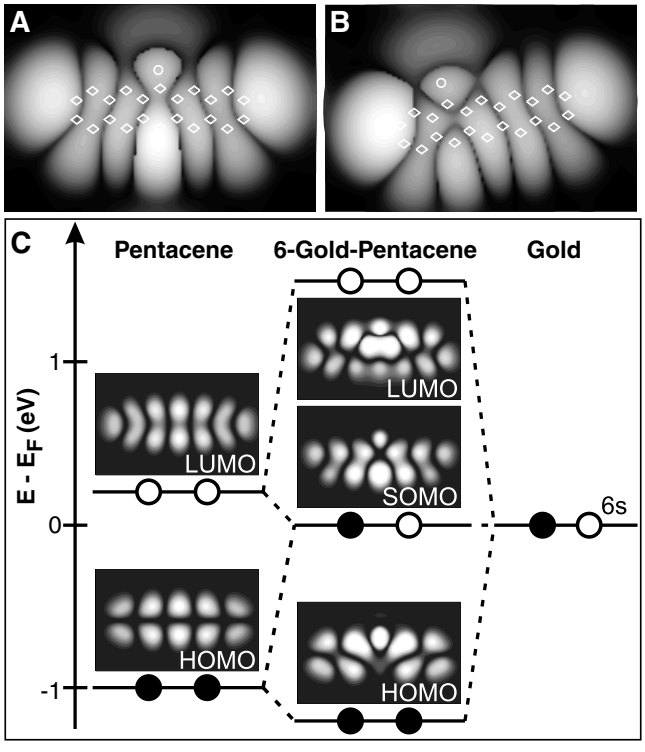

Fig. 3. Simulated STM images of the adsorbed 6-gold-pentacene (**A**) and 5-gold-pentacene (**B**) complexes as given by the topographic image of the constant, integrated LDOS. The energy range of the LDOS integral ($E_F \rightarrow E_F +$ 0.5 eV) includes the unoccupied part of the SOMO. The apparent heights are about 3 Å. The positions of the C atoms and the Au atom are indicated by diamonds and a circle, respectively. The image sizes are 15-by-23 Å. (**C**) Schematic diagram of the calculated one-electron energy levels and density maps of the frontier orbitals participating in the formation of the 6-gold-pentacene. This orbital set includes the HOMO and LUMO of the pentacene molecule; the HOMO, LUMO, and SOMO of the adsorbed complex; and the Au (6s)-derived orbital. All energies and density maps refer to adsorption on a NaCl bilayer on Cu(100). Unoccupied and occupied states are represented by open and filled circles, respectively. The density maps are 16-by-10 Å in size and correspond to LDOS maps taken at a distance of ~0.8 Å above the molecular plane.

simple three-state model. The HOMO of the complex is predominantly a bonding combination of the Au(6ŝ) state with the HOMO of pentacene, whereas the LUMO is an antibonding combination with the pentacene's LUMO. The remaining SOMO is a linear combination of the Au(6ŝ) state with both the HOMO (with antibonding character) and the LUMO (with bonding character). The apparent sideways bending of this state is purely an electronic effect. This bending and the nodal structure of the STM image are understood from the mixing of the HOMO and LUMO in the given phase relation, resulting in an enhanced amplitude on the side of the long axis of the pentacene molecule that is opposite from the Au atom. Furthermore, we find that the addition of the Au atom to the molecule is electrophilic, as there is a small net electron transfer to Au due to the larger electronegativity of the Au atom than of the pentacene molecule.

The calculations also show a stable adsorption configuration for the 5-gold-pentacene. The simulated STM image of this complex (Fig. 3B) is similar to the experimental image shown in Fig. 2J. The large difference in the apparent height between the ends of the complex is an electronic rather than a geometric effect, because the complex lies almost parallel to the surface.

Finally, DFT calculations on free gold-pentacene complexes without the NaCl/Cu(100) substrate reveal that these complexes are also stable and have similar geometric configuration and bond lengths, as well as orbitals and charge redistribution, to the adsorbed complexes. The main difference is an upward energy shift of the LUMO of the adsorbed complexes compared with a free complex because of their interaction with the occupied Cl^- 3p states.

Our DFT analysis confirms that the bond formation is an addition reaction of the gold atom to a pentacene's benzene ring, with a covalent character to create a radical complex. Aromatics usually prefer substitution over addition reactions that maintain their delocalized π-electronic system (*20*). However, in contrast to a reaction taking place in solution, the hydrogen atom in our case would have no alternate bonding partner.

Apart from the aspects of a contact formation, our findings also show new routes to selectively alter the electronic structure and chemical reactivity of large molecules with a delocalized electronic system. Control of the energetics of molecular resonances has been demonstrated before by the doping of a single molecule (*21*). The organometallic bond formation in our experiment even transforms a closed-shell molecule into a radical. This "engineering" of the orbital structure by creating different isomers controls both the nodal structure itself as well as the relative weight of the probability distribution in different parts of the molecule.

References and Notes

1. A. H. Flood, J. F. Stoddart, D. W. Steuerman, J. R. Heath, *Science* **306**, 2055 (2004).
2. B. C. Stipe *et al.*, *Phys. Rev. Lett.* **78**, 4410 (1997).
3. H. J. Lee, W. Ho, *Science* **286**, 1719 (1999).
4. S.-W. Hla, L. Bartels, G. Meyer, K.-H. Rieder, *Phys. Rev. Lett.* **85**, 2777 (2000).
5. J. R. Hahn, W. Ho, *Phys. Rev. Lett.* **87**, 166102 (2001).
6. J. Repp, G. Meyer, S. M. Stojković, A. Gourdon, C. Joachim, *Phys. Rev. Lett.* **94**, 026803 (2005).
7. J. Repp, G. Meyer, F. E. Olsson, M. Persson, *Science* **305**, 493 (2004).
8. D. M. Eigler, E. K. Schweizer, *Nature* **334**, 524 (1990).
9. J. Repp, G. Meyer, S. Paavilainen, F. E. Olsson, M. Persson, *Phys. Rev. Lett.* **95**, 225503 (2005).
10. X. H. Qiu, G. V. Nazin, W. Ho, *Phys. Rev. Lett.* **92**, 206102 (2004).
11. In the example shown, the bond was formed by running a tunneling current of $I = 2.5$ pA through the LUMO of the pentacene at a bias voltage of $V = +1.75$ V. The high bias voltage required for manipulation results from the electronic resonances of the adsorbate and is not a measure of the energy barrier of the process induced.
12. G. Pacchioni, L. Giordano, M. Baistrocchi, *Phys. Rev. Lett.* **94**, 226104 (2005).
13. In the present case, the two similar orbital images for both polarities of the bias voltage are not a result of the type of bipolar tunneling, as observed recently for a copper-phthalocyanine molecule on an alumina film (*14*). Also, tunneling at bias voltages of several volts results in IET-induced bond breaking even at an extremely low current of <1 pA. Thus, the HOMO and the LUMO of the complexes could not be measured experimentally.
14. S. W. Wu, G. V. Nazin, X. Chen, X. H. Qiu, W. Ho, *Phys. Rev. Lett.* **93**, 236802 (2004).
15. The Au-pentacene complex was adsorbed on a slab of four layers of Cu with 54 Cu atoms per layer and two layers of NaCl molecules in a super cell. All atoms except the two lowermost Cu layers were geometrically relaxed. The surface Brillouin zone was sampled using a 2×2 wave-vector mesh. The plane-wave basis set was truncated at a kinetic energy of 400 eV.
16. F. E. Olsson, M. Persson, *Surf. Sci.* **540**, 172 (2003).
17. G. Kresse, D. Joubert, *Phys. Rev. B* **59**, 1758 (1999).
18. G. Kresse, J. Furthmüller, *Phys. Rev. B* **54**, 11169 (1996).
19. J. Tersoff, D. R. Hamann, *Phys. Rev. Lett.* **50**, 1998 (1983).
20. K. P. C. Vollhardt, N. E. Schore, *Organic Chemistry* (W. H. Freeman & Co., New York, 2002).
21. R. Yamachika, M. Grobis, A. Wachowiak, M. F. Crommie, *Science* **304**, 281 (2004).

22. We thank R. Allenspach and S. Billeter for fruitful discussions. We acknowledge partial funding by the Academy of Finland; the Swedish Research Council (V.R.); the European Union projects CHIC, AMMIST, NANOSPECTRA, and NANOMAN; and allocation by computer resources by the Swedish National Allocations Committee.

10 February 2006; accepted 5 April 2006
10.1126/science.1126073

Carbon Nanotubes as High-Pressure Cylinders and Nanoextruders

L. Sun,[1] F. Banhart,[1]* A. V. Krasheninnikov,[2,3] J. A. Rodríguez-Manzo,[4] M. Terrones,[4] P. M. Ajayan[5]

Closed-shell carbon nanostructures, such as carbon onions, have been shown to act as self-contracting high-pressure cells under electron irradiation. We report that controlled irradiation of multiwalled carbon nanotubes can cause large pressure buildup within the nanotube cores that can plastically deform, extrude, and break solid materials that are encapsulated inside the core. We further showed by atomistic simulations that the internal pressure inside nanotubes can reach values higher than 40 gigapascals. Nanotubes can thus be used as robust nanoscale jigs for extruding and deforming hard nanomaterials and for modifying their properties, as well as templates for the study of individual nanometer-sized crystals under high pressure.

Because the covalent bond between two carbon atoms in graphite is one of the strongest known, a graphene plane consisting of a hexagonal arrangement of carbon atoms could be considered as a tearproof net at the nanoscale. Carbon nanotubes, which consist of cylindrically closed graphene sheets, therefore exhibit extreme mechanical properties that have been already demonstrated (*1–8*) and used in various applications (*9–11*). Although the rupture of nanotubes under axial tensile load has already been studied (*7*, *12*, *13*), their strength against internal pressure remains unexplored. Because nanotubes can be filled with various materials (*14–17*), the pressure-holding capacity of nanotubes may be tested by observing the behavior of encapsulated compressible materials upon tube contraction.

The contraction of nanotubes can be caused by knocking carbon atoms out from the tube lattice and allowing the atomic network to reconstruct. Such a contraction has been observed in spherical carbon onions under electron irradiation (*18*). Previous studies (*19–24*)

[1]Institut für Physikalische Chemie, Universität Mainz, 55099 Mainz, Germany. [2]Accelerator Laboratory, University of Helsinki, Post Office Box 43, FIN-00014, Finland. [3]Laboratory of Physics, Helsinki University of Technology, Post Office Box 1100, Helsinki 02015, Finland. [4]Advanced Materials Department, Instituto Potosino de Investigación Científica y Tecnológica, Camino a la Presa San José 2055, Col. Lomas 4a. sección, 78216 San Luis Potosí, México. [5]Department of Materials Science and Engineering, Rensselaer Polytechnic Institute, Troy, NY 12180–3590, USA.

*To whom correspondence should be addressed. E-mail: Banhart@uni-mainz.de

showed that nanotubes are self-healing structures under irradiation. Vacancies are mobile at sufficiently high temperature and coalesce to form divacancies, which ultimately mend by reconstruction of the lattice (*24*), reducing surface area and generating local tension in the graphene sheet. The collapse of hollow nanotubes under electron irradiation has been observed (*21*, *23*, *25*, *26*); however, the pressure effects experienced inside the cores during collapse have not been studied. In the present work, we observed the dynamics and compressibility of encapsulated nanowires inside collapsing nanotubes and demonstrated that even hard materials such as iron carbide or cobalt can be extruded under the pressures prevailing inside nanotubes.

Multiwalled carbon nanotubes (MWNTs) encapsulating Fe, Fe_3C, or Co nanowires were produced by means of a modified ethanol-metallocene–based chemical vapor deposition process. A solution was prepared by dissolving 3 weight percent of a metallocene (ferrocene or cobalt acetylacetonate) in ethanol (for Fe) or toluene (for Co); the solution was then sonicated and transferred to the reservoir of a sprayer (*27*–*29*). Subsequently, the metallocene solution was atomized and directed into a quartz tube in the presence of a high-purity Ar flow. The nanotubes grew inside the silica tube at 950°C for Fe and 850°C for Co. The filled nanotubes were dispersed ultrasonically in ethanol and placed onto grids for carrying out in situ electron microscopy experiments. Electron irradiation and imaging were done in a transmission electron microscope (TEM) (FEI Tecnai F-30) with a field emission gun and an acceleration voltage of 300 kV. A heating stage (Philips) was used to hold the specimens at a temperature of 600°C during the irradiation experiments and in situ imaging. At this temperature, defects in graphitic structures are mobile so as to prevent agglomeration that would lead to a rapid destruction of the nanotubes (*19*, *24*). Irradiation was carried out at beam current densities of 100 to 600 A/cm^2.

Figure 1 shows the evolution of a nanotube with nine shells containing a Fe_3C crystal under electron irradiation at 600°C. The initial configuration is shown in Fig. 1A. After 12 min of irradiation with an electron beam (approximately 80 nm in diameter and 200 A/cm^2 in intensity), the tube shrank and deformed the diameter of the Fe_3C crystal from 9 to 7 nm (Fig. 1B) and after another 9 min (Fig. 1C) to 6 nm. Because of the compressive deformation, the carbide wire increased in length. As the collapse of the tube started in the empty region, the wire slid through the hollow in the axial direction. The schematic in Fig. 1D shows the geometry. Some graphitic material aggregated inside the tube (Fig. 1, B and C), forming a new shell around the carbide crystal and some graphitic filaments in the collapsing hollow. The graphitic aggregates are due to the transfer of carbon interstitials into the tube (*21*). Initially, the end of the crystalline rod is often faceted (Fig. 1A), but aggregation of graphitic shells at the end of the crystal causes the appearance of a meniscus (Fig. 1, B and C). Therefore, the deformation and extrusion of the crystal are caused by the graphitic shells and not by a wetting effect. Heating alone does not result in the observed phenomenon. The collapse of the tubes and the extrusion of encapsulated material occur only under electron irradiation, not under heating. Additional heating of the specimen by the electron beam is negligible because the inelastic energy loss of the electrons is low and nanotubes are excellent heat conductors, so the transferred energy can dissipate into the environment.

The TEM image series (Fig. 2) shows the extent to which a Fe_3C crystal can be deformed inside the nanotube. Irradiation of the section at the end of the wire leads to a non-uniform collapse of the tube. The hollow noncollapsed part of the tube fills up with graphitic filaments (Fig. 2B). Carbon material migrates from the open side of the channel (top of each panel in Fig. 2) and aggregates to the end of the Fe_3C wire by closing the inner hollow with graphene sheets. Therefore, the number of shells increases locally. The tube now collapses in the region of the carbide crystal by deforming the crystal considerably (Fig. 2, D and E). The diameter of the Fe_3C wire decreases from 9 to 2 nm while the solid carbide is squeezed through the hollow core downward along the tube axis, as in an extrusion process. The final collapse of the tube pinches and cuts off the thinned wire (Fig. 2F) while the rest of the wire continues moving downward (the imaged section of the tube was slightly shifted during imaging). The deformation rate of the Fe_3C crystal is approximately 4 nm/min in the direction of the tube axis and 1 nm/min perpendicular to the axis. Qualitatively, the extrusion process (Figs. 1 and 2 for Fe_3C) is the same as when β-Co crystals (face-centered cubic) are encapsulated in nanotubes (fig. S1)

The compressive effect is also seen in the lattice spacings of the graphitic shells and the encapsulated crystals. In the nanotubes, a reduced spacing between the shells is seen close to the solid core. The spacing between the two innermost layers (next to the core) is 10 to 13% less than the spacing between the outer layers. Between the second and third shell, the reduction is typically less than 5%, whereas for all other shells no significant deviation from the value of graphite can be measured. The local pressure cannot be calculated in a straightforward way from the inter-shell spacing of the tube, because each shell resists outer pressure and the diameter of the shells is determined by the defect configuration. However, a change in lattice spacing in the encapsulated crystals can be used to estimate the local pressure, although the lattice resolution of the TEM is not sensitive enough to detect minute changes in spacings in this instance. In the Fe_3C nanocrystals, up to 6% compression in the radial direction was observed. For Co crystals in collapsing nanotubes, a compression of up to 3.5% was measured. Lattice distortions by shear forces were also detectable (fig. S2).

No visible crystallographic defects such as stable dislocations or twins were observed during the deformation of the crystals within the temporal resolution of this experiment (Fig. 1 and figs. S1 and S2). This is important because it shows that nanoscale crystals do not

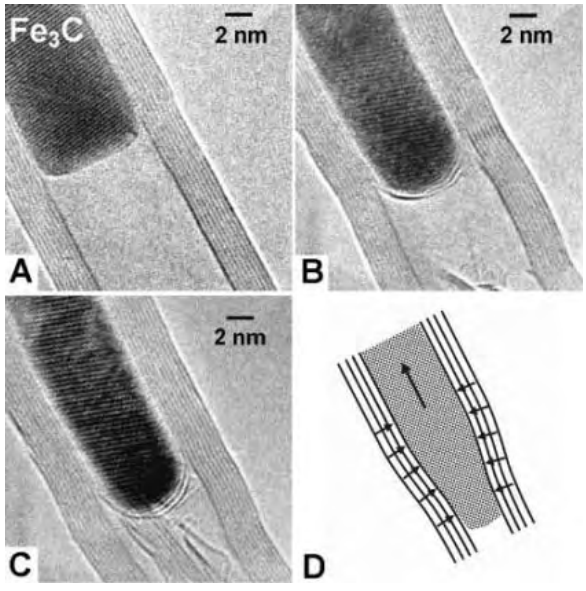

Fig. 1. MWNT with a Fe_3C crystal (dark region) in the inner core under electron irradiation at a specimen temperature of 600°C. The shrinkage of the tube leads to a deformation (thinning) of the Fe_3C crystal. Tubes before irradiation (**A**) and after 12 min (**B**) and 21 min (**C**) of irradiation are shown. The lattice fringes in (A) and in (B) and (C) originate from different sets of lattice planes because of a slight rotation of the tube under irradiation. (**D**) Simplified geometry of the system. Compressive forces (indicated by the small arrows) from the tube shells lead to a thinning of the crystal and its sliding along the tube axis (indicated by the large arrow).

deform in the same way as do macroscopic crystals, although the formation of defects has been observed in some metals encapsulated in carbon onions (*30*). Because the strain rate is low, we can consider that plastic deformation occurs above the theoretical shear stress rather than the yield stress as in bulk crystals. Such a behavior under plastic deformation is also a testimony to the large stresses that develop inside collapsing nanotubes. When the irradiation is interrupted, the compressive forces continue to have a slight effect for a short duration until the deformation stops. This technique allows for a direct observation of deformation dynamics in nanocrystals under large compression; however, the possible irradiation effects in the crystals also have to be taken into account.

In order to understand the mechanism of irradiation-mediated contraction of nanotube shells and to estimate the pressure inside the contracting tube, we used a continuum theory model in which the forces acting on the shells are functions of shell radii and inter-shell spacing (Fig. 3A). We used atomistic computer simulations to parameterize the model as described in the supporting online material. Knock-on displacements of carbon atoms in the energetic electron beam create vacancies and interstitials in the graphitic lattice of the nanotubes. In the metal and carbide cores, however, no considerable radiation effects occur because the displacement threshold energy in metals and carbides is higher than that in graphite. At 600°C, interstitials between the shells of MWNTs can migrate away from the contracting region where the pressure is high, so one can assume that no interstitials are left in the irradiated area. Metastable interstitial-vacancy complexes are also not stable at 600°C and will annihilate. Single vacancies are mobile enough to form divacancies (*24*), which are energetically favorable over single vacancies and are practically immobile (because the migration energy is more than 5 eV). Thus we can further assume that only double vacancies are present. Although all contracting shells should give rise to a pressure buildup in the inner core, it is instructive to evaluate first the pressure exerted only by the inner shell.

We calculated the total energy and the equilibrium atomic structure of single-walled carbon nanotubes (SWNTs) with various concentrations n of divacancies. Figure 3B shows the atomic network of a (10, 10) SWNT with $n = 0.05$. We found that the average equilibrium diameter $R_0(n)$ of the empty tube decreased linearly with n after relaxation because of the atomic network reconstruction. Having relaxed the atomic network for a particular n, we calculated the pressure P inside the SWNT as a function of nanotube radius R for various n (Fig. 3C). In practice, as the filling of the tube should increase R with respect to $R_0(n)$, we evaluated P numerically as the derivative of the total energy with respect to R for $R > R_0(n)$. For all n, P first increased linearly with R, and then showed a nonlinear regime. Finally, P abruptly dropped when the bonds near vacancies started breaking at the critical radius $R_c(n)$. We found that, for any n, the nonlinear dependence of P on R for $R_0 < R < R_c$ can be almost perfectly fitted by a square polynomial function [as in (*31*)].

Knowing the pressure as a function of the tube radius, one can calculate the maximum pressure inside the tube for any concentration of defects. For an incompressible inner core, P as a function of defect concentration is defined by the intersection of the vertical line drawn at the radius of the intact tube with the load curves. The pressure inside a SWNT as a function of n is shown in Fig. 3D. If we assume that the tube is filled with an incompressible material, there exists an upper limit on pressure, because the tube breaks at a certain concentration of vacancies. For a (10, 10) SWNT, the highest possible, double-vacancy concentration is $n \approx 0.06$. In reality, the highest vacancy concentration should be smaller, beacuse high experimental temperatures favor transitions between metastable configurations with close energies, resulting in the collapse of the tube. As follows from our simulations, the pressure inside a single shell can be as high as 20 GPa, and we are still not in the instability region (gray area in Fig. 3D).

To account for pressure buildup due to other shells, we calculated the total pressure P_{tot} inside MWNTs composed of two or more shells with divacancies. We assumed that the relations among tube radius, pressure, and double-vacancy concentration as calculated for the (10, 10) SWNT are qualitatively correct for nanotubes with any chiralities and diameters. We further assumed that the concentration of irradiation-induced defects is the same in all shells. To describe the forces between the shells, we adopted an analytical approach with parameters derived from experiments and used previously in a model of contracting graphitic shells in carbon onions (*32*). The balance of vacancy-induced and inter-shell forces, and the counter force from the incompressible material in the core in the MWNT, makes it possible to derive a system of nonlinear equations for equilibrium radii of all shells, which can be solved numerically.

The pressure P_{tot} in the inner core of MWNTs filled with an incompressible material (where the radius of the inner tube is equal to that of a pristine tube) is presented in Fig. 3D for various numbers of shells. P_{tot} increases because of additional contributions from other shells, and its value can be 40 GPa or higher. This value is slightly below the highest external pressure (60 GPa) seen to collapse nanotubes under experimental conditions (*33*). The

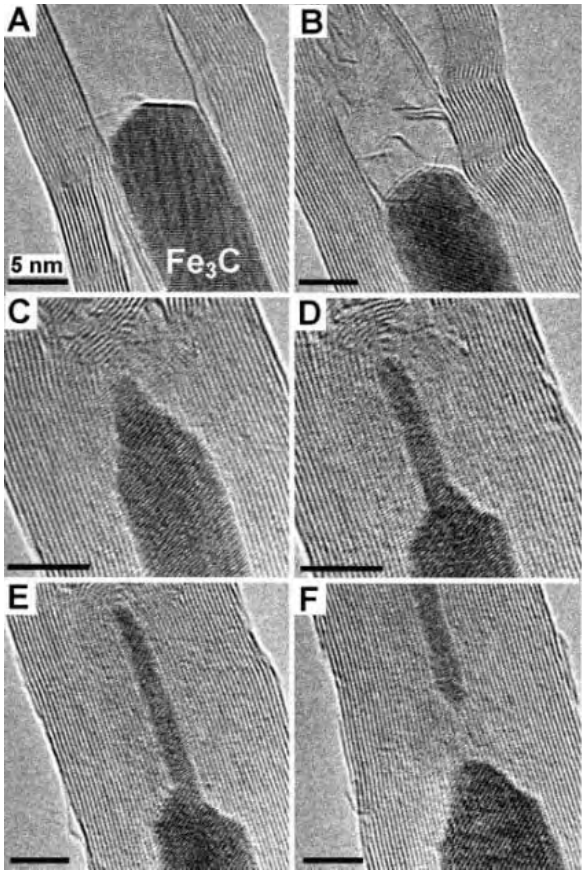

Fig. 2. Evolution of a MWNT partly filled with a Fe_3C nanowire under electron irradiation with an electron beam (about 60 nm in diameter and 200 to 400 A/cm^2 in intensity) during a total period of 50 min at a specimen temperature of 600°C. (**A**) Tube before irradiation. (**B** to **E**) Irradiation leads to a collapse of the tube and deformation of the Fe_3C crystal. (**F**) Tube collapse cuts off the thinned Fe_3C crystal. Different sets of lattice planes are seen in (A), (B), and (C) to (F). Scale bars, 5 nm.

pressure saturates quickly, and in practice does not change when the number of shells exceeds 6. This is because interstitials are absent in the high-pressure region because of the tubular geometry of the system, as a result of which the interstitials have a high probability to migrate away from the region with enhanced pressure. The open space and weak interaction between the shells allow for a decrease in shell radii and thus reduce P_{tot}. This also gives rise to a drop in inter-shell spacing, and the spacing is smaller the closer the shells are to the core. At a concentration of divacancies of 0.04, the inter-shell distance between the innermost and the next shell decreases by 15% relative to that of a pristine tube. Although a certain relaxation had already occurred when the experimental images were recorded, the measured inter-shell spacings of 10 to 13% match well with the theoretical value (unrelaxed situation). The effect of pressure on the lattice contraction of the encapsulated crystals can be estimated by using the compression modulus of bulk crystals. If we assume a pressure of 40 GPa and the measured compression modulus of bulk Fe_3C (the extrapolation according to the Birch-Murnaghan equation) (*34*), a reduction of lattice spacings of 5% can be expected. This value is close to the measured lattice compressions in Fe_3C (≤6%) and Co (≤3.5%).

Our results demonstrate the high strength of carbon nanotubes against internal pressure. The ultimate internal pressure (~40 GPa) that nanotubes can resist is only an order of magnitude below the pressure in the center of Earth (~360 GPa) or the highest pressure that has been achieved in diamond anvil cells (~400 GPa). The advantage of the present experiment is that individual nanometer-sized crystals can be studied in situ and deformed under high pressure, although irradiation effects in the crystals might occur and have to be considered. The behavior of the encapsulated crystals is monitored directly with high spatial and temporal resolution. Carbon nanotubes thus offer a template for use as compression/extrusion cells to study pressure-induced phase transformations and deformations of various solid nanomaterials.

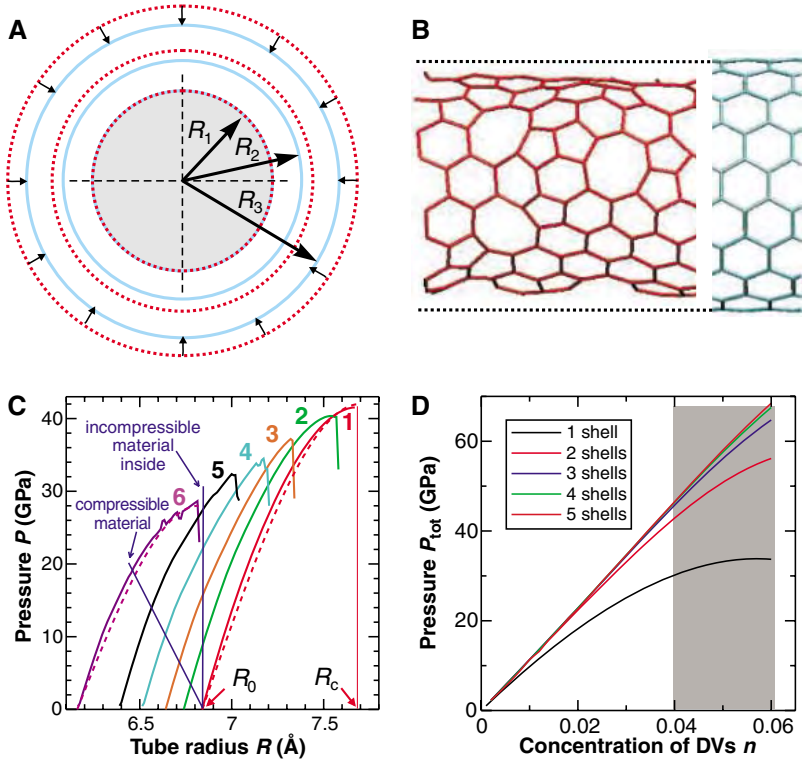

Fig. 3. (**A**) Schematic cross section of a MWNT contracting (indicated by the small arrows) because of the removal of atoms from the shells (solid blue circles) under the electron beam. The dashed red circles indicate the shells in the pristine tube. The inner core of the tube (gray circle) is filled with an incompressible material. Shell radii (R) are indicated by vectors. (**B**) Atomic networks of a pristine (10, 10) SWNT without (right) and with (left) double vacancies. There is a decrease in the average tube radius due to the reconstruction of the atomic network near vacancies. (**C**) Pressure versus tube radius (pressure-strain) curves corresponding to different divacancy concentrations n. Curve 1 corresponds to $n = 0$, 2 to $n = 0.007$, 3 to $n = 0.018$, 4 to $n = 0.028$, 5 to $n = 0.039$, and 6 to $n = 0.061$. Dashed lines are analytical fits to the simulation data. The straight blue lines illustrate the determination of pressure inside a SWNT filled with incompressible and compressible material; the intersections of the blue lines with pressure-strain curves give pressures for the corresponding divacancy concentrations. (**D**) Pressure inside a SWNT calculated as described above. The total pressure inside a MWNT with different numbers of shells is also shown as a function of n. DVs n, divacancy concentrations n.

References and Notes

1. M. M. J. Treacy, T. W. Ebbesen, J. M. Gibson, *Nature* **381**, 678 (1996).
2. E. W. Wong, P. E. Sheehan, C. M. Lieber, *Science* **277**, 1971 (1997).
3. J. P. Lu, *Phys. Rev. Lett.* **79**, 1297 (1997).
4. A. Krishnan, E. Dujardin, T. W. Ebbesen, P. N. Yianilos, M. M. J. Treacy, *Phys. Rev. B* **58**, 14013 (1998).
5. E. Hernández, C. Goze, P. Bernier, A. Rubio, *Phys. Rev. Lett.* **80**, 4502 (1998).
6. P. Poncharal, Z. L. Wang, D. Ugarte, W. A. de Heer, *Science* **283**, 1513 (1999).
7. M. Zhang *et al.*, *Science* **309**, 1215 (2005).
8. B. I. Yakobson, C. J. Brabec, J. Bernholc, *Phys. Rev. Lett.* **76**, 2511 (1996).
9. M. Cadek, J. N. Coleman, V. Barron, K. Hedicke, W. J. Blau, *Appl. Phys. Lett.* **81**, 5123 (2002).
10. A. B. Dalton *et al.*, *Nature* **703**, 423 (2003).
11. A. H. Barber, S. R. Cohen, H. D. Wagner, *Appl. Phys. Lett.* **82**, 4140 (2003).
12. M.-F. Yu *et al.*, *Science* **287**, 637 (2000).
13. M. Motta, Y. L. Li, I. Kinloch, A. Windle, *Nano Lett.* **5**, 1529 (2005).
14. P. M. Ajayan, S. Iijima, *Nature* **361**, 333 (1993).
15. S. C. Tsang, Y. K. Chen, P. J. F. Harris, M. L. H. Green, *Nature* **372**, 159 (1994).
16. Y. Maniwa *et al.*, *J. Phys. Soc. Jpn.* **71**, 2863 (2002).
17. Y. Gogotsi, N. Naguib, J. A. Libera, *Chem. Phys. Lett.* **365**, 354 (2002).
18. F. Banhart, P. M. Ajayan, *Nature* **382**, 433 (1996).
19. F. Banhart, *Rep. Prog. Phys.* **62**, 1181 (1999).
20. J. X. Li, F. Banhart, *Nano Lett.* **4**, 1143 (2004).
21. F. Banhart, J. X. Li, A. V. Krasheninnikov, *Phys. Rev. B* **71**, 241408 (2005).
22. F. Banhart, J. X. Li, M. Terrones, *Small* **1**, 953 (2005).
23. A. V. Krasheninnikov, F. Banhart, J. X. Li, A. S. Foster, R. M. Nieminen, *Phys. Rev. B* **72**, 125428 (2005).
24. A. V. Krasheninnikov, P. O. Lehtinen, A. S. Foster, R. M. Nieminen, *Chem. Phys. Lett.* **418**, 132 (2006).
25. P. M. Ajayan, V. Ravikumar, J.-C. Charlier, *Phys. Rev. Lett.* **81**, 1437 (1998).
26. N. G. Chopra, F. M. Ross, A. Zettl, *Chem. Phys. Lett.* **256**, 241 (1996).
27. F. Lupo *et al.*, *Chem. Phys. Lett.* **410**, 384 (2005).
28. R. Kamalakaran *et al.*, *Appl. Phys. Lett.* **77**, 3385 (1998).
29. M. Mayne *et al.*, *Chem. Phys. Lett.* **338**, 101 (2001).
30. J. Li, F. Banhart, *Adv. Mater.* **17**, 1539 (2005).
31. T. Xiao, K. Liao, *Phys. Rev. B* **66**, 153407 (2002).
32. M. Zaiser, *Mater. Res. Soc. Symp. Proc.* **540**, 243 (1999).
33. Z. Wang *et al.*, *Proc. Natl. Acad. Sci. U.S.A.* **101**, 13699 (2004).
34. J. Li *et al.*, *J. Phys. Chem. Minerals* **29**, 166 (2002).

35. Support from the Deutsche Forschungsgemeinschaft (grant BA 1884/4-1) is gratefully acknowledged. P.M.A. acknowledges support from NSF DMR grant on Inter-American Collaboration between the Rensselaer Polytechnic Institute and the Instituto Potosino de Investigación Científica y Tecnológica. We also thank the Consejo Nacional de Ciencia y Tecnología (CONACYT)–Mexico for scholarship (J.A.R.M.) and the following grants: 45772 (M.T.), 41464-Inter-American Collaboration (M.T., P.M.A.), 2004-01-013-SALUD-CONACYT (M.T.), and PUE-2004-CO2-9 Fondo Mixto de Puebla (M.T.). The authors thank the four reviewers of this paper for particularly useful comments.

Supporting Online Material

www.sciencemag.org/cgi/content/full/312/5777/1199/DC1
Materials and Methods
Figs. S1 and S2
References

4 January 2006; accepted 7 April 2006
10.1126/science.1124594

Earthquake Rupture Stalled by a Subducting Fracture Zone

D. P. Robinson,* S. Das, A. B. Watts

We showed that the rupture produced by the great Peru earthquake (moment magnitude 8.4) on 23 June 2001 propagated for ~70 kilometers before encountering a 6000-square-kilometer area of fault that acted as a barrier. The rupture continued around this barrier, which remained unbroken for ~30 seconds and then began to break when the main rupture front was ~200 kilometers from the epicenter. The barrier had relatively low rupture speed, slip, and aftershock density as compared to its surroundings, and the time of the main energy release in the earthquake coincided with the barrier's rupture. We associate this barrier with a fracture zone feature on the subducting oceanic plate.

In the past three decades, the complexity of the earthquake rupture process arising from the variation of the material properties on the fault, and the effect of this variation on earthquake rupture speed and ground motion, have been extensively studied theoretically (*1*–*4*). Such studies have suggested that earthquakes can propagate around or jump over relatively strong patches ("barriers") on the fault and continue to rupture. The increased stress on these patches caused by the rupture of surrounding regions can cause the patches themselves to rupture, if the critical stress required for failure is reached, while a dynamic fracture still continues on other parts of the fault. Examples of barriers both large (≈ 1500 km^2) and small (≈ 50 km^2) that remain unbroken at the end of the dynamic rupture process are known (*5*, *6*), but the actual phenomenon of rupture around large barriers that then rupture during the earthquake has never previously been seen. In this study, we present an observation of this phenomenon from the great [moment magnitude (M_w) 8.4] Arequipa, Peru, earthquake on 23 June 2001.

At the time of its occurrence, this earthquake was the largest in magnitude to occur worldwide since 1965 and remains the third largest since then. It occurred in a ~1000-km-long seismic gap on the plate boundary where the Nazca plate subducts under the South American plate, and it caused extensive damage in nearby population centers with a large local tsunami that was observed throughout the Pacific (*7*). The 2001 earthquake only partially filled the rupture zone of the 1868 earthquake. The remaining unbroken region, together with the rupture zone of the 1877 earthquake immediately to its south, remains one of the world's major seismic gaps (Fig. 1), a 600-km zone with the potential to have a M_w 9 earthquake and generate a large tsunami. Historically, great earthquakes have occurred both to the immediate north (for example, in 2001 and 1868) and south (for example, in 1877) of the Arica Bend. Thus, there is at least one example in the seismic cycle of these two zones being coupled (*8*, *9*).

The aftershocks of the 2001 earthquake, which we have relocated, using the method of joint hypocenter location (*9*) (figs. S1 and S2), suggest the presence of an essentially unilateral rupture extending from northwest to southeast, over a rectangular zone ~400 km by 150 km in area, and striking at 300° to 310°. We analyzed broadband seismograms, openly available from the Federation of Digital Seismic Networks, to recover the rupture process details, using the method developed by Das and Kostrov (*9*–*11*). The fault area, source time, and integral equation relating seismograms to the fault slip rate were discretized, leading to a system of linear equations. Constraints such as "positivity" (that is, no back-slip is permitted on the fault) were used to stabilize the problem, which was solved using the method of linear programming.

Our preferred solution (*9*) shows that the earthquake has a complex rupture history (Figs. 2 and 3 and movie S1). The unilateral rupture initially propagates ~70 km to the southeast and then circumvents a ~6000-km^2 barrier, after which it continues propagating farther to the southeast. At ~48 s after initiation, although the earthquake rupture is 180 km in length along strike, it has reached less than 15% of its seismic moment (*9*). About 54 s after initiation, the initially unbroken barrier commences rupturing and its rupture induces a large slip in the vicinity of the barrier, particularly in the shallow regions updip of it. The barrier ruptures completely in ~36 s at an average speed of ~2.8 km/s, which is lower than the average rupture speed of ~3.5 km/s (the local shear wave speed in the medium) over the rest of the fault. The initially unbroken barrier is also a region of relatively lower slip. About 200 km southeast of the hypocenter, a second barrier is encircled entirely by the rupture between ~36 to 60 s and breaks soon thereafter. The time of the major moment pulse, seen ~66 s after rupture initiation in the moment-rate function (inset, Fig. 3), is associated primarily with the rupturing of the first barrier and to a lesser degree with that of the second. The first barrier is a very robust feature of our solution that fits the data well (*9*). The second barrier is less well-constrained than the first because of its smaller size and later timing in the rupture process. It is important to point out that models that include a healing front behind which no further slip is permitted, and thereby constrain the rupture to occur only within a prescribed rupture front and the healing front, cannot reproduce the behavior of ruptures in which initially unbroken regions break at substantially later times, as that which occurred in this earthquake.

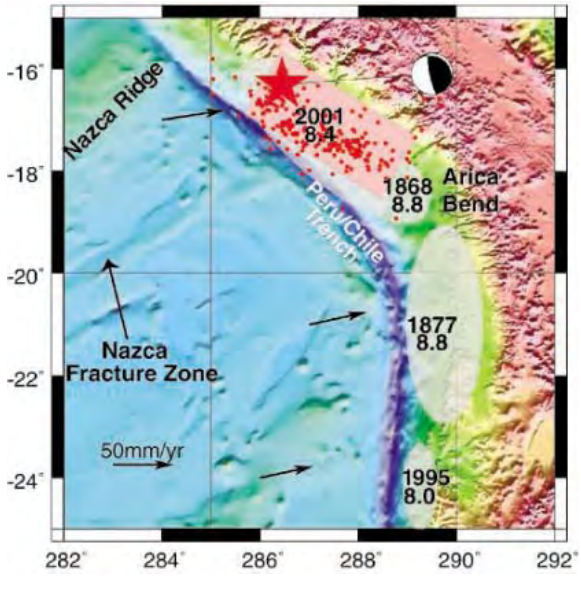

Fig. 1. Tectonic setting of the 2001 Peru earthquake, with bathymetry constructed from a General Bathymetric Chart of the Ocean (GEBCO) 1′ × 1′ grid (*24*). The shading of the bathymetry shows its slope in the direction of an artificial sun at an azimuth of 160° (dark shades represent gentle slopes, light shades represent steep slopes). Black arrows show the plate motion vectors of the Nazca plate relative to the South American plate. Approximate rupture zones of known great (magnitude ≥ 8.0) earthquakes in the region since the mid-19th century (*8*) are shown as light ovals, labeled with magnitude and year of occurrence. The rupture zone of the 2001 earthquake is shown as a red rectangle, and its epicenter is depicted by a red star. Red dots denote the aftershocks, which have been relocated, observed for 24 hours after the main earthquake (*9*). The centroid-moment tensor solution (*9*) is plotted as a black and white circle. The Nazca Ridge and Arica Bend are marked in place and a black arrow points to the location of the Nazca Fracture Zone, the subduction of which leads to the rupture complexity of this earthquake.

Department of Earth Sciences, University of Oxford, Parks Road, Oxford, OX1 3PR, UK.

*To whom correspondence should be addressed. E-mail: David.Robinson@earth.ox.ac.uk

To determine the cause of the barriers, we have examined the available marine geophysical data (*12*–*16*) in the region of the subducting oceanic plate. The oceanic crust immediately adjacent to the earthquake rupture zone is 45 to 50 million years old and was generated by seafloor spreading at the fossil Pacific/Farallon ridge. Despite relatively fast half-spreading rates (~50 mm/year), the bathymetry is not smooth but is complex and in places highly irregular. The most notable bathymetric feature is a 25- to 50-km-wide ridge that rises to ~700 m above the expected depth of the oceanic crust (Fig. 3), flanking a 20- to 25-km-wide trough that is up to ~300 m deeper than the expected depth. The ridge and trough are separated by a distinctive southeast-facing scarp that can be traced from the seaward wall of the trench in the northeast, across the outer rise, to the Nazca Fracture Zone in the southwest (*15*), a distance of some 275 km (Figs. 1 and 3 and fig. S4). The ridge, scarp, and trough features resemble an oceanic fracture zone and may represent either a northeastern extension of the Nazca Fracture Zone (*16*) or some form of fracture that developed in the plate as a response to slab-induced plate boundary forces (*17*). Irrespective of its origin, the fracture zone feature aligns very well with the first barrier and, we suggest, increases the coupling between the two sides of the fault, resulting in the highly heterogeneous earthquake rupture history. The nonuniformity of the aftershock distribution (Fig. 1 and figs. S1 and S2) over the fault mirrors the complexity of the rupture history. In fact, the trapezoidal shape of the first barrier (Fig. 2), which has relatively low slip, coincides with a trapezoidal region of lower aftershock density, visible both in the 24-hour and the 6-month aftershock distributions. This finding contrasts with the usual observation that regions of higher slip have fewer aftershocks (*18*).

The fracture zone feature can be traced on ship track profiles conducted over large distances, which show variations between profiles (of up to several hundreds of meters) in the amplitude of the ridge and trough (fig. S5). We suggest that the higher slip in the shallower depth in this part of the fault reflects a morphologically more subdued segment of the fracture zone feature. The cause of the second barrier is not as clear. Available bathymetric data suggest that there is no fracture zone feature on the subducting oceanic crust immediately seaward of the second barrier. There are, however, a number of large seamounts in the region (such as seamount X on mw853 in Fig. 3), and we speculate that such a feature may be the cause of the second barrier.

The notion that subduction of bathymetric features increases the seismic coupling on the subduction zone has been suggested by a number of previous workers (*19*–*21*), and specific examples related to seamount subduction (*21*) have been discussed. The influence of subducting bathymetric features on the behavior of earthquake ruptures is important in the context of truly great earthquakes, such as the M_w 9.1 and the M_w 8.7 earthquakes of 2004 and 2005 in Sumatra (*22*), where segmentation of the plate boundary caused these two earthquakes to occur 3 months apart. If these two had occurred as one even larger earthquake, its effects would have been even more catastrophic. The physical origin of this segmentation is unknown but is likely to be due to features on the subducting oceanic plate.

The results of this study have important implications for our understanding of the principles of the mechanics of earthquakes, because the time delay of ruptures at barriers can be used to estimate fracture energy (*3*), which is a measure of fault strength. They also shed light on how ruptures propagate through materials with non-uniform strength properties, which is relevant to the understanding of fracture in all materials for engineering applications (*2*). Finally, such rupture complexity also has a profound influence on the ground shaking, and hence damage, caused by earthquakes, because high-frequency damaging waves are generated when the rupture changes speed (*3*, *23*).

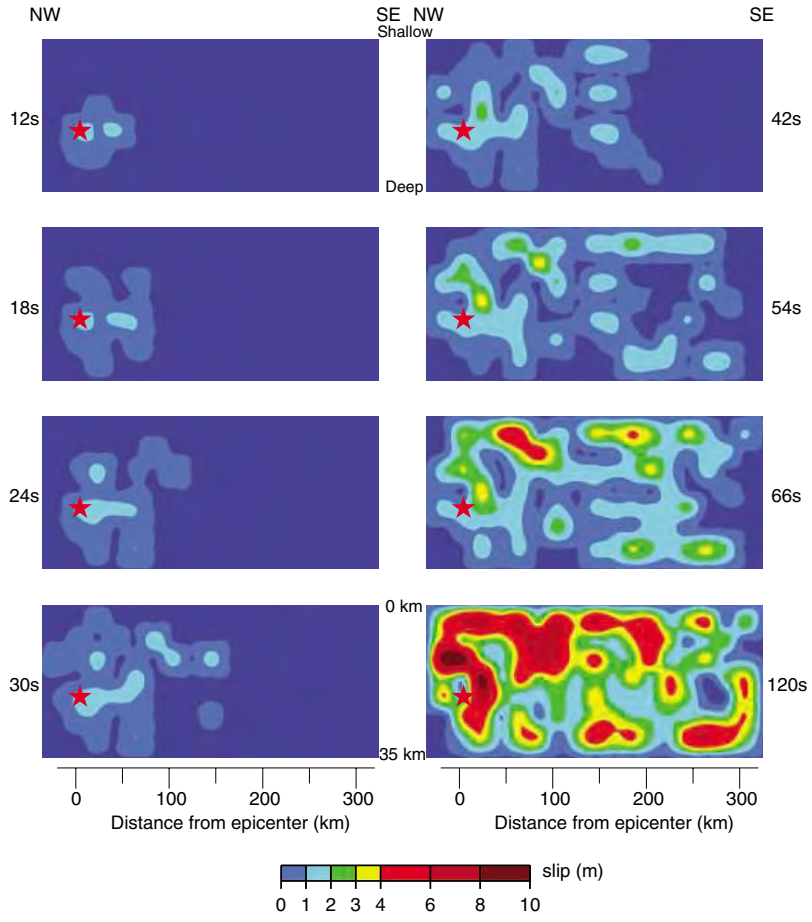

Fig. 2. Frames showing the dynamic rupture process for our preferred solution (*9*) at selected times marked on the side of each frame. See movie S1 for the full rupture history. The slip contours are plotted on the rectangular fault, which is viewed from the fault-normal direction. In each rectangle, the height represents fault depth from top (shallow edge, 0 km depth) to bottom (deep edge, ~35 km depth), and the width represents direction from left (northwest) to right (southeast). The left edge of the barrier, located ~70 km from the epicenter, is seen from 12 to 42 s, and its trapezoidal shape is seen at 42 s. Slip on the barrier starts at 48 s (movie S1) and is seen at 54 s. The rupture of the barrier induces a large slip (red) at shallow depth. For the comparison of data with solution synthetics, see the supporting online material (SOM) (fig. S3). The average slip over the fault was ~3.5 m, giving an average stress drop of ~0.8 MPa. The average slip in the region of the first barrier was ~2.8 m.

References and Notes

1. B. V. Kostrov, S. Das, *Principles of Earthquake Source Mechanics* (Cambridge Univ. Press, New York, 1988).
2. L. B. Freund, *Dynamic Fracture Mechanics* (Cambridge Univ. Press, New York, 1990).
3. M. T. Page, E. M. Dunham, J. M. Carlson, *J. Geophys. Res.* **110**, B11302 (2005).
4. S. Das, K. Aki, *J. Geophys. Res.* **82**, 5658 (1977).
5. C. Henry, S. Das, J. H. Woodhouse, *J. Geophys. Res.* **105**, 16097 (2000).
6. K. B. Olsen, R. Madariaga, R. J. Archuleta, *Science* **278**, 834 (1997).
7. A. Rodriguez-Marek, C. Edwards, Eds. *Southern Peru Earthquake of 23 June 2001 Reconnaissance Report,* special issue of *Earthquake Spectra* **19**, (2003).

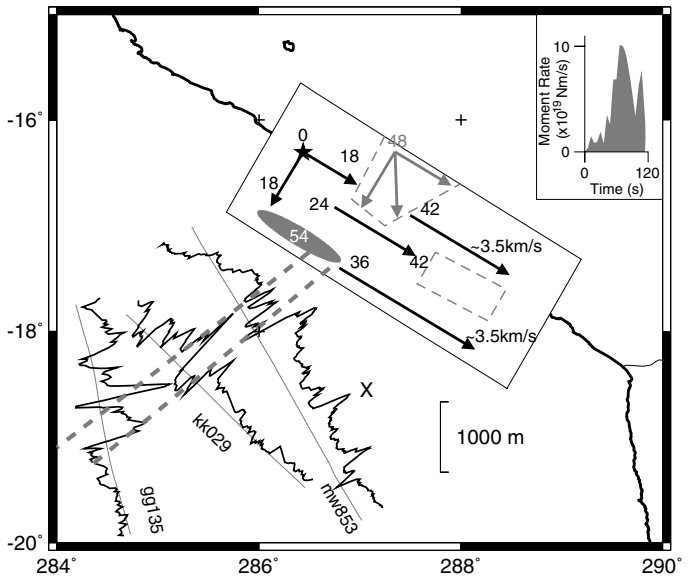

Fig. 3. Schematic representation of the rupture process. The epicenter is indicated by a black star. The two barriers are delineated by thin gray dashed lines within the central rectangle. Arrows showing earthquake rupture direction are labeled with start and selected end times (in seconds) of segments. Arrow color indicates the primary rupture (black) and the rupture of barriers (gray). Approximate rupture speeds (kilometers per second) are also indicated. The solid gray oval, shallower than the first barrier, indicates the region of high shallow slip induced by the rupture of this barrier, with the number indicating start time (54 s) when this shallow slip was induced. The three jagged black lines show the residual bathymetry (the observed bathymetry minus the bathymetry expected for the age of the oceanic crust) projected orthogonally onto ship tracks shown as three thin gray lines. Ship tracks (mw853, kk029, and gg135) are labeled according to their cruise identification in the Geophysical Data System database. The black X on bathymetric profile mw853 represents the location of a seamount. The two thick gray dashed lines show the ridge and trough features that can be correlated on each ship track (see the SOM for more details), interpreted in this study to be the physical origin of the large barrier that stalls the earthquake. The graph (inset, top right) depicts the moment-rate function.

8. D. Comte, M. Pardo, *Nat. Hazards* **4**, 23 (1991).
9. Materials and methods are available as supporting material on *Science* Online.
10. S. Das, B. V. Kostrov, *J. Geophys. Res.* **95**, 6899 (1990).
11. S. Das, B. V. Kostrov, *Phys. Earth Planet. Inter.* **85**, 293 (1994).
12. E. M. Herron, *Geol. Soc. Am. Bull.* **83**, 1671 (1972).
13. W. J. Schweller, L. D. Kulm, R. A. Prince, in *Nazca Plate: Crustal Formation and Andean Convergence, A Volume Dedicated to George P. Woollard*, L. D. Kulm, J. Dymond, E. J. Dasch, D. M. Hussong, Eds. (Geological Society of America, Boulder, CO, 1981), pp. 323–350.
14. A. V. Judge, M. K. McNutt, *J. Geophys. Res.* **96**, 16625 (1991).
15. D. W. Handschumacher, in *Geophysics of the Pacific Ocean Basin and Its Margin, A Volume in Honor of George P. Woollard*, G. H. Sutton, M. H. Manghnani, R. Moberly, Eds. (American Geophysical Union, Washington, DC, 1976), pp. 177–202.
16. S. C. Cande *et al.*, *Magnetic Lineations of the World's Ocean Basins, Scale 1:27,400,000* (map, *American Association of Petroleum Geologists*, Tulsa, OK, 1989).
17. S. Cloetingh, R. Wortel, *Tectonophysics* **132**, 49 (1986).
18. S. Das, C. Henry, *Rev. Geophys* **41**, 10.1029/2002RG000119 (2003).
19. J. Kelleher, W. McCann, *J. Geophys. Res.* **81**, 4885 (1976).
20. M. Cloos, *Geology* **20**, 601 (1992).
21. C. H. Scholz, C. Small, *Geology* **25**, 487 (1997).
22. R. Bilham, *Science* **308**, 1126 (2005).
23. R. Madariaga, *Geophys. J. R. Astron. Soc.* **51**, 625 (1977).
24. British Oceanographic Data Centre, *The GEBCO Digital Atlas*, Centenary Edition (CD-ROM) (Liverpool, UK, 2003).

25. D.P.R. is supported by a U.K. Natural Environmental Research Council (NERC) studentship NER/S/A/2003/11309 and a Schlumberger Cooperative Awards in the Sciences of the Environment (CASE) grant. The work is supported in part by NERC grant NE/C518806/1.

Supporting Online Material

www.sciencemag.org/cgi/content/full/312/5777/1203/DC1
Materials and Methods
Figs. S1 to S5
References
Movie S1

3 February 2006; accepted 7 April 2006
10.1126/science.1125771

Reduced Radiative Conductivity of Low-Spin (Mg,Fe)O in the Lower Mantle

Alexander F. Goncharov,* Viktor V. Struzhkin, Steven D. Jacobsen†

Optical absorption spectra have been measured at pressures up to 80 gigapascals (GPa) for the lower-mantle oxide magnesiowüstite (Mg,Fe)O. Upon reaching the high-spin to low-spin transition of Fe^{2+} at about 60 GPa, we observed enhanced absorption in the mid- and near-infrared spectral range, whereas absorption in the visible-ultraviolet was reduced. The observed changes in absorption are in contrast to prediction and are attributed to *d-d* orbital charge transfer in the Fe^{2+} ion. The results indicate that low-spin (Mg,Fe)O will exhibit lower radiative thermal conductivity than high-spin (Mg,Fe)O, which needs to be considered in future geodynamic models of convection and plume stabilization in the lower mantle.

Silicate perovskite $(Mg,Fe)SiO_3$ and magnesiowüstite (Mg,Fe)O are the major constituents of Earth's lower mantle. Because of partially filled *d*-electron orbitals, the presence of Fe in these minerals strongly influences the radiative component of conduction and thus their ability to transfer heat effectively (*1*). Pressure- and temperature-dependent thermal conductivity of minerals (*2*, *3*) is now thought to control some aspects of mantle convection and plume stability (*4*–*7*). In addition to the presence of large so-called superplumes (*8*, *9*), the complex seismic structure of Earth's lower mantle also reveals lateral heterogeneities that have been explained by compositional and thermal variation, partial melting, and phase transformations (*10*–*13*). The recent discovery of a spin-pairing high-spin (HS) to low-spin (LS) electronic transition of iron in silicate perovskite (*14*) and magnesiowüstite (*15*) have also been invoked to explain these anomalies. In (Mg,Fe)O, the HS-LS transition between 50 and 70 GPa strongly influences its bulk elastic properties (*16*, *17*) and is expected to blue-shift iron absorption bands in the infrared (IR) (*1*, *18*), although the transport properties of low-spin (Mg,Fe)O at high pressure have remained only speculative. Here, we provide experimental evidence for reduced radiative conductivity in LS-(Mg,Fe)O from optical absorption spectra through the spin-pairing transition in magnesiowüstite single crystals with varying iron contents spanning possible lower-mantle compositions.

Absorption spectra were obtained at pressures up to 80 GPa for high-quality single-crystal samples of $[Mg_{(1-x)}Fe_x]O$ with $x = 0.06$, 0.15, and 0.25 by a proper referencing of the transmission spectra measured through the sample (*19*) (fig. S1). The measurements were carried out in a diamond anvil cell with Ne or Ar pressure media (*19*). At low pressure, the $(Mg_{0.94}Fe_{0.06})O$ sample shows a broad absorption maximum ~8000 to 10,000 cm^{-1}, resulting from electronic transitions between Fe^{2+} d-orbitals of T_{2g} and E_g symmetry split by the crystal field, and an absorption tail in the visible-ultraviolet (UV) range that was assigned

Geophysical Laboratory, Carnegie Institution of Washington, 5251 Broad Branch Road, NW, Washington, DC 20015, USA.

*To whom correspondence should be addressed. E-mail: goncharov@gl.ciw.edu

†Present address: Department of Geological Sciences, Northwestern University, Evanston, IL 60208, USA.

to electron charge transfer between Fe^{2+} and O^{2-} ions (*1*, *18*). We assume Fe^{3+}-O^{2-} charge transfer also contributes to the absorption edge but note that the ferric iron content of the samples is very low (*19*).

In agreement with earlier studies up to 30 GPa (*20*–*22*), applying pressure red-shifts the absorption edge in the UV range, which causes the overall absorption in the near-IR region to increase with pressure. The relatively low iron concentration in the $(Mg_{0.94}Fe_{0.06})O$ sample (Fig. 1) allows us to observe a modification of the crystal-field levels through the spin-pairing transition (Fig. 2). Two new absorption bands gradually appear above 40 GPa. At the same time, the T_{2g}-E_g transition of the high-spin phase becomes less prominent, although at higher pressure a band close to this energy persists. We assign the newly observed higher energy bands to the A_{1g}-T_{2g} and A_{1g}-A_{2g} transitions, while the one similar to the T_{2g}-E_g band is assigned to the A_{1g}-T_{1g} transition. Transformation of the crystal-field energy levels (Fig. 2) is related to the change of the electronic ground state (T_{2g} to A_{1g}), i.e., the HS to LS transition. We relate the pressure point at which the new crystal field bands appear to the onset of transition pressure and note that the spectra continue to change at higher pressure as the LS state is more populated. Accordingly, we observe a decrease of the absorption coefficient in the visible-UV range. On decompression, the spectral changes are reversible without hysteresis.

With increasing pressure, the high-energy absorption edge of $(Mg_{0.75}Fe_{0.25})O$ (Fig. 3) red-shifts, as previously noted in experiments below 30 GPa (*20*, *21*). The T_{2g}-E_g crystal-field band shows a moderate blue shift and a gradual decrease of intensity, which is difficult to quantify accurately because of the steep background. However, contrary to prediction, the broad absorption in the near-IR range increases with pressure due to the red-shift of the absorption edge up to ~55 to 65 GPa, where above that, pressure shift is no longer observed (see inset to Fig. 3). The large overall absorption makes it more difficult to observe the spin-crossover modifications than in the 6% Fe samples, but the spin transition is detected by following the decrease of T_{2g}-E_g band intensity and subsequent decrease of the absorption in the visible range. Similar behavior is observed for the sample with 15% Fe, except that the A_{1g}-T_{2g} spin transition near 15,000 cm^{-1} is observed above 60 GPa. In general, the absorption edge is less steep in HS (Mg,FeO) than in LS (Mg,Fe)O.

The pressure shift of the absorption edge for (Mg,Fe)O with the 15% and 25% Fe is similar (−0.03 eV/GPa), but the absorption edge shift is only about (−0.01 eV/GPa) in the low-Fe content (6%) sample. Further support for nonlinear behavior at low-Fe concentrations is observed by directly comparing the absorption spectra for the various compositions at high pressure (Fig. 4). The spectra, normalized to the iron concentration, do not scale particularly well, especially for the low iron concentration (*23*). Nevertheless, at lower frequencies (<12,000 cm^{-1}), the absorption coefficients of materials with high iron content scale almost perfectly. The strong UV through near-IR absorption in Fe bearing (Mg,Fe)O originates from the UV band, which red-shifts under pressure (*20*, *21*, *24*). This absorption changes dramatically at the spin-pairing transition. Given a nonlinear compositional dependence of the pressure shifts, it is difficult to accept that it originates from the Fe-O charge transfer bands, as has been suggested (*1*). Indeed, one would expect the same pressure shift for samples with different Fe content and a linear scaling with the Fe content in this case. Moreover, the charge-transfer gap in transition metal oxides is typically wide and almost does not depend on pressure (*25*).

We propose that the bulk of the observed UV-visible absorption in HS-(Mg,Fe)O at iron content above 10 to 12% (fig. S2) originates from charge transfer *d-d* transitions between adjacent Fe^{2+} sites (*26*). The importance of this absorption mechanism is often neglected (*18*). The strong pressure, spin state, and Fe-concentration dependence of the corresponding excitations, which is governed by the strength of the *d-d* Coulomb interaction (figs. S3 and S4), can be explained if Fe in magnesiowüstite is randomly distributed in the lattice so that coupling between different iron sites strongly depends on the local environment. In particular, the anomalous behavior of the x = 0.06 sample can be reconciled because this composition is well below the percolation limit (~12% Fe) for the face-centered cubic lattice (*27*). Below this limit, the number of adjacent Fe sites is relatively small because of random distribution of Fe^{2+} ions. When the iron

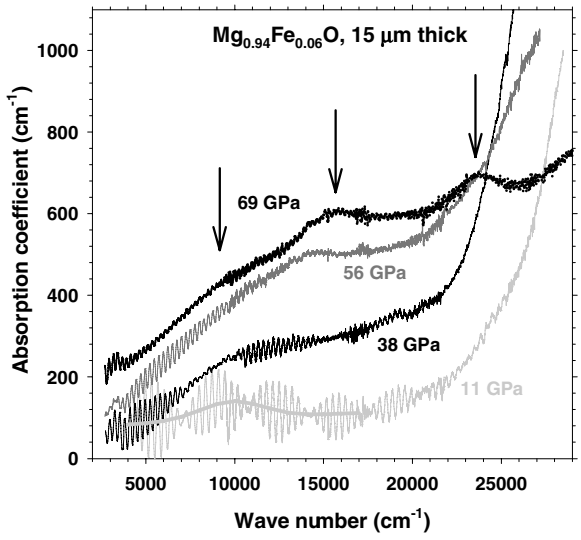

Fig. 1. Optical absorption spectra of (Mg,Fe)O containing 6% Fe at various pressures and 300 K. The absorption coefficient has been calculated using $k = A*\ln 10/d$, where $A = \log_{10}(I_0/I)$, I_0 and I are the transmission signals for the reference and sample configuration, respectively, and d is the sample thickness measured at ambient conditions from the white-light interferometry and calculated at high pressure using an isothermal equation of state over this pressure range (*16*). Ripples in the spectra at low pressures are interference fringes resulting from multiple reflections between the parallel polished sample surfaces. The beats that can be seen in interference fringes are due to a multiple interference with the beams reflected from the culet surfaces. This complex interference pattern is smoothed (thick gray line) for the 11-GPa spectrum for clarity. Vertical arrows designate new crystal-field transitions, which are characteristic of the low-spin phase.

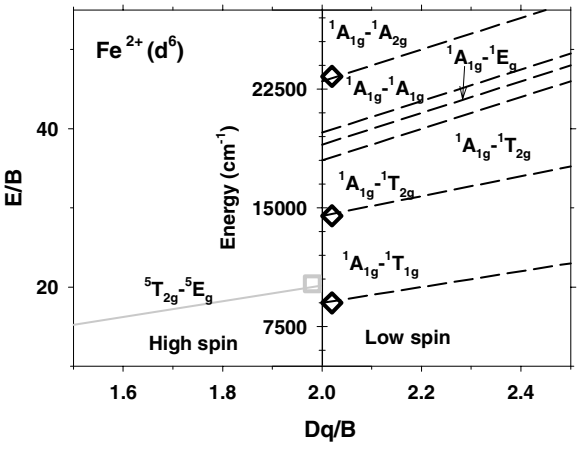

Fig. 2. The Tanabe-Sugano (*29*) diagram for Fe^{2+} (d^6). E is the energy, B is the interelectronic repulsion parameter, Dq is a crystal field strength parameter. The vertical line at Dq/B = 2 corresponds the spin-pairing transition. Only the terms relevant for spin-allowed optical transitions are shown [adapted from Figgis (*30*)]. The crystal field is assumed to be of cubic O_h octahedral symmetry. The thick gray square and thick black diamonds correspond to the positions of the absorption bands measured in the high- and low-spin phases, respectively. The energies of these bands are scaled (B = 500 cm^{-1}) to match the T_{2g}-E_g transition in the high-spin phase near the spin-pairing transition.

concentration in (Mg,Fe)O is above the percolation threshold, an interconnected network of overlapping (adjacent) 3d orbitals occurs through the structure. Thus, the absorption coefficient and its pressure dependence are greatly enhanced above this limit. Application of pressure broadens the zone formed by the *d-d* charge-transfer transitions, resulting in a decrease of the observed optical gap. Naturally, this coupling changes at the spin-pairing transition when the ground state changes its spin, which is revealed in our spectra by a change in intensity, shape, and spectral positions (Figs. 1, 3, and 4). A more detailed study on thinner samples (<8-μm thickness) is necessary to reveal fine structure of the pressure and state dependence of the *d-d* charge-transfer gap. Finally, we note that because the spin-pairing transition is observed from optical absorption spectra (Figs. 1 to 4), this study also provides an important cross-check of the HS to LS transition pressure previously inferred from x-ray emission spectroscopy (*14*, *16*) and Mössbauer spectroscopy (*17*). A plot of the HS to LS transition pressure as a function of composition inferred from the optical spectra is shown in fig. S5.

In contrast to previous notions, the radiative component of thermal conductivity in low-spin (Mg,Fe)O is remarkably low. We invoke a previously overlooked absorption mechanism in low-spin iron-bearing materials, which appears to become dominant at high pressure and results from charge fluctuations between *d*-orbitals of adjacent Fe sites. Increasing Fe concentration and the spin-pairing transition results in greater absorption in the near-IR range, indicative of reduced radiative conductivity, and therefore the radiative component of thermal conductivity may be blocked. The absorption spectra will modify at high temperatures corresponding to the conditions of Earth's mantle (*28*), but we do not expect the change of relative intensity in the HS and LS phases because they are determined by the same physical mechanisms.

The notion of reduced thermal conductivity in the lower mantle may challenge existing theories on the stability of superplumes, which appear to require enhanced thermal conductivity to mitigate excessive temperature gradients. It is possible that the reduced radiative component of heat transfer in low-spin phases is compensated by elevated lattice conduction (low-spin phase lattice is stiffer), both of which contribute to the overall thermal conductivity of the lower mantle.

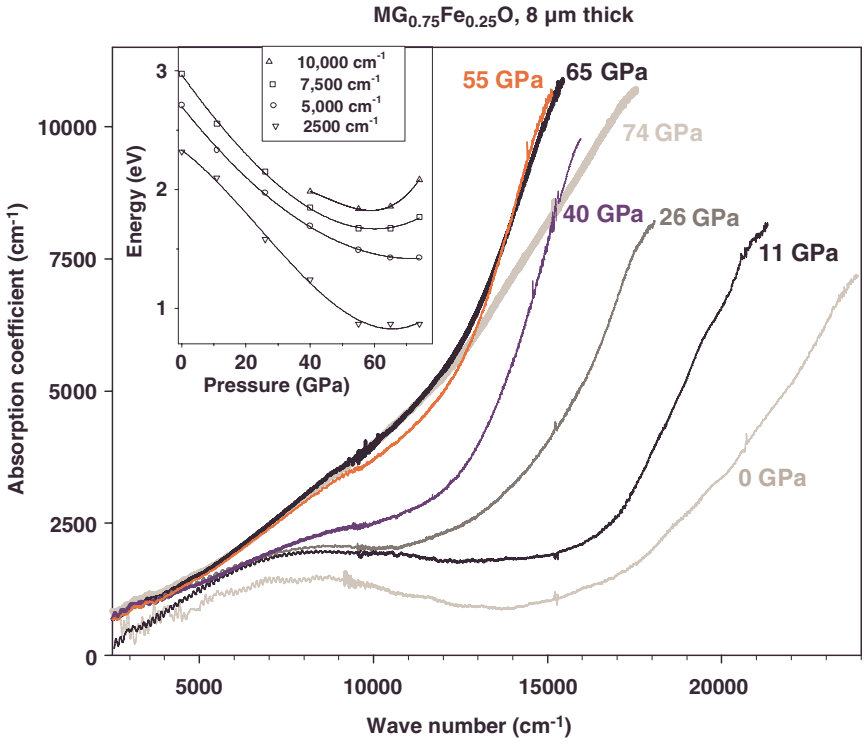

Fig. 3. Optical absorption spectra of magnesiowüstite (x = 0.25) at elevated pressure and 300 K. The absorption coefficient has been calculated in the same manner as it has been described for Fig. 1. The inset shows the pressure dependence of the points with equal absorption.

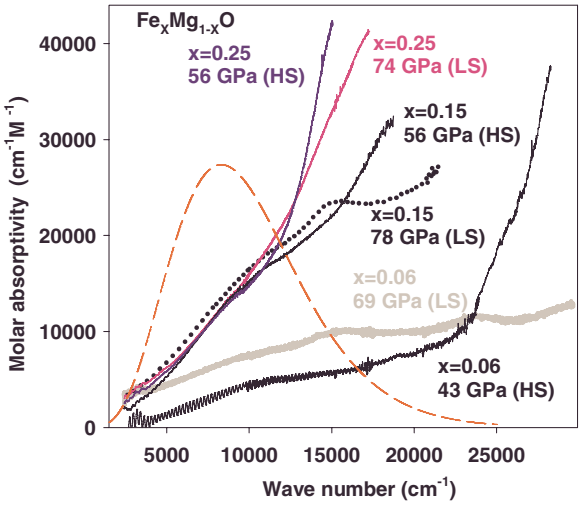

Fig. 4. Molar absorptivity (ε) for the high- and low-spin magnesiowüstite with different iron content (x). The values of ε are calculated from Beer's law $A = \varepsilon x d$, where A is absorbance and d is the sample thickness. Spectra are shown for the sample with x = 0.06 in the high-spin state at 43 GPa (black) and in the low-spin state at 69 GPa (gray). Spectra are shown for x = 0.15 in the high-spin state at 56 GPa (black) and in the low-spin state at 78 GPa (black dotted curve). The spectra are blue for x = 0.25 in the high-spin state at 56 GPa and pink for x = 0.25 in the low-spin state at 74 GPa. The dashed (red) line represents the calculated blackbody radiation (arbitrary units) at 2400 K, close to lower mantle conditions.

References and Notes

1. R. G. Burns, *Mineralogical Applications of Crystal Field Theory* (Cambridge Univ. Press, Cambridge, UK, 2nd ed. 1993).
2. A. M. Hofmeister, *Science* **283**, 1699 (1999).
3. A. M. Hofmeister, *J. Geodynamics* **40**, 51 (2005).
4. F. Dubuffet, D. A. Yuen, *Geophys. Res. Lett.* **27**, 17 (2000).
5. F. Dubuffet, D. A. Yuen, E. S. G. Rainey, *Nonlin. Proc. Geophys.* **9**, 311 (2002).
6. C. Matyska, D. A. Yuen, *Earth Planet. Sci. Lett.* **234**, 71 (2005).
7. T. K. B. Yanagawa, M. Nakada, D. A. Yuen, *Phys. Earth Planet. Int.* **146**, 163 (2004).
8. A. M. Dziewonski, *J. Geophys. Res.* **89**, 5929 (1984).
9. W.-J. Su, A. M. Dziewonski, *Nature* **352**, 121 (1991).
10. T. Lay, Q. Williams, E. J. Garnero, *Nature* **392**, 461 (1998).
11. L. H. Kellogg, B. H. Hager, R. D. van der Hilst, *Science* **283**, 1881 (1999).
12. P. J. Tackley, *Science* **288**, 2002 (2000).
13. R. D. van der Hilst, H. Kárason, *Science* **283**, 1885 (1999).
14. J. Badro *et al.*, *Science* **305**, 383 (2004).
15. J. Badro *et al.*, *Science* **300**, 789 (2003).
16. J. F. Lin *et al.*, *Nature* **436**, 377 (2005).
17. S. Speziale, A. Milner, V. E. Lee, S. M. Clark, M. P. Pasternak, R. Jeanloz, *Proc. Natl. Acad. Sci. U.S.A.* **102**, 17918 (2005).
18. D. M. Sherman, *J. Geophys. Res.* **96**, 14299 (1991).
19. Materials and methods are available as supporting material on *Science* Online.
20. H. K. Mao, *Carnegie Inst. Yr. Bk.* **72**, 554 (1972).
21. H. K. Mao and P. M. Bell, *Science* **176**, 403 (1972).
22. T. J. Shankland, A. G. Duba, A. Woronow, *J. Geophys. Res.* **79**, 3273 (1974).
23. T. Goto, T. J. Ahrens, G. R. Rossman, Y. Syono, *Phys. Earth Planet. Int.* **22**, 277 (1980).
24. R. M. Abu-Eid, K. Langer, *Naturwiss.* **65**, 256 (1978).

25. A. Shukla, J.-P. Rueff, J. Badro, G. Vanko, A. Mattila, F. M. F. de Groot, F. Sette, *Phys. Rev. B* **67**, 081101 (2003).
26. J. Zaanen, G. A. Zawatzky, J. W. Allen, *Phys. Rev. Lett.* **55**, 418 (1985).
27. C. D. Lorenz, R. M. Ziff, *Phys. Rev. E* **57**, 230 (1998).
28. T. J. Shankland, U. Nitsan, A. G. Duba, *J. Geophys. Res.* **84**, 1603 (1979).
29. Y. Tanabe, S. Sugano, *J. Phys. Soc. Jpn.* **9**, 753 (1954).
30. B. N. Figgis, *Introduction to Ligand Fields* (Wiley, New York, London, Sydney, 1966).
31. We acknowledge support by the U.S. Department of Energy (DOE) Office of Basic Energy Sciences and the DOE National Nuclear Security Administration, NSF, and the W. M. Keck Foundation. We thank R. J. Hemley and H.-K. Mao for valuable comments and S. J. Mackwell for help with sample synthesis.

Supporting Online Material
www.sciencemag.org/cgi/content/full/312/5777/1205/DC1
Materials and Methods
Figs. S1 to S5
References

31 January 2006; accepted 7 April 2006
10.1126/science.1125622

Structure of the Eukaryotic Thiamine Pyrophosphate Riboswitch with Its Regulatory Ligand

Stéphane Thore, Marc Leibundgut, Nenad Ban*

Riboswitches are untranslated regions of messenger RNA, which adopt alternate structures depending on the binding of specific metabolites. Such conformational switching regulates the expression of proteins involved in the biosynthesis of riboswitch substrates. Here, we present the 2.9 angstrom–resolution crystal structure of the eukaryotic *Arabidopsis thaliana* thiamine pyrophosphate (TPP)–specific riboswitch in complex with its natural ligand. The riboswitch specifically recognizes the TPP via conserved residues located within two highly distorted parallel "sensor" helices. The structure provides the basis for understanding the reorganization of the riboswitch fold upon TPP binding and explains the mechanism of resistance to the antibiotic pyrithiamine.

Riboswitches are conserved regions of mRNA that bind specific metabolites and regulate gene expression (*1*–*4*). This RNA-based mechanism of genetic control is believed to be of ancient origin (*5*) and is broadly distributed among bacteria, where it regulates ~4% of all genes [for reviews, see (*6*–*8*)]. Riboswitches use diverse mechanisms to alter gene expression, including sequestration of the ribosome binding site (*1*, *9*), formation of a transcription-terminating hairpin structure (*10*–*12*), or direct cleavage of their mRNAs, thus functioning as ribozymes (*13*, *14*).

Thiamine pyrophosphate (TPP) is an essential cofactor in bacteria, archaea, and eukaryotes. Its production is tightly regulated by TPP-binding riboswitches, which have been identified in thiamine-biosynthetic genes in all kingdoms (*15*). The mechanism of the regulation of gene expression by TPP has been most extensively studied for the *Escherichia coli* TPP riboswitch. Binding of the ligand to the 5′-untranslated region of the *thiM* gene, which is involved in the biosynthesis of thiamine, turns the riboswitch structure "off" and reduces translation of the mRNA by sequestering the ribosome binding site (*1*). Eukaryotic riboswitches conform to the consensus sequence and secondary structure of the TPP riboswitches found in bacteria and archaea. They bind TPP with a similar affinity and undergo the same conformational changes as their bacterial counterparts (*15*). In fungi and plants, TPP riboswitches are found either in introns or in the 5′- or 3′-untranslated regions of their target genes where they regulate, for example, mRNA splicing (*15*, *16*). TPP-responsive riboswitches display an apparent dissociation constant of ~50 nM, with the binding of TPP to the riboswitch dependent on the presence of Mg^{2+} ions (*1*, *15*, *17*). Such a high affinity relies on specific recognition of the pyrimidine ring and the pyrophosphate group of TPP (*1*). TPP riboswitches are

ETH Zurich, Institute of Molecular Biology and Biophysics, 8092 Zurich, Switzerland.

*To whom correspondence should be addressed. E-mail: ban@mol.biol.ethz.ch

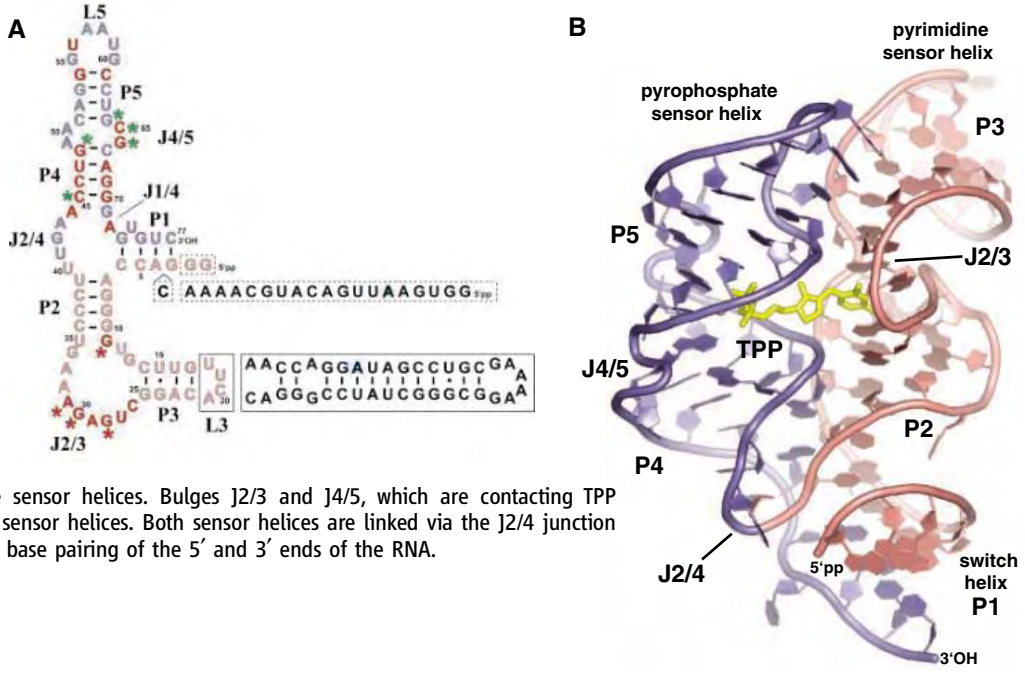

Fig. 1. Structure of the TPP riboswitch from *A. thaliana*. (**A**) Secondary-structure diagram of the TPP-binding domain located in the 3′ region of the *thiC* gene. For crystallization, the P1 helix was shortened by one and the 5′ sequence replaced by two guanines (boxed, dash lines), and the extension following P3 was replaced by the L3 tetraloop (boxed, solid lines). Color code: Pyrophosphate sensor helix (blue); pyrimidine sensor helix (pink); residues involved in pyrophosphate (green asterisks) or pyrimidine binding (red asterisks); conserved nucleotides (red). (**B**) Overall structure of the *A. thaliana* riboswitch. The TPP riboswitch binds TPP with its pyrophosphate and pyrimidine sensor helices. Bulges J2/3 and J4/5, which are contacting TPP (yellow), introduce sharp kinks into the sensor helices. Both sensor helices are linked via the J2/4 junction and switch helix P1, which is formed by base pairing of the 5′ and 3′ ends of the RNA.

attractive targets for antimicrobial drugs such as pyrithiamine, which exerts its toxic effects by binding TPP riboswitches in bacteria and fungi (*16*, *18*).

Here, we describe the crystal structure of the complex between TPP and the eukaryotic *Arabidopsis thaliana* riboswitch (AtRs), which is located in the 3′ region of the *thiC* gene. The ThiC protein homolog in *E. coli* catalyzes the conversion of 5-aminoimidazole ribotide to hydroxymethyl pyrimidine phosphate in the thiamine-biosynthetic pathway. Because of its localization adjacent to the polyadenylate tail, it has been proposed that the TPP binding to the riboswitch regulates mRNA processing and stability of the *thiC* genes in plants (*15*). The riboswitch structure reveals a complex overall fold of AtRs and the details of interactions that govern its high specificity for TPP. The architectural features of AtRs provide the basis for understanding the reorganization of the mRNA fold upon TPP binding and explain the resistance to the pyrithiamine antibiotic.

For AtRs structure determination, we chose an RNA segment representing the complete sequence of the *A. thaliana* TPP-binding riboswitch (Fig. 1A). The in vitro–transcribed RNA was refolded in the presence of TPP and crystallized from 1,6-hexanediol at neutral pH. Phases were calculated using multiple wavelength anomalous dispersion data collected from a crystal derivatized with osmium. The experimentally phased electron density map allowed tracing of the phosphodiester backbone and defining the register of the sequence based on the discrimination between purines and pyrimidines (fig. S1A). The model was completed by iterative rebuilding guided by sigma-a–weighted difference Fourier maps. The TPP molecule was positioned in the last stage of refinement into the simulated annealed omit map (fig. S1B). The final model contains two copies of the full-length RNA in complex with TPP and refines to a final R/R_{free} of (18.3/25.0)% (*19*).

The highly conserved secondary structure of the TPP-binding riboswitches consists of five helices, termed P1 to P5 (Fig. 1A). The helix P1 is formed by the 5′ and 3′ end of the riboswitch RNA and is expected to be disrupted in the absence of TPP. In *E. coli*, alternative structures of the "switch" P1 helix have been shown to expose the ribosome binding site (*1*). Helices P1, P2, and P4 together with junctions J1/4 and J2/4 form the central three-way junction. Bulges J2/3 and J4/5 connect helices P2 with P3 and P4 with P5, respectively. Terminal loops L3 and L5 close helices P3 and P5. The structure of AtRs has overall dimension of 56 Å by 40 Å by 22 Å and consists of two major helices, which are arranged in a parallel manner (Fig. 1B). One of them is formed by coaxial stacking of the switch helix P1 and helices P2 and P3, and the other consists of stacked helices P4 and P5. Such an organization of a three-way junction has been observed in several other RNA structures, including the guanine riboswitch, despite its less complex secondary structure (*20*–*22*). Helices P2/P3 and P4/P5 are severely distorted by internal bulges J2/3 and J4/5, which are involved in TPP binding (Fig. 1B). Helices P2/P3 and P4/P5 are joined at their base by junction J2/4, which forms a sharp kink.

According to their interaction with different parts of the TPP, the parallel helices P2/P3 and P4/P5 can be considered as "pyrimidine sensor" and "pyrophosphate sensor" helices, respectively (Figs. 1B and 2). The TPP binding sites on each of the two sensor helices form deep binding pockets, which tightly accommodate the pyrimidine ring on one side and the pyrophosphate on the other.

The TPP bound to the AtRs riboswitch has its pyrimidine and thiazole rings in an extended conformation resembling those observed in structures of free TPP (Fig. 1B) (*23*). This is different from the V-conformation of enzyme-bound TPP, where it functions as a cofactor (*24*). The pyrophosphate group adopts a bent conformation observed in both the free and the enzyme-complexed form of TPP (Fig. 2B) (*23*, *24*).

The high specificity of AtRs for the TPP is explained by inspection of the contact area (Fig. 2). The contacts between the pyrophosphate of the TPP and the AtRs riboswitch are localized in the internal loop J4/5 in the pyrophosphate sensor helix P4/P5 (Fig. 2A). Residues G64, C65, and G66 from the J4/5 bulge interact with the pyrophosphate moiety directly (Fig. 2, A and B), and residues G66 and G48 coordinate a putative bridging Mg^{2+} ion (Fig. 2B). The Mg^{2+} ion has been modeled based on high-resolution Mg^{2+}-bridged pyrophosphate structures as found in the Protein Data Bank and subjected to refinement. An alternative conformation of the pyrophosphate that includes an additional Mg^{2+} ion would also explain the electron density but did not refine stably at the current resolution. The large J2/3 bulge is responsible

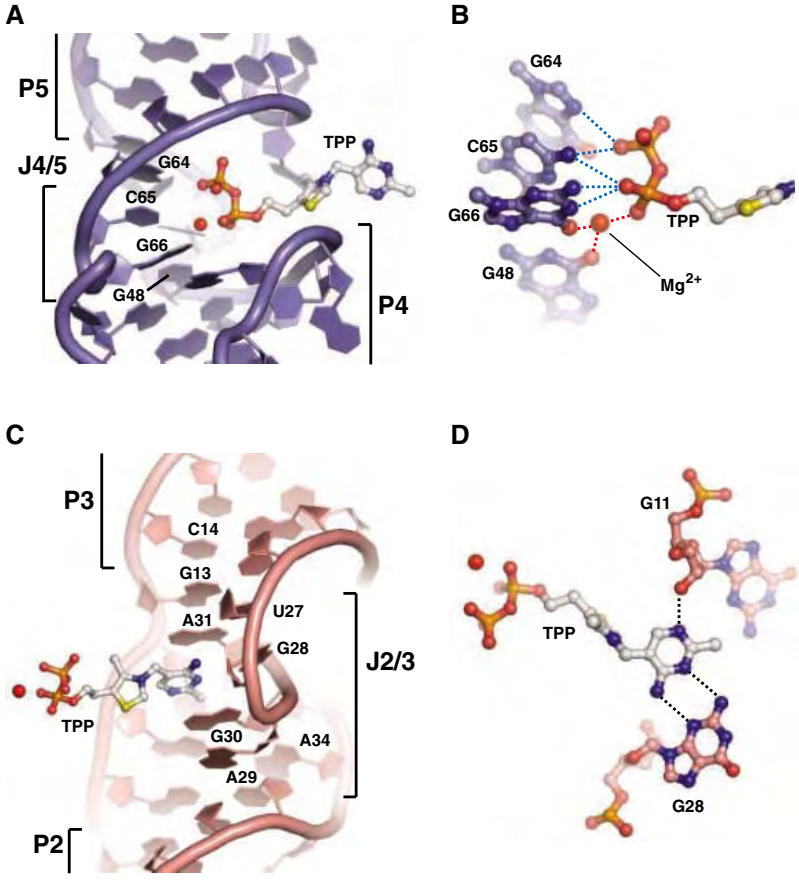

Fig. 2. Detailed views of TPP binding by the sensor helices. (**A**) The pyrophosphate sensor helix contacts the pyrophosphate moiety of TPP via a deep cleft formed by bases G64, C65, G66, and G48 of the J4/5 bulge. (**B**) G64, C65, G66, and G48 form a network of hydrogen bonds coordinating the putative Mg^{2+} ion (red sphere) and the pyrophosphate. (**C**) The pyrimidine ring of TPP is inserted into the pyrimidine sensor helix at the J2/3 bulge region by stacking between bases G30 and A31. (**D**) G28 adopts a "flipped out" conformation. This allows base pairing with the pyrimidine ring of TPP. The ring is additionally stabilized by a hydrogen contact with the ribose of base G11.

for direct recognition of the pyrimidine ring of the TPP. Residues U27 to A33, which form the longer segment of the bulge, fold in a helical stack extruded from the major groove of the pyrimidine sensor helix (Fig. 2C). Such arrangements of vertically stacked nucleotide bases were also observed in the crystal structures of several tRNAs and in the hairpin ribozyme (*25*, *26*). The extrusion starts with a trans-Watson-Crick/Hoogsteen base pair between residues U27 and A31 and ends with a cis-Watson-Crick/Hoogsteen base pair between U12 and A33. Residue A31 adopts a C2′-endo conformation, allowing the stacking of the additional TPP pyrimidine ring between bases G30 and A31 (Fig. 2C). The flipped G28 forms specific hydrogen bonds with the pyrimidine ring. This interaction mimics a Watson-crick/sugar edge base pair (Fig. 2D). The N1′ position of the TPP pyrimidine ring forms a hydrogen bond with the 2′ oxygen of the conserved residue G11 (Fig. 2D). The central thiazole ring of TPP is in proximity of the phosphate group of residue C45. However, this contact is unlikely to be very discriminating because biochemical experiments have shown that TPP-related molecules containing larger rings replacing the thiazole moiety can also be accommodated by the riboswitch (*1*).

In addition to the TPP-mediated contacts, two other major interaction areas connect the sensor helices. The first region includes contacts between loop L5 and the base of helix P3 that resemble GAAA tetraloop/receptor interactions (Figs. 3A and 4A) (*27*). These contacts are probably only present when the TPP is bound to the internal loops of the sensor helices and properly orients the tip of loop L5 (Fig. 3A). A similar observation was made in the case of the Hammerhead ribozyme where interactions between terminal loops stabilize the functional conformation (*28*, *29*). The second region of interaction involves residues in the three-way junction (Fig. 3A). This region is located between the TPP-binding part of both sensor helices and the switch helix P1. Residues A72, G42, C38, and

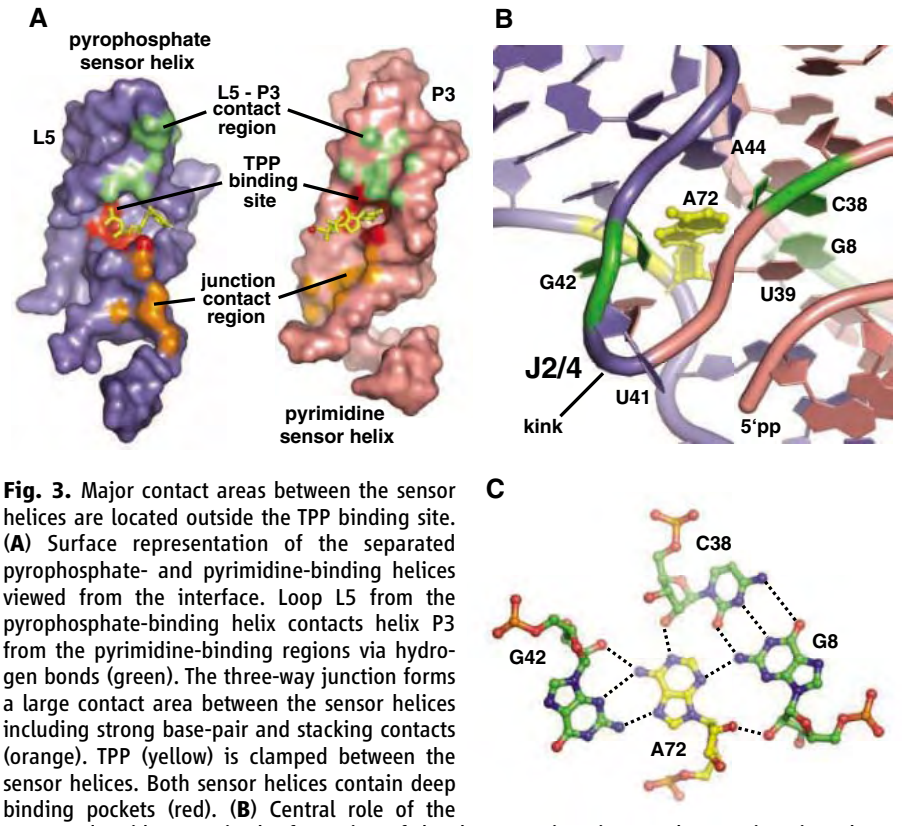

Fig. 3. Major contact areas between the sensor helices are located outside the TPP binding site. (**A**) Surface representation of the separated pyrophosphate- and pyrimidine-binding helices viewed from the interface. Loop L5 from the pyrophosphate-binding helix contacts helix P3 from the pyrimidine-binding regions via hydrogen bonds (green). The three-way junction forms a large contact area between the sensor helices including strong base-pair and stacking contacts (orange). TPP (yellow) is clamped between the sensor helices. Both sensor helices contain deep binding pockets (red). (**B**) Central role of the conserved residue A72 in the formation of the three-way junction. At the J2/4 junction, the RNA backbone undergoes a sharp kink at residue U41 between the pyrophosphate (blue) and pyrimidine (pink) sensor helices. A72 (yellow) serves as an assembly platform by forming hydrogen bonds with G8, C38, and G42 (green) and stacking with A44 and the ribose of U39 on both sides of the kink region. (**C**) The detailed view of the plane around A72 shows the extended network of hydrogen bonds formed with bases C38, G42, and G8, thereby joining together four different RNA strands.

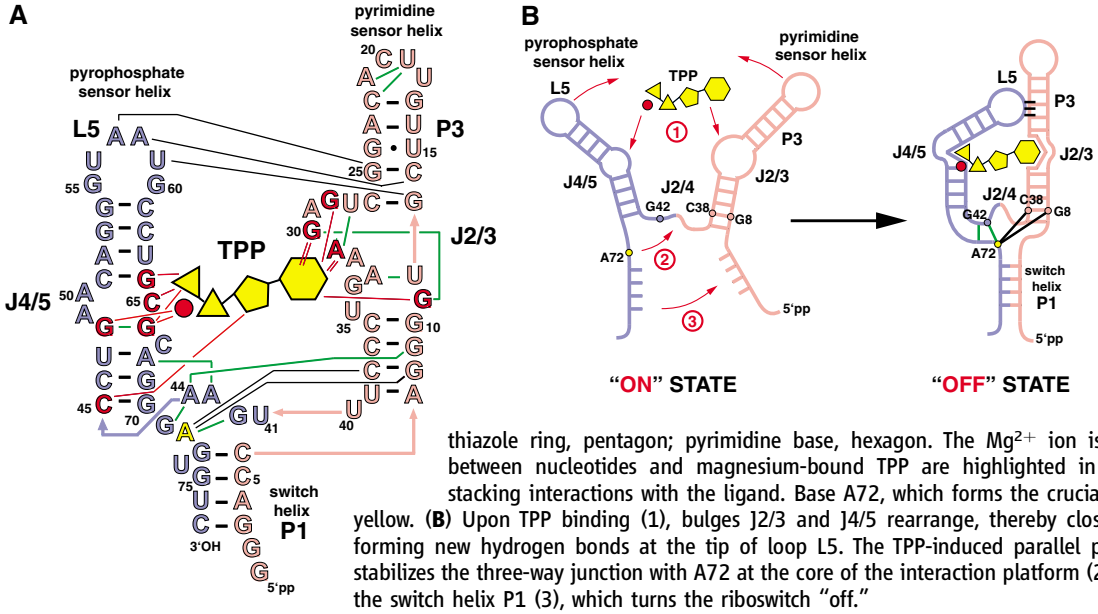

Fig. 4. Model of the coupling between TPP binding and structural rearrangements in the TPP riboswitch. (**A**) Summary of the contacts observed between the pyrophosphate (blue) and pyrimidine (pink) sensor helices, TPP, and the switch region. Watson-Crick base pairs are indicated in black, nonstandard base pairs are shown in green, and hydrogen bonds are indicated with thin black lines. TPP is schematically drawn in yellow: phosphates, triangles; thiazole ring, pentagon; pyrimidine base, hexagon. The Mg^{2+} ion is shown as a red dot. Contacts between nucleotides and magnesium-bound TPP are highlighted in red. Red double-lines indicate stacking interactions with the ligand. Base A72, which forms the crucial assembly platform, is shown in yellow. (**B**) Upon TPP binding (1), bulges J2/3 and J4/5 rearrange, thereby closing the sensor helix clamp and forming new hydrogen bonds at the tip of loop L5. The TPP-induced parallel positioning of the sensor helices stabilizes the three-way junction with A72 at the core of the interaction platform (2) and promotes the formation of the switch helix P1 (3), which turns the riboswitch "off."

G8 build an interaction platform, which stabilizes the kink in the J2/4 junction between the two sensor helices (Fig. 3, B and C). The extensive contacts within the interaction platform include residues from distant parts of the primary structure. This observation underscores the critical role of the platform in stabilizing the TPP-bound state of the riboswitch.

Residue A72 is mutated in a pyrithiamine-resistant strain of *Aspergillus oryzae* (*16*). The phosphorylated form of the well-known antibiotic pyrithiamine (PTPP) exerts its activity by directly interacting with TPP riboswitches (*18*). Both A72 and C38 mutations have also been selected in a screen for pyrithiamine resistance in bacteria (*18*). These nucleotides are key residues within the interaction platform, which stabilizes the three-way junction (Fig. 3, B and C). Biochemical experiments indicate that TPP and PTPP are still able to bind to the riboswitch despite the mutations (*18*). Our structural data are in agreement with these experiments and show that the TPP binding pocket would remain unaffected by the A72 or C38 mutations. Instead, these mutations likely disturb the correct folding of the three-way junction and prevent the coupling between TPP binding and the formation of the switch helix P1.

The structure of the AtRs riboswitch described here provides structural insights into the TPP-induced mechanism of shifting between its ligand-free "on" and the ligand-bound "off" conformational states. In the *thiM* gene from *E. coli*, where the TPP riboswitch is also found, the "on" state promotes translation of the mRNA, whereas the "off" state inhibits translation. Previous in-line probing experiments on the *E. coli* TPP riboswitch, in which the spontaneous RNA cleavage rate in the presence and absence of the ligand was monitored, revealed reduced cleavage of the "switch" helix P1 residues upon binding of the TPP (*1*). This indicates that helix P1 is not formed in the "on" state. Based on the structural and biochemical data, we propose a model for the sequence of events leading to the "off" state of the riboswitch (Fig. 4B): (1) TPP binding promotes the parallel disposition of the sensor helices. (2) Consequently, the interaction platform is assembled, forming a strong kink at the J2/4 junction. (3) The folding of the three-way junction reduces the entropic penalty for the formation of the switch helix P1. Therefore, if the formation of the three-way junction is impaired by one of the mutations, the TPP will still be able to bind to the sensor helices but will nevertheless be unable to turn the riboswitch "off."

The structure of the AtRs riboswitch reveals how thiamine pyrophosphate is recognized with high specificity and high affinity, rationalizes the mechanism of resistance to the well-known antibiotic pyrithiamine, and demonstrates which regions of the riboswitch are critical for the stability of its "off" conformation. The results presented here provide a good starting point for structure-based in vivo and in vitro experiments aimed at studying the mechanism of TPP riboswitch-regulated gene expression in general.

References and Notes

1. W. Winkler, A. Nahvi, R. R. Breaker, *Nature* **419**, 952 (2002).
2. D. A. Rodionov, A. G. Vitreschak, A. A. Mironov, M. S. Gelfand, *Nucleic Acids Res.* **31**, 6748 (2003).
3. V. Epshtein, A. S. Mironov, E. Nudler, *Proc. Natl. Acad. Sci. U.S.A.* **100**, 5052 (2003).
4. A. Nahvi, J. E. Barrick, R. R. Breaker, *Nucleic Acids Res.* **32**, 143 (2004).
5. A. G. Vitreschak, D. A. Rodionov, A. A. Mironov, M. S. Gelfand, *Trends Genet.* **20**, 44 (2004).
6. W. C. Winkler, R. R. Breaker, *Annu. Rev. Microbiol.* **59**, 487 (2005).
7. E. Nudler, A. S. Mironov, *Trends Biochem. Sci.* **29**, 11 (2004).
8. J. K. Soukup, G. A. Soukup, *Curr. Opin. Struct. Biol.* **14**, 344 (2004).
9. W. C. Winkler, S. Cohen-Chalamish, R. R. Breaker, *Proc. Natl. Acad. Sci. U.S.A.* **99**, 15908 (2002).
10. A. S. Mironov *et al.*, *Cell* **111**, 747 (2002).
11. M. Mandal, R. R. Breaker, *Nat. Struct. Mol. Biol.* **11**, 29 (2004).
12. W. C. Winkler, A. Nahvi, N. Sudarsan, J. E. Barrick, R. R. Breaker, *Nat. Struct. Biol.* **10**, 701 (2003).
13. W. C. Winkler, A. Nahvi, A. Roth, J. A. Collins, R. R. Breaker, *Nature* **428**, 281 (2004).
14. J. A. Doudna, J. R. Lorsch, *Nat. Struct. Mol. Biol.* **12**, 395 (2005).
15. N. Sudarsan, J. E. Barrick, R. R. Breaker, *RNA* **9**, 644 (2003).
16. T. Kubodera *et al.*, *FEBS Lett.* **555**, 516 (2003).
17. T. Yamauchi *et al.*, *FEBS Lett.* **579**, 2583 (2005).
18. N. Sudarsan, S. Cohen-Chalamish, S. Nakamura, G. M. Emilsson, R. R. Breaker, *Chem. Biol.* **12**, 1325 (2005).
19. Materials and methods, table S1, and fig. S1 are provided as supporting material on *Science* Online.
20. H. W. Pley, K. M. Flaherty, D. B. McKay, *Nature* **372**, 68 (1994).
21. A. Lescoute, E. Westhof, *RNA* **12**, 83 (2006).
22. R. T. Batey, S. D. Gilbert, R. K. Montange, *Nature* **432**, 411 (2004).
23. C. H. Carlisle, D. S. Cook, *Acta Crystallogr. B* **25**, 1359 (1969).
24. Y. A. Müller, G. E. Schulz, *Science* **259**, 965 (1993).
25. P. B. Rupert, A. R. Ferre-D'Amare, *Nature* **410**, 780 (2001).
26. D. Moras *et al.*, *J. Biomol. Struct. Dyn.* **3**, 479 (1985).
27. J. H. Cate *et al.*, *Science* **273**, 1678 (1996).
28. M. De la Pena, S. Gago, R. Flores, *EMBO J.* **22**, 5561 (2003).
29. A. Khvorova, A. Lescoute, E. Westhof, S. D. Jayasena, *Nat. Struct. Biol.* **10**, 708 (2003).

30. We acknowledge the support of B. Blattmann at the National Center of Competence in Research (NCCR) robotic nanoliter crystallization facility and members of the Ban lab for critical reading of the manuscript. Special thanks to C. Maris and F. Allain for initial nuclear magnetic resonance titration experiments and to F. Meylan and S. Pitsch for advice on nucleic acid derivatization. Data collection was performed at the Swiss Light Source (SLS) of the Paul Scherrer Institut (PSI) in Villigen. We are grateful to C. Schulze-Briese, A. Wagner, and S. Gutmann at the SLS whose efforts made these experiments possible. This work was supported by the Swiss National Science Foundation (SNSF) and the NCCR Structural Biology program of the SNSF. S.T. is recipient of a long-term fellowship from the European Molecular Biology Organization. The coordinates and structure factors have been deposited in the Protein Data Bank with accession code 2CKY.

Supporting Online Material

www.sciencemag.org/cgi/content/full/1128451/DC1
Materials and Methods
Fig. S1
Table S1
References

7 April 2006; accepted 25 April 2006
Published online 4 May 2006;
10.1126/science.1128451
Include this information when citing this paper.

Yersinia YopJ Acetylates and Inhibits Kinase Activation by Blocking Phosphorylation

Sohini Mukherjee,[1] Gladys Keitany,[1] Yan Li,[2,3] Yong Wang,[1] Haydn L. Ball,[2,3] Elizabeth J. Goldsmith,[3] Kim Orth[1]*

Yersinia species use a variety of type III effector proteins to target eukaryotic signaling systems. The effector YopJ inhibits mitogen-activated protein kinase (MAPK) and the nuclear factor κB (NFκB) signaling pathways used in innate immune response by preventing activation of the family of MAPK kinases (MAPKK). We show that YopJ acted as an acetyltransferase, using acetyl–coenzyme A (CoA) to modify the critical serine and threonine residues in the activation loop of MAPKK6 and thereby blocking phosphorylation. The acetylation on MAPKK6 directly competed with phosphorylation, preventing activation of the modified protein. This covalent modification may be used as a general regulatory mechanism in biological signaling.

The bacterial pathogen *Yersinia pestis* is the causal agent of plague, also known as the Black Death (*1*). Two related pathogens, *Y. pseudotuberculosis* and *Y. enterocolitica*, cause gastroenteritis (*2*). All three *Yersinia* species harbor a virulence pathogen that encodes a type III secretion system and secrete effector proteins, referred to as Yops (*Yersinia* outer proteins) (*2*). Yops are delivered by this system into a eukaryotic

cell to cripple the host defense system (*3*, *4*). The *Yersinia* species effector protein, YopJ, disrupts signaling essential for eukaryotic cells to elicit an immune response by inhibiting the evolutionarily conserved MAPK and NFκB signaling pathways (*2*, *3*, *5*, *6*). YopJ contains a catalytic domain that is similar to Clan CE of cysteine proteases, which includes the adenoviral protease (AVP) family and the ubiquitin-like protein protease (Ulp-1) family (*7*). Mutation of the putative catalytic cysteine residue to an alanine in YopJ (YopJ-C/A) abolishes its ability to inhibit the MAPK and the NFκB signaling pathways (*7*). YopJ binds MAPK kinases, including MAPKK1, MAPKK3, MAPKK4, MAPKK5, and the related kinase that activates the NFκB pathway, IκB kinase β (IKKβ), and prevents their activation (*5*). The mechanism by which this binding leads to inactivation of these kinases is unknown.

A cell-free signaling system was developed to recapitulate the inhibition of the MAPK and the NFκB signaling pathways by YopJ (*5*–*8*). Mammalian extracellular signal–regulated kinase (ERK) signaling was activated by addition of recombinant B-Raf to a membrane-free cytosolic lysate (cleared lysate), as demonstrated by the appearance of phosphorylated ERK (Fig. 1A). By contrast, activation of ERK signaling was diminished in cleared lysate isolated from cells transfected with YopJ (Fig. 1A). The catalytic activity in YopJ was required for this inhibition. Addition of B-Raf to cleared lysate isolated from cells expressing mutant YopJ-C/A lead to activation of the ERK pathway (Fig. 1A). For activation of the NFκB pathway, we added a purified active form of recombinant TNF (tumor necrosis factor) receptor–associated factor 6 (TRAF6) (T6RZC) (*9*). When T6RZC was added to control and YopJ-C/A cleared lysates, the pathway was activated, as indicated by the phosphorylation of IκB (Fig. 1B). However, the addition of T6RZC to YopJ cleared lysate did not result in activation of the NFκB pathway (Fig. 1B). Similarly, when other exogenous stimuli [including NF-κB–inducing kinase (NIK), MAPK kinase kinase 1, and activated Ras-V12 membranes] were added to the lysates, signaling was blocked only in the YopJ lysates. No obvious changes were observed in the molecular weight or the stability of MAPKK1 and MAPKK2 (MAPKK1,2) or IKKβ in the lysates (Fig. 1C). These observations were consistent with previous genetic, microbial, and cellular studies on the activity of YopJ and provided a method for analyzing inhibition of signaling by YopJ in vitro (*5*–*8*).

To test whether YopJ acted directly on the MAPKKs and IKKβ, we coexpressed a representative member of this group of kinases, human MAPKK6 (rMAPKK6), with either active YopJ (rMAPKK6-J) or the catalytically inactive form of YopJ (rMAPKK6-C/A) in bacterial cells. We then assessed whether the various rMAPKK6s could be activated in our in vitro signaling assay. Although both rMAPKK6 and rMAPKK6-C/A were robustly phosphorylated when added to cleared lysate, the rMAPKK6-J was not activated by phosphorylation by the upstream signaling machinery (Fig. 1D). Therefore, coexpression of YopJ with MAPKK6 in bacteria produced a kinase that could not be activated by the upstream signaling machinery.

Studies on the YopJ-inactivated rMAPKK6 were undertaken to determine the biochemical nature of the modifications. Although all the rMAPKK6s were indistinguishable by SDS–polyacrylamide gel electrophoresis (PAGE) and gel filtration (fig. S1), mass spectrometry revealed that the total mass of rMAPKK6-J was larger than that of either rMAPKK6 or rMAPKK6-C/A. The majority of YopJ-inactivated rMAPKK6 showed an increase in mass of 126 atomic mass units (amu), whereas smaller populations of rMAPKK6-J exhibited increases in mass of 84 amu or 42 amu (Fig. 2A). We hypothesized that YopJ altered the mass of rMAPKK6 by adding single, double, or triple post-translational modifications equal to a mass of 42 amu.

We analyzed tryptic peptides for all three rMAPKK6s (rMAPKK6, rMAPKK6-J, and rMAPKK6-C/A) by using liquid chromatography followed by tandem mass spectrometry (*10*). After obtaining a complete data set for all the predicted tryptic peptides, we found that rMAPKK6-J, but not rMAPKK6 or rMAPKK6-C/A, contained two tandem peptides [peptide A, MAPKK6 195 to 210 amino acids, and peptide B, MAPKK6 211 to 224 amino acids] modified by acetylation with a consequent increase of 42 amu for each peptide (Fig. 2, B and C). In another partially cleaved tryptic peptide (MAPKK6 195 to 224 amino acids) that contained both peptides A and B, we observed multiple acetylated sites. Peptide A in the rMAPKK6-J protein was modified by acetylation on Ser^{207} (Fig. 2B), and peptide B was modified by acetylation on Thr^{211} (Fig. 2C). In the third peptide, it appeared that Lys^{210} and Ser^{207} and/or Thr^{211} were modified by acetylation. Modification of the lysine contributes to the inefficient cleavage of this peptide by trypsin. Residues 195 to 224 map to the end of β strand 9 and the activation loop in MAPKK6, which contains Ser^{207} and Thr^{211}, the sites that are phosphorylated to activate MAPKK6. Although the serine and threonine residues are conserved throughout the MAPKK superfamily, the lysine residue is not (Fig. 2D). We predict that this residue is modified in a YopJ-dependent manner because of its

[1]Department of Molecular Biology, [2]Protein Chemistry Technology Center, [3]Department of Biochemistry, University of Texas Southwestern Medical Center, Dallas, TX 75390, USA.

*To whom correspondence should be addressed. E-mail: Kim.Orth@utsouthwestern.edu

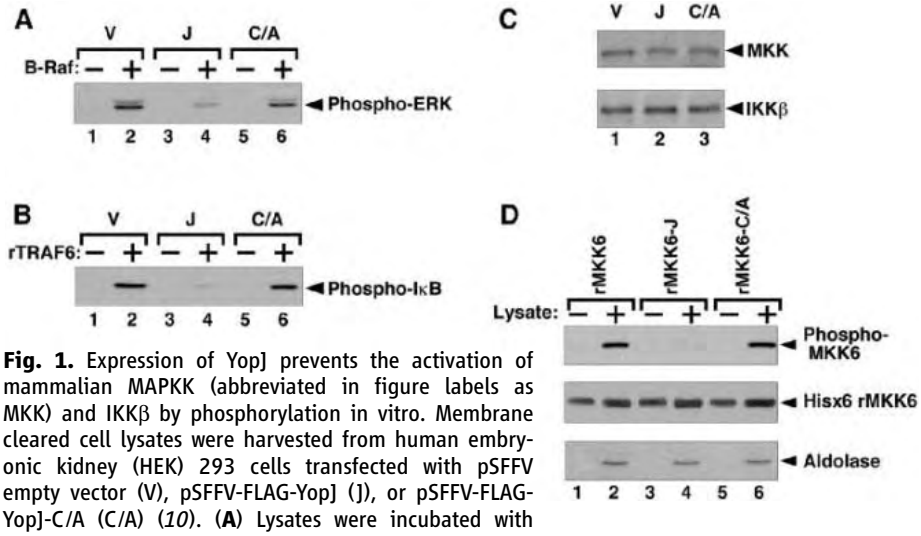

Fig. 1. Expression of YopJ prevents the activation of mammalian MAPKK (abbreviated in figure labels as MKK) and IKKβ by phosphorylation in vitro. Membrane cleared cell lysates were harvested from human embryonic kidney (HEK) 293 cells transfected with pSFFV empty vector (V), pSFFV-FLAG-YopJ (J), or pSFFV-FLAG-YopJ-C/A (C/A) (*10*). (**A**) Lysates were incubated with purified B-Raf for 10 min at 37°C, followed by immunoblotting with antibody to phospho-ERK. (**B**) V, J, and C/A lysates were incubated with rTRAF6 (*9*) for 10 min at 37°C, followed by immunoblotting with antibody against phospho-IκB (anti-phospho-IκB). (**C**) V, J, and C/A lysates were immunoblotted with antibodies to MAPKK1,2 and IKKβ. (**D**) YopJ coexpressed with rMAPKK6 in bacteria is not phosphorylated by upstream signaling machinery. Purified rMAPKK6, rMAPKK6-J, and rMAPKK6-C/A were incubated with serum-stimulated cleared lysate for 10 min at 37°C, followed by analysis with antibody to phospho-MAPKK6 (anti-phospho-MAPKK6) (lanes 2, 4, and 6). rMAPKK6 was detected by immunoblotting with antibody to Hisx4. Aldolase immunoblotblot was a load control for lysate.

coincidental location in the activation loop. The observation that YopJ covalently modifies the representative MAPKK, MAPKK6, by acetylation on the same residues that are used for activation of the kinase suggests a mechanism for the inhibition of MAPKKs and IKKβ: namely, acetylation prevents phosphorylation.

YopJ can bind and inhibit MAPKKs and IKKβ but not IKKα (fig. S2) (*5*), and all of these kinases contain serine and/or threonine residues in their activation loop that must be phosphorylated to activate the kinase (Fig. 2D) (*11*). rMAPKK6, coexpressed with YopJ and shown to be acetylated at Ser^{207} and Thr^{211} (Fig. 2, B and C), was not phosphorylated by upstream signaling machinery (Fig. 1D). These observations support our hypothesis that YopJ functions to modify the MAPKKs without noticeably changing their migration pattern on SDS-PAGE (Fig. 1C and fig. S1).

To determine whether YopJ directly functions as an acetyltransferase, we performed a transferase reaction in the presence of ^{14}C-labeled acetyl–coenzyme A (CoA) (*12*). rMAPKK6 was modified with the ^{14}C-labeled acetyl moiety only in the presence of recombinant YopJ expressed as a glutathione *S*-transferase fusion protein (GST-YopJ) and the labeled acetyl donor [^{14}C]acetyl-CoA (Fig. 3A). The ^{14}C label was associated with both rMAPKK6 and GST-YopJ (Fig. 3B). Based on this and analysis of the GST-YopJ protein beads, rMAPKK6 associated with GST-YopJ was the source of the ^{14}C label (Fig. 3C). Thus, YopJ requires both an intact catalytic site and acetyl-CoA to acetylate rMAPKK6. We did not observe any band in reactions that contained only GST-YopJ and [^{14}C]acetyl-CoA, indicating that the charging of YopJ with a [^{14}C]acetyl moiety might be transient, labile, and/or dependent on the presence of a substrate or that the reaction proceeds through direct transfer. Similarly, we have observed that rMAPKK1 was also modified by [^{14}C]acetyl moiety in a YopJ-dependent manner (fig. S4). These experiments show that YopJ acts as an acetyltransferase to modify MAPKKs.

To demonstrate that the modification on rMAPKK6 by YopJ prevents activation via phosphorylation, we used our in vitro signaling system. Pretreatment of rMAPKK6 in the presence of both YopJ and acetyl-CoA diminished the ability of the upstream signaling machinery to activate rMAPKK6 by phosphorylation (Fig. 3D). Hence, the acetylation of a MAPKK by YopJ prevents phosphorylation and activation of this kinase.

YopJ protein is delivered into the cytoplasm of a host cell by a type III secretion system, where it inhibits the activation of the MAPKKs and IKKβ (*5*). Previously, adding recombinant YopJ to lysates did not show an inhibitory affect on signaling pathways. However, by using an acetyl-CoA–supplemented cleared lysate, we observed that addition of GST-YopJ but not GST-YopJ-C/A resulted in the inhibition of the NFκB signaling pathway in vitro (Fig. 3E). Thus, as observed during infection, when delivered to a lysate, YopJ uses acety-CoA to target and inactivate MAPKKs and IKKβ.

The mechanism of YopJ inhibition is elegant in its simplicity. On the basis of current studies on a representative kinase, MAPKK6, we propose that YopJ blocks signaling of the MAPKK and NFκB pathways by binding and acetylating critical residues in the activation loop of MAPKKs and IKKβ, respectively, thereby preventing these residues from being phosphorylated.

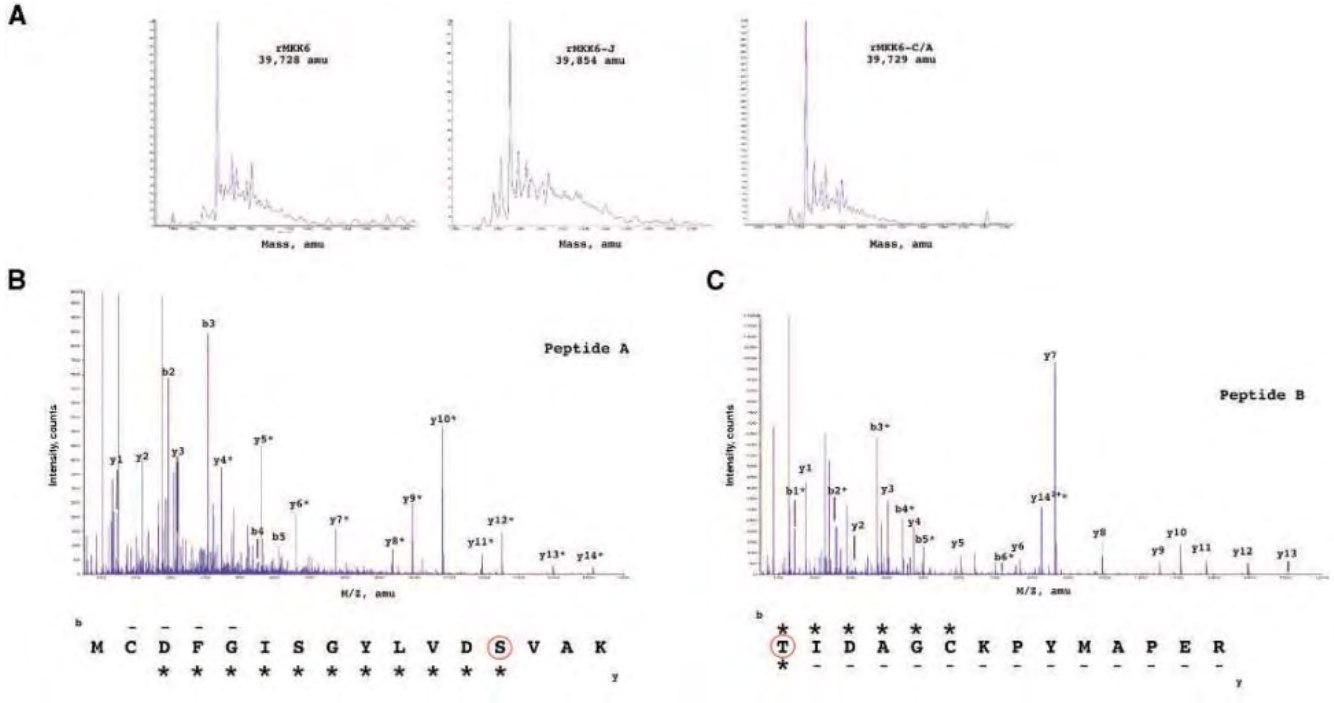

Fig. 2. rMAPKK6-J is acetylated on Ser^{207} and Thr^{211} residues in its activation loop. (**A**) Reconstructed molecular mass profiles of rMAPKK6, rMAPKK6-J, and rMAPKK6-C/A. (**B** and **C**) Electrospray ionization (ESI) tandem mass spectrometry (MS/MS) spectra of modified tryptic peptide A [mass-to-charge ratio (*m/z*) of 902.4 ($z = 2$)] and peptide B [*m/z* of 825.9 ($z = 2$)] from rMAPKK6-J. The b and y ions are marked on the MS/MS spectra. The amino acid sequence for each peptide is shown below (*18*). Acetylated residues are designated with a red circle. Masses that show an increase of 42 amu are marked with an asterisk. Two ions related to acetylated peptide B were detected, *m/z* of 825.9 ($z = 2$) and *m/z* of 833.9 ($z = 2$). MS/MS data of both ions indicated that peptide B was modified by acetylation on Thr^{211}. The only difference between these two ions is that Met^{220} is oxidized in *m/z* of 833.9. Figure 3C shows the MS/MS spectrum of *m/z* 825.9. A corresponding figure defining the b and y ions is presented in fig. S3. (**D**) Alignment of the activation loop of the MAPKK superfamily with conserved serine and/or threonine residues that are indicated by asterisks.

Analysis of the predicted secondary structure of YopJ demonstrated similarities with the protease AVP (*13*). Because of the similarities between AVP and its distant relative, Ulp1, it was proposed that YopJ might act as an Ulp1-like protease or a general hydrolase (*7*). Inconsistent with this earlier hypothesis is the observation that YopJ selectively targets MAPKKs and IKKβ without any obvious changes in their migration on SDS-PAGE (*2*–*6*, *8*) (Fig. 1C and fig. S1). However, because YopJ shares similarities with a family of cysteine proteases, this provides mechanistic insight into the chemistry of YopJ catalysis (*7*). A likely first step in the reaction is that YopJ is acetylated on Cys^{172} by formation of a thioester bond, and in the second step of the reaction this bond is attacked, not by a water molecule, but by a hydroxyl moiety on a serine or threonine residue of MAPKK, resulting in the formation of an acetylated amino acid. The substrate specificity determined by a bacterial effector protein, YopJ, and its interaction with target host proteins, MAPKKs and IKKβ, illustrates a common mechanism used by many bacterial effectors to ensure that their potent activity does not harm the bacterial host (*3*).

We find that YopJ-dependent acetylation occurs on the critical serine or threonine residues, thereby directly competing with the posttranslational modification, phosphorylation. Although the possibility exists that this is a unique modification developed by pathogenic bacteria to affect signaling in eukaryotic cells, a major characteristic of bacterial effector proteins is that they usurp or mimic a eukaryotic activity and refine this activity to produce an extremely efficient mechanism to combat eukaryotic signaling. Therefore, a more appealing hypothesis is that the modification of phosphorylatable residues by acetylation is a commonly used eukaryotic mechanism that simply has not been detected previously. Our findings support the provocative hypothesis that modification of amino acids other than lysine by acetylation is used to regulate eukaryotic cellular machineries. Enzymes that acetylate lysines have been studied for many years, including the eukaryotic and bacterial N-acetyltransferases that use acetyl-CoA and a catalytic triad, which appears similar to papain-like cysteine proteases (Cys-Glu/Asp-His) (*14*–*16*). Immunoblotting and the interpretation of tandem mass spectrometry data by MASCOT are commonly used for the identification of lysine acetylation (*17*). However, these assays do not detect acetylation of serines and threonines. In view of the current finding, a more careful manual analysis of liquid chromatography followed by tandem mass spectrometry data may be required to determine whether an amino acid other than lysine is modified by acetylation. The characterization of a bacterial effector as a Ser or Thr acetyl transferase presents a previously unknown paradigm to be considered for other biological signaling pathways.

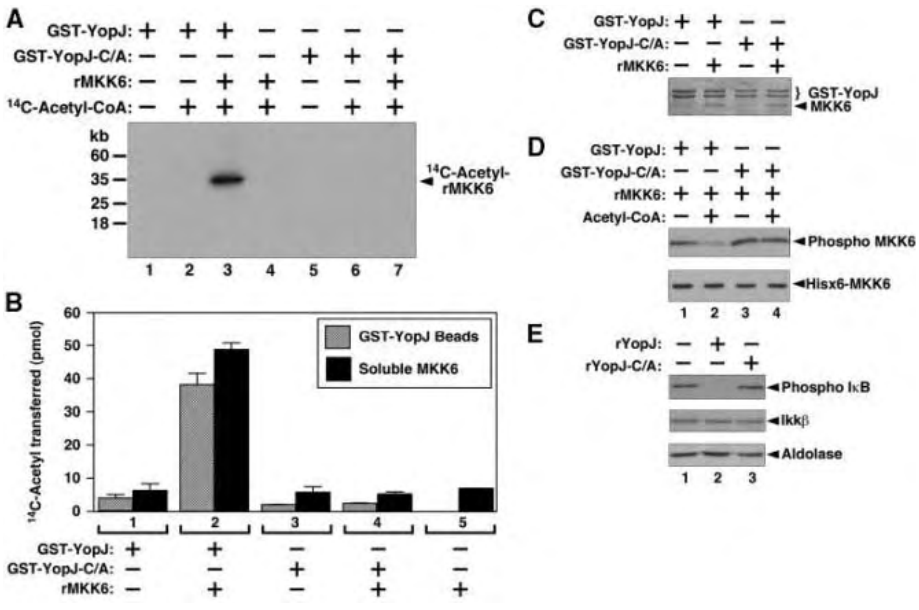

Fig. 3. In vitro acetylation by YopJ prevents phosphorylation of rMAPKK6 and activation of NFκB pathway. (**A**) Purified recombinant GST-YopJ or GST-YopJ-C/A was incubated with and without rMAPKK6 in the presence and absence of ^{14}C-labeled acetyl-CoA for 1 hour at 30°C. Samples were separated by SDS-PAGE and analyzed by autoradiography. (**B**) Purified recombinant GST-YopJ or GST-YopJ-C/A bound to glutathione sepharose beads was incubated with and without 200 pmol of rMAPKK6 in the presence and absence of 35 μM [^{14}C]acetyl-CoA. YopJ beads were washed, and supernatants were trichloroacetic acid (TCA)–precipitated, followed by measurement of the associated radiolabel. (**C**) Bead samples from (B) were separated by SDS-PAGE, followed by staining with Coomassie blue. (**D**) Purified recombinant GST-YopJ and GST-YopJ-C/A were incubated with rMAPKK6 in the presence and absence of acetyl-CoA for 1 hour at 30°C, followed by incubation with serum-stimulated cleared lysate for 10 minutes at 37°C and immunoblot analysis with anti-phospho-MAPKK6. (**E**) Acetyl-CoA (50 μM) was added to cleared lysate (10 mg/ml), followed by addition of recombinant GST-YopJ or GST-YopJ-C/A (100 ng), and incubated for 1 hour at 30°C. Lysates were then incubated with rTRAF6 (*9*) for 10 min at 37°C, followed by immunoblotting with anti-phospho-IκB, anti-IKKβ, and aldolase.

References and Notes

1. B. J. Hinnebusch, *Curr. Issues Mol. Biol.* **7**, 197 (2005).
2. G. I. Viboud, J. B. Bliska, *Annu. Rev. Microbiol.* **59**, 69 (2005).
3. K. Orth, *Curr. Opin. Microbiol.* **5**, 38 (2002).
4. L. Navarro, N. M. Alto, J. E. Dixon, *Curr. Opin. Microbiol.* **8**, 21 (2005).
5. K. Orth *et al.*, *Science* **285**, 1920 (1999).
6. S. Yoon, Z. Liu, Y. Eyobo, K. Orth, *J. Biol. Chem.* **278**, 2131 (2003).
7. K. Orth *et al.*, *Science* **290**, 1594 (2000).
8. L. E. Palmer, A. R. Pancetti, S. Greenberg, J. B. Bliska, *Infect. Immun.* **67**, 708 (1999).
9. L. Deng *et al.*, *Cell* **103**, 351 (2000).
10. Materials and methods can be found on *Science* Online.
11. G. Hardie, S. Hanks, Eds., *The Protein Kinase FactsBook* (Academic Press, San Diego, CA, 1995), p. 418.
12. W. Gu, R. G. Roeder, *Cell* **90**, 595 (1997).
13. J. Ding, W. J. McGrath, R. M. Sweet, W. F. Mangel, *EMBO J.* **15**, 1778 (1996).
14. A. M. Bode, Z. Dong, *Sci. STKE* **2005**, re4 (2005).
15. E. Sim, M. Payton, M. Noble, R. Minchin, *Hum. Mol. Genet.* **9**, 2435 (2000).
16. E. W. Brooke *et al.*, *Bioorg. Med. Chem.* **11**, 1227 (2003).
17. S. Y. Roth, J. M. Denu, C. D. Allis, *Annu. Rev. Biochem.* **70**, 81 (2001).
18. Single-letter abbreviations for the amino acid residues are as follows: A, Ala; C, Cys; D, Asp; E, Glu; F, Phe; G, Gly; H, His; I, Ile; K, Lys; L, Leu; M, Met; N, Asn; P, Pro; Q, Gln; R, Arg; S, Ser; T, Thr; V, Val; W, Trp; and Y, Tyr.

19. We thank M. Phillips, M. Cobb, E. Olson, J. Goldstein, and M. Brown for insightful discussions and critical reading of the manuscript; H. Zui, S. Sprang, L. Hooper, and J. Humphreys for their helpful conversations; Z. J. Chen, M. White, and K. L. Guan for their generous supply of reagents; and the members of the Orth lab, A. Tizenor, A. Haughey, and W. Simpson for their generous support and assistance. S.M. participation was in partial fulfillment of degree requirements. K.O. thanks R. Taussig, M. Phillips, Y. M. Chook, M. Cobb, and R. Bassel-Duby for years of unconditional support and friendship. K.O., S.M., G.K., Y.W., and E.J.G. were supported by grants from NIH National Institute of Allergy and Infectious Diseases (R01-AI056404 and R21-DK072134) and the Welch Research Foundation (I-1561 and I-1128). K.O. is a Beckman Young Investigator and C. C. Caruth Biomedical Scholar.

Supporting Online Material

www.sciencemag.org/cgi/content/full/312/5777/1211/DC1
Materials and Methods
Figs. S1 to S4
References and Notes

1 March 2006; accepted 6 April 2006
10.1126/science.1126867

A Regulatory SNP Causes a Human Genetic Disease by Creating a New Transcriptional Promoter

Marco De Gobbi,[1*] Vip Viprakasit,[2*] Jim R. Hughes,[1] Chris Fisher,[1] Veronica J. Buckle,[1] Helena Ayyub,[1] Richard J. Gibbons,[1] Douglas Vernimmen,[1] Yuko Yoshinaga,[3] Pieter de Jong,[3] Jan-Fang Cheng,[4] Edward M. Rubin,[4] William G. Wood,[1] Don Bowden,[5] Douglas R. Higgs[1]‡

We describe a pathogenetic mechanism underlying a variant form of the inherited blood disorder α thalassemia. Association studies of affected individuals from Melanesia localized the disease trait to the telomeric region of human chromosome 16, which includes the α-globin gene cluster, but no molecular defects were detected by conventional approaches. After resequencing and using a combination of chromatin immunoprecipitation and expression analysis on a tiled oligonucleotide array, we identified a gain-of-function regulatory single-nucleotide polymorphism (rSNP) in a nongenic region between the α-globin genes and their upstream regulatory elements. The rSNP creates a new promoterlike element that interferes with normal activation of all downstream α-like globin genes. Thus, our work illustrates a strategy for distinguishing between neutral and functionally important rSNPs, and it also identifies a pathogenetic mechanism that could potentially underlie other genetic diseases.

The human α-globin cluster, located at the telomeric region of chromosome 16 (16p13.3), includes an embryonic gene (ζ), two minor α-like genes [α^D (also called μ) and θ], two α genes (α2 and α1), and two pseudogenes (ψα1 and ψζ) (*1*, *2*). Upstream of these genes are four highly conserved cis elements (MCS-R1 to MCS-R4) of which MCS-R2 (also known as HS-40) plays the major role in regulating expression of the cluster (*2*, *3*) (Fig. 1). Previous analyses of mutations that down-regulate globin gene expression and cause thalassemia have elucidated many of the general mechanisms underlying human molecular disease (*4*). Down-regulation of one or two of the four α-globin genes (αα/αα) causes anemia with mild red blood cell changes; so-called α thalassemia trait. However, when α-globin gene expression is reduced to less than ~50% of normal, excess β-globin chains form tetramers (β4, called HbH), which precipitate in the red blood cell, causing a more severe form of anemia called HbH disease (*5*). In nearly all cases of α thalassemia, the molecular basis for their reduced levels of α-globin expression can be readily identified (*4*, *5*).

We have studied 148 individuals from Melanesia with α thalassemia, including 5 with HbH disease, in whom none of the previously described molecular defects could be found. The pattern of inheritance suggested that individuals with HbH disease are homozygotes for a codominant defect, referred to here as $(\alpha\alpha)^T$, causing α thalassemia with a predicted genotype of $(\alpha\alpha)^T/(\alpha\alpha)^T$ (table S1). To determine which process in gene expression had been affected, we analyzed a Melanesian individual (patient L, table S1) with a well-defined phenotype of HbH disease. In situ RNA hybridization to detect primary transcripts in erythroid cells from patient L detected substantially fewer nuclear transcripts from the α-globin genes than from the β-globin genes (Fig. 2), which is consistent with a mutation reducing α-globin RNA transcription.

DNA fluorescence in situ hybridization studies in two affected individuals showed that the α-globin cluster was present at its normal location at the tip of chromosome 16. Extensive analysis of the α-globin cluster and the surrounding 300 kb revealed no evidence for any deletions or chromosomal rearrangements in the patients with α thalassemia. Where tested, the pattern of DNA methylation appeared normal. Sequence analysis of the major (α2 and α1) and minor (α^D and θ) α-like genes and their regulatory elements revealed only the wild-type sequences or known neutral single-nucleotide polymorphisms (SNPs).

Having excluded all currently known α thalassemia mutations, we reasoned that the Melanesian form was either due to a cis-acting mutation in a previously unrecognized regulatory element or resulted from a gain-of-function mutation that negatively regulates α-globin expression. Alternatively, it was possible that α thalassemia in these individuals was due to a trans-acting mutation. By analyzing linkage to a variable number of tandem repeats (VNTR) (*6*) located ~8.5 kb from the α-globin genes (Fig. 1), we found that all individuals with the $(\alpha\alpha)^T$ mutation shared a common VNTR allele (fig. S1), demonstrating that this is a cis-linked defect. Further association studies, using known SNPs, showed that the $(\alpha\alpha)^T$ haplotype extends from the 16p telomere, with loss of association immediately downstream of the α-globin cluster (coordinate 168,467 in Fig. 1) defining the centromeric border of the region containing the cis-acting mutation. We estimated that the frequency of the $(\alpha\alpha)^T$ defect in the island population is ~0.04 (fig. S1).

We therefore resequenced the $(\alpha\alpha)^T$ haplotype by isolating bacterial artificial chromosomes (BACs) from a library constructed from the peripheral blood DNA of patient L with the Melanesian type of HbH disease [$(\alpha\alpha)^T/(\alpha\alpha)^T$]. BACs spanning the α-globin cluster and the surrounding ~213 kb of DNA (coordinates 21,059 to 234,236) were sequenced (DQ431198), and we identified 283 SNPs and/or sequence differences (Fig. 1) by comparison with the current wild-type sequence (National Center for Biotechnology Information database build 35, coordinates 1 to 223478), consistent with estimates of the frequency of SNPs throughout the genome (*7*). This now presented a situation analogous to a common, largely unsolved problem in human genetics: how to identify a functionally important single nucleotide change from all other SNPs within a relatively large (~213 kb) genomic interval (*8*, *9*).

To search for functional changes associated with these SNPs, we constructed a tiled array representing all regions of nonrepetitive DNA throughout the terminal 223.5 kb of chromosome 16. RNA expression profiles obtained with the use of complementary DNA from normal (αα/αα) or mutant [$(\alpha\alpha)^T/(\alpha\alpha)^T$] erythroblasts were compared. Two prominent differences were observed in the mutant erythroblasts (Fig. 1). First a major new peak of RNA transcription (beyond the quantitative range of the array) from the same DNA strand as α-globin (fig. S2) was observed between coordinates 149,682 and 153,390 (Fig. 1, A and B). Quantitative reverse transcription polymerase chain reaction (RT-PCR) showed that expression from this region was >1000 fold higher in the mutant than in the wild-type chromosome (Fig. 1C). Second, by RT-PCR we observed an ~80-fold decrease in expression of the α^D gene immediately downstream of this peak (Fig. 1, A and B). The decreased level of α2 and α1 gene expression detected by quantitative RT-PCR (table S2) was not detected on the array, again because globin expression lies beyond the quantitative range. No other substantial differences in the pattern of RNA expression were seen across the 223.5-kb region (Fig. 1, A and B).

[1]Medical Research Council Molecular Haematology Unit, Weatherall Institute of Molecular Medicine, John Radcliffe Hospital, Oxford, OX3 9DS, UK. [2]Department of Pediatrics, Siriraj Hospital, Mahidol University, Bangkok, Thailand. [3]BACPAC Resources, Oakland Research Institute Children's Hospital, Oakland, CA, USA. [4]Genome Science, Genomic Division, Lawrence Berkeley National Laboratory, CA, USA. [5]Department of Anatomy and Cell Biology, Monash University, Melbourne, Australia.

*These authors contributed equally to this work.
‡To whom correspondence should be addressed. E-mail: doug.higgs@imm.ox.ac.uk

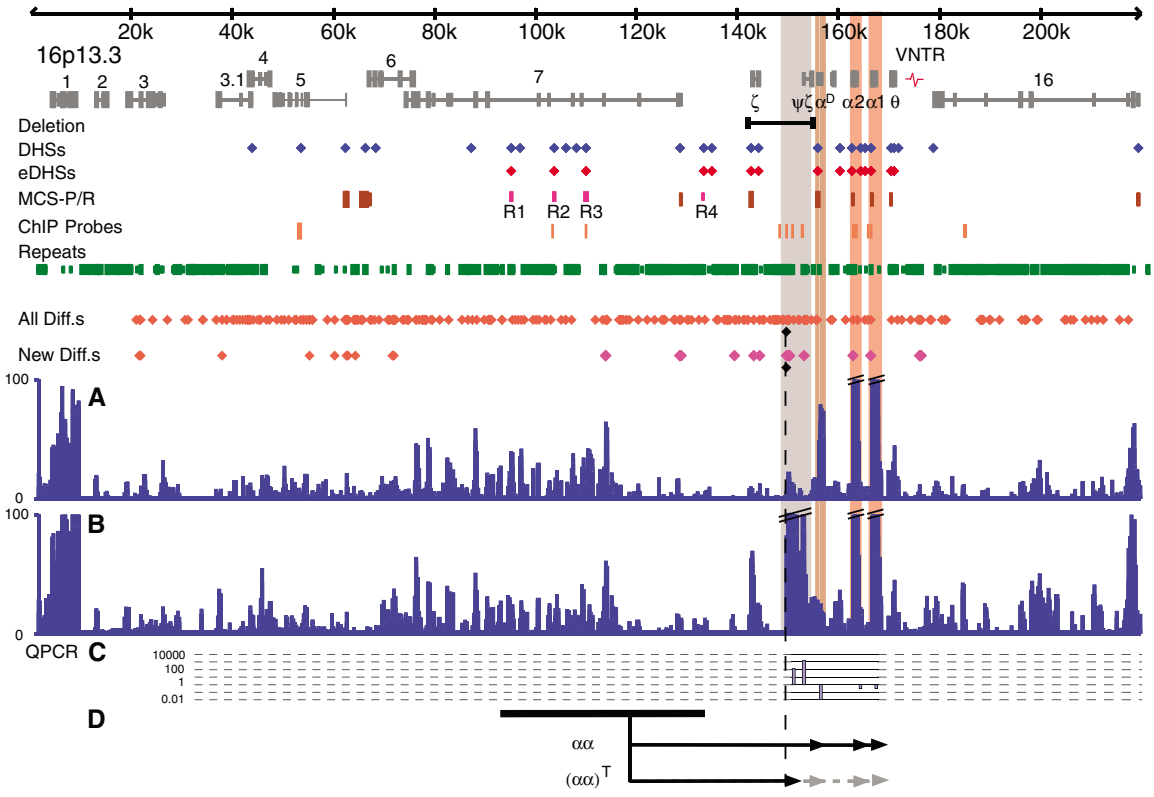

Fig. 1. Overview of the α-globin cluster and identification of a rSNP. The genes located in the telomeric region of chromosome 16 are numbered as in (*1*), and the globin genes are labeled. The VNTR (3′ hypervariable region) is shown as a red zigzag line. A deletion (*15*) removing the region containing the rSNP is shown as a black line. Below this, all DNAse1 hypersensitive sites (DHSs) and erythroid-specific sites (eDHSs) are shown (*3*, *10*, *16*). MCS-P/R summarizes all evolutionarily conserved promoter and regulatory sequences across this region (*2*). Probes used to profile ChIP products are shown in pink, and repeats are shown in green. Below this, all sequence differences between the $(\alpha\alpha)^T$ and wild-type αα chromosome are shown. "New Diffs" refers to newly identified sequence differences that are not known to be polymorphic SNPs. SNPs analyzed in genetic linkage studies described in this paper are shown in purple. The rSNP described here is shown as a black diamond in "All Diffs" and "New Diffs." A dashed vertical line runs from these diamonds through the array data. Below, the patterns of gene expression recorded on a custom-tiled Affymetrix array spanning this telomeric region in primary erythroid cells from (**A**) a normal individual (αα/αα) and (**B**) patient L with the $(\alpha\alpha)^T/(\alpha\alpha)^T$ genotype are shown. The peak of ζ-globin expression in the $(\alpha\alpha)^T$ chromosome results from cross-hybridization to the highly expressed abnormal transcripts across the homologous ψζ gene. (**C**) Estimates of the differences in RNA expression between normal and abnormal chromosomes, based on independent quantitative PCR (QPCR), are shown below (on a logarithmic scale). (**D**) Representation of how one or more of the conserved regulatory elements (contained within the region spanned by the horizontal black bar) normally interact with the α-globin promoters [αα] and how they are proposed to interact less effectively (dashed lines) in the abnormal $(\alpha\alpha)^T$ chromosome. The direction of transcription of the globin genes and the new promoter, created by the C allele of SNP 195, are indicated by the arrows.

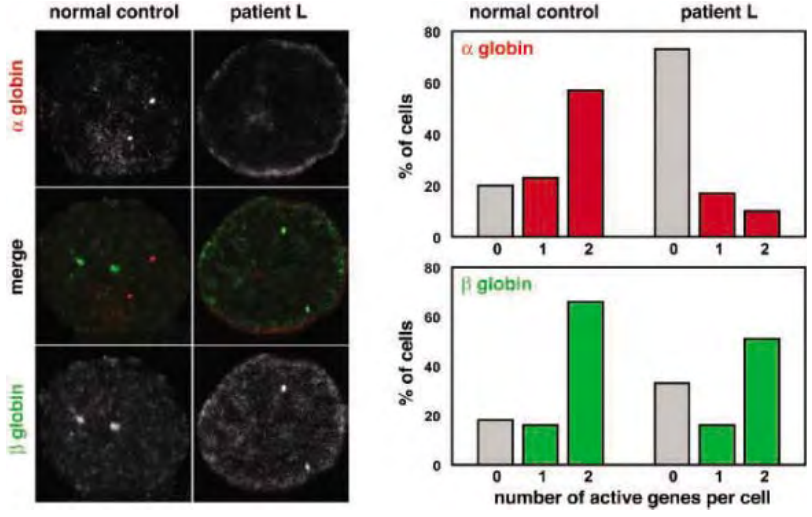

Fig. 2. In situ RNA analysis demonstrating reduced primary α-globin transcripts in patient L. Nascent α-globin (red) and β-globin (green) transcripts in intermediate erythroblasts from a normal control and from patient L [with the $(\alpha\alpha)^T/(\alpha\alpha)^T$ genotype] are shown. (**Left**) Representative nuclei show β-globin transcripts in both patient and control, but α-globin transcripts are present only in the normal control. (**Right**) The proportion of nuclei containing none, one, or two signals were recorded from the analysis of 100 cells.

The region underlying this new peak of expression is unremarkable, containing 3.7 kb of poorly conserved, predominantly noncoding sequence, although the tail of the peak extends into the ψζ-globin gene. This region contains 17 SNPs, 10 of which have been previously characterized in nonthalassemic individuals. We therefore analyzed the segregation of the remaining seven SNPs and, as controls, six additional SNPs from nonrepetitive regions of the α cluster (Fig. 1), within affected families. In addition, we performed genetic linkage studies in 15 nonthalassemic Melanesian individuals (αα/αα), 22 with α thalassemia trait $[\alpha\alpha/(\alpha\alpha)^T]$, and 5 with HbH disease $[(\alpha\alpha)^T(\alpha\alpha)^T]$. Six of the seven SNPs underlying the new peak of transcription were found on both the normal αα and abnormal $(\alpha\alpha)^T$ chromosomes. Only the C allele of SNP 195 (C or T, located at coordinate 149709) segregated with thalassemia in the affected families and showed complete association with the $(\alpha\alpha)^T$ haplotype (table S2). This allele was not found in a separate analysis of 131 nonthalassemic, Melanesian individuals. SNP 195 changes the sequence

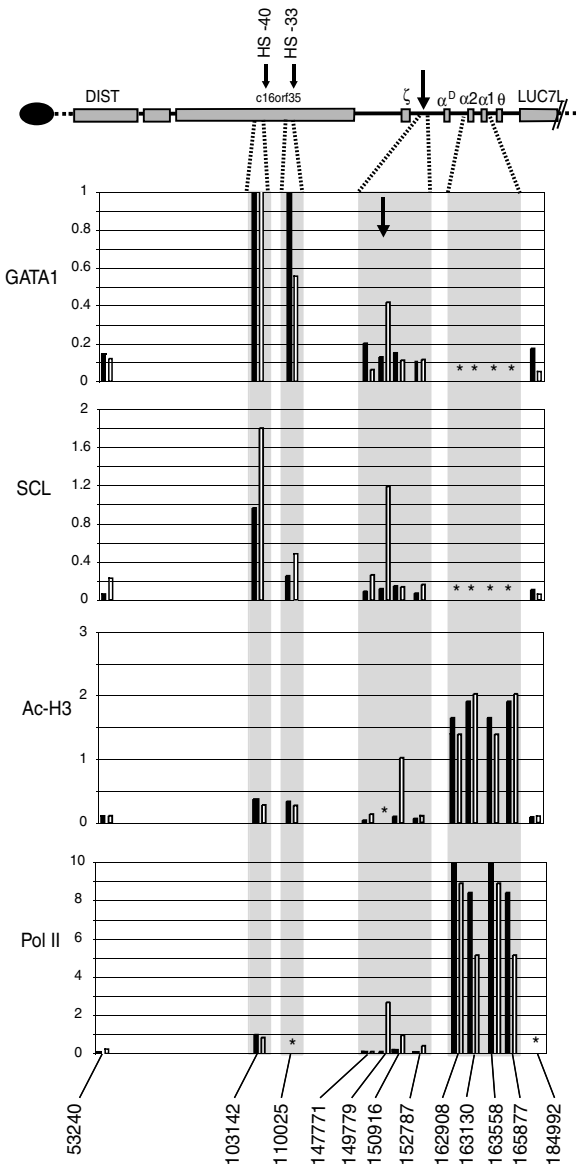

Fig. 3. Chromatin immunoprecipitation demonstrating the acquisition of a new transcription factor binding site (arrowed). The new binding site is located at coordinate 149709. Names of transcription factors and chromatin modifications are shown at left. Chromatin immunoprecipitation was performed as previously described (*10*) using primers and antibodies described in the supporting online material (*17*). The degree of enrichment in a normal individual (black columns) and in an individual with the $(\alpha\alpha)^T/(\alpha\alpha)^T$ genotype (white columns) is shown on the *y* axis, and coordinates of the regions sampled by QPCR are shown on the *x* axis. Asterisks indicate where insufficient primary cells were available for analysis.

5′-TAATAA-3′ (T allele) to 5′-TGATAA-3′ (C allele), potentially creating a new binding site for the key erythroid transcription factor GATA-1. Conventional in vitro electromobility gel shift assays and supershifts, using an antibody to GATA-1, demonstrated that this SNP creates a potential GATA-1 binding site (fig. S3). A chromatin immunoprecipitation (ChIP) profile using quantitative real-time PCR across the α-globin cluster (coordinates 53195 to 185030) showed that in addition to binding the known regulatory elements, GATA-1 also binds at the C allele of SNP 195 in vivo (Fig. 3). The C allele also nucleates the binding of a pentameric erythroid complex including the transcription factors SCL, E2A, LMO2, and Ldb-1 (Fig. 3), which are frequently found with GATA-1 at erythroid regulatory elements (*10*, *11*). ChIP profiles using antibodies that recognize modified histones [H4Ac, H3Ac, and H3K4me2 (Fig. 3 and fig. S4)] demonstrated that binding of GATA-1 at the C allele is associated with a new peak of active chromatin in the α-globin cluster. Finally, we showed that the C allele, unlike the T allele, binds RNA polymerase II (Fig. 3).

Expression of the α-globin genes normally occurs late in erythropoiesis after what appears to be a well-defined order of transcription factor binding to the upstream regulatory elements (MCS1 to MCS4), followed by recruitment of the pre-initiation complex and RNA polymerase II. These events are thought to result in the formation of a DNA/protein complex including one or more of the regulatory elements and the α-globin promoter(s) (*10*). We and others have shown that the insertion of active heterologous promoters (such as PGK Neo) in some regions of the α-globin cluster can disrupt α-globin expression, probably as a result of preferential interaction of the heterologous promoter with the upstream elements, out-competing the endogenous α-globin promoters (*12*–*14*). SNP 195 creates a new promoterlike element between the upstream regulatory elements and their cognate promoters. This element, when activated, causes significant down-regulation of the α^D, α2, and α1 genes that lie downstream (Fig. 1D), thereby causing α thalassemia.

These findings not only demonstrate an additional mechanism causing human genetic disease but also illustrate two important points when searching for SNPs that may influence gene expression (*9*). First, to distinguish functional from nonfunctional SNPs, it has been suggested that searches should be concentrated in areas of the genome likely to contain cis-regulatory elements (*8*) (such as multispecies conserved elements). The gain-of-function regulatory SNP (rSNP) identified here, located in a region of the α-globin cluster that we know may be deleted with no discernible effect on α-globin expression (Fig. 1) (*15*), demonstrates that SNPs in such areas should not be dismissed as of no potential importance. Second, the use of densely tiled arrays for analysis of transcription and ChIP profiles provides a rapid and efficient in vivo strategy to distinguish nonfunctional from functional rSNPs that may underlie the altered patterns of expression responsible for a wide range of human genetic diseases.

References and Notes

1. J. Flint *et al.*, *Nat. Genet.* **15**, 252 (1997).
2. J. R. Hughes *et al.*, *Proc. Natl. Acad. Sci. U.S.A.* **102**, 9830 (2005).
3. D. R. Higgs *et al.*, *Genes Dev.* **4**, 1588 (1990).
4. M. H. Steinberg *et al.*, Eds., *Disorders of Hemoglobin* (Cambridge Univ. Press, Cambridge, 2001).
5. D. R. Higgs *et al.*, *Blood* **73**, 1081 (1989).
6. A. P. Jarman, R. D. Nicholls, D. J. Weatherall, J. B. Clegg, D. R. Higgs, *EMBO J.* **5**, 1857 (1986).
7. R. Sachidanandam *et al.*, *Nature* **409**, 928 (2001).
8. J. C. Knight, *J. Mol. Med.* **83**, 97 (2005).
9. T. Pastinen, T. J. Hudson, *Science* **306**, 647 (2004).
10. E. Anguita *et al.*, *EMBO J.* **23**, 2841 (2004).
11. I. A. Wadman *et al.*, *EMBO J.* **16**, 3145 (1997).
12. C. Esperet *et al.*, *J. Biol. Chem.* **275**, 25831 (2000).
13. A. Leder, C. Daugherty, B. Whitney, P. Leder, *Blood* **90**, 1275 (1997).
14. E. Anguita *et al.*, *Blood* **100**, 3450 (2002).
15. P. Winichagoon *et al.*, *Nucleic Acids Res.* **10**, 5853 (1982).
16. P. Vyas *et al.*, *Cell* **69**, 781 (1992).
17. Materials and methods are available as supporting material on *Science* Online.
18. M.D.G. is a Ph.D. student in Pharmacology and Experimental and Clinical Therapy at the University of Turin, Italy. We thank J. Sloane Stanley, J. Sharpe, J. Green, J. Brown, N. Ventress, K. Clark, and the Oxford Computational Biology Research Group for technical support. V.V. is supported by the Thailand Research Fund.

Supporting Online Material

www.sciencemag.org/cgi/content/full/312/5777/1215/DC1
Materials and Methods
Figs. S1 to S4
Tables S1 and S2
References

21 February 2006; accepted 25 April 2006
10.1126/science.1126431

AXR4 Is Required for Localization of the Auxin Influx Facilitator AUX1

S. Dharmasiri,[1*†] R. Swarup,[2*] K. Mockaitis,[1*] N. Dharmasiri,[1†] S. K. Singh,[3] M. Kowalchyk,[3] A. Marchant,[3] S. Mills,[4] G. Sandberg,[3] M. J. Bennett,[2‡] M. Estelle[1‡]

The AUX1 and PIN auxin influx and efflux facilitators are key regulators of root growth and development. For root gravitropism to occur, AUX1 and PIN2 must transport auxin via the lateral root cap to elongating epidermal cells. Genetic studies suggest that AXR4 functions in the same pathway as AUX1. Here we show that AXR4 is a previously unidentified accessory protein of the endoplasmic reticulum (ER) that regulates localization of AUX1 but not of PIN proteins. Loss of AXR4 resulted in abnormal accumulation of AUX1 in the ER of epidermal cells, indicating that the *axr4* agravitropic phenotype is caused by defective AUX1 trafficking in the root epidermis.

Polar auxin transport plays an important role in a wide variety of plant growth processes (*1*, *2*). Studies indicate that the polarity of auxin transport is determined by the asymmetric localization of members of the PIN family of auxin efflux facilitators (*1*, *2*). The polarity of PIN localization can change rapidly in response to environmental and developmental signals, resulting in localized changes in auxin concentration and distribution (*3*–*5*). In the case of PIN1, proper localization is associated with continuous recycling of the protein through the endomembrane system and the activity of a guanosine diphosphate/guanosine triphosphate exchange factor protein called GNOM (*6*, *7*). Recent studies indicate that the auxin influx facilitator AUX1 is also asymmetrically localized in some root tissues (*8*). For example, AUX1 is preferentially localized to the upper plasma membrane of protophloem cells, where it is proposed to facilitate acropetal transport of auxin from the phloem into the root apex. However, the proteins that regulate AUX1 localization are not known.

The *AXR4* gene was identified in a screen for *Arabidopsis* mutants that are resistant to the auxin 2,4-D (*9*, *10*). The *axr4* phenotype is markedly similar to *aux1*, with defects in lateral root formation and gravitropism (*9*–*13*). The gravitropic defects of *aux1* and *axr4*, but not of the auxin response mutants *axr2* and *axr3*, can be rescued by the membrane-permeable auxin 1-naphthaleneacetic acid (*14*, *15*). Similarly, *aux1* and *axr4* confer selective resistance to various auxins (*14*, *15*). Genetic analysis of *aux1* *axr4* double mutants suggests that these two genes function in the same pathway to regulate auxin-related developmental processes in the primary root (*11*). To probe this functional relationship further, we performed a principal component analysis on indole-related metabolites from root tissue of wild-type and various mutant genotypes, including *axr4* and *aux1*. The results (Fig. 1A) indicate that *aux1* and *axr4* cluster together, implying that these mutations disrupt a related biological process. Neither mutant overlaps with any of the auxin signaling mutants (*axr1*, *axr2*, and *axr3*), supporting the view that like *aux1*, the *axr4* mutation disrupts a process distinct from auxin signaling.

To investigate the function of *AXR4*, we isolated the gene by positional cloning. Fine mapping localized the gene to a 750-kb region on chromosome 1. We then used ATH1 (Affymetrix) whole-genome microarrays to compare gene expression in wild-type and *axr4* roots. The results (Fig. 1B) show that the expression profiles in the two genotypes are very similar. However, expression of the *At1g54990* gene was decreased by a factor of ~6 in the mutant as compared to the wild type. Because this gene lies within the interval that includes *AXR4*, we next characterized *At1g54990* in four *axr4* alleles. Sequencing of *At1g54990* from the *axr4-1* and *axr4-2* alleles, mutants derived from T-DNA–mutagenized and γ-irradiated populations, revealed the presence of an insertion at positions 954 and 849, respectively (Fig. 1C). Sequence analysis of two new ethylmethane sulfonate–induced mutants revealed point mutations at positions 141 (*axr4-3*) and 412 (*axr4-4*), each of which result in stop codons. To confirm that *At1g54990* is *AXR4*, we introduced the *At1g54990* cDNA under control of the *cauliflower mosaic virus* (*CaMV*) *35S* promoter into *axr4-2* plants. When these transgenic plants were transferred to medium containing auxin, they responded like the wild-type line, with decreased root elongation (Fig. 1D). Together with our analysis of the *axr4* alleles, these results indicate that *At1g54990* encodes *AXR4*.

The expression of *AXR4* was initially analyzed using two different approaches: reverse transcription–polymerase chain reaction (RT-

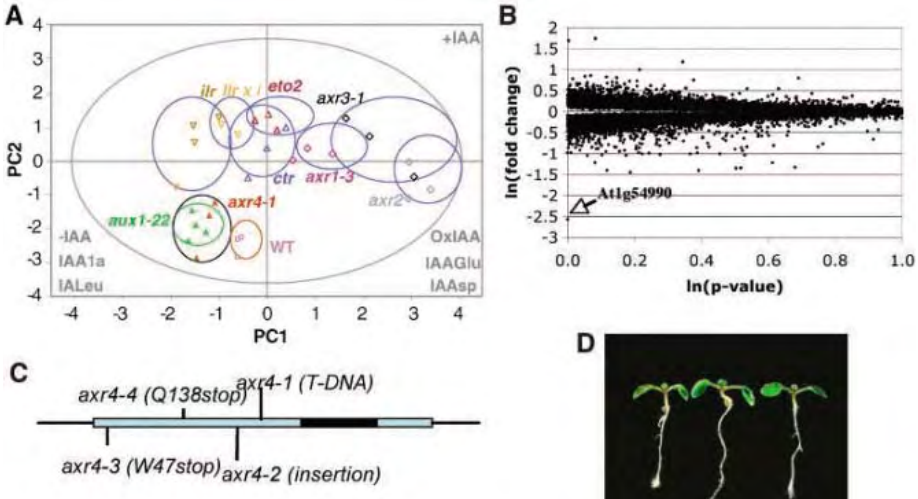

Fig. 1. *AXR4* encodes a previously unidentified protein required for auxin influx. (**A**) Principal component analysis of auxin (IAA, indole-3-acetic acid) and its metabolites in various genotypes. (**B**) Transcript profile variation between wild-type (wt) and *axr4-2* roots. Quadruplicate microarray samples (*24*) were analyzed. Natural logarithm of the mean signal change (*axr4*/wt) is plotted against the significance of signal variation (natural logarithm of *P*-value). Arrow indicates data point for At1g54990, which showed expression in the mutant that was reduced relative to wild-type levels by a factor of 5.95 ($P = 9.64 \times 10^{-4}$). (**C**) Structure of the *AXR4* gene with the positions of the *axr4* mutant alleles indicated. Colored bars indicate exons and the black bar, an intron. (**D**) Phenotype of *Col-0*, *axr4-2*, and *axr4-2 35S::AXR4* (left to right) seedlings on auxin. Four-day-old seedlings were transferred to medium containing 85 nM 2,4-D and photographed after 3 days.

[1]Department of Biology, Indiana University, Bloomington, IN 47405, USA. [2]School of Biosciences, University of Nottingham, Loughborough LE12 5RD, UK. [3]Umeå Plant Science Centre, SLU, Umeå, Sweden. [4]School of Computer Science and Information Technology, University of Nottingham, Nottingham NG7 2UH, UK.

*These authors contributed equally to this work.
†Present address: Department of Biology, Texas State University–San Marcos, San Marcos, TX 78666, USA.
‡To whom correspondence should be addressed. E-mail: malcolm.bennett@nottingham.ac.uk (M.J.B.), maestell@indiana.edu (M.E.)

PCR) (Fig. 2A) and promoter reporter experiments using transgenic lines expressing GUS under the control of the *AXR4* promoter (Fig. 2, B to D). RT-PCR experiments indicated that *AXR4* mRNA is most abundant in root tissue, with lesser amounts in rosette leaves, stems, and flowers and very little in mature siliques. Examination of the *AXR4::GUS* lines indicated that expression of *AXR4* is highest in the root tip (Fig. 2B). We also observed GUS staining in the vascular tissue of the root and hypocotyl and at sites of lateral root initiation (Fig. 2, C and D).

AXR4 appears to be unique in the *Arabidopsis* genome. A single copy of an *AXR4*-like sequence is present in all plant genomes sequenced to date (fig. S1), indicating that it is conserved among higher plants. AXR4 is 473 amino acids in length and is predicted to contain a single transmembrane domain close to the N terminus, suggesting that it is an integral membrane protein (*16*) (fig. S2). In addition, the protein contains an α/β hydrolase fold, indicating that it is a member of the α/β hydrolase superfamily. To investigate the subcellular localization of AXR4, we generated *35S::AXR4-GFP* (green fluorescent protein) and *AXR4::AXR4-GFP* constructs and introduced them into *axr4-1* and *axr4-2* plants. The *axr4-1 35S::AXR4-GFP* and *axr4-2 AXR4::AXR4-GFP* plants displayed a wild-type phenotype, indicating that the AXR4-GFP fusion is functional (fig. S3). To investigate whether AUX1 and AXR4 are colocalized, we crossed the *35S::AXR4-GFP* line with a line carrying the *AUX1::AUX1-YFP* (yellow fluorescent protein) transgene (*17*). Confocal laser microscopy of root cells of F_1 seedlings (*8*) revealed that AXR4-GFP does not colocalize with AUX1 at the plasma membrane (Fig. 2, G to I), suggesting that AXR4 is localized to another cellular membrane. To investigate this possibility, we tested colocalization of AXR-GFP with a selection of endomembrane compartment markers (fig. S4). AXR4-GFP was detected at the periphery of the cell and surrounding the nucleus (Fig. 2, F and G), mimicking the distribution of markers for the endoplasmic reticulum (ER) such as BiP (*18*) (Fig. 2, J to L) rather than the punctate pattern exhibited by the golgi apparatus marker γ-COP (fig. S4). Pixel correlation analysis (fig. S5) confirmed that the AXR4-GFP signal overlaps most significantly with markers for the ER (fig. S4), strongly suggesting that AXR4 is localized to the ER. The localization of AXR4 to the ER has also been independently determined using a proteomics-based technique termed LOPIT (localization of organelle proteins by isotope tagging) (*19*).

Although AXR4 and AUX1 do not colocalize, the genetic and physiological studies described above suggest that the two proteins function together to regulate auxin transport. Given its localization to the ER, we examined whether AXR4 might regulate AUX1 trafficking. The location of AUX1 was determined in wild-type and *axr4* roots. Localization of AUX1 to the plasma membrane is asymmetric (at the upper side) in wild-type protophloem cells (Fig. 3C), mainly axial (at both upper and lower sides) in the epidermis (Fig. 3A), and without clear polarity in the lateral root cap (LRC) (Fig. 3A). The asymmetric localization of AUX1 was abolished in *axr4* root epidermal cells (Fig. 3B; compare to Fig. 3A), whereas AUX1 was localized to an intracellular compartment in *axr4* protophloem cells (Fig. 3G; compare to Fig. 3C). AUX1 localization was not markedly altered in the LRC of *axr4* roots, suggesting

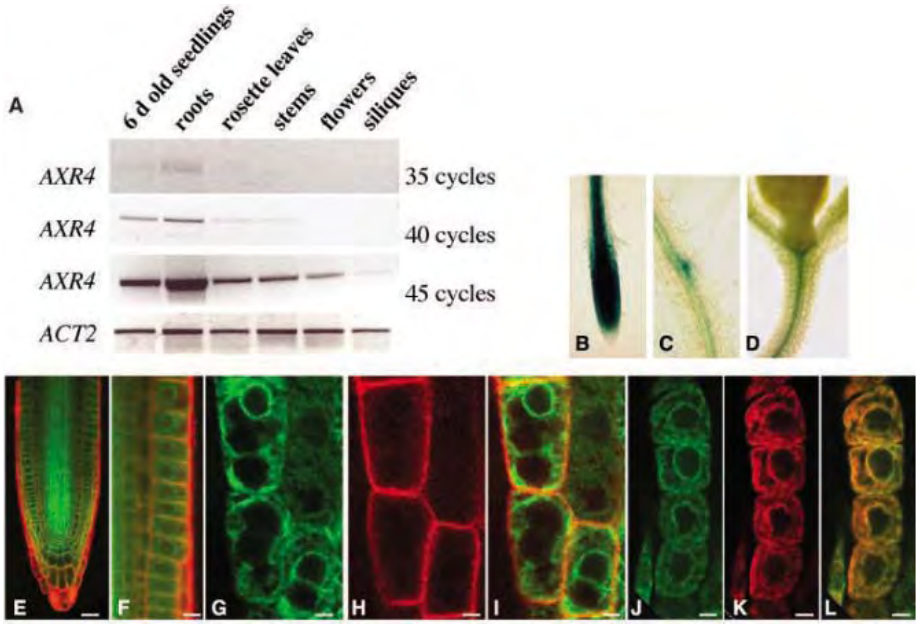

Fig. 2. Expression of *AXR4* and localization of the AXR4 protein. (**A**) *AXR4* RNA levels in various tissues determined by RT-PCR. (**B** to **D**) *AXR4::GUS* seedlings showing *AXR4* expression in the root tip (B), stele and lateral root primorida (C), and hypocotyl (D). (**E**) AXR4-GFP localization in root cells using confocal imaging. (**F**) Expression of AXR4-GFP around nuclei and at cell margins. (**G**) AXR4-GFP localization in root epidermal cells. (**H**) AUX1-YFP localization in root epidermal cells. (**I**) Superimposed confocal images of AXR4-GFP and AUX1-YFP localization. (**J**) AXR4-GFP localization in root cells using antibodies to GFP (anti-GFP). (**K**) BiP localization in root cells using anti-BiP. (**L**) Superimposed confocal images of AXR4-GFP and BiP localization.

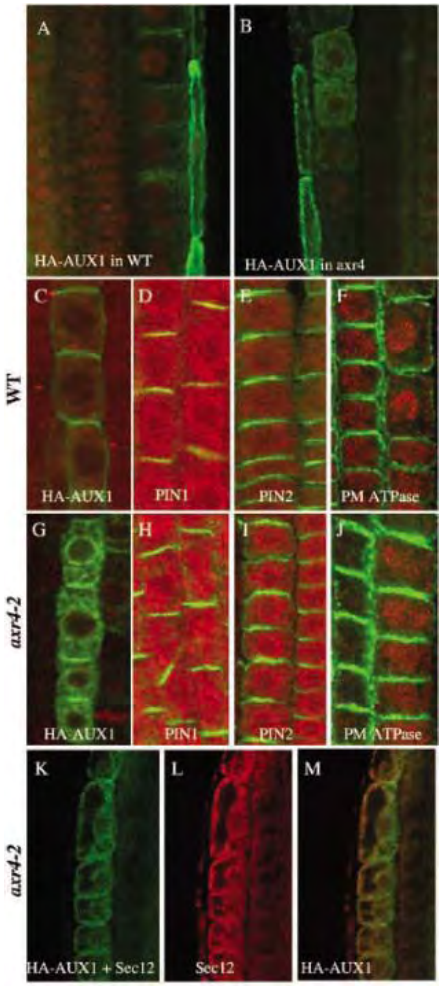

Fig. 3. ER-localized AXR4 is required for AUX1 plasma membrane trafficking. (**A** and **B**) Hemagglutinin (HA)–AUX1 localization in the LRC and epidermis of *Col-0* (A) and *axr4-2* (B). (**C** and **G**) HA-AUX1 localization in the protophloem of *Col-0* (C) and *axr4-2* (G). (**D** and **H**) PIN1 localization in *Col-0* (D) and *axr4-2* (H). (**E** and **I**) PIN2 localization in *Col-0* (E) and *axr4-2* (I). (**F** and **J**) Localization of plasma membrane H^+-ATPase in *Col-0* (F) and *axr4-2* (J). (**K**) HA-AUX1 localization in *axr4-2*. (**L**) Sec12 localization in *axr4-2*. (**M**) Superimposed images of HA-AUX1 and Sec12 in *axr4-2*.

that AXR4 may not be required for AUX1 trafficking in these cells. However, additional studies are required to confirm this possibility. These observations prompted us to investigate whether the trafficking of other membrane proteins is also dependent on AXR4 function. The auxin efflux facilitator PIN1 is normally found on the lower side of vascular cells (*5*) (Fig. 3D), whereas PIN2 is localized to the lower side of cortical cells and the upper side of epidermal cells (*5*) (Fig. 3E). We found that both PIN1 and PIN2 are localized normally in *axr4* roots (Fig. 3, H and I). The localization of other plasma membrane proteins such as proton adenosine triphosphatase (PM H^+-ATPase) is also normal in the *axr4* mutant (Fig. 3, F and J). The *axr4* mutation therefore appears to selectively disrupt trafficking of AUX1. We next investigated where AUX1 accumulates in the *axr4* background by using a selection of endomembrane compartment markers (fig. S6). Pixel correlation analysis revealed that AUX1 overlaps most significantly with markers from the ER (fig. S6) like Sec12 (Fig. 3, K to M), suggesting that loss of AXR4 causes AUX1 to accumulate in the ER.

Recent work has demonstrated that for root gravitropism to occur, AUX1 must be expressed in both the LRC and expanding epidermal cells in order to transport gravity-induced lateral auxin gradients from gravisensing columella cells to graviresponsive epidermal cells (*20*). Localization results suggest that the gravitropic defect of *axr4* seedlings is caused by the failure to traffic AUX1 to the plasma membrane in the epidermis (Fig. 3B). As a result, the *axr4* mutation is expected to disrupt the AUX1-dependent transfer of the lateral auxin gradient from the LRC to expanding epidermal cells. Consistent with this model, the auxin-responsive reporter *IAA2::GUS* is expressed normally in the LRC but is almost undetectable in the epidermis of the *axr4* mutant (compare fig. S7, A and C). In contrast, *IAA2::GUS* expression is not detected in either the LRC or epidermal cells in the *aux1* background (fig. S7B). The pattern of *IAA2::GUS* expression is consistent with the fact that AUX1 remains functional in the *axr4* LRC but not in the epidermal cells. The *axr4* mutant is resistant to 2,4-D, and because AUX1 may be functional in the LRC in *axr4* mutants, this would suggest that functional AUX1 in the LRC alone is not sufficient for 2,4-D–sensitive root growth. We tested this possibility by transactivating AUX1 in the LRC or LRC plus epidermal cells (fig. S8) using Gal4 driver lines M0013 and J0951, respectively (*20*). When *AUX1* was expressed in LRC alone using the GAL4 line M0013, the *aux1* M0013≫AUX1 line exhibited an auxin-resistant root phenotype like that of *axr4* (fig. S8, E and F) (*20*). However, when *AUX1* was also expressed in the epidermal cells using the GAL4 line J0951, normal auxin response was restored (fig. S8, B and F). Our results suggest that the *axr4* phenotype, including auxin-resistant root growth and reduced gravitropism, is caused by defective AUX1 trafficking in epidermal cells.

AXR4 joins a growing list of ER accessory proteins that facilitate trafficking of plasma membrane proteins through the secretory pathway (*21–23*). In yeast cells, the Shr3 protein acts as a molecular chaperone of amino acid permeases, preventing their inappropriate aggregation in the ER membrane (*21*). Other structurally unrelated accessory proteins also appear to function as molecular chaperones of their cognate substrates (*21*). Although unrelated to Shr3p, AXR4 may have a similar function. Alternatively, because AXR4 is a member of the α/β hydrolase superfamily, it may facilitate AUX1 polar trafficking by posttranslationally modifying AUX1, causing it to be recognized as cargo destined for a particular plasma membrane face of the plant cell. However, validation of this or other mechanisms awaits further experimentation.

References and Notes

1. J. Friml, K. Palme, *Plant Mol. Biol.* **49**, 273 (2002).
2. R. Swarup, M. Bennett, *Dev. Cell* **5**, 824 (2003).
3. E. Benkova *et al.*, *Cell* **115**, 591 (2003).
4. D. Reinhardt *et al.*, *Nature* **426**, 255 (2003).
5. I. Blilou *et al.*, *Nature* **433**, 39 (2005).
6. N. Geldner *et al.*, *Cell* **112**, 219 (2003).
7. N. Geldner, J. Friml, Y. D. Stierhof, G. Jurgens, K. Palme, *Nature* **413**, 425 (2001).
8. R. Swarup *et al.*, *Genes Dev.* **15**, 2648 (2001).
9. L. Hobbie, M. Estelle, *Plant J.* **7**, 211 (1995).
10. C. Simmons, F. Migliaccio, P. Masson, T. Caspar, D. Soll, *Physiol. Plant.* **93**, 790 (1995).
11. C. Timpte, C. Lincoln, F. B. Pickett, J. Turner, M. Estelle, *Plant J.* **8**, 561 (1995).
12. F. B. Pickett, A. K. Wilson, M. Estelle, *Plant Physiol.* **94**, 1462 (1990).
13. J. L. Mullen *et al.*, *Plant Physiol.* **118**, 1139 (1998).
14. M. Yamamoto, K. T. Yamamoto, *J. Plant Res.* **112**, 391 (1999).
15. A. Marchant *et al.*, *EMBO J.* **18**, 2066 (1999).
16. R. Schwacke *et al.*, *Plant Physiol.* **131**, 16 (2003).
17. R. Swarup *et al.*, *Plant Cell* **16**, 3069 (2004).
18. A. J. Crofts, N. Leborgne-Castel, M. Pesca, A. Vitale, J. Denecke, *Plant Cell* **10**, 813 (1998).
19. T. B. J. Dunkley *et al.*, *Proc. Natl. Acad. Sci. U.S.A.* **103**, 6518 (2006).
20. R. Swarup *et al.*, *Nat. Cell Biol.* **7**, 1057 (2005).
21. J. Kota, P. O. Ljungdahl, *J. Cell Biol.* **168**, 79 (2005).
22. E. Gonzalez, R. Solano, V. Rubio, A. Leyva, J. Paz-Ares, *Plant Cell* **17**, 3500 (2005).
23. M. Kottgen *et al.*, *EMBO J.* **24**, 705 (2005).
24. Materials and methods are available as supporting material on *Science* Online.

25. This work was supported by grants from the NIH (to M.E.), Biotechnology and Biological Sciences Research Council (BBSRC) Plant Microbial Sciences (to M.J.B. and R.S.), BBSRC Centres for Integrative Systems Biology (to S.M. and M.J.B.), BBSRC JREI2003 (to M.J.B.), Gatsby Charitable Foundation (to M.J.B.), The University of Nottingham (to M.J.B. and R.S.), European Space Agency (to M.J.B.), The Swedish Foundation for Strategic Research (to A.M.), and Swedish Research Council (to S.K.S.). Microarray studies were done at the Center for Medical Genomics at Indiana University School of Medicine. The Center for Medical Genomics is supported in part by grants from the Indiana 21st Century Research and Technology Fund and the Indiana Genomics Initiative of Indiana University (INGEN), which is supported in part by the Lilly Endowment. We are grateful to R. Jerome for processing of microarray samples and to M. Stephens for assistance with array analyses.

Supporting Online Material

www.sciencemag.org/cgi/content/full/312/5777/1122847/DC1
Materials and Methods
SOM Text
Figs. S1 to S8
References

21 November 2005; accepted 21 April 2006
Published online 11 May 2006;
10.1126/science.1122847
Include this information when citing this paper.

CRACM1 Is a Plasma Membrane Protein Essential for Store-Operated Ca^{2+} Entry

M. Vig,[1]* C. Peinelt,[2] A. Beck,[2] D. L. Koomoa,[2] D. Rabah,[1] M. Koblan-Huberson,[1] S. Kraft,[1] H. Turner,[2] A. Fleig,[2] R. Penner,[2]* J.-P. Kinet[1]*

Store-operated Ca^{2+} entry is mediated by Ca^{2+} release–activated Ca^{2+} (CRAC) channels following Ca^{2+} release from intracellular stores. We performed a genome-wide RNA interference (RNAi) screen in *Drosophila* cells to identify proteins that inhibit store-operated Ca^{2+} influx. A secondary patch-clamp screen identified CRACM1 and CRACM2 (CRAC modulators 1 and 2) as modulators of *Drosophila* CRAC currents. We characterized the human ortholog of CRACM1, a plasma membrane–resident protein encoded by gene *FLJ14466*. Although overexpression of CRACM1 did not affect CRAC currents, RNAi-mediated knockdown disrupted its activation. CRACM1 could be the CRAC channel itself, a subunit of it, or a component of the CRAC signaling machinery.

Receptor-mediated signaling in nonexcitable cells, immune cells in particular, involves an initial rise in intracellular Ca^{2+} due to release from the intracellular stores. The resulting depletion of the intracellular stores induces Ca^{2+} entry through the plasma membrane through CRAC channels (*1–4*). This phenomenon is central to many physiological processes such as T cell proliferation, gene transcrip-

tion, and cytokine release (*3*, *5*–*7*). Biophysically, CRAC currents have been well characterized (*2*, *8*, *9*), but the identity of the CRAC channel itself and the pathway resulting in its activation are still unknown. Recently, STIM1 (for stromal interaction molecule in *Drosophila*) was identified as an essential component of store-operated calcium entry (*10*, *11*). This protein is located in intracellular compartments that likely represent parts of the endoplasmic reticulum (ER). It has a single transmembrane-spanning domain with a C-terminal Ca^{2+}-binding motif that appears to be crucial for its hypothesized function as the ER sensor for luminal Ca^{2+} concentration. When stores become depleted, STIM1 redistributes into distinct structures (punctae) that move toward and accumulate underneath the plasma membrane. Whether or not STIM1 actually incorporates into the plasma membrane is controversial (*10*, *12*, *13*). Although STIM1 is required to activate CRAC currents, its presence or even its translocation appears not to be sufficient to mediate CRAC activation, because lymphocytes from patients with severe combined immunodeficiency (SCID) appear to have normal amounts of STIM1 levels and normal function, yet fail to activate CRAC channels (*14*). This suggests that other molecular components may participate in the store-operated Ca^{2+} entry mechanism.

To identify genes encoding the CRAC channel or other proteins involved in its regulation, we performed a high-throughput, genome-wide RNA interference (RNAi) screen in *Drosophila* S2R+ cells. The effect of knockdown of each of the ~23,000 genes was tested by fluorescence measurements of intracellular Ca^{2+} concentration in 384-well microplates with an automated fluorometric imaging plate reader (FLIPR, Molecular Devices). Changes in $[Ca^{2+}]_i$ were measured in response to the commonly used SERCA [sarcoplasmic and endoplasmic reticulum calcium adenosine triphosphatase (ATPase)] inhibitor thapsigargin, which causes depletion of Ca^{2+} from intracellular stores. An example of responses from this primary screen is illustrated in Fig. 1A, obtained from microplate no. 60. All 63 plates contained wells in which double-stranded RNA (dsRNA) against *Rho1* served as negative control and dsRNA against *stim1* as positive control. Higher resolution graphs of the real-time $[Ca^{2+}]_i$ imaging data are shown in Fig. 1, B and C, from cells treated with dsRNA against *Rho1* (mock) and *stim1*, as well as two genes we later identified as CRAC modulators 1 and 2 (CRACM1 and CRACM2). On the basis of inhibitory efficacy relative to positive and negative controls, we identified ~1500 genes that reduced Ca^{2+} influx to varying degrees (table S1). After eliminating numerous genes based on artifactual fluorescence signals or because they represent known housekeeping genes, cell cycle regulators, and so on, we eventually arrived at 27 candidate genes (table S2) that were subsequently evaluated in a secondary screen using single-cell patch-clamp assays.

From the secondary patch-clamp screen, we identified two novel genes that are essential for CRAC channel function, CRACM1 (encoded by *olf186-F* in *Drosophila* and *FLJ14466* in human) and CRACM2 (encoded by *dpr3* in *Drosophila*, with no human ortholog). We measured CRAC currents in *Drosophila* Kc cells after inositol 1,4,5-trisphosphate (IP_3)–mediated depletion of Ca^{2+} from intracellular stores. Both untreated control wild-type cells and cells treated with an irrelevant dsRNA against *Rho1* (mock) responded by rapidly activating a Ca^{2+} current with the time course (Fig. 1D) and inwardly rectifying current-voltage (*I*/*V*) relation (Fig. 1E) typical of I_{CRAC} in mammalian (*2*) and *Drosophila* (*15*) cell types. In contrast, CRAC currents were essentially abolished in cells treated with dsRNA for CRACM1 and CRACM2. In some of the experiments on CRACM1, we also applied ionomycin (10 μM) extracellularly on top of the 20 μM IP_3 included in the patch pipette to ensure complete store depletion, but this also failed to induce I_{CRAC} (fig. S1C). Similarly, CRAC currents were also absent when passive store depletion was induced by the Ca^{2+} chelator

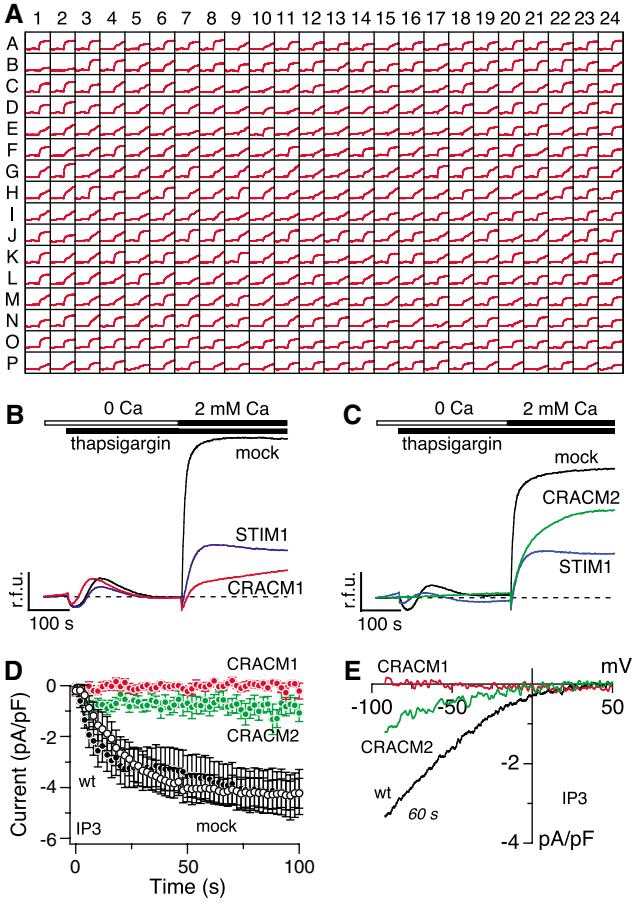

Fig. 1. Identification of CRACM1 and CRACM2 as crucial regulators of store-operated Ca^{2+} entry in *Drosophila*. (**A**) Ca^{2+} signals measured in *Drosophila* S2R+ cells in the primary high-throughput screen using FLIPR. Representative FLIPR raw data file showing 384 mini-graphs, each of which represents fluo-4 fluorescence change in an individual well with respect to time. Each plate contained the negative control dsRNA *Rho1* in well A1 and the positive control dsRNA *stim1* in well B1. (**B**) Fluo-4 fluorescence changes in relative fluorescence units (r.f.u.) obtained from cells treated with the indicated dsRNAs. Cells were kept in Ca^{2+}-free solution and exposed to thapsigargin (2 μM), followed by addition of 2 mM Ca^{2+}. The traces are representative of two independent repeats of the primary screen. (**C**) Same protocol as in (B) but for cells treated with CRACM2 dsRNA. (**D**) Normalized average time course of IP_3-induced (20 μM) I_{CRAC} measured in *Drosophila* Kc cells. Currents of individual cells were measured at −80 mV, normalized by their respective cell size, averaged and plotted versus time (±SEM). Cytosolic calcium was clamped to 150 nM with 10 mM BAPTA and 4 mM $CaCl_2$. Traces correspond to untreated control [wild type (wt), black filled circles, n = 10); Rho1 dsRNA (mock, open circles, n = 8); CRACM1 dsRNA (red circles, n = 6); and CRACM2 dsRNA (green circles, n = 9)]. (**E**) Averaged current-voltage (*I*/*V*) data traces of I_{CRAC} extracted from representative cells at 60 s for currents evoked by 50-ms voltage ramps from −100 to +100 mV with leak currents subtracted and normalized to cell size (pF). Traces correspond to untreated control (wt, n = 9); CRACM1 dsRNA (n = 5); and CRACM2 dsRNA (n = 6).

[1]Department of Pathology, Beth Israel Deaconess Medical Center and Harvard Medical School, Boston, MA 02215, USA. [2]Center for Biomedical Research at The Queen's Medical Center and John A. Burns School of Medicine at the University of Hawaii, Honolulu, HI 96813, USA.

*To whom correspondence should be addressed. E-mail: mvig@bidmc.harvard.edu (M.V.); rpenner@hawaii.edu (R.P.); jkinet@bidmc.harvard.edu (J.-P.K.)

BAPTA [(1,2-bis(*o*-aminophenoxy)ethane-*N*,*N*,*N*′,*N*′-tetraacetic acid)] (fig. S1, A and B).

We studied the human ortholog of CRACM1, a 37.7-kD protein encoded by gene *FLJ14466*, to confirm that its function is conserved across species and that it is involved in store-operated Ca^{2+} entry. We used small interfering RNA (siRNA)–mediated silencing of human CRACM1 in human embryonic kidney cells (HEK293) and human T cells (Jurkat). The selective knockdown of CRACM1 message was confirmed by semiquantitative reverse transcription polymerase chain reaction (RT-PCR) analysis (Fig. 2A). Two different CRACM1-specific siRNA sequences caused a 60 to 70% inhibition of calcium influx in response to thapsigargin-induced store depletion in HEK293 cells (Fig. 2B). Patch-clamp recordings obtained from siRNA-treated cells, responding to intracellular IP_3 perfusion, demonstrated a nearly complete inhibition of CRAC currents (Fig. 2, D and E). In Jurkat cells, siRNA-mediated inhibition of Ca^{2+} influx was close to 20% (Fig. 2C) and not as dramatic as in the HEK293 cells. However, I_{CRAC} in Jurkat cells was effectively reduced by both siRNA sequences (Fig. 2, F and G). The differences in the efficacy of suppressing the changes in $[Ca^{2+}]_i$ in HEK293 and Jurkat cells (see Fig. 2, B and C) are likely due to the different magnitudes of I_{CRAC} in these two cell types. CRAC current densities in HEK293 cells (~0.5 pA/pF) are much smaller than typically seen in Jurkat cells (~2.5 pA/pF), and a further inhibition may explain the more dramatic reduction in the Ca^{2+} signal than that observed in Jurkat cells (note that the remaining CRAC current densities in siRNA-treated Jurkat cells, while strongly reduced, are ~0.4 pA/pF and comparable to the normal CRAC current densities of untreated HEK293 cells). Taken together, these data indicate that CRACM1 is also a key modulator of store-operated CRAC currents in human cells.

Given that the knockdown of CRACM1 inhibited CRAC activation, we wanted to know whether overexpression would enhance Ca^{2+} influx and CRAC current densities. HEK293, Jurkat, and RBL-2H3 cells were infected with a Myc-tagged CRACM1 and green fluorescent protein (GFP) retrovirus, and overexpression of the protein was confirmed in HEK293 cells by immunoprecipitation followed by Western blotting (Fig. 3A). However, we did not detect any increase in CRAC current amplitudes above control levels in either HEK293 (Fig. 3B) or Jurkat cells (fig. S2A) and only a slight increase in RBL cells (fig. S2B). These data suggest that CRACM1, although necessary for CRAC activation, does not in and of itself generate significantly larger CRAC currents.

An important question is whether CRACM1 localizes to the ER (as does STIM1) or to the plasma membrane. To address this question, we tagged CRACM1 on either end (Myc–C terminus and flag–N terminus) and transfected the constructs into HEK293 cells. After 24 hours, immunofluorescence confocal analysis revealed no staining in intact cells expressing either construct, which suggested that both tags are intracellular. After permeabilizing the cells, both constructs were detected by the fluorescent antibody and showed predominant peripheral staining of the plasma membrane (Fig. 3, C and D). These data fit well with the hydropathy profile of CRACM1, which predicts a topology of four transmembrane domains, with both ends facing the cytosol (fig. S2C).

In summary, our results demonstrate that the protein CRACM1 is essential for store-operated Ca^{2+} influx via CRAC channels. Although the overexpression of CRACM1 does not alter the magnitude of CRAC currents, the plasma membrane localization of this protein and the presence of multiple transmembrane domains point

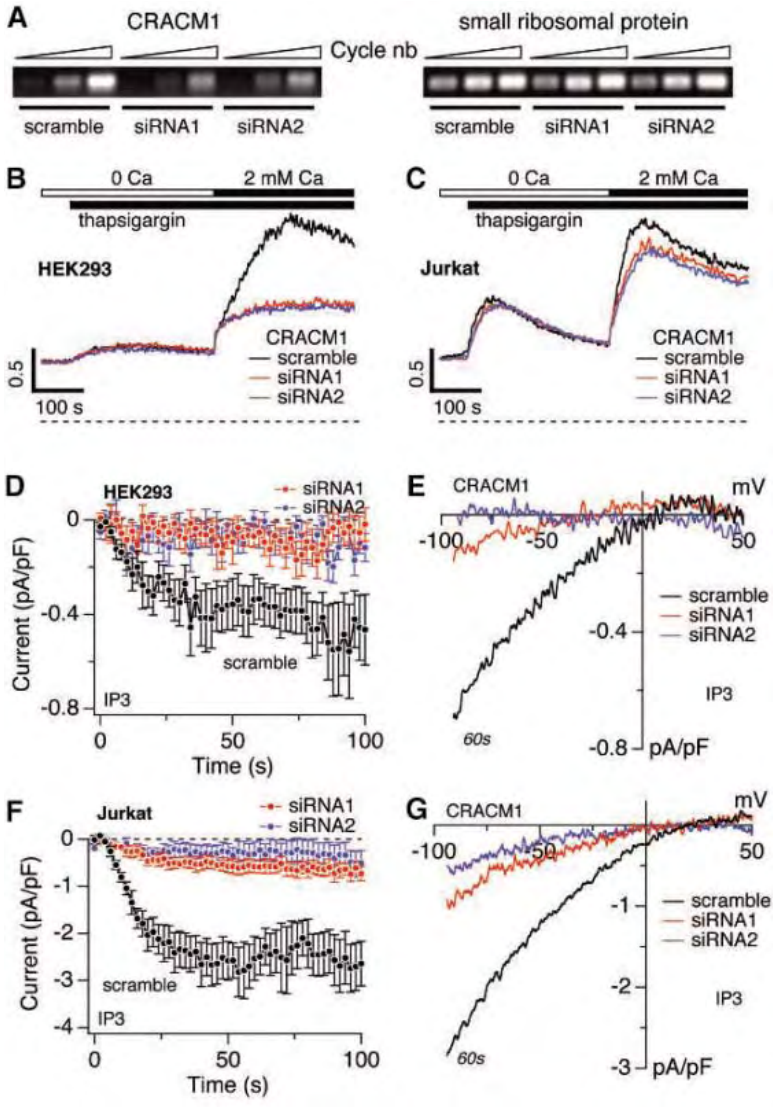

Fig. 2. Suppression of store-operated Ca^{2+} entry and I_{CRAC} by CRACM1 siRNA. (**A**) (Left) RT-PCR of CRACM1 mRNA from HEK293 cells infected with the indicated CRACM1-specific siRNAs and a scrambled sequence control. (Right) Control with primers specific for small ribosomal protein. (**B**) Fura 2–AM (pentaacetoxymethyl ester) fluorescence measurements of $[Ca^{2+}]_i$ in cells treated with scramble (control) or the two CRACM1-specific siRNAs in HEK293 cells. Cells were kept in Ca^{2+}-free solution and exposed to thapsigargin (2 μM), followed by addition of 2 mM Ca^{2+}. The traces are representative of three independent experiments. (**C**) Same protocol as in (B), but for Jurkat cells. The traces are averages of three independent experiments. (**D**) Normalized average time course of IP_3-induced (20 μM) I_{CRAC} measured in HEK293 cells treated with the indicated siRNAs (n = 9 to 13 for each group). $[Ca^{2+}]_i$ was clamped to near zero by 10 mM BAPTA. (**E**) Current-voltage (I/V) data traces of I_{CRAC} from representative cells at 60 s for currents evoked by 50-ms voltage ramps from −100 to +100 mV in cells treated with the indicated siRNAs (n = 7 to 10). (**F** and **G**) Same as panel (D) and (E), but for Jurkat cells (n = 8 to 9).

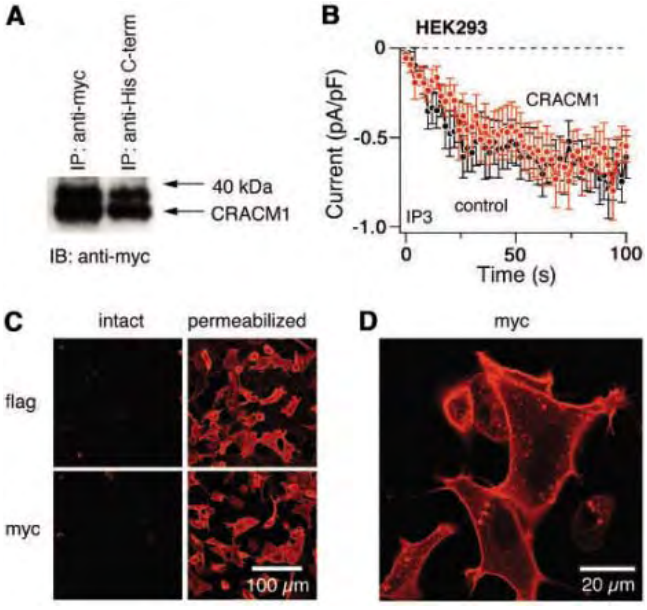

Fig. 3. Overexpression of CRACM1. (**A**) Analysis of HEK293 cells for overexpression of CRACM1 by immunoprecipitation with antibodies against Myc or C-terminal His and immunoblotting with antibody against Myc. Control immunoprecipitation from empty vector-transfected cells did not show any bands. (**B**) Normalized average time course of IP_3-induced (20 μM) I_{CRAC} measured in HEK293 cells. Currents of individual cells were measured at –80 mV, normalized by their respective cell size, averaged, and plotted against time (± SEM). Cytosolic calcium was clamped to near zero by using 10 mM BAPTA. Traces correspond to cells transfected with GFP alone (control, black circles, $n = 13$) and cells transfected with GFP plus CRACM1 (red circles, $n = 14$). (**C**) Immunofluorescence localization of CRACM1 in HEK293 cells visualized by confocal microscopy. Immunostaining for CRACM1–flag–N terminus (top) or CRACM1–Myc–C terminus (bottom) in intact (left) and permeabilized cells (right). (**D**) Same as bottom right panel of (C), but at higher magnification of selected cells to illustrate plasma membrane staining.

toward a direct role for CRACM1 in store-operated calcium influx. A number of possible functions can be envisioned for CRACM1. First, CRACM1 could function as the CRAC channel itself. In this scenario, the unaltered CRAC currents in CRACM1 overexpressing cells might be due to a limiting factor upstream of CRAC channel activation (e.g., STIM1). Second, CRACM1 could be a subunit of a multimeric channel complex, in which case the other subunit(s) could become the limiting factor(s) during overexpression. Finally, CRACM1 might function as a plasma membrane acceptor or docking protein, possibly for STIM1 or some other as-yet-unidentified component of the signaling machinery that ultimately leads to CRAC channel activation and store-operated Ca^{2+} entry.

References and Notes

1. J. W. Putney Jr., *Cell Calcium* **11**, 611 (1990).
2. M. Hoth, R. Penner, *Nature* **355**, 353 (1992).
3. A. B. Parekh, R. Penner, *Physiol. Rev.* **77**, 901 (1997).
4. A. B. Parekh, J. W. Putney Jr., *Physiol. Rev.* **85**, 757 (2005).
5. M. Partiseti *et al.*, *J. Biol. Chem.* **269**, 32327 (1994).
6. R. S. Lewis, *Annu. Rev. Immunol.* **19**, 497 (2001).
7. M. M. Winslow, J. R. Neilson, G. R. Crabtree, *Curr. Opin. Immunol.* **15**, 299 (2003).
8. M. Hoth, R. Penner, *J. Physiol.* **465**, 359 (1993).
9. A. Zweifach, R. S. Lewis, *Proc. Natl. Acad. Sci. U.S.A.* **90**, 6295 (1993).
10. J. Liou *et al.*, *Curr. Biol.* **15**, 1235 (2005).
11. J. Roos *et al.*, *J. Cell Biol.* **169**, 435 (2005).
12. S. L. Zhang *et al.*, *Nature* **437**, 902 (2005).
13. M. A. Spassova *et al.*, *Proc. Natl. Acad. Sci. U.S.A.* **103**, 4040 (2006).
14. S. Feske, M. Prakriya, A. Rao, R. S. Lewis, *J. Exp. Med.* **202**, 651 (2005).
15. A. V. Yeromin, J. Roos, K. A. Stauderman, M. D. Cahalan, *J. Gen. Physiol.* **123**, 167 (2004).

16. We thank B. Mathey-Prevot, N. Ramadan, M. Booker, and staff at the *Drosophila* RNAi Screening Center at Harvard Medical School for assistance with the screen; V. Yu and M. Xie (Synta Pharmaceuticals, Lexington, MA) for help with using FLIPR; M. Bellinger for help with cell culture; and A. Dani for stimulating discussions and help with imaging experiments. Supported in part by NIH grants 5-R37-GM053950 (J.P.K.), R01-AI050200 and R01-NS040927 (R.P.), R01-GM065360 (A.F.).

Supporting Online Material

www.sciencemag.org/cgi/content/full/1127883/DC1
Materials and Methods
Figs. S1 and S2
Tables S1 and S2

24 March 2006; accepted 17 April 2006
Published online 27 April 2006;
10.1126/science.1127883
Include this information when citing this paper.

Regulation of Adult Bone Mass by the Zinc Finger Adapter Protein Schnurri-3

Dallas C. Jones,[1*] Marc N. Wein,[1*] Mohamed Oukka,[2,4] Jochen G. Hofstaetter,[3,5] Melvin J. Glimcher,[3] Laurie H. Glimcher[1,4]†

Genetic mutations that disrupt osteoblast function can result in skeletal dysmorphogenesis or, more rarely, in increased postnatal bone formation. Here we show that Schnurri-3 (Shn3), a mammalian homolog of the *Drosophila* zinc finger adapter protein Shn, is an essential regulator of adult bone formation. Mice lacking Shn3 display adult-onset osteosclerosis with increased bone mass due to augmented osteoblast activity. Shn3 was found to control protein levels of Runx2, the principal transcriptional regulator of osteoblast differentiation, by promoting its degradation through recruitment of the E3 ubiquitin ligase WWP1 to Runx2. By this means, Runx2-mediated extracellular matrix mineralization was antagonized, revealing an essential role for Shn3 as a central regulator of postnatal bone mass.

In contrast to their role in embryonic development, few genes are known to regulate osteoblast function during postnatal skeletal remodeling (*1*–*3*). The transcription factor Runx2 is an essential component of skeletogenesis, as evidenced by the human autosomal dominant disease cleidocranial dysplasia, an inherited disorder of bone development characterized by clavicular hypoplasia and cranial and facial abnormalities, which is caused by Runx2 mutations (*4*–*6*). $Runx2^{-/-}$ mice also exhibit a complete lack of both intramembranous and endochondral ossification due to the absence of osteoblasts, resulting in an unmineralized skeleton (*6*, *7*). Runx2 is required for early commitment of mesenchymal stem cells into osteoprogenitors, and it also functions later in osteoblast differentiation to regulate the formation of the extracellular matrix (*8*).

Schnurri-3 (Shn3), a large zinc finger protein, was originally identified as a DNA

[1]Department of Immunology and Infectious Diseases, Harvard School of Public Health, Boston, MA 02115, USA. [2]Center for Neurologic Diseases, Brigham and Women's Hospital, Cambridge, MA 02139, USA. [3]Laboratory for the Study of Skeletal Disorders and Rehabilitation, Department of Orthopaedic Surgery, Harvard Medical School and Children's Hospital, Boston, MA 02115, USA. [4]Department of Medicine, Harvard Medical School, Boston, MA 02115, USA. [5]Ludwig Boltzmann Institute of Osteology, Vienna, A-1120 Austria.

*These authors contributed equally to this work.
†To whom correspondences should be addressed. E-mail: lglimche@hsph.harvard.edu

binding protein of the heptameric recombination signal sequence required for V(D)J recombination of immunoglobulin genes (*9*); however, it also functions as an adapter protein in the immune system (*10*). To determine the function of Shn3 in vivo, we generated mice bearing a null mutation in the *Shn3* gene that resulted in no detectable Shn3 mRNA or protein (fig. S1A) (*11*). Shn3$^{-/-}$ mice were born healthy at expected Mendelian ratios, with no apparent gross abnormalities. However, digital radiographic, histological, and quantitative micro computerized tomography (μ-QCT) analysis revealed increased bone mass of the long bones, calvariae, and vertebrae of mature, 8-week-old male and female Shn3$^{-/-}$ mice (Fig. 1, A to G, and fig. S1B). Like neonatal wild-type (WT) controls, Shn3$^{-/-}$ mice displayed normal skeletal morphogenesis with no premature cartilage mineralization in skeletal tissue undergoing endochondral ossification (fig. S1C). Kinetic analysis revealed initial changes in skeletal architecture in Shn3$^{-/-}$ mice between ages 1 and 2 weeks (fig. S1D).

Shn3$^{-/-}$ mice exhibited an age-associated progression of the high–bone mass phenotype with virtual obliteration of the long bone marrow cavity by 7 months (Fig. 1H). Shn3 mRNA was detected in osteoblasts, whole bone, and, to a lesser extent, in osteoclasts (Fig. 1J and fig. S1C). Histomorphometric analysis in 8-week-old mice revealed a fivefold increased bone formation rate (BFR) in Shn3$^{-/-}$ compared with WT animals with comparable osteoblast surface [Ob.S/bone surface (BS)] and osteoid thickness (OS.Th) (Fig. 1K and fig. S1E).

In vivo osteoclast populations and in vitro osteoclast differentiation and function were comparable between Shn3$^{-/-}$ and WT mice (figs. S1E and S2, A and B). Furthermore, transfer of WT bone marrow (BM) failed to decrease trabeculation in femurs of recipient Shn3$^{-/-}$ mice (Fig. 1L), indicating that the increased bone mass present in Shn3$^{-/-}$ mice results from increased bone formation by osteoblasts rather than by osteoclast defects.

Similar numbers of alkaline phosphatase–positive osteoblasts with comparable growth curve kinetics (fig. S3A) were obtained from WT and Shn3$^{-/-}$ BM and calvarial cultures (Fig. 2A). However, Shn3$^{-/-}$ cultures had an increased number of mineralized nodules that were generally larger than those formed in WT cultures (Fig. 2B). Shn3$^{-/-}$ calvarial osteoblasts expressed increased levels of bone sialoprotein (BSP) and osteocalcin (OCN) mRNA but similar levels of alkaline phosphatase (ALP) mRNA compared with WT osteoblasts (Fig. 2, C and E). Shn3$^{-/-}$ osteoblasts showed elevated expression levels of both Osterix and ATF4 mRNA and of ATF4 protein, which are key transcriptional regulators of osteoblast biology (Fig. 2, F to H) (*12*, *13*). Shn3 thus regulates the expression of genes that are important in bone formation and mineralization. Expression of LRP5 mRNA was comparable between WT and Shn3$^{-/-}$ osteoblasts (fig. S3B), and Shn3 overexpression did not alter LRP5/Wnt/β-catenin–dependent transcription (fig. S3, C and D) (*14*, *15*).

The genes overexpressed in Shn3$^{-/-}$ osteoblasts are all direct Runx2 targets (*13*, *16*), suggesting that Shn3 might inhibit osteoblast activity through Runx2. Indeed, Shn3$^{-/-}$ osteoblasts contained elevated levels of Runx2 protein and Runx2 DNA binding,

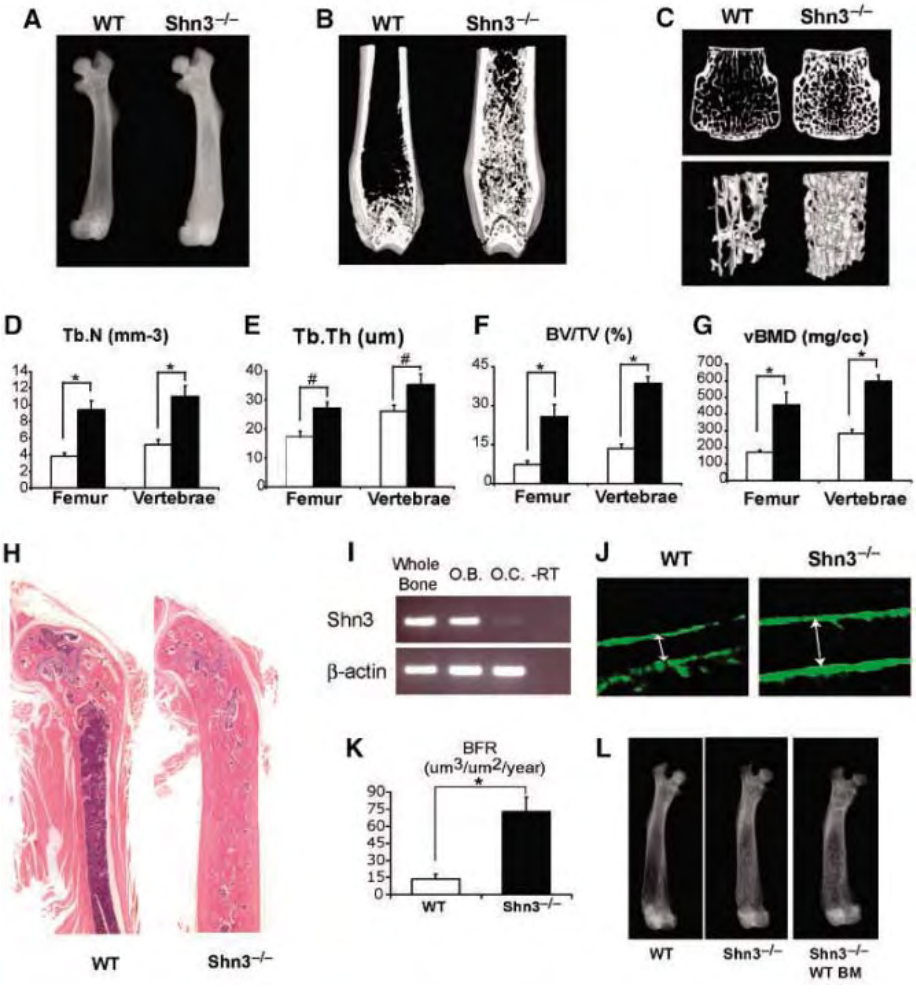

Fig. 1. Mature Shn3$^{-/-}$ mice have markedly increased bone mass. (**A**) Digital radiography of femurs isolated from 8-week-old female WT and Shn3$^{-/-}$ mice. (**B**) Three-dimensional μ-QCT image of distal femurs isolated from Shn3$^{-/-}$ and WT control mice. (**C**) Two-dimensional (upper panel) and three-dimensional (lower panel) μ-QCT images of fourth lumbar vertebrae from WT and Shn3$^{-/-}$ mice. (**D** to **G**) Analysis of μ-QCT femur images from WT mice (open bars) and Shn3$^{-/-}$ mice (filled bars) for trabecular number (Tb.N.), trabecular thickness (Tb.Th.), bone volume per tissue volume (BV/TV), and volumetric bone mineral density (vBMD). (*$P < 0.01$, #$P < 0.05$). (**H**) Femurs from 7-month-old Shn3$^{-/-}$ and WT mice were sectioned and stained with hemtoxylin and eosin. (**I**) Analysis of Shn3 mRNA expression in whole bone, osteoblasts (O.B.), osteoclasts (O.C.), and no reverse transcriptase control (–RT) by reverse transcriptase polymerase chain reaction (RT-PCR). (**J**) Dual calcein-labeling of tibial bone from WT and Shn3$^{-/-}$ mice was visualized by fluorescent micrography. Arrows point to individual calcein dye formats. (**K**) BFR is significantly increased in Shn3$^{-/-}$ mice (solid bar) when compared with control WT mice (open bar) (*$P < 0.02$). (**L**) Radiographs of femurs from control WT mice, control Shn3$^{-/-}$ mice, and Shn3$^{-/-}$ mice 4 weeks after WT BM transfer.

even though Runx2 mRNA levels were comparable between Shn3$^{-/-}$ and WT osteoblasts (Fig. 2, I to K, and fig. S4A). Shn3 overexpression in 293T cells led to a dose-dependent decrease in steady-state Runx2 protein levels (fig. S4B). Furthermore, overexpression of Shn3 accelerated Runx2 degradation kinetics and promoted Runx2 ubiquitination (Fig. 3, A to C). Additionally, we detected specific ubiquitin ligase activity with immunopurified Shn3/Runx2 complexes in in vitro ubiquitination assays (Fig. 3D).

We next tested whether Shn3 regulated Runx2 protein stability by physical interaction. Runx2 specifically coimmunoprecipitated Shn3 in cotransfection studies, and the interaction with Shn3 was mediated via the Runx2 Runt (DNA binding) domain (fig. S4C). The Shn3/Runx2 interaction is likely direct, because in vitro translated Shn3 associated with recombinant GST-Runx2 (Fig. 3E). Endogenous Runx2 and Shn3 also interacted in differentiated MC3T3-E1 osteoblastic cells (Fig. 3F) (*17*).

Although Runx2 potently activated transcription from a multimerized OSE2-luciferase reporter construct (*18*), coexpression of Shn3 inhibited Runx2 activity in a dose-dependent manner (Fig. 3G). In control experiments, Shn3 by itself had no effect on OSE2-luc activity (Fig. 3G), nor did it bind to the OSE2 element, showing that this effect was through Runx2 (fig. S4D). In addition to decreasing steady-state protein levels of Runx2, Shn3 inhibited binding of Runx2 to the canonical OSE2 Runx2 binding site (fig. S4D). From these studies, we conclude that Shn3 physically associates with Runx2, and this association leads to decreased Runx2 protein stability, thereby decreasing Runx2 DNA binding and transactivation function.

Although Shn3 could promote the ubiquitination of Runx2, Shn3 itself contains no canonical E3 ubiquitin ligase domains [really interesting novel gene (RING), homology to E6AP carboxyl terminus (HECT), or U box, see (*19*, *20*) for reviews]. Additionally, various recombinant protein fragments of Shn3 possessed no detectable in vitro E3 ubiquitin ligase activity (fig. S4D), leading us to hypothesize that Shn3 may associate with another E3 ubiquitin ligase to promote Runx2 ubiquitination. Although Runx2 was ubiquitinated by overexpressed Smurf1, a member of the HECT domain–containing Nedd4 family of E3 ligases (*21*), Runx2 protein levels are normal in Smurf1-deficient mice, suggesting another Nedd4 family E3 ligase might regulate Runx2 ubiquitination in vivo (*22*). Expression levels in mature osteoblasts revealed WWP1, another Nedd4 family E3 ubiquitin ligase, to be up-regulated during osteoblast differentiation in vitro (fig. S5A).

Coimmunoprecipitation experiments revealed association of Shn3 with WWP1 but not with Smurf1 or Smurf2 (Fig. 4A, left). Additionally, endogenous WWP1 immunoprecipitates from differentiated MC3T3-E1 osteoblast cells reproducibly contained 95-kD Shn3 immunoreactive species (Fig. 4A, right).

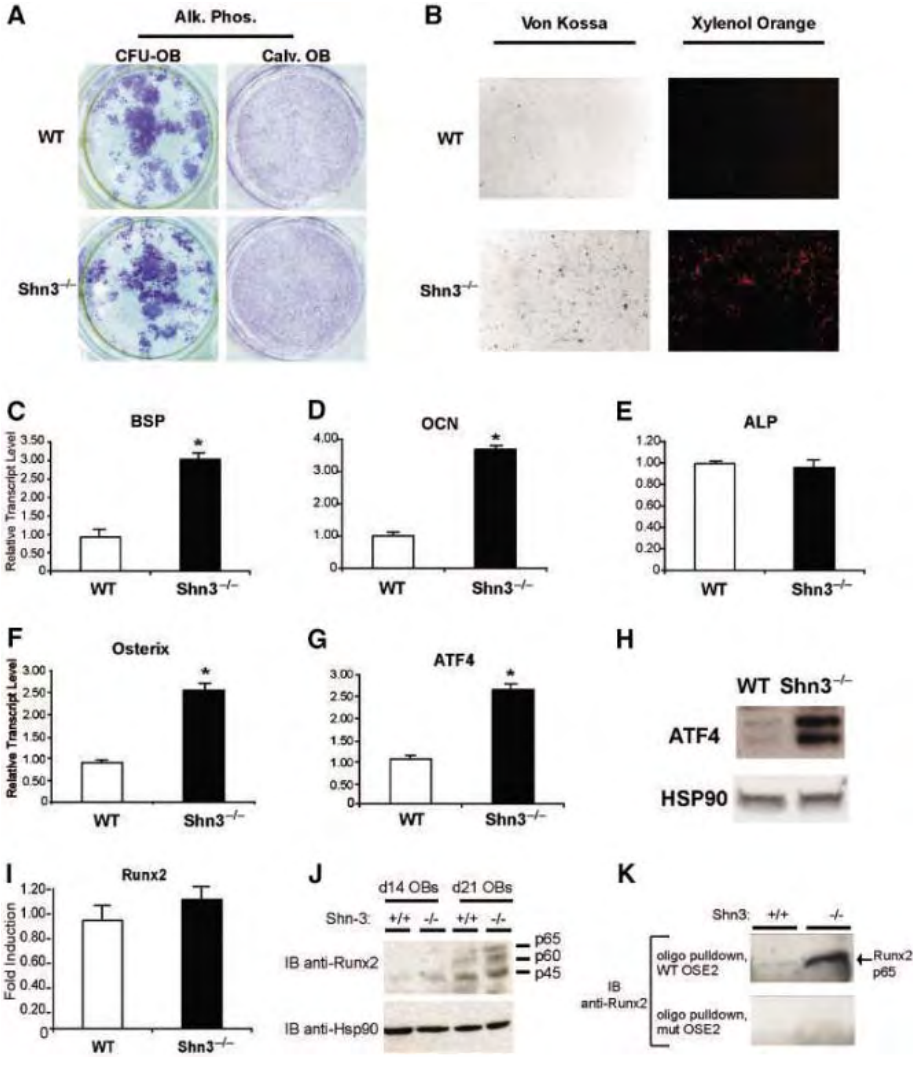

Fig. 2. Analysis of Shn3$^{-/-}$ and WT osteoblast activity in vitro. (**A**) Analysis of colony-forming unit (CFU)-OB derived from WT and Shn3$^{-/-}$ bone marrow reveal a similar number of ALP-positive colonies. Equivalent numbers of ALP-positive cells were also observed in calvarial (calv.) osteoblasts isolated from WT and Shn3$^{-/-}$ mice. Alk. Phos., alkaline phosphatase. (**B**) Calvarial osteoblast cultures generated from WT and Shn3$^{-/-}$ mice were also stained with von Kossa and xylenol orange at day 21 of culture. (**C** to **F**) Expression of BSP, OCN, ALP, and Osterix were analyzed at day 14 of culture in WT osteoblasts (open bars) and Shn3$^{-/-}$ osteoblasts (solid bars) by quantitative (Q)-PCR. The ordinate axis indicates the relative copy of mRNA per copy of β-actin mRNA (*$P < 0.01$). (**G** and **H**) WT and Shn3$^{-/-}$ osteoblasts were analyzed for the expression of ATF4 mRNA and protein by Q-PCR and Western blot, respectively. (**I**) Runx2 mRNA levels are comparable in Shn3$^{-/-}$ and WT osteoblasts at day 14 of culture as determined by Q-PCR. (**J**) Western blot analysis of whole cell extracts generated from Shn3$^{-/-}$ and WT osteoblasts for levels of Runx2 protein present in osteoblasts at both day 14 and day 21 of culture. (**K**) Runx2 DNA binding was determined from nuclear extracts generated from WT or Shn3$^{-/-}$ osteoblasts. Runx2 binding to either WT (upper panel) or mutant (lower panel) OSE2 probe was detected by Western blotting after oligonucleotide pulldown.

We detected an interaction between overexpressed Runx2 and WWP1 in 293T cells that was enhanced by Shn3 coexpression (Fig. 4B). The WWP1/Runx2 interaction likely occurs between the Runt domain of Runx2 and the WW domain of WWP1, because an in vitro translated fragment of WWP1 containing its WW domain coprecipitated with GST-Runx2 (fig. S5, B to D). An interaction between endogenous WWP1 and Runx2 p65 isoform was also detected in the ROS 17/2.8 osteoblast cell line (Fig. 4C). WWP1 overexpression led to dose-dependent reductions in steady-state levels of Runx2 protein, which was reversed by brief treatment with the proteosome inhibitor MG132 (fig. S5E). Consistent with the effects of WWP1 overexpression on Runx2 protein levels, WWP1 overexpression also inhibited Runx2 function in luciferase assays, which could be potentiated by Shn3 coexpression (fig. S5F). Finally, WWP1 promoted low levels of Runx2 ubiquitination when overexpressed in 293T cells. However, when coexpressed with Shn3, WWP1 synergized to promote Runx2 ubiquitination (Fig. 4D).

To further investigate the role of WWP1 in osteoblasts, levels of endogenous WWP1 were reduce using lentiviral delivered RNA interference (LV RNAi) (Fig. 4E and fig. S6A) (*11*). RNAi-mediated knockdown of WWP1, but not the related E3 ligase Itch, led to pronounced up-regulation of BSP, OCN, and ATF4 mRNA (Fig. 4E). Runx2 mRNA levels were similar between green fluorescent protein (GFP) RNAi- and WWP1 RNAi-expressing cells, despite increased Runx2 protein levels (Fig. 4F).

To determine if Shn3-mediated repression of Runx2 function depended on WWP1, C3H10T1/2 cells were transduced with GFPi or WWP1i lentiviruses. In subsequent luciferase reporter assays, Runx2 function was enhanced in WWP1i cells. Moreover, Shn3-mediated Runx2 repression was largely WWP1-dependent (fig. S6B).

We also analyzed primary calvarial osteoblasts transduced with WWP1 or GFP RNAi-expressing lentiviruses. Much like Shn3-deficient osteoblasts (Fig. 2), WWP1 knockdown osteoblasts showed dramatic up-regulation of Runx2 targets BSP, OCN, and ATF4 at the mRNA level (Fig. 4G) and elevated levels of theRunx2 protein (Fig. 4H), whereas Runx2 mRNA levels were comparable between WWP1 RNAi cells and controls. Furthermore, knockdown of WWP1 in these cultures led to increased numbers of mineralized matrix nodules (Fig. 4I).

Taken together, these data suggest a model in which the formation of a multimeric complex between Runx2, Shn3, and the E3 ubiquitin ligase WWP1 in mature osteoblasts inhibits Runx2 function. Shn3 is an integral adapter protein in this complex, as it enhances the ability of WWP1 to promote Runx2 polyubiquitination and proteasome-dependent degradation. RING domain E3 ubiquitin ligases are known to function in multimeric complexes (*23*); however, less is known about the regulation of HECT E3 ligases by protein-protein interactions (*24*, *25*). Additionally, future studies will be required to address the possibility

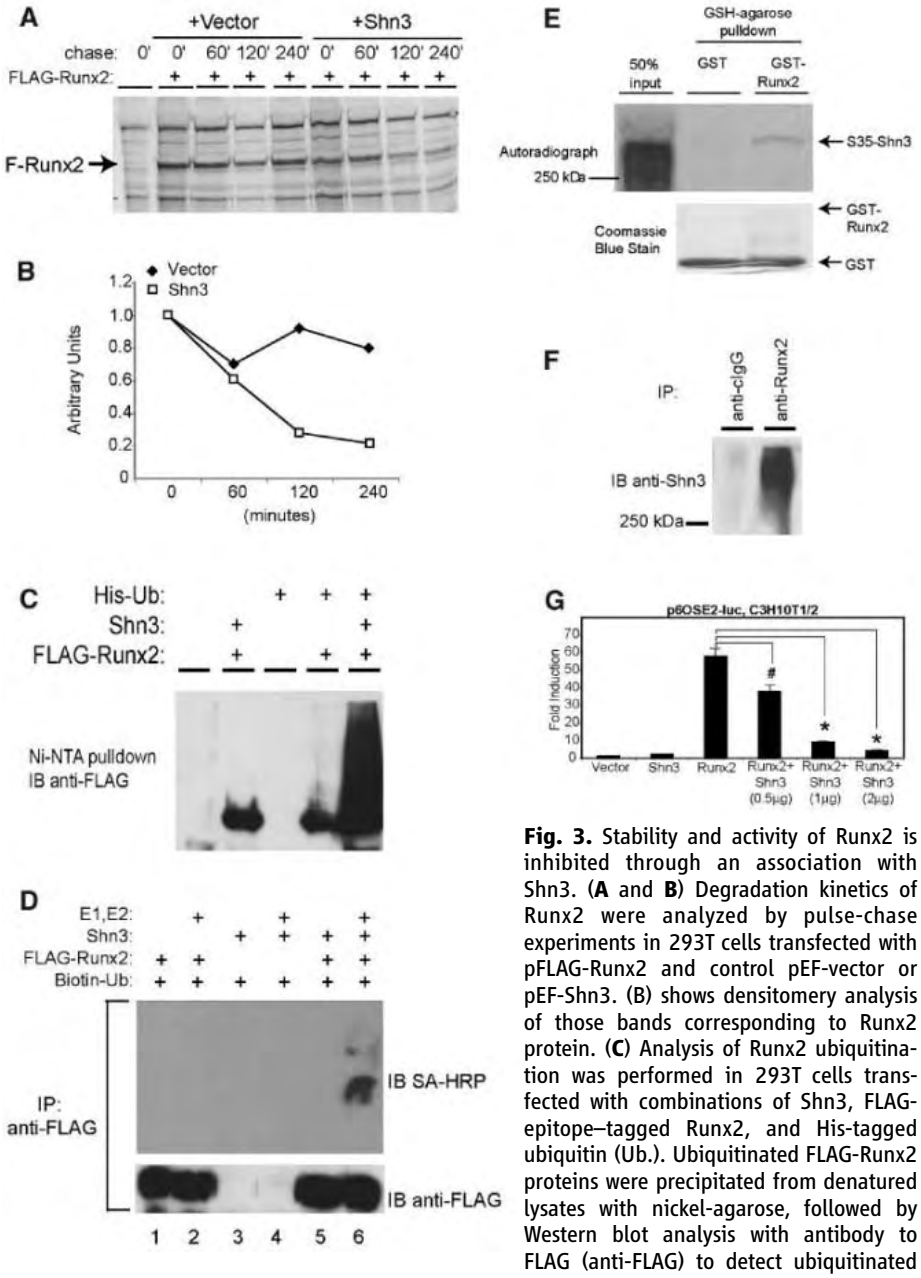

Fig. 3. Stability and activity of Runx2 is inhibited through an association with Shn3. (**A** and **B**) Degradation kinetics of Runx2 were analyzed by pulse-chase experiments in 293T cells transfected with pFLAG-Runx2 and control pEF-vector or pEF-Shn3. (B) shows densitomery analysis of those bands corresponding to Runx2 protein. (**C**) Analysis of Runx2 ubiquitination was performed in 293T cells transfected with combinations of Shn3, FLAG-epitope–tagged Runx2, and His-tagged ubiquitin (Ub.). Ubiquitinated FLAG-Runx2 proteins were precipitated from denatured lysates with nickel-agarose, followed by Western blot analysis with antibody to FLAG (anti-FLAG) to detect ubiquitinated Runx2 protein. (**D**) In vitro ubiquitination assays were performed on lysates from 293T cells that were transfected with FLAG-Runx2 and/or Shn3. FLAG-epitope–tagged proteins that were immunoprecipitated from transfected cell lysates were incubated in vitro with ubiquitin, biotinylated-ubiquitin, and recombinant E1 and E2. Reactions were then subjected to SDS-polyacrylamide gel electrophoresis (PAGE) analysis followed by blotting with streptavidin-horseradish peroxidase to detect the presence of biotin-ubiquitinated proteins. (**E**) S35-labeled in vitro translated full length Shn3 protein was incubated with glutathione S-transferase (GST) or GST-Runx2. Protein complexes were precipitated with glutathione-agarose followed by SDS-PAGE and autoradiography to detect interaction between Shn3 and Runx2. Parallel Coomassie stain of GST and GST-Runx2 protein is shown below. (**F**) Coimmunoprecipitation experiments were conducted in BMP2-differentiated MC3T3-E1 cells. Runx2 protein was immunoprecipitated from cell lysates with anti-Runx2, followed by Western blot analysis with anti-Shn3 to detect Shn3 interaction. (**G**) C3H10T1/2 cells were transfected with p6xOSE2-Luc reporter, a Runx2 expression plasmid and increasing amounts of the Shn3 expression plasmid. Results were normalized to the expression of the pRL-TK plasmid (#$P < 0.05$).

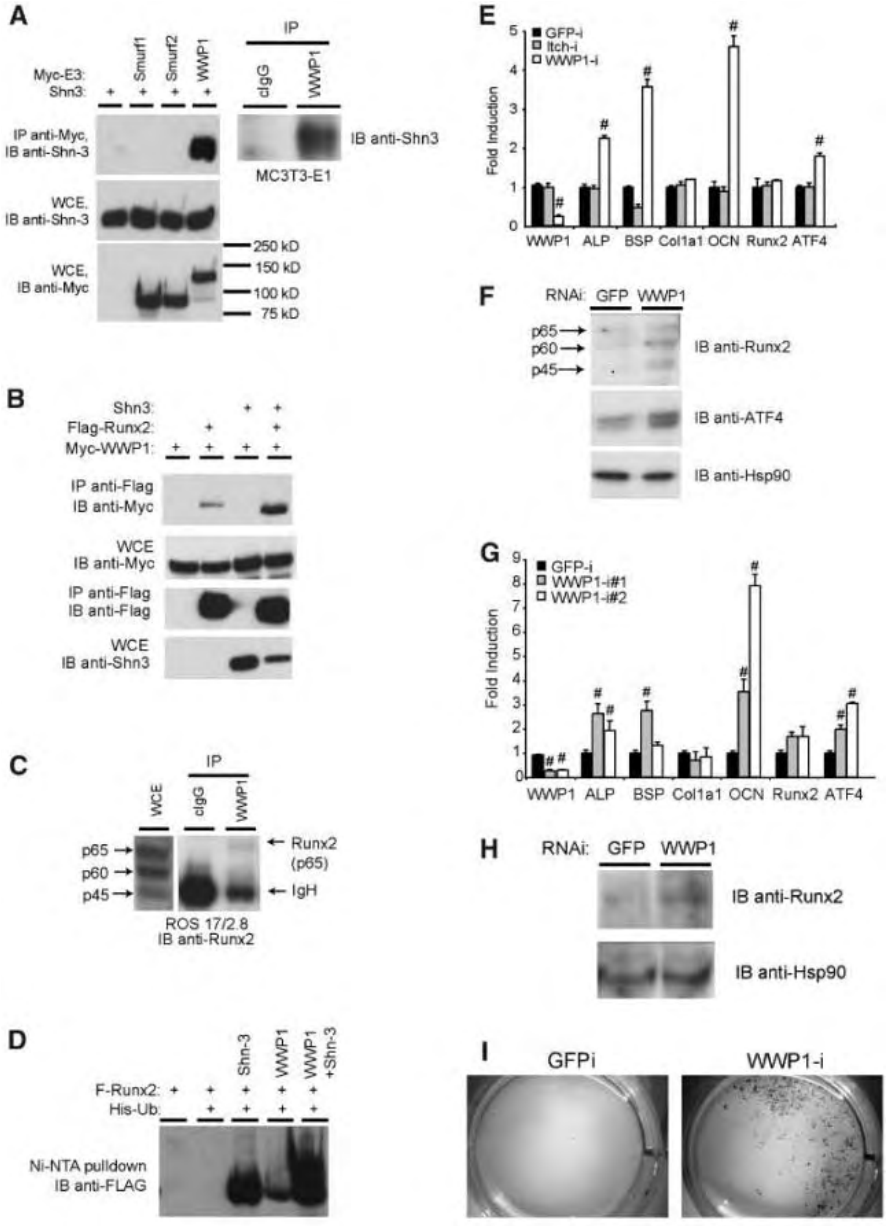

Fig. 4. Shn3 interacts with WWP1 to enhance the ubiquitination of Runx2. (**A**) The left panel shows analysis of association between Shn3 and three members of HECT domain-containing E3 ligases in 293T cells transfected with pEF-Shn3 and Myc-Smurf1, Myc-Smurf2, or Myc-WWP1. Myc-epitope tagged proteins were immunoprecipitated from cell lysates with anti-Myc, followed by Western blot analysis with anti-Shn3 to detect Shn3 interaction. The right panel shows MC3T3-E1 cells differentiated in vitro, endogenous WWP1 was immunoprecipitated, followed by SDS-PAGE and anti-Shn3 immunoblotting. (**B**) Analysis of association between WWP1 and Runx2. 293T cells were transfected as indicated, followed by anti-FLAG (Runx2) immunoprecipitation and anti-Myc (WWP1) immunoblotting. (**C**) Rat osteosarcoma 17/2.8 cell lysates were immunoprecipitated with anti-WWP1, and endogenous Runx2 proteins in immunoprecipiates were determined by immunoblotting. (**D**) Analysis of Runx2-ubiquitination was performed in 293T cells transfected with FLAG-Runx2 and combinations of Myc-WWP1 and Shn3 as described in Fig. 3C. (**E**) RNAi-expressing MC3T3-E1 cells were differentiated with BMP2/ascorbic acid/β-glycerophosphate, and expression of the indicated genes was analyzed by Q-PCR. Values are shown relative to GFPi-expressing cells (#$P < 0.05$). (**F**) Lysates from MC3T3-E1 cells in (B) were analyzed by immunoblotting for Runx2, ATF4, and Hsp90 protein levels. (**G**) RNAi-expressing primary calvarial osteoblasts were analyzed for expression of the indicated genes by Q-PCR. Values are shown relative to GFPi-expressing cells (#$P < 0.05$). (**H**) Lysates from cells in (D) were analyzed by immunoblotting for Runx2 and Hsp90 protein levels. (**I**) Osteoblasts expressing RNAi against GFP or WWP1 were cultured for 14 days followed by von Kossa staining to reveal the presence of mineralized matrix nodules.

that increased levels of Shn3/WWP1 substrates other than Runx2 may contribute to the osteosclerotic phenotypes observed in their absence.

Because the high–bone mass phenotype we observe becomes more pronounced with age, we propose the Shn3 belongs to the small group of factors that regulate postnatal osteoblast activity (*13*, *26*). Compounds designed to block Shn3/WWP1 function may serve as therapeutic agents for the treatment of osteoporosis.

References and Notes

1. Y. Yoshida *et al.*, *Cell* **103**, 1085 (2000).
2. S. Kim *et al.*, *Genes Dev.* **17**, 1979 (2003).
3. M. L. Johnson, K. Harnish, R. Nusse, W. Van Hul, *J. Bone Miner. Res.* **19**, 1749 (2004).
4. B. Lee *et al.*, *Nat. Genet.* **16**, 307 (1997).
5. S. Mundlos *et al.*, *Cell* **89**, 773 (1997).
6. F. Otto *et al.*, *Cell* **89**, 765 (1997).
7. T. Komori *et al.*, *Cell* **89**, 755 (1997).
8. P. Ducy *et al.*, *Genes Dev.* **13**, 1025 (1999).
9. L. C. Wu *et al.*, *Nucleic Acids Res.* **21**, 5067 (1993).
10. M. Oukka *et al.*, *Mol. Cell* **9**, 121 (2002).
11. Materials and methods are available as supporting material on *Science* Online.
12. K. Nakashima *et al.*, *Cell* **108**, 17 (2002).
13. X. Yang *et al.*, *Cell* **117**, 387 (2004).
14. Y. Gong *et al.*, *Cell* **107**, 513 (2001).
15. D. A. Glass II *et al.*, *Dev. Cell* **8**, 751 (2005).
16. G. S. Stein *et al.*, *Oncogene* **23**, 4315 (2004).
17. N. Zamurovic, D. Cappellen, D. Rohner, M. Susa, *J. Biol. Chem.* **279**, 37704 (2004).
18. P. Ducy, R. Zhang, V. Geoffroy, A. L. Ridall, G. Karsenty, *Cell* **89**, 747 (1997).
19. C. M. Pickart, *Cell* **116**, 181 (2004).
20. C. Patterson, *Sci. STKE* **2002**, pe4 (2002).
21. R. J. Ingham, G. Gish, T. Pawson, *Oncogene* **23**, 1972 (2004).
22. M. Yamashita *et al.*, *Cell* **121**, 101 (2005).
23. P. K. Jackson, A. G. Eldridge, *Mol. Cell* **9**, 923 (2002).
24. M. Scheffner, J. M. Huibregtse, R. D. Vierstra, P. M. Howley, *Cell* **75**, 495 (1993).
25. A. A. Ogunjimi *et al.*, *Mol. Cell* **19**, 297 (2005).
26. M. N. Wein, D. C. Jones, L. H. Glimcher, *Immunol. Rev.* **208**, 66 (2005).

27. The authors thank G. Karsenty, B. Olsen, K. Miyazono, B. Williams, N. Hacohen, and the RNAi Consortium at the Broad Institute for kindly providing reagents; A. Erlebacher and E. Gravallese for helpful advice; T. Aliprantis, M. Grusby, and G. Karsenty for thoughtful comments on the manuscript; and L. de Elizalde for expert manuscript preparation. Supported by NIH grants AI29673 (L.H.G.) and AR46983 (L.H.G., M.J.G.), a grant from The Peabody Foundation (M.J.G.), postdoctoral fellowships from the Arthritis Foundation (D.J.) and the Irvington Institute (M.O.), and by the Medical Scientist Training Program at Harvard Medical School (M.W.).

Supporting Online Material

www.sciencemag.org/cgi/content/full/312/5777/1223/DC1
Materials and Methods
Figs. S1 to S6
References

16 February 2006; accepted 25 April 2006
10.1126/science.1126313

Pituitary Adenoma Predisposition Caused by Germline Mutations in the *AIP* Gene

Outi Vierimaa,[1*] Marianthi Georgitsi,[3*] Rainer Lehtonen,[3] Pia Vahteristo,[3] Antti Kokko,[3] Anniina Raitila,[3] Karoliina Tuppurainen,[4] Tapani M. L. Ebeling,[2] Pasi I. Salmela,[2] Ralf Paschke,[5] Sadi Gündogdu,[6] Ernesto De Menis,[7] Markus J. Mäkinen,[4] Virpi Launonen,[3] Auli Karhu,[3] Lauri A. Aaltonen[3]†

Pituitary adenomas are common in the general population, and understanding their molecular basis is of great interest. Combining chip-based technologies with genealogy data, we identified germline mutations in the *aryl hydrocarbon receptor interacting protein* (*AIP*) gene in individuals with pituitary adenoma predisposition (PAP). AIP acts in cytoplasmic retention of the latent form of the aryl hydrocarbon receptor and also has other functions. In a population-based series from Northern Finland, two *AIP* mutations account for 16% of all patients diagnosed with pituitary adenomas secreting growth hormone and for 40% of the subset of patients who were diagnosed when they were younger than 35 years of age. Typically, PAP patients do not display a strong family history of pituitary adenoma; thus, *AIP* is an example of a low-penetrance tumor susceptibility gene.

Pituitary adenomas are common benign neoplasms, accounting for approximately 15% of intracranial tumors. Most common hormone-secreting pituitary tumor types oversecrete prolactin or growth hormone (GH); the oversecreted hormones, together with local compressive effects, account for substantial morbidity. Oversecretion of GH causes acromegaly or gigantism. Acromegaly is characterized by coarse facial features, protruding jaw, and enlarged extremities. Because of the slow development of the potentially severe symptoms of untreated acromegaly, including cardiac manifestations, the condition is difficult to diagnose early (*1*). Gigantism refers to excessive linear growth that occurs as a result of GH oversecretion when epiphyseal growth plates are still open, in childhood and adolescence. Genetic predisposition to pituitary tumors is believed to be rare (*2*).

We detected three clusters of familial pituitary adenoma in Northern Finland [supporting online material (SOM) text]. The most notable cluster displayed three cases of acromegaly or gigantism. Genealogy data reaching back to the 1700s had been generated by family members from the publicly available official population registries. Two first clusters could be linked by genealogy (Fig. 1A), and the third appeared separate (Fig. 1B). We hypothesized that a previously uncharacterized form of low-penetrance pituitary adenoma predisposition (PAP) would contribute to the disease burden in Northern Finland. We had previously characterized a population-based cohort of 54 patients diagnosed with GH-secreting pituitary adenoma (somatotropinoma) between 1980 and 1999 in Oulu University Hospital (OUH) (*3*). We identified pituitary adenoma patients in Northern Finland by using data on this cohort, patient interviews, and a computerized search for all cases with archived samples of pituitary adenomas at the OUH from 1978 to 2000. These data were linked to the pedigree information to identify additional affected relatives. Altogether, 11 affected individuals in family 1 were identified (Fig. 1A). The PAP phenotype—very-low-penetrance susceptibility to somatotropinoma and prolactinoma—did not fit well to any of the known familial pituitary adenoma syndromes, including multiple endocrine neoplasia type 1 (MEN1), Carney complex (CNC), isolated familial somatotropinoma (IFS), and familial isolated pituitary adenoma (*1*, *2*, *4*). These syndromes are familial, and the low penetrance of PAP appeared unique. By low penetrance, we refer to hereditary predisposition that relatively rarely leads to actual disease but which may cause much more effect on population level than high-penetrance disease susceptibility, which typically is very uncommon.

To identify the PAP locus, we performed whole-genome single-nucleotide polymorphism genotyping for 16 individuals from family 1 (Fig. 1A) (*5*) (SOM text). Before any linkage information was obtained, we opted to perform two alternative affected-only analyses. One analysis considering only individuals with acromegaly or gigantism (somatotropinoma or mixed adenoma) as affected (high stringency), and the other considered individuals with any pituitary adenoma as affected (low stringency). We did this because the number of phenocopies for acromegaly and gigantism is much lower than that for prolactinoma.

Linkage analysis using high-stringency criteria provided evidence for linkage in chromosome 11q12–11q13 (*5*) (fig. S1), a region previously implicated in isolated familial somato-

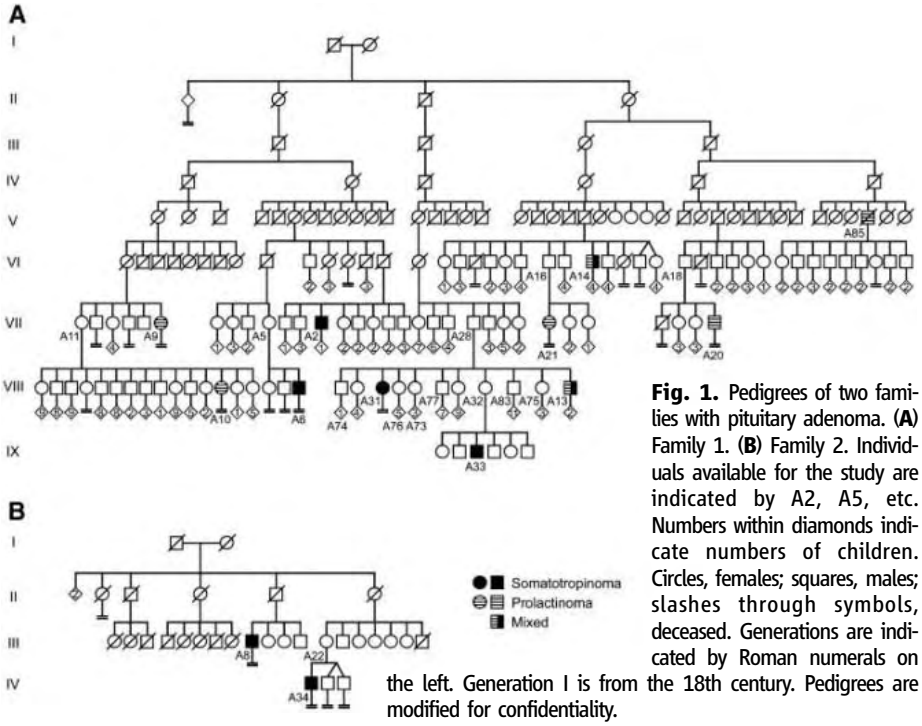

Fig. 1. Pedigrees of two families with pituitary adenoma. (**A**) Family 1. (**B**) Family 2. Individuals available for the study are indicated by A2, A5, etc. Numbers within diamonds indicate numbers of children. Circles, females; squares, males; slashes through symbols, deceased. Generations are indicated by Roman numerals on the left. Generation I is from the 18th century. Pedigrees are modified for confidentiality.

[1]Department of Clinical Genetics, [2]Department of Internal Medicine, Oulu University Hospital, 90029 Oulu, Finland. [3]Department of Medical Genetics, Molecular and Cancer Biology Research Program, 00014 University of Helsinki, Helsinki, Finland. [4]Department of Pathology, University of Oulu, 90014 Oulu, Finland. [5]Medical Department III, Leipzig University, 04103 Leipzig, Germany. [6]Division of Endocrinology-Metabolism and Diabetes, Cerrahpaşa Medical Faculty, University of Istanbul, 34303 Istanbul, Turkey. [7]Department of Internal Medicine, General Hospital, 31100 Treviso, Italy.

*These authors contributed equally to this work.
†To whom correspondence should be addressed. E-mail: lauri.aaltonen@helsinki.fi

tropinoma and including the *MEN1* gene (*6*–*11*). Notably, no *MEN1* mutations were detected in our sample set, compatible with published reports on familial pituitary adenoma (*6*, *12*–*17*). We genotyped this candidate locus using 36 markers in families 1 and 2 (table S1). The added maximum logarithm of the odds (LOD) score for these two families was 7.1 with high-stringency criteria. Families 1 and 2 shared the linked haplotype, which segregated perfectly with acromegaly, providing unambiguous evidence for disease locus identification. The linked region was between 61.7 and 69.0 megabases (Mb) (Ensembl, version 36, December 2005), harboring 295 genes. Although analysis with low-stringency criteria also showed linkage at this locus (*5*), two individuals with prolactinoma appeared to represent phenocopies (A9 and A10). The data derived using the high-stringency criteria was considered the cornerstone of subsequent gene identification efforts.

To detect genes with aberrant expression in blood samples of PAP patients and carriers, we obtained expression profiles for 16 individuals (nine PAP carriers from families 1 and 2, and seven controls) (*5*). There were 172 probe sets that mapped in the linked region. The two lowest *P* values were obtained for the two separate probe sets representing *AIP* (also known as *XAP2* and *ARA9*, GenBank no. U78521.1) ($P = 0.00026$ and $P = 0.00114$) (table S2). Thus, *AIP* was chosen as the prime candidate for mutation analysis. One other gene, *galectin-12* (*LGALS12*), was also chosen on the basis of decreased expression (table S2) and an association of *galectin-3* to pituitary tumorigenesis (*18*). No difference was detected in *MEN1* expression. The coding region of *AIP* was sequenced from normal tissue DNA. A nonsense mutation Q14X (where Q is Gln), perfectly segregating with the GH secreting adenoma phenotype in families 1 and 2, was identified (Fig. 2A). The mutation was absent in 209 local blood donors. *LGALS12* analysis was negative.

To evaluate the contribution of *AIP* in the population-based material (*3*), we had DNA available from 45 of the 54 acromegaly patients belonging to the study cohort, including four cases from families 1 and 2. Out of 45 patients from the population-based cohort, 6 displayed Q14X, and one displayed IVS3-1G>A, affecting the splice acceptor site of exon 4 (Fig. 2B). We screened 219 local blood donors for the latter change, with negative results. The age at diagnosis, sex, and size of adenoma were compared between PAP ($n = 7$) and *AIP* mutation–negative ($n = 38$) patients. Differences in tumor size or sex distribution were not observed. PAP patients were significantly younger than mutation-negative patients (24.7 ± 10.7 versus 43.6 ± 11.9 years, $P = 0.0003$). For identification of PAP patients, young age at onset is a useful indicator; six out of the fifteen patients diagnosed under 35 years of age (40%) in the population-based series had PAP. In addition, we screened 10 unselected Finnish sporadic acromegaly patients, from which DNA and appropriate authorization was available, and found Q14X in 2 of them, a result compatible with findings in the population-based cohort.

Loss of heterozygosity analysis was possible in eight tumors from mutation-positive individuals, including five somatotropinomas, one mixed-type tumor, and two prolactinomas; loss of the wild-type allele was detected in all cases, showing that these tumors were null with respect to *AIP* (fig. S2). This finding strengthened the notion that PAP is associated with predisposition to both prolactinomas and somatotropinomas and indicated that *AIP* is likely to act as a tumor suppressor.

The possible role of *AIP* in pituitary adenoma predisposition in other populations was studied in three families with two affected individuals. Normal DNA from one German (*15*) and one Turkish familial somatotropinoma case, as well as two Italian siblings with somatotropinoma (*16*) were analyzed. Whereas no mutation was detected in the German and Turkish sample, the Italian siblings displayed a nonsense mutation R304X (where R is Arg) in exon 6 (Fig. 2C). The change was absent in 203 Caucasian controls from the United Kingdom and the Centre d'Etude du Polymorphisme Humain (CEPH) (*5*), as well as in 52 local (Treviso) blood donors. The phenotype in the siblings resembled that seen in Finns: young age at onset and no visible evidence of dominant transmission (table S6).

These data strongly associate loss-of-function mutations of *AIP* to PAP. AIP was identified by its interaction with the hepatitis B virus X protein (*19*). AIP forms a complex with the aryl hydrocarbon receptor (AHR) and two 90-kD heat-shock proteins (HSP90) (*20*) (Fig. 3). The R304X mutation removes the AHR binding region (*21*, *22*). AHR is a ligand-activated transcription factor that regulates a variety of xenobiotic metabolizing enzymes (*23*). Dioxin-like chemicals display high affinity to AHR, which mediates most of the toxic responses of these agents. AHR also participates in cellular signaling pathways (*24*). AIP modulates the subcellular localization of AHR and prevents the AHR from undergoing nucleocytoplasmic shuttling (*25*). It also binds to and attenuates the activity of PDE4A5—a phosphodiesterase that modulates cyclic adenosine monophosphate (cAMP) signaling—as well as PPARα (*26*, *27*). The mechanisms by which AIP exerts its tumor-suppressive action in the

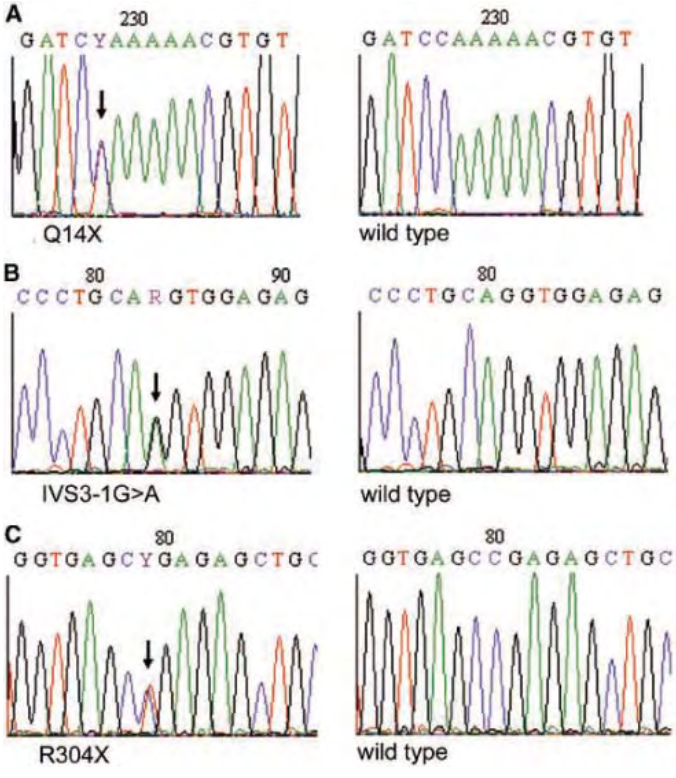

Fig. 2. *AIP* germline mutations found in Finnish and Italian PAP cases. **(A)** A Finnish nonsense mutation Q14X in exon 1. **(B)** A Finnish splice site mutation IVS3-1G>A. **(C)** An Italian nonsense mutation R304X in exon 6. Each mutated base is indicated by an arrow. The respective wild-type sequences are depicted on the right and shown for comparison.

Fig. 3. Schematic figure of AIP. FK506-binding protein (FKBP)—homology region and tetratricopeptide repeats (TPRs) are shown as colored boxes. The regions necessary for interaction with AHR and HSP90 proteins are shown with black lines. The exon boundaries of the AIP gene are marked with dashed lines. Identified germline *AIP* mutations in PAP patients are indicated by black triangles.

pituitary remain to be determined. Further work on the functional role of AIP should prove informative in revealing key cellular processes involved in genesis of pituitary adenomas, including potential drug targets.

It has not been previously realized that genetic predisposition to pituitary adenoma, in particular the GH-oversecreting type, can account for a substantial proportion of cases. Our study not only reveals this aspect of the disease but also provides molecular tools for efficient identification of predisposed individuals. Without preexisting risk awareness, the patients are typically diagnosed after years of delay, leading to substantial morbidity. Simple tools for efficient clinical follow-up of predisposed individuals are available, underlining the importance of our findings.

Our results suggest that inherited tumor susceptibility may be more common than previously thought. The identification of the PAP gene indicates that it is possible to identify the causative genetic defects in the low-penetrance conditions even in the absence of a strong family history.

References and Notes

1. A. P. Heaney, S. Melmed, *Nat. Rev. Cancer* **4**, 285 (2004).
2. L. A. Frohman, K. Eguchi, *Growth Horm. IGF Res.* **14**, S90 (2004).
3. R. Kauppinen-Mäkelin *et al.*, *J. Clin. Endocrinol. Metab.* **90**, 4081 (2005).
4. A. F. Daly, M.-L. Jaffrain-Rea, A. Beckers, *Horm. Metab. Res.* **37**, 347 (2005).
5. Materials and Methods are available as supporting material on *Science* Online.
6. S. Yamada *et al.*, *J. Clin. Endocrinol. Metab.* **82**, 239 (1997).
7. R. V. Thakker *et al.*, *J. Clin. Invest.* **91**, 2815 (1993).
8. M. R. Gadelha *et al.*, *J. Clin. Endocrinol. Metab.* **85**, 707 (2000).
9. B. S. Soares, L. A. Frohman, *Pituitary* **7**, 95 (2004).
10. B. S. Soares, K. Eguchi, L. A. Frohman, *J. Clin. Endocrinol. Metab.* **90**, 6580 (2005).
11. D. C. Luccio-Camelo *et al.*, *Eur. J. Endocrinol.* **150**, 643 (2004).
12. M. R. Gadelha *et al.*, *J. Clin. Endocrinol. Metab.* **84**, 249 (1999).
13. C. Tanaka *et al.*, *J. Clin. Endocrinol. Metab.* **83**, 960 (1998).
14. A. Verloes, A. Stevenaert, B. T. Teh, P. Petrossians, A. Beckers, *Pituitary* **1**, 273 (1999).
15. F. Ackermann *et al.*, *Exp. Clin. Endocrinol. Diabetes* **107**, 93 (1999).
16. E. De Menis, T. R. Prezant, *Pituitary* **5**, 11 (2002).
17. P. Benlian *et al.*, *Eur. J. Endocrinol.* **133**, 451 (1995).
18. D. Riss *et al.*, *Cancer Res.* **63**, 2251 (2003).
19. N. Kuzhandaivelu, Y. S. Cong, C. Inouye, W. M. Yang, E. Seto, *Nucleic Acids Res.* **24**, 4741 (1996).
20. L. A. Carver, C. A. Bradfield, *J. Biol. Chem.* **272**, 11452 (1997).
21. D. R. Bell, A. Poland, *J. Biol. Chem.* **275**, 36407 (2000).
22. J. R. Petrulis, G. H. Perdew, *Chem. Biol. Interact.* **141**, 25 (2002).
23. B. K. Meyer, G. H. Perdew, *Biochemistry* **38**, 8907 (1999).
24. J. L. Marlowe, A. Puga, *J. Cell. Biochem.* **96**, 1174 (2005).
25. R. S. Pollenz, E. J. Dougherty, *J. Biol. Chem.* **280**, 33346 (2005).
26. G. B. Bolger *et al.*, *J. Biol. Chem.* **278**, 33351 (2003).
27. W. K. Sumanasekera, E. S. Tien, R. Turpey, J. P. Vanden Heuvel, G. H. Perdew, *J. Biol. Chem.* **278**, 4467 (2003).

28. We thank S. Marttinen, R. Mattlar, O. Kajula, I.-L. Svedberg, I. Vuoristo, and M. Aho for technical assistance, the Center for Scientific Calculations for computational capacity and advice, and P. Ellonen and P. Kristo for sequencing services. Funded by the Academy of Finland (grants 213183, 212901, the Center of Excellence in Translational Genome-Scale Biology), the Sigrid Jusélius Foundation, the Cancer Society of Finland, the Research and Science Foundation of Farmos, the Foundation for Technological Advancement, and the Bodossakis Foundation. The study was approved by the appropriate ethics review committee, and the participating family members gave their informed consent. We gratefully acknowledge the participants for their valuable help.

Supporting Online Material

www.sciencemag.org/cgi/content/full/312/5777/1228/DC1
Materials and Methods
SOM Text
Figs. S1 and S2
Tables S1 to S6
References

10 February 2006; accepted 31 March 2006
10.1126/science.1126100

Strong Top-Down Control in Southern California Kelp Forest Ecosystems

Benjamin S. Halpern,[1]* Karl Cottenie,[1,2] Bernardo R. Broitman[1,3]

Global-scale changes in anthropogenic nutrient input into marine ecosystems via terrestrial runoff, coupled with widespread predator removal via fishing, have created greater urgency for understanding the relative role of top-down versus bottom-up control of food web dynamics. Yet recent large-scale studies of community regulation in marine ecosystems have shown dramatically different results that leave this issue largely unresolved. We combined a multiyear, large-scale data set of species abundances for 46 species in kelp forests from the California Channel Islands with satellite-derived primary production and found that top-down control explains 7- to 10-fold more of the variance in abundance of bottom and mid-trophic levels than does bottom-up control. This top-down control was propagated via a variety of species-level direct and indirect responses to predator abundance. Management of top-down influences such as fishing may be more important in coastal marine ecosystems, particularly in kelp forest systems, than is commonly thought.

Understanding the relative importance of top-down (consumer-driven) versus bottom-up (resource-driven) control of food webs has long been a focus of ecological studies (*1*–*4*). Anthropogenic nutrient enrichment of the environment through the use of fertilizers has become globally widespread (*5*), with most of these additions being transported to coastal systems via runoff. The abundances of large top-predators have been dramatically reduced in most of the world's oceans (*6*, *7*). How ecosystems respond to changes in the relative strength of top-down and bottom-up forces will affect conservation and restoration efforts aimed at mitigating or reversing these impacts.

Recent studies of large-scale marine ecosystems have drawn contrasting conclusions about the direction of control of community structure, offering strong evidence for either bottom-up control (*8*–*10*) or top-down regulation (*11*, *12*). Kelp forest communities have provided strong evidence of top-down control mediated through trophic cascades (*4*, *13*). However, the likelihood and strength of trophic cascades vary greatly among kelp forest systems (*13*), and there is evidence that kelp distribution and abundance can be controlled from the bottom up by nutrient levels (*14*), which in turn determine the abundance of species belonging to higher trophic levels (*15*). It is in part because kelp (such as *Macrocystis pyrifera*) respond so quickly to nutrients (via growth) or to storm disturbance or grazing (through mortality) that hypotheses of top-down versus bottom-up control are often tested in kelp forest ecosystems; changes in primary production or predator abundance (that in turn affect grazer species) are quickly incorporated into the community and can then be measured.

We used a multiyear data set of species abundances measured at 16 different kelp forest sites around the Channel Islands, California, and combined it with satellite-derived estimates of ocean primary production (from the Sea-Viewing Wide Field-of-View Sensor or SeaWiFS) at each site (*16*) to test whether ecosystem trophic dynamics are driven more by predation or primary production (Fig. 1). The northern Channel Islands lie in the middle of a dynamic oceanographic boundary formed by the convergence and mixing of the cold California Current and the warmer Southern

[1]National Center for Ecological Analysis and Synthesis, 735 State Street, Santa Barbara, CA 93101, USA. [2]Department of Integrative Biology, University of Guelph, Guelph, Ontario, Canada. [3]Department of Ecology, Evolution, and Marine Biology, University of California, Santa Barbara, CA 93106, USA.

*To whom correspondence should be addressed. E-mail: halpern@nceas.ucsb.edu

California Countercurrent. The strong spatial variability in primary production is driven in large part by the complex bathymetry of the region (*16*), spans the entire range of typical values seen for the northeast Pacific (*9*), and is positively correlated with nutrient levels (*17*). This variability in production in turn generates large variations in community structure and dynamics around the islands (*17*–*19*). The spatial heterogeneity in productivity in this transition zone and the detailed spatial and temporal scales of the data make it an ideal system for a robust test of the role of top-down versus bottom-up regulation of community structure.

Abundance data were available for 4 algal, 27 invertebrate, and 15 fish species; each of the 46 species was classified as predators (12 fishes and 4 invertebrates), herbivores (1 fish and 9 invertebrates), planktivores (2 fishes and 14 invertebrates), or algae (4 species). Details on how these data were processed before analyses are provided in Halpern and Cottenie (*18*) and are summarized in the supporting online material (also see the species listed in table S1). We used variation decomposition based on redundancy analysis to isolate the effect of predator abundance versus primary production variables on the abundance of herbivore, planktivore, or algal trophic levels within the kelp forest community. This technique is the multivariate extension of linear regression (with corresponding R^2) that measures the amount of variation (computed as the percentage of the total variation in the community matrix) that can be attributed exclusively to either top-down or bottom-up variables, after eliminating confounding spatial and temporal variables (*20*, *21*). In particular, we included and controlled for spatial, temporal, and environmental variables to account for (and therefore remove) the effect of inherent small-scale differences in populations and communities, population cycles, El Niño events, and biophysical drivers of species and community dynamics such as temperature [see (*18*) for specific variables and their treatment]. We tested all direct food web paths (Fig. 2) with secondary and primary predators as separate and summed explanatory variables, because there were only two secondary predator species. We also conducted analyses with herbivores and planktivores treated as the same trophic level. A forward selection procedure was used to isolate which predator species and primary production variables were the most important for driving the results. To further test whether differences in primary production drove variation in abundance across sites, we used linear regression analysis with annual or winter monthly average primary production as the independent variable and the summed abundances of predators or entire communities as the dependent variable.

Despite the strong spatial (Fig. 1) and temporal gradient in primary production across the waters surrounding the islands, we found little evidence of bottom-up control and a 7- to 10-fold larger influence of top-down relative to bottom-up regulation of kelp forest community structure (Fig. 3). When controlling for spatial, temporal, and environmental variables, overall predator abundance had a significant effect on algal, herbivore, and planktivore abundances, explaining 11 to 20% of abundance patterns of autotroph and primary consumer trophic levels, whereas local primary production had no significant effect (<2% explained in all cases; Fig. 3 and table S2). Top-down effects were nearly twice as strong for algae as for herbivores or planktivores. These overall results were largely driven by the abundance of primary predators, because these predators alone also explained a significant, although slightly smaller, amount of the variation in the abundance of other trophic levels, although secondary predators alone did not explain a significant amount of the variation in the abundance of the other trophic levels. Neither predator abundance nor entire community abundance was significantly correlated with annual or winter local primary production ($P > 0.50$ in all cases). Forward selection models isolated two key predator species that drove the top-down effects on algae, herbivores, and planktivores. For all trophic paths in the food web, spiny lobster (*Panulirus interruptus*) and Kellet's whelk (*Kelletia kelletii*) were significantly important species, likely due to their strong impacts on key grazers of kelp (urchins) and algae (limpets and snails). Kelp rockfish (*Sebastes atrovirens*) and striped seaperch (*Embiotoca lateralis*) also explained a significant amount of the variation in algal abundance. Both fishes eat a variety of small invertebrates that are not major consumers of algae, and so the mechanism of control on algal abundance is not clear. This top-down control is much stronger for algae as compared to that of mid-level trophic levels; in other words, the trophic cascade is accentuated rather than attenuated. The top-down control was largely mediated through these few key species, an effect that would have been missed had all species' abundances been lumped into trophic levels, as in past studies of community regulation.

Our results suggest that, regardless of local patterns of primary production, the

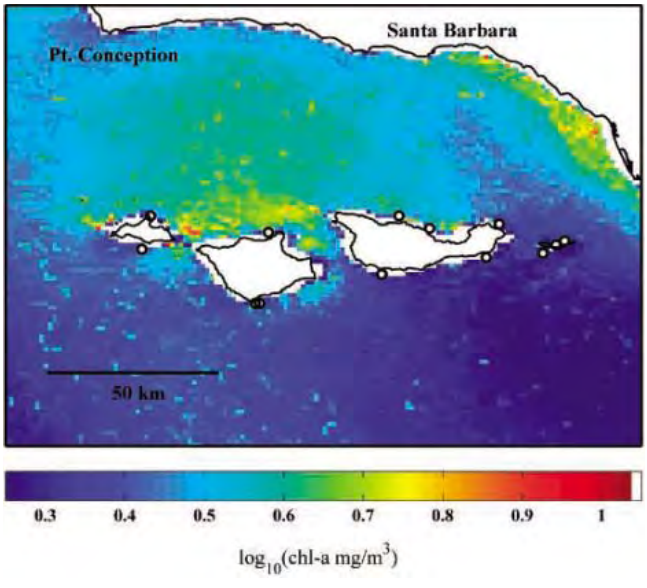

Fig. 1. Map of the northern Channel Islands and location of the Kelp Forest Monitoring Program (KFMP) sites (open circles) and the long-term mean SeaWiFS chlorophyll a concentration across the region.

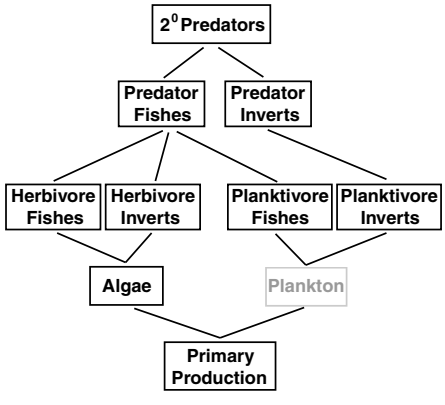

Fig. 2. Schematic of the kelp forest food web analyzed. Lines indicate paths of trophic interactions, as determined by the feeding habits of species included in analyses. Primary production was measured by concentrations of chlorophyll a. Plankton abundances are shaded gray because no measurements were available for phytoplankton or zooplankton.

abundance of top predators is markedly influencing the structure of this benthic ecosystem. We focused here on determining which variables explained the variation of species' abundances across space and time, because biomass data were not available, and so we were unable to calculate the effect size per se of top-down control. Previous experimental studies of rocky intertidal ecosystems have found similarly strong top-down regulation (*22*, *23*), suggesting that such control may be typical for coastal ecosystems. Although the range of primary production values in our study included a broad range of typical values, it did not include some of the more extreme possible values, in particular those that occur during strong El Niño years; indeed, benthic communities in coastal ecosystems have been shown to be influenced by nutrient input in these cases (*24*). Coastal ecosystems are heavily fished, highly variable in natural productivity, and subject to high levels of anthropogenic nutrient input, and so it is particularly important to understand how such coastal systems are regulated.

Almost all ecosystem-scale tests of the direction of community control have only been able to look for correlations at a single (albeit large) site, given the challenges of conducting repeated sampling over large scales. A notable exception (*9*) found bottom-up control of top trophic levels at the oceanwide and regional (and replicated) scales. Our study is well replicated at a spatial scale relevant to most community and ecosystem dynamics, while still spanning a similar (although narrower) range of productivity seen across the entire northeast Pacific. Our results suggest that the importance of bottom-up control in coastal ecosystems may often be overestimated.

Top-down regulation was the dominant and only significant factor controlling algal abundance, in contrast to past work showing the sensitivity of giant kelp to nutrient levels and local-scale disturbance regimes (*14*). Our study had a relatively large spatial scale and broad taxonomic coverage, which likely explains these differences in results. Given that kelp is a foundation species for the ecosystem, this top-down regulation of kelp dynamics is likely to have community-wide consequences (*25*). For the midlevel trophic groups, top-down control is still highly significant, but explains less of the variation than that for the indirect control of algae. We have shown elsewhere that these differences in community structure are driven primarily by site-based variables (such as habitat or recruitment) and not by climate variables (such as local temperature, regional disturbance regimes, or El Niño–Southern Oscillation events) (*18*). In fact, the combination of spatial, temporal, and environmental variables included in our analyses also explained a significant amount of variation in community structure for mid-level trophic groups but not for algae (table S2). We anticipate that local-scale recruitment dynamics may be driving the differences in community structure not explained by top-down control, because recruitment limitation has been noted in other studies of kelp forest and intertidal communities in the region of our study (*19*, *26*). If local-scale predator abundance and recruitment dynamics are indeed the driving forces for the community dynamics of coastal ecosystems, then the difference in the scales of community regulation may be a fundamental reason for the different results among different systems, in particular between pelagic and benthic ecosystems.

Future efforts to manage and protect coastal ecosystems will be challenging, given all of the threats that these systems face. Our results suggest that efforts to control activities that affect higher trophic levels (such as fishing) will have far larger impacts on community dynamics than efforts to control, for example, nutrient input, except when these inputs are so great as to create anoxic zones (i.e., dead zones). In fact, as predators return to systems in response to conservation and restoration efforts, top-down regulation should become even more important than we found in our study, although the role of any particular species in this control of community dynamics may decrease. In contrast, if humans continue to "fish down" coastal food webs, essentially removing the agents of community control, large ecosystems by default become controlled by bottom-up rather than top-down factors, making these systems even more sensitive to future nutrient inputs.

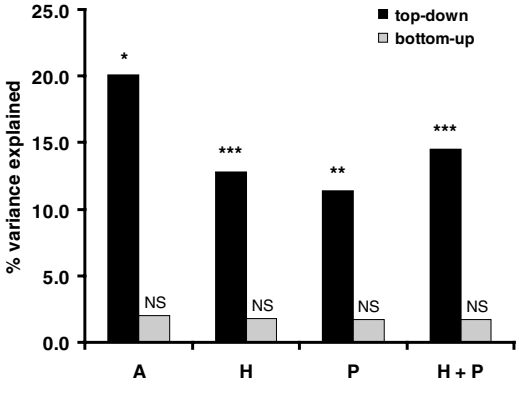

Fig. 3. Percent variance in community structure explained by bottom-up versus top-down variables for different trophic levels. A, algae; P, planktivores; H, herbivores. Significance values are indicated for variance decomposition analyses testing whether the abundance of that trophic level is explained by predator abundance (black bars) or primary production (gray bars). *$P < 0.05$, **$P < 0.01$, ***$P < 0.001$; NS, not significant.

References and Notes

1. S. R. Carpenter, J. F. Kitchell, J. R. Hodgson, *Bioscience* **35**, 634 (1985).
2. M. D. Hunter, P. W. Price, *Ecology* **73**, 724 (1992).
3. M. E. Power, *Ecology* **73**, 733 (1992).
4. J. A. Estes, M. T. Tinker, T. M. Williams, D. F. Doak, *Science* **282**, 473 (1998).
5. P. M. Vitousek *et al.*, *Ecol. Appl.* **7**, 737 (1997).
6. D. Pauly, V. Christensen, J. Dalsgaard, R. Froese, F. Torres, *Science* **279**, 860 (1998).
7. J. B. C. Jackson *et al.*, *Science* **293**, 629 (2001).
8. A. J. Richardson, D. S. Schoeman, *Science* **305**, 1609 (2004).
9. D. M. Ware, R. E. Thomson, *Science* **308**, 1280 (2005).
10. W. J. Mitsch, J. G. Gosselink, *Wetlands* (Van Nostrand Reinhold, New York, ed. 2, 2001).
11. B. Worm, R. A. Myers, *Ecology* **84**, 162 (2003).
12. K. T. Frank, B. Petrie, J. S. Choi, W. C. Leggett, *Science* **308**, 1621 (2005).
13. R. S. Steneck *et al.*, *Environ. Conserv.* **29**, 436 (2002).
14. P. K. Dayton, M. J. Tegner, P. B. Edwards, K. L. Riser, *Ecol. Monogr.* **69**, 219 (1999).
15. M. H. Graham, *Ecosystems* **7**, 341 (2004).
16. M. P. Otero, D. A. Siegel, *Deep-Sea Res. II* **51**, 1129 (2004).
17. C. A. Blanchette, B. R. Broitman, S. D. Gaines, *Mar. Biol.* 10.1007/s00227-005-0239-3 (2006).
18. B. S. Halpern, K. Cottenie, *Global Change Biol.*, in press.
19. B. R. Broitman, C. A. Blanchette, S. D. Gaines, *Limnol. Oceanogr.* **50**, 1473 (2005).
20. See supporting online material.
21. L. Legendre, P. Legendre, *Numerical Ecology* (Elsevier, New York, 1998).
22. J. C. Castilla, *Trends Ecol. Evol.* **14**, 280 (1999).
23. B. A. Menge, *J. Exp. Mar. Biol. Ecol.* **250**, 257 (2000).
24. L. R. Vinueza, G. M. Branch, M. L. Branch, R. H. Bustamante, *Ecol. Monogr.* **76**, 111 (2006).
25. K. D. Lafferty, *Ecol. Appl.* **14**, 1566 (2004).
26. D. C. Reed, P. T. Raimondi, M. H. Carr, L. Goldwasser, *Ecology* **81**, 2011 (2000).

27. Thanks to D. Kushner and the U.S. National Park Service for providing the Kelp Forest Monitoring Program (KFMP) data and to D. Siegel for the Institute for Computational Earth System Science (ICESS) chlorophyll a composites. B. Silliman, K. Selkoe, F. Micheli, and three anonymous reviewers provided valuable comments on earlier versions of this manuscript. Support was provided by the National Center for Ecological Analysis and Synthesis (B.S.H. and K.C.), the A. W. Mellon Foundation (B.R.B.), and the David H. Smith postdoctoral program funded by The Nature Conservancy (B.S.H.).

Supporting Online Material

www.sciencemag.org/cgi/content/full/312/5777/1230/DC1
Materials and Methods
Tables S1 and S2
References

11 April 2006; accepted 26 April 2006
10.1126/science.1128613

Dispensing Safety Caps

These caps, designed in a variety of configurations, help control dangerous, costly laboratory mishaps that can compromise the health and safety of staff and require emergency clean-up and down time. The T series cap is designed to maintain a steady flow equilibrium while preventing the escape of gaseous vapors that can contaminate the work environment. With an optional integrated check valve and filter, the T cap prevents the introduction of unwanted ambient debris. The combined air inlet and check valve configuration enables air to flow into the bottle to replace the removed liquid while preventing particulate contamination. The Q Series or C Series bottle caps can prevent measurement mistakes when transferring liquids. These caps, fitted with optional on/off valves, allow for foolproof, precision operation of individual fluid lines to carefully control a chemical reaction. Because these safety valves can be shut with precision, the caps are useful for transporting and handling fluids to and from individual stations within the laboratory.

Bio-Chem Valve and Omnifit. For information 973-263-3001 www.bio-chemvalve.com

Total RNA from Tissue

The RNeasy FFPE Kit is designed to purify total RNA from formalin-fixed, paraffin-embedded (FFPE) tissue sections. Special lysis and incubation conditions reverse formalin crosslinking, which would otherwise block downstream applications. The purified RNA delivers maximal performance in applications such as real-time reverse transcription-polymerase chain reaction. The specially developed lysis buffer efficiently releases RNA from FFPE samples while avoiding further RNA degradation. Optimized binding conditions allow purification of all usable RNA down to 70 nucleotides. The procedure can be completed in as little as 70 minutes.

Qiagen For information 800-426-8157 www.qiagen.com

Cancer Study Antibody Array

The Panorama p53 Pathways Antibody Array is designed for studying the expression patterns of proteins known to be involved in p53 pathways. The array enables the analysis of cell or protein extracts and contains 112 antibodies spotted in duplicate onto a nitrocellulose slide along with Cy3 and Cy5 positive controls and a negative control. The regulatory protein p53 is involved in a variety of signaling pathways that could be crucial to understanding the development and progression of cancer.

Sigma-Aldrich For information 314-286-7616 www.sigma-aldrich.com

One-Step Cell Lysis and Protein Purification

The HIS-Select iLAP 5 ml Column is a patent-pending method that combines cell lysis and histidine-tagged protein purification steps into one step, allowing fast, efficient, and non-denaturing protein extraction directly from microbial cultures. It maximizes the speed and efficiency of recombinant protein extraction while eliminating sample loss. The column contains highly specific HIS-Select nickel chelate matrix and highly efficient CelLytic Express, both present in a convenient tablet format. The single-use, disposable column is designed for the simultaneous, direct lysis of a 5-ml bacterial culture and affinity capture of the target histidine-tagged protein without any additional manipulation required (such as centrifugation). As the culture is lysed in the column, the target protein is captured on the same highly selective HIS-Select Affinity Gel.

Sigma-Aldrich For information 314-286-7431 www.sigma-aldrich.com

Silicon Drift Detector

The Quantax Quad is an innovative energy-dispersive spectroscopy (EDS) system for x-ray microanalysis on electron microscopes. It features the unique XFlash Quad detector, the first four-channel 40 mm^2 silicon drift detector (SDD) for EDS systems mounted on electron microscopes. The novel Quantax Quad delivers fast results across a broad range of applications. It is especially suitable for field emission scanning electron microscopes and low vacuum scanning electron microscopes. Cooled by Peltier elements, the XFlash Quad detector requires no liquid nitrogen and is vibration-free and maintenance-free.

Bruker AXS For information 609-771-4473 www.bruker-biosciences.com

ICP Emission Spectrometer

The ICPE-9000 Multitype ICP (inductively coupled plasma) Emission Spectrometer is suitable for analyzing substances from metals to pharmaceuticals and offers reduced running costs, stable performance, high sensitivity, and low contamination. Its advanced technology includes a large-scale, one-inch charge-coupled device (CCD) detector with increased pixel size and an Echelle spectrometer that allows high-speed measurements with increased resolution. It is equipped with mini-torch technology that reduces argon gas consumption by half compared with conventional torches. Because the ICPE-9000's spectrometer (equipped with semiconductor detectors) is maintained under a vacuum, contamination and decline in sensitivity do not occur over long-term use, and high-purity gas for internal purging is not required. The instrument's software includes qualitative database calibration (for automatic wavelength selection and fast calibration), a method development assistant, an automatic wavelength selection system, an interference database, and a method diagnosis assistant.

Shimadzu Scientific Instruments
For information 800-477-1227 www.ssi.shimadzu.com592K

Newly offered instrumentation, apparatus, and laboratory materials of interest to researchers in all disciplines in academic, industrial, and government organizations are featured in this space. Emphasis is given to purpose, chief characteristics, and availability of products and materials. Endorsement by *Science* or AAAS of any products or materials mentioned is not implied. Additional information may be obtained from the manufacturer or supplier by visiting www.science.labvelocity.com on the Web, where you can request that the information be sent to you by e-mail, fax, mail, or telephone.

POSITIONS OPEN

ASSISTANT/ASSOCIATE/FULL PROFESSOR
The Allan and Alfie Norville Endowed Chair for Heart Disease in Women Research

The University of Arizona (U of A) College of Medicine invites applications for a tenure-track **ENDOWED CHAIR POSITION** in Cardiovascular Research broadly focused on Women's Heart Issues. The successful candidate will be a member of the newly formed, and rapidly expanding, Cardiovascular Research Program that will occupy a floor of the new Medical Research Building. This program represents a tremendous opportunity for growth in cardiovascular research.

A competitive recruiting package is offered. Applicants must have a Ph.D., M.D., or equivalent degree, an active extramurally funded research program and scholarly publications. Candidates with research experience in modern molecular approaches are particularly encouraged to apply. The candidate will benefit from a highly collaborate environment and will have a primary appointment in a basic science or clinical department, and will be a member of the U of A Sarver Heart Center. Interested applicants should go to **website: http: //www.uacareertrack.com** and search for Job 35047. In addition, send a letter with curriculum vitae, a state of the applicant's research interests with emphasis on how their research might impact Women's Cardiovascular Health issues, and the names of three individuals as references to: **Dr. Carol Gregorio, c/o Chris Martin, University of Arizona, 1501 N. Campbell Avenue, P.O. Box 245044, Tucson, AZ 85724.** Review of applications will begin August 1, 2006, and will continue until the position is filled. For more information contact **Drs. Gordon Ewy (e-mail: gaewy@aol.com), Carol Gregorio (e-mail:gregorio@u.arizona.edu)** or see **website: http://www.heart.arizona.edu.** *The U of A is an Equal Employment Opportunity/Affirmative Action Employer and encourages applications from minorities, women, persons with disabilities, and veterans.*

FACULTY POSITION IN STRUCTURAL BIOLOGY
Wayne State University, School of Medicine

The Department of Biochemistry and Molecular Biology (**website: http://www.med.wayne.edu/biochem**) seeks applicants with a strong record of research accomplishments for a **TENURE-TRACK POSITION** in structural biology, in areas related to human disease. Candidates in all fields will be considered, but preference will be given to investigators in the area of infectious disease or drug design. The position is available at any level; junior candidates are particularly encouraged to apply. Core facilities include 600 MHz and 700 MHz NMR spectrometers, Rigaku FR-D generator and HTC area detector, and high performance fluorescence and CD spectrometers. The successful candidate will have guaranteed access to the Michigan Life Sciences Corridor 900 MHz NMR facility in Lansing or the LS-CAT at Argonne APS. E-mail a statement of research interests, curriculum vitae, and names of three or more references as a single PDF file to: **Robert Johnson, Chair of the Search Committee** at **e-mail: rmjohns@med.wayne.edu.** *Wayne State University is an Equal Opportunity Employer and encourages applications from women and minorities.*

FACULTY POSITION IN NEUROSCIENCE

The Department of Biomedical Sciences at Marquette University invites applications for a tenure-track faculty position at the level of **ASSISTANT PROFESSOR.** The successful candidate will be expected to develop an independent, extramurally funded research program that expands the Departmental research focus in neuroscience. Candidate is expected to participate in teaching undergraduate histology/graduate neuroscience courses. Send curriculum vitae, description of research interests, and the names of three references to: **Dr. Doug Lobner, Department of Biomedical Sciences, Marquette University, P.O. Box 1881, Milwaukee, WI 53201-1881 (e-mail: doug.lobner@mu.edu).** *Affirmative Action/Equal Opportunity Employer.*

POSITIONS OPEN

FACULTY POSITION IN MASS SPECTROMETRY AND PROTEOMICS

Applications are invited for a faculty position at the rank of **RESEARCH ASSISTANT PROFESSOR.** The Feist-Weiller Cancer Center **(website: http://www.fwcconline.org/)** at Louisiana State University Health Sciences Center-Shreveport (LSUHSC-S) seeks a research-track faculty member with broad expertise in mass spectrometry and proteomics research who will have an academic appointment in the Department of Biochemistry and Molecular Biology **(website: http://www.shrevebiochem.com)** and will have laboratory and office space in the Research Core Facility (RCF). This facility maintains and operates state-of-the-art technologies primarily for the benefit of LSUHSC-S researchers that include MALDI-TOF-MS and LC-MS-MS. The successful candidate is expected to operate the mass spectrometry component of the RCF. This will involve active collaborations with other LSUHSC-S researchers, establishing additional mass spectrometry techniques at LSUHSC-S, developing proteomics capabilities, and writing extramural grant proposals to augment existing mass spectrometry capabilities. Applicants should have a doctoral degree and postdoctoral research experience in mass spectrometry and/or proteomics. Please send curriculum vitae, a brief statement of current research interests and experience in mass spectrometry, and the names of three references to: **Robert E. Rhoads, Ph.D., Professor and Head, Department of Biochemistry and Molecular Biology, Louisiana State University Health Sciences Center-Shreveport, 1501 Kings Highway, Shreveport, LA 71130-3932.**

RESEARCH FACULTY POSITIONS AVAILABLE

One of the most prominent research institutes in Taiwan, the Institute of Atomic and Molecular Sciences, Academia Sinica, invites qualified candidates to apply for tenure-track Research Fellow (Principal Investigator) positions in the following research fields: biophysical science, nano-science, surface science, molecular dynamics, atomic physics, ultrafast and high-field optics, and interdisciplinary field in physical chemistry or chemical physics. For detailed academic activities of our Institute, please visit **website: http://www.iams.sinica.edu.tw.** Applicants should send full curriculum vitae by air-mail or e-mail, including a list of publications, a research proposal, and at least three letters of recommendation to: **Dr. Jim J. Lin, Room 335, P.O. Box 23-166, Institute of Atomic and Molecular Sciences, Academia Sinica, Taipei, Taiwan 106. E-mail: jimlin@po.iams.sinica.edu.tw; fax: 886-2-2362-0200.** To ensure timely processing, all application materials must be received by August 31, 2006.

ASSISTANT PROFESSOR, ECOLOGY, ASHLAND UNIVERSITY. One year, full-time, temporary position, Ph.D. required. Position primarily involves teaching ecology to nonmajors, with the possibility of teaching other courses in an area of specialization. Facilities are available for research activities, including directing undergraduate research. Send letter of application, statement of teaching philosophy, curriculum vitae, transcripts, and three letters of recommendation to: **Ecology Search, Department of Biology/Toxicology, Ashland University, Ashland, OH 44805.** See **website: http://www.ashland.edu.** Application review begins June 1, 2006. *Ashland University is an Equal Opportunity Employer and is committed to diversity in the workplace.*

RESEARCH ASSOCIATE IN GENOMIC ANALYSIS

The Edward Via Virginia College of Osteopathic Medicine (VCOM) invites applications for a Research Associate in Genomic Analysis of Human Arthritis and Obesity. VCOM is a postbaccalaureate professional medical college located in Blacksburg, Virginia. For more information on this position, please visit our **website: http://www.vcom.vt.edu.**

Careers in Translational Medicine

From Bench to Bedside

Translational medicine facilitates the rapid, effective application of results in the research laboratory to patients in the clinic. To work in the field, individuals need both a broad understanding of basic life science and a passionate interest in human health. BY PETER GWYNNE

For individuals seeking a career in life science, the ability to think in multidisciplinary terms has become little short of essential. Nowhere is that ability more necessary than at the conjunction of basic science and clinical medicine. Translational medicine, as the field is known, aims to convert research results into clinical developments of use to actual patients. It demands an understanding of both basic research and clinical medicine, and it is growing in popularity. "This is the hot area," says Roger Narayan, associate professor in the joint department of biomedical engineering at the University of North Carolina.

Defining translational medicine isn't easy. Indeed, it has almost as many definitions as practitioners. "It reminds me of the story about the blind men and elephant; people tend to define translation as part of drug development," jokes Edward Spack, senior director of biosciences business development at SRI International. "Speak to anybody from any company or academic institution and they'll have a new focus on it and a host of names," adds Trevor Mundel, global head of early clinical development at the Novartis Institutes for BioMedical Research.

However, researchers agree on the broad outlines of the field. "I define it as a global approach to extracting clinically useful information from advances in basic science and bringing those advances directly into clinical care," says Ann Harris, director of the human molecular genetics program at Children's Memorial Hospital's Children's Memorial Research Center and Northwestern University. Robin Miskimins, professor of basic biomedical sciences at the University of South Dakota, takes a similar view. "I think of it as medicine that seeks to implement the newest in treatment options by taking them from the research options to usable medical technology in as few steps as possible," she points out.

Children's Memorial Research Center
http://www.childrensmrc.org

National Institute of Child Health and Human Development
http://www.nichd.nih.gov

Northwestern University
http://www.northwestern.edu

Novartis Institutes for BioMedical Research
http://www.nibr.novartis.com

SRI International
http://www.sri.com

University of North Carolina
http://www.unc.edu

University of South Dakota
http://www.usd.edu

Bridge Building

Irwin Arias, adjunct investigator and head of the unit of cellular polarity at the National Institute of Child Health and Human Development and professor of physiology and medicine at Tufts University, summarizes those thoughts. "To me, translational medicine is a term that means almost the same thing as bridge building between science and medicine; others call it bench to bedside," he explains. "The principle is: How do you link up the incredible advances in science with better medicine? As with the metaphorical structure, this type of bridge building requires many different structural components. There is no single cure-all."

In almost all cases, the field involves movement of intellectual property from the laboratory to the clinic. "It's hard to overestimate the amount of good medical treatment that comes out of good basic research," Miskimins says. However, the activity can also move in the opposite direction. "A lot of people talk about the reverse of the bench to the bedside approach: taking things you can learn from the patient population to gain new insights into fundamental biology," Narayan explains.

Translational medicine has a history. "It's not a new concept," asserts Arias, whom many observers regard as the godfather of the field. "The link between medicine and science was very strong in the 1950s, 1960s, and into the 1970s. It was not unheard of then for basic scientists to attend grand rounds." But rapid advances in fundamental biology since then have focused basic researchers more on their lab work while changes in the nature of health care have made it increasingly difficult for clinical researchers to collaborate with their colleagues in fundamental science.

Those factors still hinder the progress of translational medicine. "Today, the opportunities to improve medical diagnosis and treatment based on science are extraordinary," Arias says. "But we're frustrated by changes in the health delivery system and medical education and the high degree of specialization in the progress of basic science." CONTINUED »

Careers in Translational Medicine


IRWIN ARIAS

Several Specialists

Success in translational medicine demands a wide variety of capabilities. "You have all the basic medical science disciplines – biochemistry, chemistry, pharmacology, physiology, and toxicology, as well as some of the physical sciences and engineering," Narayan says. "All these areas that can interface with clinical medicine are now doing so. Federal and private funding are making it possible." An understanding of development and application can also help. "Basic research is only part of the training needed," Spack explains. "Chemists may be good basic chemists but lack experience in formulation. Some companies have very strong engineers but little knowledge of regulatory affairs. Universities often lack regulatory expertise. One of the advantages we have here at SRI is technological divisions that can bring groups to bear on multidisciplinary challenges such as medical devices."

Recruiters don't ignore specialized skills. "All our translational medicine studies are based on biochemical or imaging markers," Novartis's Mundel says. "So our scientists need great familiarity with imaging techniques and their deficiencies."

However, a feel for multidisciplinary matters certainly helps scientists involved in translational medicine. "Those working most successfully are working across disciplinary boundaries," Northwestern's Harris points out. That doesn't necessarily demand broad training. "The skills don't need to be in one person, but must exist within the team," Narayan explains. "You can be largely trained as a specialist in one field," Harris agrees. "What's most important is to think broadly and think about subjects in a variety of ways. You need to be able to communicate with the people caring for patients – listening to them as well as explaining what you are doing."

Not many individuals fill the necessary criteria. "The number of people who fit into this is vanishingly small," Mundel says. "Within the cardiovascular metabolism area I must have reviewed 286 CVs of interested people. We got this down to a short list of six to eight scientists. Ultimately the one who joined us had actual clinical experience."


ANN HARRIS

Pathobiology for Ph.D.s

The most obvious candidates to participate in translational medicine are M.D.-Ph.D.s. "But those programs have a relatively fixed number of people coming through the pipeline," Arias says. "However, every medical school has basic science graduate programs that train Ph.D.s, most of whom have interest in pathobiology. Here at the National Institutes of Health, we offer Ph.D. students, postdocs, and staff who are interested in learning about disease and medical problems a course called "Demystifying Medicine." The course is similar to one we started at Tufts School of Medicine 18 years ago that trains Ph.D.s in pathobiology. The NIH program is generic and attracts people from all institutes."

Arias bases the course on a simple fact: "It's a lot easier to demystify medicine for bright Ph.D.s than to take chief residents and put them in a laboratory," he explains. The course exposes students to clinical and basic science presentations in a format based on old fashioned grand medical rounds, frequently including interviews with patients.

Ph.D.s have responded enthusiastically to the program. Slightly more than 100 scientists joined the course in 2001, the first year that Arias offered it. In the current year, he recalls, over 900 have registered and, on average, 350 regularly attend on site or electronically. Requirements for registration are simple. "The course is self-selecting," Arias says. "The one ingredient is that participants share a deep and sometimes passionate interest in human health." The program is accessible worldwide through the NIH's video archive and the Demystifying Medicine website (http://www1.od.nih.gov/oir/DemystifyingMed).

Scientists with that passion now have a few other options for training in translational medicine. "The National Cancer Institute has started a similar course solely focused on cancer biology, which is more detailed and more like a traditional course," Arias says. "MIT has an ambitious program that involves bioengineers." Whoever offers them, the courses have so far produced similarly positive results. "About a third of students selecting this kind of program after finishing their postdoctoral work are in tenure track positions in some of the best clinical departments," Arias reports.


ROBIN MISKIMINS

Mentors and Role Models

A few universities have started programs that require researchers to understand the basics of translational medicine. "We're starting an M.D.-Ph.D. program in the fall and looking for mentors and role models; we're specifically looking for people with M.D. and Ph.D. degrees," the University of South Dakota's Miskimins says. Finding those individuals presents one unique problem. "They see the winter here and don't come back," Miskimins says. "But it's getting easier to attract them."

Students have shown more enthusiasm. "They are quite academically diverse, including chemistry majors, biology majors, a psychology major, and some who have bummed around a while before deciding what they want to do next," Miskimins says. "All had a strong interest in medicine and then got hooked on research. They decided that making a contribution to the patients they would see as physicians would be an exciting way to go."

Harris's program, started at Northwestern two years ago and funded largely by philanthropic donations, aims to develop practical links between the lab and the clinic. "The program already has three principal investigators (PIs) who are working on genetic aspects of neurological disease – projects that tie in clearly with CONTINUED »

Visit **www.sciencecareers.org** and plan to attend upcoming meetings and job fairs that will help further your career.

Baylor Institute for Immunology Research
Dallas, Texas

Investigator in Infectious Diseases

Baylor Institute for Immunology Research (BIIR) in Dallas, TX is seeking a recognized leader in the field of bacteriology/virology to study the pathogenesis on the human immune system of microbes, such as HIV, hepatitis C and influenza virus. The $3 million Max and Gayle Clampitt Chair for Immunology Research is available to support this faculty position, as well as additional generous start up funds. The NIAID has recently designated BIIR as one of the nationwide Centers for Translational Research on Human Immunology and Biodefense. BIIR is the center of a network of scientists working at Yale University, The Rockefeller University, NIAID, the University of Texas Southwestern Medical Center and the University of New Mexico. Thus, this individual will play a major role in the Baylor/NIAID Center for Translational Research on Human Immunology and Biodefense and will work closely with BIIR researchers in a variety of existing projects as well as the development of new projects. BIIR is a highly-collaborative and energetic research facility that focuses on dendritic cells (DCs), the initiators of immune responses. A priority of BIIR is to design the vaccines of the future, based on either ex vivo generated DCs or recombinant fusion proteins composed of antibodies specific to DCs fused to microbial antigens. The overarching aim at BIIR is to quickly translate relevant research findings to the clinical setting in the form of novel therapeutic and diagnostic tools.

Post-doctoral Fellowships are also available.

BAYLOR
Institute for
Immunology Research
Baylor Research Institute

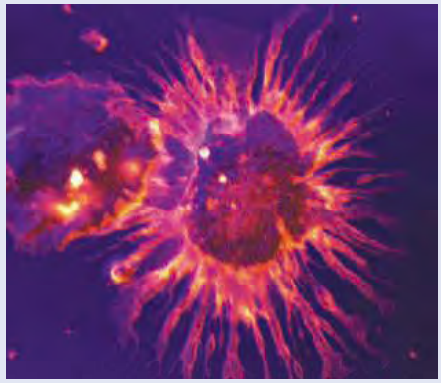

Interstitial dendritic cell

The Baylor Institute for Immunology Research was established in 1996 with a mission to translate recent discoveries in immunology from the laboratory to the patient bedside. The study of dendritic cells, the initiators of immune responses, represents a unifying theme of research for BIIR scientists. BIIR is housed in a 44,500 ft2 facility solely dedicated to research.

BIIR contains advanced core facilities including flow cytometry, confocal microscopy, microarrays, immunomonitoring, monoclonal antibody generation, humanized SCID mice, an animal facility with a BSL-2+ lab (a BSL3+ lab is in development) and a cGMP core dedicated to dendritic cell vaccines. We have a clinical group conducting IRB-FDA approved, investigator-initiated clinical trials.

Submit resume in confidence to:
Jacques Banchereau, PhD, Director
3434 Live Oak, Dallas, TX 75204

For information contact:
Cindy Samuelsen
(214)820-7451
cindysa@baylorhealth.edu

Visit the BIIR website: www.biir.org

Careers in Translational Medicine

clinical issues that the neurologists and psychologists at Children's Memorial Hospital are dealing with," Harris says. "All three are basic scientists, but they are very much crossing the boundary between the molecular advances at the bench and their use in developing new treatments."

Harris's requirements for qualified individuals resemble those of Miskimins. "The big recruitment of the moment is for PIs, but we have openings for postdocs also," she says. "The most important thing is that candidates have to be outstanding basic scientists who are creative and innovative. They also have to be able to see the bigger picture – the application of their research to clinical problems."

At the University of North Carolina, meanwhile, Narayan wants scientists with practical experience. "I'm looking for people who can translate a lot of our research in novel materials into practical devices," he says. "We want multidisciplinary and interdisciplinary skills in processing, characterizing, and modeling devices, as well as preclinical testing, animal modeling, and the clinical end of testing on human subjects. We want people who can take a device and interact with a clinical subject for testing and evaluation."

ROGER NARAYAN

Accelerating the Transition

However well academic programs work, they often fail to bridge the gap between research and usable products, in the form of drugs and devices intended to improve human health. That has emerged as a particular problem in recent years, as pharmaceutical and biotechnology companies have focused more on the later stages of their drug pipelines. "Early in this decade I saw a shift of money and emphasis on the drugs already in the clinic and a real need to chaperone new drugs," SRI's Spack recalls.

In response, his company linked up with Stanford University and the University of California faculties at Berkeley, San Diego, and San Francisco to create PharmaSTART, a consortium intended to accelerate the transition of new drugs from discovery into clinical use. "We're providing development plans that lay out roadmaps for how to make the transition, including advice on funding sources," says Spack, who is PharmaSTART's senior director. "We're also providing a forum for discussions on translational medicine with angel investors, the U.S. Food and Drug Administration, and other interested parties. And we're bringing groups together for translational development grant opportunities."

The consortium's variety of programs creates a demand for versatile recruits. "We're getting all sorts of projects, from gene therapy for an orphan disease to a small molecule for cancer," Spack says. "We need to triage projects quickly, to understand what the clinical application is, and to fill the pathways. So we need people with broad experience who can communicate with basic scientists: people who can translate translation. It also requires a certain level of marketing savvy to understand opportunities, some business acumen, and some feel for government." Fortunately, he adds, "we don't necessarily need all those skills in one person."

Industrial-style thinking is also crucial to Novartis as it recruits scientists for its work on translational medicine. "In the universities it's very difficult to have the sort of cross-fertilization that you need for translational medicine," Mundel explains. "There's also not the volume. We see projects turning over on a yearly basis; academics tend to think in spans of five years, 10 years, and more." Mundel seeks mainly senior scientists who can train their own replacements in what he calls "a kind of translational medicine university inside the company."

EDWARD SPACK

Traits for Success

What personality traits make for successful specialists in translational medicine? "It is important that they can communicate well with scientific and nonscientific stakeholders, such as ethics committees, internal review boards, regulatory agencies, and – importantly – research subjects," Narayan says.

Collegiality is equally critical. "Some people seem to have a certain knack of being able to work in a matrix without being trapped by it," Mundel says. "I see very bright people coming in and generating so many antibodies to their activities that they can't be successful." Harris agrees that the solo scientist has no place in translational medicine. "The people who are going to be successful in this field are not solely focused and completely absorbed by their research," she says. "They need to be energetic and to go out into the clinic. The field takes an outgoing, enthusiastic, highly energetic person."

Miskimins sees the need for two other characteristics. "One is problem-solving skills," she says. "You're going to deal with hospitals, drug companies, patients, and others, and encounter all sorts of hurdles and rules and regulations; you'll have to find solutions. The other factor is persistence. Not everything works the first time. You need the will to work at it when things aren't going well."

A former science editor of Newsweek, *Peter Gwynne (pgwynne767@aol.com) covers science and technology from his base on Cape Cod, Massachusetts, U.S.A.*

Others
call it research.

We call it changing the medical textbooks.




For 30 years, Genentech has been at the forefront of the biotechnology industry, using human genetic information to discover, develop, commercialize and manufacture biotherapeutics that address significant unmet medical needs. Today, Genentech manufactures and commercializes multiple biotechnology products that have helped patients suffering from serious diseases and conditions, including breast cancer, colorectal cancer, non-Hodgkin's lymphoma, lung cancer, rheumatoid arthritis, cystic fibrosis and allergic asthma. The company is the leading provider of anti-tumor therapeutics in the United States.

Genentech's research organization features world-renowned scientists who are some of the most prolific in their fields and in the industry. Our more than 650 scientists have consistently published important papers in prestigious journals and have secured more than 5,500 patents worldwide (with an equal number pending). Genentech's research organization combines the best of the academic and corporate worlds, allowing researchers not only to pursue important scientific questions but also to watch an idea move from the laboratory into development and out into the clinic. We are proud of our long history of groundbreaking science leading to first-in-class therapies, and we hope you'll consider joining us as we continue the tradition.

Our continued growth has created opportunities in Research in our South San Francisco headquarters. Please take this opportunity to learn about Genentech, where the creativity and openness of an academic environment meet the rigorous dedication of industry-leading professionals focused on improving and extending people's lives.

Seeking Cancer Research Professionals

Postdoctoral Fellows, Research Associates and Scientists in the following areas:

- Angiogenesis
- Antibody Engineering
- Assay Technology
- Bioinformatics
- Biomedical Imaging
- Cell Biology
- Immunology
- Medicinal Chemistry
- Molecular Biology
- Molecular Diagnostics
- Molecular Oncology
- Pathology
- Protein Chemistry
- Protein Engineering
- Translational Oncology
- Tumor Biology

Please visit us at booth #4813 at the ASCO Career Fair, June 3-5 in Atlanta, GA.

To learn more about these opportunities, please visit **www.gene.com/careers**. Please use "Ad - Science" when a "source" is requested. Genentech was named #1 on FORTUNE's 2006 "100 Best Companies to Work For" list. Genentech is an equal opportunity employer.

Genentech
IN BUSINESS FOR LIFE
www.gene.com

National Cancer Institute

U.S. DEPARTMENT OF HEALTH AND HUMAN SERVICES
National Institutes of Health

Be at the Forefront of Clinical Cancer Prevention Research

Join the NCI's Cancer Prevention Fellowship Program

The Cancer Prevention Fellowship Program offers research training in clinical cancer prevention and in other multidisciplinary aspects of cancer prevention science. Physicians, nurses, and other clinical scientists have the opportunity to combine their interest in cancer prevention research with their clinical acumen to become leaders in the field of cancer prevention and control. The program is sponsored by the Department of Health and Human Services, the National Institutes of Health, the National Cancer Institute (NCI), and the Division of Cancer Prevention.

What will I get out of the program?

- Master in clinical investigation (M.S.) or public health (M.P.H.) degree
- NCI Summer Curriculum in Cancer Prevention
- Mentored research at the NCI or at the Food and Drug Administration (FDA)
- Clinical privileges at nearby medical institutions at which research is carried out
- Experience in clinical prevention protocol review
- Professional development and leadership training

What areas of cancer prevention research are available?

- Behavioral intervention research
- Biomarkers and other basic (translational) research
- Chemoprevention
- Design and analysis of cancer prevention trials
- Development and research-related review of drugs, biologics, or medical devices
- Epidemiology (environmental, genetic, molecular, nutritional)
- Ethical issues in clinical prevention
- Evaluation and outcomes research of clinical prevention practices
- Nutritional intervention studies
- Screening and early detection

Am I eligible?

You must have a doctoral degree (M.D., Ph.D., or equivalent). Foreign education must be comparable to that received in the United States. You must also be a citizen or a permanent resident of the United States at the time of application (September 1).

How long is the program?

The typical duration is 3 years (year 1: master's degree; years 2-3: NCI Summer Curriculum in Cancer Prevention and mentored research).

How do I obtain more information?

Visit our website: **http://cancer.gov/prevention/pob** or request a catalog.

To receive a catalog*, contact:

Douglas L. Weed, M.D., M.P.H., Ph.D.
Director
Cancer Prevention Fellowship Program
National Cancer Institute
6130 Executive Boulevard (EPN)
Suite 321, MSC 7361
Bethesda, MD 20892-7361

* Please provide home address, telephone, e-mail, and where you heard about the program.

How do I apply?

Apply online at **http://cancer.gov/prevention/pob** or send your application materials directly to the Cancer Prevention Fellowship Program director, as described on our website and in our catalog.

When are applications due?

Applications are due September 1, 2006 for entry into the program in July 2007.

Further inquiries:

Program Coordinator
Cancer Prevention Fellowship Program
Phone: (301) 496-8640
Fax: (301) 402-4863
E-mail: cpfpcoordinator@mail.nih.gov

Selection for these positions will be based solely on merit, with no discrimination for non-merit reasons, such as race, color, gender, national origin, age, religion, sexual orientation or physical or mental disability. NIH provides reasonable accommodations to applicants with disabilities. If you need reasonable accommodation during any part of the application and hiring process, please notify us. The decision on granting reasonable accommodation will be handled on a case-by-case basis. **THE DHHS/NIH/NCI IS AN EQUAL OPPORTUNITY EMPLOYER**

AWARDS

Supporting the Career Development of U.S. and Canadian Physician-Scientists Whose Work Bridges the Gap between Basic Research and Patient Care

2007 Clinical Scientist Awards in Translational Research

The Burroughs Wellcome Fund is an independent private foundation dedicated to advancing the biomedical sciences by supporting research and other scientific and educational activities.

BURROUGHS WELLCOME FUND

919.991.5100
www.bwfund.org

Deadline: September 1, 2006
$750,000 over five years for established physician-scientists

- Candidates must have an M.D. or M.D.–Ph.D. degree, hold an appointment or joint appointment in a subspecialty of clinical medicine, and hold a current license to practice medicine in the U.S. or Canada.
- Candidates must be academic investigators at the assistant professor or early associate professor level, holding a tenure-track or equivalent position at the time of application.
- BWF is interested particularly in supporting investigators who will bring novel ideas and new approaches to translational research.
- Degree-granting institutions in the United States and Canada may nominate from two to four candidates.

Complete program information, eligibility guidelines, and application forms are available on BWF's website at **www.bwfund.org**.

CAREERS IN TRANSLATIONAL MEDICINE

Positions @ NIH

The National Institutes of Health

Hire the World's Best Scientists

Advertise your positions to the more than 3800 doctoral scientists and clinicians who are in training at the National Institutes of Health

Reach scientists who are at the forefront of their fields

Access a population large enough to guarantee interest in your position

Post new positions with a click of your mouse

Visit the NIH Virtual Job Fair @ www.training.nih.gov/careers

Office of Intramural Training and Education

For students, recent graduates, and postdoctoral, research, and clinical fellows.

Your on-line guide to training with the best at the world's largest biomedical research institution.

In Bethesda, Maryland, and at other NIH laboratories.

Office of Intramural Training
and Education
Bethesda, Maryland
20892
800.445.8283

opportunity *clicks*

www.training.nih.gov

Fogarty International Center
National Institutes of Health

The Fogarty International Center (FIC), the international component of the NIH, addresses global health challenges through innovative and collaborative research and training programs and supports and advances the NIH mission through international partnerships. This position is located in the Division of International Training and Research responsible for managing research and training grants and fellowships awarded by FIC. Grants support a diverse array of projects in infectious diseases, including HIV/AIDS, TB and malaria, chronic diseases including those related to mental health, injury and tobacco use, and the supporting disciplines of global health, including environmental sciences, population science, economics, bioethics and informatics. A growing number of these grants are highly interdisciplinary and include social and behavioral sciences.

FIC is looking for a behavioral or social scientist who will identify and administer extramural research and training awards in an array of global health relevant fields, including psychology, sociology, economics, anthropology, and health systems. Broad research experience, including experience in developing countries, strong communication and organizational skills are important. In addition to his/her own portfolio of grants, the candidate will work with existing program officers to strengthen the behavioral and social sciences linkages among the various extramural programs and other FIC divisions.

The vacancy announcement contains application procedures and lists all mandatory information, which you must submit with your application. To obtain the announcement which will be available on **05/01/2006**, and posted under **#FIC-06-119716**, you may visit the OPM website **http://www.usajobs.opm.gov/**. Applications and all supporting documentations must be received by **7/7/2006.**

WWW.NIH.GOV

Health Research in a Changing World

Fighting Diseases and Improving Lives

Director, Division of Extramural Activities (DEA)

The National Institute of Allergy & Infectious Diseases (NIAID) is seeking exceptional and visionary leaders for the position of Director, Division of Extramural Activities (DEA), NIAID. A $4.4 billion organization, the NIAID supports well over 100 major research programs and initiatives within three broad, distinct mission areas: Biodefense research, AIDS research, and the NIAID traditional research mission of immunologic and infectious diseases.

The Division of Extramural Activities (DEA) serves NIAID's extramural research community and the Institute by overseeing research policy and management for scientific review, grants and contracts. Annually, the NIAID awards approximately 6000 grants for 2.5 billion dollars. Within the last year NIAID awarded over 1 billion dollars in research and development contracts for Bioshield/Biodefense efforts and over 150 million dollars in small purchases and station support contracts making NIAID the largest servicing center for contracts at NIH.

DEA is responsible for the development and over sight of the NIAID phasing of initiatives and provides guidance and review of all solicitations affecting NIAID programs. In addition, DEA is responsible for managing NIAID's research training and international programs, and conducting initial peer review for funding mechanisms with Institute-specific needs. In addition to providing broad policy guidance to Institute management, DEA also oversees all of NIAID's chartered committees, including the National Advisory Allergy and Infectious Diseases Council (NAAIDC); disseminates information to its extramural community, and develops extramural staff training.

The DEA is comprised of 14 Offices, Branches, and Programs with approximately 210 scientific and administrative federal staff.

The Director, DEA reports to the Director, NIAID and provides overall executive direction and scientific leadership for the DEA. Specifically, develops, directs and coordinates DEA program activities; manages resource allocations to include staff, physical and financial resources; maintains staff through recruitment and training efforts and ensures effective program operations. In addition, the successful candidate will serve as an advisor to the Director, NIAID on extramural policy issues. Also, will serve the Institute in the following capacities: Integrity Officer for cases involving research misconduct; the Representative and Spokesperson to scientific societies, research organizations, institutional officials, and small business representatives; Representative on the Extramural Policy Management Committee for NIH and Liaison for NIAID and other Institutes for resolving disputes between officials regarding scientific issues.

Applicants must possess an M.D., Ph.D., or equivalent degree and must demonstrate the following: (1) worked independently in planning, organizing, and conducting biomedical research in fields consistent with the mission of the NIAID; (2) served effectively, in research program administration in these fields which must include managing policies and procedures associated with extramural research administration; and (3) acquired an understanding of the history, interests, internal dynamics, and relationships of the Institutes and Centers of the National Institutes of Health and of organizations in which health research is conducted. This experience may be gained via senior level research experiences as a principal investigator of a grant or contract, or may otherwise be gained through active involvement in initiating research projects, developing protocols, conducting studies, documenting findings, interpreting results in a published report (journal), supervising staff, and managing the budget. Preference will be given to those known and respected within their profession, both nationally and internationally, as distinguished individuals of outstanding scientific competence and those that possess a record as a senior scientific administrator/executive leader.

APPLICATION PROCESS: Applicants must be a U.S. citizen. Salary is commensurate with experience and a full package of benefits is available including retirement, health and life insurance, long term care insurance, leave and savings plan (401K equivalent). Curriculum vitae and bibliography to: **Ms. Lisa Poindexter-Steed**, Office of Workforce Effectiveness and Resources, NIAID, 6610 Rockledge Drive, Room 2109, Bethesda, Maryland, 20892-2520 and reference announcement number **DIRDEA-06-01**. The application review process will begin **June 16, 2006**. Direct inquiries to: Ms. Poindexter-Steed via email: lsteed@niaid.nih.gov or at 301-496-9687. Information regarding the Institute is available on our website at **www.niaid.nih.gov**. All information provided by applicants will remain confidential and will only be reviewed by authorized officials of the NIAID.

The Welsh Centre for Integrative Research in the Rural Environment (WCIRRE)

WCIRRE integrates research at the two universities in sustainability and resilience in the rural landscape, uniting more than 50 international scientists with expertise from molecular biology through ecology to the social sciences, with unifying themes of environmental change, health, conservation and sustainability. With £2.7 million we are now recruiting high calibre researchers to complement and reinforce existing strengths and create a leading international centre of excellence.

In the School of Agricultural and Forest Sciences, Bangor

* Chair in Environmental Systems

To work in areas such as risk assessment, land use and climate change; livestock-wildlife-human disease; food chains; life cycle analysis; application of integrative modelling techniques.

* Lecturer in Conservation
* Research Lecturer in Ecological Modelling

In the Institute of Rural Sciences, Aberystwyth

* Chair in Ecological Modelling

To develop novel integrative approaches towards understanding of ecological processes up to the landscape scale, in the context of rural land use and its production and service outputs.

* Lecturer in Grazing Ecology
* Research Lecturer in Environmental Systems

In the School of Biological Sciences, Bangor

* Chair in Environmental Genomics

To utilise state-of-the-art genomic and post-genomic equipment to investigate organism function within ecosystems, and so advance evolutionary and ecological theory and applications.

In the Institute of Biological Sciences, Aberystwyth

* Research Lecturer in Environmental Genomics/ Metabolomics

Salary and Terms

The Chair positions are permanent and within the Professorial range (minimum £44,818 p.a.), the Lecturer positions are 5-years and within the Lecturer range (£24,352 - £36,959 p.a.), and Research Lecturers are 3-years and within the Research 1A range (currently £20,044 - £30,002 p.a.).

Further details for posts at Aberystwyth: http://www.aber.ac.uk/human-resources/en/vacancies.htm and at Bangor: http://www.bangor.ac.uk/jobs/ Informal enquiries to Prof Jamie Newbold (cjn@aber.ac.uk, +44 1970 622242) and Dr John Healey (j.healey@bangor.ac.uk, +44 1248 383703) in Bangor.

Closing date for Chairs: 16 JUNE 2006, for other posts see web-sites above.

PRIFYSGOL CYMRU UNIVERSITY OF WALES **BANGOR**

Prifysgol Cymru Aberystwyth 1872 The University of Wales

PRIFYSGOL CYMRU • UNIVERSITY OF WALES BANGOR 1884

Wedi Ymrwymo i Gyfle Cyfartal • Committed To Equal Opportunities

---

USF HEALTH UNIVERSITY OF SOUTH FLORIDA

http://hsc.usf.edu • 12901 Bruce B. Downs Blvd, MDC 02 • Tampa, FL 33612

ASSISTANT/ASSOCIATE PROFESSOR
School of Basic Biomedical Sciences

The School of Basic Biomedical Sciences within the College of Medicine at USF Health, seeks outstanding scientists in the areas of Neurosciences, Cardiovascular, Allergy, Immunology & Infectious Diseases and Cancer Pathobiology for six tenured/tenure earning faculty positions at the level of Assistant/Associate Professor. These faculty can have appointments in the departments of Molecular Medicine, Molecular Pharmacology & Physiology, or Pathology & Cell Biology.

Currently, the College of Medicine has over 540 fulltime core faculty, over 450 medical students, and over 150 students in the biomedical graduate program. As a result of a recent reorganization, a School of Basic Biomedical Sciences has been established to serve as the home for all basic and translational research within the College. With the objective of doubling its extramural funding in the next five years, faculty of the College of Medicine have outlined a bold strategic plan which includes recruitment of over 50 new tenured/tenure earning faculty and the establishment of state of the art Core facilities.

USF Health consists of the colleges of Medicine, Nursing, and Public Health. Also included are the schools of Basic Biomedical Sciences and Physical Therapy. In partnership with its affiliated hospitals, USF Health's research funding last year was $134 million – more than half of which came from federal sources. It has research and clinical affiliations with H. Lee Moffitt Cancer Center, the Johnnie B. Byrd Sr. Alzheimer's Research Institute, the Tampa General Hospital, the All Children's Hospital, the Shriner's Hospital for Children, and the James A. Haley and Bay Pines VA Medical Centers. USF is one of only 95 public and private universities in the U.S. that have been designated as Carnegie Comprehensive Doctoral Research University/Very High Research Activity.

Minimum requirements for Assistant Professor include a MD, PhD, or MD/PhD with a minimum of two years of experience as a junior faculty and evidence of continued growth as an educator, mentor, and a productive researcher. For Associate Professor, a minimum of five years of continuous and productive accomplishment as an Assistant Professor or equivalent is required. The successful candidate is expected to have a distinguished record of scholarly activity, NIH R01 and other extramural funding and teaching experience in a medical/graduate curriculum. Ability to build interdisciplinary programs and experience with successfully mentoring graduate and medical students and postdoctoral-fellows is also required.

Applicants should submit, by email, a letter summarizing their qualifications and interests in the position, future research plans, curriculum vitae and the names and contact information of five references. Completed applications must be submitted to **Ms. Vanessa Ayer (vayer@health.usf.edu)**. Competitive start-up packages and salaries will be provided commensurate with experience. Review of Applications will begin June 5, 2006 and will continue until all positions are filled.

USF Health is committed to increasing its diversity and will give individual consideration to qualified applicants for this position with experience in ethnically diverse settings, who possess varied language skills, or who have a record of research issues that support/benefit diverse communities or teaching a diverse student population. The University of South Florida is an Equal Opportunity / Affirmative Action / Equal Access Institution. For disability accommodations, contact Vanessa Ayer at 813-974-8349 within 5 days of an event. According to Florida law, search records, including applications and search committee meetings, are open to the public.

50 YEARS

VCU

TENURE TRACK FACULTY POSITION DIRECTOR OF FUNCTIONAL LIPIDOMICS/METABOLOMICS INITIATIVE

Virginia Commonwealth University School of Medicine

Virginia Commonwealth University School of Medicine is developing a new initiative in functional lipidomics/metabolomics and invites applications for a tenure-track faculty position Nos. F1996 and F1997 to spearhead this initiative. Candidates should have a research program with a record of sustained productivity and current extramural funding. Substantial resources are available to support recruitment of an outstanding investigator in the general area of lipidomics or metabolomics. Candidates will be considered for the rank of Assistant, Associate or full Professor, based upon qualifications and experience. Applicants should have a M.D., Ph.D. or equivalent degree and will be expected to contribute to the University's teaching mission as well as develop vigorous collaborative efforts with other VCU researchers. VCU's research expertise is spread across several programs having national prominence in terms of NIH-funded research ranking. VCU has a very active and expanding critical mass of investigators whose research is focused on metabolism and signaling of bioactive lipids in cancer, inflammation, atherosclerosis, heart and lung disorders, cholesterol and bile acid metabolism in liver disorders, and insulin resistance and fatty liver disease. These programs have a history of strong and successful research and training programs. However, this search is not necessarily focused on existing areas of strength and invites outstanding applications covering any aspect of lipidomics or metabolomics.

More information about the School of Medicine and Departments, and this open position can be found at **http://www.vcu.edu/biochem/department/pos.shtml**and**http://www.pubinfo.vcu.edu/facjobs/facjob.asp?Item=2290**. Applicants should submit by email a CV, names and e-mail addresses of three references, and a summary of research and teaching interests to: **Dr. Robert F. Diegelmann (rdiegelm@vcu.edu)**, Department of Biochemistry, Virginia Commonwealth University School of Medicine.

Virginia Commonwealth University is an Equal Opportunity/Affirmative Action Employer. Women, persons with disabilities, and minorities are encouraged to apply.

biology COB

Editor-in-Chief

The Company of Biologists, a not-for-profit publisher, is seeking to appoint an Editor-in-Chief to launch and lead an exciting, new international monthly journal covering cutting edge research at the interface of biology and medicine, with an emphasis on model organisms.

The Editor-in-Chief will have the following responsibilities:

- Building the journal and developing its profile in the scientific community
- Quality, scope and intellectual calibre of the journal content
- Liaison with academic editors, members of the advisory board and peer reviewers
- Management of the in-house editorial team
- Editorial budget management.

To meet the challenge of this role, the ideal candidate will have biomedical research experience, a proven editorial track record and outstanding managerial and communication skills. The imaginative flair needed to launch a high profile new journal will be essential, as well as the commitment to developing it into a top-ranking publication. To this end, a proven ability to interact with senior scientists is required. Experience of journal launches would be a definite advantage.

The successful candidate will probably be located in the UK, but for the right person this may be negotiable. The salary will be competitive and will reflect the critical importance and responsibilities of this position. Applicants should send by email a CV and a brief covering letter explaining their interest in and qualifications for the post. [Additional information about the post can be obtained informally from Mrs Miriam Ganczakowski, Human Resources Officer.]

Written application and CV to be received no later than 23 June, 2006.

Mrs M. Ganczakowski
Human Resources Officer
The Company of Biologists Limited
Bidder Building, 140 Cowley Road, Cambridge CB4 0DL
Fax: 01223 426070
Email: miriam@thecob.demon.co.uk

PRINCIPAL ADVISER ON NEUROSCIENCE

The Gatsby Charitable Foundation

The Trustees of the Gatsby Charitable Foundation are looking for a Principal Adviser on neuroscience to help develop further their activities in this subject. They intend to try to make a significant contribution to the development of this science in the UK, on a scale similar to their activities in plant science.

The ideal candidate for this post will have the following characteristics:

- A strong personal interest in the area and commitment to it.
- A PhD and post-doctoral (research) experience at a high level in relevant areas.
- A genuine understanding of the science, in all its breadth, with a desire to make a significant contribution to its advancement.
- Happy to do a lot of international travel.

The role will be based in Cambridge, UK.

Salary will be sufficient to attract and retain a person of the calibre we seek.

Funding for this position is not intended to support research undertaken by the applicant him/herself.

Applicants should, in the first instance, email their curriculum vitae and a brief covering letter stating the reasons for their application to **contact@gatsby.org.uk**

Please put "Application for Gatsby Principal Adviser on Neuroscience" in the email subject heading.

Informal enquiries can be made to Lisa Page-Berelian by email l.page-berelian@gtep.co.uk or by telephone +44 (0) 20 7410 0330.

The closing date for applications is 30 June 2006.

Further information about The Gatsby Charitable Foundation can be found on the website www.gatsby.org.uk

MAX PLANCK INSTITUTE FOR CHEMICAL ECOLOGY

Nicotiana attenuata-oxylipin signalling **Group Leader position** in the **Dept of Molecular Ecology** at MPI for Chemical Ecology

We are looking for a

Postdoctoral scientist

with proven leadership abilities and training in molecular biology, ecology, or analytical chemistry and an interest in combining these skills to study plant-mediated interactions (with competitors, herbivores, pathogens) in a native tobacco, *Nicotiana attenuata*. The objective is to study traits important for *N. attenuata*'s ecological interactions by genetic transformation with subsequent tests of performance in *N. attenuata*'s native habitat. More than 50 different transformants are available, many that dissect oxylipin-signalling, and the resistance that it mediates, hence candidates with an interest in oxylipin-related resistance are particularly encouraged to apply. The position, which will be funded for 5 years (pending a successful 2nd year review), comes with a generous supply budget, technical support for plant transformation, vector construction, microarray construction and hybridization, plant growth, secondary metabolite analysis, access to field sites (see: http://www.ice.mpg.de/itb/home_en.htm for more information) and support for PhD students. Applicants should have an excellent knowledge of molecular biology and English communication skills.

The Max Planck Institute is an equal opportunity employer, committed to the hiring, advancement and fair treatment of individuals without regard to race, colour, religion, sex, age, national origin, ethnicity, disability or any other protected status designated by federal state or local law.

Review of applications will begin July, 2006. Please send CV, description of research interests, 3 references via mail or email (baldwin@ice.mpg.de) to:

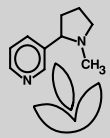

Prof. Ian T. Baldwin
MPI for Chemical Ecology
Hans-Knöll-Straße 8
07745 Jena
Germany

Research Opportunities
Virginia Bioinformatics Institute

Associate and Full Professorships in Bioinformatics

The Virginia Bioinformatics Institute (VBI) at Virginia Tech has built an internationally recognized scientific program with significant extramural funding. Areas of strength among the 16 research groups at VBI include infectious diseases, ranging from the molecular to the population scale, systems biology approaches to study stress response in several organisms, modeling and simulation of biological networks, functional genomics, metabolomics, proteomics and bioinformatics/computational biology. Candidates are expected to have an established research program and a track record of extensive extramural research funding.

About VBI. Established in 2000 by the Commonwealth of Virginia, the Institute is a part of Virginia Tech (VT) and has its own 130,000 sq ft research facility with state-of-the-art core laboratory and computational facilities. VBI strongly emphasizes synergistic interactions among faculty and is organized around the concept of team science. VBI places strong emphasis on systems biology and bioinformatics rather than organizing research according to academic disciplines. Instead, research areas represented at VBI organize themselves around the specific needs of individual research projects. Extensive national and international collaborations complement the expertise of the faculty, including strong interactions with several biomedical research centers. Faculty entrepreneurial activities are strongly encouraged and the university provides support for the establishment of commercial ventures.

State-of-the-art facilities. VBI is currently establishing a facility in the Washington, DC area, as part of Virginia Tech's expansion into that region. Faculty members whose programs will not require laboratory facilities will have the option of basing their primary research operation there. Faculty whose research programs require laboratory facilities will necessarily be primarily located at VBI's on-campus facility in Blacksburg, where state-of-the-art laboratory facilities are available. The new faculty may also have the option of joint affiliations with other departments at Virginia Tech and two prominent medical schools on the East Coast. Reference posting 042478.

Along with a strong research environment, the Institute actively participates in "Genetics, Bioinformatics, and Computational Biology" (GBCB), an interdepartmental Ph.D. program, widely recognized for its strengths in computational and experimental sciences, which attracts outstanding students with an interdisciplinary research focus.

Research Opportunities at VBI:

- Associate and Full Professorships in Bioinformatics, posting 042478
- AIDS Therapy Modeler Postdoctoral Associate, posting 042829
- Bacterial Genome Annotator Postdoctoral Associate, posting 042721
- Bioinformatics Scientists, postings 060012 and 060043
- Computational Biologist Postdoctoral Associate, posting 042479
- Computer Support Specialist, posting 043222
- Functional Genomicist Postdoctoral Associate, posting 060336
- IT Production Lead, posting 043200
- Metabolomics Specialist Postdoctoral Associate, posting 041979
- Metabolomics Specialist, posting 060044
- Microfluidics and Mass Spectrometry Specialist Postdoctoral Associate, posting 043287
- Molecular Biologist, posting 060045
- Nucleotide Metabolism Modeler Postdoctoral Associate, posting 060105
- Proteomics Specialist, posting 042940
- Software Engineer or Senior Software Engineer, posting 060286
- Software Quality Engineer Lead, posting 043285
- Systems Administrator, posting 043168

For more Information:

To apply, visit www.jobs.vt.edu and search by posting number.
To learn more about VBI and our research, please visit us at www.vbi.vt.edu

To learn more about the Interdisciplinary PhD program in Genetics, Bioinformatics, and Computational Biology (GBCB), visit http://www.grads.vt.edu/academics/programs/gbcb/index.html

VBI

VirginiaTech
Invent the Future

If you want to contribute your bit in alleviating human sufferings

If you are committed to scientific excellence

If your thrust is on Innovation in Life Sciences

Then Zydus Research Centre is just the right place for you

Zydus Research Centre (ZRC) is the research and development wing of Zydus Cadila, a global healthcare provider which aims to be a top ten global generic company by 2010 and a global research driven company by 2020.

Founded in the year 2000, ZRC is located at Ahmedabad, Gujarat, India and has 230 scientists working on cutting edge technologies in 14 scientific disciplines.

The research programme is focused on developing new therapies for diabetes, dyslipidemia, obesity, cardiovascular disorders, inflammation, arthritis and pain management. Within a short span of time, ZRC has developed a rich pipeline of New Chemical Entities (NCEs) which are at various stages of clinical and pre-clinical evaluation – ZYH1 (Phase II), ZYH2 (IND), ZYI1 (IND), ZYO1 (pre-clinical) and many are under biological testing. Our research in biologics has led to the development of several therapeutic proteins, vaccines and diagnostic kits.

ZRC is in the process of expanding its team and offers opportunities for outstanding R & D professionals, scientists and managers in the following areas:

- Medicinal Chemistry
- Combinatorial Chemistry
- Bioinformatics
- High Throughput Screening
- Pharmacology
- Molecular Biology
- Biotechnology (Upstream & Downstream Processing)
- Toxicology and Pathology
- Drug Metabolism and Pharmacokinetics
- Intellectual Property Management
- QA & Regulatory
- Clinical Research

Openings exist at various levels depending on your expertise and skills. Please visit **http://www.zyduscadila.com/R&D/research.asp** for detailed job profile and applying online.

ZRC provides a creative environment conducive for growth that encourages continuous learning and unravels the hidden potential.

Interested candidates can e-mail their resume giving full details of their experience, achievements and aspirations to **zrc@zyduscadila.com**. Candidates can also send in their resume indicating the post and area of specialisation on the envelope to:

The President,
Zydus Research Centre,
Sarkhej-Bavla N.H. No 8A, Moraiya, Ahmedabad – 382213.
Gujarat, India.

INNOVATION Zydus Research Centre IN LIFE SCIENCE

Zydus dedicated to life

ETH
Eidgenössische Technische Hochschule Zürich
Swiss Federal Institute of Technology Zurich

C-BSSE
Center of Biosystems Science and Engineering

The Center of Biosystems Science and Engineering of ETH Zurich in Basel

ETH Zurich established a new interdisciplinary Center of Biosystems Science and Engineering (C-BSSE) located in Basel (**www.bsse.ethz.ch**). The C-BSSE, which is an autonomous center of excellence active in the area of systems biology, is an integral part of SystemsX, the Swiss Initiative in Systems Biology (**www.systemsx.ch**). The Center will take a lead in combining biological, nanoscientific and computational approaches to study the behavior of single cells in isolation or in their interaction with other cells by following a tight integration of biological science and engineering at a conceptual and application level. The main research area of C-BSSE will be the study of perturbed biological systems, including the characterization of the dynamics of complex regulatory and metabolic networks down to the single molecule level, the simulation of systems behavior with the help of mathematical models, and the reconstitution and engineering of cellular and whole organ functions. The scientific concept will be realized with a structure for C-BSSE that gives approximately equal weight to experimentation, theory, and technology development. The Center has appointed a Director in Experimental Biology and is negotiating with senior candidates for the other areas. In addition, C-BSSE seeks to fill three positions at the assistant professor level (tenure track) in the following areas:

Assistant Professor of Experimental Quantitative Cell Biology
Candidates should have a strong background in quantitative analyses of cellular processes. Potential areas of research interests include, but are not limited to, a comprehensive description of gene regulatory networks to assess cellular functions and to achieve the ability to induce cellular plasticity required for regeneration and tissue engineering, and the uncovering of the routes of communication among cellular communities and deciphering the intracellular consequences. Methodological and technological approaches yielding data amenable to modeling and simulation will be considered preferentially.

Assistant Professor of Computational Biology
Candidates should demonstrate exceptional potential to develop an innovative research program in computational biology targeted towards biosystems sciences and engineering. Specific research areas include, but are not limited to, analysis and integration of heterogeneous experimental data sets (e.g. from genomics and proteomics), modeling, and inference and modeling of cellular networks, multi-scale simulation, systems analysis of network structures and dynamics, and optimal experimental design.

Assistant Professor of Synthetic Biology/ Engineering of Biological Systems
Candidates should demonstrate exceptional potential to develop an innovative research program in the rational engineering of complex biological systems. Current areas of interest include, but are not limited to, the manipulation and reconstruction of multi-component biological systems (genetic circuits, enzyme systems, modular protein complexes). With such an engineering perspective, other areas will be considered, such as the development of experimental tools to measure and image single molecular events in living cells, and the implementation of basic technologies such as the development and application of micro-scale devices to study the influence of signaling molecules on multi-cell dynamics and organization.

Assistant professorships at ETH Zurich have been established to promote the careers of younger scientists. The initial appointment is for four years with the possibility of renewal for an additional two-year period and promotion to a permanent position. The successful candidates will work in an open interactive research environment and are expected to have demonstrated ability to collaborate in an interdisciplinary research field at the interface of biological, computational, and engineering sciences. Courses at Master level may be taught in English.

Please submit your application together with a curriculum vitae, a list of publications, a list of on-going projects, and a detailed research plan **to the President of ETH Zurich, Prof. Dr. Ernst Hafen, Raemistrasse 101, CH-8092 Zurich, no later than June 30, 2006.** ETH Zurich specifically encourages female candidates to apply with a view towards increasing the proportion of female professors.

MEDICAL OFFICERS AND INTERDISCIPLINARY SCIENTISTS
PANDEMIC INFLUENZA VACCINE

The Center for Biologics Evaluation and Research, Food and Drug Administration, Department of Health and Human Services is searching for outstanding physicians and scientists to assist in the Center's Pandemic Influenza Vaccine initiative. Center staff conducts biomedical research to provide a strong scientific base for the regulation of blood and blood-related products, vaccines, allergenic products, and gene therapies according to statutory authorities in order to protect and enhance the public health. In conjunction with regulatory and research responsibilities, the Center statistically evaluates clinical and pre-clinical studies of human biological products and vaccines and epidemiologically evaluates post-marketing studies and adverse biological reactions.

The Pandemic Influenza Vaccine initiative is to protect critical workers and the US population in the anticipation of an influenza pandemic as quickly as possible through the establishment of a pandemic influenza vaccine manufacturing capacity. FDA has dramatically expanded its pandemic influenza program in the clinical, statistical, epidemiological, manufacturing and facilities areas this past year. FDA will be required to perform additional data reviews and facility inspections both for assuring adequate annual flu vaccine and in response to the potential for a pandemic.

QUALIFICATIONS:

- **Physicians:** Applicants must have an M.D. or equivalent degree from an accredited institution and additional research experience. Graduates of foreign medical schools must submit a copy of their ECFMG certificates.
- **Scientists:** (Other than M.D.) An advanced degree in one or more of the following disciplines is highly desirable: Biology, Microbiology, Chemistry, Biochemistry; Toxicology/Pharmacology, or Mathematical Statistician.

CANDIDATES FOR CIVIL SERVICE OR COMMISSIONED CORPS APPOINTMENTS MUST BE U.S. CITIZENS. NON-U.S. CITIZENS MAY BE ELIGIBLE FOR SERVICE FELLOWSHIP APPOINTMENTS OR OTHER POST-DOCTORAL PROGRAMS.

SALARY:

- **Physicians:** salaries range from Selected Federal White-Collar Pay Schedules, $97,213 - $114,882. In addition, physicians may also be eligible for a Physician's Comparability Allowance (PCA) of $4,000 to $24,000 per annum, or be appointed under Title 42 Excepted Service not to exceed $114,882. Salary and benefits are commensurate with education and experience. Positions may be filled by appointment in the US Public Health Service, Commissioned Corps.
- **Scientists:** salaries range from Selected Federal White-Collar Pay Schedules $52,468 - $114,882. Salary and level of responsibility are commensurate with education and experience.

LOCATION: CBER is actively recruiting applicants to fill positions located in Bethesda and Rockville, Maryland, involved in the regulation of biological and related products in support of the Pandemic Influenza Vaccine.

HOW TO APPLY: Applications are accepted and should indicate availability for employment. Interested candidates should submit a current Curriculum Vitae/Resume and cover letter to: **Food and Drug Administration, Center for Biologics Evaluation and Research; 1401 Rockville Pike, HFM-123, Rockville, MD 20852-1448; ATTENTION: Recruitment Coordinator**.

Additional information: **http://www.fda.gov/cber/inside/hirebkg.htm**.

FDA IS AN EQUAL OPPORTUNITY EMPLOYER. SMOKE FREE ENVIRONMENT.
**FDA provides reasonable accommodations to applicants/employees with disabilities.*

Associate director for Computational Neuroscience

International Neuroinformatics Coordinating Facility (INCF)

The INCF is an independent international organization established through a collaborative effort of 10 OECD member countries, following recommendations of the OECD Global Science Forum. The INCF consists of a Secretatiat, hosted by the Karolinska Institutet in Stockholm, and national nodes in each of the member countries. The mission of the INCF is to coordinate and facilitate the development of 1) database applications for neuroscience data, 2) analytical tools, and 3) modeling and simulation capabilities pertaining to nervous system functions.

The INCF Secretariat is currently under establishment and will have a staff of around 10 persons. INCF is now announcing a position as Deputy Director / Associate Director for Computational Neuroscience. The candidate should have a well established track record in computational neuroscience/neuroinformatics. The Associate Director will be responsible for coordination of developments of simulation and modeling tools, and the development of new interfaces between tools and databases. Salary level is subject to negotiation.

The application should contain a CV, a list of publications, a declaration of why the candidate is interested in this position, and a brief proposal of how the candidate would approach this task. The review of the applications will commence on August 1, 2006.

For information, contact: Executive Director, Professor Jan Bjaalie
Email: **jan.bjaalie@incf.se** Tel: **+46-70-5787092**

The application should be submitted to INCF, Karolinska Institutet, Nobels väg 15 A, SE-171 77 Stockholm, Sweden.

The **Division of Endocrinology and Metabolism/ Department of Medicine** at **Georgetown University Medical Center** invites applications for two tenure-track physician/scientist positions at the level of Assistant/Associate Professor.

Description of Program: The **Division of Endocrinology and Metabolism** is a multidisciplinary clinical and research division, and the home of vigorous NIH-funded programs in basic laboratory and clinical research. The Division is composed of 9 faculty members with active basic and clinical research programs in renal physiology, diabetes, obesity, thyroid disorders, vasopressin and oxytocin physiology, vitamin D metabolism, gender differences, regulation of food intake, and the renin-angiotensin-aldosterone system.

Targeted Areas of Research: The program seeks investigators with outstanding accomplishments and future promise in the following (but not limited to) scientific areas: diabetes, metabolic syndrome, and neuroendocrinology of obesity.

Candidates must have the following qualifications: PhD, MD, or MD/PhD degrees and a minimum of four years of postdoctoral experience (or equivalent). Appointees are expected to establish and maintain an outstanding research program, to bring or develop substantial external research funding, and to become leaders in departmental and programatic activities, including involvement in basic and/or clinical research in the areas of diabetes, metabolic syndrome and neuroendocrine control of obesity. Rank and salary are negotiable, but will be determined by the applicant's qualifications and prior employment history.

Interested applicants should submit a brief cover letter, CV and contact details of three potential references. Applicants should forward the required documents to: **Christine Maric, PhD, FAHA, FASN, Director, Diabetes Research, Center for the Study of Sex Differences, Georgetown University Medical Center, Washington, DC 20007. Email: cm255@georgetown.edu**.

GUMC is an Equal Opportunity/Affirmative Action Employer and encourages applications from women and minority candidates.

UCLA

Academic Administrator
Full Time Position

The Academic Administrator is responsible for overall program administration of the UCLA Undergraduate Minor in Biomedical Research, an interdisciplinary minor for approximately 400 students governed by a Faculty Advisory Committee, which includes faculty members from the biomedical sciences in both the College and the Medical School and reports jointly to the Dean of Life Sciences and the Vice Provost for Undergraduate Education.

Duties include the following: approve admission of students to the minor, recruit instructors from the ladder faculty for seminar courses, manage the placement of undergraduates in laboratories, manage mechanisms to provide individual career advice and mentoring to students to facilitate their acceptance and transition to postgraduate programs (MD, MSTP, PhD), monitor research laboratory training programs to ensure high standards of excellence, recruit and supervise lecturers, supervise graduate research mentors and counseling staff, prepare formative, summative and longitudinal assessments of the minor, serve as one of the instructors for the lower division course, train graduate students, postdocs and new faculty in mentoring undergraduate researchers in the minor.

Qualifications include a Ph.D. degree in a life science discipline (Biology, Microbiology, Physiology, Biochemistry, Neuroscience, Genetics or other related field); experience in undergraduate teaching at a university level; demonstrated skill in teaching undergraduate research-based laboratories at a university level; ability to conduct undergraduate seminars based on current biomedical research; experience mentoring undergraduate students in issues related to biomedical research.

Salary range of $54,240 – $70,272, commensurate with qualifications and experience. Please send curriculum vitae, written statement of teaching interests and background, and at least three letters of reference by **June 12, 2006** to: **UCLA Life Sciences Academic Coordinator Search ATTN: Ms. Grace Angus, 621 Charles E. Young Dr. South, Box 951606, Los Angeles, CA 90095-1606**.

UCLA is an Equal Opportunity/Affirmative Action Employer. Women and minorities are encouraged to apply.

LABORATORY CHIEF, LABORATORY OF METHODS DEVELOPMENT AND QUALITY CONTROL

The Division of Bacterial, Parasitic and Allergenic Products, Office of Vaccines Research and Review, Center for Biologics Evaluation and Research, Food and Drug Administration, Department of Health and Human Services has an immediate opening for a productive scientist to serve as the Chief of the Laboratory of Methods Development and Quality Control. The successful candidate will lead mission-oriented research and regulatory activities related to laboratory methods used in the evaluation of vaccines for bacterial and parasitic diseases, including immunoassays to monitor vaccine response and bioassays to assess product quality. The focus is on the development, evaluation, and application of assay methods; projects are not restricted to a specific product area. Individuals with a doctoral degree are highly preferred. The position is located on the NIH campus in Bethesda, MD. Salary is commensurate with experience.

Candidates should send a resume and names/contact information including e-mail addresses for three references to: **Dr. Richard Walker, Director, Division of Bacterial Products, Center for Biologics Evaluation and Research, HFM-425, 1401 Rockville Pike, Rockville, Maryland 20852, or send to Richard.Walker@fda.hhs.gov**.

The DHHS and FDA are Equal Opportunity Employers.

THE UNIVERSITY OF CHICAGO

Host-Pathogen Interactions
Department of Microbiology

The Department of Microbiology at the University of Chicago invites applications for a faculty position at the rank of Assistant Professor (although candidates of all ranks will be considered). Applicants should have a Ph.D. or M.D., Ph.D. degree and relevant postdoctoral training. The successful applicant is expected to develop an extramurally supported research program focusing on host-pathogen interactions of parasitic or bacterial infectious agents. Candidates are expected to contribute to departmental teaching.

The University of Chicago maintains extensive core facilities in support of microbiological research. Competitive salaries and start-up packages will be provided. Applicants should submit a cover letter, curriculum vitae, and a statement of research interests emphasizing career goals. Review of applications will begin on **September 15, 2006** and will continue until position is filled. Completed applications and letters from three referees should be sent to: **Olaf Schneewind, Search Committee, Department of Microbiology, 920 East 58th Street, Room 1117, Chicago, Illinois, 60637**.

The University of Chicago is an Affirmative Action/Equal Opportunity Employer.

RESEARCH POSITIONS

Positions available at the rank of **Research Assistant Professor, Research Instructor** and **Post-Doctoral Fellow** for **NIH and VA funded Laboratory** to study mechanisms responsible for myocardial dysfunction in a variety of cardiomyopathy models using a combination of cutting-edge and classic techniques at the in vivo, organ, tissue, cellular and molecular levels. This laboratory is part of the new **CENTER FOR INTEGRATIVE RESEARCH IN CARDIOVASCULAR SCIENCES (CIRCS) at WEST VIRGINIA UNIVERSITY SCHOOL OF MEDICINE**.

Interested applicants with relevant training and experience, particularly in molecular biology and protein-protein interactions, should submit a copy of their curriculum vitae and the names and contact numbers of three references to:

Mitchell S. Finkel, M.D.
West Virginia University
School of Medicine
Departments of Medicine, Physiology and Pharmacology
PO Box 9157
Morgantown, WV 26506-9157
mfinkel@hsc.wvu.edu

WVU is an Equal Opportunity/Affirmative Action Employer. Women and Minorities are encouraged to apply.

Wellman Center for Photomedicine

Assistant or Associate Professor

The Wellman Center for Photomedicine at Harvard Medical School and the Harvard University-Massachusetts Institute of Technology Division of Health Sciences and Technology (HST) are collaborating in the search for a candidate at either the Assistant or Associate Professor level who will establish new research programs in photodynamic therapy (PDT) in areas such as (but not limited to) cancer research, infectious diseases, and fluorescence imaging. The candidate will be expected to promote and foster multidisciplinary research with joint faculties within Wellman, HST, and the larger MGH and Harvard research communities.

The Wellman Center, located on the campus of the Massachusetts General Hospital, will be the primary physical location for this faculty member. The Wellman Center for Photomedicine (WCP) conducts basic and applied research to investigate the use of optical technologies in medicine and biology (**http://www.mgh.harvard.edu/wellman**); this is where the only first-line clinical application of PDT for treatment of choroidal neovascularization secondary to age-related macular degeneration (Visudyne) was co-developed. Ongoing translational programs at WCP emphasize the development of imaging technologies, tissue optics, and new combination treatments, such as PDT with differentiation and immune therapies, and PDT of disease-specific molecular targets. Active PDT research at WCP focuses on cancer (ovarian, prostate, skin, GI, head & neck), cardiovascular and infectious diseases, immunology, and ophthalmology.

The ideal candidate would combine a record of achievement in scientific research and a demonstrated interest in translational research, with an M.D., a Ph.D. or an M.D.-Ph.D. A strong publication record and evidence of ability to obtain independent peer-reviewed funding is expected. Although there is interest in a candidate with a program in cancer biology, applicants in a wide range of research disciplines will be considered as long as there is a commitment to developing PDT research (see additional PDT program information at **http://www.dartmouth.edu/~pdt/**).

Applicants should submit the following: (i) curriculum vitae, (ii) a statement of teaching interests, (iii) a statement of research interests and goals demonstrating commitment to PDT, (iv) brief ideas of potential collaborative possibilities with WCP and HST faculty (**http://hst.mit.edu**), (v) plans for future funding, and (vi) reprints of selected recent publications. Applicants also need to make arrangements to have three letters of recommendation sent on their behalf directly to the Search Committee Chair. Although applications will be accepted until the position is filled, complete applications (with at least three references in hand) will be reviewed beginning **July 14, 2006**, and should be mailed to: **Tayyaba Hasan, Ph.D., Chair of WCP/HST PDT Faculty Search Committee, c/o Susan Weeks, Wellman Center for Photomedicine/MGH, 40 Blossom Street BAR 604, Boston, MA 02114**. Electronic versions of the application materials should also be sent to **sweeks@partners.org**.

Massachusetts General Hospital, Harvard University and Massachusetts Institute of Technology are Equal Opportunity Employers. Women and minorities are encouraged to apply.

ROPES & GRAY

FISH & NEAVE IP GROUP OF ROPES & GRAY

Ropes & Gray LLP
Fish & Neave Intellectual Property Group
Patent Agent/Technical Advisor Program
Boston and New York City

The Fish & Neave Intellectual Property Group of Ropes & Gray LLP is an internationally known intellectual property law practice of over 200 lawyers. We are seeking Ph.D. candidates, nearing the completion of their studies and thesis defense, or recent Ph.D. graduates, working in academia or industry to join our Patent Agent/Technical Advisor Program. The candidates' Ph.D. degrees should be in the areas of synthetic organic chemistry, cellular biology, immunology, molecular biology, neurobiology, pharmaceutical sciences, bioinformatics, genomics, proteomics, polymer chemistry, or biochemistry.

The positions are full-time. We train the Patent Agent/Technical Advisor to prepare and to prosecute patent applications and to perform other tasks relating to our practice, including litigation, transactions, counseling and licensing. After one year with the firm, the Patent Agent/Technical Advisor also attends law school, either days or nights. During the last 15 years, more than 60 Ph.D's have joined our program and more than 40 have graduated from law school and are now working as intellectual property lawyers in biopharmaceuticals. The remainder are continuing their law school studies. Benefits: competitive salary; full law school tuition (with book allowance); medical benefits; 20-days paid vacation.

E-mail resumes with complete undergraduate and graduate transcripts to:
hiringprogram@ropesgray.com

Students may also mail their materials to:
Ms. Heather C. Fennell
Legal Recruitment Manager
Ropes & Gray LLP
Fish & Neave Intellectual Property Group
1251 Avenue of the Americas
New York, NY 10020

Incyte Corporation is focused on becoming a leading drug discovery and development company by building a proprietary product pipeline of novel, small molecule drugs. We have assembled a talented drug discovery and development team that has extensive experience in a number of therapeutic areas. We have several active internal drug discovery programs focused on the identification of drugs for inflammation, cancer, and diabetes. Our assets, including a highly experienced team with prior industry success in bringing important new drugs to market put us in a strong position to make a difference in healthcare as well as improve the lives of patients. We are currently recruiting for a Research Investigator/Sr. Research Investigator in our Applied Technology Group located in Wilmington, Delaware.

Research Investigator/Sr. Research Investigator

The position in this dynamic group is to provide the chemistry group with biological assays for leads identification, leads optimization, and SAR studies. The assays vary from enzymatic assays, membrane and cell binding assays, to cell based functional assays. The responsibilities include assay selection, development, and more importantly assay implementation and data management. Thorough mechanistic understanding of a variety of cell based and biochemical assays is required. Hands on experience with commonly used assay detection platforms and data management are pluses. We are seeking a Ph.D. in cell/molecular biology, biochemistry, pharmaceutical chemistry, or related fields.

Incyte provides a dynamic environment with a growing pipeline and an outstanding team to advance our programs. We offer a highly competitive compensation and benefits package. **For consideration please forward your resume with salary requirements to: careers@incyte.com, job code LL6443YL.** Equal Opportunity Employer M/F/V/D.

Incyte

Featured Employers

Search **ScienceCareers.org** for job postings from these employers. Listings updated three times a week.

Abbott Laboratories www.abbott.com

Genentech www.gene.com

Institute for One World Health
www.oneworldhealth.org

Kelly Scientific Resources
www.kellyscientific.com

Novartis Institutes for BioMedical Research
www.nibr.novartis.com

Pfizer Inc.
www.pfizer.com

Pierce Biotechnology, Inc.
www.piercenet.com

If you would like to be a featured employer, call 202-326-6543.

ScienceCareers.org
We know science AAAS

TERRY FOX MOLECULAR ONCOLOGY GROUP
LADY DAVIS INSTITUTE FOR MEDICAL RESEARCH
MCGILL UNIVERSITY

FACULTY POSITION
MOLECULAR ONCOLOGY

The Lady Davis Institute of McGill University is expanding its program in Molecular Oncology. An ASSISTANT PROFESSOR tenure-track position is available for candidates with research interests in the molecular and cellular basis of cancer with preference for applicants that use genetic mouse models. Applicants should have a Ph.D. and/or M.D. with relevant postdoctoral experience. Candidates will be judged on their potential to develop a vigorous independent research program that can attract extramural support.

The Lady Davis Institute for Medical Research and the Sir Mortimer B. Davis-Jewish General Hospital at McGill University houses over 50 independent research labs that cover the full range of basic and clinical research in oncology, neuroscience, endocrinology, and viral pathogenesis. We offer highly attractive salary and start-up packages and an exceedingly high quality of life in Montreal, one of North America's greatest and most lively cities.

Applicants should have an MD and/or PhD or the equivalent. Please send a letter outlining your current and future research interests, a copy of your CV and the names and addresses of three references to: **Chair of Search Committee, Lady Davis Institute for Medical Research/McGill University, 3755 Côte Ste-Catherine Road, Montréal, Québec, CANADA, H3T 1E2.**

Send email inquiries and applications to: **gdipancr@ldi.jgh.mcgill.ca**
Application deadline: **October 15, 2006**
More information can be found at: **http://www.jgh.ca/research/ldi/index.html**

In accordance with Canadian Immigration requirements, priority will be given to Canadians and permanent residents of Canada. McGill University is committed to equity in employment.

THE STATE UNIVERSITY OF NEW JERSEY
RUTGERS

Cell Biologist /Neurobiologist

The Department of Cell Biology and Neuroscience at Rutgers University, Piscataway, invites applications for two tenure-track positions at the Assistant Professor level. Applicants should have a Ph.D. or M.D. and an outstanding record of research productivity. Candidates in fields such as cell cycle regulation, cell differentiation, developmental neurobiology, immunology, and synaptic plasticity, at either the molecular or systems level, are strongly encouraged to apply.

The successful candidate will be expected to establish a high-quality, independent research program supported by external peer-reviewed funding, and to contribute to graduate and undergraduate education. The Department offers excellent state-of-the-art facilities and a competitive start-up package. Interested individuals are encouraged to apply on line through the CBN website (**http://cbn.rutgers.edu**) or send a curriculum vitae, a brief statement of research plans, and the names and addresses of three references to: **CBN Search Committee, c/o Virginia Marano (marano@biology.rutgers.edu), Nelson Laboratories, 604 Allison Road, Piscataway, NJ 08854**. The positions will be open until filled but applications postmarked before **August 15, 2006** will be considered first.

Rutgers University is an Equal Opportunity/ Affirmative Action Employer.

The U.S. Forest Service North Central Research Station seeks a **RESEARCH ECOLOGIST** to develop a more comprehensive understanding of biogeochemical cycles in forests. We are looking for a creative individual dedicated to advancing our understanding of forest carbon cycling. The position is in a work unit focused on belowground processes in ecosystems, and is located on the Michigan Technological University campus in Houghton, Michigan, on the beautiful Keweenaw Peninsula. This is a permanent, full-time appointment (GS-12/13/14/15; $62,291.00 to $133,850.00) with flexible work schedule, full health and retirement (including 401[k]-type), and vacation and sick leave benefits. The desired candidate will have a Ph.D. and research experience in the application of the principles and concepts of biogeochemistry to forest ecosystem science. Early to mid-career scientists seeking a synergistic environment and community of excellence are encouraged to consider joining our team. Adjunct faculty status and the ability to train graduate students are both possibilities.

The position is scheduled to open on **30 May 2006** for a period of 30 days. To receive the job announcement contact **Linda Kolodziej** at **651-649-5023** or via e-mail **lkolodziej@fs.fed.us**. The early alert describing the position in more detail can be found at **http://www.ncrs.fs.fed.us/4159**.

The U. S. Department of Agriculture Forest Service is an Equal Opportunity Provider and Employer.

Professor of Neurosurgery

As part of its Meningioma Project, The Department of Neurosurgery at Brigham and Women's Hospital seeks a scientist to fill the Kathleen and Steven Haley endowed Professorship of Neurosurgery at Harvard Medical School. The candidate should have a MD and/or PhD degree or equivalent with a significant record of achievement in the fundamental problems of biology, chemistry, genetics or other science broadly relevant to brain tumors. He or she should be willing to devote further work to studies of meningiomas and have a track record of programmatic collaborations.

Interested candidates should send their CV to :

Dr. Peter Black
Chair, Department of Neurosurgery
Brigham & Women's Hospital
75 Francis Street, Boston, MA 02115

Harvard Medical School and Brigham & Women's Hospital are Equal Opportunity/Affirmative Action Employers. Women and minorities are particularly encouraged to apply.

BRIGHAM AND WOMEN'S HOSPITAL
HARVARD MEDICAL SCHOOL

POSITIONS OPEN

The Department of Physical Therapy and Rehabilitation Sciences at the University of Kansas Medical Center invites applications for a tenure-track faculty member at the rank of **ASSISTANT/ASSOCIATE PROFESSOR.** Applicants must have a Ph.D.; a background in physical therapy or rehabilitation science is preferred. Applications for the position should have well-documented interests in research related to neurological rehabilitation; a research agenda that adds to our existing programs is preferred. The successful applicant will be expected to establish and maintain an active research program, obtain external funding and mentor Ph.D. students. Teaching responsibilities will be modest and based on the successful applicant's area of expertise.

The Department of Physical Therapy and Rehabilitation Sciences at the University of Kansas Medical Center is a well-established program offering an entry-level DPT degree, a postprofessional DPT degree, a Ph.D. in Rehabilitation Science, and a joint DPT-Ph.D. degree. The program is ranked 10th in the nation among physical therapy programs at public institutions by U.S. News and World Report. The faculty has diverse research expertise in the areas of stroke and Parkinson's disease, diabetes, chronic pain, peripheral joint injuries and scoliosis; and work with colleagues in the Hogland Brain Imaging Center, the Landon Center on Aging, and the General Clinical Research Center. Generous laboratory space and equipment are available. To learn more about the Department, please visit our **website: http://www.ptrs.kumc.edu.**

Interested individuals should apply online at **website: https://jobs.kumc.edu.** Applications will be accepted immediately. Position J0020282. Paid for by KUMC.

Questions can be directed to:

Patricia S. Pohl, Ph.D., PT
Mail Stop 2002
University of Kansas Medical Center
3901 Rainbow Boulevard
Kansas City, KS 66160
Telephone: 913- 588-4564
E-mail: ppohl@kumc.edu

An Equal Opportunity/Affirmative Action Employer.

POSITIONS OPEN

ASSOCIATE OR FULL PROFESSOR CARDIOVASCULAR RESEARCH

We seek an established investigator with outstanding research accomplishments to complement and extend the cardiovascular research strengths in our Department and our Institution. Medical College of Georgia has a strong cardiovascular research community with specific interests in myocardial disease, diabetes, hypertension, endothelial dysfunction, atherosclerosis, inflammation, oxidative stress, angiogenesis, nitric oxide, eicosanoids, adhesion proteins, ion channels, and development of physical cardiovascular risk factors. We seek an applicant with a strong record of productivity and an extramurally funded research program, particularly a program involving cardiac and vascular dysfunctions and diseases. Physician–scientists are encouraged to apply. We offer a substantial startup package commensurate with rank, and outstanding core facilities are available for microarray technology, genetically modified animals, cell imaging, electron microscopy, primate research, and clinical collaborations. The successful applicant for this position will also participate in teaching programs for professional and graduate students. Please send curriculum vitae, summary of professional and research goals, and the names and addresses of three references to: **Cardiovascular Search Committee, Department of Pharmacology and Toxicology, Medical College of Georgia, Augusta, GA 30912-2300. E-mail: wcaldwel@mail.mcg.edu** and visit the Department **website: http://www.mcg.edu/SOM/phmtox/index.html.** Application review will begin July 1, 2006. *MCG is an Equal Employment Opportunity/Affirmative Action Equal Access Employer.*

POSITIONS OPEN

DEPARTMENT CHAIR

The Department of Biochemistry and Molecular Biology at Colorado State University invites applications for a new Chair. The successful candidate will have an internationally recognized research program complementing one or more existing strengths of the Department in cellular biochemistry, structural biology, and eukaryotic gene expression. The University has initiatives in infectious disease and genomics/proteomics that might be of interest to candidates. The Chair will provide vision and dynamic leadership in guiding the Department's research, teaching, and service missions. Required credentials include a Ph.D. degree in biochemistry or related field with research, teaching, and service experience commensurate with an appointment as a tenured Professor. Further information can be found at **website: http://www.bmb.colostate.edu/index.cfm.** To apply, submit a cover letter, curriculum vitae, and statements of research and service experience, departmental leadership philosophy, and vision for undergraduate/graduate education to **website: http://www.natsci.colostate.edu/searches/biochem/.** Applicants should provide names and contact information online for three references as soon as possible to allow references time to write letters. Referees will receive instructions by e-mail for submitting letters online, or may mail them to: **Biochemistry and Molecular Biology Chair Search, c/o Department of Biology, 1878 Campus Delivery, Colorado State University, Fort Collins, CO 80523-1878.** For full consideration, applications should be received by September 15, 2006, although applications will be considered until the position is filled. *Colorado State University is an Equal Employment Opportunity/Affirmative Action employer.*

Additional job postings not featured in this issue can be viewed online at **website: http://www.sciencecareers.org.** New jobs are added daily!

Fonds
InBev-Baillet Latour
Fund

The

InBev-Baillet Latour Health Prize - 2007

consists of sum of

150.000 €

and will have as theme

"Neurosciences"

The purpose of the Prize is to recognise the scientific merits of the laureate and to encourage him or her, by this individual award, in the pursuit of his or her creative research. Exceptionally, the Prize may be shared by two persons who have closely worked together over a long period.

The Prize is open to scientists of all nationalities, who have not previously received in their own name an equivalent Prize rewarding the work which is submitted for the "InBev-Baillet Latour Health Prize".

Nominations for 2007 marked "Confidential" should be postmarked no later than **September 15th 2006** and sent to the Secretary General of the National Fund for Scientific Research F.N.R.S., rue d'Egmont 5, BE - 1000 Brussels, Belgium.

The regulations of this Prize and the proposing form are available at the InBev-Baillet Latour website (**www.inbev-baillet-latour.be**) and at the F.N.R.S. website (**www.fnrs.be**).

POSITIONS OPEN

RESEARCH ASSOCIATE 4 OR 5
(Nuclear Magnetic Resonance Spectroscopist)

The College of Basic Sciences at Louisiana State University, Baton Rouge, is seeking a highly qualified, experienced Nuclear Magnetic Resonance (NMR) spectroscopist. Required qualifications: Master's degree in chemistry, biology or physics; solution state experience with modern multi-dimensional homonuclear and heteronuclear NMR (preferably in an academic or industrial NMR service facility); knowledge of relevant hardware and software; excellent interpersonal and communication skills. Additional qualifications desired: Ph.D.; experience in solid state NMR. Responsibilities: equipment troubleshooting and maintenance, cryogen fills, spectrometer calibration, user training and experiment design. Opportunities for collaboration with several research groups (organic; organometallic; materials science; environmental; biochemical) exist.

The NMR Facility instrumentation includes a Varian Systems 700 MHz 3-channel spectrometer with a cold probe; a Varian Inova 500 MHz 3-channel spectrometer with robotic sample changer; a Bruker DPX 400 MHz 2-channel spectrometer with high resolution probes in addition to HR-MAS probes; a Bruker AV 400 MHz wide bore (solid state) 3-channel (plus lock) spectrometer; a Bruker ARX 300 MHz 2-channel spectrometer; and a Bruker DPX 250 MHz 2-channel spectrometer. All spectrometers are equipped with Z-gradients. Computing platforms include IRIX (SGI), Linux, and OS X (MAC). Funding is currently in place to purchase a 400 MHz spectrometer with a high-power gradient amplifier and a diffusion probe.

Title and salary will be dependent upon qualifications and credentials of applicant chosen. An offer of employment is contingent on a satisfactory pre-employment background check. Review of applications will begin June 30, 2006, and will continue until candidate is selected. Applicants should send curriculum vitae (including e-mail address) and arrange to have three letters of reference sent to: **Dr. Robert Hammer, c/o College of Basic Sciences, 338 Choppin Hall, Louisiana State University, Ref: 005164, Baton Rouge, LA 70803.**

Louisiana State University is an Equal Opportunity/Equal Access Employer.

MEDICAL INFORMATION RESEARCHER/WRITER

PinnacleCare, a growing health management company based in Baltimore, Maryland, is seeking a medical Researcher/Writer. The successful candidate will perform information research mostly among biomedical journals to discover the latest findings in disease mechanism, diagnosis, current treatment options, and clinical trials and then write reports in clear, concise, and plain English.

Candidates should have a Ph.D., preferably in a field of clinical science. An M.D. is not required but is favored. Scientists graduated recently with a Ph.D. strongly encouraged to apply.

Please e-mail or fax your curriculum vitae/resume to: **Benjamin Yang, M.D., Ph.D., Director of Research, PinnacleCare; e-mail: resumes@pcistaff.com,** or **fax: 410-637-3431.**

CHIEF MEDICAL OFFICER

Highly intelligent individual with exceptional communication skills sought by prominent Manhattan family to research and coordinate family medical and healthcare issues. Act as liaison with leading medical researchers and consultants in academia and industry, with full responsibility for technical, financial, and administrative functions. Considerable weight given to evidence of unusual academic or other intellectual distinction. Ph.D. or M.D. required, clinical experience a plus but not essential. Possible entrepreneurial opportunities involving delivery of ultrahigh-end medical care to other, similar families. Full-time position. Excellent compensation with significant upside potential and management possibilities. Resume to **e-mail: fmc4@spsfind.com.**

POSITIONS OPEN

PROGRAM DIRECTORS
Plant Developmental Biologist, AD-401-4
Behavioral Neuroscientist, AD-401-4
Two Permanent Positions, NSF
Division of Integrative Organismal Biology
Annual salary ranges from $91,407 to $142,449

The Division of Integrative Organismal Biology (IOB) in the Directorate for Biological Sciences at the National Science Foundation is seeking qualified candidates for two positions as Program Director, one in plant developmental biology and a second in behavioral neuroscience. IOB supports integrative research in emerging areas of organismal biology of plants and animals including neuroscience, developmental biology, ecological and evolutionary physiology, and behavior. More information about IOB can be found on **website: http://www.nsf.gov/div/index.jsp?div=IOB.**

Appointment to these positions is to be filled as a permanent Program Director. Applicants must possess a Ph.D. in biology or in an equivalent discipline. In addition, six or more years of successful research, research administration, or managerial experience beyond the Ph.D. is required. The announcements which include position requirements and application procedures are located on NSF's Division of Human Resource Management **website: http://www.nsf.gov/about/career_opps/** or can be obtained by contacting **Myra Loyd** at **telephone: 703-292-4363.**

The announcement number for the Plant Developmental Biologist position is E20060102-Permanent; the announcement number for the Behavioral Neuroscientist position is E20060103-Permanent. Hearing impaired individuals may **telephone: TDD 703-292-8044.** Applications must be received by June 30, 2006.

NSF is an Equal Opportunity Employer committed to employing a highly qualified staff that reflects the diversity of our nation.

POSITIONS OPEN

SIX POSTDOCTORAL POSITIONS available at the Hormel Institute, University of Minnesota, Austin, Minnesota, to study signal transduction in tumor promotion, chemoprevention, and early development (see review articles: *Science* STKE, re4, 2005; *Prog. Nucleic Acid Res. Mol. Biol.*, **79:**237-97, 2005; *Nature Review Cancer* **4:**793-805, 2004; *Science* STKE, re2, 2003). We are seeking self-motivated Ph.D.s with experience in biochemistry, molecular and cellular biology specializing in one of three categories as follows: (1) signal transduction, functional genomics, models such as mouse transgenic/knockout, *Xenopus,* zebrafish; (2) proteomics, protein crystallization, X-ray crystallography, and structure refinement; (3) computational biology to work with the Hormel Institute, IBM (Blue Gene/L, Rochester, Minnesota) and the University of Minnesota Supercomputing Institute focusing on computational and modeling aspects involving protein-protein interactions in cell signaling, small molecule interactions with proteins, and developing focus chemical libraries for screening protein targets. Experience with molecular simulation packages such as Gaussian03, AMBER, LAMMPS, docking programs, bioinformatics software and commonly used molecular modeling interface. Please send your curriculum vitae and the names and telephone numbers of three references to: **Dr. Zigang Dong, The Hormel Institute, University of Minnesota, 801 16th Avenue N.E., Austin, MN 55912. Fax: 507-437-9606; e-mail: zgdong@hi.umn.edu.** These positions will be open until qualified candidates are found. *The University of Minnesota is committed to the policy that all persons shall have equal access to its programs, facilities, and employment without regard to race, color, creed, religion, national origin, sex, age, marital status, disability, public assistance status, veteran status, or sexual orientation.*

POSTDOCTORAL POSITION at Boston University Medical Center and the Whitaker Cardiovascular Institute. Position available to study the molecular mechanisms of oxidative signaling in vascular cells and animal models of cardiovascular disease. Work involves development and analyzing transgenic mice. Previous experience in molecular biology and transgenics is desirable. Send resume and three references to **Diane Lobel** at **e-mail: drlobel@bu.edu,** or **Diane Lobel, 715 Albany Street, Room 507, Boston, MA 02118.**

The College of Life Science at Fujian Normal University, China, invites applications for tenure-track faculty positions at the **ASSOCIATE PROFESSOR** and **PROFESSOR** level. Individuals expertised in the area of developmental biology, cell biology, and neurobiology are encouraged to apply. The positions offer an attractive startup package and excellent laboratory space. Candidates should have a Ph.D., suitable postdoctoral research experience, and an ability to develop innovative research programs. For further information visit **website: http://life.fjnu.edu.cn** or contact: **Professor Yanding Zhang, Dean of the College.**

MARKETPLACE

In the Frantic World of Gene Expression...
A Moment of Clear-ity

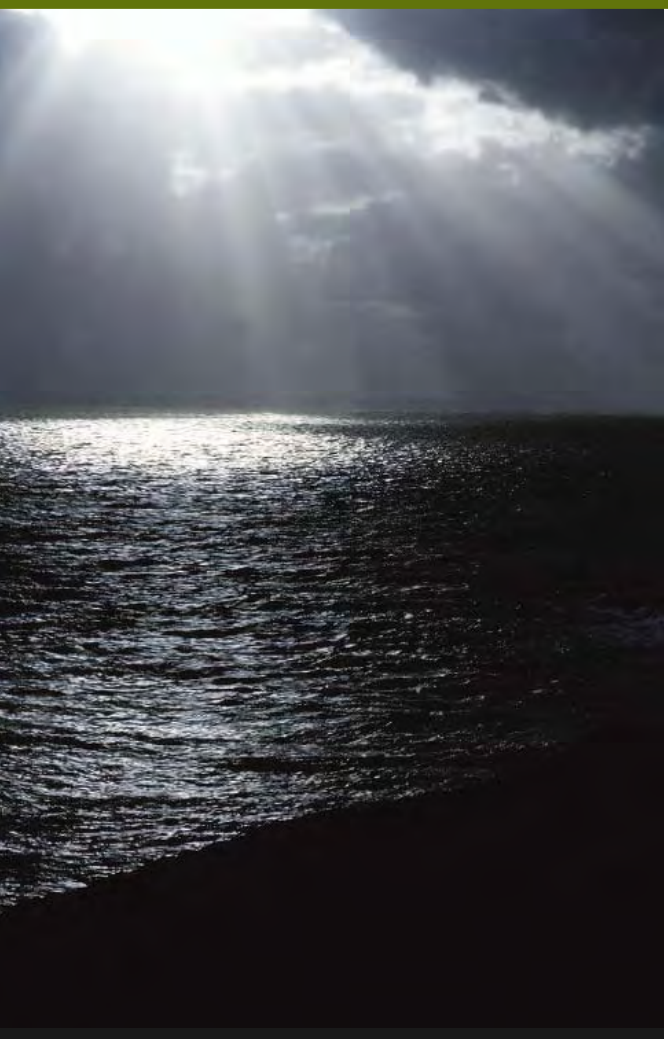

GLOBINclear™-Systems

Globin mRNA Removal from Human, Mouse, and Rat Samples

- Remove >95% of contaminating globin mRNA
- Detect an average of 50% more genes after globin mRNA removal
- Reduce patient to patient variability in assay sensitivity
- Provide greater representation of the genome — low 3'/5' ratios
- Preserve expression profiles — no RNase H treatments that degrade mRNA

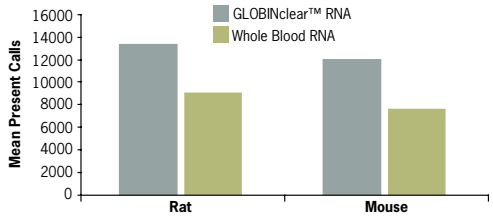

Using GLOBINclear™-Mouse/Rat Results in Higher Gene Detection in Array Analysis. Triplicate GLOBINclear-Mouse/Rat reactions were performed with pooled total RNA samples derived from either mouse or rat blood. The processed RNA was then amplified with MessageAmp™ II-96 to synthesize biotinylated aRNA probe for GeneChip® array analysis. Biotinylated aRNA was then hybridized to triplicate Affymetrix microarrays (Mouse430A_2 or Rat230_2 GeneChips). GLOBINclear processing resulted in an increase in genes called present of 46% and 56% for rat and mouse, respectively.

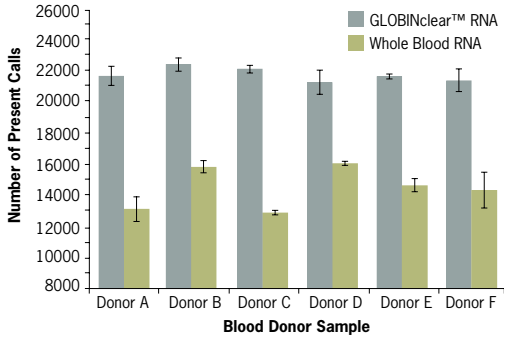

GLOBINclear™-Human Treatment Increases the Number of Genes Detected in Array Analysis. Duplicate arrays (Affymetrix® GeneChip® U133 Plus 2.0) were hybridized with two GLOBINclear-treated whole blood total RNA samples for each donor shown. Duplicate arrays were also hybridized with untreated total RNA samples from each donor. GLOBINclear-treated samples demonstrated a clear and consistent increase in features 'present' (average increase of 50%). Ambion's MessageAmp™ II-96 aRNA Amplification Kit was used to prepare biotinylated aRNA for hybridization using 1 µg input RNA.

GLOBINclear™-Systems employ a novel, non-enzymatic technology to remove >95% of the globin mRNA from whole blood. The resulting RNA is a superior template for RNA amplification or synthesizing labeled cDNA for array analysis and quantitative RT-PCR.

Learn more at
www.ambion.com/prod/globin

Ambion, Inc.
U.S. 800-888-8804 • Canada 800-445-1161
U.S. tel +1-512-651-0200 • fax +1-512-651-0201

Ambion (Europe) Ltd
tel +44 (0)1480-373-020
fax +44 (0)1480-373-010

Ambion K.K. (Japan)
tel +81 (0)3-5638-2181
fax +81 (0)3-5638-2182

For a list of Ambion direct free phone numbers and distributors in your country, go to www.ambion.com/contact

Ambion®
THE RNA COMPANY®
An Applied Biosystems Business